frontiers | Research Topics

Sustainable planning and life-cycle thinking of energy infrastructure

Edited by
Nallapaneni Manoj Kumar, Idiano D'Adamo, Subrata Hait, Anshu Priya, Sofiane Kichou and Massimo Gastaldi

Published in
Frontiers in Energy Research

ISSN 1664-8714
ISBN 978-2-8325-2328-5
DOI 10.3389/978-2-8325-2328-5

About Frontiers

Frontiers is more than just an open access publisher of scholarly articles: it is a pioneering approach to the world of academia, radically improving the way scholarly research is managed. The grand vision of Frontiers is a world where all people have an equal opportunity to seek, share and generate knowledge. Frontiers provides immediate and permanent online open access to all its publications, but this alone is not enough to realize our grand goals.

Frontiers journal series

The Frontiers journal series is a multi-tier and interdisciplinary set of open-access, online journals, promising a paradigm shift from the current review, selection and dissemination processes in academic publishing. All Frontiers journals are driven by researchers for researchers; therefore, they constitute a service to the scholarly community. At the same time, the *Frontiers journal series* operates on a revolutionary invention, the tiered publishing system, initially addressing specific communities of scholars, and gradually climbing up to broader public understanding, thus serving the interests of the lay society, too.

Dedication to quality

Each Frontiers article is a landmark of the highest quality, thanks to genuinely collaborative interactions between authors and review editors, who include some of the world's best academicians. Research must be certified by peers before entering a stream of knowledge that may eventually reach the public - and shape society; therefore, Frontiers only applies the most rigorous and unbiased reviews. Frontiers revolutionizes research publishing by freely delivering the most outstanding research, evaluated with no bias from both the academic and social point of view. By applying the most advanced information technologies, Frontiers is catapulting scholarly publishing into a new generation.

What are Frontiers Research Topics?

Frontiers Research Topics are very popular trademarks of the *Frontiers journals series*: they are collections of at least ten articles, all centered on a particular subject. With their unique mix of varied contributions from Original Research to Review Articles, Frontiers Research Topics unify the most influential researchers, the latest key findings and historical advances in a hot research area.

Find out more on how to host your own Frontiers Research Topic or contribute to one as an author by contacting the Frontiers editorial office: frontiersin.org/about/contact

Sustainable planning and life-cycle thinking of energy infrastructure

Topic editors

Nallapaneni Manoj Kumar — City University of Hong Kong, SAR China
Idiano D'Adamo — Sapienza University of Rome, Italy
Subrata Hait — Indian Institute of Technology Patna, India
Anshu Priya — Amity University, India
Sofiane Kichou — Czech Technical University in Prague, Czechia
Massimo Gastaldi — University of L'Aquila, Italy

Citation

Kumar, N. M., D'Adamo, I., Hait, S., Priya, A., Kichou, S., Gastaldi, M., eds. (2023). *Sustainable planning and life-cycle thinking of energy infrastructure*. Lausanne: Frontiers Media SA. doi: 10.3389/978-2-8325-2328-5

Table of contents

frontiers | Frontiers in Energy Research

TYPE Editorial
PUBLISHED 18 April 2023
DOI 10.3389/fenrg.2023.1196826

OPEN ACCESS

EDITED AND REVIEWED BY
Michael Carbajales-Dale,
Clemson University, United States

*CORRESPONDENCE
Nallapaneni Manoj Kumar,
nallapanenichow@gmail.com,
manllapan2-c@my.cityu.edu.hk

RECEIVED 30 March 2023
ACCEPTED 11 April 2023
PUBLISHED 18 April 2023

CITATION
Kumar NM, D'Adamo I, Hait S, Priya A, Kichou S and Gastaldi M (2023), Editorial: Sustainable planning and lifecycle thinking of energy infrastructure. *Front. Energy Res.* 11:1196826. doi: 10.3389/fenrg.2023.1196826

Editorial: Sustainable planning and lifecycle thinking of energy infrastructure

Nallapaneni Manoj Kumar[1,2,3]*, Idiano D'Adamo[4], Subrata Hait[5], Anshu Priya[1,6], Sofiane Kichou[7] and Massimo Gastaldi[8]

[1]School of Energy and Environment, City University of Hong Kong, Kowloon, Hong Kong SAR, China, [2]Center for Research and Innovation in Science, Technology, Engineering, Arts, and Mathematics (STEAM) Education, HICCER—Hariterde International Council of Circular Economy Research, Palakkad, Kerala, India, [3]Swiss School of Business and Management Geneva, Genève, Switzerland, [4]Department of Computer, Control and Management Engineering, Sapienza University of Rome, Roma, Italy, [5]Department of Civil and Environmental Engineering, Indian Institute of Technology Patna, Bihar, India, [6]Centre for Plant and Environmental Biotech, Amity Institute of Biotechnology, Amity University, Noida, India, [7]Czech Technical University in Prague, University Centre for Energy Efficient Buildings, Buštěhrad, Czech Republic, [8]Department of Industrial and Information Engineering and Economics, University of L'Aquila, L'Aquila, Italy

KEYWORDS

energy infrastructure, renewable energy, smart microgrids, circular economy, SDG7, clean energy policy, sustainable and resilient energy systems, integrated energy infrastructures

Editorial on the Research Topic
Sustainable planning and lifecycle thinking of energy infrastructure

1 Energy infrastructure

Energy infrastructure refers to the systems, structures, and facilities that are designed to generate, transmit, and distribute energy (Bridge et al., 2018). Energy infrastructure is a critical component of modern societies and is essential for powering homes, businesses, and industries (Goldthau, 2014; Pandey, 2020). The types of energy infrastructure vary depending on the energy source and other things in its value chain. For example, traditional utilities like gas and pipelines, power generation systems for fossil fuels and renewable ones, electrical transmission lines, electrical metering and distribution systems, smart systems, storage facilities, advanced electric and electronic systems, and various types of power control systems (Bridge et al., 2018; Pandey, 2020). In addition, today's energy infrastructure includes many directly or indirectly related industrial systems and numerous interdependent sectors like transportation (electric vehicles) (Nallapaneni, 2022a), food and agriculture (farm machinery, drying, agrivoltaics) (Chand et al., 2021; Nallapaneni et al., 2021; Poonia et al., 2022).

Energy infrastructure can also refer to the policies, regulations, and institutions that govern energy production and consumption (Goldthau, 2014; Bridge et al., 2018). These can include things like energy conservation programs, renewable energy standards, and energy market regulations. Furthermore, energy communities represent a new social model for the energy transition (D'Adamo et al., 2022). Overall, energy infrastructure is a complex and multifaceted system that plays a crucial role in the functioning of modern societies and is a key driver of global economic growth and competitiveness.

2 Importance of planning energy infrastructure and its implementation

Planning is crucial for energy infrastructure because the development and operation of energy infrastructure can have significant environmental, economic, and social impacts. They are often large-scale and require long-term investments; if we want to list the reasons; there are several reasons, some are listed below.

2.1 Environmental impact

Energy infrastructure projects can have significant environmental impacts, including land-use changes, habitat destruction, air and water pollution, and others. Proper planning can help identify potential environmental impacts and mitigate them through the use of cleaner technologies, siting decisions, and other measures.

2.2 Cost-effectiveness

Energy infrastructure projects are often large and expensive, so careful planning is needed to ensure that they are cost-effective. This includes identifying the most efficient and effective technologies, optimizing the project design, and ensuring that the project is built and operated in a way that maximizes its energy output and minimizes its operating costs.

2.3 Social acceptance

Energy infrastructure projects can also have significant social impacts, including displacement of communities, impacts on cultural resources, and impacts on public health and safety. Proper planning can help identify potential social impacts and develop strategies to mitigate them, including engaging with local communities, developing public health and safety plans, and providing adequate compensation and support for affected communities.

2.4 Regulatory compliance

Energy infrastructure projects are subject to a range of regulatory requirements, including environmental permits, land-use approvals, and safety regulations. Proper planning is essential to ensure that the project is designed and implemented in compliance with all applicable regulations and requirements.

2.5 Interdependencies

Energy infrastructure projects have seen many technological advancements in recent years, especially from an application point of view in various other infrastructure sectors. As a result, systems like renewable-powered desalination (Vishnupriyan et al., 2021), agrivoltaics (Nallapaneni et al., 2021), grapevoltaics (Nallapaneni and Chopra, 2021a; Kumar and Chopra, 2023), vehicle-integrated photovoltaics (Mamun et al., 2022), floating solar (Kumar et al., 2022), urban wind turbines (Dilimulati et al., 2018), integrated renewables-battery energy storage systems (Cucchiella et al., 2017) and others have become popular and created interdependencies in the context of climate change mitigation and decarbonization (Zhongming et al., 2018). Such interdependencies suggest the need for effective planning and better implementation of energy infrastructure to ensure the competitiveness of the energy and the other dependent sectors.

To summarise, proper planning is essential for energy infrastructure projects to ensure that they are designed and implemented in a way that is sustainable, cost-effective, and beneficial to society as a whole. However, when we think of planning and implementation, planning based on conventional feasibility studies is insufficient and should be from a life-cycle perspective (Kumar et al., 2023). Also, Sustainable Development Goal 7 (SDG7) advocates having energy infrastructure developments confined to set targets and indicators, broadly promoting the goal "ensure access to affordable, reliable, sustainable and modern energy for all" (UN SDG, 2022). On the other side, the energy infrastructure's technology and policy drivers are rapidly changing, whereas the regulatory framework and permitting systems surrounding the energy infrastructure are currently designed for another age, making it difficult for implementation, modernization, expansion, decommissioning, and end-of-life (Nallapaneni, 2021; D'Adamo et al., 2023; Molla et al., 2023). Considering all such considerations, it is better to apply "sustainable planning and life-cycle thinking" to the energy infrastructure.

3 Approaches for sustainable planning and lifecycle thinking of energy infrastructure

There are several approaches for planning energy infrastructure, depending on factors such as the type of energy infrastructure being planned, the project's scale, and the project's goals. Some common approaches include.

3.1 Integrated resource planning (IRP)

IRP is a comprehensive planning process that considers all potential resources, including renewable energy, demand management, and energy efficiency measures. This approach aims to balance the cost, reliability, and environmental impacts of different resource options to meet the needs of customers (Beecher, 1995).

3.2 Scenario planning

Scenario planning involves developing multiple scenarios for the future based on different assumptions about energy demand, prices, and technological advancements. This approach helps planners identify potential risks and opportunities and develop strategies to address them (Ringland, 1998).

3.3 Stakeholder engagement

Stakeholder engagement involves involving a diverse group of stakeholders in the planning process, including community members, industry experts, and policymakers. This approach can help ensure that the infrastructure meets the needs of all stakeholders and that their concerns are addressed (Kujala et al., 2022).

3.4 Cost-benefit analysis (CBA)

CBA is a method of evaluating the costs and benefits of different energy infrastructure options. This approach can help identify the most cost-effective options for meeting energy needs (Layard, 1994).

3.5 Techno-economic assessment (TEA)

TEA is a method used to evaluate the feasibility and economic viability of energy infrastructure projects, such as renewable energy generation, transmission, and distribution. The TEA approach takes into consideration various factors such as the availability of natural resources, energy demand and consumption patterns, environmental impact, and regulatory framework. This can help make informed decisions on which energy infrastructure projects to pursue based on their economic and technical viability and their potential to meet the energy needs of the community while minimizing environmental impact (Burk, 2018).

3.6 Life cycle assessment (LCA)

LCA is a method of assessing the environmental impacts of different energy infrastructure options throughout their entire life cycle, from raw material extraction to disposal. This approach can help identify the most environmentally sustainable options (Hauschild et al., 2018).

3.7 Integrated TEA and LCA

Integrated TEA and LCA is a comprehensive approach that combines the evaluation of the economic and technical aspects of a technology or project with an analysis of its environmental impact over the entire life cycle of the product or service (Yuan et al., 2022). By integrating TEA and LCA, decision-makers can better evaluate the overall sustainability of a technology or project by considering not only its financial and technical feasibility but also its environmental impact. The combined approach enables the identification of trade-offs between economic and environmental goals and helps to identify opportunities for improvements in both areas.

3.8 Design in line with SDG7

Design in line with SDG7 refers to the practice of designing energy infrastructure and its systems and service following the targets of SDG7, i.e., to ensure access to affordable, reliable, sustainable, and modern energy for all. It was first proposed by (Kumar et al., 2020; Nallapaneni and Chopra, 2021b) for designing hybrid microgrids, see Figure 1A.

3.9 RePLiCATE approach

RePLiCATE stands for Resilience Performance Life Cycle Analysis and Techno-Economics, Figure 1B. It is a framework proposed for the first time by (Nallapaneni, 2021) in his doctoral thesis, later in his young scientist talk in the HKICE Young Scientist Seminar Series at the Hong Kong Institute for Clean Energy, City University of Hong Kong, for sustainable and resilient planning of advanced clean energy systems (Nallapaneni, 2022b). RePLiCATE combines LCA, TEA, and resilience assessment to evaluate the environmental, economic, and social impacts of advanced clean energy systems across their life cycle stages (Nallapaneni, 2021; Nallapaneni, 2022b). The framework aims to provide decision-makers with a comprehensive understanding of the trade-offs between different performance indicators and identify sustainable and resilient strategies for energy infrastructure planning (Nallapaneni and Chopra, 2021a; Kumar and Chopra, 2023). Furthermore, RePLiCATE can also be integrated with the various SDGs to understand the energy infrastructure performance on a regional level based on the principles and methods as proposed by (D'Adamo et al., 2021).

4 Discussion on the research topic collection

This Research Topic in Frontiers in Energy Research intends to collect contributions that enable the sustainable transformation of energy infrastructure during its implementation, modernization, expansion, decommissioning, and end-of-life from a science, technology, engineering, and policy perspective. The overall response from the research, academic, and industry community for this Research Topic was amazing. A total of 22 articles were published and briefly fall under energy infrastructure dedicated to the power sector and other interdependent and dependent sectors.

4.1 Energy and supporting infrastructure dedicated to power sector

In energy infrastructure planning, first and foremost is to know the influential factors that influence the intentions of energy use and type of energy use, *etc.* Nazir & Tian (2022) investigated various factors influencing the intention to use renewable energy in energy infrastructure, such as social media exposure, relative advantage, ease of use, awareness, cost, attitude, and purchase intention, especially in Pakistan. The study uses the theory of planned behavior and the unified theory of acceptance and proposes hypotheses that are tested using structured questionnaires on a sample of 497 respondents. The findings show that attitude has a significant mediating effect on the relationship between purchase intention and factors such as social media exposure, relative

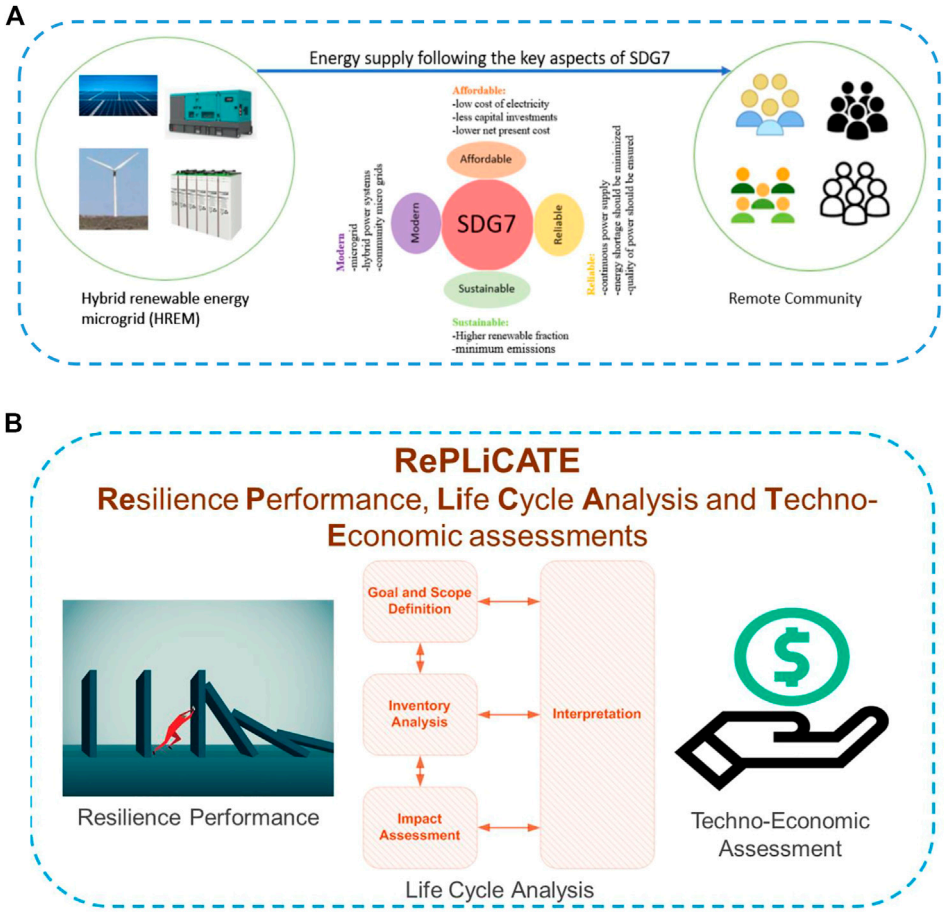

FIGURE 1
Approaches for Sustainable Planning and Lifecycle Thinking of Energy Infrastructure. **(A)** Energy Systems Design in line with SDG7. Adopted from authors own sources (Kumar et al., 2020; Nallapaneni and Chopra, 2021b); **(B)** RePLiCATE Approach. Adopted from authors own sources (Nallapaneni, 2021; Nallapaneni, 2022b).

advantage, ease of use, awareness, and cost. The study suggests that marketing approaches can be used to enhance customer purchase intention and help make decisions in the renewable energy sub-sector.

After understanding the intentions of use, energy systems design and placing them in the network either in a decentralized or centralized way matters. This phase is crucial where system design and related parameters or optimization that affect overall feasibility is given more importance. For instance, in (1). Navothna & Thotakura (2022) analyzes the performance of a 1 MWp solar photovoltaic (PV) plant in GITAM (Deemed to be University) in Andhra Pradesh, India. The study calculates efficiency, capacity factor, and performance ratio using simulated data and analyzes the PV modules' light-induced degradation and degradation rate. (2). Desai et al. proposed the adoption of bifacial solar panels in rooftop PV systems in India and investigated the feasibility. The goal is to enhance energy generation as compared to mono-facial solar panels. The study presents the technical and economic advantages of using bifacial Si-modules in a typical 5-kW single-phase solar rooftop PV system. The study finds that bifacial modules generate more than 10% excess energy compared to the poly c-Si systems. Finally, the study finds that an optimized bifacial system tilted between 15° and 20° will reduce the levelized cost of electricity (LCOE) by 5.5% as compared to the traditional poly c-Si system. (3). Same et al. (2022) proposed a hybrid renewable energy system (HRESs) and a control system for a refugee camp to provide affordable, reliable, and clean energy. The techno-economic feasibility of the system was evaluated under load following, cycle charging, and predictive control strategy. The results showed that the predictive control strategy was the most suitable, with the lowest cost and highest eco-friendliness and energy efficiency. The total net present cost for electrification of the refugee camp was $3,809,822.54, and the cost of electricity generated was $0. 2018 per kWh. The hybridization of the diesel generator under the predictive control strategy could avoid 991,240.32 kg of emissions annually. (4). Zhou et al. investigated the impact of displacement selections and heat exchanger arrangement on the performance of a 300 MW geothermal-aided power generation (GAPG) power plant. The results showed that using geo-fluid to displace high-grade extraction steam only can prevent silica scaling in the heat exchanger system, which can improve the performance of the GAPG plant. Additionally, the parallel arrangement of the heat exchanger is more effective than the series arrangement in terms of additional power output. The study also found that the GAPG plant has the potential to reduce carbon dioxide emissions by 13%, which

highlights the environmental benefits of this technology. (5). Sivadanam et al. address the impact of inverter-based resources (IBRs) on the synchronous inertia of interconnected power systems (IPSs) and the need for faster frequency response requirements. The study proposes a stochastic and iterative-based optimization for load frequency control (LFC) using a hybrid energy storage system (HESS) with plug-in hybrid electric vehicles (PHEVs) and a superconducting magnetic energy storage (SMES) device. Two types of tie lines are investigated with optimal parameters recorded using particle swarm optimization (PSO) and biogeography-based optimization (BBO). The proposed BBO-based LFC ensures precision and accuracy, indicating improved IPS dynamic performance in smart cities. (6). Hussien et al. propose a method to minimize torque ripples in a surface-mounted permanent magnet synchronous motor using the variable switching frequency technique of pulse width modulation. The goal is to achieve high-performance operation of a motor-generator set. The effectiveness of the proposed control strategies is confirmed through obtained results to ensure controllability.

While developing infrastructure, it is crucial to check on the government subsidies and policies, if not atleast its outcome how the policy is performing to realise the climate goals. Wang et al. investigated the impact of government subsidies on pollution reduction in power companies in China. A fixed-effects panel data model was used to investigate the influence of subsidies on pollution reduction and how the mechanism works. The study found that subsidies can significantly reduce pollution, especially sulfur dioxide emissions and soot. Additionally, the results indicated that subsidies encourage power companies to reduce emissions through end-of-pipe control and green innovation. The study also found that subsidies have a better effect on regions with stronger environmental regulations, less economically developed regions, big-scale companies, and companies with low slack.

Other key aspect in infrastructure is its management, security and risk. For instance, in (1). Kong et al. described the design of a security risk management and control system for power trading institutions based on a Bayesian network to reduce the impact of risk on power trading projects. The risk evaluation is performed and effectively identifies risks; overall the system has high-risk management and control efficiency, with near-practical application value. (2). Zhang et al. proposed a simulation method to study the impact of the spot market on safety risks and generation benefits in the evolving electricity market considering actual cascade hydropower station (CHS). The hydraulic power matching among the CHSs is examined and the proposed method can help in making bidding decisions in spot transactions and can be useful during the transition period of electricity reform. This can also provide insights into the impact of new modes of a transaction on the electricity market and can help in identifying potential risks and opportunities. (3). Li and Hu (2022) addressed the Research Topic of accurately measuring and managing energy risk, which is critical for economic development and energy security. Instead of Value at Risk (VaR) method that is commonly available, this study proposes the use of Conditional VaR (CVaR) based on non-parametric kernel (NPK) framework. The results indicate that the NPK framework backed CVaR method is more effective in measuring actual energy risk and in carrying out risk hedging. Overall, the paper offers a more accurate and effective method to measure and manage energy risk, which is essential for promoting economic growth and energy security.

4.2 Energy and supporting infrastructure for interdependent and dependent sectors

Developing energy and supporting infrastructure from the context of interdependent and dependent sectors will lead to many new research areas. For instance, the Research Topic of co-producing energy and water is investigated by Murillo-Alvarado and Cardenas-Gil (2022) where they propose a mathematical optimization model to determine the feasibility of installing solar power generation plants and two scenarios are analyzed; one with variation in the operating time of the thermal storage system and the other with the incorporation of the rainwater harvesting system. Wu and Chul-Soo (2023) explored another application, i.e., the integration of solar photovoltaic collectors with vertical-green balconies in old high-rise buildings for water heating application. The study aims to conduct a preliminary research study on such integration possibilities with old buildings and explore various benefits such as water heating, energy-saving rate. The study suggests that the process-specific rationalization plan can be applied in future urban architecture renovation.

From a transportation sector application and its electrification point of view, (1). Chakraborty et al. presented the importance of sustainable mobility and the use of hydrogen fuel-based vehicular technologies to reduce greenhouse gas (GHG) emissions in the transportation sector. The study also provides an overview of various technologies with a different perception. (2). Tian et al. focuses on the effective utilization of coal liquefaction residue (CLR) through fluidized bed pyrolysis process that introduces green hydrogen and green oxygen to the process, achieving near-complete utilization of carbon and hydrogen elements in the CLR and producing high-quality liquid fuels and syngas. This new process can achieve almost near-zero carbon dioxide (CO_2) emission in the entire unit which can facilitate sustainable development and improve the efficiency of coal conversion technology. (3). Chowdary and Sura (2022) proposes a solution to address concerns about charging infrastructure for electric vehicles (EVs) by designing and modeling a grid-connected photovoltaic-based microgrid. The study aims to analyze a hypothetical EV population charging while considering realistic EV loads and simulating the charging process. The study also analyzes the impact of weather parameters on power production and the impact of scaled EV sessions on microgrid power balances. The proposed solution could help address concerns about charging infrastructure for EVs and promote the adoption of renewable energy sources in the transportation sector. (4). Though renewables support transportation sector, there are some incidents where energy infrastructure may be considered as a risk. For instance, the wind turbines may be considered as potential obstructions to air traffic. Weigel et al. presented a multi-aspect holistic evaluation of aircraft detection lighting systems (ADLS) using a framework previously developed by the authors based on multi-criteria analysis (MCA), LCA, and expert interviews. The study presents information on potential implementation risks, bottlenecks, and levers for life cycle improvement.

From a supporting infrastructure for energy infrastructure, i.e., pipeline and gas network point of view, (1). Wang et al. used

a stochastic process analysis of Research Topic evolution to trace and predict the technology trend of coal slurry pipeline transportation from patent texts. The study provides directions for sustainable research and development (R&D) activities in coal slurry pipeline transportation technology, facilitating interdisciplinary discussions and providing objective data for future decision-making by scientists and R&D managers in this field. (2). Wang et al. examined the impact of China's third-party access policy on the efficiency of its natural gas network. They identify that the policy has resulted in a decoupling of gas trade and transport, which has led to underutilization of transmission resources due to the contractual arrangements between entry and exit capacities in the commercial network. To address this Research Topic, the authors propose a mathematical programming with equilibrium constraints (MPEC) model that integrates the allocations of commercial capacity and physical flows. Overall, the study highlights the importance of considering both commercial and physical aspects of natural gas transportation when designing policies to support the sustainable development of energy mix and low-carbon targets.

From an energy technology implementation and policy realisation to achieve decoupling and sustainability point of view, (1). Ao et al. examined the mediating role of innovation in the circular economy approach of energy-related enterprises in managing waste resources and reducing carbon emissions. They show that waste resource utilization positively affects the quality of new energy products, but it does not significantly impact the innovation of these products. On the other hand, carbon reduction behavior by companies in developing countries positively impacts new energy product innovation, but it does not significantly affect product quality. The study validates the existence of a relationship between waste resource utilization, new energy product innovation, and product quality. The findings can help energy-related enterprises improve their new energy product development activities and contribute to reducing waste and carbon emissions. (2). Xie et al. investigated the relationship between carbon emissions and economic growth in Fujian Province, China, based on evidence, as part of China's "double carbon" target to reduce emissions while achieving economic growth. The study emphasizes the importance of the concept of ecological civilization in achieving the "double carbon goal" and the need for accelerating measures that guide the integration of urban and rural areas with critical infrastructure where energy is considered one critical commodity. (3). Han et al. examined the decoupling of China's CO_2 emissions and economic growth using the environmental Kuznets curve model for long-term decoupling and the Tapio model for short-term decoupling. They showed that the influence of industrial and energy structures inhibited CO_2 emissions, but population structure may endorse them. The study recommends that China should strengthen and optimize its energy structure to match its industrial structure.

5 Conclusion

The Research Topic "Sustainable Planning and Life Cycle Thinking of Energy Infrastructure" explored various aspects of planning and implementing sustainable energy infrastructure. Based on the received response in this call, we covered a broad range of Research Topic related to energy infrastructure planning, including renewable energy systems, energy storage, grid integration, and policy impact and role of energy in decarbonization. Apart from planning, the Research Topic also focused on the need to adopt a life cycle thinking approach to energy infrastructure development; this approach involves considering the entire life cycle of energy systems, from production and distribution to end-of-life disposal. By taking a holistic view of energy infrastructure, it is possible to identify opportunities to reduce environmental impacts, improve resource efficiency, and enhance social and economic sustainability. However, the response towards life cycle thinking of energy infrastructure in this call was not too much. Also, from the approaches mentioned in Section 3, the point of view for sustainable planning and lifecycle thinking of energy infrastructure in the received response from various authors was only limited to fewer approaches.

To conclude, the articles included in the Research Topic provided insights into the strategies and technologies that can be employed to promote sustainable energy infrastructure. For instance, several articles explored the use of renewable energy sources, such as solar, geothermal, hydrogen, and wind power, to reduce greenhouse gas emissions and promote energy independence. Other articles discussed the importance of energy storage technologies, such as batteries and pumped hydro; mobility, such as hydrogen- and electric-based, and their integration into the grid. Few other articles focused on technology implementation and policy support in realizing economic growth and decarbonization. In addition, the Research Topic emphasized the importance of considering social and economic factors when planning energy infrastructure. For instance, several articles discussed the role of community engagement and participation in energy infrastructure decision-making. Others explored the potential for energy infrastructure to create new jobs and economic opportunities in local communities.

Overall, the Research Topic collected interesting articles and highlighted the need for a comprehensive, integrated approach like RePLiCATE (Figure 1B) to energy infrastructure planning and development following SDG7 (Figure 1A) and other applicable tools or techniques as per the changing global policies. We strongly believe that by considering technical, environmental, social, and economic factors under the RePLiCATE approach, it is possible to create sustainable energy systems that meet the needs of present and future generations.

Author contributions

All authors listed have made a substantial, direct, and intellectual contribution to the work and approved it for publication.

Acknowledgments

The Research Topic Editors would like to take the opportunity to thank the authors who responded to the call. We are also deeply

indebted to the reviewers whose input was indispensable to select the published papers.

Conflict of interest

The authors declare that the research was conducted in the absence of any commercial or financial relationships that could be construed as a potential conflict of interest.

Publisher's note

All claims expressed in this article are solely those of the authors and do not necessarily represent those of their affiliated organizations, or those of the publisher, the editors and the reviewers. Any product that may be evaluated in this article, or claim that may be made by its manufacturer, is not guaranteed or endorsed by the publisher.

References

Beecher, J. A. (1995). Integrated resource planning fundamentals. *J. Am. Water Works Assoc.* 87 (6).

Bridge, G., Özkaynak, B., and Turhan, E. (2018). Energy infrastructure and the fate of the nation: Introduction to special issue. *Energy Res. Soc. Sci.* 41, 1–11. doi:10.1016/j.erss.2018.04.029

Burk, C. (2018). "Techno-economic modeling for new technology development," in *Chemical engineering progress*, 43–52.

Chand, A. A., Prasad, K. A., Mar, E., Dakai, S., Mamun, K. A., Islam, F. R., et al. (2021). Design and analysis of photovoltaic powered battery-operated computer vision-based multi-purpose smart farming robot. *Agronomy* 11 (3), 530. doi:10.3390/agronomy11030530

Cucchiella, F., D'Adamo, I., and Gastaldi, M. (2017). The economic feasibility of residential energy storage combined with PV panels: The role of subsidies in Italy. *Energies* 10, 1434. doi:10.3390/en10091434

D'Adamo, I., Ferella, F., Gastaldi, M., Ippolito, N. M., and Rosa, P. (2023). Circular solar: Evaluating the profitability of a photovoltaic panel recycling plant. *Waste Manag. Res.*, 734242X221149327. 0734242X221149327. doi:10.1177/0734242X221149327

D'Adamo, I., Gastaldi, M., Imbriani, C., and Morone, P. (2021). Assessing regional performance for the sustainable development goals in Italy. *Sci. Rep.* 11, 24117. doi:10.1038/s41598-021-03635-8

D'Adamo, I., Gastaldi, M., and Morone, P. (2022). Solar collective self-consumption: Economic analysis of a policy mix. *Ecol. Econ.* 199, 107480. doi:10.1016/j.ecolecon.2022.107480

Dilimulati, A., Stathopoulos, T., and Paraschivoiu, M. (2018). Wind turbine designs for urban applications: A case study of shrouded diffuser casing for turbines. *J. Wind Eng. Industrial Aerodynamics* 175, 179–192. doi:10.1016/j.jweia.2018.01.003

Goldthau, A. (2014). Rethinking the governance of energy infrastructure: Scale, decentralization and polycentrism. *Energy Res. Soc. Sci.* 1, 134–140. doi:10.1016/j.erss.2014.02.009

Hauschild, M. Z., Rosenbaum, R. K., and Olsen, S. I. (2018). *Life cycle assessment*. Cham: Springer International Publishing. Available at: https://doi.org/10.1007/978-3-319-56475-3Book.

Kujala, J., Sachs, S., Leinonen, H., Heikkinen, A., and Laude, D. (2022). Stakeholder engagement: Past, present, and future. *Bus. Soc.* 61 (5), 1136–1196. doi:10.1177/00076503211066595

Kumar, N. M., Chakraborty, S., Yadav, S. K., Singh, J., and Chopra, S. S. (2022). Advancing simulation tools specific to floating solar photovoltaic systems–Comparative analysis of field-measured and simulated energy performance. *Sustain. Energy Technol. Assessments* 52, 102168. doi:10.1016/j.seta.2022.102168

Kumar, N. M., Chopra, S. S., Chand, A. A., Elavarasan, R. M., and Shafiullah, G. M. (2020). Hybrid renewable energy microgrid for a residential community: A techno-economic and environmental perspective in the context of the SDG7. *Sustainability* 12 (10), 3944. doi:10.3390/su12103944

Kumar, N. M., and Chopra, S. S. (2023). Integrated techno-economic and life cycle assessment of shared circular business model based blockchain-enabled dynamic grapevoltaic farm for major grape growing states in India. *Renew. Energy* 209, 365–381. doi:10.1016/j.renene.2023.03.064

Kumar, N. M., Islam, S., Podder, A. K., Selim, A., Bajaj, M., and Kamel, S. (2023). Lifecycle-based feasibility indicators for floating solar photovoltaic plants along with implementable energy enhancement strategies and framework-driven assessment approaches leading to advancements in the simulation tool. *Front. Energy Res.* 11, 1075384. doi:10.3389/fenrg.2023.1075384

Layard, P. R. G. (1994). *Cost-benefit analysis*. Cambridge University Press.

Mamun, K. A., Islam, F. R., Haque, R., Chand, A. A., Prasad, K. A., Goundar, K. K., et al. (2022). Systematic modeling and analysis of on-board vehicle integrated novel hybrid renewable energy system with storage for electric vehicles. *Sustainability* 14 (5), 2538. doi:10.3390/su14052538

Molla, A. H., Shams, H., Harun, Z., Kasim, A. N. C., Nallapaneni, M. K., and Rahman, M. N. A. (2023). Evaluation of end-of-life vehicle recycling system in India in responding to the sustainability paradigm: An explorative study. *Sci. Rep.* 13 (1), 4169. doi:10.1038/s41598-023-30964-7

Nallapaneni, M. K. (2021). *Leveraging blockchain and smart contract technology for sustainability and resilience of circular economy business models*. City University of Hong Kong. Doctoral DissertationPhD-SEE-55632135.

Nallapaneni, M. K., and Chopra, S. S. (2021). "Blockchain-enabled dynamic grapevoltaic farms for selected wine risk regions on a global level and the potential opportunities for symbiotic industrial networks," in *6th AIEE energy symposium current and future challenges to energy security: The energy transition, a pathway from* (Milan, Italy.

Nallapaneni, M. K., Chopra, S. S., and D'Adamo, I. (2021). "Agrivoltaics for the co-production of soybeans-solar photovoltaics energy and the opportunities for developing synergetic industrial networks in India," in *5th international conference on alternative fuels, energy and environment (ICAFEE 2021): Future and challenges: Future and challenges*.

Nallapaneni, M. K., and Chopra, S. S. (2021). "Design and analysis of microgrids in line with SDG7 for residential communities in the global south," in *International symposium on sustainable systems and technology (ISSST 2021)*. ISSST-2021.

Nallapaneni, M. K. (2022). "RePLiCATE: A framework for sustainable and resilient planning of advanced clean energy systems," in *HKICE young scientist seminar series* Hong Kong Institute for Clean Energy, City University of Hong Kong. HKICE_YS20221125, 1.

Nallapaneni, M. K. (2022). "U.S.A.'s interstate highway modernization and financing issues: Could road-integrated wind and solar photovoltaics offer support?," in *Nallapaneni's self archive*, 0001. doi:10.13140/RG.2.2.30563.63523/3

Pandey, V. (2020). "Energy infrastructure for sustainable development," in *Affordable and clean energy*, 1–13.

Poonia, S., Singh, A. K., Jain, D., Kumar, N. M., and Singh, D. (2022). Techno-Economic Analysis of Integrated Solar Photovoltaic Winnower-Cum Dryer for Drying Date Palm Fruit. *Sustainability* 14 (20), 13686. doi:10.3390/su142013686

Ringland, G. (1998). *Scenario planning*. Chichester, UK: John Wiley and Sons.

UN SDG (2022). *Goal 7- Ensure access to affordable, reliable, sustainable and modern energy for all*. United Nations. Available at: https://sdgs.un.org/goals/goal7.

Vishnupriyan, J., Arumugam, D., Kumar, N. M., Chopra, S. S., and Partheeban, P. (2021). Multi-criteria decision analysis for optimal planning of desalination plant feasibility in different urban cities in India. *J. Clean. Prod.* 315, 128146. doi:10.1016/j.jclepro.2021.128146

Yuan, X., Kumar, N. M., Brigljević, B., Li, S., Deng, S., Byun, M., et al. (2022). Sustainability-inspired upcycling of waste polyethylene terephthalate plastic into porous carbon for CO_2 capture. *Green Chem.* 24 (4), 1494–1504. doi:10.1039/d1gc03600a

Zhongming, Z., Linong, L., Xiaona, Y., Wangqiang, Z., and Wei, L. (2018). *Renewables are the key to a climate-safe world*. IRENA.

frontiers in Energy Research

ORIGINAL RESEARCH
published: 17 February 2022
doi: 10.3389/fenrg.2022.837007

The Influence of Consumers' Purchase Intention Factors on Willingness to Pay for Renewable Energy; Mediating Effect of Attitude

Mehrab Nazir[1]* *and Jian Tian*[2]*

[1]School of Economics and Management, Jiangsu University of Science and Technology, Changzhou, China, [2]School of Economics and Management, Jiangsu University of Science and Technology, Zhenjiang, China

OPEN ACCESS

Edited by:
Idiano D'Adamo,
Sapienza University of Rome, Italy

Reviewed by:
Ahmed Imran Hunjra,
Ghazi University, Pakistan
Muhammad Mohsin,
Jiangsu University, China
Irfan Ali,
Aligarh Muslim University, India

***Correspondence:**
Mehrab Nazir
mehrabnazir9@gmail.com
Jian Tian
tianjian@just.edu.cn

Specialty section:
This article was submitted to Sustainable Energy Systems and Policies, a section of the journal Frontiers in Energy Research

Received: 16 December 2021
Accepted: 17 January 2022
Published: 17 February 2022

Citation:
Nazir M and Tian J (2022) The Influence of Consumers' Purchase Intention Factors on Willingness to Pay for Renewable Energy; Mediating Effect of Attitude. Front. Energy Res. 10:837007. doi: 10.3389/fenrg.2022.837007

Low market adoption has been a real challenge to Pakistan`s renewable energy growth. This research investigated the factors that influence the intention to use renewable energy in Pakistan. This research was conducted to examine the influences of renewable energy and marketing factors on purchase intention through attitude. It analyzed seven concepts: social media exposure, relative advantage, ease of use, awareness, cost, attitude, and purchase intention and deliberated their relationships. The conceptual framework is based on the theory of planned behavior and the unified theory of acceptance. The primary purpose of this study is to examine the influence of (social media exposure, relative advantage, ease of use, awareness, and cost) on purchase intention with the indirect effect of attitude. Proposed hypotheses have been tested using structured questionnaires through SPSS (AMOS) based on a sample of 497 respondents from Pakistan. Structural equation modeling technique was used to analyze the studied variables' relationships (social media exposure, relative advantage, ease of use, and ease of use, awareness, and cost) and attitude with purchase intention. Study findings show that attitude has a major mediating effect on the relationship between purchase intention and (social media exposure, relative advantage, ease of use, awareness, and cost). The main findings revealed interesting consumer purchase intention regarding renewable energy technology. The results showed a significant positive relationship between influential determinants (social media exposure, relative advantage, ease of use, awareness, and cost) and purchase intention towards the use of renewable energy technology. This study suggests that these marketing approaches can be used as a brand marketing strategy to enhance customer purchase intention. The study's findings will help in making decision in the renewable energy sub-sector. Furthermore, the findings of this study could be used as a reference by the government when making decisions about renewable energy deployment.

Keywords: social media, relative advantage, ease of use, awareness, cost, attitude, purchase intention

1 INTRODUCTION

The widespread usage of fossil fuels has caused many environmental issues, including environmental disruption and degradation (Irfan et al., 2020). Climate change is another phenomenon that harms human existence and the environment (Handmer and Dovers, 2013). In recent years, political and economic discussions have focused on environmental issues and climate change (Grafakos et al., 2020). The utilization of renewable energy in Pakistan is in a developing stage; individuals are more concerned about social norms, the environment, and the advantages of utilizing renewable energy generation technologies (RETs) as renewable energy knowledge grows (Irfan et al., 2021a). In general, attitudes are essential predictors of pro-environmental behavior, such as renewable energy (Yorkovsky and Zysberg, 2021). However, the technology acceptance model identifies attitude as a mediator between purchase intention and renewable energy components towards the utilization of renewable energy. In light of the foregoing and the findings of studies such as those by Patil et al. (2020), we attempted to investigate the role of attitude as a mediator in the relationship of the Unified theory of acceptance and use of technology (UTAUT) principal components with the behavior intention of the consumer.

Increasing demand for electricity utilization with the possibility of depleting fossil fuels has contributed to the need to rapidly grow renewable energy sources (REs) to satisfy consumer demand (Woldeyohannes et al., 2016). Nonetheless, the global energy consumption of these energy sources remains at a minimum level (Painuly, 2001; Rezaei and Ghofranfarid, 2018). This can be said to be right about the developing countries with a large energy market; there seems to be low acceptance for consumers' renewable energy sources. Due to the rapid proliferation in population and economic growth, electricity consumption has risen enormously (Chen and Sivakumar, 2021). Many developing countries still use fossil fuels to generate electricity, including Pakistan. However, fossil fuels cannot be dependent as a prime energy source because of their high cost and adverse environmental impacts (Iqbal et al., 2018). Governments are trying to solve the current energy crisis and track the existing ecological and economic situation by finding economic and sustainable sources (Merino-Rodríguez et al., 2019). The conventional forms of energy generation to renewable sources are due to the need of the public and regulatory authorities for producing and consuming renewable energy (Ikram et al., 2020).

Several national policies were introduced to promote optimal utilization of Pakistan's energy resources (conventional and renewable), for sustainable development. Such included the National Energy Policy (Kamran and Reviews, 2018). Recently, there has been an increase in renewable energy installations across various world countries at least at a small scale level (Murshed et al., 2020). However, Pakistan electricity consumers have low acceptance of green energy, thus investigating the factors that might be responsible for to enhance the consumption of renewable energy (Irfan et al., 2021a). Pakistan has participated in global movements against climate change; therefore, research into consumer behavior toward intention to use renewable energy provides valuable insights both locally and internationally. Numerous research attributed the lack of willingness to use small-scale renewable energy for household energy to lack of consumer confidence, lack of adequate policy, low public awareness, prices, financing constraints, low community acceptance, lack of skilled human resources, weak technology dissemination strategies (Devine-Wright, 2007; Painuly, 2001; Sesan, 2008; Wüstenhagen et al., 2007). While attitude on the intention to use renewable energy have been well studied in developed countries but neglected in developing countries (Irfan et al., 2021a). In particular, the results of studies conducted in the industrialized world cannot be effectively generalized to developing nations (Dewan and Kraemer, 2000) due to their very different social, cultural, economic, political, and legal contexts (Spanos et al, 2002). Many scholars have worked on the Pakistan renewable energy market (Solangi et al., 2021). Some consider the consumer perception of renewable energy technologies while others extensively researched the potentials, policies, constraints, and current status of the generation capacities. Increasing demand for electricity utilization with the possibility of depleting fossil fuels has contributed to the need to rapidly grow renewable energy sources (renewable energy technologies) to satisfy consumer demand. Few types of research have concentrated on the individual point of view on renewable energy in Pakistan. Recently, no detailed research has targeted the households, their socio-economic perceptions (income level), and intention to purchase RE technologies. There are few studies on the motivational reasons behind the intention to purchase, and actual demand remains very low. So the major factors affecting people's intention to use RE are not fully evaluated in Pakistan.

Many factors affected the market of Pakistan's renewable energy. Authors have mentioned policy constraints, financial cost, technical and institutional problems, infrastructure, human capacity, etc. According to (Irfan et al., 2021a), substantial financial investment; inadequate infrastructure, technology, less research and innovation, lack of power purchase agreements, inadequate environmental support and public awareness are some significant barriers to renewable energy fast growth and use in Pakistan**.** However, Pakistan is a developing state and is not known especially for its support for RE due to many obstacles like economic, political, technical, and social barriers (Irfan et al., 2020). The nation relies largely on electricity supply from fossil fuels. The national economy can't fulfill the demand by the expensive electricity generation of manufactured fossil fuels from other countries. So there are severe energy shortages in Pakistan.

These considerations may differ among technologies or nations. This research focuses on different aspects in Pakistan and tries to evaluate the intention to adopt renewable energy. The issue imposed is, "What variables drive customers' RE buying intention in Pakistan?" Thus, the study explores characteristics that explain customer propensity to acquire RE technology. This study claims that variables impacting intention to acquire RE technology and results will benefit stakeholders. Few studies have

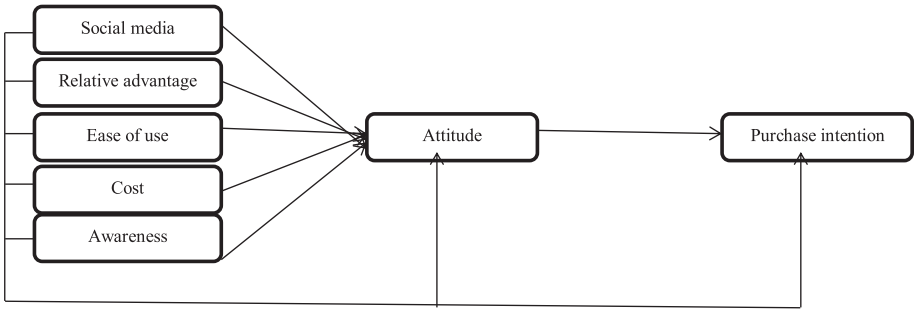

FIGURE 1 | The conceptual framework is based on a survey of the literature. The research found that social media, relative advantage, ease of use, cost and awareness will influence purchase intention with the indirect effect of attitude. This study considers that social media, relative advantage, ease of use, cost and awareness also directly impact consumer attitude. These components have radically altered attitude towards purchase intention.

emphasized the individual's perspective on RE in Pakistan. Recently, no extensive research has addressed the households, their socio-economic attitudes (income level), and intention to acquire RE technology. So, Pakistan's primary elements impacting people's intention to use RE are not thoroughly investigated. Furthermore, effective evaluation of the desire to acquire RE technology assists stakeholders when making investment decisions and designing goods and market strategies. For testing, parameters such as social media exposure, relative benefit, cost, subjective norms, ease of use, awareness, attitude, and purchase intention were used. Because developing nations must understand the processes involved in the move from conventional to renewable energy, this research focuses on elements and theories essential to pre-purchase intention to utilize renewable energy.

The rest of the study is structured as follows. **Section 2** presents the literature review that supports the hypotheses' construction and is followed by **Section 3**, where methodological procedures are detailed. Results are presented in **Section 4**. The paper ends with the discussion and conclusion section, followed by the cited references.

2 LITERATURE REVIEW

2.1 Supportive Theories

These studies have generated important exploratory themes. The theory of planned behavior helps construct initial consumer behavior models, but it doesn't go in-depth into all the possible influences. The unified theory of acceptance and use of technology (UTAUT) is applied in adopting renewable energy technologies in the new environmental area (Aggarwal, 2020). Various researchers and analysts have suggested that many hypotheses analyze customer behavior intention and identify the socio-economic variables that influence purchasing intention in the current era (Rezaei and Ghofranfarid, 2018). But according to the study by Rezaei et al. (2018), one of the most significant theories is a unified theory of acceptance and use of technology (UTAUT), which has been applied in many research fields. The main aspects of the advanced UTAUT theory involve behavioral intention, perceived behavioral control, relative advantages, awareness, and attitude as the most significant driver of individual behavior (Claudy et al, 2013). Researchers have studied consumer intentions to use renewable energy technologies in developing countries in recent years. This idea is how people are aware of current technologies, their latest advantages, and disadvantages, and how to utilize them. The most destructive factor of using technology is a lack of knowledge; a lack of knowledge makes it far more difficult to accept new technology (Alam et al., 2014).

Researchers have studied consumer intentions to use renewable energy technologies in developing countries in recent years. Hosseini et al. (2018) used the theory of planned behavior to evaluate consumer intentions to develop RE technologies in different nations. Alam et al. (2014) discovered that the intention to use renewable energy (RE) is affected by perceptions of behavioral control, ease of use, relative advantage, cost, and consumer awareness. Vand et al. (2019) surveyed Chinese customers to assess their attitudes toward renewable energy (RE). The study's findings suggest that low awareness and low-income levels provide severe barriers to the use of renewable energy (RE). Düştegör et al. (2015) conducted a study in Saudi Arabia and found that financial incentives and government subsidy programmes are the most motivating factors in renewable energy (RE) adoption. Pakistan's renewable energy programme has recently received little research attention towards using RETs. According to Irfan et al. (2021b), Pakistan faces a severe energy crisis, which can be solved by off-grid solar power. Wang et al. (2020) used multiple sources of renewable energy (RE) to supplement fossil fuel generation in the country. The authors found that wind, solar, and biomass energy had great opportunities to utilize energy.

2.2 Research Model and Hypothesis Development

Researchers agreed that the adoption of any given technology is heavily affected by many multidimensional variables, including economic, social, and regulatory aspects (Wolsink M. 2020). Due to the high cost of the technology, the lengthy payback time, and the social effects, it has become increasingly challenging to deploy RETs. Numerous studies have used the TPB framework to

investigate the impact of various variables on behavior, and these studies recognize that this model is appropriate and logical (Elhoushy S. and El-Said, O. A. 2020). The global energy consumption of these energy sources remains at a minimum level (Woldeyohannes et al., 2016). The findings of many studies have shown community acceptance as a critical concern for the growth of RES (Wolsink M. 2020). In other words, the development of renewable energy sources is not just dependent on their economic and technological support. Due to the rapid proliferation in population and economic growth, electricity consumption has risen enormously (Murshed et al., 2020). Many developing countries still use fossil fuels to generate electricity, including Pakistan. However, because of their high cost and negative environmental impacts, fossil fuels cannot be used as a primary energy source (Iqbal et al., 2018). Governments are trying to solve the current energy crisis and track the existing ecological and economic situation by finding economic and sustainable sources (Merino Rodríguez et al., 2019). The conversion of conventional forms of energy generation to renewable sources is due to the need of the public and regulatory authorities to produce and consume renewable energy (Ikram et al., 2020).

This model recognized the appropriateness and robustness of TPB for evaluating consumer intention to utilize RETs in Pakistan. Environmental concerns may be seen as being conscious of ecological degradation for customers. The cost is the total price for consumers to buy the technology, and awareness refers to how consumers know the RETs and their advantages. Including these contexts allows us to make the framework sufficiently broad to study the variables that may play an important role in influencing the intention of consumers to use RETs.

2.3 Hypotheses

2.3.1 Social Media Exposure

Social media is a web-based tool that enables people to develop, reproduce, and exchange information (Laitinen and Sivunen 2020). Social media plays a significant role in sharing information from one person to another. Companies are trying to use social media to engage with their consumers about products (Chopra et al., 2020). The authors found that social media has enormous potential to raise awareness and increase purchases of sustainable products. Marketing researchers stated that social media channels are helpful to facilitate customers' brand connections (Erkan and Evans, 2016). Erlangga, H. (2021) discovered that social media messaging boosts consumer enthusiasm to buy products. In contrast, social media interactions directly impact consumers' purchase decisions towards renewable energy technology (Wang et al., 2020). Consumer attitudes, perceptions, and purchase decisions are all influenced by social media in each stage of the purchasing process (Pop et al., 2021). The social media activities of consumers have a favorable influence on pro-environmental behaviors such as the reduction, reuse, and recycling of waste materials (Trang et al., 2019). RE is more likely to be trusted by consumers through regular and pleasant social media experiences (Sun et al., 2020). Most scholars feel that social media has played an essential role in the overall flow of purchase intentions (Taillon et al., 2020). The quantity and nature of media coverage of environmental disasters and conflicts have made many concerns a significant societal issue. Therefore, Mazis and Raymond (1997) stated that advertisers use various mediums to communicate product benefits to the target audience. Social media advertisements can be used to deliver detailed information and create a brand image, and product packaging may be utilized to attract consumers at the point of sale (Voorveld et al., 2018). Different social media channels are often coordinated into one integrated promotion. However, Liwafa and Utami (2021) explained that social media exposure allows understanding or perceiving an advertising message towards clients through specific media channels. Social media exposure is an important driving force for innovation dissemination and impacts innovators (Zhang et al., 2021). The strongest influence on the flow of social media exposure is that it conveys innovative knowledge quickly to a broad population (Sohn and Kim, 2020). Based on the previous work, media exposure can be argued as an essential predictor of purchasing intention. Therefore.

H1: Social media exposure has a positive effect on the purchase intention.

2.3.2 Relative Advantage

The extent to which an inventive technology is considered to be superior to those that occurred before it or its closest alternative is referred to as relative advantage (Gkartzonikas and Gkritza, 2019). Consumers acknowledge the usage of renewable energies and other socio-economic, environmental benefits (Irfan et al., 2021a). The limited penetration of RE might be attributed to its low relative advantage and accessible power sources in several world regions. According to the evidence, the intention is an excellent predictor of renewable energy purchase behavior and an important component in analyzing people's actual purchasing activity (Rezaei and Ghofranfarid, 2018). The consumer's behavioral intention of adoption relates to their desire to utilize a potential goods or services. This research aims to better recognize customers' behavioral intentions to use renewable energy. Several variables can influence buy intention as a dependent variable, described as the mind's capacity to behave in a specific way to make a purchase (Kusumawati and Mangkoedihardjo 2021). The examined factors include relative advantage effects on purchasing intention attitudes. The constructs selected for the study were taken from the theories mentioned above and were supposed to impact purchasing intention. Furthermore, a previous study revealed a relative benefit that directly impacts the buying intention to utilize RE. Relative advantage directly impacts the attitude, which acts as a mediator in the interaction with intention (Rezaei and Ghofranfarid, 2018; Esa and Zahari, 2016). This research, therefore, argues that:

H2: The relative advantage has a positive effect on customer's purchase intention.

2.3.3 Perceived Ease of Use

The degree to which a technology is supposed to be challenging to use is measured by perceived ease of use (Moslehpour et al., 2018). According to Chen et al. (2020), perceived ease of use is an individual's belief in the ability of an individual component to be simple to use (Tahar et al., 2020). Energy sources are relatively simple, inexpensive, and have a more significant market

perception. Researchers revealed that renewable energy, such as solar energy, has several technological challenges that consumers must overcome (Adenle, 2020). Renewable energy installations, use, maintenance, and technicalities influence public perception. Renewable energy solutions that are easy to install, user-friendly, family-friendly, and comparable to living standards are more likely to influence adoption intention (Ashinze et al., 2021).

H3: Perceived ease of use has a significant positive effect on the customer's purchase intention.

2.3.4 Cost

Renewable energy costs include maintenance, installation and the opportunity cost of implementing RE (Ashinze et al., 2021). According to research, costs were also a significant factor in reducing the adoption and integration of renewable energy solutions, mainly in emerging nations with relatively low incomes (Barnett-Howell et al., 2021). It is primarily a fact that the minimum capital necessary for installing renewable energy is greater than the minimum required by conventional energy. Previous research found a direct and significant relationship between cost and technology adoption (Sarker et al., 2020). According to Irfan et al. (2021a), the consumer perception of renewable energy benefits was demonstrated by three primary outcomes: energy savings, environmental benefits, and the independence of conventional power sources. The customer's impression of product cost depends on the person's social development and financial expertise (Kumar et al., 2020). The current research will provide insights into the perceived cost of renewable energy and its impact on client purchasing intentions. This study now provides insight into perceived costs and their effect on consumer intention.

H4: Cost has a positive effect on the customer purchase intention.

2.3.5 Awareness

The extent to which customers are aware of current technology, its benefits, and drawbacks and can keep up with new developing technological updates is defined as awareness (Waris et al., 2020). The term of awareness refers to the ability of prospective consumers to obtain appropriate information about RE's fundamental usage, economic prospects, and environmental implications (Kumar et al., 2020). One key element of UTAUT that directly impacts the behavioral desire to utilize renewable energy sources is awareness (Kardooni and Ghofranfarid, 2018). A higher degree of awareness is likely to boost the acceptance of RE technologies among new users (Mirza et al., 2009). Awareness is a key component in the choice of customers to acquire new technologies. Numerous research found that knowledge of the consumer's desire to utilize renewable energy sources was beneficial (Alam et al., 2014). Furthermore, green energy knowledge encourages clients to develop a good perception of RE marketing and enhance their purchase incentive to prevent ecological threats (McEachern et al., 2005).

H5: Awareness has a positive effect on the customer purchase intention.

2.3.6 Attitude

Attitude is a person's positive or negative feelings about performing the target behavior (Ashinze et al., 2021). Attitude is an essential component of the theory of planned behavior which refers to assessing a person's behavior as favorable or unfavorable (Amoako et al., 2020). Consumer attitudes may be seen as favorable or negative emotions towards the usage of RETs. The origins of these good or negative emotions may be based on their anticipated environmental, economic, or social consequences and advantages. Attitude (ATT) is a key part of the TPB, which assesses an individual's behavior as favorable or unfavorable (Hamid and Ban, 2021). Attitude can be seen as positive or negative customer opinions regarding the use of RETs. The existing literature demonstrates that attitude is closely linked with the intention of RETs.

Moreover, Najar and Hamid Rather (2021) validated a favorable link between behavior and the intentions of customers to buy energy-efficient household equipment. The attitude was also favorably linked to the consumer's energy reduction intentions (Ali et al., 2021). They also showed the favorable impact of attitudes on the intention of consumers to buy RET. Existing research indicates that the mindset is favorably linked to the intention of customers to use RETs. Consumers think that green energy helps avoid global warming and climate harm lowers our dependence on conventional power and improves air quality (Suraya et al., 2020). Some researchers suggested that attitude is a strong predictor of household power consumption (Chen and Aklikokou, 2020). Numerous studies have confirmed a favorable connection between attitude and customers' willingness to buy energy-efficient home equipment. The attitude has also been shown to be favorably linked to consumer energy reduction intentions (Ali, 2021), showing that this mindset strongly affects the intention of customers to buy energy-efficient goods. This study further explained the concept by examining the mediator's role as a link between variables such as relative advantage, subjective norm; ease of use and awareness as well as the cost and intention to use in the framework of an ideal model, this study hopes to learn more about this topic.

H6: Attitude has a positive effect on purchase intention.

H7: Attitude moderates the relationship between purchase intention and social media exposure.

H8: Attitude moderates the relationship between purchase intention and cost.

H9: Attitude moderates the relationship between purchase intention and relative advantage.

H10: Attitude moderates the relationship between purchases intention and awareness.

H11: Attitude moderates the relationship between purchase intention and ease of use.

2.4 Conceptual Framework

On based of **Figure 1**, the conceptual framework is based on a survey of the literature. The research found that social media, relative advantage, ease of use, cost and awareness will influence purchase intention with the indirect effect of attitude. This study considers that social media, relative advantage, ease of use, cost and awareness also directly impact consumer attitude. These components have radically altered attitude towards purchase intention.

TABLE 1 | Demographic characteristics.

Variable	Category	Frequency	Percentage
Gender	Male	387	77.9
	Female	110	22.1
Age (Years)	20–30	237	47.7
	31–40	82	16.5
	41–50	60	12
	51–60	76	15.3
	61-above	42	8.5
Qualification	Bachelors	245	49.3
	Masters	96	19.3
	Postgraduates	75	15.1
	Diplomas	56	11.3
	Others	25	5.0
Income	1–10,000	26	5.2
	10,000–20,000	59	11.9
	20,000–30,000	83	16.7
	30,000–40,000	197	39.6
	40,000-above	132	26.6

3 METHODOLOGY

3.1 Sample Selection and Collection

This section discusses the methodology, including sample selection and description, data collection, regression model, data analysis, and this is also used to apply statistical tests for testing the hypothesis. The main focus of our current study is to measure "A multidimensional model of renewable energy: Linking purchase intentions, attitude, and user behavior." To achieve the objectives of the study, the planned strategy is to explore the respondents' views towards social media exposure, relative advantage, awareness, perceived ease of use, and attitude. After eliminating questionnaires with error, a total number of 497 respondents was used and analyzed with using statistical software SPSS (Amos). We used the non-probability convenience sampling technique. One of the main advantages of this sampling strategy is that it permitted researchers to collect data from a large number of participants in a very short space of time (Comrey A., and Lee H. 1992). Primary data was collected from the respondents from different Punjab, Pakistan. The hypothesis is measured based upon a scale used by (Roberts and Ko, 2005) in their study. Advertisement is the key instrument of the marketing field, which drives the consumer's probability, understanding, tendency, and selection and effectively promotes and sells the product and services. The customers' attitude towards the purchase intention is measured by the factors of RE., which have an influential impact on consumers' purchase intention. The constructed scale of consumer purchase intention is based on (Baker and Churchill's, 1977), which is used to assess the physical attractiveness of models in promotion as well as the customer's intent to purchase goods.

The usefulness of this research hugely depends on the efficiency of data collection and analysis. (Raykov and Marcoulides, 2006), stated that multicollinearity consistency can easily provide unstable estimates of regression coefficients. IBM SPSS is employed to test for multicollinearity between independent variables. A list of measured items and the sources of each part are presented separately in a table. A coding operation was undertaken at this stage, through which the categories of data are transformed into symbols that were tabulated and counted. Collected data will be coded and modeled using AMOS/SPSS Software.

The hypothesized relationship among observed variables is estimated based on the structural model-direct model and mediation model for testing the indirect effect in the second process. This presented two structural models used for analysis. "Bootstrapping" is qualitative research that includes an estimation of the importance of the indirect impact and meaning of the point estimate. The "Test of mediation" gives two estimates of the indirect effect and tests their ranges but quantifies confidence intervals for the point estimates (Mallinckrodt et al., 2006).

The demographic characteristics of the sample are given in **Table 1** and discussed as follows. Most participants were men (n = 497, 77.9%), with Baker and Churchill's, 1977 an age distribution between 20 and 30 years old (47.7%). In the case of educational background, most individuals reported a bachelor's degree (245, 49.3%). In total, 197 participants (39.6%) specified that their monthly income was between 30,000 and 40,000 rupees.

4 DATA ANALYSIS

4.1 Findings

Different statistical approaches were used for data analysis. The structural equations modeling (SEM) technique was used to analyze the data. SEM can be used to evaluate the connection between variables. Anderson and Gerbing (1988) suggested that the SEM method consists of two stages (measuring model and the structural model). In the measuring model, the researcher verified every latent variable to estimate the structural model by doing confirmatory factor analysis (CFA). For the present study, latent variables were analyzed to ascertain the statistical relation between the seven variables. Stephens and Sommer (1996) recommended that the loading factor of all items should not be less than .50. The results of the CFA contributed to the model's modification. With the results of SEM, the researcher inspected the relationship with latent variables because it indicates the direct or indirect influence of the latent variable on other latent variables. The anticipated linkages between these variables are explicitly specified in the SEM. In SEM, the researcher is enabled to know what was stated and what facts were presented in the proposed model (Hair et al., 1995). The greater the link between proposed relationships and data patterns, the better they show a good fit between model and data. The estimation procedure helps to assess whether or not the suggested model fits the data. Decisions concerning the modification to be raised also depend on fit statistics. There are some types of model fit statistics, such as absolute fit indices, incremental fit, comparative fit, and finally parsimony indices. Each model fit statistic consists of several fit indexes where some thumb rules are applied to the minimum score or value to get a good fit (Byrne, 2001).

TABLE 2 | Variables of exploratory factor analysis, descriptive statistics, and confirmatory factor analysis.

Indicator	Measurable variables	Factor loading	CR	AVE	Cα
Social Media	SM1	.955	.974	.925	.973
	SM3	.946			
	SM3	.951			
Relative advantage	RD1	.916	.971	.870	.971
	RD2	.900			
	RD3	.933			
	RD4	.871			
	RD5	.886			
Awareness	AW1	.924	.969	.864	.969
	AW2	.879			
	AW3	.909			
	AW4	.906			
	AW5	.856			
Ease of use	EU1	.905	.946	.813	.945
	EU2	.863			
	EU3	.876			
	EU4	.796			
Cost	CT1	.865	.946	.778	.946
	CT2	.838			
	CT3	.864			
	CT4	.814			
	CT5	.759			
Attitude	AT1	.914	.941	.841	.940
	AT2	.877			
	AT3	.894			
Purchae intention	PI1	.914	.938	.834	.937
	PI2	.908			
	PI3	.855			

SM, social media; CT, cost; RD, relative advantage; AW, awareness; EU, ease of use; AT, Attitude; PT, purchase intention.

The availability of alternative fit indices caused several challenges for the evaluation process (Kline, 2012). As pointed out by Kenny and McCoach (2003), there is no consistent standard measure in model evaluations; they endorsed the root mean square approximation error (RMSEA), the comparative fit index (CFI), and Tucker-Lewis coefficient (TLI). Bentler's (1990) suggested fit indices are TLI, Incremental fit index (IFI), and Fan et al. (1999) supported RMSEA, TLI, and CFI to be fit indicators. Since it is unlikely that all fit measures can be samples, these fit indices are used for reporting the quality of the two models in the current study. Keep the common fit indexes, and the root mean square fit error (RMSEA), the incremental fit index (IFI), the Tucker-Lewis coefficient (TLI), and the comparative fit index were used for confirming and supporting the proposed model (CFI). For RMSEA, the value should be less than .06 to a closer model, which would be best if the value is equal to. 08. Meanwhile, if the value exceeds .01, it shows that the model does not fit well (Hu and Bentler, 1999). For IFI, the values closer to one show a good fit (Bollen, 1989), and values greater than .90 would be good for TLI and CFI (Hair et al., 1995). In the second step, structural equation modeling was used to test the statistical relationships between independent variables (social media exposure, relative advantage, awareness, cost, and perceived ease of use) and the dependent variable (purchase intention). In the third phase, we checked the statistical link of the mediating variable (attitude) between the independent and dependent variables.

4.2 Measurement Instruments

This research used a quantitative approach to analyze customers' perceptions about factors of renewable energy and its effect on attitude and purchase intention. The study assessed six variables that measure the purchase intention of renewable energy technology and consumers' experiences. The questionnaire considered all research variables and a five-point Likert scale. The first construct is renewable energy. According to the research of (Wu et al., 2018), renewable energy is operationalized into five dimensions: Eighteen items of factors of renewable energy were classified into five dimensions (social media exposure, relative advantage, perceived ease of use, awareness, and cost). Due to poor factor loading, I deleted one item of social media exposure and one item of cost. A total of sixteen items were considered. Four items of mediating variable (attitude) and three items of purchase intention were selected. However, due to poor factor loading of one item, I deleted one item, and overall two items are considered for purchase intention.

Moreover, **Table 2** shows the detailed measurement items, including Cronbach's alpha, average variance extracted (AVE),

TABLE 3 | Discriminant validity of the constructs.

	Purchase intention	Social media	Relative advantage	Cost	Awareness	Attitude	Ease use
Purchase intention	.913						
Social media	.446	.962					
Relative advantage	.411	.338	.933				
Cost	.326	.323	.385	.882			
Awareness	.299	.241	.334	.419	.929		
Attitude	.457	.498	.356	.080	.137	.917	
Ease use	.256	.243	.164	.186	.163	.234	.902

TABLE 4 | Path analysis Regression Weights: (Group number 1 - Default model).

	—	—	Estimate	S.E.	C.R.	*p*	Decision
Attitude	<---	Social media	.442	.033	10.832	***	Accepted
Attitude	<---	Relative advantage	.259	.036	6.204	***	Accepted
Attitude	<---	Cost	–.186	.036	–4.260	***	Accepted
Attitude	<---	Awareness	.003	.030	.069	.945	Not Accepted
Attitude	<---	Ease use	.118	.034	3.089	.002	Accepted
Purchase intention	<---	Social media	.171	.042	3.869	***	Accepted
Purchase intention	<---	Relative advantage	.159	.041	3.780	***	Accepted
Purchase intention	<---	Cost	.130	.041	3.013	.003	Accepted
Purchase intention	<---	Awareness	.099	.034	2.476	.013	Not Accepted
Purchase intention	<---	Ease use	.085	.039	2.262	.024	Accepted
Purchase intention	<---	Attitude	.271	.051	6.094	***	Accepted

****This symbol mean our hypothesis are accepted on base of threshold.*

and composite reliability (CR) for all research variables. According to the outcomes shown in **Table 2**, the CR of every construct varies from .938 to .974, showing that all indicators are under the recommended level. Furthermore, the values of the AVE confirmed the constructs' validity by more than .5 (Kao and Hung, 2008; Kao and Lin, 2016). AVE values ranged from .778 up to .925, which indicates that the average explanatory power of the variables used in this study was satisfactory and it is appropriate for advanced analysis. The convergent validity of each estimation item was tested using factor loadings, and the values of all measures are between 0.796 and 0.955, which exceeds the benchmark value of 0.5. (Hair et al., 1995, 2010).

Finally, this statistical measurement was tested with a confidence interval (CI) and Percentile 90% CI through the software (Amos). To satisfy the discriminant validity criteria, the square root of a construct's AVE must be greater than the correlations between the component and the others in the research (Fornell and Larcker, 1981). The diagonal items in **Table 3** are the square root values of AVEs, while the other components are Pearson correlation coefficients between the variables. As a result, the measurement's discriminant validity is satisfactory.

4.3 Structure Equation Model

The proposed direct, indirect, and mediating hypotheses were statistically tested with the structural equation model (SEM) using the Amos software. Basically, SEM provides the complete direction and consideration of the proposed hypothetical model and also provides accuracy without any incorrect standard error estimations. First, we checked the direct effects of independent variables (social media exposure, relative advantage, awareness, cost, and perceived ease of use) on the dependent variable (purchase intention) with path analysis in the table. We also used the bootstrap of 1,000 samples to check the indirect effect (Gunzler et al., 2013) of attitude between the independent variables (social media exposure, relative advantage, awareness, cost, and perceived ease of use) and dependent variable (purchase intention).

According to the findings of **Table 4**, Five dimensions of renewable energy are considered to check the statistical relation, (social media exposure (β = .171 p < .001), relative advantage (β = .159, p < .001), ease of use (β = .085, p < .001), and cost (β = .130, p < .001) have positive significant influence on purchase intention, while (awareness (β = .099, p < .001), has no any positive significant effect on purchase intention. Moreover, the second direct effects of social media exposure (β = .442 p < .001), relative advantage (β = .259, p < .001), ease of use (β = .118, p < .001), and cost (β = -.186, p < .001) have positive significant effect on attitude while (awareness (β = .003, p < .001), has no any positive significant effect on attitude. On the other hand, the mediating variable (attitude (β = 0.271, p < .001) also has a statistically significant positive direct effect on purchase intention.

4.4 The Direct and Indirect Effects

The mediated hypotheses propose that factors of renewable energy (social media exposure, relative advantage, awareness, cost, and ease of use) indirectly impact purchase intention through attitude. Estimated results of **Table 5** illustrated that attitude (β = 0.271, p < .001) has a significant positive impact on purchase intention, so it is proven that there exists a mediation between (social media exposure, relative benefits, consciousness,

TABLE 5 | Direct, indirect, and total effect.

	Ease use	Awareness	Cost	Relative advantage	Social media	Attitude	Purchase Intention
Direct effect							
Attitude	.118	.003	–.186	.259	.442	.000	.000
Purchase intention	.085	.099	.130	.159	.171	.271	.000
Indirect effect							
purchase intention	.032	.001	–.050	.070	.120	.000	.000
Total effect							
purchase intention<	.117	.100	.080	.229	.291	.271	.000

cost, perceived ease of use) and purchase intention through attitude. The empirical outcomes supported the above assumption, indicating that attitude would affect purchase intention. Additionally, this study demonstrated that attitude mediates the relations between (social media exposure and ease of use) and purchase intention, while attitude has no mediating effect between relative advantage, awareness, and cost) and purchase intention. Therefore, green companies should focus on renewable energy channels to enhance their consumer attitude to raise their purchase intention to satisfy their customer's environmental needs.

5 DISCUSSION

This research is designed to check the significance of RE as a sustainable source of clean energy and its components on the one hand, and the attitude that mediates the relationship between (social media exposure, relative advantage, awareness, perceived ease of use, and cost) and purchase intention on the other hand. The main objective of this study is to investigate the multidimensional factors that affect renewable purchase intention. According to the consequences of result of H1, there is a significant direct relationship between social media exposure and purchase intention (Lee et al.,. 2021). So, the perceived value of social media advertising is severely impacted by intrusiveness and privacy concerns about the use of renewable energy (Arora and Agarwal, 2019). In accordance with the findings of H2, there is also an optimistic direct relation between the relative advantage and purchase intention. As a result, the more significant perceived comparative advantage of renewable energy accelerates the adoption of renewable energy. However, past research has confirmed the concept that relative advantage directly influences purchase intention, and these results are supported by the study (Rezaei and Ghofranfarid, 2018). With the results of H3, there is also a significant direct connection between perceived ease of use and the purchase intention of RE. Individuals in Pakistan have strong ideas about accepting renewable energy, which may exchange from one person to another, but further qualitative research is needed to understand this dynamic. This study supports studies (Irfan et al., 2021a; Waris et al., 2020). The indirect results supported and verified how easy it is to use renewable energy significantly impacted the purchase intention through attitude. These outcomes align with the study (Liobikienė et al., 2021). Hence, my results support a significant effect of perceived ease of use and purchase intention. These results relatively matched with previous results. The Pakistani respondents felt that this technology was simple to use, maintain, and comprehend.

The results of hypothesis four verified this theory (Aggarwal, 2020). The study found a positive correlation between how much an organization's employees think RE costs and their attitudes regarding purchasing and using RE. If the cost of the product increases, it diversely affects purchase intention because consumers always want to decrease the cost of any product. So a product's perceived cost is crucial to uptake. While the result of H5 revealed no significant direct relationship between awareness and purchase intention, These consequences align with the studies (Rezaei et al., 2018; Liobikienė et al., 2021). As established by the initial factors, and as evident from the resultant findings, the relationship between intentions to use and determinants (social media exposure, relative advantage, ease of use, cost, and awareness) of renewable energy did not have a significant positive impact on purchase intention. In contrast, with the indirect effect of attitude, some factors (perceived ease of use and social media exposure) positively affected purchase intention. As a rule, the model's predictive capacity is boosted significantly when the attitude component's presence as a mediating variable is factored in. Attitude is a crucial mediator between renewable energy determinants and purchase intention. The idea that attitude is a substantial mediating factor in the relationship between renewable energy determinants and purchase intention was proven by hypotheses H6, H7, H8, H9, and H10. In simpler terms, if the citizens of Pakistan feel better about their attitude, then their motivation to use energy sources improves. This helps to boost consumer interest in RE. As a result, increasing people's interest in renewable energy sources should be possible through reinforcing their beliefs in the efficacy of RE.

6 MANAGERIAL IMPLICATIONS

With a deep focus on exploring the factors of renewable energy (RE) on consumer purchase intention, the current research provides practical implications for organizations, stakeholders, and government policymakers. The study has provided light on the effects that impact the purchase of sustainable renewable energy (Masukujjaman et al., 2021). Managers and policymakers may use these findings to provide suggestions to enhance renewable energy through renewable energy components (Wang et al., 2020). This study improves the relationships of

renewable energy sources (REs) between all renewable energy (RE)-related components and influences consumer purchases towards renewable energy. This energy sector deeply affects the economy of Pakistan (Abbasi, et al., 2020). So the investment in renewable energy (RE) is accumulating in Pakistan, which will help with falling costs and technological advancements in fulfilling consumer demand. Thus, renewable energy (RE) companies should improve their working techniques to protect the environment and focus on consumer demands. To do this, a company should simplify its transactions, payments, and credit allocation methods to minimize its energy consumption. To improve this attribute, a renewable energy (RE) company should focus on marketing factors (social media exposure and ease of use) to enhance consumers' intention towards renewable energy (RE). To that end, organizers should raise awareness of the factors determining optimal usage to stimulate young people's interest in renewable energy. These awareness efforts should also stress the framework used and provided in this research to understand better the links examined here and their implications for business management. Helping the environment with renewable energy, which was the study's primary goal, may assist in creating significant changes in economic growth and a better community.

7 CONCLUSION, LIMITATIONS AND FUTURE RESEARCH

This research aims to analyze individual intentions to use renewable energy in Pakistan based on numerous psychological models, theories, and comprehensive frameworks. The study found that people are more likely to choose renewable energy if they have a positive opinion about it and plan to buy it. My research model consists of a multidimensional model with five independent variables (social media exposure, relative advantage, awareness, cost, and perceived ease of use), one mediating variable (attitude) to check the effect of these variables on one dependent variable (purchase intention) towards the use of renewable energy technology. This study extended the theory of planned behavior to completely assess the aspects that influence public acceptance and use of the RE, which is this study's significant contribution. The study findings reveal interesting discoveries that have major policy considerations and practical ideas for decision-making. Social media exposure does not help with the convenience of use or their level of awareness towards the use of renewable energy technology. Customers' purchase intention is a critical predictor of RE's intentions to follow through with the behavior. Several advantages of the proposed strategy are obvious to those who examine the usage of renewable energy in Pakistan. These approaches provide new insights and understanding of renewable energy in Pakistan. The study also provides valuable information for policymakers to aid them in expanding the use of renewable energy in rural areas.

Despite the fact that the research findings are consistent with theoretical expectations, the present study has limitations. Firstly, a limited sample size was selected, which has an impact on the generalizability of the results. So it is necessary for the next researcher to use sample size more than 500 to get a proper findings. Second, the data was gathered in general but did not take into account the country's rural and urban parts. In urban and rural areas, socioeconomic characteristics such as awareness, income, and education may vary. Future studies should address this restriction by doing research in the countryside. This important component may be taken into account in future research to enhance the current body of knowledge from a Pakistan viewpoint. Finally, a number of variables influence the RE sector; nevertheless, only the most important ones were examined. This limitation may be addressed by evaluating the effect of other potential variables such as risk perception, confidence in RETs, and moral responsibilities.

There are various limitations to this study, as well as potential areas for further research. The renewable energy technology sector is still in its early stages and faces several challenges, and the first is that the demand for renewable energy is increasing quickly. The environmental impact of renewable energy technology is still a topic of discussion. This article cannot critically examine renewable energy technology aspects, but consumer responses may be affected due to intense public discussions over it. Future research should concentrate on renewable energy technology's ecological performance measured by Life Cycle Assessment (LCA) studies. Then these studies' findings can be applied to future consumer research. For example, future research might consider the number of improved renewable energy technologies that customers find appealing. Furthermore, while technological advances will help reduce costs in the near future, renewable energy technology is now supplied at greater prices than its potential competitors. Studies have looked at whether or not consumers are ready to pay a higher for product lines that have environmental benefits. The results show that they are, even though the exact increase depends mainly on customer characteristics (Stigka et al., 2014), product purchase frequency (Morone et al., 2021), and consumers' overall price sensitivity (Niedermeier et al., 2021). Future studies could produce a more thorough evaluation of consumers' desire to pay for renewable energy technology. Renewable energy technology features depend on product and brand, qualities, and distinct consumer characteristics.

Furthermore, the capacity of attitudes and intention to purchase predict actual conduct is questionable, especially in environmental behavior (Papista and Krystallis, 2013). There's also an inconsistency between what people say they're willing to spend and what they end up paying (Barber et al., 2012). Future research should investigate if consumers are willing to buy different types of renewable energy technology in a real-life situation (i.e. field experiment) and add more objective behavioral data (e.g. utilizing real purchase data) to make the results more robust and generalizable. Future studies could concentrate on demographic differences between nations and how these affect the evaluation of renewable energy technologies. And also, it would be great to look deeper into specific nation demographics or cultural aspects that influence how consumers evaluate renewable energy products and possibly

shed light on why some countries receive renewable energy products better than others.

DATA AVAILABILITY STATEMENT

The raw data supporting the conclusion of this article will be made available by the authors, without undue reservation.

ETHICS STATEMENT

The studies involving human participants were reviewed and approved by School of Economics and Management, Jiangsu University of Science and Technology, Zhenjiang, China. Written informed consent for participation was not required for this study in accordance with the national legislation and the institutional requirements.

AUTHOR CONTRIBUTIONS

Conceptualization, JT; methodology, MN; software, MN; validation, MN and MN; formal analysis, MN; investigation MN; data curation, Meharb Nazir; writing—original draft preparation, MN; writing—review and editing, JT and MN.; supervision, JT; funding acquisition, JT.

REFERENCES

Abbasi, K., Jiao, Z., Shahbaz, M., and Khan, A. (2020). Asymmetric Impact of Renewable and Non-renewable Energy on Economic Growth in Pakistan: New Evidence from a Nonlinear Analysis. *Energy Exploration & Exploitation* 38 (5), 1946–1967. doi:10.1177/0144598720946496

Adenle, A. A. (2020). Assessment of Solar Energy Technologies in Africa-Opportunities and Challenges in Meeting the 2030 Agenda and Sustainable Development Goals. *Energy Policy* 137, 111180.

Agarwal, R. N. (2020). The Role of Effective Factors in Utaut Model on Behavioral Intention. *Beman* 10 (3), 5–23. doi:10.24818/beman/2020.10.3-01

Alam, S. S., Nik Hashim, N. H., Rashid, M., Omar, N. A., Ahsan, N., and Ismail, M. D. (2014). Small-scale Households Renewable Energy Usage Intention: Theoretical Development and Empirical Settings. *Renew. Energ.* 68, 255–263. doi:10.1016/j.renene.2014.02.010

Ali, B. (2021). Consumer Attitudes Towards Healthy and Organic Food in the Kurdistan Region of Iraq. *Manag. Sci. Lett.* 11 (7), 2127–2134.

Ali, M. R., Shafiq, M., and Andejany, M. (2021). Determinants Of Consumers' Intentions Towards The Purchase Of Energy Efficient Appliances In Pakistan: An Extended Model Of The Theory Of Planned Behavior. *Sustainability* 13 (2), 565.

Amoako, G. K., Dzogbenuku, R. K., and Abubakari, A. (2020). Do Green Knowledge and Attitude Influence the Youth's Green Purchasing? Theory of Planned Behavior. *Int. J. Product. Perform. Manag.*

Anderson, J. C., and Gerbing, D. W. (1988). Structural Equation Modeling in Practice: A Review and Recommended Two-Step Approach. *Psychol. Bull.* 103 (3), 411.

Arora, T., and Agarwal, B. (2019). Empirical Study on Perceived Value and Attitude of Millennials towards Social media Advertising: a Structural Equation Modelling Approach. *Vision* 23 (1), 56–69. doi:10.1177/0972262918821248

Ashinze, P. C., Tian, J., Ashinze, P. C., Nazir, M., and Shaheen, I. (2021). A Multidimensional Model of Sustainable Renewable Energy Linking Purchase Intentions, Attitude and User Behavior in Nigeria. *Sustainability*, 13(19), 10576.

Baker, M. J., and Churchill, G. A., Jr (1977). The Impact of Physically Attractive Models on Advertising Evaluations. *J. Market. Res.* 14 (4), 538–555.

Barber, S., Boyen, X., Shi, E., and Uzun, E. (2012). "Bitter to Better—How to Make Bitcoin a Better Currency," in *International Conference on Financial Cryptography and Data Security*. Berlin, Heidelberg: Springer, pp. 399–414.

Barnett-Howell, Z., Watson, O. J., and Mobarak, A. M. (2021). *The Benefits and Costs of Social Distancing in High-and Low-Income Countries*. Transactions of the Royal Society of Tropical Medicine and Hygiene.

Bentler, P. M. (1990). Comparative Fit Indexes in Structural Models. *Psychol. Bull.*, 107(2), 238.

Bollen, K. A. (1989). A New Incremental Fit index for General Structural Equation Models. *Sociological Methods Res.* 17 (3), 303–316. doi:10.1177/0049124189017003004

Byrne, B. M. (2001). Structural Equation Modeling with AMOS, EQS, and LISREL: Comparative Approaches to Testing for the Factorial Validity of a Measuring Instrument. *Int. J. Test.* 1 (1), 55–86. doi:10.1207/s15327574ijt0101_4

Claudy, M. C., Peterson, M., and O'Driscoll, A. (2013). Understanding the Attitude-Behavior Gap for Renewable Energy Systems Using Behavioral Reasoning Theory. *J. Macromarketing* 33 (4), 273–287. doi:10.1177/0276146713481605

Chen, L., and Aklikokou, A. K. (2020). Determinants of E-Government Adoption: Testing the Mediating Effects of Perceived Usefulness and Perceived Ease of Use. *Int. J. Public Admin.* 43 (10), 850–865.

Chen, Y., and Sivakumar, V. (2021). Invesitigation of Finance Industry on Risk Awareness Model and Digital Economic Growth. *Annals Operat. Res.* 1–22.

Chopra, C., Gupta, S., and Manek, R. (2020). Impact of Social Media on Consumer Behaviour. *Int. J. Creat. Res. Thougts* 8 (6), 1943–1961.

Devine-Wright, P. (2007). "Reconsidering Public Attitudes and Public Acceptance of Renewable Energy Technologies: a Critical Review," in *Beyond Nimbyism: A Multidisciplinary Investigation of Public Engagement with Renewable Energy Technologies*. Manchester Architecture Research Centre, University of Manchester, 15.

Dewan, S., and Kraemer, K. L. (2000). Information Technology and Productivity: Evidence from Country-Level Data. *Manage. Sci.* 46 (4), 548–562. doi:10.1287/mnsc.46.4.548.12057

Düştegör, D., Sultana, N., Felemban, N., and Al-Qahtani, D. (2015). "Public Acceptance of Renewable Energy and Smart-Grid in Saudi Arabia." in IEEE 8th GCC Conference & Exhibition. IEEE, 1–6.

Erkan, I., and Evans, C. (2016). The Influence of Ewom in Social Media on Consumers' Purchase Intentions: An Extended Approach to Information Adoption. *Comput. Human Behav.* 61, 47–55.

Esa, E., and Zahari, A. R. (2016). Corporate Social Responsibility: Ownership Structures, Board Characteristics and the Mediating Role of Board Compensation. *Procedia Econ. Finance* 35, 35–43.

Fornell, C., and Larcker, D. F. (1981). Evaluating Structural Equation Models With Unobservable Variables and Measurement Error. *J. Market. Res.* 18 (1), 39–50.

Gkartzonikas, C., and Gkritza, K. (2019). What Have We Learned? A Review of Stated Preference and Choice Studies on Autonomous Vehicles. *Transport. Res. Part C* 98 323–337.

Grafakos, S., Viero, G., Reckien, D., Trigg, K., Viguie, V., Sudmant, A., and Dawson, R. (2020). Integration of Mitigation and Adaptation in Urban Climate Change Action Plans in Europe: A Systematic Assessment. *Renew. Sustain. Energy Rev.* 121, 109623.

Gunzler, D., Chen, T., Wu, P., and Zhang, H. (2013). Introduction to Mediation Analysis With Structural Equation Modeling. *Shanghai Arch. Psychiatry* 25 (6), 390.

Hair, J. F., Anderson, R., Tatham, R., and Black, W. (1995). *Multivariate Data Analysis: With Readings*. Englewood Cliffs: Prentice-Hall.

Hair, J. F., Babin, B. J., and Anderson, R. E. (2010). *A GLOBAL PERSPECTIVIE*. Kennesaw: Kennesaw State University.

Hamid, S., and Bano, N. (2021). Behavioral Intention of Traveling in the Period of COVID-19: An Application of the Theory of Planned Behavior (TPB) and Perceived Risk. *Int. J. Tour. Cities*.

Handmer, J., and Dovers, S. (2013). *Handbook of Disaster Policies and Institutions: Improving Emergency Management and Climate Change Adaptation*. London: Routledge.

Hosseini, A., Zolfagharzadeh, M. M., Asghar Sadabadi, A., Aslani, A., Jafari, H., and Journal, A. E. (2018). Social Acceptance of Renewable Energy in Developing Countries: Challenges and Opportunities. *Distributed Generation Altern. Energ. J.* 33 (1), 31–48. doi:10.1080/21563306.2018.11969264

Hu, L. T., and Bentler, P. M. (1999). Cutoff Criteria for Fit Indexes in Covariance Structure Analysis: Conventional Criteria vs. New Alternatives. *Struct. Equ. Model.* 6 (1), 1–55.

Irfan, M., Hao, Y., Ikram, M., Wu, H., Akram, R., Rauf, A., et al. (2021a). *Assessment of the Public Acceptance and Utilization of Renewable Energy in Pakistan*. Sustainable Production and Consumption. 27, 312–324. doi:10.1016/j.spc.2020.10.031

Irfan, M., Hao, Y., Ikram, M., Wu, H., Akram, R., and Rauf, A. (2021b). Assessment of the Public Acceptance and Utilization of Renewable Energy in Pakistan. *Sustain. Prod. Consum.* 27, 312–324.

Ikram, M., Zhang, Q., Sroufe, R., Shah, S. Z. A., and Consumption (2020). Towards a Sustainable Environment: The Nexus between ISO 14001, Renewable Energy Consumption, Access to Electricity, Agriculture and CO2 Emissions in SAARC Countries. *Sustainable Prod. Consumption* 22, 218–230. doi:10.1016/j.spc.2020.03.011

Iqbal, T., Dong, C.-q., Lu, Q., Ali, Z., Khan, I., Hussain, Z., et al. (2018). Sketching Pakistan's Energy Dynamics: Prospects of Biomass Energy. *J. Renew. Sust. Energ.* 10 (2), 023101. doi:10.1063/1.5010393

Irfan, M., Zhao, Z.-Y., Li, H., Rehman, A., and Research, P. (2020). The Influence of Consumers' Intention Factors on Willingness to Pay for Renewable Energy: a Structural Equation Modeling Approach. *Environ. Sci. Pollut. Res.* 27 (17), 21747–21761. doi:10.1007/s11356-020-08592-9

Kao, C., and Hung, H. T. (2008). Efficiency Analysis of University Departments: An Empirical Study. *Omega* 36 (4), 653–664.

Kao, T. W. D., and Lin, W. T. (2016). The Relationship Between Perceived E-Service Quality and Brand Equity: A Simultaneous Equations System Approach. *Comput. Human Behav.* 57, 208–218.

Kamran, M., and Reviews, S. E. (2018). Current Status and Future success of Renewable Energy in Pakistan. *Renew. Sust. Energ. Rev.* 82, 609–617. doi:10.1016/j.rser.2017.09.049

Kenny, D. A., and McCoach, D. B. (2003). Effect of the Number of Variables on Measures of Fit in Structural Equation Modeling. *Struct. Equ. Model.* 10 (3), 333–351.

Kline, R. B. (2012). *Assumptions in Structural Equation Modeling*.

Kumar, M., Patel, A. K., Shah, A. V., Raval, J., Rajpara, N., Joshi, M., and Joshi, C. G. (2020). First Proof of the Capability of Wastewater Surveillance for COVID-19 in India Through Detection of Genetic Material of SARS-Cov-2. *Sci. Total Environ.* 746, 141326.

Kusumawati, D. I., and Mangkoedihardjo, S. (2021). Problems and Use of Cyanobacteria for Environmental Improvement–A. *J. Arid. Agric.* 7, 9–14.

Laitinen, K., and Sivunen, A. (2020). *Enablers of and Constraints on Employees' Information Sharing on Enterprise Social Media*. Information Technology and People.

Liobikienė, G., Dagiliutė, R., and Juknys, R. (2021). The Determinants of Renewable Energy Usage Intentions Using Theory of Planned Behaviour Approach. *Renew. Energy* 170, 587–594.

Liwafa, A., and Utami, C. W. (2021). The Effect of Digital Marketing and Service Quality on Consumer Brand Choice of Handmadeshoesby. *KnE Soc. Sci.* 354–365.

Lee, J., Kim, C., and Lee, K. C. (2021). Investigating the Negative Effects of Emojis in Facebook Sponsored Ads for Establishing Sustainable Marketing in Social Media. *Sustainability* 13 (9), 4864. doi:10.3390/su13094864

Mallinckrodt, B., Abraham, W. T., Wei, M., and Russell, D. W. (2006). Advances in Testing the Statistical Significance of Mediation Effects. *J. Counsel. Psychol.* 53 (3), 372.

Masukujjaman, M., Alam, S. S., Siwar, C., and Halim, S. A. (2021). Purchase Intention of Renewable Energy Technology in Rural Areas in Bangladesh: Empirical Evidence. *Renew. Energ.* 170, 639–651. doi:10.1016/j.renene.2021.01.125

Mazis, M. B., and Raymond, M. A. (1997). Consumer Perceptions of Health Claims in Advertisements and on Food Labels. *J. Consum. Aff.* 31 (1), 10–26.

McEachern, M., Seaman, C., Padel, S., and Foster, C. (2005). Exploring the gap between Attitudes and Behaviour. *Br. Food J.*

Merino-Rodríguez, I., Herrera, I., and Valdés-Riquelme, H. (2019). Environmental Assessment of Energy Scenarios for a Low-Carbon Electrical Network in Chile. *Sustainability* 11 (18), 5066.

Mirza, U. K., Ahmad, N., Harijan, K., and Majeed, T. (2009). Identifying and Addressing Barriers to Renewable Energy Development in Pakistan. *Renew. Sustain. Energ. Rev.* 13 (4), 927–931. doi:10.1016/j.rser.2007.11.006

Morone, P., Caferra, R., D'Adamo, I., Falcone, P. M., Imbert, E., and Morone, A. (2021). Consumer Willingness to Pay for Bio-Based Products: Do Certifications Matter. *Int. J. Prod. Econ.* 240, 108248. doi:10.1016/j.ijpe.2021.108248

Moslehpour, M., Pham, V. K., Wong, W. K., and Bilgiçli, İ. (2018). E-Purchase Intention of Taiwanese Consumers: Sustainable Mediation of Perceived Usefulness and Perceived Ease of Use. *Sustainability* 10 (1), 234.

Murshed, M., Abbass, K., Rashid, S. J. I. J. o. F., and Economics (2020). *Modelling Renewable Energy Adoption across South Asian Economies: Empirical Evidence from Bangladesh*. India: Pakistan and Sri Lanka.

Najar, A. H., and Hamid Rather, A. (2021). Mediating Role of Guest's Attitude Toward the Impact of UGC Benefits on Purchase Intention of Restaurants; Extending Social Action and Control Theories. *J. Foodserv. Bus. Res.* 24 (3), 249–273.

Niedermeier, A., Emberger-Klein, A., and Menrad, K. (2021). Which Factors Distinguish the Different Consumer Segments of green Fast-moving Consumer Goods in Germany. *Bus Strat Env* 30 (4), 1823–1838. doi:10.1002/bse.2718

Painuly, J. P. (2001). Barriers to Renewable Energy Penetration; a Framework for Analysis. *Renew. Energ.* 24 (1), 73–89. doi:10.1016/S0960-1481(00)00186-5

Papista, E., and Krystallis, A. (2013). Investigating the Types of Value and Cost of Green Brands: Proposition of a Conceptual Framework. *J. Bus. Ethics* 115 (1), 75–92.

Patil, P., Tamilmani, K., Rana, N. P., and Raghavan, V. (2020). Understanding Consumer Adoption of Mobile Payment in India: Extending Meta-UTAUT Model With Personal Innovativeness, Anxiety, Trust, and Grievance Redressal. *Int. J. Inform. Manage.* 54, 102144.

Pop, R. A., Săplăcan, Z., Dabija, D. C., and Alt, M. A. (2021). The Impact of Social Media Influencers on Travel Decisions: The Role of Trust in Consumer Decision Journey. *Curr. Issues Tour.*, 1–21.

Raykov, T., and Marcoulides, G. A. (2006). On Multilevel Model Reliability Estimation From the Perspective of Structural Equation Modeling. *Struct. Equ. Model.* 13 (1), 130–141.

Rezaei, R., and Ghofranfarid, M. (2018). Rural Households' Renewable Energy Usage Intention in Iran: Extending the Unified Theory of Acceptance and Use of Technology. *Renew. Energ.* 122, 382–391. doi:10.1016/j.renene.2018.02.011

Rezaei, A. H., Keshavarz, M. H., Tehrani, M. K., and Darbani, S. M. R. (2018). Quantitative Analysis for the Determination of Aluminum Percentage and Detonation Performance of Aluminized Plastic Bonded Explosives by Laser-Induced Breakdown Spectroscopy. *Laser Phys.* 28 (6), 065605.

Roberts, W. C., and Ko, J. M. (2005). Frequency by Decades of Unicuspid, Bicuspid, and Tricuspid Aortic Valves in Adults Having Isolated Aortic Valve Replacement for Aortic Stenosis, With or Without Associated Aortic Regurgitation. *Circulation* 111 (7), 920–925.

Sarker, U., Oba, S., and Daramy, M. A. (2020). Nutrients, Minerals, Antioxidant Pigments and Phytochemicals, and Antioxidant Capacity of the Leaves of Stem Amaranth. *Sci. Rep.* 10 (1), 1–9.

Sesan, T. (2008). *Status of Renewable Energy Policy and Implementation in Nigeria*. United Kingdom: Institute of Science and Society, Faculty of Social Sciences, Law and Education, University of Nottingham.

Solangi, Y. A., Longsheng, C., and Shah, S. A. A. (2021). Assessing and Overcoming the Renewable Energy Barriers for Sustainable Development in Pakistan: An Integrated AHP and Fuzzy TOPSIS Approach. *Renew. Energ.* 173, 209–222. doi:10.1016/j.renene.2021.03.141

Sohn, J. W., and Kim, J. K. (2020). Factors That Influence Purchase Intentions in Social Commerce. *Technol. Soc.* 63, 101365.

Spanos, Y. E., Prastacos, G. P., and Poulymenakou, A. (2002). The Relationship between Information and Communication Technologies Adoption and Management. *Inf. Manage.* 39 (8), 659–675. doi:10.1016/s0378-7206(01)00141-0

Stigka, E. K., Paravantis, J. A., and Mihalakakou, G. K. (2014). Social Acceptance of Renewable Energy Sources: A Review of Contingent Valuation Applications. *Renew. Sustain. Energ. Rev.* 32, 100–106. doi:10.1016/j.rser.2013.12.026

Stephens, G. K., and Sommer, S. M. (1996). The Measurement of Work to Family Conflict. *Educ. Psychol. Meas.* 56 (3), 475–486.

Sun, Y., Wang, Z., Zhang, B., Zhao, W., Xu, F., Liu, J., and Wang, B. (2020). Residents' Sentiments Towards Electricity Price Policy: Evidence From Text Mining in Social Media. *Resour. Conserv. Recycl.* 160, 104903.

Suraya, I., Nurmansyah, M. I., Rachmawati, E., Al Aufa, B., and Koire, I. I. (2020). The Impact of Large-Scale Social Restrictions on the Incidence of Covid-19: A Case Study of Four Provinces in Indonesia. *Kesmas*.

Tahar, A., Riyadh, H. A., Sofyani, H., and Purnomo, W. E. (2020). Perceived Ease of Use, Perceived Usefulness, Perceived Security and Intention to Use E-Filing: The Role of Technology Readiness. *J. Asian Finance Econ. Bus.* 7 (9), 537–547.

Taillon, B. J., Mueller, S. M., Kowalczyk, C. M., and Jones, D. N. (2020). Understanding the Relationships Between Social Media Influencers and Their Followers: The Moderating Role of Closeness. *J. Prod. Brand Manage.* 29 (6).

Trang, H. L. T., Lee, J. S., and Han, H. (2019). How do Green Attributes Elicit Pro-Environmental Behaviors in Guests? The Case of Green Hotels in Vietnam. *J. Travel Tour. Market.* 36 (1), 14–28.

Vand, B., Hast, A., Bozorg, S., Li, Z., Syri, S., and Deng, S. (2019). Consumers' Attitudes to Support Green Energy: A Case Study in Shanghai. *Energies* 12 (12), 2379. doi:10.3390/en12122379

Voorveld, H. A., Van Noort, G., Muntinga, D. G., and Bronner, F. (2018). Engagement With Social Media and Social Media Advertising: The Differentiating Role of Platform Type. *J. Adv.* 47 (1), 38–54.

Wang, Y., Xu, L., and Solangi, Y. A. (2020). Strategic Renewable Energy Resources Selection for Pakistan: Based on SWOT-Fuzzy AHP Approach. *Sust. Cities Soc.* 52, 101861. doi:10.1016/j.scs.2019.101861

Waris, A., Atta, U. K., Ali, M., Asmat, A., and Baset, A. J. N. M. (2020). COVID-19 Outbreak: Current Scenario of Pakistan. *New Microbes New Infect.* 35, 100681.

Woldeyohannes, A. D., Woldemichael, D. E., and Baheta, A. T. (2016). Sustainable Renewable Energy Resources Utilization in Rural Areas. *Renew. Sustain. Energy Rev.* 66, 1–9.

Wu, T., Yang, S., and Tan, J. (2020). Impacts Of Government R&D Subsidies on Venture Capital and Renewable Energy Investment-an Empirical Study in China. *Resour. Policy* 68, 101715.

Wüstenhagen, R., Wolsink, M., and Bürer, M. J. (2007). Social Acceptance of Renewable Energy Innovation: An Introduction to the Concept. *Energy Policy* 35 (5), 2683–2691. doi:10.1016/j.enpol.2006.12.001

Yorkovsky, Y., and Zysberg, L. (2021). Personal, Social, Environmental: Future Orientation and Attitudes Mediate the Associations between Locus of Control and Pro-environmental Behavior. *Athens J. Soc. Sci.* 8, 83–98.

Zhang, Y., Gao, J., Cole, S., and Ricci, P. (2021). How the spread of User-Generated Contents (UGC) Shapes International Tourism Distribution: Using Agent-Based Modeling to Inform Strategic UGC Marketing. *J. Trav. Res.* 60 (7), 1469–1491.

Conflict of Interest: The authors declare that the research was conducted in the absence of any commercial or financial relationships that could be construed as a potential conflict of interest.

Publisher's Note: All claims expressed in this article are solely those of the authors and do not necessarily represent those of their affiliated organizations, or those of the publisher, the editors, and the reviewers. Any product that may be evaluated in this article, or claim that may be made by its manufacturer, is not guaranteed or endorsed by the publisher.

frontiers | Frontiers in Energy Research

BRIEF RESEARCH REPORT
published: 06 April 2022
doi: 10.3389/fenrg.2022.857948

Analysis on Large-Scale Solar PV Plant Energy Performance–Loss–Degradation in Coastal Climates of India

*Bhogula Navothna and Sandhya Thotakura**

Department of Electrical, Electronics and Communication Engineering, Gandhi Institute of Technology and Management (Deemed to be University), Visakhapatnam, India

This article presents a detailed analysis of the performance, rate of degradation, and power and energy loss of a 1 MWp scale solar photovoltaic (PV) plant in the academic institution GITAM (Deemed to be University), located in the coastal region of Andhra Pradesh, India. The PV plant consists of 3,078 polycrystalline PV modules of 325 Wp rating, installed on the rooftop of the institute buildings. The annual energy generated is 1684.881 MWh. In this study, performance analysis involves the calculation of efficiency, capacity factor, and performance ratio with data simulated using the PVsyst tool. Degradation analysis involves energy light-induced degradation (LID) and degradation rate (DR). The predicted result provides an estimate for optimal functioning of PV plant with an annual capacity factor, performance ratio, and energy loss of 11.3%, 87.9%, and –26%, respectively. Energy loss by light-induced degradation is predicted as –2.7%/year, and the degradation rate of module per year is –0.6% to –5%.

Keywords: photovoltaic, performance parameters, energy loss, degradation rate, PV SYST

OPEN ACCESS

Edited by:
Sofiane Kichou,
Czech Technical University in Prague, Czechia

Reviewed by:
Sunanda Sinha,
Malaviya National Institute of Technology, India
Satish Kumar Yadav,
University of Lucknow, India

***Correspondence:**
Sandhya Thotakura
sandhyathotakura@gmail.com

Specialty section:
This article was submitted to Sustainable Energy Systems and Policies, a section of the journal Frontiers in Energy Research

Received: *19 January 2022*
Accepted: *02 March 2022*
Published: *06 April 2022*

Citation:
Navothna B and Thotakura S (2022) Analysis on Large-Scale Solar PV Plant Energy Performance–Loss–Degradation in Coastal Climates of India. Front. Energy Res. 10:857948. doi: 10.3389/fenrg.2022.857948

INTRODUCTION

The focus on increasing renewable resources has become one of the crucial methods to overcome the scarcity of electricity after the depletion of traditional energy sources and reduce atmospheric issues by utilizing fossil fuels. Decommissioning and dismantling conventional energy plants such as nuclear and thermal are implemented worldwide. Solar power, biomass, and hydropower are all excellent sources of renewable energy. The total installed capacity is 378.43 GW as of 31.10.2020 in India. Among this electricity mix, renewable energy sources contribute 36.2% (according to a report on load generation 2019–2020 by the Ministry of Power, Government of India, listed on its website: https://powermin.gov.in/en/content/power-sector-glance-all-india). The power generating capacity has to be increased to reach peak energy demand. Owing to the several advantages of solar energy resources over the other non-conventional sources, solar energy can increase the electricity generation capacity. The benefits of employing solar energy resources are abundant: eco-friendliness, decreased tariff, less maintenance, and reliability (Thapar et al., 2018). Research presented the initiative policies made by the government of India on encouraging grid-connected roof-top photovoltaic (PV) systems and off-grid systems.

The research by Subramaniyan et al. (2018) discussed the contribution of non-conventional resources such as solar and wind power and the estimation of these resources with a peak period technique in Rajasthan. In the study presented by Rodrigues et al. (2019), feasibility analysis to install

a grid-connected PV plant to the state university of Campinas is estimated using two simulation tools, one of which is PVsystV6 and the other is Helioscope. The performance rate of the proposed plant is about 81.2 and 80.83% in PVsyst and Helioscope, respectively. In a performance study of a 100 kWp grid-connected solar PV system, the performance ratio (PR) is observed to be 80% using PVsyst V6.52 software (Kumar et al., 2017a). In the research conducted by Kumar and Sudhakar (2015) on a 10 MWp solar photovoltaic plant, the largest PV plant located at Ramagundem, the PR is observed to be 86.12% and capacity utilization factor (CUF). A performance study of PV systems situated in Eastern India exhibited a PR of 0.78, PV efficiency of 13.42%, and system efficiency of 12.05% (Sharma and Goel, 2017). In a performance analysis carried out by Yadav et al. (2015) on a 1 kWp PV system located in Hamirpur, the PR and average solar radiation are recorded as 0.724 and 4.4 kWh/m^2, respectively, on a specific day. In a degradation study conducted in the semi-arid climate on a c-si photovoltaic system for four years, the highest PR of 76.46% is spotted in the presentation (Kumar and Malvoni, 2019). In a performance analysis carried out by Kumar et al. (2016) on a 10 KW roof-top photovoltaic system, the capacity factor is noticed as 17.8%, 18.5%, and 19.3% with two crystalline silicon-type and one thin-film-type technology, respectively. In an article by Thotakura et al. (2020), research was carried out on the performance of 1 MW scale grid-tied roof-top solar PV plants in a coastal region in India having tropical wet and dry conditions. Real-time data are monitored and compared with PVGIS, PV Watts, and PVsyst software simulation tools. The megawatt plant's capacity factor is 21.77%, with an annual energy generation of 168.488 MWh.

The operational performance was analyzed by Sudhakar et al. (2021) on a 2 MWp solar plant in Kerala, India, and an average performance ratio and capacity utilization factor of 73.39 and 15.41% were stated. Because of the monsoon season, there is a reduction of 35% in energy generation, mainly due to cloudy and rainy weather conditions. Dahmoun et al. (2021), in their research, published the literature on the operational performance analysis of a grid-tied 23.92 MWp solar PV plant located in Algeria for a period of 36 months. They reported a 5.46 kWh/kWp/day of an annual average daily array, 4.95 kWh/kWp/day of final yield, 82.02% of PR, and 20.64% of CUF. The real-time data are compared with the PVsyst and solar GIS tools and found a strong coincidence. The article by Bansal et al. (2021) presented a study on a 5 MW grid-integrated solar PV plant installed with crystalline silicon modules investigated for seven years. The authors checked the degradation analysis and performance assessment in Gujarat, India, which has hot and dry climate. It is mentioned that, from 2013 to 2016, the yearly average PR, CUF, inverter efficiency, and PV system efficiency of 73%, 17–18%, 96%, and 10.29–10.415% are attained and during 2017–2019, the values are in the range of 70% of PR, CUF of 14–16%, respectively.

The study by Ameur et al. (2022) covered six-year working data of a 5.94 kWp PV system comprising 2.04 kWp polycrystalline, 2.04 kWp monocrystalline (m-Si), and 1.86 kWp amorphous (a-Si) technologies to estimate the long-term performance and degradation rate for different climatic conditions of Ifrane, Morocco. Correlating with the present study technology, the polycrystalline system has a degradation rate of 0.36 ± 0.01%/year and 0.28 ± 0.004%/year with linear regression and classical seasonal decomposition statistical techniques and a performance ratio of 84.32%. In the literature (Makrides et al., 2010; Sharma et al., 2014; Sinha and Chandel, 2014; Gökmen et al., 2016; Kichou et al., 2016; Khandelwal and Shrivastava, 2017; Kumar et al., 2016; Kumar et al., 2017a; Kumar et al., 2017b; Jiang et al., 2016; Dubey et al., 2017; Sharma and Goel, 2017; Vasita et al., 2017; Atluri et al., 2018; Bhullar and Lalwani, 2018; Kichou et al., 2018; Prakhya and Reddy, 2018; Sudhakar and Samykano, 2018; Kumar N. et al., 2019; Kumar and Subathra, 2019; Navothna et al., 2020; Aoun, 2020; Thapar and Sharma, 2020), the researchers addressed about the performance factors, losses, and efficiency of solar PV plants located in various climatic regions. Few authors adopted simulation tools PVGIS, PV Watts, and PVsyst to compare with the monitored data. However, this kind of exploration is site specific, as various factors influence the technical activity of the solar PV plant of the region in which it is located. This analysis has not been carried out in the present study location (coastal region, Visakhapatnam, India) to the best of the authors' knowledge.

In the present study, the analysis of grid-connected PV systems near coastal areas is evaluated using the PVsyst simulation tool. Analyzing performance parameters is also essential to improve the solar photovoltaic system installations. Hence, the following are the present study's goals:

- To model and comprehend the operation of a roof-top grid-connected PV system installed on the rooftops of an educational institution Gandhi Institute of Technology and Management, Visakhapatnam, Andhra Pradesh, India
- To comprehend the energy conversion process and explore the various energy losses of roof-top polycrystalline solar PV systems built in the coastal region
- Degradation estimation of the photovoltaic plant

In the present study, performance specifications are identified, which are helpful for the feasibility analysis of the solar PV system in coastal areas. The results obtained from this study will create awareness of the potential of such a system being used to control the problem of energy scarcity and increase the use of non-conventional energy sources in various parts of the world. The developing countries can be global leaders in utilizing these sources.

SYSTEM DESCRIPTION

In the present study, a 1 MWp roof-top solar photovoltaic power plant connected to the grid was assembled on an educational Institute, Gandhi Institute of Technology and Management, Vishakhapatnam, located in the coastal region of Andhra Pradesh, India, is discussed. The plant consists of 23 PV arrays

installed at 15 building terraces and 23 inverters with a capacity of 20 kWp/50 kWp. The plant is located in latitude 17° 48′ 8.208″ N and longitude 83°23′ 6.54″ E. The detailed electrical specifications of the PV plant and the geometrical site map are provided in **Supplementary Data**.

FRAMEWORK AND METHODOLOGY

The performance study of the grid-connected PV system installed on the rooftops of academic buildings includes the normalized parameters that characterize the operating performance of the PV system. The parameters considered for the assessment in the present study location are array energy, net array energy output, array efficiency, grid energy, net energy output of PV system, system efficiency, capacity factor, performance ratio, loss, and degradation rate. The performance of this system can be compared to that of other PV systems under various working situations once these parameters have been determined. To predict and analyze the working of the PV system, the data related to the plant and selective simulation tools are required. The current study indicates the performance parameters of the solar plant located in a coastal area. The critical parameters and their equations for analysis are also furnished (Malvoni et al., 2017a). The methodology for the analysis is illustrated as follows:

- The critical data for the analysis of PV plants such as the geographical specification of the study location (coordinates, weather conditions, temperature, solar irradiation, and wind speed), PV module, and inverter specifications are accumulated.
- One of the most widely used PV system simulation tools is identified. In this study, PVsyst is preferred for the performance and irradiation analysis of the PV system.
- Performance parameters of the solar PV plant are studied in detail and presented with their equations. The energy and efficiency parameters are estimated.
- Degradation analysis of the solar PV plant is analyzed by mainly focusing on the light-induced degradation (LID) and degradation rate (DR).

PVsyst Software Tool

PVsyst software is one of the most widely used simulation tools in the design and calculation of basic considerations of photovoltaic systems PVSyst (2021). Modeling in PVsyst starts with system sizing, which comprises desired power rating or available area, PV module, and inverter sizing. Based on the given input specifications, the PVsyst will propose module configurations for further simulation study. This software updates weather details of the selected location, which helps in evaluating output parameters. PVsyst tool gives monthly global irradiance, diffuse irradiance, temperature, and wind speed of the selected location. Based on these data, the trajectory of the Sun, which provides information on losses that occur during period of a year, is also given. The results of the simulation tool include total energy produced, performance ratio, and specific energy. By utilizing these results, energy yield, capacity factor, and efficiency of PV array and PV system can be calculated. The existing PV system behavior and further expansion of the system can be carried out Photovoltaic Software (2021).

Array Energy [E_{AE}]

It is the energy generated by a photovoltaic array. Array energy mainly depends on the area of the total array of the PV system [A_A], solar radiation [I_s] incident on PV modules, and the efficiency of the PV module [η_{PV}], how successfully it transforms solar energy into electrical energy. The area of the total array [A_A] of the PV system is calculated by considering the total number of PV modules multiplied by the area of individual modules. The extra space to accommodate the panels in specified orientation and between the strings is also added. The area used by the total arrays of the installed PV system is 12,000 m^2. Therefore, the array energy is expressed as a product of all the mentioned three parameters, as shown in the following equation:

$$E_{AE} = A_A \times I_s \times \eta_{pv}, kWh. \quad (1)$$

Net Array Energy Output [D_{EA}]

A solar array is a group of solar modules joined in series and parallel. Hence the net array energy output mainly depends on the area of the total arrays of the PV system, the efficiency of the PV module for the incident solar irradiation, and the full capacity of the solar PV plant. It is also expressed as the ratio of energy array to the entire plant capacity (PC), as shown in the following equation:

$$D_{EA} = \frac{E_{AE}}{PC}, kWh. \quad (2)$$

Array Efficiency [η_A]

Any system's efficiency is determined by the input it receives and the output it produces. The efficiency of an array is determined by the input, which is the solar irradiation dispersed across the entire array, and the generated output energy as expressed in the following equation:

$$\eta_A = \frac{E_{AE}}{A_A \times I_S} \times 100. \quad (3)$$

Grid Energy [E_{GE}]

The existing plant is an integrated grid system, the energy generated by the PV arrays is converted to AC and pumped into the grid *via* inverters. Solar energy generation depends on solar irradiation, and energy conversion depends on the inverter's performance and losses. Hence the grid energy is expressed in **Eq. 4** as a product of array energy [E_{AE}], the efficiency of the inverter [η_{inv}], and loss efficiency [η_{LOSS}].

$$E_{GE} = E_{AE} \times \eta_{inv} \times \eta_{LOSS}, kWh. \quad (4)$$

Net Energy Output of the PV System [D_{EG}]

It is the solar PV system's net energy output, expressed as a ratio of energy injected into the grid to the capacity of the solar PV plant, as shown in the following equation:

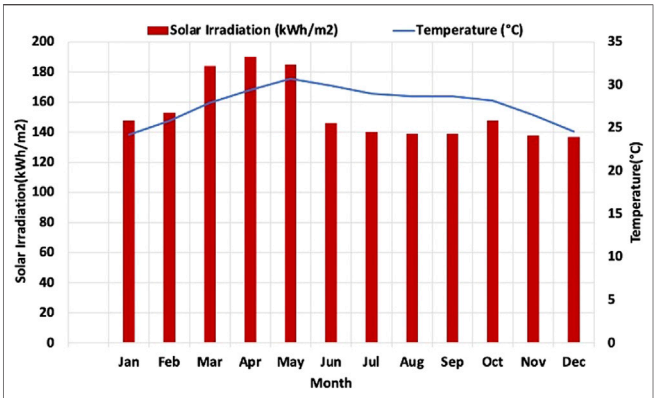

FIGURE 1 | Monthly solar irradiation and ambient temperature.

$$D_{EG} = \frac{E_{GE}}{PC}, kWh \Big/ kW\,p. \tag{5}$$

System Efficiency [η_{sys}]

A solar System's efficiency is commonly defined as the ratio of solar energy input to electrical energy output. The system efficiency depends on many parameters, whereas here, it is declared as the ratio of grid energy [E_{GE}] to the solar irradiation [I_s] and the area of total PV arrays [A_A].

$$\eta_{sys} = \frac{E_{GE}}{A_A \times I_S} \times 100. \tag{6}$$

Capacity Factor [F_c]

The capacity factor can be defined as the actual electricity production divided by a power plant's maximum feasible electrical output over some time, as shown in the following equation:

$$F_c = \frac{D_{EG}}{OH} \times 100. \tag{7}$$

Performance Ratio [PR]

The performance ratio (PR) is a frequently used term for assessing the relative performance of solar panels with different designs, technologies, capacities, and locations. PR is calculated using **Eq. 8**, where it is expressed as a percentage ratio of net grid energy output [D_{EG}] to the reference energy yield [Y_R].

$$PR = \frac{D_{EG}}{Y_R} \times 100. \tag{8}$$

Loss and Degradation Rate [DR]

Loss and degradation rate are the two essential parameters for analyzing the performance of PV systems. In a survey conducted by the National Centre for PV Research and Education at the Indian Institute of Technology, Bombay, and National Institute of Solar Energy, Haryana, it is assumed that the deterioration in crystalline silicon modules would vary from −0.6 to −5%/year (Dubey et al., 2016; Dubey et al., 2017). The mathematical equation for degradation rate can be expressed as (Kumar et al., 2019)

$$\%DR = \frac{12*m}{c} \times 100, \tag{9}$$

where m: slope and c: intercept. These values are considered for the present study directly from the literature (Kumar N. M. et al., 2019).

RESULTS AND DISCUSSION

Analysis of Solar Radiation and Ambient Temperature

The solar irradiation and ambient air temperature of the study location from January 2020 to December 2020 are shown in **Figure 1**. Monthly solar irradiation and ambient temperature are obtained for analysis from the PVsyst simulation software tool. The annual average horizontal global solar irradiation is observed as 153.91 kWh/m^2. The maximum Sun irradiation of 190 kWh/m^2 is recorded in April, and the lowest in December, with 137 kWh/m^2. The maximum ambient temperature is in May at 30.7°C and the minimum in December at 24.6°C.

Energy Analysis

Figure 2A presents the estimated energy yields and energy given to the grid of the PV system. The total amount of energy generated from the PV system is 1780.878 MWh. The PV system yield ranges between 118.537 MWh in July and 178.499 MWh in March. Each year, the total quantity of AC energy put into the grid is about 1684.881 MWh. In July, the AC energy output was 118.537 MWh, while in March, it was 169.306 MWh. It is observed that the difference between DC and AC energy yields is caused by energy loss. This energy loss is due to module temperatures and various system constituents (Sharma and Goel, 2017). The PV system's average efficiency in each month is estimated and shown in **Figure 2A** for extensive examination of PV system performance. The average annual efficiency of the total system is 16.3%, whereas the array efficiency varies between 16.24% (July) to 16.48% (May). In **Figure 2B**, the variation of specific energy over 1 year is presented. The total yearly electricity yielded from the PV system was 1774 kWh/kWp. The least and maximum possible monthly definite energy predicted are 125 kWh/kWp in July and 178 kWh/kWp in March, respectively. The total yearly energy at grid end is 1679 kWh/kWp, with a minimum monthly specific energy of 118 kWh/kWp predicted in July and a maximum of 169 kWh/kWp in March. The total annual energy delivered into the grid is estimated to be around 1684.881 MWh, with a minimum of 3,823 kWh anticipated in July and a maximum of 5,617 kWh during April. The average amount of energy injected every hour into the grid is forecasted to be 159 kWh in July and 234 kWh in April, which are presented in **Figure 2C**.

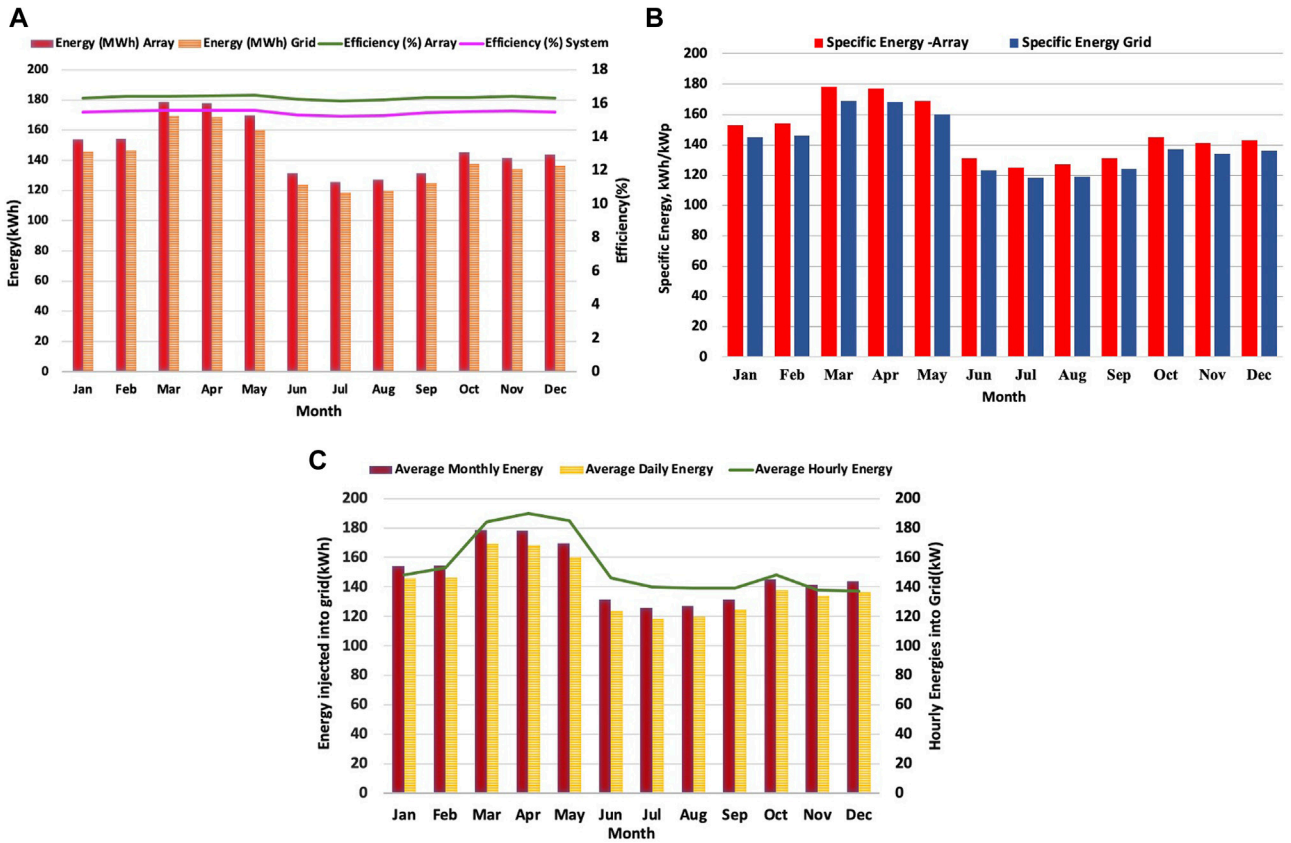

FIGURE 2 | (A) Estimated energy generated and efficiency of the PV plant **(B)** Monthly specific energy output of the plant **(C)** Average monthly and hourly energy injected into grid by the PV plant.

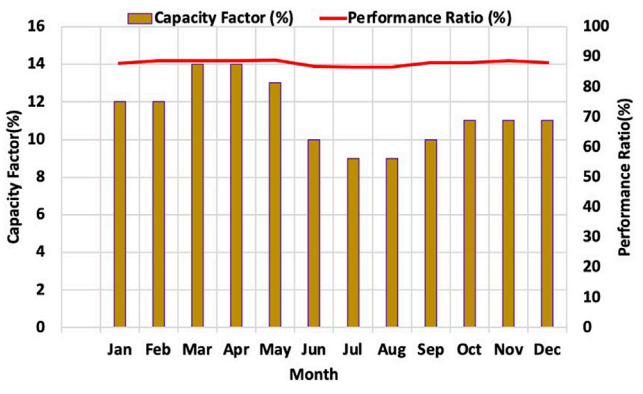

FIGURE 3 | Monthy average capacity factor and performance ratio.

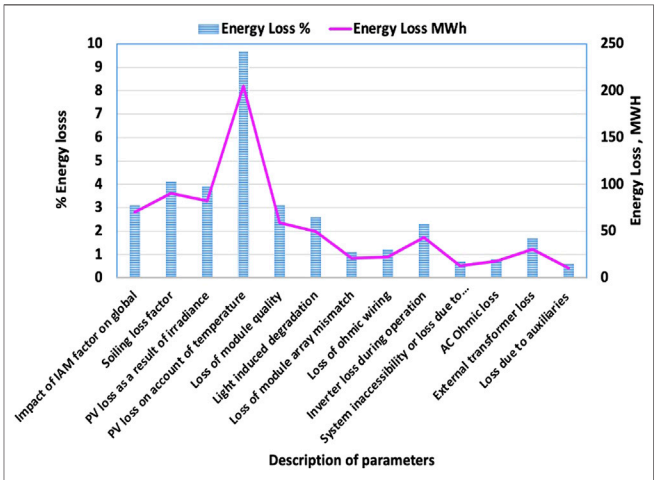

FIGURE 4 | Energy loss estimation of PV plant.

Capacity Factor (F_c) and Performance Ratio (PR)

The two key performance indicators of the PV system are capacity factor and performance ratio. The yearly average capacity factor was 11.3%, with the least forecasted value of 9% in August and a peak forecasted value of 14% in March. The average annual performance ratio was 87.96%, with the least indicated with a value of 86.51% in July and peak forecasted with 88.79% in May. **Figure 3** displays the F_c and

TABLE 1 | Performance correlation with existing roof-top PV plants.

Location	Solar plant capacity	Energy (MWh)	F_C (%)	PR (%)	Energy loss (%)	References
Kerman	11 kWp	-	23.81	82.92	-	Edalati et al. (2015)
Hoon City	14 MWp	24,964	-	76.9	-	Kagilik and Tawel (2015)
Hamirpur	100 kWp	01.36	15.40	72.4	32.0	Ramoliya (2015)
Hyderabad	100 kWp	161.60	18.44	80	20.0	Dubey et al. (2016)
Southern Italy	960 kWp	1262.10	15.60	84.4	26.1	Malvoni et al. (2017b)
Chandigarh	200 kWp	292.9	16.70	77.3	26.5	Kumar et al. (2017b)
Ahmedabad	~150 kWp	150.79	-	75.1–82.5	-	Vasita et al. (2017)
Bhubaneswar	~100 kWp	14.96	-	78	-	Sharma and Goel (2017)
South America	27 kWp	37	15.5	74.5	-	Raghoebarsing and Kalpoe (2017)
Haryana	50 kWp	-	-	87	-	Berwal et al. (2017)
Gujarat	25 MWp	50,091	22.80	80.1	-	Bhullar and Lalwani (2018)
Brazil	7.82 MWp	82.7	-	81.2	-	Rodrigues et al. (2019)
Tamil Nadu	83 kWp	5.499	-	52	-	Aravindan et al. (2019)
Palestine	7.68 kWp	-	-	76	-	Ibrik and Hashaika (2019)
Odisha	100 kWp	-	16.17	80	-	Mohanty (2020)
Manisa, Turkey	30 kWp	45.59	17.35	83.61	-	Ates and Singh (2021)
Tamil Nadu	5.00 kWp	7.144	16.31	76.83	-	Duraivelu and Elumalai (2021)
Saudi Arabia	467 kWp	-	15–18	80–86	-	Minai et al. (2022)
Vishakhapatnam	1.00 MWp	1684.81	11.33	87.9	26.0	Present study, 2022

PR of the PV plant. Even though the capacity utilization factor and performance ratio both depends on the energy yield of the solar PV system, there are other individual parameters that each of them depends on. Capacity factor also depends on the operating time of the PV plant, whereas performance ratio is proportional to reference energy yield, which makes the difference in their final values.

Loss Analysis

In this section, the energy losses are evaluated in a 1 MW roof-top connected PV system over 12 months using a PV system modeling technique and are presented in **Figure 4**. The energy loss varies from -0.7% (−12900.311 kWh) to −9.7% (−204877.98 kWh). The minimum foreseen worth is because of auxiliaries (−0.6%), system inaccessibility (−0.7%), and from the side of the electrical converter, there are losses in the AC resistance unit (0.7%). The temperature was the source of the greatest anticipated energy loss (9.7%). Nonetheless, the loss in energy due to solar irradiance levels on the PV module (3.9%), module quality loss (−3.1%), and light-induced deterioration are all significant (2.6%), and also the electrical converter operational loss (−2.3%) is additionally limiting the effectiveness of the PV system. The total energy losses are estimated as 715.76 MWh, with a total energy loss of 34.9%.

Degradation Analysis

The loss in the performance of the solar modules due to exposure to sunlight is named light-induced degradation (LID). Accurate measurement of power loss over time is marked as degradation rate (DR), where these two parameters play as vital performance indicators of a PV system. The observations show a LID of -2.7%, which accounts for the energy loss value of −49,588.921 kWh/year for the PV system. Estimated energy loss because of the degradation rate within 1 MW crystalline PV plant ranges from −10,689.3 to −89,099.5 kWh/year, respectively.

Correlation With the Present-Day Literature

The forecasted parameter in this study is equated with different PV systems based on the given performance information in their literature. The findings of this investigation appear to be consistent with those of previous studies, as shown in **Table 1**. This study helps the investors and researchers function of PV plants in the coastal areas.

CONCLUSION

The present case study involves a detailed analysis of the performance of a 1 MW power solar PV plant for coastal weather conditions in Visakhapatnam, India, mainly using the energy outputs, losses, and degradation rate. As per the weather conditions of the location, the following observations are made:

- The annual average horizontal global solar irradiation at the present study location is recorded as 153.91 kWh/m^2, with maximum sun irradiation of 190 kWh/m^2 in April and the lowest value of 137 kWh/m^2 during December
- The total energy generation from the 1 MW power plant is estimated as 1780.878 MWh
- Each year, the AC energy injected into the grid is 1684.881 MWh
- The average annual efficiency of the entire plant is approximated as 16.3%, whereas the PV array efficiency may vary between 16.24 and 16.48%
- The yearly average capacity factor of the solar PV plant is around 11.3%
- With the polycrystalline panels, the 1 MW power PV plant operates with the PR% of 87.9%, with the highest PR value of 88.79% in May due to the highest solar irradiation during the summer season
- The energy losses are −26%
- Under these climatic circumstances, the degradation rate of a photovoltaic array is between −0.6 and −5% every year

DATA AVAILABILITY STATEMENT

The original contributions presented in the study are included in the article/**Supplementary Material**, further inquiries can be directed to the corresponding author.

AUTHOR CONTRIBUTIONS

Conceptualization, writing—review and editing, and supervision: ST; data curation, formal analysis, investigation, and writing: BN,.

ACKNOWLEDGMENTS

The authors thank GITAM (Deemed to be University) for providing the data for conducting this study.

SUPPLEMENTARY MATERIAL

The Supplementary Material for this article can be found online at: https://www.frontiersin.org/articles/10.3389/fenrg.2022.857948/full#supplementary-material

REFERENCES

Ameur, A., Berrada, A., Bouaichi, A., and Loudiyi, K. (2022). Long-term Performance and Degradation Analysis of Different PV Modules under Temperate Climate. *Renew. Energ.* 188, 37–51. doi:10.1016/j.renene.2022.02.025

Aoun, N. (2020). Performance Analysis of a 20 MW Grid-Connected Photovoltaic Installation in Adrar, South of Algeria. *Adv. Stat. Model. Forecast. Fault Detect. Renew. Energ. Syst.* 85, 1–12. doi:10.5772/intechopen.89511

Aravindan, M., Balaji, V., Saravanan, V., and Arumugam, M. (2019). Performance Evaluation of Roof Top Solar Photovoltaic Systems in Tamilnadu. *Ijape* 8 (3), 265–276. doi:10.11591/ijape.v8.i3.pp265-276

Ates, A. M., and Singh, H. (2021). Rooftop Solar Photovoltaic (PV) Plant - One Year Measured Performance and Simulations. *J. King Saud Univ. - Sci.* 33 (3), 101361. doi:10.1016/j.jksus.2021.101361

Atluri, K., Hananya, S. M., and Navothna, B. (2018). "Performance of Roof-Top Solar PV System with Crystalline Solar Cells," in Proceedings of the 2018 National Power Engineering Conference (NPEC), Madurai, IndiaMarch 2018 (Piscataway, New Jersey, United States: IEEE). doi:10.1109/npec.2018.8476721

Bansal, N., Pany, P., and Singh, G. (2021). Visual Degradation and Performance Evaluation of Utility Scale Solar Photovoltaic Power Plant in Hot and Dry Climate in Western India. *Case Stud. Therm. Eng.* 26, 101010. doi:10.1016/j.csite.2021.101010

Berwal, A. K., Kumar, S., Kumari, N., Kumar, V., and Haleem, A. (2017). Design and Analysis of Rooftop Grid Tied 50 kW Capacity Solar Photovoltaic (SPV) Power Plant. *Renew. Sustain. Energ. Rev.* 77, 1288–1299. doi:10.1016/j.rser.2017.03.017

Bhullar, S. S., and Lalwani, M. (2018). "Performance Analysis of 25 MW Grid-Connected Solar Photovoltaic Plant in Gujarat, India," in Proceedings of the 2018 3rd International Innovative Applications of Computational Intelligence on Power, Energy and Controls with their Impact on Humanity (CIPECH), Ghaziabad, India, November 2018 (Piscataway, New Jersey, United States: IEEE). doi:10.1109/cipech.2018.8724370

Dahmoun, M. E.-H., Bekkouche, B., Sudhakar, K., Guezgouz, M., Chenafi, A., and Chaouch, A. (2021). Performance Evaluation and Analysis of Grid-Tied Large Scale PV Plant in Algeria. *Energ. Sustain. Develop.* 61, 181–195. doi:10.1016/j.esd.2021.02.004

Dubey, R., Chattopadhyay, S., Kuthanazhi, V., John, J., Ansari, F., Rambabu, S., et al. (2016). *All-India Survey of PV Module Reliability: 2016*. Gurugram: NCPRE, IITB and NISE.

Dubey, R., Chattopadhyay, S., Kuthanazhi, V., Kottantharayil, A., Singh Solanki, C., Arora, B. M., et al. (2017). Comprehensive Study of Performance Degradation of Field-mounted Photovoltaic Modules in India. *Energy Sci Eng* 5 (1), 51–64. doi:10.1002/ese3.150

Duraivelu, R., and Elumalai, N. (2021). Performance Evaluation of a Decentralized Rooftop Solar Photovoltaic System with a Heat Recovery Cooling Unit. *Environ. Sci. Pollut. Res.* 28 (15), 19351–19366. doi:10.1007/s11356-020-12104-0

Edalati, S., Ameri, M., and Iranmanesh, M. (2015). Comparative Performance Investigation of Mono- and Poly-Crystalline Silicon Photovoltaic Modules for Use in Grid-Connected Photovoltaic Systems in Dry Climates. *Appl. Energ.* 160, 255–265. doi:10.1016/j.apenergy.2015.09.064

Gökmen, N., Hu, W., Hou, P., Chen, Z., Sera, D., and Spataru, S. (2016). Investigation of Wind Speed Cooling Effect on PV Panels in Windy Locations. *Renew. Energ.* 90, 283–290. doi:10.1016/j.renene.2016.01.017

Ibrik, I., and Hashaika, F. (2019). Techno-economic Impact of Grid-Connected Rooftop Solar PV System for Schools in Palestine: a Case Study of Three Schools. *Ijeep* 9 (3), 291–300. doi:10.32479/ijeep.7593

Jiang, F., Zou, X., and Liu, H. (2016). "Performance Test and Analysis of a PV Power Plant in Hami," in Proceedings of the 2016 Chinese Control and Decision Conference (CCDC), Yinchuan, China, May 2016 (Piscataway, New Jersey, United States: IEEE). doi:10.1109/ccdc.2016.7532103

Kagilik, A., and Tawel, A. (2015). Performance Analysis of 14 MW Grid-Connected Photovoltaic System. *jsesd* 4 (1), 11–21. doi:10.51646/jsesd.v4i1.78

Khandelwal, A., and Shrivastava, V. (2017). "Viability of Grid-Connected Solar PV System for a Village of Rajasthan," in Proceedings of the 2017 International Conference on Information, Communication, Instrumentation and Control (ICICIC), Indore, India, August 2017 (Piscataway, New Jersey, United States: IEEE). doi:10.1109/icomicon.2017.8279175

Kichou, S., Abaslioglu, E., Silvestre, S., Nofuentes, G., Torres-Ramírez, M., and Chouder, A. (2016). Study of Degradation and Evaluation of Model Parameters of Micromorph Silicon Photovoltaic Modules under Outdoor Long Term Exposure in Jaén, Spain. *Energ. Convers. Manag.* 120, 109–119. doi:10.1016/j.enconman.2016.04.093

Kichou, S., Wolf, P., Silvestre, S., and Chouder, A. (2018). Analysis of the Behaviour of Cadmium telluride and Crystalline Silicon Photovoltaic Modules Deployed Outdoor under Humid continental Climate Conditions. *Solar Energy* 171, 681–691. doi:10.1016/j.solener.2018.07.028

Kumar, N. M., and Malvoni, M. (2019). A Preliminary Study of the Degradation of Large-Scale C-Si Photovoltaic System under Four Years of Operation in Semi-arid Climates. *Results Phys.* 12, 1395–1397. doi:10.1016/j.rinp.2019.01.032

Manoj Kumar, N., and Subathra, M. S. P. (2019). Three Years Ahead Solar Irradiance Forecasting to Quantify Degradation Influenced Energy Potentials from Thin Film (A-Si) Photovoltaic System. *Results Phys.* 12, 701–703. doi:10.1016/j.rinp.2018.12.027

Shiva Kumar, B., and Sudhakar, K. (2015). Performance Evaluation of 10 MW Grid Connected Solar Photovoltaic Power Plant in India. *Energ. Rep.* 1, 184–192. doi:10.1016/j.egyr.2015.10.001

Kumar, N. M., Reddy, P. R. K., Sunny, K. A., and Navothana, B. (2016). "Annual Energy Prediction of Roof Mount PV System with Crystalline Silicon and Thin Film Modules," in Proceedings of the Special Section on: Current Research Topics in Power, Nuclear and Fuel Energy, SP-CRTPNFE 2016, from the International Conference on Recent Trends in Engineering, Science and Technology 2016, Hyderabad, India, October 2016, 24–31.

Kumar, N. M., Das, P., and Krishna, P. R. (2017a). "Estimating Grid Feed in Electricity from Roof Integrated Si-Amorph PV System Based on Orientation, Tilt and Available Roof Surface Area," in Proceedings of the 2017 International Conference on Intelligent Computing, Instrumentation and Control Technologies (ICICICT), Kerala, India, July 2017 (Piscataway, New Jersey, United States: IEEE).

Kumar, N. M., Kumar, M. R., Rejoice, P. R., and Mathew, M. (2017b). Performance Analysis of 100 kWp Grid Connected Si-Poly Photovoltaic System Using PVsyst Simulation Tool. *Energ. Proced.* 117, 180–189. doi:10.1016/j.egypro.2017.05.121

Kumar, N. M., Gupta, R. P., Mathew, M., Jayakumar, A., and Singh, N. K. (2019a). Performance, Energy Loss, and Degradation Prediction of Roof-Integrated Crystalline Solar PV System Installed in Northern India. *Case Stud. Therm. Eng.* 13, 100409. doi:10.1016/j.csite.2019.100409

Kumar, N., Sudhakar, K., and Samykano, M. (2019b). Techno-economic Analysis of 1 MWp Grid Connected Solar PV Plant in Malaysia. *Int. J. Ambient Energ.* 40 (4), 434–443. doi:10.1080/01430750.2017.1410226

Kumar, A. P. (2016). "Analysis of Hybrid Systems: Software Tools," in Proceedings of the 2016 2nd International Conference on Advances in Electrical, Electronics, Information, Communication and Bio-Informatics (AEEICB), Chennai, India, February 2016 (Piscataway, New Jersey, United States: IEEE). doi:10.1109/aeeicb.2016.7538302

Kumar, N. M. (2017). "Simulation Tools for Technical Sizing and Analysis of Solar PV Systems," in Proceedings of the 6th World Conference on Applied Sciences, Engineering and Technology (WCSET-2017), Ponorogo, Indonesia, August 2017.

Makrides, G., Zinsser, B., Georghiou, G. E., Schubert, M., and Werner, J. H. (2010). "Evaluation of Grid-Connected Photovoltaic System Performance Losses in Cyprus," in Proceedings of the 7th Mediterranean Conference and Exhibition on Power Generation, Transmission, Distribution and Energy Conversion (MedPower 2010), Agia Napa, November 2010. doi:10.1049/cp.2010.0883

Malvoni, M., De Giorgi, M. G., and Congedo, P. M. (2017a). Study of Degradation of a Grid Connected Photovoltaic System. *Energ. Proced.* 126, 644–650. doi:10.1016/j.egypro.2017.08.263

Malvoni, M., Leggieri, A., Maggiotto, G., Congedo, P. M., and De Giorgi, M. G. (2017b). Long Term Performance, Losses and Efficiency Analysis of a 960 kW P Photovoltaic System in the Mediterranean Climate. *Energ. Convers. Manag.* 145, 169–181. doi:10.1016/j.enconman.2017.04.075

Minai, A. F., Usmani, T., Alotaibi, M. A., Malik, H., and Nassar, M. E. (2022). Performance Analysis and Comparative Study of a 467.2 kWp Grid-Interactive SPV System: A Case Study. *Energies* 15 (3), 1107. doi:10.3390/en15031107

Mohanty, R. C. (2020). Performance Evaluation of One MW On-Grid SPV Power Generation Plant in Odisha, India. *Indian J. Nat. Sci.* 10 (58), 18084–18091.

Navothna, B., Kondamudi, S. C., and Thotakura, S. (2020). Review of Photovoltaic Systems Performance Influencing Factors. *J. Green Eng.* 10, 9052–9067.

Photovoltaic Software (2021). General Description of PV GIS Software. Available at: https://photovoltaic-software.com/pv-softwares-calculators/online-free-photovoltaic-software/pvgis (Accessed February 20th, 2021).

Prakhya, R. K., and Reddy, C. L. (2018). Estimating the Performance Ratio and Degradation Factor of Roof-Toproof-Top Solar PV Plant. *CVR J. Sci. Technol.* 14, 32–37. doi:10.32377/cvrjst1407

PVSyst (2021). General Description of the PVsyst Software. Available at: http://files.pvsyst.com/help/general_descr.htm (Accessed January 30th, 2021).

Raghoebarsing, A., and Kalpoe, A. (2017). Performance and Economic Analysis of a 27-kW Grid-Connected Photovoltaic System in Suriname. *IET Renew. Power Generation* 11 (12), 1545–1554. doi:10.1049/iet-rpg.2017.0204

Ramoliya, J. V. (2015). Performance Evaluation of Grid-Connected Solar Photovoltaic Plant Using PVSYST Software. *J. Emerging Tech. Innovative Res. (Jetir)* 2 (2), 7.

Rodrigues, A., Silva, E., and Seixas, S. (2019). "Performance Analysis of PV System Grid Connected Using Simulation Tools," in Proceedings of the the 13th Latin-American Congress On Electricity Generation and Transmission, Santiago de Chile, Chile, October 2019.

Sharma, R., and Goel, S. (2017). Performance Analysis of a 11.2 kWp Roof Top Grid-Connected PV System in Eastern India. *Energ. Rep.* 3, 76–84. doi:10.1016/j.egyr.2017.05.001

Sharma, D. K., Verma, V., and Singh, A. P. (2014). Review and Analysis of Solar Photovoltaic Softwares. *Int. J. Curr. Eng. Technol.* 4 (2), 725–731.

Sinha, S., and Chandel, S. (2014). Review of Software Tools for Hybrid Renewable Energy Systems. *Renew. Sustain. Energ. Rev.* 32, 192–205. doi:10.1016/j.rser.2014.01.035

Subramaniyan, S., Mathew, M., and Hossain, J. (2018). "Renewable Energy Capacity Value Estimation Using Peak Period Method in Rajasthan," in Proceedings of the 2018 3rd International Conference for Convergence in Technology (I2CT), Pune, India, April 2018 (Piscataway, New Jersey, United States: IEEE). doi:10.1109/i2ct.2018.8529338

Sudhakar, K., and Samykano, M. (2018). "Performance of Utility Scale PV Plant in Malaysia and India: a Comparative Study," in Proceedings of the 2018 4th International Conference on Electrical Energy Systems (ICEES), Chennai, India, February 2018 (Piscataway, New Jersey, United States: IEEE).

Sudhakar, K., Ngui, W., and Kirpichnikova, I. (2021). Energy Analysis of Utility-Scale PV Plant in the Rain-Dominated Tropical Monsoon Climates. *Case Stud. Therm. Eng.* 26, 101123. doi:10.1016/j.csite.2021.101123

Thapar, S., and Sharma, S. (2020). Factors Impacting Wind and Solar Power Sectors in India: A Survey-Based Analysis. *Sustainable Prod. Consumption* 21, 204–215. doi:10.1016/j.spc.2020.01.001

Thapar, S., Sharma, S., and Verma, A. (2018). Analyzing Solar Auctions in India: Identifying Key Determinants. *Energ. Sustain. Develop.* 45, 66–78. doi:10.1016/j.esd.2018.05.003

Thotakura, S., Kondamudi, S. C., Xavier, J. F., Quanjin, M., Reddy, G. R., Gangwar, P., et al. (2020). Operational Performance of Megawatt-Scale Grid Integrated Roof-Toproof-Top Solar PV System in Tropical Wet and Dry Climates of India. *Case Stud. Therm. Eng.* 18, 100602. doi:10.1016/j.csite.2020.100602

Vasita, J., Shakhiya, Q., and Modi, J. (2017). "Feasibility Study and Performance Evaluation of a Grid-Connected Roof-Toproof-Top Solar PV System," in Proceedings of the 2017 International Conference on Information, Communication, Instrumentation and Control (ICICIC), Indore, India, August 2017 (Piscataway, New Jersey, United States: IEEE).

Yadav, P., Kumar, N., and Chandel, S. (2015). "Simulation and Performance Analysis of a 1 kWp Photovoltaic System Using PVsyst," in 2015 International Conference on Computation of Power, Energy, Information and Communication (ICCPEIC), Melmaruvathur, India, April 2015 (Piscataway, New Jersey, United States: IEEE). doi:10.1109/iccpeic.2015.7259481

Conflict of Interest: The authors declare that the research was conducted in the absence of any commercial or financial relationships that could be construed as a potential conflict of interest.

NOMENCLATURE

PV Photovoltaic

LID Light-induced degradation

DR Degradation rate

E_{AE} Array energy (kWh)

A_A Array area of PV system (m^2)

I_S Incident solar radiation on the surface (kWh/m^2)

η_{pv} Efficiency of the PV module (%)

D_{EA} Net array energy output (kWh)

PC Plant capacity (kWh)

$\boldsymbol{\eta_A}$ Array efficiency (%)

E_{GE} Grid energy (kWh)

η_{inv} Inverter efficiency (%)

η_{LOSS} Loss efficiency (%)

D_{EG} Net energy output of PV system (kWh)

F_c Capacity factor (%)

OH Operating hours (h)

PR Performance ratio (%)

Y_R Reference energy yield (h/d)

frontiers | Frontiers in Energy Research

BRIEF RESEARCH REPORT
published: 28 June 2022
doi: 10.3389/fenrg.2022.869890

Feasibility Assessment of Bifacial Rooftop Photovoltaic Systems in the State of Gujarat in India

Alpesh Desai[1]*, *Indrajit Mukhopadhyay*[1,2] and *Abhijit Ray*[1,2]*

[1]Department of Solar Energy, School of Technology, Pandit Deendayal Energy University (PDEU), Gandhinagar, India, [2]Solar Research Development Centre (SRDC), Pandit Deendayal Energy University (PDEU), Gandhinagar, India

Bifacial solar photovoltaic (PV) modules are one of the recent interventions in the widespread commercial deployment of solar energy. This study intends to analyze the adoption of bifacial solar panels in rooftop PV systems to enhance energy generation as compared to their mono-facial counterparts. The technical and economic advantages of a typical 5-kW single-phase solar rooftop photovoltaic system using bifacial Si-modules are presented and compared with those using traditional polycrystalline Si (poly c-Si) modules in the urban location of the state of Gujarat in India. This methodology allows one to find optimal performance under the same irradiation and load conditions. As the majority of terraces in this location have a surface of white or gray tiles, which have a high albedo factor, bifacial modules generate more than 10% excess energy as compared to the poly c-Si systems. Although bifacial modules have an initial cost higher than the polycrystalline counterparts, the cost of their balance of system and space is reduced by 2 to 13%, respectively. Analysis shows that a 5kW bifacial technology can generate an excess of 13 MWh as compared to the traditional poly-Si over a period of 25 years. Finally, it is seen that an optimized bifacial system that is tilted between 15 and 20° will reduce the levelized cost of electricity (LCOE) by 5.5% as compared to the traditional poly c-Si system.

Keywords: rooftop solar, bifacial modules, distributed energy systems, solar efficiency, LCOE, technoeconomic environment, solar in India

OPEN ACCESS

Edited by:
Massimo Gastaldi,
University of L'Aquila, Italy

Reviewed by:
Aneesh A. Chand,
University of the South Pacific, Fiji
Mobi Mathew,
Deakin University, Australia
Sonali Goel,
PhD, India

***Correspondence:**
Alpesh Desai
alpesh.dphd18@sot.pdpu.ac.in
Abhijit Ray
abhijit.ray@sse.pdpu.ac.in

Specialty section:
This article was submitted to Sustainable Energy Systems and Policies, a section of the journal Frontiers in Energy Research

Received: *05 February 2022*
Accepted: *19 April 2022*
Published: *28 June 2022*

Citation:
Desai A, Mukhopadhyay I and Ray A (2022) Feasibility Assessment of Bifacial Rooftop Photovoltaic Systems in the State of Gujarat in India. Front. Energy Res. 10:869890. doi: 10.3389/fenrg.2022.869890

1 INTRODUCTION

India has a huge renewable energy potential across the country. Solar energy is one of the key sources of clean energy, and the country has taken various initiatives to promote the utility scale and decentralized or distributed systems as well in the last 5 years. The Indian government has already revised the solar target from 20 to 100 GW, which is promising as well as challenging. Among this 100 GW target, 40 MW will be achieved through the decentralized mode and the rest 60 GW from utility-scale solar projects. Out of 8 GW of solar rooftop deployment in India, Gujarat state has installed around 2 GW, which includes 1.2 GW of residential rooftop systems aggregating to more than 1,00,000 houses. In the decentralized solar project, the rooftop photovoltaic (PV) system has received a priority. The majority of solar PV rooftop systems are expected to be deployed in urban and semi-urban areas. As in India, the majority of residential terraces are flat surfaces, so there is great scope for an elevated structure where one can get the benefits of reflection from the rear side of PV modules. Available open space is always a constraint for the installation of solar PV systems, and in this context, traditional rooftop systems are the best possible solution. It is also proven that the traditional rooftop solar PV system would play a notable role in distributed energy generation to mitigate the energy demand of various load segments. It

has been adopted in a widespread manner across residential, commercial, and industrial users; however, the selection of solar panels is still a concern. In many cases, questions are raised about lower energy production and efficiency issues. Despite the apparent benefits of bifacial modules, their applications still suffer from a lack of visibility into the performance gain that they can provide. On the other hand, self-energy in the same building will be highly accepted in all major urban areas, and the same will be added to rooftop solar potential. The rooftop systems' acceptability is therefore high for the consumption categories, including industrial, commercial, and residential levels. In industries where the sheds or terraces permit the structural load, deployment is expected as it directly saves energy consumption. In the same way, developing rural areas and semi-urban areas are also expected to adopt solar PV rooftop systems (Estimating The Rooftop Solar Potential Of Greater Mumbai, 2015; Press Information Bureau, Government of India Cabinet, 2015). To meet the demand-supply and reduce the transmission and distribution line losses, battery energy storage could be used. In a grid-connected solar rooftop system, a hybrid inverter is used, which is connected to both the grid and the battery. This hybrid inverter-based grid-tie solar rooftop system allows the inverter to store the excess energy in a battery which could be used later on as per the building/house energy demand. However, policy and regulation for the use of battery storage-based hybrid inverters in the rooftop solar system is in the development stage in India (Estimating The Rooftop Solar Potential Of Greater Mumbai, 2015; Thanh et al., 2021). A solar PV rooftop system may comprise various technologies such as thin-film and silicon. In silicon-based technology, polycrystalline, monocrystalline, and bifacial solar module technologies have been found since 1977. Among them, bifacial (BF) module technologies were specially developed for space applications. In BF-modules, Glass-on-Glass technology captures additional light from the rear side, which increases the overall generation. Recently, there has been technological advancement in the production of polycrystalline to bifacial module production from five busbars to multi-busbar (Hubner et al., 1997; Cuevas, 2005; Guerrero-Lemus et al., 2016; Dullweber et al., 2017; Kenny et al., 2018; Ayala, 2019; Baumann et al., 2019; Jang and Lee, 2020). The improvement of silicon module efficiencies is mainly attributed to p-type and n-type PID-free passivated emitter and rear cell technology (PERC) and heterojunction (HJT) solar cell manufacturing. They are also incorporated into bifacial solar cells to achieve analogous efficiencies to the traditional mono-facial ones. A bifacial PV module can absorb irradiance on both sides. The performance of a bifacial PV module is influenced by module tilt and azimuth, similar to a mono-facial PV module. It is, however, more influenced by the diffuse irradiance factor (DIF), height, and albedo than a mono-facial PV module. The performance of the BF module PV system has been analyzed on various reflective surfaces/materials such as white surfaces, multi-color tiles, grass, etc., under different environmental conditions. Due to front and rear side glass, BF modules produce more energy throughout their life at a lower operating cost (Hubner et al., 1997; Cuevas, 2005; Guerrero-Lemus et al., 2016; Dullweber et al., 2017; Kenny et al., 2018; Ayala, 2019; Baumann et al., 2019; Jang and Lee, 2020). Still, in the laboratory and field, advanced-level research is underway to get higher efficiency and faster deployment in the market (Hubner et al., 1997; Joge et al., 2003; Cuevas, 2005; Branker et al., 2011; Yang et al., 2011; Chu and Majumdar, 2012; Chu et al., 2016; Guerrero-Lemus et al., 2016; Deline et al., 2017; Dullweber et al., 2017; Hansen et al., 2017; Kabir et al., 2018; Kenny et al., 2018; Sun et al., 2018; Ayala, 2019; Baumann et al., 2019; Tahir Patel et al., 2019; Jang and Lee, 2020). To deploy any new technology in the solar market, one has to confirm the levelized cost of electricity (LCOE) as it widely varies with the capital investment, energy generation, post-installation operation, and maintenance cost. Currently, major deployment in India is based on the polycrystalline technology with five busbar technologies. Hence for pushing the bifacial technology, one should compare the LCOE. Bifacial technology will cater to the future market over the traditional polycrystalline market as it requires less space than polycrystalline and delivers higher energy generation than the polycrystalline technology. Overall, we can say that higher generation due to reflection and multi busbar technology results in higher LCOE (Cuevas et al., 1982; Luque et al., 1985; Chieng and Green, 1993; Solar Energy Technologies Office, 2011; Guo et al., 2013; Tyagi et al., 2013; Ueckerdt et al., 2013; Yusufoglu et al., 2014; Janssen et al., 2015; Lo et al., 2015; Castillo-Aguilella and Hauser, 2016; Fertig et al., 2016; Guerrero-Lemus et al., 2016; Ito and Gerritsen, 2016; Green et al., 2017; Stein et al., 2017; Chang et al., 2018; EIA, 2018; ITRPV, 2018; Delano Thierry Odou and Bhandari, 2020; Masrur et al., 2020). Solar radiation is available throughout the year in the Gujarat region of India. In this region, March to June, as well as October to December, are considered to generate higher solar energy than the rest of the months (Guo et al., 2013; Ito and Gerritsen, 2016; Delano Thierry Odou and Bhandari, 2020; Masrur et al., 2020). Researchers across the globe are concerned about the deployment of the bifacial system and installing the small-scale test beds to study the techno-commercial viability, while the classification of bifacial and relevant key technologies needs to be addressed. To the best of our knowledge, representative bifacial PV systems have not been studied yet in terms of their technical performance and economic as well as environmental impact in long-term use.

This study explores the Techno-Economic-Environmental analysis and design optimization of a 5kW bifacial grid-connected solar rooftop PV system and compares it with the polycrystalline system for the Gujarat region. The key objective is to find the techno-economic exploration concerning an ideally designed system with key parameters such as solar radiation (seasonal variation thereof) and performance ratio at the rooftop level.

2 MATERIALS AND METHODS

2.1 Solar PV Rooftop System Design Modeling

A typical grid rooftop system consisting of a solar PV (SPV) array, a solar grid tie inverter/power conditioning unit (PCU), a solar module mounting structure (MMS), and other balance of system (BoS) components, which include AC/DC cables,

earthling protection, lightning protection (LA), a bi-directional meter, and a solar meter, was used. All the components used in the SPV system should conform to the BIS/IEC as per the requirements of the regional electricity authority (Weatherspark, 2015). System capacity has been designed based on the module size, followed by the structure, inverter, and cable design. Here, we have designed the 5 kW rooftop system for the Gujarat region where traditional polycrystalline systems consist of 335 Wp modules which could be installed on an 8 × 2 table structure, while in the same case with the bifacial system, it consists of 385 Wp of 13 modules which could be installed on a 7 × 2 table structure. The same will reduce the BoS cost and also use 13% less space on the same terrace.

2.2 Solar Energy Generation

2.2.1 Solar Radiation on the Tilted Surface of the Solar Module

Total solar irradiance (radiation) on the tilted surface of the solar module includes reflected, direct, and diffuse radiation (Weatherspark, 2015; Torrentpower, 2015; Desai et al., 2020a; Desai et al., 20212021; Desai et al., 2020b; Sharma and Goel, 2017; Desai et al., 2019; Desai et al., 2021a).

$$I_{TR} = I_b r_d + I_b r_b + (I_b + I_d) I_r, \tag{1}$$

where r_r,r_b, and r_d are reflected, beam, and diffuse, and I_r, I_b, and I_d are beam, direct radiation, and diffuse instantaneous values, respectively.

2.2.2 Average Annual Solar Radiation on Tilted Solar Panels (Without Shading)

Using an empirical equation, we can measure the beam, direct, and diffuse radiation or estimate the total solar radiation falling on the solar module. Month wise, daily average monthly global radiation on a horizontal surface H_{ga} is given by (IRENA, 2012; Sharma and Goel, 2017; Desai et al., 2019; Desai et al., 2020b;; Desai et al., 2021a; Desai et al., 2021b; Bihari et al., 2021; Desai et al., 20212021).

$$H_{ga} = (H_{oa} + H_{ob}) * \{a + b[S_a / S_{ma}]\}, \tag{2}$$

where

H_{oa} = monthly average solar radiation at the horizontal surface,

H_{ob} = monthly average solar radiation at the horizontal surface at the rear surface,

S_a = monthly average daily sunshine hour

S_{maxa} = maximum daily sunshine hours possible at a given location.

a and b are constants.

2.2.3 Plant Performance Ratio

Solar plant performance can be identified on the basis of available solar radiation at the plant location against the generated energy. This performance Ratio (PR) is based on all types of losses, right from the solar module to grid losses, with respect to radiation and local climate conditions. The PR value generally varies between 60 and 80%, but it depends on the solar PV module temperature, DC cable loss, soiling losses, AC cable loss, transmission loss etc. PR is defined as the ratio of the final yield (Y_f = total energy fed to the grid) to reference yield of the total energy (Y_r) that the system could have produced without any losses in ideal condition (IRENA, 2012; Sharma and Goel, 2017; Desai et al., 2019; Desai et al., 2020b; Desai et al., 2021a; Desai et al., 2021b; Bihari et al., 2021; Desai et al., 20212021).

$$PR = Y_f / Y_r. \tag{3}$$

The performance ratio (PR) is mainly influenced by module mismatch loss, module temperature loss, DC cable loss, AC cable loss, incidence angle modifier (IAM) loss, soiling loss, etc.

2.2.4 Solar PV Module Efficiency

The instantaneous solar PV module efficiency is given by

$$\eta = P_{dc} / (G * A_m * 100). \tag{4}$$

As a function of temperature, it can be represented as

$$\eta_T = \eta_{Tref} * \left(1 - \beta_{ref} T - T_{ref}\right), \tag{5}$$

where

η_{Tref} = PV module efficiency at reference temperature,

β_{ref} = power temperature coefficient,

T_{ref} = reference temperature,

T = cell temperature.

$$T = T_{amb} + \{1.25 * 10 - 3\, Gt * (NOCT - 20)\}, \tag{6}$$

where

NOCT = nominal operating cell temperature,

T_{amb} = ambient temperature,

Gt = total solar irradiance in plane (IRENA, 2012; Sharma and Goel, 2017; Desai et al., 2019; Desai et al., 2020b; Desai et al., 2021a; Desai et al., 2021b; Bihari et al., 2021; Desai et al., 20212021).

2.2.5 Estimation of the Electricity Generated by the Output of a Bifacial Photovoltaic System

Bifacial energy generation from both front and back sides is estimated as per the following:

$$E_f = A_t * \eta_{PVf} * H_{ga} * PR, \tag{7}$$

$$E_r = A_t * \eta_{PVr} * H_{al} * PR, \tag{8}$$

E_f = energy from the front side (kWh),

E_r = energy from the rear side (kWh),

A_t = total solar panel area (m^2),

η_{pvf} = rear efficiency of the solar module (%),

η_{pvr} = front efficiency of the solar module (%),

H_{ga} = average annual solar radiation on the shadow free solar module,

H_{ga} = average annual solar radiation on the solar module due to albedo,

PR = performance ratio (generally vary in the range between 0.5 and 0.9, default value = 0.75) (IRENA, 2012; Sharma and Goel, 2017; Desai et al., 2019; Desai et al., 2020b;; Desai et al., 2021a; Desai et al., 2021b; Bihari et al., 2021; Desai et al., 20212021)

TABLE 1 | Component costs (All in INR and USD).

Description	Polycrystalline system	Bifacial system
1. SPV module(Wp)	335	385
Open circuit voltage (Voc) in volts	45.80	48.65
Short circuit current (Isc) in amps	9.50	9.95
Voltage at maximum power (Vmp) in volts	36.70	39.90
Current at maximum power (Imp) in amps	9.13	9.65
Total modules (nos)	15	13
Solar capacity (kW)	5	5
Total module area ($m^{2)}$	30	26
Module capex INR (USD)approx.	90,450/-(1,206$)	102,602/-(1,368$)
SPV system life (years)	25	25
2. PV inverter		
Inverter capacity (kW)	5	5
Inverter capex INR (USD)approx.	30,000/-(400$)	30,000/-(400$)
Inverter lifetime (years)	7	7
Replacement cost from 6^{th} to 25^{th}year INR (USD) approx.	45,000/- (600$)	45,000/-(600$)
3. BoS cost		
Intial capital INR (USD) approx. for 1^{st} 5 years	99,500/-(1,326.7$)	97,000/-(1,293.33$)
Replacement cost from 6^{th} to 25^{th}year INR (USD) approx.	10,000/-(133.33$)	10,000/-(133.33$)
Lifetime (years)	25	25
4. Total comprehensive O&M cost INR (USD) approx. for 25 years	65,000/-(866.66$)	65,000/-(866.66$)
5. Energy generation for 25 years (kWh) (0.8% Annual degradation considered)	173,400 (2,312$)	190,740 (2,453.2$)
6. Tariff INR (USD)approx.	7 (0.093 USD)	

(1 USD = 75 INR)*

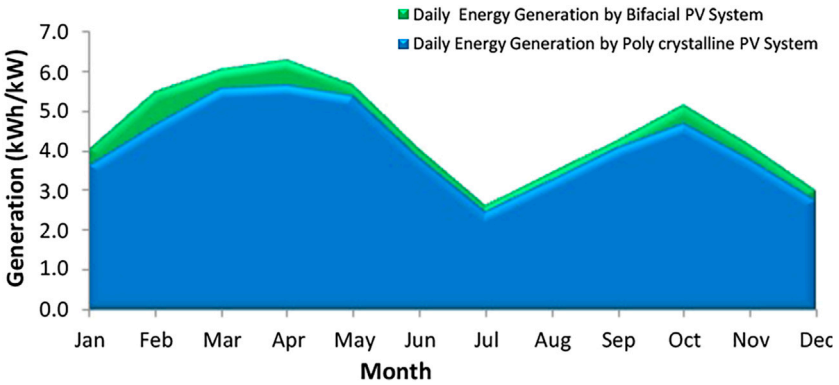

FIGURE 1 | Solar PV rooftop system daily energy.

$$\text{Total Bifacial Energy Yield } E_b = E_f + E_r. \quad (9)$$

In this section, solar generation modeling has been discussed according to this rooftop system, which generates power according to radiation and temperatures as both are the critical parameters for energy generation. Traditional polycrystalline rooftop systems generate power based on the irradiance falling on the front side of the module, whereas in bifacial rooftop systems, energy generation is possible from the front as well as the rear side. Due to this additional rear side irradiance, which is mainly due to albedo based on the color of the roof, the white roof has the highest albedo, and this will help generate more energy.

3 ECONOMIC EXPLORATION

3.1 *Levelized Cost of Electricity Generation*

Based on the capital investment, O&M expenses, and estimated revenue generation with respect to the energy throughout the life span of the plant, the LCOE of the renewable plant is calculated. As is known, renewable energy is regionally specific and the LCOE varies accordingly in a region-specific manner based on the availability of resources. In our approach, we have shown a constant cash flow analysis considering the ideal generation with the decided degradation and necessary replacement factor. A capital investment-based model is suitable for most renewable energy generation technologies, where in the case of solar or wind power fuel cost as input is zero. We have

TABLE 2 | Monthly energy generation.

Month	Effective irradiance (kWh/m^2)	Monthly energy generation by the bifacial PV system (kWh)	Monthly energy generation by the polycrystalline PV system (kWh)
January	148.4	602	543
February	167	766	651
March	212.5	937	864
April	209.2	943	848
May	201.3	876	834
June	155.2	605	574
July	127.4	406	382
August	135.2	533	505
September	158.8	639	612
October	179.4	799	728
November	152.5	621	568
December	148.4	463	425

taken a simple and constant effort-based approach, given the fact that the model could be applied to different regions and countries according to available resources. The analysis we have conducted in this study is easy to understand and has transparency (Carbon Brief, 2019). The formula used for calculating the LCOE of renewable energy technologies is as follows:

$$LCOE = \sum_{y=1}^{25} \frac{C_y + O\&M_y + \mathrm{R}_c}{E_y}, \tag{10}$$

where LCOE = levelized cost of electricity (average lifetime); Cy = yearly capital investment; O and My = yearly operation and maintenance cost; RC = replacement cost; Ey = electricity generation in the year y;

$$C_Y = C_M + C_{BOS} + C_I, \tag{11}$$

$$R_{Cy} = C_{BoSy} + C_{Iy}. \tag{12}$$

Here, capital coast C_y is the cost of the total system cost which includes the module and balance of supply material (BoS), which are the inverter, structure, cables, earthling, and LA. The installation cost of the system is also considered the capital cost. Hence, as only modules have a life span of 25 years, there are chances of component replacement during the 25-year time period, which includes the BoS material and installation costs which are considered as a replacement cost. While considering the LCOE of solar rooftop systems, in this majority, two components are available: one is the module cost as the bifacial module cost is higher than the traditional polycrystalline module cost, and the other is the structure cost, which is included in BoS. In this bifacial system the higher efficiency of the module number decreased, which directly reduced the structure size and cost.

In our section, we will estimate the LCOE cost of both polycrystalline and bifacial systems with respect to the capital investment made in each solar rooftop system.

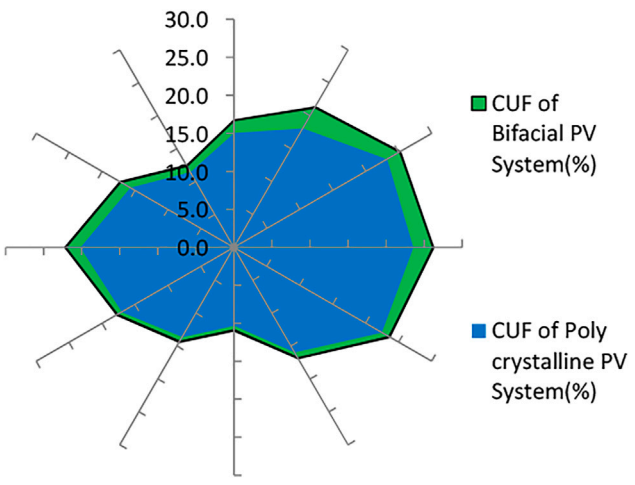

FIGURE 2 | Solar PV system monthly CUF (%).

3.2 Components' Cost and Performance Characteristics

Table 1 shows the cost summary of components, including the capital investment, replacement cost, O&M, and specifications [48].

4 RESULTS AND DISCUSSION

4.1 Technical Analysis

The actual energy generation from a bifacial system is analyzed throughout the year, as shown in **Figure 1**. The monthly energy generation is given as per **Table 1** below and is used in the calculation of system performance. From **Table 2**, it is seen that the bifacial solar PV system has a significant effect on energy generation as the collection of radiation is from the front and rear sides. Installing 5 kW rooftop systems at one place and the same orientation at the same place can produce the monthly average energy generation for a bifacial system of 682 kWh while from a traditional poly c-Si system it was 628 kWh. An average of 8% higher generation was observed than the poly c-Si system. The annual solar PV energy yield under the bifacial system was

1638 kWh/kWp as compared to the poly c-Si system, which was 1507 kWh/kWp.

Figure 1 also shows that for the rooftop PV system, daily energy for the bifacial mode varies between 2.6 and 6.3 kWh/kW/day. The daily average generation for the bifacial system is 4.5 kWh compared to the traditional polycrystalline system of 4.1 kWh. The monthly yield varies between 81 and 189 kWh/kW. The average yield for the bifacial system is 136 kWh/kW and for the Poly c-Si system it is 126 kWh/kW, as shown in **Figure 1**. The average energy generated by the bifacial system is calculated to be 8% higher than the Poly c-Si system. **Figure 2** shows that the capacity utilization factor (CUF) of the bifacial system is 18.7% whereas it is 17.2% for the poly c-Si rooftop system, which shows that the bifacial-based solar rooftop system CUF is 1.5% higher than the poly c-Si-based solar PV rooftop systems (Sampedro et al., 2020).

It was observed that the annual average PR for the bifacial system is 81 and 75.54% for the polycrystalline system. October, February, and April have a PR that is around 90% which is at par in comparison to the traditional solar PV rooftop system. Monthly average yield, annual average daily yield, annual average PR, and annual average CUF for the bifacial system and polycrystalline system are 136 kWh/kWp, 4.5 kWh/kWp, 81, and 18.72% and 126 kWh/kWp, 4.1 kWh/kWp, 75.5, and 17.22% for the solar PV System, respectively. According to the latest research conducted in the world still, we can get more than 20 to 30% higher generation in the bifacial system by modifying the roof and using the seasonal tilt-based structure, which will help to get the maximum irradiance from the rare side.

4.2 Economic Analysis

For the acceptance of the bifacial System in the market, a techno-economic-environmental analysis is needed in parallel. The economic analysis gives an idea about the internal rate of return, economic viability concerning the payback period of the project on which investment is made. To identify the economic viability we have conducted the economic analysis of the project on two financing conditions, one with the 100% equity investment and the other with a price of seven INR (0.0933 USD)/kWh. The internal rate of return (IRR) for the bifacial system is 24% against the 23% of the polycrystalline solar system which is very attractive looking to the current global financing scenario. We get the payback of the bifacial system 2 months earlier than the polycrystalline system. The LCOE for the bifacial rooftop solar system is 1.88 INR (0.0250 USD), which is 5.5% higher than the traditional polycrystalline rooftop system.

4.2 Environmental Analysis

India is the third-largest in the world for greenhouse gas emissions as the main source is coal for energy generation. Every year India emits about 7% of global emissions (IRENA, 2012; Carbon Brief, 2019; GHE, 2014; Environment and U. N. (2019-11-19), 2019; downtoearth, 2018). These emitted gases or particles are the following: monoxide (CO), carbon dioxide (CO_2), etc. Our analysis shows that throughout life, a bifacial system saves 916,525 kg of CO_2 from adding to the atmosphere and prevented 224,444 kg of uses of coal compared to the polycrystalline system which is 8% higher.

5 CONCLUSION

Bifacial module technology, which is expected to dominate PV installations in the near future, presents an emerging trend in terms of technical and economic feasibility in rooftop PV systems for energy generation. Annual average daily yield, annual average monthly yield, annual average PR, and annual average CUF for a typical 5kW bifacial PV system are found to be 4.5 kWh/kWp, 136 kWh/kWp, 81%, and 18.72%, respectively for a flat rooftop. This system can generate an excess of 13 MWh than the traditional poly-Si technology. A tilt angle between 15° and 20° will reduce LCOE by INR 0.11 (0.0015 USD), which is 5.5% higher than the traditional poly-Si rooftop system. This can be reduced further by the larger deployment of the bifacial rooftop system, as in regions such as Gujarat, which have more than 3 GW of rooftop potential, which could be enhanced by 400 MW as bifacial modules require less space. The deployment of 3 GW bifacial in place of polycrystalline silicon modules leads to a generation of 39 TWh throughout its life. The bifacial rooftop technology of the proposed scale can save 13% space, 9,16,525 kg of CO_2 emission throughout its life, and prevents the use of 2,24,444 kg coal, which is advantageous as compared to polycrystalline systems.

DATA AVAILABILITY STATEMENT

The raw data supporting the conclusion of this article will be made available by the authors without undue reservation.

AUTHOR CONTRIBUTIONS

AD and IM have conceptualized the article. AD has collected and analyzed the data. Also, AD was involved in writing the first draft, followed by corrections and proofreading. IM and AR have corrected and modified the manuscript.

SUPPLEMENTARY MATERIAL

The Supplementary Material for this article can be found online at: https://www.frontiersin.org/articles/10.3389/fenrg.2022.869890/full#supplementary-material

REFERENCES

Ayala, P. (2019). Bifacial Solar Modules System Design, Modelling, and Performance. The University of Arizona. ProQuest Dissertations Publishing, Thesis. Avaliable at: http://hdl.handle.net/10150/631283.

Baumann, T., Nussbaumer, H., Klenk, M., Dreisiebner, A., Carigiet, F., and Baumgartner, F. (2019). Photovoltaic Systems with Vertically Mounted Bifacial PV Modules in Combination with Green Roofs. *Sol. Energy* 190, 139–146. doi:10.1016/j.solener.2019.08.014

Bihari, S. P., Sadhu, P. K., Sarita, K., Khan, B., Arya, L. D., Saket, R. K., et al. (2021). "A Comprehensive Review of Microgrid Control Mechanism and Impact Assessment for Hybrid Renewable Energy Integration," in IEEE Access, 17 June 2021 (IEEE). doi:10.1109/ACCESS.2021.3090266

Branker, K., Pathak, M. J. M., and Pearce, J. M. (2011). A Review of Solar Photovoltaic Levelized Cost of Electricity. *Renew. Sustain. Energy Rev.* 15, 4470–4482. doi:10.1016/j.rser.2011.07.104

Carbon Brief (2019). *The Carbon Brief Profile: India*. Carbon Brief.

Castillo-Aguilella, J. E., and Hauser, P. S. (2016). Multi-Variable Bifacial Photovoltaic Module Test Results and Best-Fit Annual Bifacial Energy Yield Model. *IEEE Access* 4, 498–506. doi:10.1109/ACCESS.2016.2518399

Chang, N. L., Ho-Baillie, A. W. Y., Vak, D., Gao, M., Green, M. A., and Egan, R. J. (2018). Manufacturing Cost and Market Potential Analysis of Demonstrated Roll-To-Roll Perovskite Photovoltaic Cell Processes. *Sol. Energy Mater. Sol. Cells* 174, 314–324. doi:10.1016/j.solmat.2017.08.038

Chieng, Y. K., and Green, M. A. (1993). Computer Simulation of Enhanced Output from Bifacial Photovoltaic Modules. *Prog. Photovolt. Res. Appl.* 1, 293–299. doi:10.1002/pip.4670010406

Chu, S., Cui, Y., and Liu, N. (2016). The Path Towards Sustainable Energy. *Nat. Mater.* 16, 16–22. doi:10.1038/nmat4834

Chu, S., and Majumdar, A. (2012). Opportunities and Challenges for a Sustainable Energy Future. *Nature* 488, 294–303. doi:10.1038/nature11475

Cuevas, A., Luque, A., Eguren, J., and del Alamo, J. (1982). 50 Per Cent More Output Power from an Albedo-Collecting Flat Panel Using Bifacial Solar Cells. *Sol. Energy* 29, 419–420. doi:10.1016/0038-092X(82)90078-0

Cuevas, A. (2005). "The Early History of Bifacial Solar Cells," in Proceedings of the 20th European Photovoltaic Solar Energy Conference, Barcelona, Spain, January, 2005, 801–805.

Delano Thierry Odou, O., and Bhandari, R. (2020). Rabani Adamou "Hybrid Off-Grid Renewable Power System for Sustainable Rural Electrification in Benin. *Renew. Energy* 145, 1266e1279. doi:10.1016/j.renene.2019.06.032

Deline, C., MacAlpine, S., Marion, B., Toor, F., Asgharzadeh, A., and Stein, J. S. (2017). Assessment of Bifacial Photovoltaic Module Power Rating Methodologies-Inside and Out. *IEEE J. Photovoltaics* 7 (2), 575–580. doi:10.1109/jphotov.2017.2650565

Desai, A., Mukhopadhyay, I., and Ray, A. (2021). "Effect of Azimuth and Tilt Angle on Ideally Designed Rooftop Solar PV Plant for Energy Generation," in 2021 IEEE 48th Photovoltaic Specialists Conference (PVSC), Fort Lauderdale, FL, USA, 20-25 June 2021 (IEEE). doi:10.1109/PVSC43889.2021.9519091

Desai, A., Mukhopadhyay, I., and Ray, A. (2020). "Exploring Technical and Economic Feasibility of a Stand-Alone Solar PV Based DC Distribution System over AC for Use in Houses," in 2020 47th IEEE Photovoltaic Specialists Conference (PVSC), Calgary, AB, Canada, 15 June-21 Aug. 2020 (IEEE). doi:10.1109/PVSC45281.2020.9300411

Desai, A., Mukhopadhyay, I., and Ray, A. (2020). "Performance Analysis of String and Central Inverter Based Ideally Designed Utility Scale Solar PV Plant," in 2020 47th IEEE Photovoltaic Specialists Conference (PVSC), Calgary, AB, Canada, 15 June-21 Aug. 2020 (IEEE). doi:10.1109/PVSC45281.2020.9300494

Desai, A., Mukhopadhyay, I., and Ray, A. (2021). "Snail Trail Impact on Rooftop Solar PV Plant Energy Generation," in 2021 IEEE 48th Photovoltaic Specialists Conference (PVSC), Fort Lauderdale, FL, USA, 20-25 June 2021 (IEEE). doi:10.1109/PVSC43889.2021.9518985

Desai, A., Ray, A., and Mukhopadhyay, I. (2019). Theoretical Analysis of a Solar PV-Wind Hybrid Power System for Energy Generation in Kutch Region. *IOP Conf. Ser. Earth Environ. Sci.* 27, 1–10. doi:10.1088/1755-1315/322/1/012006

Desai, A., Shah, V., Mukhopadhyay, I., and Ray, A. (20212021). "Multiple MPPT Based String Inverter Effect on Annual Performance: Observations at Utility Scale Solar PV Plants," in 2020 47th IEEE Photovoltaic Specialists Conference (PVSC), Calgary, AB, Canada, 15 June-21 Aug. 2020 (IEEE).

downtoearth (2018). A Comprehensive GHG Inventory for India Is Within Reach. Avaliable at: www.downtoearth.org.

Dullweber, T., Schulte-Huxel, H., Hannebauer, H., Blankemeyer, S., Baumann, U., Schimanke, S., et al. (2017). Bifacial PERC+ Solar Cells: Status of Industrial Implementation and Future Perspectives. *Jpn. J. Appl. Phys.* 57, 08RA01. doi:10.7567/JJAP.57.08RA01

EIA (2018). Levelized Cost and Levelized Avoided Cost of New Generation Resources in the Annual Energy Outlook. *U. S. Energy Inf. Administation* 1, 20. Available: http://large.stanford.edu/courses/2018/ph241/asperger2/docs/eia-mar18.pdf (Accessed January 10, 2022).

Environment, U. N. (2019-11-19). (2019). "Emissions Gap Report 2019". UNEP - UN Environment Programme. Retrieved 2020-04-20.

Estimating The Rooftop Solar Potential Of Greater Mumbai (2015). Estimating the Rooftop Solar Potential of Greater Mumbai. Available at: http://www.ncpre.iitb.ac.in/research/pdf/Estimating_Rooftop_Solar_Potential_Greater_Mumbai.pdf (Accessed January 10, 2022).

Fertig, F., Nold, S., Wöhrle, N., Greulich, J., Hädrich, I., Krauß, K., et al. (2016). Economic Feasibility of Bifacial Silicon Solar Cells. *Prog. Photovolt. Res. Appl.* 24, 800–817. doi:10.1002/pip.2730

GHE (2014). *Greenhouse Gas Emissions in India*. USAID.

Green, M. A., Hishikawa, Y., Warta, W., Dunlop, E. D., Levi, D. H., Hohl-Ebinger, J., et al. (2017). Solar Cell Efficiency Tables (Version 50). *Prog. Photovolt. Res. Appl.* 25, 668–676. doi:10.1002/pip.2909

Guerrero-Lemus, R., Vega, R., Kim, T., Kimm, A., and Shephard, L. E. (2016). Bifacial Solar Photovoltaics - A Technology Review. *Renew. Sustain. Energy Rev.* 60, 1533–1549. doi:10.1016/j.rser.2016.03.041

Guo, S., Walsh, T. M., and Peters, M. (2013). Vertically Mounted Bifacial Photovoltaic Modules: A Global Analysis. *Energy* 61, 447–454. doi:10.1016/j.energy.2013.08.040

Hansen, C. W., Gooding, R., Guay, N., Riley, D. M., Kallickal, J., Asgharzadeh, A., et al. (2017). "A Detailed Model of Rear-Side Irradiance for Bifacial PV Modules," in 44th IEEE Photovoltaic Specialists Conference, Washington, DC, USA, 25-30 June 2017 (IEEE). doi:10.1109/pvsc.2017.8366707

Hubner, A., Aberle, A., and Hezel, R. (1997). "Temperature Behavior of Monofacial and Bifacial Silicon Solar Cells," in Conf. Rec. Twenty Sixth IEEE Photovolt. Spec. Conf. - 1997, Anaheim, CA, USA (IEEE), 223–226. doi:10.1109/PVSC.1997.654069

IRENA (2012). *White Paper on Renewable Energy Technologies: Cost Analysis Series Volume 1: Power Sector Hydro Power Issue 3/5"*. IRENA.

Ito, M., and Gerritsen, E. (2016). "Geographical Mapping of the Performance of Vertically Installed Bifacial Modules," in 32nd PVSEC (Munich: PVSEC), 1603–1609.

ITRPV (2018). International Technology Roadmap for Photovoltaic— Results 2017 Including Maturity Report 2018. Avalliable at: http://www.itrs.net/Links/2013ITRS/2013Chapters/2013Litho.pdf (Accessed January 12, 2022).

Jang, J., and Lee, K. (2020). Practical Performance Analysis of a Bifacial PV Module and System. *Energies* 13, 4389. doi:10.3390/en13174389

Janssen, G. J. M., Van Aken, B. B., Carr, A. J., and Mewe, A. A. (2015). Outdoor Performance of Bifacial Modules by Measurements and Modelling. *Energy Procedia* 77, 364–373. doi:10.1016/j.egypro.2015.07.051

Joge, T., Eguchi, Y., Imazu, Y., Araki, I., Uematsu, T., and Matsukuma, K. (2003). Basic Application Technologies of Bifacial Photovoltaic Solar Modules. *IEEJ Trans. PE* 123 (8), 947–955. doi:10.1541/ieejpes.123.947

Kabir, E., Kumar, P., Kumar, S., Adelodun, A. A., and Kim, K.-H. (2018). Solar Energy: Potential and Future Prospects. *Renew. Sustain. Energy Rev.* 82, 894–900. doi:10.1016/j.rser.2017.09.094

Kenny, P., Lopez-Garcia, J., Menendez, E. G., Haile, B., and Shaw, D. (2018). "Characterizing Bifacial Modules in Variable Operating Conditions," in 2018 IEEE 7th World Conference on Photovoltaic Energy Conversion (WCPEC) (A Joint Conference of 45th IEEE PVSC, 28th PVSEC & 34th EU PVSEC), Waikoloa Village, HI, USA, 10–15 June 2018, 1210–1214. doi:10.1109/pvsc.2018.8547853

Lo, C. K., Lim, Y. S., and Rahman, F. A. (2015). New Integrated Simulation Tool for the Optimum Design of Bifacial Solar Panel with Reflectors on a Specific Site. *Renew. Energy* 81, 293–307. doi:10.1016/j.renene.2015.03.047

Luque, A., Lorenzo, E., Sala, G., and López-Romero, S. (1985). Diffusing Reflectors for Bifacial Photovoltaic Panels. *Sol. Cells* 13, 277–292. doi:10.1016/0379-6787(85)90021-3

Masrur, H., Howlader, H. O. R., Khan, M. K. R., Guerrero, J. M., and Senjyu, T. (2020). Analysis of Techno-Economic-Environmental Suitability of an Isolated Microgrid System Located in a Remote Island of Bangladesh. *Sustainability* 12, 2880. doi:10.3390/su12072880

Press Information Bureau Government of India Cabinet (2015). Revision of Cumulative Targets Under National Solar Mission from 20,000 MW by 2021-22 to 1,00,000 MW," 17 June 2015. Available at: http://pib.nic.in/newsite/PrintRelease.aspx?relid=122566 (Accessed January 10, 2022).

Sampedro, J., Smith, S. J., Arto, I., González-Eguino, M., Markandya, A., Mulvaney, K. M., et al. (2020). Health Co-Benefits and Mitigation Costs as Per the Paris Agreement Under Different Technological Pathways for Energy Supply. *Environ. Int.* 136, 105513. doi:10.1016/j.envint.2020.105513

Sharma, R., and Goel, S. (2017). Performance Analysis of a 11.2 kWp Roof Top Grid-Connected PV System in Eastern India. *Energy Rep.* 3, 76–84. doi:10.1016/j.egyr.2017.05.001

Solar Energy Technologies Office (2011). Sunshot-Photovoltaic-Manufacturing-Initiative. Avalliable at: https://www.energy.gov/eere/solar/sunshot-photovoltaic-manufacturing-initiative (Accessed January 10, 2022).

Stein, J. S., Burnham, L., and Lave, M. Performance Results for the Prism Solar Installation at the New Mexico Regional Test Center. Technical Report. 2017.

Sun, X., Khan, M. R., Deline, C., and Alam, M. A. (2018). Optimization and Performance of Bifacial Solar Modules: A Global Perspective. *Appl. Energy* 212, 1601–1610. doi:10.1016/j.apenergy.2017.12.0410.1016/j.apenergy.2017.12.041

Tahir Patel, M., Ryyan Khan, M., Sun, X., and Alam, M. A. (2019). A Worldwide Cost-Based Design and Optimization of Tilted Bifacial Solar Farms. *Appl. Energy*. 247, 467–479. doi:10.1016/j.apenergy.2019.03.150

Thanh, T. N., Vu Minh, P., Trung, K. D., and Anh, T. D. (2021). Study on Performance of Rooftop Solar Power GenerationCombined with Battery Storage at Office Building in Northeast Region, Vietnam. *Sustainability* 13, 11093. doi:10.3390/su131911093

Torrentpower (2015) Connect.Torrentpower. Avaliable at: https://connect.torrentpower.com/tplcp/index.php/callcenter/index?pagename=Solar (Accessed January 01, 2022).

Tyagi, V. V., Rahim, N. A. A., Rahim, N. A., and Selvaraj, J. A. L. (2013). Progress in Solar PV Technology: Research and Achievement. *Renew. Sustain. Energy Rev.* 20, 443–461. doi:10.1016/j.rser.2012.09.028

Ueckerdt, F., Hirth, L., Luderer, G., and Edenhofer, O. (2013). System LCOE: What Are the Costs of Variable Renewables? *Energy* 63, 61–75. doi:10.1016/j.energy.2013.10.072

Weatherspark (2015) Average Weather in Bhuj India Year Round. Avaliable at: https://Weatherspark.Com/Y/106743/Average-Weather-In-Bhuj-India-Year-Round (Accessed January 10, 2022).

Yang, L., Ye, Q. H., Ebong, A., Song, W. T., Zhang, G. J., Wang, J. X., et al. (2011). High Efficiency Screen Printed Bifacial Solar Cells on Monocrystalline CZ Silicon. *Prog. Photovolt. Res. Appl.* 19 (3), 275–279. doi:10.1002/pip.1018

Yusufoglu, U. A., Lee, T. H., Pletzer, T. M., Halm, A., Koduvelikulathu, L. J., Comparotto, C., et al. (2014). Simulation of Energy Production by Bifacial Modules with Revision of Ground Reflection. *Energy Procedia* 55, 389–395. doi:10.1016/j.egypro.2014.08.111

Conflict of Interest: The authors declare that the research was conducted in the absence of any commercial or financial relationships that could be construed as a potential conflict of interest.

Publisher's Note: All claims expressed in this article are solely those of the authors and do not necessarily represent those of their affiliated organizations, or those of the publisher, the editors, and the reviewers. Any product that may be evaluated in this article, or claim that may be made by its manufacturer, is not guaranteed or endorsed by the publisher.

frontiers | Frontiers in Energy Research

ORIGINAL RESEARCH
published: 09 May 2022
doi: 10.3389/fenrg.2022.824421

Technical Performance Optimization of a Novel Geothermal Hybrid Power Generation System

Ying Zhou[1], *Jiyun Qin*[1]*, *Eric Hu*[2] *and Qinglei Zhang*[1]

[1]China Institute of FTZ Supply Chain, Shanghai Maritime University, Shanghai, China, [2]School of Mechanical Engineering, The University of Adelaide, Adelaide, SA, Australia

Geothermal Aided Power Generation (GAPG) technology is a geothermal hybrid power system that geothermal energy has been integrated into the fossil fired plant to preheat the feedwater, and displace the extraction steam of fossil fired plant. In such a power system, the heat exchange process between extraction steam and geo-fluid occurs in a heat exchange between. When the geo-fluid in the heat exchanger quench to lower temperature for heat transfer purpose, silica scaling would occur in the heat exchanger system. The performance of the GAPG plant would be influenced by the configuration of the heat exchanger and silica scaling in the heat exchanger. For a GAPG plant, it has two possible configurations for a heat exchanger system: series arrangement and parallel arrangement. The different configuration also impacts on the technical performance of the GAPG plant. The silica scaling in the heat exchanger system would harm the performance of the GAPG plant. In this study, a GAPG power system from a 300 MW power plant is used as a case study to understand the impact of displacement selections and heat exchanger arrangement on the performance of the GAPG plant. It was found that there is no silica scaling occurring in heat exchangers system if geo-fluid is used to displace to high-grade extraction steam only. Furthermore, the Parallel arrangement is better than the Series arrangement in terms of the additional power output. Moreover, the GAPG plant has protentional to reduce carbon dioxide emissions by 13%.

Keywords: geothermal aided power generation, configuration, power system, silica scaling, displacement selection

OPEN ACCESS

Edited by:
Idiano D'Adamo,
Sapienza University of Rome, Italy

Reviewed by:
Nallapaneni Manoj Kumar,
City University of Hong Kong, Hong Kong SAR, China
Ephraim Agyekum,
Ural Federal University, Russia

***Correspondence:**
Jiyun Qin
qin.jiyun@foxmail.com

Specialty section:
This article was submitted to Process and Energy Systems Engineering, a section of the journal Frontiers in Energy Research

Received: *30 November 2021*
Accepted: *07 January 2022*
Published: *09 May 2022*

Citation:
Zhou Y, Qin J, Hu E and Zhang Q (2022) Technical Performance Optimization of a Novel Geothermal Hybrid Power Generation System. Front. Energy Res. 10:824421. doi: 10.3389/fenrg.2022.824421

INTRODUCTION

With rapid economic development, the consumption of electricity has supplied an increasing share of the world's total consumption of energy (Christina et al., 2020). Coal is the most widely used fuel to produce electricity (Christina et al., 2020). However, with the increasing awareness of the negative environment impacts from carbon dioxide, which is emission from coal fired power plants, the use of other kinds of energy resources to produce electricity has become more attractive (Hargreaves and Jones, 2020). Renewable resources, such as geothermal energy, solar energy and wind energy, are receiving growing attention for the production of electricity purpose (Hargreaves and Jones, 2020). However, some of the renewable energy resources such as solar and wind energy have the disadvantage of being intermittent nature. Compared with other renewable energy such as solar and wind energy, geothermal energy has the advantage of being non-intermittent.

For the low to medium temperature geothermal resources in the range of 90°C–300°C, from the thermodynamic points of view, the thermal efficiency of a geothermal alone power plant is capped by

the temperature of the geothermal fluid entering geothermal power plants (Zhao et al., 2021). On the other hand, fossil fuel power plants are presently still the backbone of electricity production, which have relatively high thermal efficiency as the combustion temperature is much higher (Seyfettin, 2021). Therefore, a hybrid power plan is a practical way to efficiently use geothermal energy and reduce emission from electricity production (Hao et al., 2021).

The concept of a hybrid geothermal power plant was first presented in the late 1970s by DiPippo (DiPippo et al., 1978). It was pointed that there are three kinds of hybrid power systems (Kingston Reynolds Thom and Allardice Ltd, 1980; DiPippo et al., 1981). The first choice is integrating geothermal fluid into the boiler for superheating, the second choice is using geothermal fluid to preheating feedwater to the boiler, and the third choice is to compound these two choices. Comparing these three choices, DiPippo found that the second choice has the advantages of easy control over than other two choices. In the present study, the second choice is termed geothermal aided power generation (GAPG) technology.

The GAPG technology is a method of integrating geothermal energy into a conventional regenerative Rankine cycle (RRC) power plant technology (Hao et al., 2021). In such a technology, geothermal energy carried by the geothermal fluid is used to displace extraction steam from the steam turbine by preheating feedwater to the boiler. Therefore, the displaced extraction steam is then can be expended further in the steam turbine. The GAPG plant can be operated both for power-boosting and fuel-saving purposes by adjusting the mass flow rate of feedwater entering the boiler (Kolb, 1998).

The major thermodynamic advantage of the GAPG technology is that the efficiency of geothermal to power efficiency is no longer capped by the temperature of the geothermal fluid, but the combustion temperature of the plant. Thermodynamic analysis shows that the GAPG technology has an overall improvement in the utilisation of low to medium temperature geothermal resources (Khalifa, 1978; Khalifa et al., 1978). Kestin et al. found that, for geothermal fluid at 200°C, a GAPG plant can theoretically produce 4% more electricity than the original RRC plant and 60% more work than a geothermal alone power plant (Kestin et al., 1978). Buchta analysed a GAPG plant modified from a 200 MW power plant, and geothermal energy is used to displace extraction steam to low-pressure feedwater heaters, it was found that even for the geothermal fluid temperature at 90°C, the geothermal to power efficiency can achieve to about 10% (Buchta, 2009; Buchta and Wawszczak, 2010). For a 500 MW power plant, GAPG technology can increase electricity production by up to 19% (Zhou et al., 2014). However, it was found that the thermodynamic of the GAPG plant over other kinds of geothermal alone power plant is dependent on the distance between the geothermal well and RRC power plant (Liu et al., 2016). Except thermodynamic advantages, it was also pointed that GAPG plants have advantage of lower cost of electricity than other kinds of geothermal alone power plants (Battye et al., 2010; Borsukiewicz-Gozdur, 2010).

Besides geothermal resources, solar thermal energy can also be used for preheating purpose, this kind of renewable preheating power system is termed as Solar Aided Power Generation (SAPG) technology (Zhou et al., 2015). Previous studies found that this kind of SAPG power system still has thermodynamic and economic advantages over solar alone power plants (Zhao et al., 2016a; Zhao et al., 2016b; Zhao et al., 2016c; Waqar et al., 2017; Zhang et al., 2017; Zhang et al., 2019). However, due to the intermittent nature of solar resources, a storage system is needed for the SAPG system (Qin et al., 2017; Qin et al., 2018; Qin et al., 2022). Compared with GAPG and SAPG plant system, the GAPG power system can be operated without thermal storage system, and can overcome the disadvantage of the intermittent nature for the SAPG power system (Sudhakar et al., 2018; Kumar, 2019; Agyekum et al., 2021a; Agyekum et al., 2021b).

In a GAPG plant, the additional power is not generated directly from the geothermal heat but from displaced/saved extraction steam. Therefore, displacement of extraction steam at different stages leads to different technical benefit (Hao et al., 2021). This means that the geothermal to power efficiencies of a GAPG plant might be dependent on the displacement stage selection. Previous studies pointed that there are two possible heat exchanger arrangements for the GAPG plant, which were series arrangement and parallel arrangement (Khalifa, 1978; Khalifa et al., 1978). In the series arrangement, the heat exchanger is arranged in series with the feedwater heater system of the Rankine cycle power plant. In the parallel arrangement, the heat exchanger is arranged in parallel with the feedwater heater system of the Rankine cycle power plant. It was found that series arrange had the advantages of being easy to control. However, there is a lack of study on the performance of the GAPG plant with different heat exchanger arrangements for a given displacement selection.

In addition, a GAPG plant faces the specific problem of silica scaling in heat exchangers, which would not be allowed for the safe operation of the plant (Setiawan et al., 2019). In the GAPG technology, with the geothermal fluid from (production) well head for preheating purpose, the temperature of the geothermal fluid would be dropped. Then, the dissolved silicon dioxide might precipitate from the geothermal fluid, and the silica scaling would then occur in the heat exchangers of the GAPG plant. The precipitation rate of silicon dioxide is mainly dependent on the geothermal fluid temperature and silica concentration in the fluid. Therefore, when determining the displacement selection, the potential silica scaling problem in the heat exchangers must be considered.

In the present study, the silica scaling process in heat exchangers with different displacement selections has been considered for studying the impact of displacement selections and heat exchanger arrangement on the performance of the GAPG plant.

GEOTHERMAL AIDED POWER GENERATION

Figure 1 presents a schematic diagram of a regenerative Rankine cycle power plant. In such a power system, some steams are extracted from the steam turbine through various stages to the

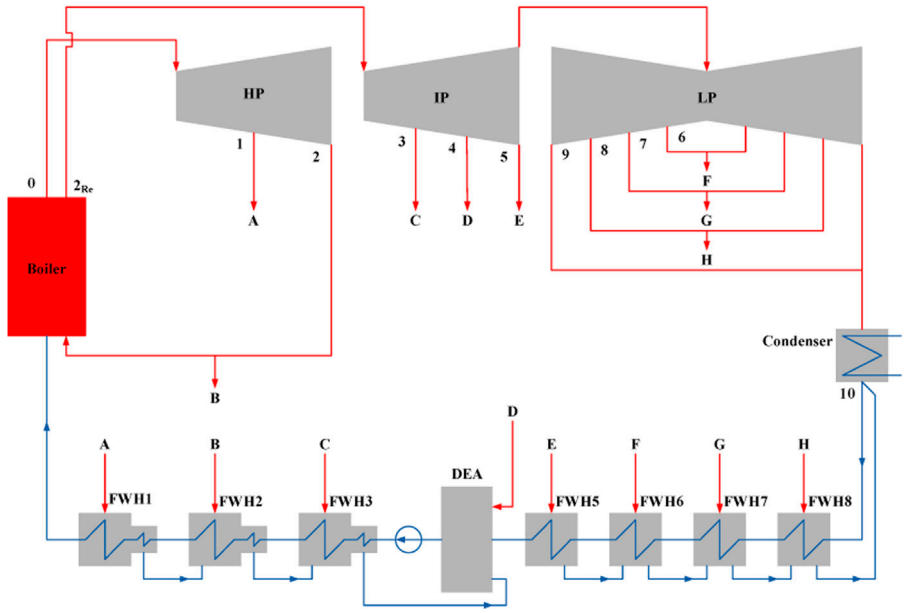

FIGURE 1 | Schematic diagram of a typical 300 MW regenerative Rankine cycle power plant with seven feedwater heater (FWH) and one deaerator.

feedwater system of the power plant. In the feedwater heater system, the extraction steam is used to preheat the feedwater of the boiler. By doing this, the overall efficiency of the RRC power plant could be increased but it would lead to a decrease in the net power output per kilogram of the steam flow through the boiler.

The GAPG plant is based on the RRC power plant. In such a plant, the geothermal energy carried by the geothermal fluid enters a heat exchanger, also termed geo-preheater, sub-system to displace extraction steam for feedwater preheating purpose. The extraction steam replaced by geothermal energy, sometimes termed as saved steam, could then expand further in the lower stages of the steam turbine to generate (more) power. After the feedwater of the RRC power plant is preheated by the geothermal fluid, the geothermal fluid is sent back to the geothermal (injection) well. In order to integrate geothermal energy into the power plant, there are two kinds of arrangement for the heat exchanger sub-system, i.e. the parallel and the series arrangements.

Figure 2 shows the schematic diagram of a GAPG plant with the parallel heat exchanger arrangement. As shown in **Figure 2**, in a parallel GAPG plant each high pressure FWHs of the RRC power plant (FWH1 to FWH3 in **Figure 2**) would potentially have one geo-preheater to transfer of the geothermal heat to the feedwater. Namely, each geo-preheater is in parallel with the displaced FWH. The FWHs that could be displaced by geothermal fluid depends on the geothermal fluid temperature. If the temperature of the geothermal fluid can be used to displace FWH1 in **Figure 2**, the temperature of the geothermal fluid at point G1 must be higher than the temperature of the feedwater at point 1. In this arrangement, shown in **Figure 2**, the valves A to C require to be adjusted according to the geothermal fluid flow rate to make sure the feedwater temperatures at the exit of each FWH remain unchanged.

Figure 3 shows the schematic diagram of the series arrangement of the heat exchanger or geo heater arrangement. As shown in **Figure 3**, in the series arrangement, there is only two heat exchangers required to preheat feedwater. The geo-preheater 1 is used to displace FWH1 to FWH3 (high pressure FWHs) and the geo-preheater 2, if allowed, is used to displace FWH5 to FWH8 (low pressure FWHs). Similarly (to the parallel arrangement), the Valves A-C, should be adjusted according to the flow rate and the temperature of the geo-fluid at point G1, to make sure the temperature of the feedwater at ws1 remain unchanged.

In a GAPG plant, besides the temperature of geo-fluid, there is another factor that would determine which stage of FWH cloud be displaced, that is silica scaling. As the geothermal fluid transfers heat (to feedwater) in geo-preheaters, its temperature drops. When the temperature of geothermal fluid drops, the dissolved silicon dioxide in the geothermal fluid would precipitate from the fluid. the precipitation rate of silicon dioxide is a function of the temperature and silica concentration of the geothermal fluid (Bhuana et al., 2009) (Sudhakar et al., 2018). The precipitation of the silicon dioxide would cause the silica scaling in the heat exchanger and pipelines, which could not be allowed to occur for the safe operation of the plant. Therefore, determining or selecting the right FWH(s) to be displaced, according to the temperature and SiO2 concentration of the geo-fluid, would help to minimize/reduce silica scaling.

SIMULATION MODEL OF THE GAPG PLANTS

To calculate the performance of the GAPG plant, a simulation model has been developed. The simulation model consists of two

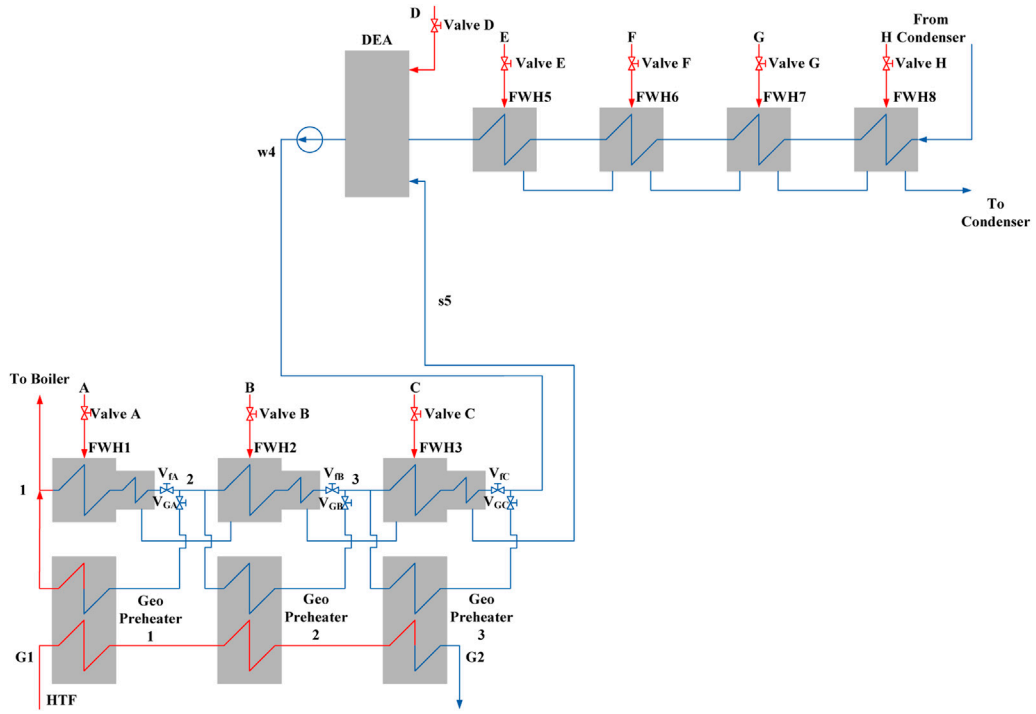

FIGURE 2 | Schematic diagram of parallel GAPG plant feedwater heater system.

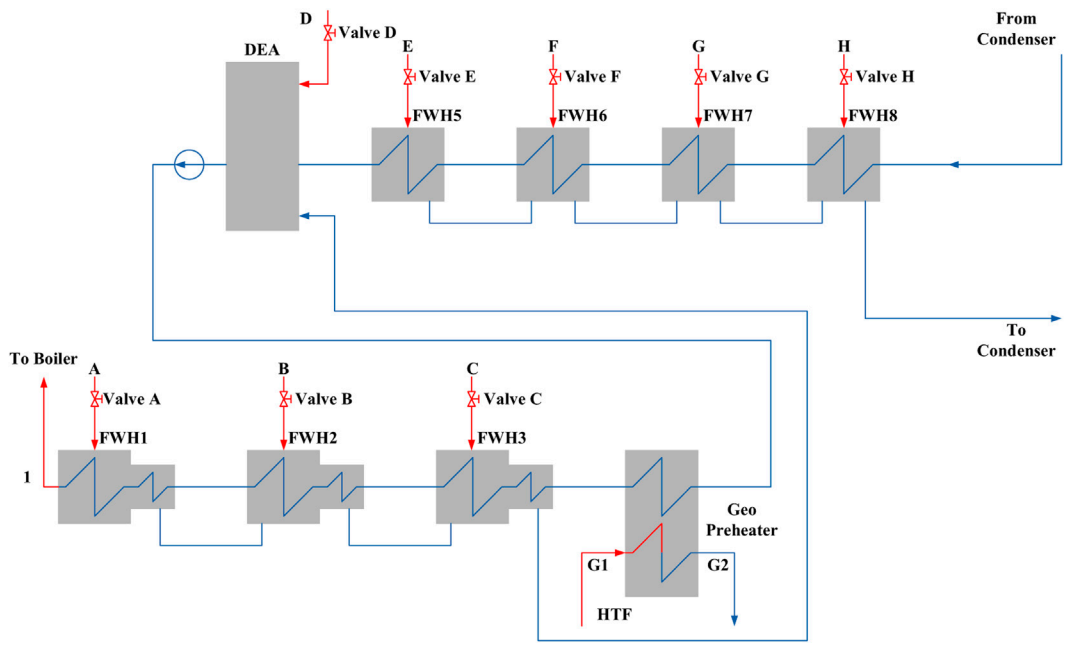

FIGURE 3 | Schematic diagram of Series GAPG plant feedwater heater system.

TABLE 1 | Temperature functions of the rate constants for silica-water reactions (Rimstidt and Barnes, 1980).

$\log k_+ = 1.174 - 2.028 \times 10^{-3}T - 4158/T$
$a_2 = -0.707$, $c_2 = -2598$

parts. The first part is used to calculate the GAPG plant's technical performance, and the second part is used to simulate the silica scaling process that occurred in the geo-preheater.

Simulation Model of GAPG Plant

For a GAPG plant, the simulation of the GAPG plant is actually simulating the energy and mass balance of the FWH system, in which the Matrix Method is often used (Huang et al., 2019). In this paper, the Matrix Method is used to simulate the extraction steam's mass flow rate variations after geothermal energy integration. Then, the power output of steam turbine can be calculated by using new calculated mass flow rate.

For a GAPG plant with 8 FWHs (including three high pressure FWHs, one deaerator, and four low pressure FWHs), and extraction steam to all high pressure FWHs has been displaced by geothermal energy, the Matrix for FWH system can be expressed as:

$$\begin{pmatrix} q_1 & \cdots & \cdots & \cdots & \cdots & \cdots & \cdots & 0 \\ r_2 & q_2 & \ddots & \ddots & \ddots & \ddots & \ddots & \vdots \\ r_3 & r_3 & q_3 & \ddots & \ddots & \ddots & \ddots & \vdots \\ r_4 & r_4 & r_4 & q_4 & \ddots & \ddots & \ddots & \vdots \\ \tau_5 & \tau_5 & \tau_5 & \tau_5 & q_5 & \ddots & \ddots & \vdots \\ \tau_6 & \tau_6 & \tau_6 & \tau_6 & r_6 & q_6 & \ddots & \vdots \\ \tau_7 & \tau_7 & \tau_7 & \tau_7 & r_7 & r_7 & q_7 & \vdots \\ \tau_8 & \tau_8 & \tau_8 & \tau_8 & r_8 & r_8 & r_8 & q_8 \end{pmatrix} \begin{pmatrix} y_A \\ y_B \\ y_C \\ y_D \\ y_E \\ y_F \\ y_G \\ y_H \end{pmatrix} + \begin{pmatrix} \dot{Q}_{Geo,1}/\dot{m}_0 \\ \dot{Q}_{Geo,2}/\dot{m}_0 \\ \dot{Q}_{Geo,3}/\dot{m}_0 \\ 0 \\ 0 \\ 0 \\ 0 \\ 0 \end{pmatrix} = \begin{pmatrix} \tau_1 \\ \tau_2 \\ \tau_3 \\ \tau_4 \\ \tau_5 \\ \tau_6 \\ \tau_7 \\ \tau_8 \end{pmatrix}, \quad (1)$$

Where, q_i (kJ/kg) is the decrease of extraction steam specific enthalpy in the ith FWH; τ_i (kJ/kg) is the increase of the feedwater specific enthalpy in the ith FWH; r_i (kJ/kg) is the decrease of the drained steam specific enthalpy from the $(i\text{-}1)^{\text{th}}$ FWH in the ith FWH; and y_i is the each stages of extraction steam mass flow rate. $\dot{Q}_{Geo,i}$ (kJ/s) is the geothermal energy input of ith FWH; and $\dot{m}_0$ (kg/s) is the boiler mass flow rate. The $\dot{Q}_{Geo}$ is equal to $\sum \dot{Q}_{Geo,i}$.

The extraction steam flow rates of each extraction steam at each FWHs with various geothermal energy integration could be calculated by **Eq. 1**.

In a GAPG plant, the increased power output after geothermal input can be termed as geothermal power output. Therefore, the power efficiency for the whole GAPG plant can be given as:

$$\eta_{Geo} = \frac{\Delta W_e}{Q_{Geo} + Q_{Boiler}}, \quad (2)$$

Where ΔW_e is the increased power output after geothermal integration; and Q_{Geo} is the geothermal energy input.

Prediction of the Silica Deposition

In a GAPG plant, the silicon dioxide becomes supersaturated as the geo-fluid flows up and quenches to a lower temperature (Chan, 1989). Polymerization happens when the concentration of silica is supersaturated and polymerization proceeds to silica (Gunnarsson and Arnórsson, 2005). The silica scaling takes place in geothermal wells, well pipes, and heat exchanger in the GAPG plant. In geothermal fluid, the rates of silica deposition and polymerization is determined by the PH and salt concentration of geothermal fluid, the residence time, and temperature of geothermal fluid (Gunnarsson and Arnórsson, 2005). The rate of silica deposition can be controlled by adjusting PH through the addition acid of by adding salt (Gunnarsson and Arnórsson, 2005). However, adding salt might still have a negative effect on the pipes of power system and environment of geothermal wells. In the present paper, it is assumed that the solubility of silicon dioxide is only controlled by the temperature of the geothermal fluid and the silica scaling occurs in the heat exchanger system of the GAPG system.

In order to optimise the displacement selections of the GAPG plant with different silica concentrations, the net precipitation rate of silicon dioxide should be calculated. The approaches taken to calculate the silica precipitation and deposition rate of silicon dioxide are quite complex and poorly understood (Brown and Bacon, 2009). A simplified approach using experimental data from Brown and Bacon is used in the present paper to calculate the deposition rate of silicon dioxide.

The precipitation rate of silicon dioxide is mainly determined by the kinetics of amorphous silica in the geothermal fluid. For a geothermal fluid at temperatures ranging from 0 to 300°C, the kinetics of amorphous silica precipitation have been determined by the study of Rimstidt and Barnes (Rimstidt and Barnes, 1980). The reversible reaction of silicon dioxide is shown as:

$$SiO_2\,(S) + 2H_2O\,(1) \leftrightarrow H_4SiO_4\,(aq).$$

For this reversible reaction, H4SiO4 (aq) is the precipitation of silicon dioxide. The net precipitation rate can be expressed as (Bhuana et al., 2009):

$$r'_{SiO_2} = -k_+\,(1 - Q/K)\,\frac{\text{mol}}{\text{L.s}}, \quad (3)$$

Where the k_+ is the forward rate constant, K is the equilibrium constant and Q is the activity quotient. The Q/K is the degree of saturation (S).

Q is then calculated by

$$Q = a_{H_4SiO_4} / \left(a_{SiO_2}\right)\left(a_{H_2O}\right)^2, \quad (4)$$

TABLE 2 | Key parameters of case study power plant (300 MW subcritical power plants).

Points in Figure 1								
Item	**Unit**	**A**	**B**	**C**	**D**	**E**	**F**	**G**	**H**
Pressure	Bar	54.41	34.62	15.76	7.56	4.86	1.87	0.632	0.226
Temperature	°C	374.9	313.2	430.4	326.3	276.5	174.9	85.9	61.6
FWH outlet temperature	°C	269	240.2	198.2	169.1	146.1	113.7	83.1	58.8
Drain steam temperature	°C	245.9	203.8	174.7	165.4	119.3	88.8	64.4	40.2
Extraction flow rate	kg/s	16.00	19.78	9.70	14.73	10.42	9.44	7.34	7.37

Outlet steam parameters of boiler, and Steam turbine

Item	Unit	Boiler	Reheater	HP turbine	IP turbine	LP turbine
Pressure	Bar	167	31.16	34.62	4.77	0.052
Temperature	°C	537	537	312.8	276.5	33.6
Flow rate	kg/s	241.5	205.8	225.6	170.9	146.8

TABLE 3 | Case study scenarios.

Scenario No	**Displaced FWHs**	**Case study power plant**	
		Geo-fluid inlet temperature (°C)	**Geo-fluid outlet temperature (°C)**
Scenario 1	Displacing extraction steam to FWH1 to FWH3	280	180
Scenario 2	Displacing extraction steam to FWH5 to FWH8	155	45
Scenario 3	Displacing extraction steam to FWH1 to FWH 8	280	45
Scenario 4	Displacing extraction steam to FWH5	180	120

Where, a_i is the activity of species *i*. In the mathematical model, a_i is calculated as the silica concentration. As SiO_2 and H_2O are present as a solid and a liquid, then a_{SiO_2} and a_{H_2O} can be calculated as "1."

Rimistidt and Barnes provide a method to calculate k_+ and K as a function of the geothermal fluid temperature (Rimstidt and Barnes, 1980). The forward rate constant k_+ and the equilibrium constant are given by:

$$\log K = a_1 + b_1 T + c_1/T, \tag{5}$$

$$\log k_+ = (a_1 + a_2) + b_1 T + (c_1 + c_2)/T. \tag{6}$$

Rimistidt and Barnes provide the a_1, a_2, b_1, c_1, c_2 which is shown in **Table 1**.

From **Eq. 3** to **Eq. 6**, the net precipitation rate of silica with various geothermal fluid temperature and silica concentration can be expressed as follows:

$$r'_{SiO_2} = 10^{(a_1+a_2)+b_1 T+\frac{c_1+c_2}{T}}\left(1 - \frac{a_{H_4SiO_4}}{10^{a_1+b_1 T+\frac{c_1}{T}}}\right)\frac{\text{mol}}{\text{L.s}}. \tag{7}$$

By using **Eq. 6**, the silica scaling process in the heat exchanger system of the GAPG plant can be simulated.

CASE STUDY

A GAPG plant, modified from a 300 MW subcritical RRC power plant, was chosen to be the study case, which is shown in **Figure 1**. The key parameters of the 300 MW power plant are given in **Table 2**. As there is no existing GAPG plant, the validation of the GAPG plant is based on the real operation data. In this study, the simulated results of the Rankine cycle plant model have been compared with real operated data with the case study plant. The simulation results for the power output and mass flow rate to the boiler without geothermal input are 303 MW and 241.5 kg/s, while the real operation data are 300 MW and 245.8 kg/s. It can be seen that the comparison results of the GAPG plant show further agreement between the simulation model and reference data.

According to **Figure 1**, the 300 MW subcritical RRC power plant has seven feedwater heaters and one deaerator. Four different displacement scenarios have been evaluated in the present study, which are given in **Table 3**.

In Scenario 1, extraction steam to FWH 1 to FWH 3 has been displaced by the geothermal energy. In Scenario 2, the geo-fluid is used to displace extraction steam to FWH5 to FWH8. In Scenario 3, all FHWs have been displaced by the geo-fluid. In Scenario 4, it is assumed that the geothermal fluid from the Scenario 1 (180°C) is used to displace extraction steam at points E only.

In the present study, the minimum temperature difference required for heat transfer in heat exchangers is assumed to be 10°C. At the (production) well, silica is present as quartz, and the concentration of silica in the reservoir ranges from 500 to 700 mg/kg SiO_2, which is dependent on the temperature at the well head (Fournier and Rowe, 1966).

RESULTS AND DISCUSSION

In this study, the silicon dioxide precipitation in the geo-preheater system for four scenarios has been simulated. Based on the simulation results, the displacement selection with

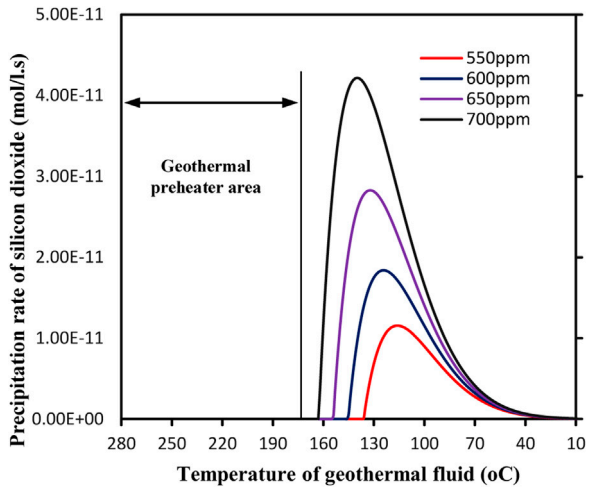

FIGURE 4 | Variation of silicon dioxide precipitation rate in the heat exchanger/geo-preheater system for scenario 1.

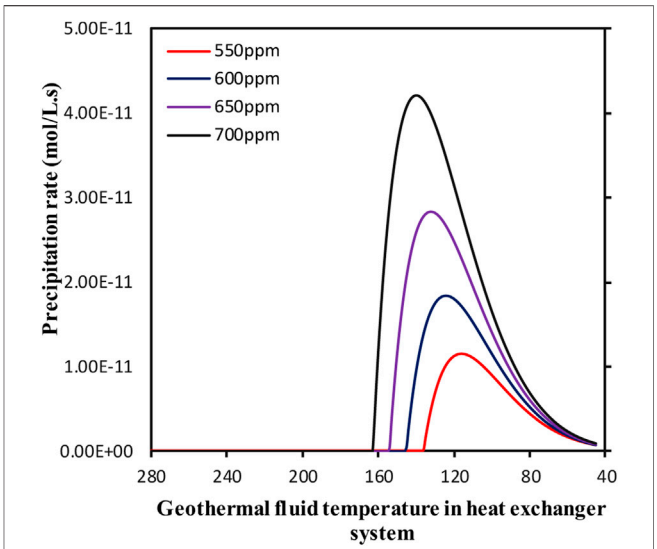

FIGURE 6 | Precipitation rate as a function of temperature in the heat exchanger system/geo-preheater for Scenario 3.

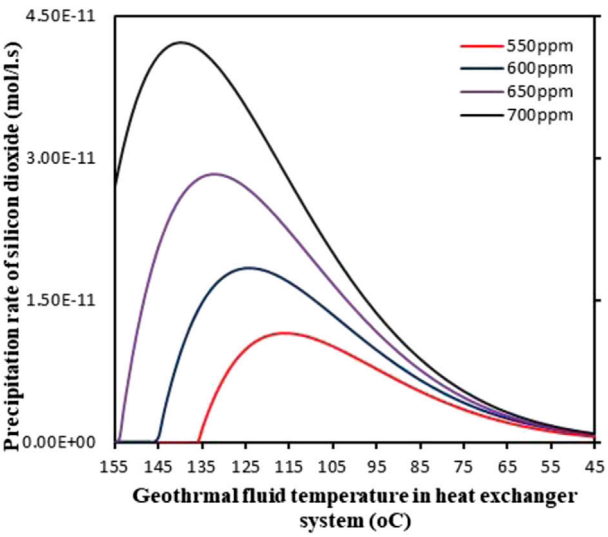

FIGURE 5 | Variation of silicon dioxide precipitation rate in the heat exchanger system/geo-preheater for Scenario 2.

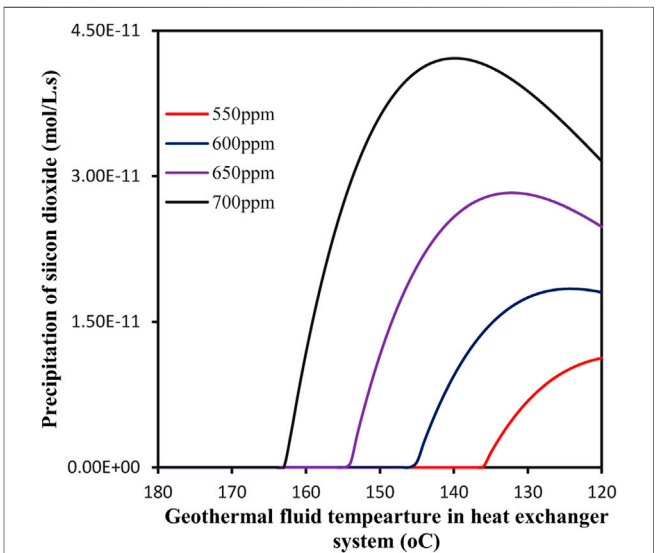

FIGURE 7 | Precipitation rate as a function of temperature in the heat exchanger system for Scenario 4.

minimum silica scaling occurring would be selected. The technical performance of the optimal displacement selection with two heat exchanger arrangements has been compared.

Silicon Dioxide Precipitation in the Geo-Preheater System

Figure 4 presents the variation of silicon dioxide precipitation rate for scenario 1. It can be found from **Figure 4** that temperature at which silicon dioxide precipitation starts and the temperature at which its rate reaches maximum depend on the silicon dioxide concentration in the geothermal fluid. When the silicon dioxide concentration is 700 mg/kg, the silicon dioxide begins to precipitate at about 162°C, and the maximum precipitation rate occurs at around 140°C. If the silicon dioxide concentration was to 550 mg/kg, these two temperatures would be 136 and 116°C, respectively. This trend provides a mechanism to decrease the precipitation of silicon dioxide in the Geo-preheater system.

For Scenario 1, the geo-fluid temperature at the inlet of the heat exchangers for the 300 MW power plant is assumed to be 280°C, and that at the outlet is 180°C. Both temperatures i.e. 280°C and 180°C are well above the precipitation starting temperature,

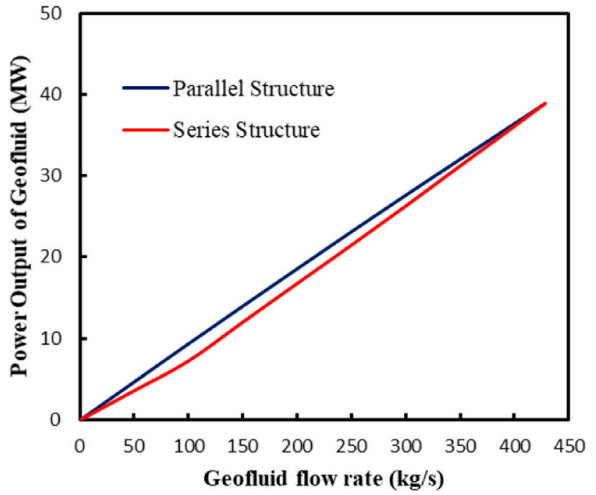

FIGURE 8 | The power output of geothermal energy of two kinds of GAPG plants with different geothermal fluid integration.

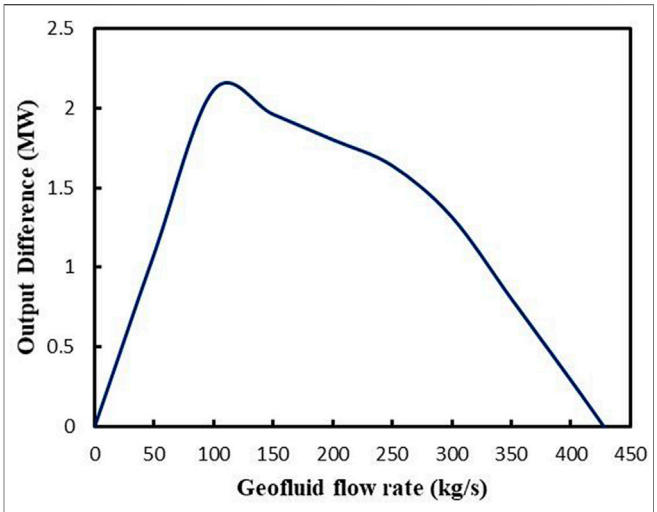

FIGURE 10 | Power output difference between two kinds of GAPG plants with the same amount of geothermal integration.

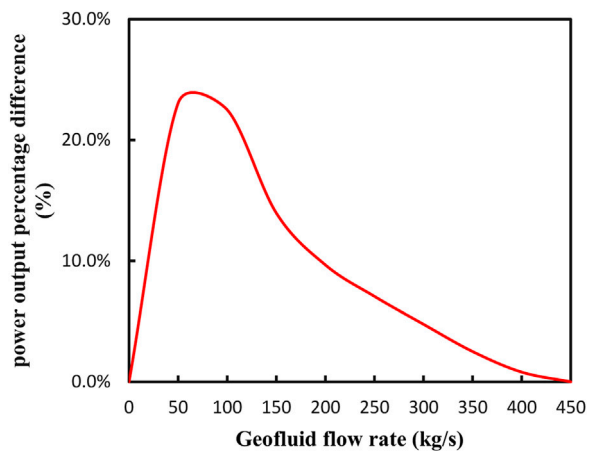

FIGURE 9 | Comparison of two kinds of GAPG plant output with same amount of geothermal integration.

according to **Figure 4**, even for the highest SiO2 concentration of 700 ppm. In other words, precipitation of silicon dioxide or silica scaling would not occur in Scenario 1.

Figure 5 presents the variations of precipitation rate in the Geo-preheater system of the GAPG plant for Scenario 2. For Scenario 2, the geothermal inlet temperature is 155°C, and the geothermal outlet temperature is 45°C. From **Figure 5**, it can be found that when the geo-fluid with the concentration of silica at 650 and 700 mg/kg, silicon dioxide begins to precipitate from geo-fluid when they enter the Geo-preheater system. When the concentrations of silica are 550 and 600 mg/kg, about 90 and 80% of the Geo-preheater system are susceptible to fouling by silicon dioxide. This means that Scenario 2 is not suitable for the GAPG plant.

The variations of precipitation rate of silicon dioxide in the Geo-preheater system for Scenario 3 is plotted in **Figure 6**. For Scenario 3, the geothermal inlet and outlet temperatures are 280°C and for 45°C. As can be seen in **Figure 6**, when the temperature decreases to about 160°C, the geothermal fluid becomes saturated. This means that about 50% of the heat exchanger system is susceptible to fouling by silicon dioxide. This area is the heat exchanger system parallel with low-pressure heat exchanger system. This means that geothermal fluid with the concentration of silica at 550–700 mg/kg is also not suitable for the GAPG plant.

Figure 7 presents the variation of silicon dioxide precipitation rate in the heat exchanger system for Scenario 4. In this Scenario, the geothermal temperature at the inlet is about 180°C, which is higher than Scenario 2. However, it can be found that there is still about 30–70% of the heat exchanger system is susceptible to fouling by silicon dioxide for the concentration of silica ranging from 550 to 700 mg/kg. This means that Scenario 4 is also not suitable for the GAPG plant.

From **Figure 4** to **Figure 7**, it can be concluded that the best displacement option for the GAPG plant is geo-fluid used to displace all high-pressure FWHs, due to the low silica scaling during the preheating process. Therefore, the technical performance of the GAPG plant with two structures for scenario 1 has been compared.

Comparison of Technical Performance of the Series and Parallel Arrangement

Figure 8 shows the Extra power output of the steam turbine after different geothermal fluid flow rate integration. **Figure 8** shows that when the FWH1 to FWH3 are fully displaced by geothermal energy, the two kinds of GAPG plants have the same power output. When the extraction steam from FWH1 to FWH3 is fully displaced by the geothermal energy, the extra output of steam turbine is 38.9 MW for both of the GAPG plants. When the extraction steam to all high pressure FWHs has been displaced, the power output can be increased by 13%. This means that if the GAPG plant has been operated for reducing boiler consumption. It has protentional to reduce the 13% of carbon dioxide emissions.

TABLE 4 | Hybrid efficiencies of two kinds of GAPG plant with different amount of geothermal energy integration.

Geothermal fluid flow rate (kg/s)	50 (%)	100 (%)	150 (%)	200 (%)	250 (%)	300 (%)	350 (%)	400 (%)	428.7 (%)
Parallel GAPG plant	46.3	46.1	45.8	45.6	45.4	45.1	44.9	44.7	44.6
Series GAPG plant	46.3	46.0	45.7	45.5	45.2	45.0	44.9	44.7	44.6

However, when the extraction steam from FWH1 to FWH3 is partly displaced by the geothermal energy, the power output of the Parallel GAPG plant is higher than the Series GAPG plant. The reason is thought that in the Series GAPG plant, the lower pressure FWH is displaced firstly, this leads to the lower power output than the Parallel GAPG plant.

Figure 9 shows the power output percentage difference of two kinds of GAPG arrangements. As shown in **Figure 9**, when 50 kg/s geothermal fluid is integrated into two kinds of GAPG plant, the extra output of the Parallel GAPG plant is 29.3% higher than the Series GAPG plant. With the increase of geothermal fluid, the power output difference percentage decrease with the amount of geothermal energy integration.

Figure 10 shows the power output difference of two kinds of the GAPG plant with different geothermal fluid input. **Figure 10** indicates that when the flow rate of geothermal fluid is integrated into two kinds of GAPG plant from 50 to 100 kg/s, the output difference increases from 1.1 to 2.1 MW. After the geothermal fluid flow rate is 100 kg/s, with the increase of geothermal fluid flow rate, the output difference of two kinds of GAPG plant decrease to 0.

Table 4 shows the hybrid efficiencies of two kinds of GAPG plant with different geothermal energy integration. The hybrid efficiency is defined as the total output of the steam turbine divided by the boiler fuel consumption and geothermal input. As shown by **Table 4**, with the same amount of geothermal thermal energy input, the two kinds of GAPG plant have almost the same hybrid efficiencies.

CONCLUSION

In a GAPG plant, geothermal fluid at different temperatures is used to displace different grade extraction steam to different stages of feedwater heater. Different displacement selections lead to different technical performances. As the rate of silica deposition is mainly dependent on the temperature of geothermal fluid, adjusting displacement selections can be used to control the silica scaling process that occurred in the heat exchanger system. Also, there are two configurations for the GAPG plant, Parallel, and Series configurations.

In this study, the silica scaling that occurred in the heat exchanger system for different GAPG plant's displacement selections is simulated to optimise displacement selections. The technical performance for the optimal displacement selections with two structures has been compared. To achieve this aim, a 300 MW subcritical power plant GAPG plant has been used as a case study. Four different displacement selections are used as scenarios for assessment. The results indicate that:

When extraction steam to all high pressure FWHs has been displaced by geo-fluid, there is no silicon dioxide scaling occurred for the GAPG plant. In other words, for scenario 1, there is no energy loss caused by silica scaling with different silico dioxide concentrations in the geothermal fluid.

When extraction steam to all low pressure FWHs has been displaced by geo-fluid, it was found that there is at least 30% of heat exchanger system is susceptible to fouling by silicon dioxide.

Considering the silicon dioxide scaling in the GAPG plant's heat exchanger system, displacement of extraction steam to all high pressure FWHs is the best displacement selection for the GAPG plant.

When geo-fluid is used to partly displace the extraction steam of the power plant, the Parallel GAPG plant's geothermal power output is higher than that of the Series GAPG plant. When the geo-fluid flow rate is 100 kg/s, there is a maximum power output difference which is 2.1 MW. However, extraction steam has been fully displaced by the geo-fluid, two kinds of GAPG plants have the same geothermal output. Under this condition, the GAPG plant has protentional to reduce the emissions of Rankine cycle power plant by 13%.

DATA AVAILABILITY STATEMENT

The original contributions presented in the study are included in the article/Supplementary Material, further inquiries can be directed to the corresponding author.

AUTHOR CONTRIBUTIONS

YZ is responsible for the investigation, conceptualization. JQ contributes to conceptualization, methodology, formal analysis. EH contributes to contributes to data curation, formal analysis. QZ contributes to investigation and validation.

ACKNOWLEDGMENTS

This paper is supported by the National Natural Science Foundation of China (51875332).

REFERENCES

Agyekum, E. B., Adebayo, T. S., Bekun, F. V., Kumar, N. M., and Panjwani, M. K. (2021). Effect of Two Different Heat Transfer Fluids on the Performance of Solar Tower CSP by Comparing Recompression Supercritical CO2 and Rankine Power Cycles, China. *Energies* 14 (12), 3426. doi:10.3390/en14123426

Agyekum, E. B., Ali, E. B., and Kumar, N. M. (2021). Clean Energies for Ghana-An Empirical Study on the Level of Social Acceptance of Renewable Energy Development and Utilization. *Sustainability* 13 (6), 3114. doi:10.3390/su13063114

Battye, D. L., Ashman, P. J., and Nathan, G. J. (2010). "Economic of Geothermal Feedwater Heating for Steam Rankine Cycles," in Progressing of Australian Geothermal Conference, Adelaide, Australia, November 16–19, 2010 (Australia: Geoscience).

Bhuana, D. S., Ashman, P. J., and Nathan, G. J. (2009). "Silica Deposition in Enhanced Geothermal Systems," in Progressing of Australia Geothermal Energy Conference, Brisbane, Australia, November 11–13, 2009 (Australia: Geoscience).

Borsukiewicz-Gozdur, A. (2010). Dual-fluid-hybrid Power Plant Co-powered by Low-Temperature Geothermal Water. *Geothermics* 39, 170–176. doi:10.1016/j.geothermics.2009.10.004

Brown, K. L., and Bacon, L. G. (2009). Pilot Plant Experiments at Wairakei Power Station. *Geothermics* 38, 64–71. doi:10.1016/j.geothermics.2008.11.004

Buchta, J. (2009). "Green Power from Conventional Steam Power Plant Combined with Geothermal Well," in Progressing of IEEE International Conference on Industrial Technology, Churchill, Australia, February 10–13, 2009 (IEEE), 2009. doi:10.1109/icit.2009.4939553

Buchta, J., and Wawszczak, A. (2010). "Economical and Ecological Aspects of Renewable Energy Generation in Coal Fired Power Plant Supported with Geothermal Heat," in Progressing of Electric Power and Energy Conference (EPEC), Halifax, Canada, August 25–27, 2010 (IEEE), 2010. doi:10.1109/epec.2010.5697179

Chan, S. H. (1989). A Review on Solubility and Polymerization of Silica. *Geothermics* 18, 49–56. doi:10.1016/0375-6505(89)90009-6

Christina, W., Petra, Z., and Andrea, S. (2020). Review of Power-To-X Demonstration Projects in Europe. *Front. Energ. Res.* 8, 191. doi:10.3389/fenrg.2020.00191

DiPippo, R., DiPippo, E. A., Kestin, J., and Khalifa, H. E. (1981). Compound Hybrid Geothermal-Fossil Power Plants: Thermodynamic Analyses and Site-Specific Applications. *J. Eng. Power* 103, 797–804. doi:10.1115/1.3230804

DiPippo, R., Khalifa, H., Correia, R., and Kestin, J. (1978). "Fossil Superheating in Geothemral Steam Ower Plants," in Progressing of the Intersoc Energy. (San Diego, CA: Convers Eng Conference 13th).

Fournier, R., and Rowe, J. (1966). Estimation of Underground Temperatures from the Silica Content of Water from hot springs and Wet-Steam wells. *Am. J. Sci.* 264, 685–697. doi:10.2475/ajs.264.9.685

Gunnarsson, I., and Arnórsson, S. (2005). Impact of Silica Scaling on the Efficiency of Heat Extraction from High-Temperature Geothermal Fluids. *Geothermics* 34, 320–329. doi:10.1016/j.geothermics.2005.02.002

Hao, L., Fu, L. J., Zhang, Y., and Xiong, &Y. Y. (2021). A Dynamic and Cooperative Control Strategy for Multi-Hybrid Energy Storage System of DC Microgrid Based on SOC. *Front. Energ. Res.* 9, 795513. doi:10.3389/fenrg.2021.795513

Hargreaves, J. J., and Jones, R. A. (2020). Long Term Energy Storage in Highly Renewable Systems. *Front. Energ. Res.* 8, 219. doi:10.3389/fenrg.2020.00219

Huang, C., Hou, H., Hu, E., Yu, G., Peng, H., Yang, Y., et al. (2019). Performance Maximization of a Solar Aided Power Generation (SAPG) Plant with a Direct Air-Cooled Condenser in Power-Boosting Mode. *Energy* 175, 891–899. doi:10.1016/j.energy.2019.03.133

Kestin, J., DiPippo, R., and Khalifa, H. (1978). Hybrid Geothermal-Fossil Power Plants. *Mech. ENgineering* 100, 28–35.

Khalifa, H., DiPippo, R., and Kestin, J. (1978). "Geothermal Preheating in Fossil-Fired Steam Power Plants," in Progressing of Intersoc Energy Convers Eng Conf 13th, San Diego, CA, August 20–25, 1978.

Khalifa, H. (1978). "Hybrid Power Plants for Geo-Pressured Resources," in Progressing of 5th Annual Geothermal Conference and Workshop, Washington, DC, June 23–25, 1981.

Kolb, G. J. (1998). Economic Evaluation of Solar-Only and Hybrid Power Towers Using Molten-Salt Technology. *Solar Energy* 62, 51–61. doi:10.1016/s0038-092x(97)00075-3

Kumar, N. M. (2019). Performance of Single-Sloped Pitched Roof Cadmium telluride (CdTe) Building-Integrated Photovoltaic System in Tropical Weather Conditions. *Beni-Suef Univ. J. Basic Appl. Sci.* 8 (1), 1–9. doi:10.1186/s43088-019-0003-2

Liu, Q., Shang, L., and Duan, Y. (2016). Performance Analyses of a Hybrid Geothermal-Fossil Power Generation System Using Low-Enthalpy Geothermal Resources. *Appl. Energ.* 162, 149–162. doi:10.1016/j.apenergy.2015.10.078

Qin, J., Hu, E., Nathan, G. J., and Chen, L. (2018). Mixed Mode Operation for the Solar Aided Power Generation. *Appl. Therm. Eng.* 139, 177–186. doi:10.1016/j.applthermaleng.2018.04.118

Qin, J., Hu, E., and Nathan, G. J. (2017). Impact of the Operation of Non-displaced Feedwater Heaters on the Performance of Solar Aided Power Generation Plants. *Energ. Convers. Manage.* 135, 1–8. doi:10.1016/j.enconman.2016.12.061

Qin, J., Zhang, Q., Hu, E., Duan, J., Zhou, Y., and Zhang, H. (2022). Optimisation of Solar Aided Power Generation Plant with Storage System Adopting Two Non-displaced Extraction Steam Operation Strategies. *Energy* 239, 121937. doi:10.1016/j.energy.2021.121937

Kingston Reynolds Thom, and Allardice Ltd (1980). *An Investigation into Hybrid Geothermal/gas Power Plants*, Auckland: New Zealand Energy Research and Development Committee.

Rimstidt, J., and Barnes, H. (1980). The Kinetics of Silica-Water Reactions. *Geochimica et Cosmochimica Acta* 44, 1638–1639. doi:10.1016/0016-7037(80)90220-3

Setiawan, F. A., Rahayuningsih, E., Petrus, H. T. B. M., Nurpratama, M. I., and Perdana, I. (2019). Kinetics of Silica Precipitation in Geothermal Brine with Seeds Addition: Minimizing Silica Scaling in a Cold Re-injection System. *Geothermal Energy* 7 (22). doi:10.1186/s40517-019-0138-3

Seyfettin, G. (2021). Can, "Steam Turbine—Quo Vadis? *Front. Energ. Res.* 8, 612731. doi:10.3389/fenrg.2020.612731

Sudhakar, K., Samykano, M., and Jayaseelan, V. (2018). "BIPV Market Growth: SWOT Analysis and Favorable Factors," in 2018 4th International Conference on Electrical Energy Systems (ICEES), Chennai, India, February 7–9, 2018 (IEEE), 412–415.

Waqar, A., Shahbaz Tanveer, M., Ahmad, J., Aamir, M., Yaqoob, M., and Anwar, F. (2017). Multi-objective Analysis of a CHP Plant Integrated Microgrid in Pakistan. *Energies* 10, 1625. doi:10.3390/en10101625

Zhang, G., Cao, Y., Cao, Y., Li, D., and Wang, L. (2017). Optimal Energy Management for Microgrids with Combined Heat and Power (CHP) Generation, Energy Storages, and Renewable Energy Sources. *Energies* 10, 1288. doi:10.3390/en10091288

Zhang, N., Hou, H., Yu, G., Hu, E., Duan, L., and Zhao, J. (2019). Simulated Performance Analysis of a Solar Aided Power Generation Plant in Fuel Saving Operation Mode. *Energy* 166, 918–928. doi:10.1016/j.energy.2018.10.014

Zhao, Y., Du, B., Chen, S., Zhao, J., Gong, Y., Bu, X., et al. (2021). Thermo-Economic Comparison Between Organic Rankine Cycle and Binary-Flashing Cycle for Geothermal Energy. *Front. Energ. Res.* 9, 759872. doi:10.3389/feart.2021.759872

Zhao, Y., Hong, H., and Jin, H. (2016a). Appropriate Feed-In Tariff of Solar-Coal Hybrid Power Plant for China's Inner Mongolia Region. *Appl. Therm. Eng.* 108, 378–387. doi:10.1016/j.applthermaleng.2016.07.062

Zhao, Y., Hong, H., and Jin, H. (2016b). Effectiveness Analysis of Solar Replacement Scenarios in a Typical Solar–Coal Hybrid System. *Energy Sourc. A-Recovery Utilization Environ. Effects* 38, 1798–1804. doi:10.1080/15567036.2014.1004003

Zhao, Y., Hong, H., and Jin, H. (2016c). Effectiveness Analysis of Solar Replacement Scenarios in a Typical Solar–Coal Hybrid System. *Energ. Sourc. Part A-Recovery Utilization Environ. Effects* 38, 1969–1974. doi:10.1080/15567036.2014.1004003

Zhou, C., Doroodchi, E., and Moghtaderi, B. (2014). Assessment of Geothermal Assisted Coal-Fired Power Generation Using an Australian Case Study. *Energ. Convers. Manage.* 82, 283–300. doi:10.1016/j.enconman.2014.03.011

Zhou, L., Li, Y., Hu, E., Qin, J., and Yang, Y. (2015). Comparison in Net Solar Efficiency between the Use of Concentrating and Non-concentrating Solar Collectors in Solar Aided Power Generation Systems. *Appl. Therm. Eng.* 75, 685–691. doi:10.1016/j.applthermaleng.2014.09.063

Conflict of Interest: The authors declare that the research was conducted in the absence of any commercial or financial relationships that could be construed as a potential conflict of interest.

Publisher's Note: All claims expressed in this article are solely those of the authors and do not necessarily represent those of their affiliated organizations, or those of the publisher, the editors and the reviewers. Any product that may be evaluated in this article, or claim that may be made by its manufacturer, is not guaranteed or endorsed by the publisher.

frontiers in Energy Research

BRIEF RESEARCH REPORT
published: 31 March 2022
doi: 10.3389/fenrg.2022.845686

Stochastic and Iterative Based Optimization for Enhancing Dynamic Performance of Interconnected Power System With Hybrid Energy Storage

*Niveditha Sivadanam *, Nagu Bhookya and Sydulu Maheswarapu*

Department of Electrical Engineering, National Institute of Technology Warangal, Warangal, India

With the growing dominance of inverter-based resources (IBRs), the synchronous inertia of the interconnected power systems (IPSs) is affected. The increase in IBRs results in a decrease in the system inertia. The decrease in inertia impacts the initial rate of decline of the frequency. Thus, there is a need for faster frequency response requirements to enhance the dynamic performance of the IPS. With the massive penetration of the plug-in hybrid electric vehicles (PHEVs) into expanding smart cities, PHEVs can act as controllable loads which support the inertial response of the system in a rapid manner. This gives a scope to monitor a large amount of EV operational data to ensure reliable operation considering extensive penetration of EVs. This study proposes a stochastic and iterative based optimization for a two-area interconnected power system (IPS) coupled with a hybrid energy storage system (HESS). The HESS uses 10,000 plug-in hybrid electric vehicles (PHEVs) in each area and a superconducting magnetic energy storage (SMES) device to aid load frequency control (LFC). The 10,000 PHEVs would contribute to massive operational data, which needs to be considered while studying the IPS dynamic performance. Here, we investigated two discrete tie lines: HVDC links parallel to the alternating current (AC) tie line and a virtual synchronous power-based (VSP)-HVDC link parallel to the AC tie line. The controller's optimal parameters are recorded using two meta-heuristic algorithms, that is, particle swarm optimization (PSO) and biogeography-based optimization (BBO) along with simultaneous coordinated tuning of secondary controller and storage units. Results are taken both in the presence and absence of a HESS with two types of tie links. The analysis is performed with typical load changes and sensitivity analysis scenarios for an accurate record of variations in the outcomes. Thus, the proposed BBO-based LFC tracks the supply and demand variations, ensuring precision and accuracy, indicating improved IPS dynamic performance in smart cities.

Keywords: electric vehicles, dynamic performance, stochastic and iterative approach, BBO for electric vehicles, meta-heuristic algorithms, hybrid energy storage, Interconnected Power System

OPEN ACCESS

Edited by:
Nallapaneni Manoj Kumar, City University of Hong Kong, Hong Kong SAR, China

Reviewed by:
Sudhakar Babu Thanikanti, Chaitanya Bharathi Institute of Technology, India
Mohamed Hussien, Tanta University, Egypt

****Correspondence:***
Niveditha Sivadanam
ns701608@student.nitw.ac.in

Specialty section:
This article was submitted to Sustainable Energy Systems and Policies, a section of the journal Frontiers in Energy Research

Received: *30 December 2021*
Accepted: *07 February 2022*
Published: *31 March 2022*

Citation:
Sivadanam N, Bhookya N and Maheswarapu S (2022) Stochastic and Iterative Based Optimization for Enhancing Dynamic Performance of Interconnected Power System With Hybrid Energy Storage. Front. Energy Res. 10:845686. doi: 10.3389/fenrg.2022.845686

Abbreviations: ACE, Area control error; AGC, Automatic generation control; BBO, Biogeography based optimization; EG, Electric grid; HESS, Hybrid energy storage system; HSI, High suitability index; HVAC, High voltage alternating current; HVDC, High voltage direct current; IPS, Interconnected power system; IBR, Inverter based resources; LFC, Load frequency control; LSI, Low suitability index; PHEV, Plug-in hybrid electric vehicles; PSO, Particle swarm optimization; SIV, Suitability index variable; SMES, Superconducting magnetic energy storage; VSP, Virtual synchronous power.

INTRODUCTION

The decarbonization of the transport and the energy sectors is no longer a choice (1). With emerging technologies, the countries in the world are trying to reach ambitious goals owing to sustainable challenges and objectives. The increasing electric mobility market for the existing interconnected power systems represents a key factor for more sustainable transport and in the energy sector in terms of energy storage and generation profile. Besides that, with the integration of sensors, information and communication technologies, and Internet of things (IoT) devices, the traditional cities are transforming to smart cities (2). The smart electric network in a smart city gives a flexibility in the interconnected power system.

The present-day power system is complex and widely interconnected, with energy demand escalating continuously. The traditional power system needs enormous capital for electricity generation and harms the environment. With the focus on improving the earth's climate, the conventional power system is being transformed into a decentralized, distributed generation. The distributed generation uses environment-sustainable sources such as solar, wind, geothermal, biomass, and small hydro to meet the growing demand. However, due to these sources' intermittent nature, the electric grid faces operational challenges like reliability, power quality, grid stability, and, in particular, frequency control.

The interconnected power system's successful operation requires matching the total generation to the total load demand and losses associated with the system. The instantaneous balance between the total generation and the total load reflects on the interconnected power system's frequency. With time, the operating point of the power system changes. Large penetration of electric vehicles (EVs) into the smart city's existing power pool raises electric grid (EG) reliability concerns, disrupting smart city transportation service. This gives a scope to monitor a large amount of EV operational data and provide inertial support for the EG to ensure reliable operation considering extensive penetration of EVs. Therefore, the system can notice the irregularities in the nominal frequency and power exchange schedules, producing undesirable effects. The two variables of interest are frequency and power exchanges between tie-links. Frequency stability is a rather important issue in a large interconnected power system. The load frequency control problem has been supplemented with significant research contributions from time to time, like controller designs incorporating parameter uncertainties, excitation control, load changes and characteristics, and AC/DC transmission links (Ibraheem and Kothari, 2005). Also, with the grid's multi-unit nature, including various conventional and renewable units, the grid frequency deviates rigorously in terms of which conventional load frequency control cannot satisfy the requirements up to the mark. Any small disturbance in one area may lead to instability in the entire grid system. The variation in system parameters is indicated by area control error (ACE) in the interconnected system due to its dependence on frequency and tie-line power. Usually, the AC tie line serves the purpose, but it is economical to use the HVDC link parallel to the AC tie line for long-distance benefits. HVDC line also improves stability due to fewer losses and the absence of reactive power. HVDC lines are also useful in avoiding loop flows in the interconnected system. In the study by Elyas et al. (2014), conventional AGC is modified for the deregulated power market and the system with renewable sources, and the system performance is analyzed with both AC and DC tie lines. In the study by Pham et al. (2016), LFC of a four-area power system with thermal units is investigated with HVDC links, and functional observers are designed for feedback control. In the study by (Kachhwaha et al., 2016), LFC of a multi-unit power system is modeled with EV and fractional order PID (FOPID), and the simulation is carried out for the cases with and without EV in which the dynamic performance of the system is enhanced with EV. In the study by Anil et al. (2016), various controllers are designed for LFC of a multi-unit power system in which HVDC with the H-infinity controller stands better than the HVDC optimal sliding mode controller and HVDC-PI controller. In the study by Johnson and Shubhanga. (2016), a 14-bus AC IEEE system is modified with an HVDC link to eliminate loop flow in the interconnected power system. Sivadanam et al. (2020) discussed the inertial response of different types of power systems which impacts the frequency control of different types of systems.

Even though load frequency control has been dealt with for more than 3 decades, the introduction of renewable energy sources, energy storage, and electric vehicles poses new challenges in power systems' operation. With massive penetration of renewable units with less or no inertia, the system's inertia gets disturbed. Usually, voltage source converters (VSCs) are used to improve transient stability in HVDC transmission. A VSC-HVDC system contains energy stored in DC link capacitors utilized for emulating inertia, and this strategy is named inertia emulation control (INEC). This is well illustrated in the study by Zhu et al. (2013) with various load changes and faults. In the study by Elyas et al. (2014), a two-area system is considered, and a derivative-based virtual inertia controller is designed in which the dynamic performance like peak overshoots is improved compared to HVDC transmission lines. In the study by Elyas et al. (2014), the concept of virtual synchronous power (VSP)-based virtual inertia emulation is proposed for AGC of the multi-unit interconnected power system. The inertia emulation process needs some energy, which can be provided by any energy storage devices. In general, SMES is preferable due to its fast-responding nature with which it can supply rapid power in a short duration of time. In the study by Praghnesh and Sinha. (2018), SMES is incorporated with thyristor-controlled phase shifters for the interconnected system, and craziness-based PSO is implemented to optimize the parameters Bhatt et al., 2010. On the other hand, PHEV can act as a distributed storage system, an effective solution for LFC in interconnected systems. In the study by Musio and Damiano (2012), the effect of PHEV on the cost of a virtual power plant is well analyzed.

Swarm intelligence techniques can be used to optimize the controller parameters for better system performance. In the study by Rupali and Chaphekar, (2015), PSO is implemented on a two-area interconnected power system. BBO is the upcoming latest and effective technique in optimization. In the study by Pham

et al. (2016), the travelling salesman problem is solved effectively using BBO. In the study by Rahman et al. (2015), three degrees of freedom PI controller is optimized using BBO. In the study by Hari Kumar and Ushakumari. (2014) conventional PID controller for a multi-unit system is replaced with a BBO optimized controller to enhance the system performance. In the study by Roy et al. (2014), BBO and oppositional BBO (OBBO) optimized controllers for the interconnected system are compared with PSO in which BBO improves system transients and settling time. Barisal and Mishra. (2018) presented automatic generation control of interconnected power systems with diverse generation sources. The work by Oshnoei et al. (2019) considered electric vehicles as a part of each area and proposed a TID controller for different load changes. Surya & Sinha. (2018) discussed the impact of ultracapacitor and thyristor control phase shifters on load frequency control using the ANFIS technique. Yang et al. (2017) proposed a two-level control using the multi-agent method for load frequency control. In the study by Ilias et al. (2016), the authors proposed optimization of PID controllers utilizing the evolutionary particle swarm optimization technique for a two-area interconnected power system. Abd-Elazim and Ali. (2016) proposed a BAT optimization technique for the design of optimum load frequency controllers for non-linear interconnected power systems. From the literature, the authors noticed the use of the following algorithms, namely, back tracking search algorithm (Madasu et al., 2017), Artificial Bee Colony (Kouba et al., 2015), Particle Swarm Optimization (Kouba et al., 2015), differential search algorithm (Guha et al., 2017), fractal search algorithm (Sivalingam et al., 2017), flower pollination algorithm (Madasu et al., 2018), harmony search algorithm (Shankar and Mukherjee, 2016), and JAYA algorithm (Annamraju and Nandiraju., 2019), for optimization of different types of controllers in the interconnected power systems. Sivadanam et al. (2020) proposed Particle Swarm Optimization and Biogeography Based Optimization algorithm (Sivadanam et al., 2021) for improving the dynamic performance of the interconnected power system.

Most of the works in the literature are implemented on the conventional power systems but with the rising growth of smart cities and introduction of IBRs, power electronic converters, energy storage systems, electric vehicles etc., the frequency control needs to be studied in different scenarios for interconnected power systems for successful operation and control of the modern electric grid. To the best of the author's knowledge, this is the first study which utilizes smart city transportation service as a variable for the frequency control of the IPS. This study uses the PHEVs as a part of the hybrid energy storage system (HESS) and utilizes aggregated PHEV demand to enable the frequency control. The main contributions and key features of the article are as follows:

i. The study includes the aggregated PHEV demand as a signal controlled by the transmission system operator as a part of smart city service.
ii. The controller parameters are tuned using optimization techniques for a large interconnected system. The robustness of the controller is analyzed with different parameters.
iii. The frequency deviations and tie-line deviations are observed for HVDC and VSP-HVDC tie-links in large, interconnected power systems.

In this study, a two-area interconnected power system with two reheat thermal units with a PID controller for secondary control is considered, and PHEV and SMES units are incorporated in each area. An HVDC link and a VSP-HVDC link are added parallel to the AC tie line in two different case studies. The system is simulated at various load changes. Simultaneous coordinated tuning of the secondary controller and storage unit parameters with PSO and BBO is carried out at different load changes, and sensitivity analysis is carried out with and without the PID controller. The steady-state and transient state analysis is carried out, and variation in frequency and tie-line power is plotted for every typical case study. Simulation is carried out in a MATLAB/SIMULINK environment.

The remaining section of the article is organized into five sections. In *Modeling of the Proposed System*, the mathematical modeling of the system will be introduced. *Biogeography Based Optimization Algorithm* deals with the optimization approach used to tune the controller parameters. The results and discussion are presented in *Results and Discussion*. *Sensitivity Analysis With HVDC and VSP- HVDC Links* deals with sensitivity analysis to verify the robustness of the proposed controller. Finally, *Conclusion* provides conclusions drawn based on case studies.

MODELING OF THE PROPOSED SYSTEM

The proposed system model consists of a two-area interconnected power system with thermal units incorporated with a hybrid energy storage system in each unit, which is modeled in two different scenarios, that is, with an HVDC link and a VSP-HVDC link.

Two-Area Interconnected System With Thermal Units

The primary regulation of AGC is required to curb the oscillations under load changes. The secondary regulation is needed to bring back the distorted value to the nominal range value, that is, to make the steady-state error zero. The PID controller is used as a secondary controller in this study, which increases the type of the system to make the steady-state error zero. A generalized multi-area interconnected system is modeled in **Figure 1**, as shown below. In **Figure 1**, B_i = bias coefficient of area-i; Δf_i, Δf_j = change in area-i and area-j frequency, respectively; ΔP_{gi} = governor output in area-i; ΔP_{Ti} = turbine output in area-i; ΔP_{SMESi} = output of SMES unit in area-i; ΔP_{tieij} = tie-line power; ΔP_{PHEVi} = output of PHEV in area-i; ΔP_i, = input power of area-i.

Hybrid Energy Storage System

The hybrid energy storage system constitutes plug-in hybrid electric vehicles which are used in the transportation sector

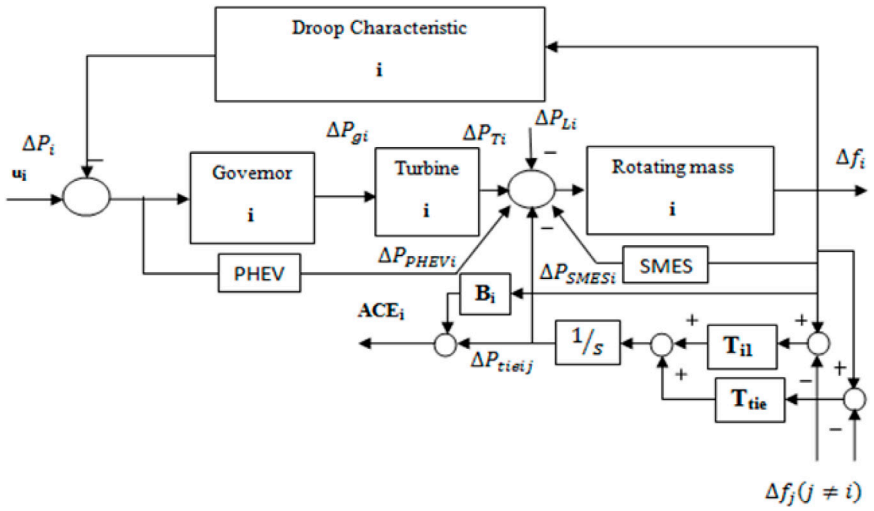

FIGURE 1 | LFC of the interconnected power system with PHEV and SMES incorporation.

and a superconducting magnetic energy storage, an electrical storage device.

Plug-In Hybrid Electric Vehicles

The carbonization of the transport sector in a city is one of the main reasons for pollution. With the use of plug-in hybrid electric vehicles (PHEVs) in the transport sector, a revolution in the world transport sector has begun to mitigate the rising global climatic changes. The technological advancements of battery systems and power electronic devices make the PHEVs a more viable option for all the common people in coming years. The adoption of PHEVs in large numbers into the interconnected power system can be used to help the electric grid in emergency situations. It will be economical if the PHEV data in an area are gathered together and then aggregated as the total PHEV demand and made available as a correction signal for the operator to meet the grid requirements, particularly active power injections. The battery state-of-charge (SOC) determines the participation factor of each PHEV.

Superconducting Magnetic Energy Storage

The superconducting magnetic energy storage (SMES) is an electrical energy storage device which has fast response time, high power capability in short time, flexible control of real power, high storage efficiency, and high-power density. The SMES uses the direct current passing through a superconducting coil which is cooled by bringing the temperature below a critical value. This produces a magnetic field, and the energy can be stored in it. To obtain the superior, several subsystems need to be designed carefully. A SMES unit consists of a sizeable superconducting coil with a cryogenic cooling system. The equivalent circuit of the SMES uses a lumped parameter model represented through a six-segment design comprising self-inductances (L_i), mutual couplings among sections (i and j, M_{ij}), AC loss resistances (R_{si}), skin effect related resistances (R_{pi}), turn-ground (shunt-C_{Shi}), and turn-turn capacitances (series-C_{Si}). This model is suitable for a frequency range from DC to a few thousand Hertz. The addition of spike capacitors (C_{Sg1} and C_{Sg2}) along with a filter capacitor C_F in parallel with grounding balance resistors (R_{g1} and R_{g2}) allows for diminishing the effect of resonances. A metal-oxide-semiconductor (MOV) protection for passing voltage surge suppression is included between your SMES product and the DC/DC converter (Molina and Mercado, 2011). The equivalent circuit of the SMES coil is shown in **Supplementary Figure S1**.

HVDC Link in Parallel With AC Tie Line

The high voltage alternating current (HVAC) which is used for transferring bulk power to long distances suffers from stability issues, reactive power control problems, etc. With the development of high voltage direct current (HVDC), there are advantages like no reactive power consumption, low losses, and possible asynchronous connections like solar, wind, etc. The growth of the alternate fuel sources led to increasing HVDC interconnections into the interconnected power system. By this interconnection of the AC tie-line parallel with the HVDC link, the frequency deviation is very low, leading to improved quality and continuity of power supply to the customers.

The variation in tie-line power now depends on both AC and DC power change, which is modeled in the following equation.

$$\Delta P_{tie} = \Delta P_{AC} + \Delta P_{DC} \quad (1)$$

The area control error (ACE) is responsible for considering the local impact on other areas in the interconnected areas. The area control error (ACE) is a function of total tie-link power and the power obtained from the hybrid energy storage system. The total tie-link power includes both the AC and DC tie-link power. The beta (β) is the frequency bias coefficient of each area. The ACE helps in achieving the load frequency control (LFC). The modified area control errors of both the areas with the inclusion of HVDC links are as follows:

$$ACE_1 = \Delta P_{tie,11} + \Delta P_{tie,12} + B_1 \Delta f_1 + \Delta P_{SMES1} + \Delta P_{PHEV1} + \Delta P_{DC1} \quad (2)$$

$$ACE_2 = a_{12}\left(\Delta P_{tie,22} + \Delta P_{tie,12}\right) + B_2 \Delta f_2 + \Delta P_{SMES2} + \Delta P_{PHEV2} + \Delta P_{DC2} \quad (3)$$

The schematic diagram of the interconnected system with HVDC is as shown in **Supplementary Figure S2A**.

VSP-HVDC Line in Parallel With AC Tie Line

Usually, conventional generators with the droop capability are responsible for providing sufficient inertia against frequency deviations in the system. However, the penetration of renewables in the modern power system imposes very low or no inertia, disturbing the system inertia. Inertia plays a significant role in damping oscillations due to sudden changes. Hence, there is a need to emulate the inertia into the system so that the system's transient stability can be improved. The inertia emulation control (INEC) strategy is proposed recently, which supports the AC network during and following disturbances, with minimal impact on the systems connected beyond the HVDC system's terminals (Rakhshani et al., 2017).

Configuration of the System With VSP-HVDC Line

The configuration of the two-area system with the VSP-HVDC line in parallel with the AC tie line is shown in **Supplementary Figure S2B**.

Derivative Control-Based Virtual Inertia Emulation

With the change in active power, the grid frequency varies. The derivative of frequency is used to adjust active power, emulating the inertia into the system by the following control law (Elyas et al., 2014) in power electronic converters.

$$P_{EM} = g\omega_0 \frac{d(\Delta\omega_0)}{dt} \quad (4)$$

where g is the gain of conversion and ω_0 is the scheduled grid frequency. This conversion process generally requires energy which can be gained by other areas or any available storage units. In this study, SMES is installed to serve the purpose. The block diagram of the control scheme for inertia emulation is in **Supplementary Figure S3**. Under various disturbances, the frequency may alter due to the change in active power. The derivative of frequency is used in the control law of the power electronic converter to regulate the active power such that system stability is retained (Rakhshani et al., 2016). A low pass filter is used due to the sensitivity of the system to the noise. The emulated power in both areas is given by the following:

$$\Delta P_{ESS1}(s) = \frac{J_1}{sT_{ESS} + 1}\left(s\Delta f_1(s)\right) \quad (5)$$

$$\Delta P_{ESS2}(s) = \frac{J_1}{sT_{ESS} + 1}\left(s\Delta f_2(s)\right) \quad (6)$$

The frequency deviation of the two-area interconnected system, including SMES and PHEV with VSP-HVDC line in parallel to the AC tie link, is given as follows:

$$\Delta f_1 = \frac{1}{2H_1 s + D_1}\left(\Delta P_1 + \Delta P_{PHEV1} - \Delta P_{SMES1} - \Delta P_{dc1} - \Delta P_{tie12} + \Delta P_{ESS1} - \Delta P_{L1}\right) \quad (7)$$

$$\Delta f_2 = \frac{1}{2H_2 s + D_2}\left(\Delta P_2 + \Delta P_{PHEV2} - \Delta P_{SMES2} - \Delta P_{dc2} + \Delta P_{tie12} + \Delta P_{ESS2} - \Delta P_{L2}\right) \quad (8)$$

BIOGEOGRAPHY BASED OPTIMIZATION ALGORITHM

Simon has introduced the BBO algorithm motivated by the migration of biological species between islands. It is constructed based on biogeography, which is the study of biological groups over time and space. It belongs to the class of metaheuristic algorithms. The effectiveness of the algorithm lies in its iterative and stochastic nature to optimize the given fitness function subjected to constraints even in a complex environment. The evolution of new species, migration of existing species, and extinction of species form the development of the algorithm. The islands which support the life are known to have high suitability indices (HSIs), and the islands which do not have favorable conditions for the growth of species are known to have low sustainability indices (LSIs). The HSI and LSI depend on the suitability index values (SIVs). The SIVs are characterized by the geography, rainfall, temperature, vegetation, etc. Based on the immigration and emigration rates, the algorithm achieves optimum solution based on SIV and HSI. The migration and mutation are the most important steps in the determination of the optimum solution.

The process of migration is based on immigration and emigration that occur among geographical regions. The parameters that control the migration process are immigration rate (λ) and emigration rate (μ).

$$\lambda = (1 - N/N_{max})I \quad (9)$$

$$\mu = EN/N_{max} \quad (10)$$

where N, E, Nmax, and I represent the number of species, maximum emigration rate, maximum species number, and maximum immigration rate.

RESULTS AND DISCUSSION

The suggested algorithm's efficacy and effectiveness can be verified by considering a two-area interconnected power system that consists of two thermal units with a hybrid energy storage system (PHEV and SMES) in each area. The test system's transfer function model is developed in MATLAB/SIMULINK, and the algorithm is created in m-file. The system's dynamic performance can be realized with two step load patterns: 0.01 pu and 0.05 pu under different scenarios. In scenario-1, the HVDC

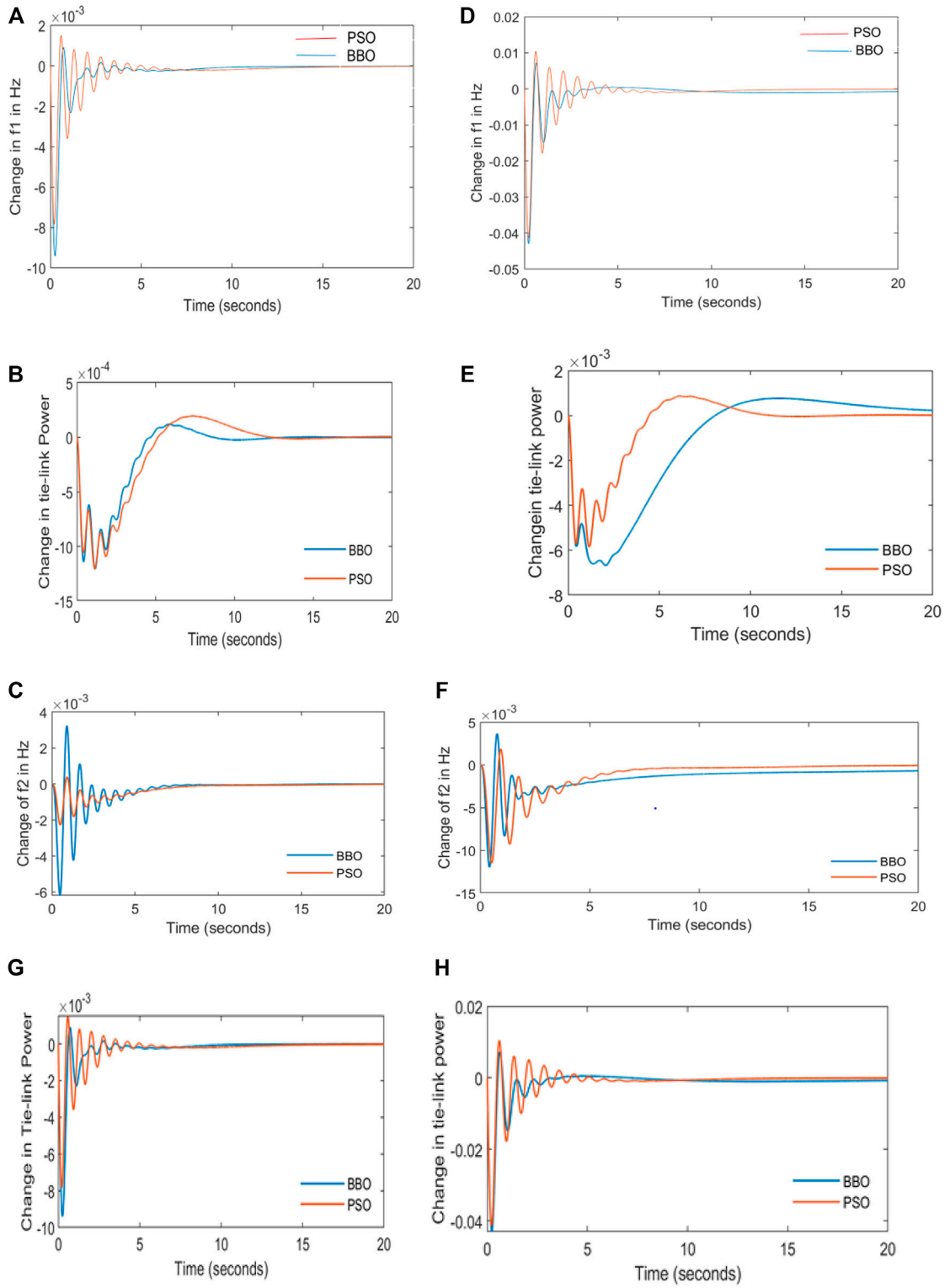

FIGURE 2 | Dynamics of Area-1 and Area-2 with and without HESS for 1% and 5% change in load with HVDC link. **(A)** Dynamics of f1 at 1% Load Change with HESS. **(B)** Dynamics of Ptie at 1% Load Change with HESS. **(C)** Dynamics of f2 at 1% Load Change with HESS. **(D)** Dynamics of f1 at 5% Load Change with HESS. **(E)** Dynamics of Ptie at 5% Load Change with HESS. **(F)** Dynamics of f2 at 5% Load Change with HESS **(G)** Dynamics of Ptie at 1% Load Change without HESS. **(H)** Dynamics of Ptie at 5% Load Change without HESS.

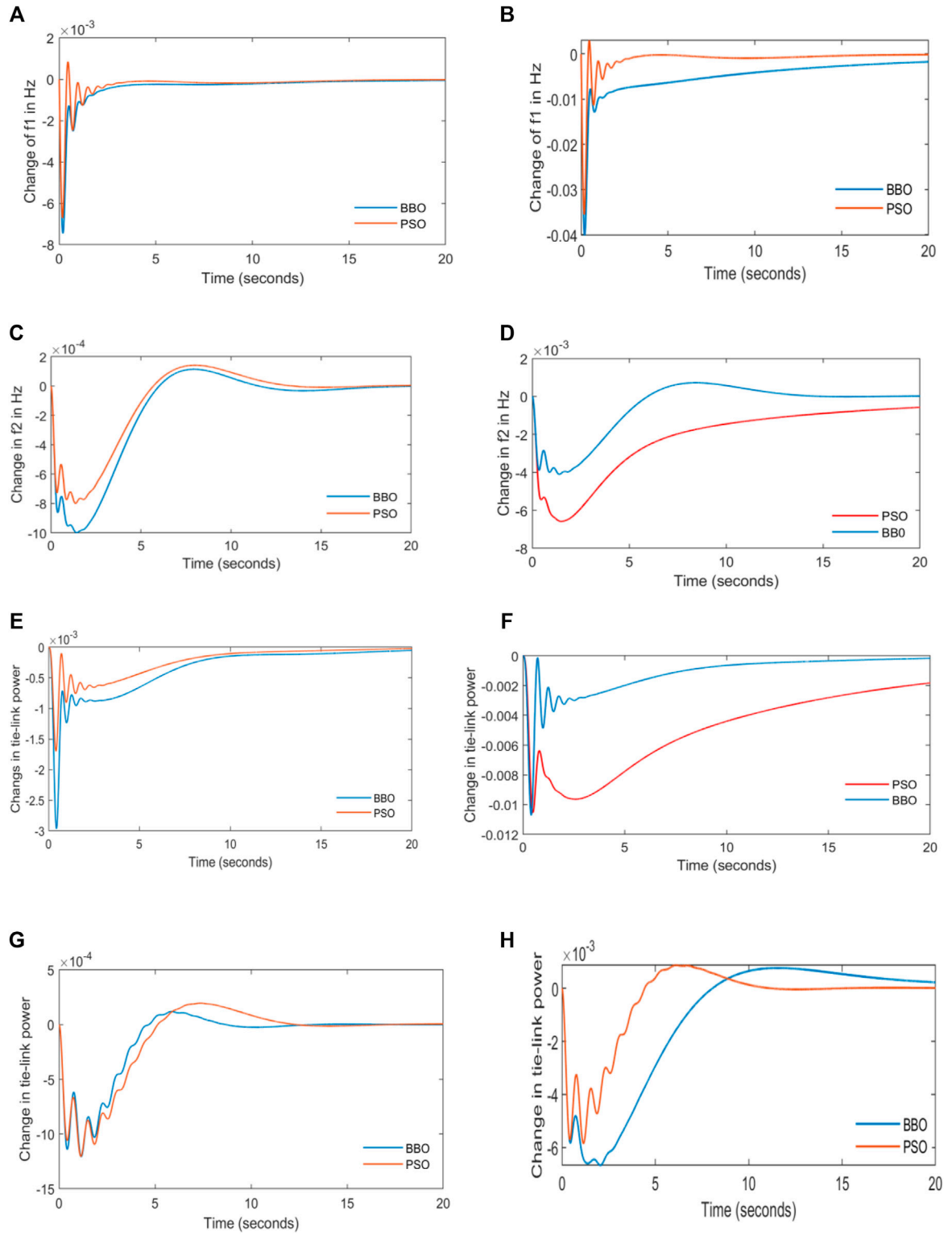

FIGURE 3 | Dynamics of Area-1 and Area-2 with and without HESS for 1% and 5% change in load with VSP-HVDC link. **(A)** Dynamics of f_1 at 1% Load Change with HESS. **(B)** Dynamics of P_{tie} at 1% Load Change with HESS. **(C)** Dynamics of f_2 at 1% Load Change with HESS. **(D)** Dynamics of f_1 at 5% Load Change with HESS. **(E)** Dynamics of P_{tie} at 5% Load Change with HESS. **(F)** Dynamics of f_2 at 5% Load Change with HESS. **(G)** Dynamics of P_{tie} at 1% Load Change without HESS. **(H)** Dynamics of P_{tie} at 5% Load Change without HESS.

link is parallel with the AC tie link, and in scenario-2, the VSP-HVDC link is in parallel with the AC tie link. The PID controller's optimal parameters are achieved by applying a technique known as Simultaneous Coordinated Control (SCC) using PSO and BBO. The objective function minimizes frequency deviation in both the areas along with stable tie-line power exchange.

Scenario-1: With HVDC Link

In this scenario, the two-area interconnected power system has an HVDC link parallel to the AC tie link. The performance of the system is analyzed at load changes of 0.01 and 0.05 pu, respectively. The plots of frequency variation and tie-line power variation are shown in the following content for typical case studies with the presence and absence of the hybrid energy storage system. **Figures 2A,D** represent variations of frequency in area-1 for 0.01 and 0.05 pu change in load. The results show that the BBO algorithm has a minimum first peak with minimum steady-state oscillations and takes less time to reach a steady-state than PSO. The magnitude of frequency deviation is more in the 0.05-pu step load pattern. **Figures 2B,E** represent the tie-line power variation, which explains that the net power schedules between area 1 and area 2 are more stable with BBO.

Figures 2C,F represent variations of frequency in area-2 for 0.01 and 0.05 pu change in load. The results show that the BBO algorithm has a minimum first peak with minimum steady-state oscillations and takes less time to reach a steady-state than PSO. The magnitude of frequency deviation is more in the 0.05-pu step load pattern. **Figures 2G,H** represent the tie-line power variation in the absence of HESS at 0.01 and 0.05 pu load disturbances. The oscillations in tie-line power in the absence of HESS are more than those of the system in HESS's presence.

Scenario-2: With VSP-HVDC Link

The two-area system is modeled with the VSP-HVDC link parallel to the AC tie line, enhancing the system inertia, thereby improving the system stability. **Figures 3A,B** represent the deviation of frequency in area-1 at 0.01 and 0.05 pu step load patterns. The results show that the BBO algorithm has a minimum first peak with minimum steady-state oscillations and takes less time to reach a steady-state than PSO.

Figures 3C,D represent variations of frequency in area-2 for 0.01 and 0.05 pu change in load. The results show that the BBO algorithm has a minimum first peak with minimum steady-state oscillations and takes less time to reach a steady-state than PSO. The magnitude of frequency deviation is more in the 0.05-pu step load pattern. **Figures 3E,F** represent the tie-line power variation at 0.01 and 0.05 pu load change, respectively, which explains that the net power schedules between area 1 and area 2 are more stable with BBO. **Figures 3G,H** represent the tie-line power variation of the system in the absence of the HESS unit in which oscillations are more than those of the system with HESS.

SENSITIVITY ANALYSIS WITH HVDC AND VSP- HVDC LINKS

Sensitivity analysis is performed for the two-area interconnected system with the HVDC link in parallel with the AC tie line, including PHEV and SMES units to demonstrate the robustness of the proposed algorithm by varying the system parameters such as gain (K_P) and time constant (T_P) of the transfer function block of the power system at 0.01 pu load change condition. The value of K_P is set to 120, 140, and 160 and T_P as 10, 15, and 20 in each case, and the system is tuned with the BBO algorithm for the optimal values of the PID controller in the presence and absence of the HESS unit. The variation in frequency and tie-line power for different K_P values are plotted in **Figures 4A–C**.

Figures 4D–F represent the variation of frequency in area-1, area-2, and tie-line power with various values of T_P. From the above plots, it is clear that with the increase in K_P and the decrease in T_P, the oscillations increased enormously, and the settling time also increased, which is undesirable.

Figures 5A–C represent the plots with the variation of K_P. **Figures 5D–F** represent the plots with the variation of T_P. It is observed that the settling time is much improved, and oscillations decreased with virtual inertia emulation when compared to the standard HVDC line. It is also observed that the change in T_P affects the system parameters compared to the change in K_P.

The performance of the system is determined by the first peak overshoot value of area-1 and area-2 frequencies (Δf_{1peak},Δf_{2peak}), first peak overshoot of change in tie-line power ($\Delta P_{(tie\text{-}peak)}$), settling time ($t_s$), the highest possible peak value in tie-line power variation ($\Delta P_{(tie\text{-}high)}$) and its corresponding time (t_p), steady-state error (e_{ss}), and oscillations, which are enlisted in the following tables.

Tables 1, **2** represent the variation of system parameters under 0.01 and 0.05 pu load changes when the system is optimized with PSO and BBO for HVDC and VSP-HVDC interconnected lines. From **Table 1**, the change in peak frequency of area-1 of the system with PSO is 7.46*10−3 Hz and improved with BBO optimization up to 6.7*10−3 Hz for 1% load change. The settling time of the area-1 proposed model when optimized with BBO is 19.70 s for 5% load change, whereas it is 68 s with PSO optimization. It can be noted that the system optimized with BBO gives better results with low peak overshoot and less settling time, indicating the fast recovery of the system to its stable operating point. The maximum peak overshoot in the tie-line power is reduced with BBO optimization.

VSP-HVDC line inclusion in the system improves the transient stability compared to the HVDC line, evident from the decrease in peak overshoot and settling time. The role of SMES is pivotal in damping oscillations, which is evident from the above analysis. The steady-state error is zero due to the presence of a PID controller in both areas. From **Table 2**, it is observed that the peak value of change in frequency of area-2 of the proposed interconnected system incorporated with HESS is 2.97*10−3 Hz with PSO, and it is decreased to 1.70*10−3 Hz with BBO optimization for 1% load change case. Also $\Delta P_{(tie\text{-}peak)}$ for 5% load change is 5.36*10−4 MW with the HESS unit, and it is increased to 5.66*10−4 MW when the HESS unit is disconnected, which demonstrates the role of the storage element in the system.

Table 3 represents the sensitivity analysis of the two-area interconnected system, including SMES and PHEV for both HVDC and VSP-HVDC line cases and their respective performance at a 1% load change condition with K_P's variation and T_P optimized with BBO technique.

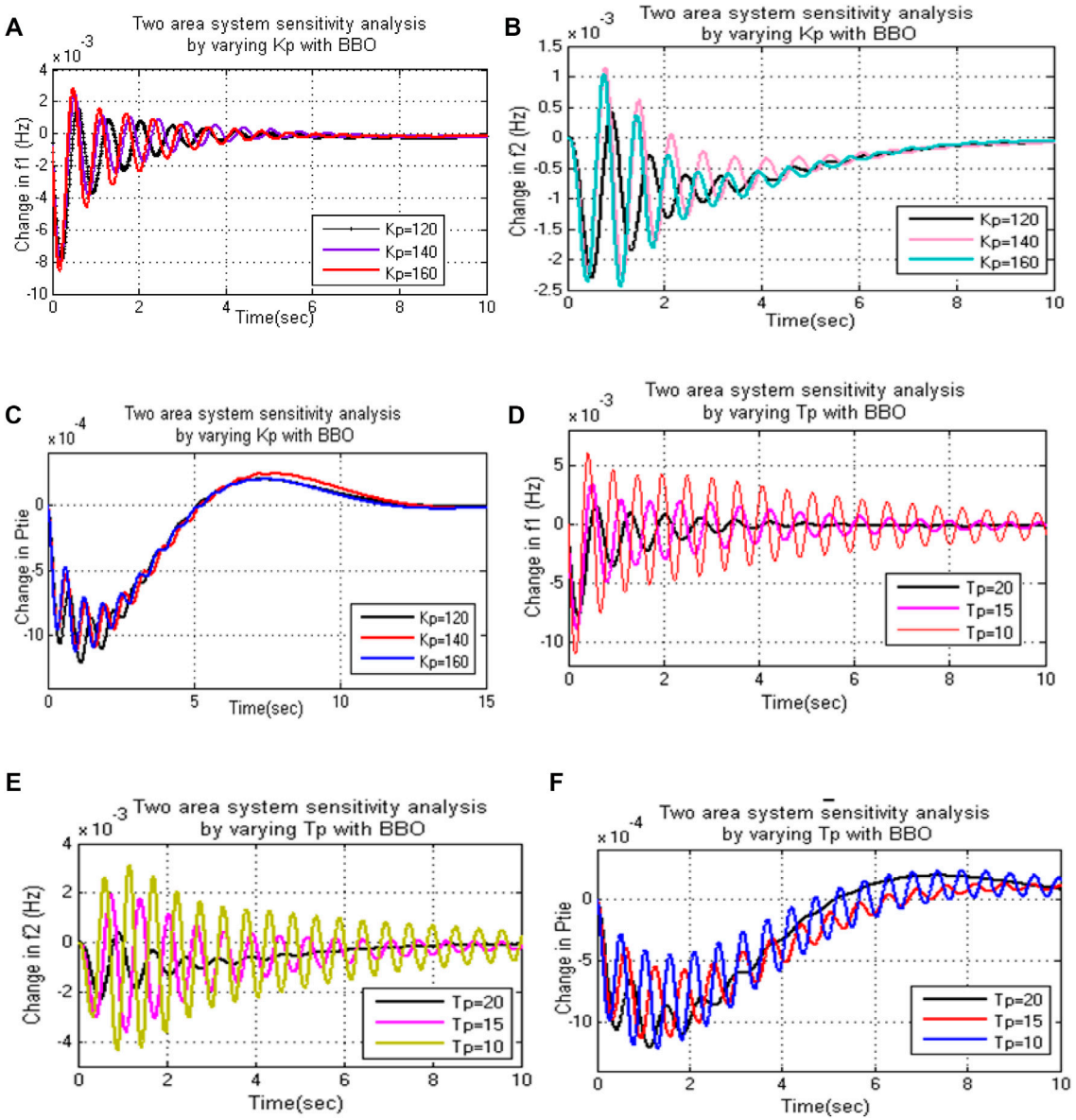

FIGURE 4 | Sensitivity analysis in the presence of HVDC link. **(A)** Effect of variation of Kp on f_1. **(B)** Effect of variation of Kp on f_2. **(C)** Effect of variation of Kp on P_{tie}. **(D)** Effect of variation of Tp on f_1. **(E)** Effect of variation of Tp on f_2. **(F)** Effect of variation of Tp on P_{tie}.

With an increase in K_P and decrease in T_P, the peak overshoot of frequency and tie-line power increased, indicating the decrease in transient stability. For the case of $T_p = 15$, the peak change in tie-line power is recorded as 0.98*10–4 MW for the HVDC tie line, whereas it is decreased to 0.85*10–4 MW with the VSP-HVDC line, which demonstrates the effect of virtual inertia emulation into the system.

CONCLUSION

The penetration of a large number of renewable units with low inertia in the present-day power systems is the severe cause for disturbing the system inertia. This criterion may lead to system frequency and tie-line power to move out of limits leading to transient instability, which is undesirable. This explains the need for virtual inertia emulation to build a secure and stable power system. This study presents a novel model of AGC of an interconnected system incorporated with the SMES and PHEV units in each area. PHEV aids in the LFC problem and SMES serve to supply energy for the virtual inertia emulation process and damp oscillations. On the other hand, PHEVs are pollution-free, which is very desirable in the present-day situation.

The performance of the two-area interconnected system is investigated with two discrete transmission lines since the transmission line plays a pivotal role in power exchange between different areas in an interconnected model. HVDC

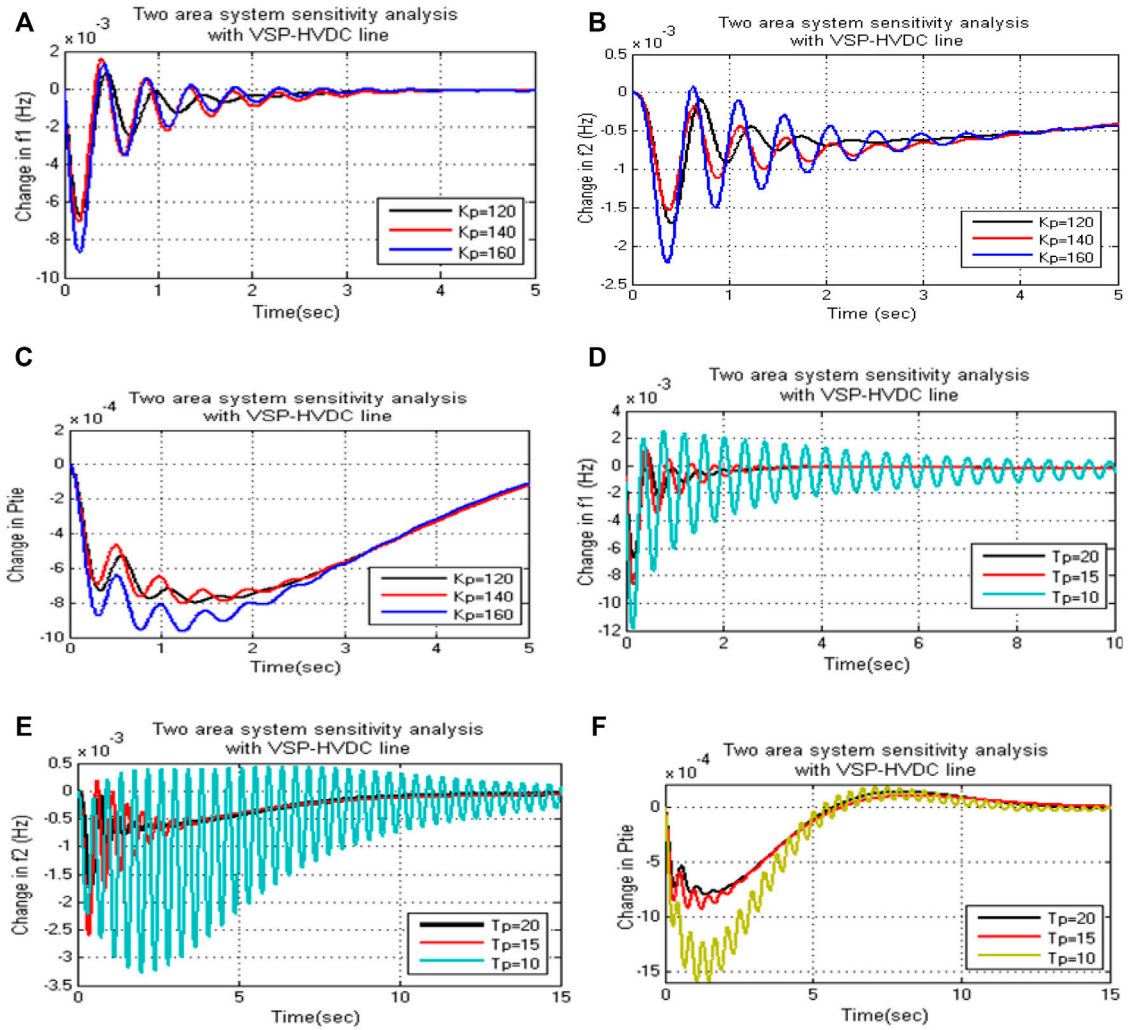

FIGURE 5 | Sensitivity analysis in the presence of VSP-HVDC link. **(A)** Effect of variation of Kp on f_1. **(B)** Effect of variation of Kp on f_2. **(C)** Effect of variation of Kp on P_{tie}. **(D)** Effect of variation of Tp on f_1. **(E)** Effect of variation of Tp on f_2. **(F)** Effect of variation of Tp on P_{tie}.

TABLE 1 | Performance analysis of the two-area interconnected system with HVDC link.

Technique used	HESS Unit	ΔP_L	Δf_{1peak} (10–3 Hz)	t_s (sec)	Δf_{2peak} (10–3Hz)	t_s (sec)	$\Delta P_{tie-peak}$ (10–4 MW)	t_s (sec)	$\Delta P_{tie-high}$ (10–4 MW)	t_p (sec)
PSO	Present	0.01	9.4112	15.74	6.1729	15.4	1.1486	16.5	1.2225	1.15
BBO		0.01	7.8653	24.80	2.2929	28.2	1.0652	25.6	1.2111	1.13
PSO		0.05	42.600	68.00	10.300	88.0	5.8123	82.0	6.9273	2.02
BBO		0.05	41.100	19.70	11.200	34.0	5.5900	24.8	6.0545	1.15
PSO	Absent	0.01	7.3482	26.30	3.0567	29.7	0.9074	25.3	1.3277	1.72
BBO		0.01	8.0545	11.70	2.7387	16.9	1.0949	17.0	1.1651	1.15
PSO		0.05	44.100	14.00	18.800	18.0	5.9236	21.2	6.3613	1.17
BBO		0.05	40.100	25.00	26.600	22.6	4.2280	26.8	4.7717	0.98

TABLE 2 | Performance analysis of the two-area interconnected system with VSP-HVDC line.

Technique used	HESS Unit	ΔP_L	Δf_{1peak} (10–3 Hz)	t_s (sec)	Δf_{2peak} (10–3 Hz)	t_s (sec)	$\Delta P_{tie-peak}$ (10–4 MW)	t_s (sec)	$\Delta P_{tie-high}$ (10–4 MW)	t_p (sec)
PSO	Present	0.01	7.4615	30.4	2.9786	38.0	0.8662	28.3	0.9978	1.43
BBO		0.01	6.7220	25.8	1.7059	32.3	0.7305	27.5	0.7994	1.37
PSO		0.05	39.800	58.5	10.400	73.1	5.3638	66.0	6.5614	1.51
BBO		0.05	35.100	28.8	10.500	34.6	3.8314	27.7	4.0863	1.40
PSO	Absent	0.01	8.0337	16.0	3.5678	20.7	1.0143	24.2	1.3768	1.50
BBO		0.01	7.4239	12.0	2.3160	15.5	0.8879	77.0	0.9278	0.94
PSO		0.05	40.700	39.6	11.600	48.8	5.6688	45.7	7.0924	1.51
BBO		0.05	38.600	14.0	13.600	17.5	4.5691	92.0	4.7316	0.96

TABLE 3 | Sensitivity analysis of the presented two-area system.

TIE LINE	Varying		Δf_{1peak} (10^{-3} Hz)	t_s (sec)	Δf_{2peak} (10^{-3} Hz)	t_s (sec)	$\Delta P_{tie-peak}$ (10^{-4} MW)	t_s (sec)	$\Delta P_{tie-high}$ (10^{-4} MW)	t_p (sec)
HVDC	Kp	120	7.8653	24.8	2.2129	28.2	1.0652	25.6	1.2111	1.13
		140	8.0823	25.6	2.2966	30.0	0.9548	25.2	1.1098	1.00
		160	8.6156	22.0	2.3536	31.4	0.9574	26.9	1.1180	0.95
	Tp	20	7.8653	24.8	2.2929	28.2	1.0652	25.6	1.2111	1.13
		15	8.9764	29.0	3.0285	30.7	0.9835	30.8	1.1407	0.95
		10	11.000	41.0	3.0187	36.1	0.9970	35.2	1.1292	1.32
VSP-HVDC	Kp	120	6.7220	25.8	1.7059	32.3	0.7305	27.5	0.7994	1.37
		140	7.0282	25.8	1.5382	33.2	0.6908	24.9	0.8050	1.23
		160	6.6718	24.2	2.2144	33.1	0.8748	26.4	0.9673	1.23
	Tp	20	6.7220	25.8	1.7059	32.3	0.7305	27.5	0.7994	1.37
		15	8.6514	23.8	2.6049	39.9	0.8549	27.0	0.9306	1.23
		10	11.900	32.9	2.2189	38.3	1.0894	84.9	1.5976	1.09

line in parallel with the AC line and VSP-HVDC line in parallel with the AC line are placed separately, and the system is optimized in each case with PSO and BBO techniques by simultaneous coordinated tuning of the secondary controller and SMES unit. Sensitivity analysis is also performed for each scenario. Results indicate that with virtual inertia emulation, the system's transient stability is improved when the system, including PHEV and SMES, is optimized with BBO. The high penetration levels of electric vehicles can lead to stability issues in the interconnected power systems. The EV charging demand needs to be carefully monitored for optimal operation of interconnected power systems. The authors would like to extend the work by increasing different penetration levels of the plug-in hybrid electric vehicles and evaluate the various combinations of hybrid energy storage systems by integrating communication delays, analyzing the filter requirements, and demanding response services offered by the load. The authors would like to add that if the total generation demanded by the load is met by renewable energy sources, the system would be sustainable (Nallapaneni and Chopra, 2021).

DATA AVAILABILITY STATEMENT

The original contributions presented in the study are included in the article/**Supplementary Material**, further inquiries can be directed to the corresponding author.

AUTHOR CONTRIBUTIONS

NS: conceptualization, methodology, validation, formal analysis, investigation, data curation, writing—original draft, and visualization. NB: resources, supervision, and writing—review and editing. SM: resources, supervision, and writing—review and editing.

SUPPLEMENTARY MATERIAL

The Supplementary Material for this article can be found online at: https://www.frontiersin.org/articles/10.3389/fenrg.2022.845686/full#supplementary-material

REFERENCES

Abd-Elazim, S. M., and Ali, E. S. (2016). Load Frequency Controller Design via BAT Algorithm for Nonlinear Interconnected Power System. *Int. J. Electr. Power Energ. Syst.* 77, 166–177. doi:10.1016/j.ijepes.2015.11.029

Anil Kumar, T., Venu, G., and Venkata Ramana, N. (2016). "Load Frequency Control of Multi Area Power System in Deregulated Environment with Robust Controllers in Coordination with Frequency Controllable HVDC Link," in International Conference on Energy Efficient Technologies for Sustainability, 473–478. doi:10.1109/iceets.2016.7583801

Annamraju, A., and Nandiraju, S. (2019). Coordinated Control of Conventional Power Sources and PHEVs Using Jaya Algorithm Optimized PID Controller for Frequency Control of a Renewable Penetrated Power System. *Prot. Control. Mod. Power Syst.* 4, 28. doi:10.1186/s41601-019-0144-2

Barisal, A. K., and Mishra, S. (2018). Improved PSO Based Automatic Generation Control of Multi-Source Nonlinear Power Systems Interconnected by AC/DC Links. *Cogent Eng.* 5, 1422228. doi:10.1080/23311916.2017.1422228

Bhatt, P., Roy, R., and Ghoshal, S. P. (2010). "GA/Particle Swarm Intelligence Based Optimization of Two Specific Varieties of Controller Devices Applied to Two-Area Multi-Units Automatic Generation Control. *Int. J. Electr. Power Energy Syst.* 32 (4), 299–310. doi:10.1016/j.ijepes.2009.09.004

Elyas, R., Remon, D., Cantarellas, A. M., Rouzbehi, K., and Rodriguez, P. (2014). "Integration of Renewable Generation for Frequency Support of HVDC/AC Interconnected Systems under Power Market Scenario," in IEEE PES General Meeting Conference & Exposition, 1–5.

Guha, D., Roy, P. K., and Banerjee, S. (2017). Study of Differential Search Algorithm Based Automatic Generation Control of an Interconnected thermal-thermal System with Governor Dead-Band. *Appl. Soft Comput.* 52, 160–175. doi:10.1016/j.asoc.2016.12.012

Hari Kumar, R., and Ushakumari, S. (2014). "Biogeography Based Tuning of PID Controllers forLoad Frequency Control in Microgrid," in International Conference on Circuits, Power and Computing Technologies [ICCPCT-2014], 797–802. doi:10.1109/iccpct.2014.7054992

Ibraheem, P. K., and Kothari, D. P. (2005). Recent Philosophies of Automatic Generation Control Strategies in Power Systems. *IEEE Trans. Power Syst.* 20 (No. 1), 346–357.

Johnson, Teena., and Shubhanga, K. N. (2016). "Loop Flow Performance of Interconnected Power Systems with HVDC Links," in IEEE 1st International Conference on Power Electronics, Intelligent Control and Energy Systems, 1–6. doi:10.1109/icpeices.2016.7853342

Kachhwaha, A., Pandey, S. K., Dubey, A. K., and Gupta, S. (2016). "Interconnected Multi-Unit Two-area Automatic Generation Control Usingoptimal Tuning of Fractional Order PID Controller along with Electrical Vehicle Loading," in IEEE 1st International Conference on Power Electronics, Intelligent Control and Energy Systems, 1–5. doi:10.1109/icpeices.2016.7853167

Kouba, N. E. Y., Menaa, M., Hasni, M., and Boudour, M. (2015). "Optimal Control of Frequency and Voltage Variations Using PID Controller Based on Particle Swarm Optimization," in 2015 4th international conference on systems and control (Sousse, Tunisia: ICSC), 424–429. doi:10.1109/icosc.2015.7152777

llias, H., Fikri, A., and Zahari, M. (2016). Optimisation of PID Controller for Load Frequency Controller in Two-Area Power System Using Evolutionary Particle Swarm Optimisation. *Int. J. Elect. Syst.* 12 (2), 315–324.

Madasu, S. D., Kumar, M. L. S. S., and Singh, A. K. (2017). Comparable Investigation of Backtracking Search Algorithm in Automatic Generation Control for Two Area Reheat Interconnected thermal Power System. *Appl. Soft Comput.* 55, 197–210. doi:10.1016/j.asoc.2017.01.018

Madasu, S. D., Sai Kumar, M. L. S., and Singh, A. K. (2018). A Flower Pollination Algorithm Based Automatic Generation Control of Interconnected Power System. *Ain Shams Eng. J.* 9, 1215–1224. doi:10.1016/j.asej.2016.06.003

Molina, M. G., and Mercado, P. E. (2011). Power Flow Stabilization and Control of Microgrid with Wind Generation by Superconducting Magnetic Energy Storage. *IEEE Trans. Power Electron.* 26 (3), 910–922. doi:10.1109/tpel.2010.2097609

Musio, M., and Damiano, A. (2012). *A Virtual Power Plant Management Model Based on Electric Vehicle Charging Infrastructure Distribution*. 3rd IEEE PES Innovative Smart Grid Technologies Europe (ISGT Europe), 1–7. doi:10.1109/ISGTEurope.2012.6465684

Nallapaneni, M. K., and Chopra, S. S. (2021). "Electric Vehicles Participation in Load Frequency Control of an Interconnected Power System Is Not Sustainable," in 6th AIEE Energy Symposium Current and Future Challenges to Energy Security: the energy transition, a pathway from low carbon to decarbonization.

Oshnoei, A., Khezri, R., Muyeen, S. M., Oshnoei, S., and Blaabjerg, F. (2019). Automatic Generation Control Incorporating Electric Vehicles. *Electric Power Components Syst.* 47, 720–732. doi:10.1080/15325008.2019.1579270

Pham, D. T., Huynh, T. T. B., and Dang, M. C. (2016). "An Improving of Migration Operator in Biogeography-Based Optimization for Solving Traveling Salesman Problem," in International Conference on Computational Intelligence and Cybernetics, 33–40.

Pham, T. N., Trinh, H., and Hien, L. V. (2016). Load Frequency Control of Power Systems with Electric Vehicles and Diverse Transmission Links Using Distributed Functional Observers. *IEEE Trans. Smart Grid* (7), 238–252. doi:10.1109/tsg.2015.2449877

Prakash, S., and Sinha, S. K. (2018). ALFC of Hybrid Multi-Generation Power System Using UC and TCPS by ANFIS Control Technique. *Int. J. Elect.* 106, 174–211. doi:10.1080/00207217.2018.1519857

Rahman, A., Chandra Saikia, L., and Sinha, N. (2015). *Load Frequency Control of a Hydro-thermal System under Deregulated Environment Using Biogeography-Based Optimized Three Degree-Of-freedom Integral-Derivative Controller*. IET Generation, Transmission & Distribution, 2284–2293. doi:10.1049/iet-gtd.2015.0317

Rakhshani, E., Remon, D., Mir Cantarellas, A., Martinez Garcia, J., and Rodriguez, P. (2017). Virtual Synchronous Power Strategy for Multiple HVDC Interconnections of Multi-Area AGC Power Systems. *IEEE Trans. Power Syst.* 32 (3), 1665–1677. doi:10.1109/tpwrs.2016.2592971

Rakhshani, E., Remon, D., Mir Cantarellas, A., and Rodriguez, P. (2016). Analysis of Derivative Control Based Virtual Inertia in Multi-Area High-Voltage Direct Current Interconnected Power Systems". *IET Gener. Transm. Distrib.* 10 (6), 1458–1469. doi:10.1049/iet-gtd.2015.1110

Roy, A., Dutta, S., and Roy, P. K. (2014). "Automatic Generation Control by SMES-SMES Controllers of Two-Area Hydro-Hydro System," in 1st International Conference on Non-Conventional Energy (ICONCE 2014), 302–307. doi:10.1109/ICONCE.2014.6808731

Rupali, R. K., and Chaphekar, S. N. (2015). "Particle Swarm Optimization Based PI Controller for Two Area Interconnected Power System," in International Conference on Energy Systems and Applications, 496–500.

Shankar, G., and Mukherjee, V. (2016). Load Frequency Control of an Autonomous Hybrid Power System by Quasi-Oppositional harmony Search Algorithm. *Int. J. Electr. Power Energ. Syst.* 78, 715–734. doi:10.1016/j.ijepes.2015.11.091

Sivadanam, N., Nagu, B., and Sydulu, M. (2020). Inertial Response and Frequency Control in Electric Vehicles Integrated Renewable and Non-renewable Power System. *J. Green Eng.* 10 (11), 10981–10993.

Sivadanam, N., Nagu, B., and Sydulu, M. (2020). Performance Optimization of an Interconnected Power System in the Presence of Plug-In Hybrid Electric Vehicles. *J. Green Eng.* 10 (9), 4910–4925.

Sivadanam, N., Bhookya, N., and Maheswarapu, S. (2021). Dynamic Performance Enhancement of Interconnected Hybrid Thermal Power System in the Presence of Electric Vehicles. *Case Stud. Therm. Eng.* 26, 101045. doi:10.1016/j.csite.2021.101045

Sivalingam, R., Chinnamuthu, S., and Dash, S. S. (2017). A Hybrid Stochastic Fractal Search and Local Unimodal Sampling Based Multistage PDF Plus (1 + PI) Controller for Automatic Generation Control of Power Systems. *J. Franklin Inst.* 354, 4762–4783. doi:10.1016/j.jfranklin.2017.05.038

Yang, S., Huang, C., Yu, Y., Yue, D., and Xie, J. (2017). *Load Frequency Control of Interconnected Power System via Multi-Agent System Method*, 45, 839–851. doi:10.1080/15325008.2015.1131764Load Frequency Control of Interconnected Power System via Multi-Agent System Method*Electric Power Components Syst.*

Zhu, J., Campbell, D. B., Grain, P. A., and AndrewChris, J. R. G. B. (2013). Inertia Emulation Control Strategy for VSC-HVDC Transmission Systems. *IEEE Trans. Power Syst.* (28), 1277–1287. doi:10.1109/tpwrs.2012.2213101

Conflict of Interest: The authors declare that the research was conducted in the absence of any commercial or financial relationships that could be construed as a potential conflict of interest.

Publisher's Note: All claims expressed in this article are solely those of the authors and do not necessarily represent those of their affiliated organizations, or those of the publisher, the editors, and the reviewers. Any product that may be evaluated in this article, or claim that may be made by its manufacturer, is not guaranteed or endorsed by the publisher.

frontiers | Frontiers in Energy Research

ORIGINAL RESEARCH
published: 30 May 2022
doi: 10.3389/fenrg.2022.870850

High-Performance Sensorless Operation of Motor-Generator Set With an Improved Torque-Ripple Minimization Strategy

Mohamed G. Hussien[1]*, *Zakaria M. Salem Elbarbary*[2,3] *and Abd El-Wahab Hassan*[1,4]

[1]Department of Electrical Power and Machines Engineering, Faculty of Engineering, Tanta University, Tanta, Egypt, [2]Electrical Engineering Department, College of Engineering, King Khalid University, Abha, Saudi Arabia, [3]Electrical Power and Machines Department, Collage of Engineering, Kafrelsheikh University, Kafrelsheikh, Egypt, [4]Department of Electrical Power and Machines Engineering, Higher Institute of Engineering (HIE), El-Shorouk Academy, El-Shorouk City, Egypt

OPEN ACCESS

Edited by:
Nallapaneni Manoj Kumar,
City University of Hong Kong, Hong Kong SAR, China

Reviewed by:
Mukesh Kumar,
Indian School of Mines, India
Narottam Das,
Central Queensland University, Australia
Tian-Hua Liu,
National Taiwan University of Science and Technology, Taiwan

***Correspondence:**
Mohamed G. Hussien
mohamed.hussien3@f-eng.tanta.edu.eg

Specialty section:
This article was submitted to Sustainable Energy Systems and Policies, a section of the journal Frontiers in Energy Research

Received: 07 February 2022
Accepted: 19 April 2022
Published: 30 May 2022

Citation:
Hussien MG, Salem Elbarbary ZM and Hassan AE-W (2022) High-Performance Sensorless Operation of Motor-Generator Set With an Improved Torque-Ripple Minimization Strategy. Front. Energy Res. 10:870850. doi: 10.3389/fenrg.2022.870850

This paper aims at minimizing the torque ripples using variable switching frequency technique of PWM (VSFPWM) of the surface-mounted permanent magnet synchronous motor (SPMSM) for a high-performance operation of a motor-generator set. The proposed system was employed to drive the promising brushless doubly-fed reluctance generator (BDFRG) with a sensorless vector-control topology. Validity of the rotor-position/speed estimation critically affects most of the sensorless control strategies. Therefore, a simple estimation method is proposed for the positioning of rotor of the generator. The presented control strategies are confirmed with some of the obtained results to assure its controllability.

Keywords: SPMSM, ripple prediction of torque, VSFPWM, BDFRG, sensorless vector-control

INTRODUCTION

The surface-mounted permanent magnet synchronous motor (SPMSM) is very attractive type nowadays in drive systems for its numerous advantages such as, high efficiency, high torque to inertia ratio, high power density, reliability, and long life (Pandav et al., 2017a). In addition, the surface-mounted PMSM is preferred than the other type interior permanent magnet synchronous motor (IPMSM) because of its lower cost due to its simple rotor design (the permanent magnet (PM) material in SPMSM is mounted on the rotor, not inside the rotor as in the case of IPMSM). The motor-generator set is very spreading in most applications such as elevators, hybrid vehicles, and high-frequency machines (Hussien and Hassan, 2019). In the context of electric power generation and large fixed electrical power systems, a motor–generator consists of an electric motor mechanically coupled to an electric generator (or alternator) (Chokkalingam et al., 2019; Bharatiraja et al., 2017). The motor runs on the electrical input current while the generator creates the electrical output current, with power flowing between the two machines as a mechanical torque; this provides electrical isolation and some buffering of the power between the two electrical systems (Pandav et al., 2017b; Sanjeevikumar et al., 2016). In this paper, the motor-generator set can be arranged as using the SPMSM as the prime mover for a generator with doubly-fed type. For the motor side, the SPMSM is supplied with a voltage-source inverter (VSI) as given in **Figure 1**.

Power electronic converter acts as an interface between the electric generator and the utility grid to adjust the generator speed of the turbine. Hence, the converter rating has to be as same

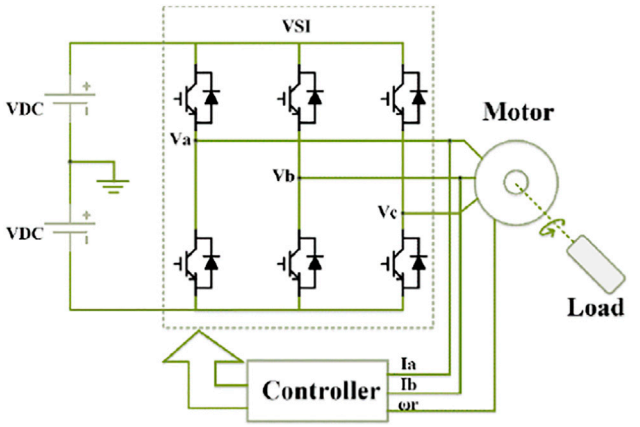

FIGURE 1 | Inverter-fed SPMSM system.

as that of the generator which consequently increases the overall system cost. In order to reduce the converter rating, the slip recovery machines can be used. The converter of these machines processes only the slip power in the rotor circuit resulting in a significant cost reduction compared to the full-capacity generating systems. These features have made the doubly-fed induction generators widely popular and attracting great attention from researchers (Xu et al., 2021).

Recently, Brushless Doubly-Fed Induction Machine (BDFIM) and the Brushless Doubly-Fed Reluctance Machine (BDFRM) have gained attention from researchers due to their self-cascaded arrangements (Xu et al., 2020). Although, both machines have common merits, the efficiency of the BDFRM is better than that of the BDFIM because of absence of rotor copper loss. Therefore, the Brushless Doubly-Fed Reluctance Generator (BDFRG) is preferable for variable-speed generating systems. Usually, BDFRG has two isolated windings arranged in the same fixed frame, i.e. the power winding (PW) and the control winding (CW). The PW is considered as the primary winding with a direct connection to the load/grid side. Furthermore, the CW is considered as the secondary winding which is generally connected through a bi-directional power electronic converter with the load/grid side (Chinthamalla et al., 2016; Hussien et al., 2022).

Different control techniques such as scalar control, vector control, and direct torque control are proposed for BDFRG. Out of various control strategies, the vector-control technique is preferred for high performance operation. The different techniques of vector control are mainly focused on the BDFRG rotor-position measurement aided with a rotor-position/speed encoder (Mousa et al., 2018). The required rotor position signal is needed to realize the desired angle of frame transformation for CW-side variables. The rotor-position/speed encoder increases cost and reliability problems which makes it undesirable in most drive systems. In recent years, sensorless vector-control strategies are adopted for estimation of rotor position/speed from the currents and voltages of the machine (Boldea et al., 2021; Kumar et al., 2019; Kumar and Das, 2018).

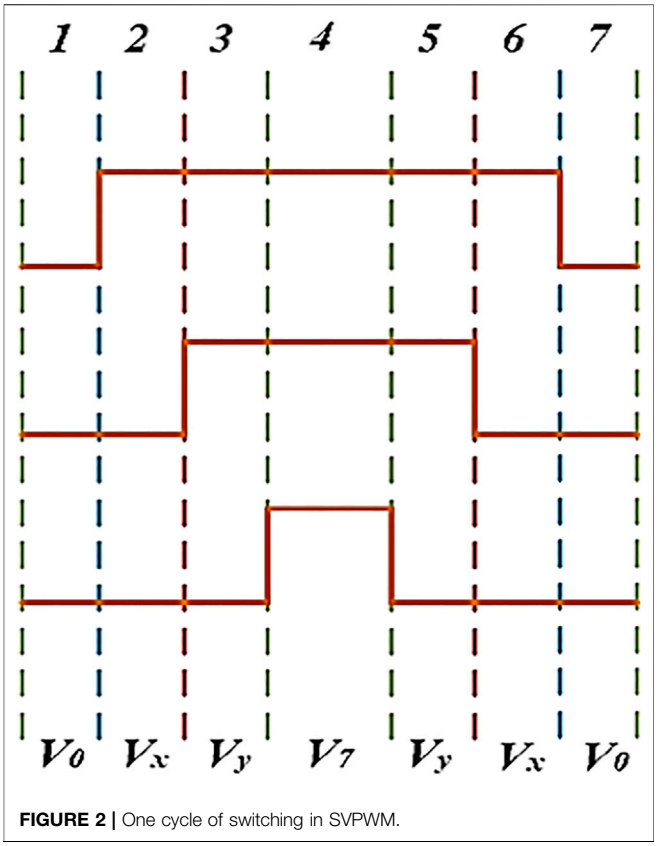

FIGURE 2 | One cycle of switching in SVPWM.

For an efficient operation of the adopted motor-generator set, this paper aims to apply the variable switching frequency PWM (VSFPWM) method for torque ripple control of the motor side (SPMSM). In addition, for the generator side (BDFRG), a new sensorless vector-control is applied and investigated for a high performance of the presented motor-generator system.

TORQUE RIPPLES MINIMIZATION CONTROL FOR SPMSM

Prediction of Current Ripple

The prediction of ripple in current is described as follows (Fei Wang and Wang, 2014; Hussien et al., 2020; Jiang and Wang, 2013).

$$\begin{bmatrix} v_{a_s} \\ v_{b_s} \\ v_{c_s} \end{bmatrix} = \begin{bmatrix} d_a^{'} \\ d_b^{'} \\ d_c^{'} \end{bmatrix} \cdot \frac{V_{dc-Link}}{2} \tag{1}$$

Aided with the SVPWM, **Figure 2**, the current ripple changes in each one cycle will considered as in **Figure 3**.

As shown in **Figure 4**, the slope of phase-A current is derived, during different zones, as

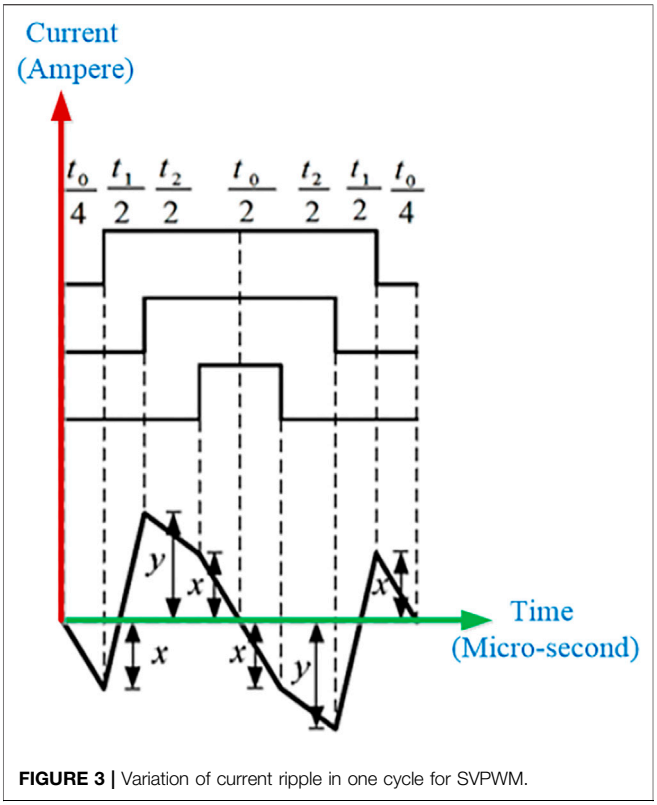

FIGURE 3 | Variation of current ripple in one cycle for SVPWM.

$$\frac{di_{a_s}}{dx} = \frac{2}{3L_s}\left(\frac{v_{b_s} + v_{c_s}}{2} - v_{a_s}\right) \tag{2}$$

$$\frac{di_{a_s}}{dx} = \frac{V_{dc-Link}}{3L_s}\left(\frac{d_b^{'} + d_c^{'}}{2} - d_a^{'}\right) \tag{3}$$

$$\frac{di_{a_s}}{dx} = \frac{2V_{dc-Link}}{3L_s}\left(1 + \frac{d_b^{'} + d_c^{'}}{4} - \frac{d_a^{'}}{2}\right) \tag{4}$$

$$\frac{di_{a_s}}{dx} = \frac{2V_{dc-Link}}{3L_s}\left(\frac{1}{2} + \frac{d_b^{'} + d_c^{'}}{4} - \frac{d_a^{'}}{2}\right) \tag{5}$$

$$\frac{di_{a_s}}{dx} = \frac{V_{dc-Link}}{3L_s}\left(\frac{d_b^{'} + d_c^{'}}{2} - d_a^{'}\right) \tag{6}$$

With the same principles, the slope of ripples for all phase currents can be given as in **Table 1** (Hussien et al., 2020). The peak level of the slope can be given as in **Eq. 7** with the values x and y to be plus or minus signs.

$$\begin{cases} x = k_1 \,.\, \dfrac{t_o}{4} \\ y = k_1 \,.\, \dfrac{t_o}{4} + k_2 \,.\, \dfrac{t_1}{2} \end{cases} \tag{7}$$

Prediction of Torque Ripple

The relationship between current ripple and PWM torque ripple is given as (Fei Wang and Wang, 2014).

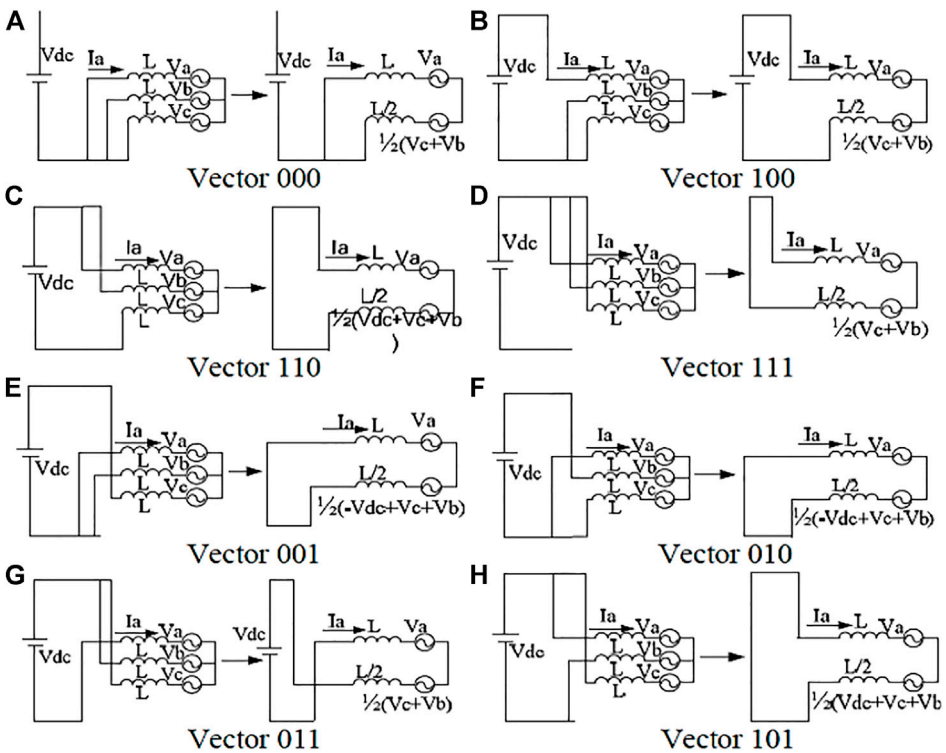

FIGURE 4 | Corresponding circuits for all vectors.

TABLE 1 | Slope of current ripple for the three phases (Hussien et al., 2020).

Vector	Phase_A	Phase_B	*Phase_C*
000	$V_{dc-Link}\ 3L_s\ (d'_b + d'_c/2 - d'_a)$	$V_{dc-Link}/\ 3L_s\ (d'_a + d'_c/2 - d'_b)$	$V_{dc-Link}/\ 3L_s\ (d'_b + d'_a/2 - d'_c)$
100	$2V_{dc-Link}/\ 3L_s\ (1 + d'_b + d'_c/4 - d'_a/2)$	$V_{dc-Link}/\ 3L_s\ (d'_a + d'_c/2 - 1 - d'_b)$	$V_{dc-Link}/\ 3L_s\ (d'_b + d'_a/2 - 1 - d'_c)$
110	$2V_{dc-Link}/\ 3L_s\ (1/2 + d'_b + d'_c/4 - d'_a/2)$	$2V_{dc-Link}/\ 3L_s\ (1/2 + d'_a + d'_c/4 - d'_b/2)$	$2V_{dc-Link}/\ 3L_s\ (d'_b + d'_a/4 - 1 - d'_c/2)$
111	$V_{dc-Link}/\ 3L_s\ (d'_b + d'_c/2 - d'_a)$	$V_{dc-Link}/\ 3L_s\ (d'_a + d'_c/2 - d'_b)$	$V_{dc-Link}/\ 3L_s\ (d'_b + d'_a/2 - d'_c)$
001	$V_{dc-Link}/\ 3L_s\ (d'_b + d'_c/2 - 1 - d'_a)$	$V_{dc-Link}/\ 3L_s\ (d'_a + d'_c/2 - 1 - d'_b)$	$2V_{dc-Link}/\ 3L_s\ (1 + d'_b + d'_a/4 - d'_c/2)$
010	$V_{dc-Link}/\ 3L_s\ (d'_b + d'_c/2 - 1 - d'_a)$	$2V_{dc-Link}/\ 3L_s\ (1 + d'_a + d'_c/4 - d'_b/2)$	$V_{dc-Link}/\ 3L_s\ (d'_b + d'_a/2 - 1 - d'_c)$
011	$2V_{dc-Link}/\ 3L_s\ (d'_b + d'_c/4 - 1 - d'_a/2)$	$2V_{dc-Link}/\ 3L_s\ (1/2 + d'_a + d'_c/4 - d'_b/2)$	$2V_{dc-Link}/\ 3L_s\ (1/2 + d'_b + d'_a/4 - d'_c/2)$
101	$2V_{dc-Link}/\ 3L_s\ (1/2 + d'_b + d'_c/4 - d'_a/2)$	$2V_{dc-Link}/\ 3L_s\ (d'_a + d'_c/4 - 1 - d'_b/2)$	$2V_{dc-Link}/\ 3L_s\ (1/2 + d'_b + d'_a/4 - d'_c/2)$

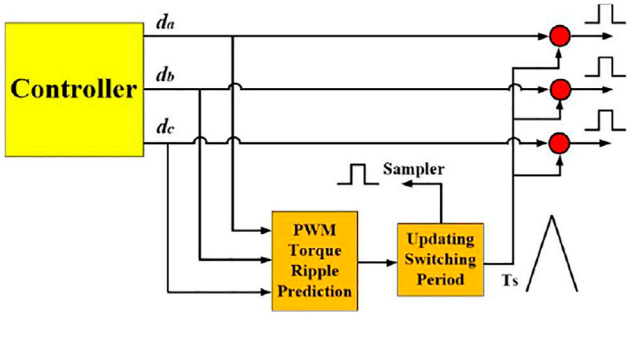

FIGURE 5 | Control diagram of VSFPWM.

$$\begin{bmatrix} \Delta i_{d\_ripple} \\ \Delta i_{q\_ripple} \end{bmatrix} = C_{abc-dq} \begin{bmatrix} \Delta i_{a\_ripple} \\ \Delta i_{b\_ripple} \\ \Delta i_{c\_ripple} \end{bmatrix} \tag{8}$$

where,

$$C_{abc-dq} = \frac{2}{3} \begin{bmatrix} \cos\theta & \cos\left(\theta - \frac{2\pi}{3}\right) & \cos\left(\theta + \frac{2\pi}{3}\right) \\ -\sin\theta & -\sin\left(\theta - \frac{2\pi}{3}\right) & -\sin\left(\theta + \frac{2\pi}{3}\right) \end{bmatrix}$$

where Δi_{a_ripple}, Δi_{b_ripple} and Δi_{c_ripple} are a real-time current ripple in *abc* coordinate, Δi_{d_ripple} and Δi_{q_ripple} are the d-q components. The angle, θ indicates the d-axis position.

The PWM torque ripple is obtained as

$$T_{ripple} = \frac{3}{2} p \psi_f \cdot \Delta i_{q\_ripple} \tag{9}$$

Then, the variable switching frequency PWM (VSFPWM) is attained based on the prediction process of torque ripple.

Torque Ripple Control-Based VSFPWM

The criteria of torque ripple minimization used in this paper is specified in **Figure 5**. The switching period can be updated according to the following relation (Hussien et al., 2020).

$$T_s = T_{sN} \cdot \frac{\Delta T_{require}}{\Delta T_{predict}} \tag{10}$$

To assure the effectiveness of the proposed VSFPWM methodology for torque ripple minimization of the SPMSM drive system, some results are given in **Figures 6–8**.

The results ensure the controllability of the presented strategy to minimize the ripples of torque using VSFPWM for the SPMSM drives.

A NEW SENSOLRESS VECTOR-CONTROL STRATEGY OF BDFIG DRIVE SYSTEMS

Dynamic Model of Generator

The complete modeling of BDFRG is presented in literature (Mousa et al., 2018) and briefly described as follows:

The power and control windings' voltage equations in dq-axis and its flux linkage relations can be expressed as:

$$\left.\begin{aligned} v_{d_p} &= r_p i_{d_p} + \frac{d}{dt}\lambda_{d_p} - \omega\lambda_{q_p} \\ v_{q_p} &= r_p i_{q_p} + \frac{d}{dt}\lambda_{q_p} + \omega\lambda_{d_p} \\ v_{d_c} &= r_c i_{d_c} + \frac{d}{dt}\lambda_{d_c} - (\omega_r - \omega)\lambda_{q_c} \\ v_{q_c} &= r_c i_{q_c} + \frac{d}{dt}\lambda_{q_c} + (\omega_r - \omega)\lambda_{d_c} \end{aligned}\right\} \tag{11}$$

where

$$\left.\begin{aligned} \omega &= P_p\,\omega_f \\ \omega_r &= \left(P_p + P_c\right)\omega_{rm} \end{aligned}\right\} \tag{12}$$

$$\left.\begin{aligned} \lambda_{d_p} &= L_p i_{d_p} + L_{pc} i_{d_c} \\ \lambda_{q_p} &= L_p i_{q_p} - L_{pc} i_{q_c} \\ \lambda_{d_c} &= L_c i_{d_c} + L_{pc} i_{d_p} \\ \lambda_{q_c} &= L_c i_{q_c} - L_{pc} i_{q_p} \end{aligned}\right\} \tag{13}$$

where

$$\left.\begin{aligned} L_p &= L_{lp} + \frac{3}{2}L_{mp} \\ L_c &= L_{lc} + \frac{3}{2}L_{mc} \\ L_{pc} &= \frac{3}{2}\mathrm{L}_{\mathrm{pc}_{\max}} \end{aligned}\right\} \tag{14}$$

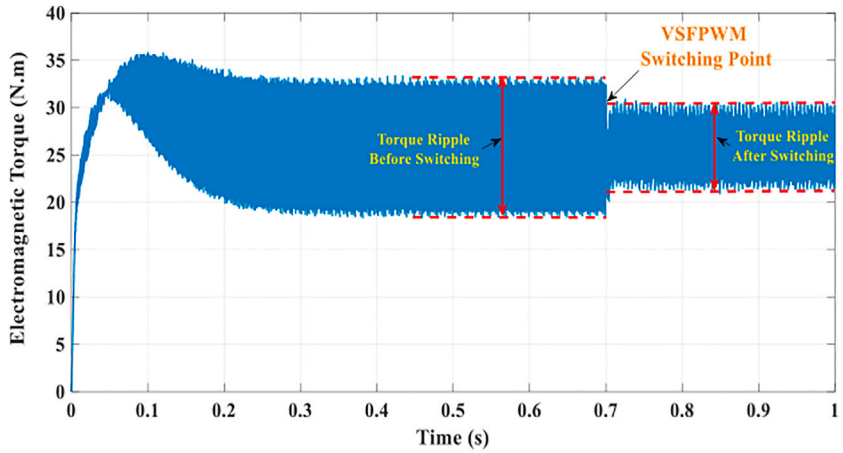

FIGURE 6 | Torque response.

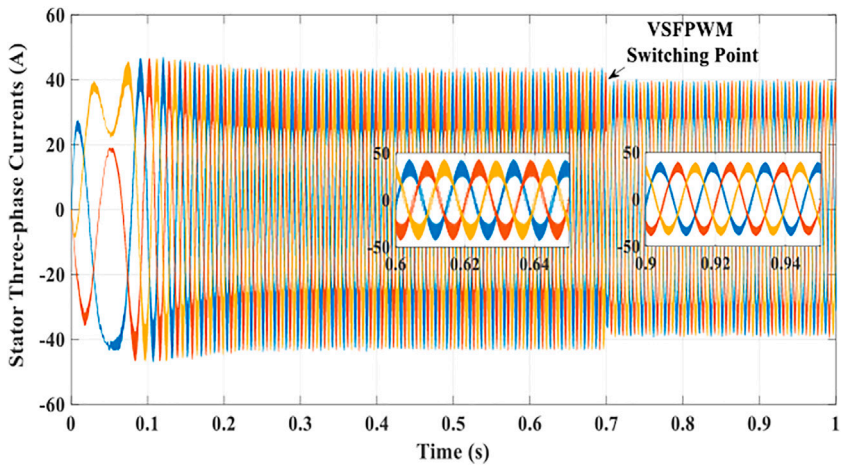

FIGURE 7 | Responses of currents.

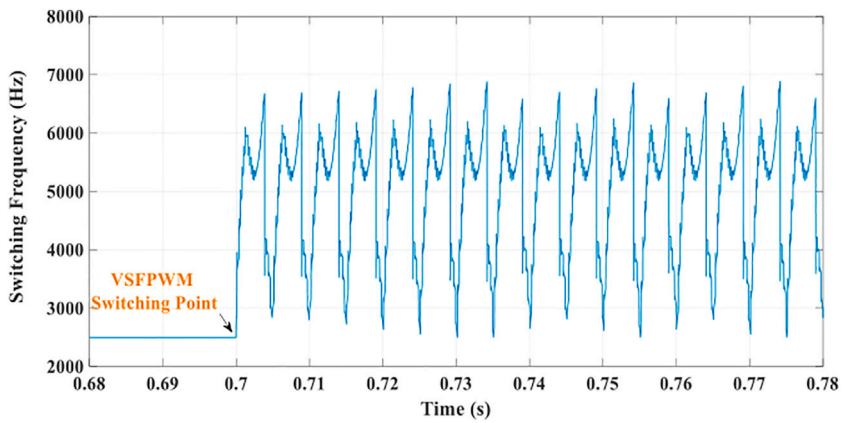

FIGURE 8 | Switching frequency variations.

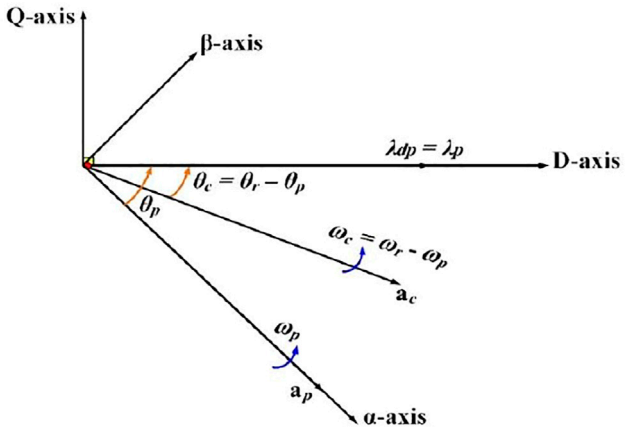

FIGURE 9 | Relationship between phase-axis of BDFRG.

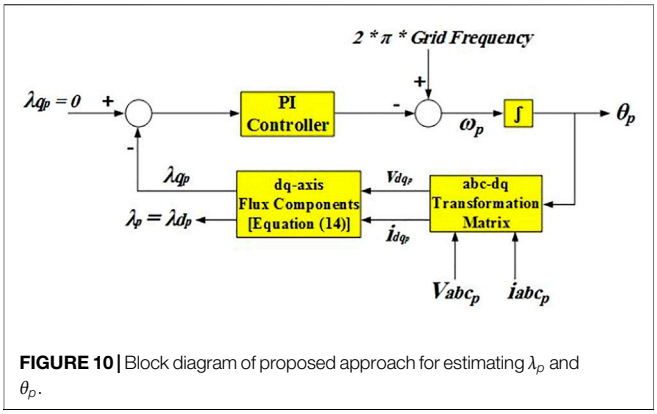

FIGURE 10 | Block diagram of proposed approach for estimating λ_p and θ_p.

With respect to vector control, the electromagnetic torque can be expressed as follows:

$$T_e = \left(\frac{3}{2}\right)\left(\frac{L_{pc}}{L_p}\right)\left(P_p + P_c\right)\left(\lambda_{d_p} i_{q_c} + \lambda_{q_p} i_{d_c}\right) \tag{15}$$

Vector-Control Based PW Field-Orientation Method

The principle advantage of the BDFRG vector-control strategy is the resultant decoupling effect between the electromagnetic torque and Q_{power} (Mousa et al., 2018). BDFRG vector control is based on the position of total power-winding's flux vector, λ_p with its d-axis. In other words, the d-axis component and total of the power-winding flux are equal i.e., $(\lambda_{d_p} = \lambda_p)$ and the q-axis component, λ_{q_p} = zero. The relationship between the phase-axis of BDFRG of the proposed flux orientation of PW is shown in **Figure 9**.

The block diagram of Phase-Locked Loop method used to estimate the flux vector magnitude of power-winding, λ_p and its angle θ_p is shown in **Figure 10** and the procedure can be summarized as follows:

Primarily, angle θ_p is initiated from summing of output signal from PI-controller and grid angular-frequency as shown in **Figure 10**. Then, angle θ_p is provided as input to the abc-dq transformation matrix to obtain voltage and current components of power-winding, V_{dq} and I_{dq} respectively in the power-winding synchronous reference frame (Mousa et al., 2018). Then the output signal is aided with **Eq. 31** to obtain the dq-axis components of λ_p as follows:

$$\left.\begin{aligned} \lambda_{d_p} &= \left(v_{q_p} - r_p\, i_{q_p}\right)/\omega_p \\ \lambda_{q_p} &= \left(-v_{d_p} + r_p\, i_{d_p}\right)/\omega_p \end{aligned}\right\} \tag{16}$$

The angular frequency, ω_p and the angle, θ_p is obtained by providing λ_{q_p} as a feedback signal, as shown in **Figure 10**. In addition, magnitude of λ_p is obtained directly from its d-axis component, as $\lambda_p = \lambda_{d_p}$. The "*Trial and error*" process is implemented for choosing PI-controller gains in order to obtain the required flux orientation at which $\lambda_{q_p} = 0$.

The torque and reactive power can be easily obtained from the proposed flux orientation of power-winding.

$$T_e = \left(\frac{3}{2}\right)\left(\frac{L_{pc}}{L_p}\right)\left(P_p + P_c\right)\lambda_p\, i_{q_c} \tag{17}$$

$$Q_{Power} = \left(\frac{3}{2}\right)\left(\frac{\omega_p}{L_p}\right)\lambda_p\left(\lambda_p - L_{pc} i_{d_c}\right) \tag{18}$$

From **Eqs. 17**, **18**, it is evident that, instantaneous electromagnetic torque and reactive-power control can be simply realized by controlling i_{q_c}&i_{d_c} respectively.

Design Procedure of the Proposed Rotor Position Observer

BDFRG rotor position can be estimated using the following relation [21]:

$$\theta_{r_{est}} = tan^{-1}\frac{Imaj\left[\left(\lambda_{p_s} - L_p i_{p_s}\right) i_{c_s}\right]}{Real\left[\left(\lambda_{p_s} - L_p i_{p_s}\right) i_{c_s}\right]} \tag{19}$$

where, i_{p_s}, i_{c_s} and λ_{p_s} are the currents of the power and control winding and space-vector flux linkage respectively.

In (Mousa et al., 2018), λ_{p_s} is obtained aided with the three-phase power-winding flux linkages which are determined as:

$$\lambda_{abc_p} = \int\left(V_{abc_p} - R_p\, i_{abc_p}\right)dt \tag{20}$$

The main issue of this rotor-position estimation method is the integration of three-phase power-winding voltages to obtain the flux linkage using **Eq. 20**. This considers the main problem of the most sensorless drive systems especially at low speed conditions. In this paper, voltage-integration problem has been overcome by the proposed simple rotor-position estimation method which is outlined as:

Aided with the dq-axis components of the power-winding flux and its angle, θ_p, the corresponding power-winding flux linkages in $\alpha\beta$-axis can be estimated as:

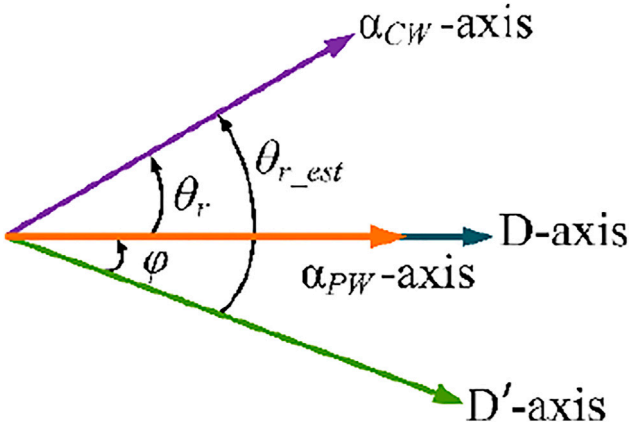

FIGURE 11 | Corresponding fictitious frame transformations with the phase axis relationship of BDFRG considering the position error.

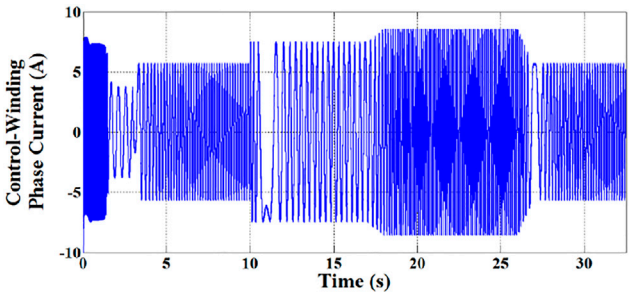

FIGURE 12 | Response of the control-winding phase-current.

$$\begin{pmatrix} \lambda_{\alpha_p} \\ \lambda_{\beta_p} \end{pmatrix} = \begin{pmatrix} \cos\theta_p & -\sin\theta_p \\ \sin\theta_p & \cos\theta_p \end{pmatrix} \begin{pmatrix} \lambda_{d_p} \\ \lambda_{q_p} \end{pmatrix} \tag{21}$$

Then, the space-vector flux linkage is given by:

$$\lambda_{p_s} = \lambda_{\alpha_p} + j\,\lambda_{\beta_p} \tag{22}$$

where the symbol "*j*" denotes the imaginary unit.

Based on **Eq. 22**, the space-vector power-winding flux linkage is estimated without voltage-integration. Hence, it can be simply used to estimate the BDFRG rotor-position using **Eq. 19**.

Stability Analysis of Proposed Position Observer

In this subsection, stability confirmation of proposed control system is clearly satisfied. Assuming that the proposed procedure initializes with an error between the position which is predicted, θ_{r_est}, and actual position, θ_r. Therefore, the actual *d-q* frame assigned on the $\alpha\beta$-axis PW stationary reference frame, used to obtain i_{c_s} referred to PW side, cannot be localized. Hence, an imaginary reference frame d'-q' is employed as shown in **Figure 11**.

The rotor position's estimation error is determined as $\varphi = (\theta_{r\_est} - \theta_r)$. Coupling component Δi_c^{PW} will be obtained in the q'-axis as a result of position error. Consequently, this term can be neglected by representing the $\varphi = 0$.

Based on the imaginary reference frame d'-q' shown in **Figure 11**,

$$\Delta i_c^{PW} = \left(e^{j\theta_{r_{est}}} - e^{j\theta_r}\right)\left(i_{c_s}\right)^{conj} \tag{23}$$

$$\Delta i_c^{PW} = \left(e^{j\varphi} - 1\right)e^{j\theta_r}\left(i_{c_s}\right)^{conj} \tag{24}$$

Therefore, aided with **Eq. 19**

$$\Delta i_c^{PW} = \frac{\lambda_{p_s} - L_p i_{p_s}}{L_{pc}}\left(e^{j\varphi} - 1\right) \tag{25}$$

The speed estimation error is considered to be

$$\Delta\omega_{rm} = K_o\left(\Delta i_c^{PW} + \frac{1}{K_i}\int \Delta i_c^{PW} dt\right) \tag{26}$$

Then, derivative of position estimation error is as follows:

$$\frac{d}{dt}\varphi = \left(p_p + p_c\right)K_o\left(\Delta i_c^{PW} + \frac{1}{K_i}\int \Delta i_c^{PW} dt\right) \tag{27}$$

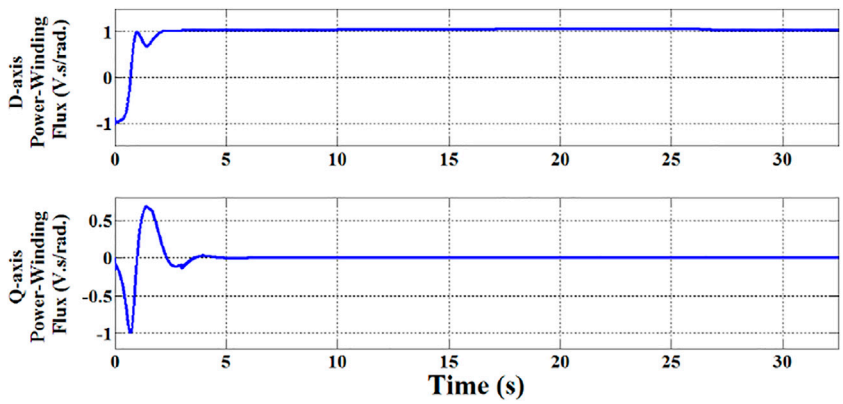

FIGURE 13 | Response of the dq-axis power-winding flux components.

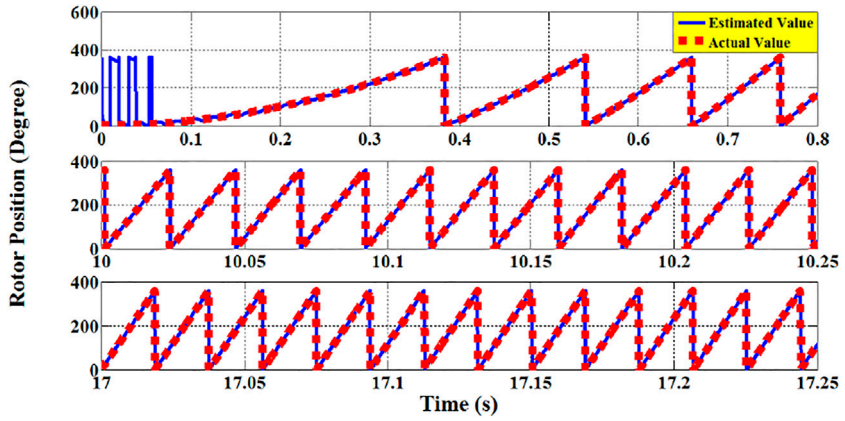

FIGURE 14 | BDFRG's actual and estimated rotor-position during different periods.

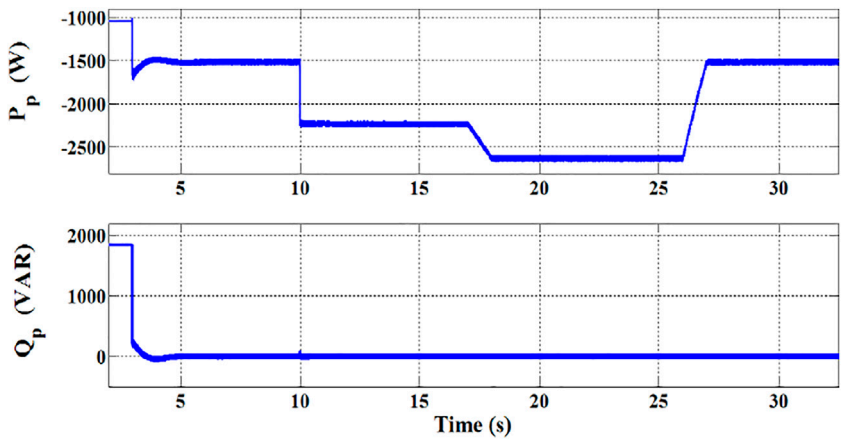

FIGURE 15 | Active and reactive power of generator PW.

where K_o and K_i are the adopted sensorless system's control parameters

$$\frac{d}{dt}\begin{bmatrix}\sigma\\ \varphi\end{bmatrix}=\begin{bmatrix}0 & G_1 f(\varphi)\\ \dfrac{G_2}{K_i} & G_2 G_1 f(\varphi)\end{bmatrix}\cdot\begin{bmatrix}\sigma\\ \varphi\end{bmatrix} \tag{28}$$

where

$$G_1=\left(\frac{\lambda_{p_s}-L_p i_{p_s}}{L_{pc}}\right)\quad,\quad G_2=\left(p_p+p_c\right)K_o$$

with $\sigma=\int \Delta i_c^{PW}dt$ and

$$f(\varphi)=\frac{e^{j\varphi}-1}{\varphi} \tag{29}$$

It is dedicated that $f(\varphi)$ is a continuous even function and $f(0)=1$. Hence, the stability domain of **Eq. 29** is projected to be symmetric at desired operating point, $\varphi=0$.

Stability of large system signal is verified by using the multi-model to represent **Eq. 29** as

$$\dot{x}=\left[\mu_1(\varphi)\cdot H_1+\mu_2(\varphi)\cdot H_2\right]\cdot x \tag{30}$$

For $0\le absolute(\varphi)\le\varphi_{max}$ with $x=[\,\sigma\quad\varphi\,]^t$

$$\left.\begin{aligned}\mu_1(\varphi)&=\frac{f(\varphi)-f(\varphi_{max})}{1-f(\varphi_{max})}\\ \mu_2(\varphi)&=\frac{1-f(\varphi)}{1-f(\varphi_{max})}\end{aligned}\right\} \tag{31}$$

$$H_1=\begin{bmatrix}0 & G_1\\ \dfrac{G_2}{K_i} & G_2.G_1\end{bmatrix},H_2=\begin{bmatrix}0 & G_1 f(\varphi_{max})\\ \dfrac{G_2}{K_i} & G_2 G_1 f(\varphi_{max})\end{bmatrix}$$

From **Eqs. 29**, **30**, it is evident that they are totally equivalent: approximation, linearization and simplification are not made. Also, considering that

$$\left.\begin{array}{c}\mu_1(\varphi)+\mu_2(\varphi)=1\\ \mu_1(\varphi)\geq 0\\ \mu_2(\varphi)\geq 0\end{array}\right\} \tag{32}$$

The quadratic Lyapunov function is determined in order to validate the stability analysis **Eq. 30**, as

$$\left.\begin{array}{c}V(x)=x^t\cdot N\cdot x\\ N=N^t>0\end{array}\right\} \tag{33}$$

From the analysis, it is evident that the proposed control system, both (29) and (30), is stable by obtaining a symmetric matrix, *N*, attaining as follows

$$\left\{\begin{array}{c}N>0\\ \left(H_1^t\cdot N+N\cdot H_1\right)>0\\ \left(H_2^t\cdot N+N\cdot H_2\right)>0\end{array}\right. \tag{34}$$

The convergence domain is obtained from maximum position error, $\varphi_{\max}$, related to linear matrix inequalities found in **Eq. 34**. From above relations, it is evident that the estimation of convergence domain can be concluded as $0 \leq absolute(\varphi) \leq 90$. This proves that the theoretical convergence domain is the largest possible which validates the stability of the proposed sensorless position observer.

RESULTS AND DISCUSSION

A sample of results is presented in this section to validate the proposed control technique. The analysis obtained are based on a six/two-pole, 4.5 kW BDFRG prototype. The overall system parameters are listed in (Mousa et al., 2018).

Initially up to 3 s, BDFRG is freely run with short-circuited CW terminals for the purpose of soft starting. Then, the partially power-rating converter is switched into the CW. The response of the CW phase-current during different periods corresponding to various wind speed is depicted in **Figure 12**. It is evident, that the over-current of converter is entirely prevented using the soft-starting method.

Figure 13 shows the response of dq-axis PW flux components. It is evident, that the q-axis component, λ_{q_p} is maintained constant at zero. This ensures the efficacy of the proposed control strategy to estimate the precise position of the PW flux, θ_p for the required power-winding flux orientation.

In addition, **Figure 14** depicts the BDFRG estimated rotor-position and the corresponding actual value. It is evident that there is a close correlation between the estimated and actual rotor-position of the generator which validates the rotor-position estimation method of the proposed sensorless control technique.

Also, the dynamic response of active and reactive power of PW is depicted in **Figure 15**. It evident that the reactive power is maintained constant at zero which ensures a unity power-factor operation.

CONCLUSION

This paper has handled an effective method for reducing the ripples of torque using VSFPWM technique for the applications of SPMSM drives. In addition, a sensorless vector-control technique for BDFRG is proposed in this paper. The results have confirmed the controllability of the prediction process for torque ripple. Moreover, the proposed VSFPWM technique has achieved a good performance for the minimization target of torque ripple. In addition, a close correlation between the generator's estimated and actual rotor-speed proves the efficacy of the proposed rotor-position/speed estimation method. Furthermore, the obtained results have assured the simplicity and capability of the presented simple sensorless observer of the adopted generator system.

DATA AVAILABILITY STATEMENT

The original contributions presented in the study are included in the article/Supplementary Material, further inquiries can be directed to the corresponding author.

AUTHOR CONTRIBUTIONS

All authors listed have made a substantial, direct, and intellectual contribution to the work and approved it for publication.

ACKNOWLEDGMENTS

The authors extend their appreciation to the Deanship of Scientific Research at King Khalid University for funding this work through General Research Project under Grant number (RGP.1/133/43).

REFERENCES

Bharatiraja, C., Sanjeevikumar, P., Mahes, A., Saxena, A., Padmapriya, K., Mithra, B. K., et al. (2017). Analysis, Design and Investigation on a New Single-phase Switched Quasi Z-Source Inverter for Photovoltaic Application. *International Journal of Power Electronics and Drive Systems* 8 (2), 853–860. doi:10.11591/ijpeds.v8.i2.pp853-860

Boldea, I., Tutelea, L. N., Wu, C., Blaabjerg, F., Liu, Y., Hussien, M. G., et al. (2021). Fractional kVA Rating PWM Converter Doubly Fed Variable Speed Electric Generator Systems: An Overview in 2020. *IEEE Access* 9, 117957–117968. doi:10.1109/access.2021.3101907

Chinthamalla, R., Sanjeevikumar, P., Karampuria, R., Jain, S., and Ertas, A. H. (2016). Viliam Fedak, "A Solar PV Water Pumping Solution Using a Three-Level Cascaded Inverter Connected Induction Motor Drive". *Eng. Sci. Technol. Int. J. (JESTECH)* 19 (4), 1731–1741.

Chokkalingam, B., Bhaskar, M. S., Padmanaban, S., Ramachandaramurthy, V. K., and Iqbal, A. (2019). Investigations of Multi-Carrier Pulse Width Modulation Schemes for Diode Free Neutral Point Clamped Multilevel Inverters. *J. Power Electron.* 19 (3), 702–713.

Fei Wang, D., and Wang, F. (2014) Current-Ripple Prediction for Three-phase PWM Converters," *IEEE Trans. Ind. Appl.* 50 (1), 531–538. doi:10.1109/tia.2013.2270224

Hussien, M. G., and Hassan, A. E. "Mathematical Analysis of the Small Signal Model for Voltage-Source Inverter in SPMSM Drive Systems," in Proceedings of the 2019 21st International Middle East Power Systems Conference (MEPCON), Cairo, Egypt, December 2019, 540–549. doi:10.1109/mepcon47431.2019.9008172

Hussien, M. G., Liu, Y., Xu, W., Junejo, A. K., and Allam, S. M. (2022). Improved MRAS Rotor Position Observer Based on Control Winding Power Factor for Stand-Alone Brushless Doubly-Fed Induction Generators. *IEEE Trans. Energy Convers.* 37 (1), 707–717. doi:10.1109/tec.2021.3110776

Hussien, M. G., Sanjeevikumar, P., Leonowicz, Z., Bo Holm-Nielsen, J., and Mihet-Popa, L. "Theoretical and Performance Analysis of PWM Control-Based Variable Switching Frequency for Torque Ripple Reduction in SPMSM Drive Systems," in Proceedings of the 2020 IEEE International Conference on Environment and Electrical Engineering and 2020 IEEE Industrial and Commercial Power Systems Europe, Madrid, Spain, June 2020 (EEEIC/I&CPS Europe), 1–5.

Jiang, D., and Wang, F. (2013) Variable Switching Frequency PWM for Three-phase Converters Based on Current Ripple Prediction. *IEEE Trans. Power Electron.* 28 (11), 4951–4961. doi:10.1109/tpel.2013.2240701

Kumar, M., Das, S., and Kiran, K. (2019). Sensorless Speed Estimation of Brushless Doubly-Fed Reluctance Generator Using Active Power Based MRAS. *IEEE Trans. Power Electron.* 34 (8), 7878–7886. doi:10.1109/tpel.2018.2882473

Kumar, M., and Das, S. (2018). Model Reference Adaptive System Based Sensorless Speed Estimation of Brushless Doubly-Fed Reluctance Generator for Wind Power Application. *IET Power Electron* 11 (Issue 14), 2355–2366. doi:10.1049/iet-pel.2018.5344

Mousa, M. G., Allam, S. M., and Rashad, E. M. (2018). Maximum Power Extraction under Different Vector-Control Schemes and Grid-Synchronization Strategy of a Wind-Driven Brushless Doubly-Fed Reluctance Generator. *ISA Trans.* 72, 287–297. doi:10.1016/j.isatra.2017.10.005

Pandav, K. M., Mahajan, S. B., Sanjeevikumar, P., Badave, S. M., and Pachagade, R. (2017a). "2.4 kW Three-phase Inverter for Aircraft Application-Hardware Implementation." in *Lecture Notes in Electrical Engineering*. (Singapore: Springer Journal Publications). doi:10.1007/978-981-10-4394-9_33

Pandav, K. M., Mahajan, S. B., and Sanjeevikumar, P. (2017b) "Frede Blaabjerg, "Three Phase Z-Source Multilevel Inverter System for Renewable Energy Application"," in Proceedings of the Intl. Conf. on Renewable Energy and Resources, OMICS International Publishing, USA, July 2017, 24–25.

Sanjeevikumar, P., Bhaskar, M. S., Pandav, K. M., Pierluigi, S., and Valentin, O. (2016) "Hexuple-Inverter Configuration for Multilevel Nine-phase Symmetrical Open- Winding Converter," in Conf. Proc., Proceedings of the IEEE First Intl. Conf. Power Electron., Intelligent Control and Energy System, IEEE-ICPEICES'16, India, July 2016, 1837–1844.

Xu, W., Hussien, M. G., Liu, Y., and Allam, S. M. (2021). Sensorless Control of Ship Shaft Stand-Alone BDFIGs Based on Reactive-Power MRAS Observer. *IEEE J. Emerg. Sel. Top. Power Electron.* 9 (2), 1518–1531. doi:10.1109/jestpe.2019.2963264

Xu, W., Hussien, M. G., Liu, Y., Islam, M. R., and Allam, S. M. (2020). Sensorless Voltage Control Schemes for Brushless Doubly-Fed Induction Generators in Stand-Alone and Grid-Connected Applications. *IEEE Trans. Energy Convers.* 35 (4), 1781–1795. doi:10.1109/tec.2020.2999629

Conflict of Interest: The authors declare that the research was conducted in the absence of any commercial or financial relationships that could be construed as a potential conflict of interest.

Publisher's Note: All claims expressed in this article are solely those of the authors and do not necessarily represent those of their affiliated organizations, or those of the publisher, the editors and the reviewers. Any product that may be evaluated in this article, or claim that may be made by its manufacturer, is not guaranteed or endorsed by the publisher.

frontiers | Frontiers in Energy Research

ORIGINAL RESEARCH
published: 15 June 2022
doi: 10.3389/fenrg.2022.896621

Investigation on Heterogeneous Influence of Government Subsidies on Pollution Reduction of Power Companies and Its Influencing Mechanism

Qin Wang[1,2], *Xiaoqi Zheng*[2]* *and Zhonggang Yue*[2]

[1]School of Economics and Management, Nanjing University of Science and Technology, Nanjing, China, [2]School of Economics, Nanjing University of Posts and Telecommunications, Nanjing, China

This study aims to investigate whether the subsidies promote pollution reduction or not by taking the power companies in China as a case study. So, we built a fixed-effects panel data model first, which is then used to verify the influence of government subsidies on pollution reduction in power companies. Additionally, how the subsidy influencing mechanism would work is also investigated. Results find that subsidies can significantly reduce power companies' pollution, especially sulfur dioxide emissions and soot. At the same time, the result also showed that the government subsidies could encourage power companies to cut emissions by taking measures like end-of-pipe control and green innovation. Also, from the perspective of heterogeneity, government subsidies have a better effect on the regions with stronger environmental regulations, less economically developed regions, big-scale companies, and companies with low slack.

Keywords: government subsides, pollution reduction, green innovation, mediating effect model, environmental management

OPEN ACCESS

Edited by:
Nallapaneni Manoj Kumar, City University of Hong Kong, Hong Kong SAR, China

Reviewed by:
Mohammad Haseeb, Wuhan University, China
Fernando Caixeta, Federal Institute of Education, Science Technology of the Triângulo Mineiro, Brazil

***Correspondence:**
Xiaoqi Zheng
zhengxiaoqi@njupt.edu.cn

Specialty section:
This article was submitted to Sustainable Energy Systems and Policies, a section of the journal Frontiers in Energy Research

Received: *15 March 2022*
Accepted: *29 April 2022*
Published: *15 June 2022*

Citation:
Wang Q, Zheng X and Yue Z (2022) Investigation on Heterogeneous Influence of Government Subsidies on Pollution Reduction of Power Companies and Its Influencing Mechanism. Front. Energy Res. 10:896621. doi: 10.3389/fenrg.2022.896621

1 INTRODUCTION

1.1 Background

As the largest developing country in the world, China is facing multiple challenges such as economic growth, employment security, and environmental governance (Ai et al., 2020). Among these, environmental governance is more stressful; as a result, emission reduction targets were set for each public and private sector company (Usman et al., 2021). Many administrative and voluntary approaches and subsidies were popped out at the federal and local levels in line with this. Compared with administrative orders and voluntary approaches, government subsidies have no negative impact on companies' output, and they can influence companies' behavior through the market force (Davis, 2017). Therefore, government subsidies can be an essential policy instrument and play an indispensable role in leading companies to allocate resources and shoulder social responsibilities (Frye and Shleifer, 1997; Wang et al., 2020). To deal with the increasingly severe environmental pollution, China's central government issued a notice about regulating the funding channels for environmental protection in early 1984. The document held that at least 80% of the fee the government levies on companies for the discharge of pollutants had to be used to subsidize companies' environmental protection. In 1994, the Ministry of Environmental Protection and the Ministry of Finance jointly issued a couple of provisions about enhancing the management of

environmental subsidies, which specially regulated the use of the means of government subsidies to stimulate companies' environmental protection. In 2003, regulations regarding the utilization and management of pollutant discharge fees regulated that the fee should be used for companies' pollution management. The interim measures for the management of special funds allocated by the Central Finance for Emission Reduction of Major Pollutants issued by the Ministry of Finance in 2007 regulated establishing national funds for emission reduction of major pollutants and encouraging provincial-level governments to enact environmental subsidy policies for local environmental protection. The 12th 5-year (from 2011 to 2015) plan requested local governments to increase the budgets for environmental gradually subsides in their annual financial plans (Ren et al.,2021). When we look at the sectors, economic growth, and environmental governance, the energy sector has a prominent role in the nation's economy. However, the stressing point is its environmental impact. Considering the case of power companies in China, they are dominated by coal as a resource for producing power, and this determines the severe effect of the electric power industry on environmental quality (Yan and Yang, 2008). In 2012, China became the most significant contributor to global sulfur dioxide (SO_2) emissions (Shi et al., 2016). The current rates rose to 33%, and coal power plants seem to be the primary sources (Zhao et al., 2013; Nakaishi et al., 2021). Noticing this, the Chinese government started emphasizing emission reduction in power companies by providing investment subsidies for technology innovation and reform through direct fiscal appropriation, finance discounts, and tax subsidies (Gao et al., 2009; Liang et al., 2015; Shi et al., 2016; Zhang et al., 2017; Hou et al., 2020; Schreifels et al., 2021). For instance, the government passed a regulation requiring the newly built coal power plants to install desulfurization units. A price subsidy for desulfurization is offered to promote this, that is, raising the price limit for electricity to 0.015 yuan per kilowatt hour. Also, to improve the development of new-energy power firms in line with environmental regulations, the government provided subsidies to the renewable power plants (including wind power plants, photovoltaic power plants, and biomass power plants) (Li, 2021). However, these measures mainly include sewage discharge permission which the power companies must apply in advance. On the other side, the local governments take compulsive measures to limit the companies' production and ensure the emission complies with standards for discharge of pollutants. But these sewage discharge permission significantly affected the power companies' pollution management costs; in many instances, their costs are increased. It became worse and burdened the companies when the business scale of sewage discharge was immense. Such burdens lead to limiting production levels to reduce the pollution management cost. But such development approaches made the national economy unsustainable.

To counter such issues, researchers like Zhang and Zhang (2011) and Wang and Zhang (2018) showed that increasing the facilities for pollution reduction and green technology innovations can save energy and reduce emissions. We reviewed end-of-pipe treatment and green innovative strategies in the following sections to understand this more thoroughly.

1.2 End-of-Pipe Treatment Strategy

The end-of-pipe treatment strategy is a passive environmental governance approach (Hart, 1995; Sharma et al., 1998); it is the first approach raised and adopted in environmental management. It is mainly introduced through the purchases and installations of pollution control equipment (for instance, the desulfurization equipment or using the raw materials which will generate fewer pollutants) when companies face pressure from external environmental regulations during electric power production. More specifically, coal ore with less sulfur content can reduce SO_2 emissions. On the other side, the waste heat recovery of soot for reheating can further reduce the cost of the resources used for heating the coal and help enhance the plant's energy efficiency. In such cases, innovative changes are needed for the plant equipment, affecting the investments where the company should be able to manage it. This is where the government subsidy comes into the picture and helps to increasing the cash flow of the subsidized companies and meet the capital demand for companies to upgrade their equipment with new technology in line with environmental regulations (Zhang and Zhang, 2011; Wang et al., 2015; Wang and Zhang, 2018; Yan et al., 2019).

1.3 Green Innovative Strategies

In the early days, the pollution management technologies adopted during the life cycle of environmental management practice were relatively few. But to meet the demand for environmental management, companies have started adopting green innovative strategies (Wang and Zhang, 2020; Wang and Li, 2021). The positive externalities of green innovations will lead to innovative social benefits being higher than private benefits; technology spillovers will result in the consequence that innovative companies cannot internalize all the innovative benefits. As a result, the companies started facing capital shortages and the burden of operating costs when engaging in green innovative activities. In such cases, the government subsidies can make up the cost of companies' green innovations and encourage companies' participation in environmental technology innovations. In addition, relevant social investors tend to invest in companies compliant with national regulations. The government's subsidies to environmental innovations have some signaling function. For instance, the companies that receive government subsidies can send specific signals to the society, telling the potential investors that they comply with the government's environmental regulations and meet the government's requirements for environmental protection so that they can get investment from the outside world (Wang and Wang, 2019; Xing et al., 2019).

From the earlier discussed end-of-pipe treatment and green innovative strategies, two hypotheses were formulated, hypothesis 1: government subsidies can help implement companies' pollution control strategies and increase the equipment investment for environmental management to reduce the emission of pollutants; hypothesis 2: government

subsidies can promote the green innovative level of power companies and reduce the emission of pollutants.

So, based on the formulated hypotheses, this article aims to study how government subsidies impact the pollution reduction of power companies from the perspectives of pollution prevention and control strategies and green innovation strategies. For this, the microdata of power companies is considered. The key contributions of the study include complementing the existing research from the microperspective of power plants combined with the emission data, followed by the analysis of the heterogeneous impact of government subsidies on the emission of pollutants from the perspective of slack that enriches the existing research. Additionally, we also bring out some operational insights that help in policy amendments.

The article structure is as follows; **Section 2** introduces the empirical approaches and variables used in the investigation. **Section 3** discusses the fundamental regression results, followed by a brief analysis of the relevant mechanisms. **Section 4** provides the conclusion and suggestions.

2 METHODS

A fixed-effects panel data model shown in **Eq. 1** was adopted to test if government subsidies can help promote pollution reduction of power companies or not.

$$Y_{ict} = \alpha + \beta S_{ict} + \gamma X_{ict} + \delta_i + \theta_t + X_c + \varepsilon_{ict}, \quad (1)$$

where the subscripts i, c, and t represent a company, the city where the company is located, and the year respectively; Y_{ict} represents the quantity of pollutants discharged by a company; S_{ict} represents the subsidy income received by the company; X_{ict} represents the control variables at the company level, including the size of a company and the years a company has been in business; δ_i represents company fixed effects; θ_t represents the year with fixed effects; X_c represents the control variables at the city level and the level of environmental regulations in regions; ε_{ict} represents error terms, and the α, β, and γ represents the coefficients.

2.1 Data Sources and the Sample Selection

The data at the prefecture and city levels are from China City Statistical Yearbooks; the data at the provincial level is from the China environment yearbook released by the Ministry of Ecology and Environment of the People's Republic of China. The power company's microdata from China industry business performance data reports are considered. This mainly covers the foremost financial variables of all state-owned and big nonstate-owned industrial enterprises in China. Then, we matched the power company's financial index data with pollution data and patent data with the China city statistical yearbook to get the indexes needed for research and analysis. However, due to data availability limitations, we only included the data from 1998 to 2014 at the company level. In addition, we eliminated the samples with a debt to assets ratio below 0, and the study also does a 10% winsorization to continuous variables to prevent the influence of extreme values on results.

2.2 Variables

While under investigation, this study accounts for numerous variables types. For instance, the explained variables, explanatory variables, control variables, and the mechanism analysis variables.

The views of Wu et al. (2018) and Xing et al. (2019) were adopted to measure the government subsidies by the amount of subsidies (denominated in millions and yuan) a company receives in the year. Moreover learning from existing literature (Nie et al., 2008; Usman and Jahanger, 2021; Wang et al., 2021), we also analyzed some other factors that may influence enterprises' pollution reduction like the characteristics of power companies, the characteristics of prefecture-level cities and the level of regional environmental regulations. The control variables of companies' characteristics include *ln*size (firm size represented by the natural logarithm of the year-end total assets), age (years a company has been in business calculated through the formula: the year it is observed deducts the year when it is founded plus one), lev (financial leverage of a company represented by the debt-to-assets ratio: long-term debt divided by total assets), ROA (earnings of a company indicated by the Return on Total Assets), and *ln*capital (profitability of a company's main businesses indicated by operating profit margin: the amount of operating profit divided by primary business income). Moreover, the factors that can be used to control the development of urbanization and industrialization like *ln*pgdp (the per-capita GDP level of the city in which a company is located), *ln*pop (density of population: year-end total population divided by the territorial area of the city), and struc2 (the ratio of the second and third industries' output value to GDP) are added. These variables are expressed in logarithmic forms, respectively. Considering the possible impact of environmental regulation, the levels of different regions on companies' emission of pollutants are considered. Also, learning from Hong et al. (2011), the pollution discharge fee is viewed as a proxy variable. The data relating to pollution discharge fees are available only at the provincial level, so we used the provincial-level pollution discharge fees (*ln*fees) to indicate the environmental regulation levels of different cities. Some researchers in the literature have already tested how intermediate variables (number of the equipment for pollution management and number of green innovations) reduce a company's emissions. Hence, we adopted the validation method of the mechanism of an intermediary function raised by Wen and Ye (2013), see **Eq. 2**.

$$M_{ict} = \alpha' + \beta' S_{ict} + \gamma' X_{ict} + \delta'_i + \theta'_t + X'_c + \varepsilon'_{ict} \quad (2)$$

where M_{ict} represents intermediate variables such as the number of facilities for pollution reduction and the number of technological innovations adopted by the power company. The rest of the variable's definitions are the same as the ones shown in **Eq. 1**. Now, in **Eq. 2**, if the regression coefficients have significance, it indicates the existence of a mechanism of action of how government subsidies influence power companies' pollution reduction.

TABLE 1 | Descriptive statistical analysis.

Variable	N	Mean	Sd	Min	p50	Max
lnSO_2	8420	13.8256	3.0545	0.0000	14.2686	17.9426
*ln*Soot	8171	12.7756	2.9664	0.0000	13.2225	17.0957
Subsidies	8530	3.0545	22.5869	0.0000	0.0000	710.2970
*ln*size	8529	12.3351	2.6747	0.0000	12.5007	19.3665
Age	8491	16.7715	15.7214	0.0000	11.0000	135.0000
ROA	8181	0.0166	0.1982	−2.6887	0.0085	14.2967
lev	8182	0.6854	0.3827	0.0000	0.6898	8.9627
*ln*capital	8391	6.5993	1.7280	0.0000	6.5795	14.8760
*ln*fees	8530	11.5477	0.4049	10.8269	11.5249	12.7289
*ln*pgdp	7962	12.8088	2.7839	2.4849	13.1651	18.2396
*ln*pop	8024	5.6020	1.2705	0.1823	6.0539	9.3557
Struc2	8023	88.6605	9.2093	46.8000	91.5600	99.8800

TABLE 2 | Benchmark regression results.

—	(1) *ln*SO_2	(2) *ln*SO_2	(3) *ln*Soot	(4) *ln*Soot
Subsidies	−0.0151***	−0.0178***	−0.0042**	−0.0050**
	(0.0051)	(0.0050)	(0.0019)	(0.0020)
N	8420	7492	8171	7326
r^2	0.0595	0.0753	0.0295	0.0381
Control	Yes	Yes	Yes	Yes
FE-year	Yes	Yes	Yes	Yes
FE-city	Yes	Yes	Yes	Yes

The proxy variable of pollution management facilities is the investment in equipment for pollution reduction, that is, the number of facilities for flue gas purification and the number of facilities for wastewater management. Regarding the measurement indexes of green technology innovations, this study learns from previous research and uses the logarithms of the number of applications for green patents (Dong and Wang, 2019; Pei Xiao et al., 2019), that is, because the patent is a strong index of green innovations (Berrone et al., 2013). The research is carried out based on the information about companies' patent applications released by the State of Intellectual Property Office of China by combining the international patent classification code of green patents listed on the green patent list, which is provided by WIPO (World Intellectual Property Organization) and the keywords (environmental protection, energy saving, pollution reduction, low carbon, cleanness, recycle, and sustainability) of the new definition of companies' green innovations raised by Lim and Prakash (2014). Research investment is also a standard index for green innovations; this study does not adopt the index because the research investment index in China industry performance data is only available till 2007. Compared with other analysis methods, the descriptive statistical analysis can more visually measure the overall level and scale of one region's green technology innovations. Hence, the study adopts the descriptive statistical analysis method; details are given in **Table 1**.

TABLE 3 | Robustness test results of substitution variables.

	(1) pSO_2	(2) pSoot
Subsidies	−0.0014***	−0.0004**
	(0.0004)	(0.0002)
*ln*size	−0.0566***	−0.0456***
	(0.0117)	(0.0120)
N	7343	7179
r^2	0.0843	0.0351
Control	YES	YES
FE-year	YES	YES
FE-city	YES	YES

3 RESULTS AND DISCUSSION

3.1 Benchmark Regression Result

The benchmark regression results shown in **Table 2** are estimated based on **Eq. 1**, where the regression formula controls the company fixed effects and year fixed effects, and standard errors cluster at the city level. It only considered core explanatory variables in column 1 and government subsidies remarkably improved the reduction of SO_2 emissions of power plants at 1%. It added control variables in column 2; the results show that the explanatory variables are still significantly negative. We can see from the coefficients that government subsidies help reduce power companies' SO_2 emissions by 0.0178 tons. Similarly, government subsidies can substantially reduce soot emissions by 0.005 tons. Therefore, benchmark regression analysis initially proves that government subsidies statistically and economically influence the emission reduction of SO_2 and soot.

3.2 Robustness Test Results

The robustness test results include the observed effects of substitution variables and the downsizing of company samples. The emission intensity of pollutants is taken as a substitution variable to reprove government subsidies' impact on pollution reduction. The emission intensity indexes required are represented by SO_2 and soot divided by the total industrial output value. There are many new types of power generation options; these include hydropower plants, solar power companies, wind power enterprises, and biomass power plants. Such a sample would cause deviations and errors. To avoid this, we only considered thermal power plants when testing the government subsidies' effects on reducing the emission of pollutants.

3.2.1 Substitution Variables

The regression results (in **Table 3**) indicate that government subsidies have a remarkable effect on reducing emission intensities of SO_2 and soot. It shows that government subsidies can help improve companies' productivity and reduce pollution under unit production value. In other words,

TABLE 4 | Government subsidies' effects on thermal power plants' emission reduction.

—	(1) $lnSO_2$	(2) lnSoot
Subsidies	−0.0207***	−0.0036*
	(0.0043)	(0.0021)
N	6930	6820
r^2	0.0972	0.0433
Control	Yes	Yes
FE-year	Yes	Yes
FE-city	Yes	Yes

TABLE 5 | Heterogeneity of enforcement of environmental regulations.

—	(1) $lnSO_2$	(2) $lnSO_2$	(3) lnSoot	(4) lnSoot
Subsidies	0.0005	−0.0250***	−0.0011	−0.0051***
	(0.0019)	(0.0026)	(0.0036)	(0.0019)
N	3580	3912	3515	3811
r^2	0.0380	0.1601	0.0365	0.0528
Control	Yes	Yes	Yes	Yes
FE-year	Yes	Yes	Yes	Yes
FE-city	Yes	Yes	Yes	Yes

government subsidies reduce the cost companies' cause to the outside world through power plants' technological improvements and green technology innovations.

3.2.2 Downsizing the Sample Size

From the results shown in **Table 4**, we can see that government subsidies have a remarkable effect on reducing SO_2 and soot emissions. Also, the parameters and coefficients of regression results are more prominent than benchmark regression results, indicating that government subsidies have a remarkable impact on thermal power companies' emissions reduction.

3.3 Analysis of Heterogeneity

This section presents the results related to the heterogeneity of enforcement of environmental regulations, levels of economic development, firm size, and the slack.

3.3.1 Heterogeneity of Enforcement of Environmental Regulations

Environmental management requires companies to increase their budgets (on pollution reduction) or reduce their benefits, so companies will have no motivation to overachieve the goal of emission reduction as requested by local environmental rules when there are some differences in the enforcement of regional environmental regulations. Generally, the companies in the regions with weak enforcement of regulations usually have a relatively low motivation to reduce the emission of pollutants, so government subsidies' effects will be ineffective. Keeping this in view, **Table 5** presents the heterogeneity of enforcement of environmental regulations results.

From **Table 5**, we can see that columns 2 and 4 are the regions with strong enforcement of environmental regulations where the government subsidies' effect on power companies' emission reduction was stronger. This observation is in line with the results reported by Chen and Chen (2018) and Cheng and Chen. (2019). They said that the regulations and measures could effectively reduce environmental pollution. Therefore, if we want government subsidies to function and perform effectively, we need to combine them with environmental regulations and policies.

TABLE 6 | Heterogeneity of levels of economic development.

—	(1) $lnSO_2$	(2) $lnSO_2$	(3) lnSoot	(4) lnSoot
Subsidies	−0.0288***	−0.0148***	−0.0077*	−0.0014
	(0.0057)	(0.0050)	(0.0046)	(0.0011)
N	3744	3734	3669	3651
r^2	0.1337	0.0657	0.0201	0.0466
Control	Yes	Yes	Yes	Yes
FE-year	Yes	Yes	Yes	Yes
FE-city	Yes	Yes	Yes	Yes

3.3.2 Heterogeneity of Levels of Economic Development

In **Table 6**, the results of the heterogeneity levels of economic development are shown. The difference in levels of regional economic development is another factor that may influence the government's subsidy effect on power companies' pollution reduction targets. This is because government subsidies' outcome depends on the relative value where the companies in more economically developed regions would exhibit low value. It might be due to the more active financial markets, and the chances for power companies to get funds are high from the market. In addition, such active markets give the power companies more access to funds. Government Subsidies have a relatively weak effect on relieving business liquidity pressure and financing pressure, so the subsidies' impact on the emission reduction of pollutants is relatively weak.

On the contrary, the effect on the power companies in less economically developed regions is strong. The sample companies in columns 1 and 3 of **Table 6** belong to the power enterprises in less economically developed regions, government subsidies' effect on the emission reduction is stronger than the power companies (in columns 2 and 4) in more economically developed regions. This concludes that government subsidies can better affect the emission reduction of power companies in less economically developed regions.

3.3.3 Heterogeneity of Firm Size

The firm size could potentially affect the emission reduction targets. For instance, when compared with small-scale companies, the investment made by big-scale companies for

TABLE 7 | Heterogeneity of firm size.

—	(1) *ln*SO_2	(2) *ln*SO_2	(3) *ln*Soot	(4) *ln*Soot
Subsidies	−0.0016	−0.0177***	0.0376	−0.0046***
	(0.0119)	(0.0048)	(0.0264)	(0.0017)
N	3586	3906	3500	3826
r^2	0.0287	0.1500	0.0270	0.0759
Control	Yes	Yes	Yes	Yes
FE-year	Yes	Yes	Yes	Yes
FE-city	Yes	Yes	Yes	Yes

TABLE 8 | Heterogeneity of low discretion slack (SR1).

	(1) *ln*SO_2	(2) *ln*SO_2	(3) *ln*Soot	(4) *ln*Soot
Subsidies	−0.0173***	−0.0124	−0.0052***	−0.0051
	(0.0053)	(0.0090)	(0.0019)	(0.0034)
N	3635	3608	3556	3521
r^2	0.1168	0.0300	0.0568	0.0312
Control	Yes	Yes	Yes	Yes
FE-year	Yes	Yes	Yes	Yes
FE-city	Yes	Yes	Yes	Yes

reducing the emission of pollutants and green innovations could potentially result in a scale effect. So, in such situations, the government subsidies' influence on the pollution reduction of companies may be heterogeneous.

Columns 1 and 3 in **Table 7** represents small-scale power companies, whereas columns 2 and 4 represent big-scale power enterprises. The observed regression results indicate that government subsidies' impact on reducing big-scale companies' emissions is more remarkable. But in the case of small-scale companies, although the influence on SO_2 emission reduction is significant, the impact on soot emission is not as impressive. So, the overall observation is that the big companies are more able to take social responsibilities. In contrast, the small companies use the subsidies they receive for production, which further encourages the companies to purchase the equipment for pollution reduction.

3.3.4 Heterogeneity of Slack

Slack belongs to companies' internal resources like surplus cash and idle production equipment. Suppose, if a company has enough slack to support green fields, its dependence on external resources will decrease, and the relative value of government subsidies to the company will be low. Generally, slack can be divided into low discretion slack (SR1) and high discretion slack (SR2). SR1 has low liquidity, and it needs more time to convert or to be utilized when facing some specific utilization (Li and Liu, 2010). For instance, idle production equipment.

TABLE 9 | Heterogeneity of high discretion slack (SR2).

—	(1) *ln*SO_2	(2) *ln*SO_2	(3) *ln*Soot	(4) *ln*Soot
Subsidies	−0.0194***	−0.0160**	−0.0061***	−0.0036
	(0.0071)	(0.0068)	(0.0018)	(0.0023)
N	3690	3739	3595	3671
r^2	0.0761	0.0832	0.0547	0.0452
Control	Yes	Yes	Yes	Yes
FE-year	Yes	Yes	Yes	Yes
FE-city	Yes	Yes	Yes	Yes

Regarding the method for measuring low discretion slack (Herold et al., 2006; Iyer and Miller, 2008; Latham and Braun, 2008; Yang et al., 2015), we used **Eq. 3**.

$$SR1 = \frac{\text{management fee of the same period}}{\text{sales income of the same period}}. \quad (3)$$

In **Table 8**, the heterogeneity of the low discretion slack (SR1) result is given. From **Table 8**, we can see that columns 1 and 3 belong to the SR1 low group, and government subsidies have a remarkable effect on companies' emissions reduction. In contrast, columns 2 and 3 belong to the SR1 high group, and government subsidies' impact on companies' emission reduction is insignificant. This indicates that if a company has a high SR1, it will not be easy for government subsidies to mobilize the company's internal organizations to use the resources for emission reduction.

High discretion slack (SR2) is not for specific utilization or needs. It has relatively high liquidity, so administrators can more easily control it. We used the quick ratio index to measure it, as shown in **Eq. 4**.

$$SR2 = qucik\ ratio = \frac{(\text{liquid assets} - \text{stock})}{\text{liquid liabilities}}. \quad (4)$$

In **Table 9**, the heterogeneity of the high discretion slack (SR2) result is given. From the measuring results of **Table 9**, it can be observed that the government subsidies' impact on the reduction of SO_2 emissions has a better effect on power companies with low SR2 (in column 1) when compared with power companies with high SR2 (in column 2). Coming to the influence of government subsidies on soot emission reduction, it is remarkable for the companies with low SR2 (in column 3) and not significant for the ones with high SR2 (in column 4). This indicates that companies with high SR2 have abundant liquid assets, and their government subsidies' relative value is low, revealing that subsidies cannot remarkably encourage them to allocate the slack to the field of pollution reduction.

Overall, the heterogeneity of slack results suggests that government subsidies significantly affect the emission reduction of power companies. The effect could be more significant for companies with scarce slack than for those with rich slack.

TABLE 10 | Pollution prevention and control strategies.

—	(1) Facilities 1	(2) Facilities 2
Subsidies	0.0076*	0.0014
	(0.0042)	(0.0020)
N	5350	6861
r^2	0.0245	0.0183
Control	Yes	Yes
FE-year	Yes	Yes
FE-city	Yes	Yes

TABLE 11 | Green innovative strategies.

—	(1) Invention	(2) Noninvention
Subsidies	0.0014*	−0.0020
	(0.0008)	(0.0061)
N	7582	7581
r^2	0.0133	0.0063
Control	Yes	Yes
FE-year	Yes	Yes
FE-city	Yes	Yes

3.4 Mechanism Analysis

This section presents the mechanism analysis test results for the hypothesis 1: government subsidies can help implement companies' pollution control strategies and increase the equipment investment for environmental management to reduce the emission of pollutants, and hypothesis 2: government subsidies can promote the green innovative level of power companies and reduce the emission of pollutants.

3.4.1 Pollution Prevention and Control Approaches

From the aforementioned results, it can be understood that subsidies positively impact pollution prevention equipment purchases. To understand this, two facility approaches, where facility one represents the number of exhaust gas pollution management facilities and facility two represents the number of wastewater pollution management facilities, are considered. The regression model shown in **Eq. 2** verifies government subsidies' influence on the number of facilities for pollution management, and the results are given in **Table 10**. From **Table 10**, it can be observed that government subsidies have a significant positive effect on the investment in facilities for fuel gas purification. However, they do not substantially impact the investment in facilities for wastewater treatment, and the influence is still positive.

3.4.2 Green Innovative Approaches

Table 11 presents the results of the green innovative strategies obtained by solving the regression model shown in **Eq. 2**. Here, invention patents are regarded as substantive innovations (invention), appearance design patents, and utility model patents as strategic innovations (noninvention) (Li and Zheng, 2016). **Table 11** results reveal that the government subsidies are helpful for the substantive innovations of power companies where the income in the form of subsidy would be allocated for improving green technologies in the company. However, government subsidies' influence on companies' nonsubstantive innovations is not notable, indicating that government subsidies cannot realize the goal of reducing company emissions through strategic innovations.

4 CONCLUSION AND THE SUGGESTION

This study investigated whether the existing subsidies will promote pollution reduction or not by taking the power companies in China as a case study. For this, a fixed-effects panel data model was built to verify the influence of government subsidies. Based on the investigation, the following conclusions were made:

- An increase of one million yuan in government subsidies could potentially reduce the SO2 and shoot emissions in power companies by 0.0178 and 0.005 tons, respectively.
- The heterogeneity results suggest that government subsidies significantly affect the emission reduction of power companies but depend upon many factors. So, it is always advised to consider the enforcement level of environmental regulations, levels of economic development, firm size, and slack. Moreover, government subsidies have a more prominent effect on the pollution reduction of regions with stronger environmental regulations, less economically developed regions, big-scale companies, and companies with low slack.
- Mechanism analysis shows that government subsidies can encourage companies to increase facilities for emission reduction and adopt green innovative technologies.

Based on the concluding remarks, we proposed the following suggestions, given that government subsidies have a more considerable marginal effect on power companies.

- Green innovations have a emission reduction effect and a knowledge spillover effect, so government subsidies not only need to encourage power companies to reduce the emission of pollutants through the two approaches but also encourage the companies to focus on green inventions and innovations.
- It is strongly advised that the government subsidies combine with environmental regulations to deal with power companies' pollution reduction.
- There is a high potential and scope for emission reduction in economically developed regions as they have better access to funds and technology. So, the government subsidies should give more support to companies in that region.
- Scale effects should be considered when providing government subsidies, especially for the big-scale companies. Given such a policy, the scale effect of pollution reduction could be realized practically.
- More considerable support should be given to the power companies whose slack is low. Hence, formulating a policy in line with slack would be better.

DATA AVAILABILITY STATEMENT

The original contributions presented in the study are included in the article/Supplementary Material; further inquiries can be directed to the corresponding author.

AUTHOR CONTRIBUTIONS

All authors listed have made a substantial, direct, and intellectual contribution to the work and approved it for publication.

FUNDING

National Natural Science Foundation of China: The measurement and influential mechanism of rebound effect of household energy consumption in China under "30/60 target" (No.72104112).

ACKNOWLEDGMENTS

We acknowledge the contributions of associate professor Wang Jingjing.

REFERENCES

Ai, H., Hu, S., Li, K., and Shao, S. (2020). Environmental Regulation, Total Factor Productivity, and Enterprise Duration: Evidence from China. *Bus. Strat. Env.* 29 (6), 2284–2296. doi:10.1002/bse.2502

Ai, H., Zhou, Z., Li, K., and Kang, Z. (2021). Impacts of the Desulfurization Price Subsidy Policy on SO2 Reduction: Evidence from China's Coal-Fired Power Plants. *Energy Policy* 157, 1–13. doi:10.1016/j.enpol.2021.112477

Berrone, P., Fosfuri, A., Gelabert, L., and Gomez-Mejia, L. R. (2013). Necessity as the Mother of 'green' Inventions: Institutional Pressures and Environmental Innovations. *Strat. Mgmt. J.* 34 (8), 891–909. doi:10.1002/smj.2041

Chen, S., and Chen, D. (2018). Air Pollution, Government Regulations & High-Quality Economic Development. *Econ. Res. J.* 2, 20–34.

Cheng, G., and Chen, X. (2019). New Path of Sustainable Development: Environmental Regulation and Technological Progress: An Empirical Test Based on Threshold Effect. *J. Anhui Normal Univ. Humanit. Soc. Sci.* 3, 69–77. doi:10.14182/j.cnki.j.anu.2019.03.009

Davis, L. W. (2017). The Environmental Cost of Global Fuel Subsidies. *Energy J.* 38, 7–27. doi:10.5547/01956574.38.si1.ldav

Dong, Z., and Wang, H. (2019). Local-Neighborhood Effect of Green Technology of Environmental Regulation. *China Ind. Econ.* 1, 100–118. doi:10.19581/j.cnki.ciejournal.2019.01.006

Frye, T., and Shleifer, A. (1997). The Invisible Hand and the Grabbing Hand. *Am. Econ. Rev.* 87, 354–358.

Gao, C., Yin, H., Ai, N., and Huang, Z. (2009). Historical Analysis of SO2 Pollution Control Policies in China. *Environ. Manag.* 43, 447–457. doi:10.1007/s00267-008-9252-x

Hart, S. L. (1995). A Natural-Resource-Based View of the Firm. *Amr* 20 (4), 986–1014. doi:10.5465/amr.1995.9512280033

Herold, D. M., Jayaraman, N., and Narayanaswamy, C. R. (2006). What Is the Relationship between Organizational Slack and Innovation? *J. Manag. Issues* 18 (3), 372–392.

Hong, T., Yu, M., and Jiang, J. (2011). Determination of Industrial Pollution-An Empirical Study Based on Pollution Demand-Supply Schedule. *Manag. Rev.* 23 (10), 3–9. doi:10.16538/j.cnki.fem.2011.08.004

Hou, B., Wang, B., Du, M., and Zhang, N. (2020). Does the SO2 Emissions Trading Scheme Encourage Green Total Factor Productivity? an Empirical Assessment on China's Cities. *Environ. Sci. Pollut. Res.* 27, 6375–6388. doi:10.1007/s11356-019-07273-6

Iyer, D. N., and Miller, K. D. (2008). Performance Feedback, Slack, and the Timing of Acquisitions. *Acad. Manag. J.* 51 (4), 808–822. doi:10.5465/amj.2008.33666024

Latham, S. F., and Braun, M. R. (2008). The Performance Implications of Financial Slack during Economic Recession and Recovery: Observations from the Software Industry (2001~2003). *J. Manag. Issues* 20 (1), 30–50.

Li, W., and Zheng, M. (2016). Is it Substantive Innovation or Strategic Innovation? the Impact of Macroeconomic Industry Policies on Micro-enterprise Innovation. *Econ. Res. J.* 4, 60–73.

Li, X., and Liu, C. (2010). High-discretion Slack Resources or Low-Discretion Slack Resources-An Empirical Study on the Structure of Organizational Slack. *China Ind. Econ.* 7, 94–103.

Li, X. (2021). Environmental Regulation, Government Subsidies and Regional Green Technology Innovation. *Econ. Surv.* 38 (03), 14–23. doi:10.15931/j.cnki.1006-1096.2021.03.002

Liang, D., Dong, H., Fujita, T., Geng, Y., and Fujii, M. (2015). Cost-effectiveness Analysis of China's Sulfur Dioxide Control Strategy at the Regional Level: Regional Disparity, Inequity and Future Challenges. *J. Clean. Prod.* 90, 345–359. doi:10.1016/j.jclepro.2014.10.101

Lim, S., and Prakash, A. (2014). Voluntary Regulations and Innovation: The Case of ISO 14001. *Public Admin Rev.* 74 (2), 233–244. doi:10.1111/puar.12189

Nakaishi, T., Takayabu, H., and Eguchi, S. (2021). Environmental Efficiency Analysis of China's Coal-Fired Power Plants Considering Heterogeneity in Power Generation Company Groups. *Energy Econ.* 102, 1–13. doi:10.1016/j.eneco.2021.105511

Nie, H., Tan, S., and Wang, Y. (2018). Innovation, Firm Size and Market Competition: From the Evidence of Firm-Level Panel Data in China. *J. World Econ.* 7, 57–66. doi:10.3969/j.issn.1002-9621.2008.07.005

Ren, S., Sun, H., and Zhang, T. (2021). Do Environmental Subsidies Spur Environmental Innovation? Empirical Evidence from Chinese Listed Firms. *Technol. Forecast. Soc. Change* 173, 1–12. doi:10.1016/j.techfore.2021.121123

Schreifels, J. J., Fu, Y., and Wilson, E. J. (2021). Sulfur Dioxide Control in China: Policy Evolution during the 10th and 11th Five-Year Plans and Lessons for the Future. *Energy Policy* 48, 779–789. doi:10.1016/j.enpol.2012.06.015

Sharma, S., and Vredenburg, H. (1998). Proactive Corporate Environmental Strategy and the Development of Competitively Valuable Organizational Capabilities. *Strat. Mgmt. J.* 19 (8), 729–753. doi:10.1002/(sici)1097-0266(199808)19:8<729::aid-smj967>3.0.co;2-4

Shi, G., Zhou, L., Zheng, S., and Zhang, Y. (2016). Environmental Subsidy and Pollution Control: an Empirical Study Based on the Power Industry. *Economics* 15, 1439–1462.

Usman, M., and Jahanger, A. (2021). Heterogeneous Effects of Remittances and Institutional Quality in Reducing Environmental Deficit in the Presence of EKC Hypothesis: a Global Study with the Application of Panel Quantile Regression. *Environ. Sci. Pollut. Res.* 28 (28), 37292–37310. doi:10.1007/s11356-021-13216-x

Usman, M., Makhdum, M. S. A., and Kousar, R. (2021). Does Financial Inclusion, Renewable and Non-renewable Energy Utilization Accelerate Ecological Footprints and Economic Growth? Fresh Evidence from 15 Highest Emitting Countries. *Sustain. Cities Soc.* 65, 102590. doi:10.1016/j.scs.2020.102590

Wang, H., Tang, X., Xu, P., and Dong, Q. (2021). Effects and Influencing Mechanism of Environmental Subsidies on Regional Innovation Ability-Based on the Perspective of Spatial Spillover. *J. Statistics* 2 (8), 53–66.

Wang, Juanru., and Zhang, Yu. (2018). Environmental Regulation, Green Technology Innovation Intention and Green Technology Innovation Behavior. *Stud. Sci. Sci.* 36 (2), 321–360.

Wang, K., Yang, G., Liu, J., and Li, X. (2015). Research on Competition for IPO Resources, Government Subsidies and Companies' Business Performance, 9. *Manag. World*, 147–157.

Wang, M., and Li, Y. (2021). Market Regulation, Product Consumption Choice and Enterprise Green Technological Innovation. *J. Eng. Manag.* 35 (2), 44–54. doi:10.13587/j.cnki.jieem.2021.02.005

Wang, X., and Wang, F. (2019). No Resource or No Motivation? Government Subsidies, Green Innovation and Incentive Strategy Selection. *Sci. Res. Manag.* 40 (7), 131–139. doi:10.19571/j.cnki.1000-2995.2019.07.013

Wang, Y., and Zhang, Y. (2020). Do State Subsidies Increase Corporate Environmental Spending? *Int. Rev. Financial Analysis* 72, 1–11. doi:10.1016/j.irfa.2020.101592

Wen, Z., and Ye, B. (2014). Analyses of Mediating Effects: The Development of Methods and Models. *Adv. Psychol. Sci.* 22 (5), 731–745. doi:10.3724/sp.j.1042.2014.00731

Wu, J., Tian, Z., and Long, X. (2018). The Impact of Government Subsidies on Corporate Innovation in Strategic Emerging Industries. *Stud. Sci. Sci.* 36 (1), 158–166.

Xiao, P., Jiang, A., and Yun, Y. (2019). Private Investment, Environmental Regulation and Green Technological Innovation-Analysis of Spatial Dubin Model Based on 11 Provinces and Cities in the Changjiang River Economic Belt. *Sci. Technol. Prog. Policy* 8, 44–51.

Xing, H., Wang, F., and Gao, S. (2019). Does Government Subsidy Promote Substantial Innovation in Enterprises: Influence Mechanism Based on Resource and Signal Transmission Attributes. *Mod. Econ. Res.* 3, 57–64.

Yan, G., and Yang, J. (2008). Implementing Mechanism of Total Emission Control SO2 in Power Sector. *Environ. Sci. Technol.* 5, 134–138.

Yan, X., Jin, X., and Tong, T. (2019). Research Hotspots and Development Outline of China's Environmental Regulations: Based on Visualization Analysis of CNKI. *Jiang Xi Soc. Sci.* 5, 99–110.

Yang, J., Liu, Q., and Shi, J. (2015). The Value of Corporate Green Innovation Strategy. *Sci. Res. Manag.* 36 (1), 18–25.

Zhang, G., and Zhang, X. (2011). Review and Prospect of the Green Innovation Research Outline in Foreign Countries. *Foreign Econ. Manag.* 33 (8), 25–32.

Zhang, J., Zhang, Y.-x., Yang, H., Zheng, C.-h., Jin, K., Wu, X.-c., et al. (2017). Cost-effectiveness Optimization for SO 2 Emissions Control from Coal-Fired Power Plants on a National Scale: A Case Study in China. *J. Clean. Prod.* 165, 1005–1012. doi:10.1016/j.jclepro.2017.07.046

Zhao, X., and Ma, C. (2013). Deregulation, Vertical Unbundling and the Performance of China's Large Coal-Fired Power Plants. *Energy Econ.* 40, 474–483. doi:10.1016/j.eneco.2013.08.003

Conflict of Interest: The authors declare that the research was conducted in the absence of any commercial or financial relationships that could be construed as a potential conflict of interest.

Publisher's Note: All claims expressed in this article are solely those of the authors and do not necessarily represent those of their affiliated organizations, or those of the publisher, the editors, and the reviewers. Any product that may be evaluated in this article, or claim that may be made by its manufacturer, is not guaranteed or endorsed by the publisher.

frontiers | Frontiers in Energy Research

ORIGINAL RESEARCH
published: 13 July 2022
doi: 10.3389/fenrg.2022.904079

Performance Verification of Bayesian Network–Based Security Risk Management and Control System for Power Trading Institutions

Shuqin Kong, Lin Tian, Jiansheng Sheng, En Lu, Jingqing Luo and Yun Xu*

Guangdong Power Exchange Center Co. Ltd, Guangzhou, China

Risk in power trading is unavoidable for various reasons. The impact of this risk would vary based on the trading characteristics that mainly depend on the market design and power purchase agreements. So, a security risk management and control system for power trading institutions based on a Bayesian network is designed to reduce the risk of power trading projects. As a part of the network, we first provided the overall architecture of the risk management and control system, which includes a malicious network behaviour detection module, controller selection module, data transmission module, and management and control result visualisation module. Second, the hardware test design was implemented by analysing each module's working principle and function. Based on the hardware design of the system, the regression analysis method is used to evaluate the risk of power transactions, followed by market fluctuation prediction to obtain the prediction result induced risks. The relationship between security risks and risk-influencing factors is analysed using the Bayesian network. The initial list of risks is established, the uncertain risk factors are reasoned, and the security risk management and control model of power trading institutions is tested to achieve the goal of risk management and control. The experimental results show that this method's risk management and control efficiency are high. At the same time, this method effectively realised comprehensive risk identification by reducing the loss to power enterprises and has near-practical application value.

Keywords: Bayesian network, electricity trading, risk control, virtual link, regression analysis method

OPEN ACCESS

Edited by:
Nallapaneni Manoj Kumar, City University of Hong Kong, Hong Kong SAR, China

Reviewed by:
Benyoh Emmanuel Kigha Nsafon, Kyungpook National University, South Korea
Premkumar M., GMR Institute of Technology, India

****Correspondence:***
Shuqin Kong
shuqing_kong@163.com

Specialty section:
This article was submitted to Sustainable Energy Systems and Policies, a section of the journal Frontiers in Energy Research

Received: *25 March 2022*
Accepted: *10 June 2022*
Published: *13 July 2022*

Citation:
Kong S, Tian L, Sheng J, Lu E, Luo J and Xu Y (2022) Performance Verification of Bayesian Network–Based Security Risk Management and Control System for Power Trading Institutions. Front. Energy Res. 10:904079. doi: 10.3389/fenrg.2022.904079

1 INTRODUCTION

Network technologies (NTs) are being widely used in many applications. NTs mainly use data systems to manage and deliver digital resources through a computer network built specifically for a particular sector (Syuntyurenko and Gilyarevskii, 2021). Various industries currently use computer hardware and system software that maintain NTs. However, with the rapid development of information technology, the application scope of NTs has gradually expanded, especially for the emerging fields (cloud computing and big data) (Syuntyurenko and Gilyarevskii, 2021). The rise of NTs has greatly facilitated the stakeholders' engagement and brought solid support for enterprise development and national progress (Charwand and Gitizadeh, 2018; Rinalini and Prakash, 2018). Although the convenience of using NTs has brought numerous opportunities, the increase in the number of users, software defects, diversification of network attack types, and other factors have

increased the respective risk coefficient. Depending on the application and service (critical or non-critical), the impact of risk varies.

Considering the power and energy sector, NTs play a crucial role in power trading. At present, power transactions between the seller and buyer in the power industry are usually carried out through the network. A minor defect will lead to the whole system's collapse and failure, putting the power trade and system at risk. The impact of this risk would vary based on the trading characteristics that mainly depend on the market design and power purchase agreements. Therefore, risk management and control of power transactions are of great practical significance to ensure the security of power transactions and enable the smooth operation of power services (Ito et al., 2018; Jack et al., 2018). To better understand the power transaction risk and mitigation measures that are already presented in the literature, we have conducted a brief review and found that only a few studies exist. Gao et al. (2017) designed a risk management method based on a system dynamics model for a power construction project. From the perspective of safety and benefit, the system dynamics model is constructed. Using the system dynamics model, the risk management system is divided into five subsystems: equipment setting, environmental safety, and safety management. Using Vensim_ PLE software, Gao et al. (2017) simulated the risk of a power construction project and obtained the relevant data at the initial stage of the project. They also obtained the safety scheme using an analytic hierarchical process. The system effectively coordinated with the quantities and improved production efficiency, but failed to produce comprehensive risk identification results. Yan et al. (2018) designed a risk management model for power selling companies considering the adoption of new energy resources. A conditional value risk theory model was used to analyse the power purchase proportion of power selling companies upon considering the conditions of new energy resources. At the same time, based on the principal–agent principle, a power sales model was established to analyse the impact of electricity price parameters on power purchase decision-making. Combined with results from the analysis of the two models, effective risk management was realised by Yan et al. (2018). Though this method has delivered a significant decision on risk, it failed to provide insights into economic loss–related decisions that occur in power enterprises' operations. Wang et al. (2018), using a scenario method, simulated some random variables in the context of power selling and purchasing. The variables include spot prices and electricity demand. The results from Wang et al. (2018) revealed that sales and purchase decision-making and risk depend on the existing contracts. It was also observed that renewable energy penetration also has some impact. In another study, Lu et al. (2020) designed a visualisation system for power grid operation risk management and control. The system followed a five-tier architecture, including a network communication layer, model base support layer, data support layer, dynamic editing layer, and application system layer. The system is also enabled with an underlying support platform where relevant functions between various modules are built. Later, based on digital perception technology, the three-dimensional modelling of the power operation scene was carried out by Lu et al. (2020) to demonstrate the risk scene visually. The experimental results show that the system can visually display the scene of power risk and provide support for power risk management and control decision-making. However, the system has the problem of a long response time.

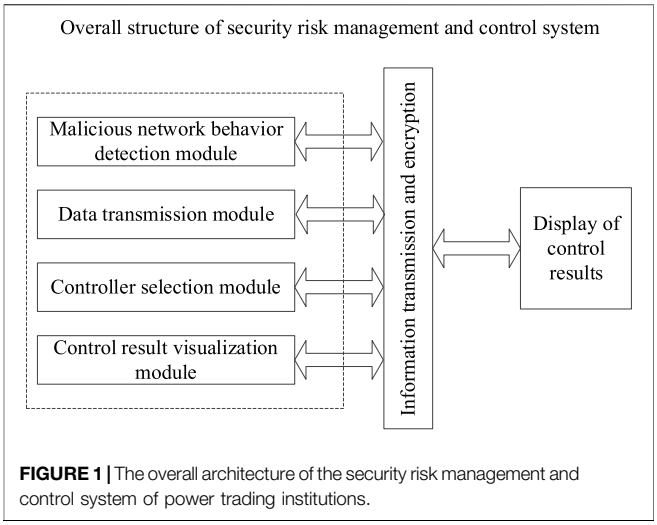

FIGURE 1 | The overall architecture of the security risk management and control system of power trading institutions.

Based on the previous literature study, it is clear that the existing risk management approaches have certain limitations. There is a strong need to improve security in power trading. In order to improve the security of power trading and reduce the risk of power construction projects, this article proposed a Bayesian network–based security risk management and control system. This proposed method will assist power trading institutions with risk-free power transactions. The system improves the comprehensiveness of risk identification, reduces the economic losses of power enterprises, and enables the rapid control of safety risks.

The article is divided into five sections: **Section 2** provides the design of the security risk management and control system, **Section 3** provides various security risk control methods used in this study, and the performance results of the proposed method are presented in **Section 4**, followed by critical conclusions in **Section 5**.

2 DESIGN OF A SECURITY RISK MANAGEMENT AND CONTROL SYSTEM

2.1 Overall Architecture

Security risk management and control of power trading institutions are classified under the power trading system's technical field. In such fields, every system has built an architecture upon which the system's function would depend. Even for our proposed system, there is a need for architecture. The overall architecture of the risk management and control system includes a malicious network behaviour detection module, controller selection module, data transmission module, and management and control result visualisation module. In **Figure 1**, the overall architecture of the system is presented.

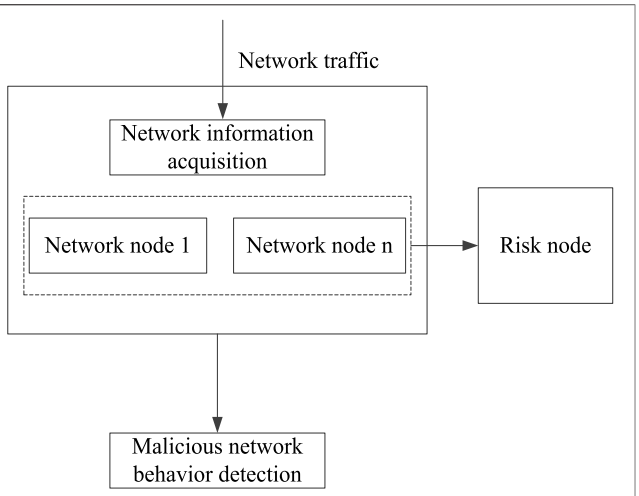

FIGURE 2 | Workflow of the malicious network behaviour detection module.

According to **Figure 1**, under the joint action of the four modules, the effective control of malicious network attacks can be realised, and the control results can be displayed to relevant personnel to help them make corresponding decisions. Therefore, the risk control system designed in this article has a good counteracting effect. Applying the system to the power trading environment can effectively prevent trading risks in the power trading market and assist power enterprises in making scientific decisions.

2.2 System Hardware Module Analysis

The overall architecture of the risk management and control system shown in **Figure 1** can realise the effective control of safety risks under the joint action of various hardware modules. The specific functions and working principles of each module are provided in the following sections.

2.2.1 Malicious Network Behaviour Detection Module

Risk detection and identification are crucial in security risk management and control. Traditionally, the malicious network behaviour detection module is studied as very important research content in signal processing. It is widely used in many fields, such as communication networks and computer networks, to effectively ensure network security (Choi et al., 2019). At this stage, power trading is usually carried out through the network. Therefore, detecting malicious network behaviour in power trading networks is vital. In **Figure 2**, the workflow diagram of the malicious network behaviour detection module is presented.

According to **Figure 2**, the malicious network behaviour detection module mainly comprises the connection relationship between network nodes. When there is a risk, the node with a problem can be marked as a risk node. Because the risk node often presents randomness, the association rule method is used to deal with the risk node. After excluding the risk node, malicious network behaviour detection can be realised.

2.2.2 Data Transmission Module

In security risk management and control, a large amount of data are bound to be generated. Dealing with these data is essential, given that it is a factor related to the effect of risk management and control. Usually, the mobile network will transmit data through a virtual link. The link will carry the data to the mobile network and then forward the data using the virtual link through the routing configuration to reach the desired terminal system location (Wu et al., 2021). **Figure 3** shows how the data transmission is done.

From **Figure 3**, the virtual link seems logical from the data source to the receiving end. Here, the data source refers to the source terminal system. The receiving end refers to the terminal system, that is, the power trading organisation. Virtual links can transmit a variety of data in one-to-one or one-to-many connections. In each virtual link, there is a fixed bandwidth. The bandwidth again differs from one virtual link to another link. In this case, it is necessary to isolate each virtual link to make it independent so that the virtual link will not affect other links during use. At the same time, it will not occupy the bandwidth of other links, which ensures the independence of virtual links and shortens the security risk management and control time. Overall, it will improve the management and control efficiency.

2.2.3 Controller Module Selection

The rapid development of network and information technology has led to a sharp increase in data. Large amounts of data bring convenience to people but make the extraction and mining of data more difficult. In the context of power trading, the power transaction data are the internal information of electrical enterprises. Hence, the privacy-sensitive data in power transactions should be encrypted to improve the accuracy of the data and ensure that confidential information is not leaked. Specifically, the migration controller is used to encrypt the data. The primary function of the migration controller is to decide

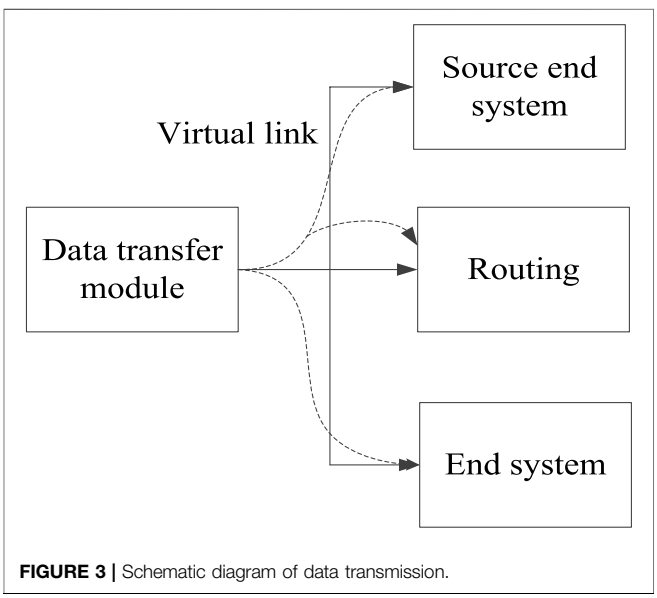

FIGURE 3 | Schematic diagram of data transmission.

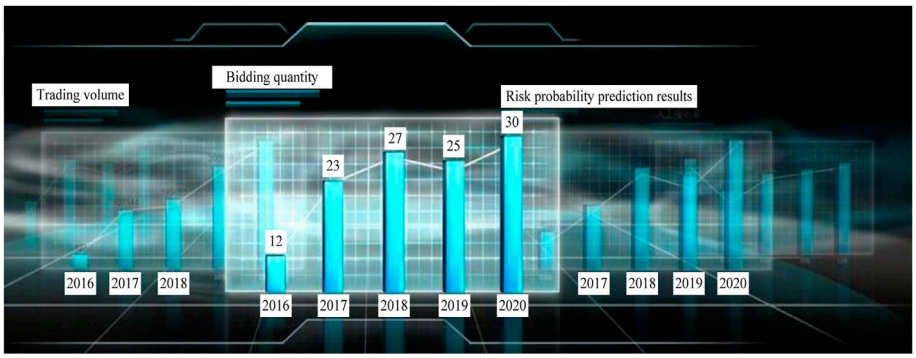

FIGURE 4 | Control result visualisation interface.

which data to encrypt and directly selects the data with encryption requirements (Chen, 2021). The data selection process of the traditional target server is more complex, and the migration controller has the advantage of a light workload.

2.2.4 Control Result Visualisation Module

Power transaction data and risks can be effectively processed with the help of the modules discussed in **Sections 2.2.1–2.2.3**. Therefore, the visual display of control results is the last link of the security risk control system. The results will be displayed to help relevant personnel make power transaction decisions and judgements. **Figure 4** shows the visualisation interface of control results.

It can be seen from **Figure 4** that in the visual interface, the power transaction data and power risk prediction data of power enterprises over the years can be obtained intuitively. Such data can assist relevant personnel in transaction decision-making.

3 SECURITY RISK CONTROL METHODS

Based on the system hardware design, in order to realise the rapid and comprehensive control of security risk, we further studied the security risk management and control methods of power trading institutions.

3.1 Power Transaction Risk Prediction

The operational risk of power trading institutions in all trading links is analysed in a decentralised manner. The regression analysis method as proposed by Goli and Drechsler (2020) is used to assess the risk of power trading so as to realise the risk prediction. **Eq. 1** provides the formulated objective function for risk prediction:

$$f(c) = \ln\sqrt{1-\Delta p} \times \sum_{i=1}^{N} p_i, \tag{1}$$

where $f(c)$ represents the objective function, specifically the electricity transaction cost; Δp represents the risk variation coefficient; p_i represents the state transition matrix; and N represents the number of factors affecting the transaction risk in the electricity market.

The power transaction risk characteristics are represented by the set E, and the global optimisation of the power transaction risk characteristic sequence is carried out to obtain the extreme global value $E_{best}(i)$ and the extreme individual value $A_{best}(i)$. The mathematical notations for $E_{best}(i)$ and $A_{best}(i)$ are given in **Eqs 2**, **3**.

$$E_{best}(i) = \sum_{i=1}^{N}\left(\frac{e_i - f_1}{e_i - f_2}\right), \tag{2}$$

$$A_{best}(i) = \frac{a_j}{\sum_{j=1}^{N} a_j} \Big/ I_{ij}, \tag{3}$$

where e_i represents the risk factor; f_1 and f_2 represents the risk probability distribution density; a_j represents the electricity purchase demand of the electricity transaction; I_{ij} represents the electricity transaction compensation.

Based on **Eqs. 2**, **3**, the market transaction cost proportion of the power transaction risk assessment is obtained using **Eq. 4**. Upon solving **Eq. 4**, the optimal solution for the objective function shown in **Eq. 1** is achieved.

$$p_d^2 = \frac{\sum_{i=1}^{N} p_i w_i}{E_{best}(i) + A_{best}(i)}, \tag{4}$$

where w_i represents the market size.

The benefit gain output of power trading risk B_g is evaluated using:

$$B_g = E^2\left[L(n)^2\right] - w_i, \tag{5}$$

where $L(n)$ represents the equity gain of the power company.

Based on the aforementioned five steps, a quantitative evaluation of power transaction risk is estimated. At the same time, future market fluctuations are predicted, and risk prediction is realised.

3.2 Realisation of Security Risk Management and Control

Based on power trading risk prediction results as per **Section 3.1**, the Bayesian network is used to establish power trading

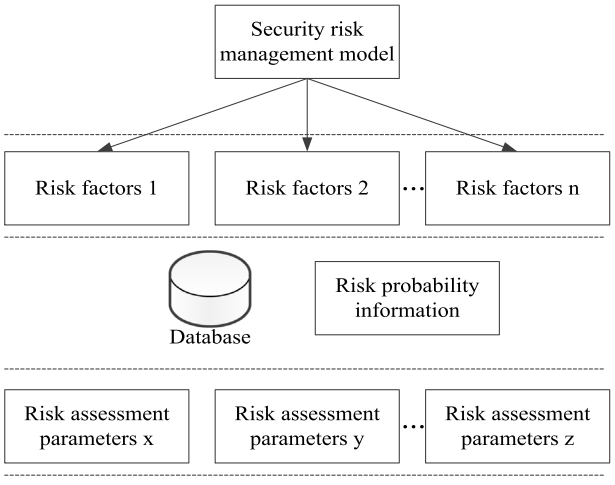

FIGURE 5 | Security risk control model of power trading institutions based on a Bayesian network.

institutions' security risk management and control models. The Bayesian inference and control knowledge are then transformed into a wide range of empirical analyses (Nie et al., 2018; Sierra et al., 2018; Duan et al., 2020). Here, we analyse the relationship between security risk and risk-influencing factors through a Bayesian network to achieve the purpose of risk control. The security risk management and control model of power trading institutions based on a Bayesian network is shown in **Figure 5**.

According to **Figure 5**, the risk management and control model mainly selects the risk characteristics of power transactions from the set E and then establishes an initial list of risks and a Bayesian network structure. Then, the uncertain risk factors are inferred by the Bayesian network (Zhu et al., 2019; Kang et al., 2020; Lou et al., 2020), and the posterior probability of risk occurrence is obtained using

$$P_e^2 = D^2 - [\log_2 R(x)], \tag{6}$$

where D^2 represents the objective probability and $R(x)$ represents the risk probability correction function.

The risk probability information is obtained according to the established risk management and control model, clearly including the entire power transaction stage. Since a large amount of probabilistic information is obtained in risk management and control, the Bayesian network nodes represent and store this information (Roostaei et al., 2021; Yan et al., 2021).

Considering the real-time variability of risk, the conditional transition probability reflects the risk variation coefficient. **Equation 7** is used to estimate the conditional transition probability:

$$T_\alpha = \left[\left(\hat{X} - X\right)^T Q^{-1}\left(\hat{X} - X\right)\right], \tag{7}$$

where X and $\hat{X}$, respectively, represent the risk attributes before and after transfer and Q represents the degree of transfer of attributes.

Assuming that η_1 is the risk attribute before the transfer and η_2 is the risk attribute after the transfer, the transfer process expression between the two is given in:

$$\eta_1 \to \eta_2 = X_{r1}^g + T_\alpha \cdot \left(X_{r1}^g - X_{r2}^g\right), \tag{8}$$

where X_{r1}^g and X_{r2}^g represent the risk impact structure, as given in **Eqs 9**, **10** (Zhao et al., 2021):

$$X_{r1}^g = \frac{x(y+1)}{n \times x}, \tag{9}$$

$$X_{r2}^g = \frac{(x+y)z}{n \times x}, \tag{10}$$

where x, y, and z represent risk assessment parameters.

Upon the successful execution of the aforementioned steps, the design of the security risk management and control method is completed. Then, the effective management and control of the risks in each stage of the power trading project are realised.

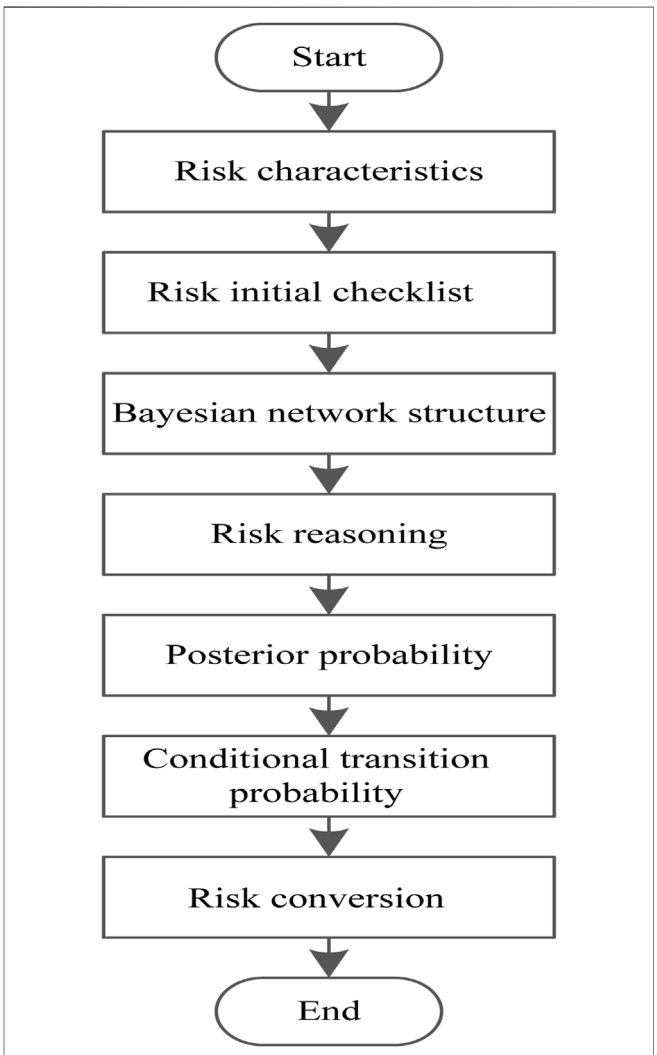

FIGURE 6 | Flow chart of safety risk management and control of power trading institutions.

TABLE 1 | Descriptive statistical results of relevant information of electric power enterprises.

Parameter	Specific value
Transaction price	0.515 yuan
Market transaction electricity	2.34 billion kWh
Electricity direct transaction electricity	1.75 billion kWh
Accumulatively organise and complete the market transaction electricity	970 million kWh
Coal power investment ratio	58%

TABLE 2 | Comparison of results of safety risk management and control efficiency of power trading institutions.

Number of experiments/time	Control time/s		
	This study	Method by Lu et al. (2020)	Method by Gao et al. (2017)
5	12.2	15.7	13.8
10	12.7	16.8	14.6
15	13.5	17.3	17.4
20	13.8	18.9	18.5
25	14.6	19.5	19.2

TABLE 3 | Comparison results of the number of identified attack types.

Type of attack	Attack type identification results		
	This study	Method by Lu et al. (2020)	Method by Gao et al. (2017)
DOS	√	√	×
MAC spoofing	√	×	×
Buffer overflow	√	√	√
Flood attack	√	√	√
Smurf attack	√	×	√

"√"means that the network attack can be identified; "×" means that the network attack cannot be identified.

Figure 6 shows the flow chart of safety risk management and control of power trading institutions.

4 RESULTS AND COMPARISON

Simulation experiments are conducted to test the proposed method's performance for realising security risk management and control between the power trading institutions. Results are shown for the proposed method; in addition, the results are compared with the methods proposed in the literature to verify the effectiveness of our method.

4.1 Simulation Experiment Environment Settings

The experimental hardware platform consists of a Core i7-2350M processor, 8 GB memory, and the Windows 10 operating system. SPSS 22.0 simulation software was used to process experimental data to ensure the accuracy of experimental results. Taking a large power enterprise as the test object, the performance evaluation of the system application was carried out. We collected power transaction data of the enterprise from the past 2 years to obtain a sample dataset containing 3,000 sample values. From this set, some samples are randomly selected to verify the effect of safety risk management and control. **Table 1** shows the results of a descriptive statistical analysis of the relevant information about the power company.

In the aforementioned experimental environment, the control effects of different methods are verified. The results are analysed in **Sections 4.2**.

4.2 Analysis of System Performance Verification Results

4.2.1 Comparison of Safety Risk Management and Control Efficiency

Using the management and control time as an evaluation index for prediction efficiency, we verified power trading institutions' safety risk management and control efficiency. The methods proposed by [5] and [6] are compared with the proposed method, respectively. The comparison results of the safety risk management and control time of power trading institutions are shown in **Table 2**.

According to the results shown in **Table 2**, as the number of experiments continues to increase, the safety risk management and control time of the power trading institutions of the three methods gradually increases. When the number of the experiment is 5 times, the control time of the method proposed by Lu et al. (2020) is 15.7 s and the control time of the method proposed by Gao et al. (2017) is 13.8 s. At the same time, the prediction time using the method proposed in this study is only 12.2 s, which is 25.09% and 12.30% lower than the results obtained by Lu et al. (2020) and Gao et al. (2017), respectively. When the experiment number is 25 times, the control time of the method proposed by Lu et al. (2020) is 19.5 s and the control time of the method proposed by Gao et al. (2017) is 19.2 s. At the same experiment number, the control prediction time using the method proposed in this article is 14.6 s. For the increased

TABLE 4 | Comparison of economic losses in safety risk control.

Quarter first quarter	Economic loss/yuan		
	This study	Method by Lu et al. (2020)	Method by Gao et al. (2017)
Second quarter	123,564.2	200,147.3	236,571.2
Third quarter	98,523.6	174,025.6	198,746.3
Fourth quarter	10,254.9	154,217.6	210,360.1
Quarter	150,263.4	185,247.0	220,304.7

experiment number, the observed difference in prediction time is 28.74% and 27.22%, respectively, when compared to the results provided by Lu et al. (2020) and Gao et al. (2017). Overall, it can be seen that the control time of our proposed method is shorter, indicating that the security risk control efficiency of this method is higher.

4.2.2 Comparison of Security Risk Management and Control System

The number of identified attack types evaluates the comprehensiveness of the risk management, and control effect is evaluated. **Table 3** shows the test results of the number of identified attack types after applying the three methods.

After analysing the experimental results from **Table 3**, it can be seen that our proposed method can accurately identify the five types of attacks, and the identification results are more comprehensive. However, when we use the method by Lu et al. (2020) to identify the attack type, only two network attacks are identified. The MAC spoofing and Smurf attack are also lost. At the same time, the method by Gao et al. (2017) shows the same result, but the lost spoofings are DOS and MAC. So, it can be seen that the identification results of our method are more comprehensive, which shows that it is well suitable for the security risk control of power trading institutions. It can also effectively be used to realise the operational risk management of power trading, thereby improving the profitability of commercial power enterprises and their risk control ability.

4.2.3 Comparison of Economic Losses

The ultimate goal of security risk control of power trading institutions is to reduce the economic losses caused by risks and improve the economic benefits of power enterprises. Therefore, taking 2019 as a representative year, the economic losses after risk control by different methods are compared. The comparison results for economic loss are shown in **Table 4**.

If we observe **Table 4** for the method proposed in this article, the economic loss is 382,606.1 yuan. In contrast, the economic loss for the methods by Lu et al. (2020) and Gao et al. (2017) are 574,837.5 yuan and 986,982.3 yuan, respectively. From this, it can be seen that the economic loss under our proposed control method is the lowest, that is, 40.15% lower than the results provided in Lu et al. (2020) and 88.25% lower than the results provided in Gao et al. (2017). Overall, it can be understood that this method can effectively reduce the economic loss of the power enterprise transaction and may have a positive effect by improving the economic development of the enterprise.

To sum up, the control effect of the method in this article is better than that of the traditional method. It has a positive effect on control efficiency, risk identification, and economic loss, which thoroughly verifies its effectiveness.

5 CONCLUSION

This study aimed to resolve the risk-related problems faced by power trading institutions and the ineffectiveness of the existing methods to tackle such risk. This article proposed a Bayesian network–based security risk management and control system for power trading institutions. The Bayesian network was able to thoroughly analyse the relationship between security risks and risk factors. At the same time, a security risk management and control model for power trading institutions is established to achieve risk management and control. The experimental results showed a positive outcome. The comparisons with the traditional method highlighted the advantages of risk management and control efficiency, the comprehensiveness of risk identification results, and control of power enterprise losses.

DATA AVAILABILITY STATEMENT

The original contributions presented in the study are included in the article/Supplementary Material; further inquiries can be directed to the corresponding author.

AUTHOR CONTRIBUTIONS

Conceptualisation: SK, LT, JS, EL, JL, and YX; methodology: SK; software: SK, EL, JL, and YX; validation: LT, JS, and EL; formal analysis: SK, JL, and YX; investigation: YX; resources: SK; data curation: SK, EL, JL, and YX; writing—original draft preparation: YX; writing—review and editing: YX and LT; visualisation: SK; supervision: SK; project administration: SK; and funding acquisition: SK. All authors have read and agreed to the published version of the manuscript.

FUNDING

This work is supported by the Science and technology project support of China Southern Power Grid Corporation (GDKJXM20201925).

REFERENCES

Charwand, M., and Gitizadeh, M. (2018). Risk-Based Procurement Strategy for Electricity Retailers: Different Scenario-Based Methods. *IEEE Trans. Eng. Manag.* 67 (1), 141–151. doi:10.1109/TEM.2018.2864132

Chen, M. (2021). Accounting Data Encryption Processing Based on Data Encryption Standard Algorithm. *Complexity* 2021 (5), 1–12. doi:10.1155/2021/7212688

Choi, C., Esposito, C., Lee, M., and Choi, J. (2019). Metamorphic Malicious Code Behavior Detection Using Probabilistic Inference Methods. *Cognitive Syst. Res.* 56 (8), 142–150. doi:10.1016/j.cogsys.2019.03.007

Duan, Z., Wang, L., and Sun, M. (2020). Efficient Heuristics for Learning Bayesian Network from Labeled and Unlabeled Data. *Intell. Data Anal.* 24 (2), 385–408. doi:10.3233/ida-194509

Gao, C. Y., Shao, H., Bi, H., Zhang, Z., and Song, X. (2017). System Dynamics Model for Electric Construction Project Risk Management. *China Saf. Sci. J.* 27 (10), 137–143. doi:10.16265/j.cnki.issn1003-3033.2017.10.023

Goli, M., and Drechsler, R. (2020). PREASC: Automatic Portion Resilience Evaluation for Approximating SystemC-Based Designs Using Regression Analysis Techniques. *ACM Trans. Des. Autom. Electron. Syst.* 25 (5), 1–28. doi:10.1145/3388140

Ito, H., Hanai, K., Saito, N., Kojima, T., Yoshiyama, S., and Fukui, S. (2018). Electricity System Reform Requirements: A Novel Implementation to Grid Management and Control. *IEEE Power Energy Mag.* 16 (2), 46–56. doi:10.1109/mpe.2017.2779552

Jack, M. W., Suomalainen, K., Dew, J. J. W., and Eyers, D. (2018). A Minimal Simulation of the Electricity Demand of a Domestic Hot Water Cylinder for Smart Control. *Appl. Energy* 211 (1), 104–112. doi:10.1016/j.apenergy.2017.11.044

Kang, Y-L., Feng, L-L., and Zhang, J-A. (2020). Research on Subregional Anomaly Data Mining Based on Naive Bayes. *Comput. Simul.* 37 (10), 303–306,316. doi:10.3969/j.issn.1006-9348.2020.10.064

Lou, C., Li, X., and Atoui, M. A. (2020). Bayesian Network Based on an Adaptive Threshold Scheme for Fault Detection and Classification. *Ind. Eng. Chem. Res.* 59 (34), 15155–15164. doi:10.1021/acs.iecr.0c02762

Lu, D., Zhang, Z. Q., Yu, X. P., Li, P. L., Mi, C. M., and Xu, J. (2020). Research on Architecture and Function of Grid Operation Risk Control Visualisation System. *J. Nanjing Univ. Sci. Technol.* 44 (01), 87–93.

Nie, S., Zheng, M., and Qiang, J. (2018). The Deep Regression Bayesian Network and its Applications: Probabilistic Deep Learning for Computer Vision. *IEEE Signal Process. Mag.* 35 (1), 101–111. doi:10.1109/msp.2017.2763440

Rinalini, L., and Prakash, G. C. (2018). Risk-Based Coalition of Cooperative Microgrids in Electricity Market Environment. *IET Generation Transm. Distribution* 12 (13), 3230–3241. doi:10.1049/iet-gtd.2017.1562

Roostaei, J., Colley, S., Mulhern, R., May, A. A., and Gibson, J. M. (2021). Predicting the Risk of GenX Contamination in Private Well Water Using a Machine-Learned Bayesian Network Model. *J. Hazard. Mater.* 411 (10), 125075. doi:10.1016/j.jhazmat.2021.125075

Sierra, L. A., Yepes, V., García-Segura, T., and Pellicer, E. (2018). Bayesian Network Method for Decision-Making about the Social Sustainability of Infrastructure Projects. *J. Clean. Prod.* 176 (1), 521–534. doi:10.1016/j.jclepro.2017.12.140

Syuntyurenko, O. V., and Gilyarevskii, R. S. (2021). Trends and Risks of Network Technologies. *Sci. Tech. Inf. Proc.* 48 (2), 97–106. doi:10.3103/s0147688221020088

Wang, L., Zhang, L., Zhang, F., and Jin, D. (2018). Decision-Making and Risk Assessment of Purchasing and Selling Business for Electricity Retailers. *Autom. Electr. Power Syst.* 42 (1), 47–54. doi:10.7500/AEPS20170522001

Wu, Y., Pickavet, M., and Colle, D. (2021). Analysis of Interference on Mirror-Aided Non-LOS Backhaul Data Transmission in VLC Attocell Networks. *Photonic Netw. Commun.* 41 (7), 189–201. doi:10.1007/s11107-021-00928-w

Yan, H., Zhao, W., and Liu, W. (2018). A Risk Management Model of Power Retailers Considering the Participation of New Energy. *Proc. CSEE* 38 (23), 6947–6954+7128. doi:10.13334/j.0258-8013.pcsee.172693

Yan, H., Wang, F., Yan, G., and He, D. (2021). Hybrid Approach Integrating Case-Based Reasoning and Bayesian Network for Operational Adjustment in Industrial Flotation Process. *J. Process Control* 103 (12), 34–47. doi:10.1016/j.jprocont.2021.05.003

Zhao, Y., Tong, J., and Zhang, L. (2021). Rapid Source Term Prediction in Nuclear Power Plant Accidents Based on Dynamic Bayesian Networks and Probabilistic Risk Assessment. *Ann. Nucl. Energy* 158 (3), 108217. doi:10.1016/j.anucene.2021.108217

Zhu, J., Zhang, W., and Li, X. (2019). Fatigue Damage Assessment of Orthotropic Steel Deck Using Dynamic Bayesian Networks. *Int. J. Fatigue* 118 (1), 44–53. doi:10.1016/j.ijfatigue.2018.08.037

Conflict of Interest: SK, LT, JS, EL, JL, and YX were employed by the company, Guangdong Power Exchange Center Co., Ltd.

frontiers | Frontiers in Energy Research

TYPE Original Research
PUBLISHED 01 September 2022
DOI 10.3389/fenrg.2022.959150

OPEN ACCESS

EDITED BY
Nallapaneni Manoj Kumar,
City University of Hong Kong, Hong Kong SAR, China

REVIEWED BY
Gaurav Saini,
Indian Institute of Engineering Science and Technology, Shibpur, India
Aneesh A. Chand,
University of the South Pacific, Fiji
Ali Thaeer Hammid,
Imam Sadiq University, Iran

*CORRESPONDENCE
Wei-Bin Huang,
xhuang2002@163.com

SPECIALTY SECTION
This article was submitted to Sustainable Energy Systems and Policies, a section of the journal Frontiers in Energy Research

RECEIVED 01 June 2022
ACCEPTED 01 August 2022
PUBLISHED 01 September 2022

CITATION
Zhang S, Ma G-W, Huang W-B, Tao C-H, Yang B-Q and Xue Y-L (2022), Simulation of hydraulic power matching–based risk and economic evaluation among cascade hydropower stations in spot transactions. *Front. Energy Res.* 10:959150. doi: 10.3389/fenrg.2022.959150

Simulation of hydraulic power matching–based risk and economic evaluation among cascade hydropower stations in spot transactions

Shuai Zhang[1], Guang-Wen Ma[1], Wei-Bin Huang[1]*, Chun-Hua Tao[2], Bing-Quan Yang[3] and Yu-Lin Xue[3]

[1]College of Water Resource & Hydropower, Sichuan University, Chengdu, China, [2]Dadu River Hydropower Development Co., Ltd., Chengdu, China, [3]Power China Hydropower Development Group Co., Ltd., Chengdu, China

The electricity market is evolving rapidly from pre-bid to spot markets, where the transactions between producers and consumers have become crucial and are vulnerable to safety risks. In addition, the new modes of transaction are also becoming popular and are said to have some risks. To reveal the impact of the new electricity transaction mode—spot market—on the safety risk and generation benefit, this article presents a simulation method connecting the transaction results and operation process. To verify the effectiveness of the proposed method, an actual cascade hydropower station (CHS) in the Dadu River basin, Southwestern China, which comprises eight hydropower stations, is selected. Hydraulic power matching among the CHSs is discriminated from four aspects with multiple indicators combined with the reality of a hydropower-dominated market in Sichuan, China. The dispatching decision-making process of hydropower generators is described with a multi-objective optimization model and then solved with a fast search strategy based on the classical output calculation method in hydrology. The security risks and economic damage hidden in the day-ahead market on a certain day are discovered and analyzed. The technology proposed provides support for bidding decisions in spot transactions and satisfies the reality during the transition period of electricity reform.

KEYWORDS

electricity spot market, cascade hydropower stations, hydraulic power matching, multi-objective optimization, risk and economic evaluation

1 Introduction

Hydropower is and will be playing a critical role in global carbon neutrality and climate change; its global installed capacity is 1,360 GW (Wang et al., 2022). In China, the installed capacities reached 350 GW (Wang et al., 2022). The scale continues to expand globally and in China with the increasing demand and governmental commitment to

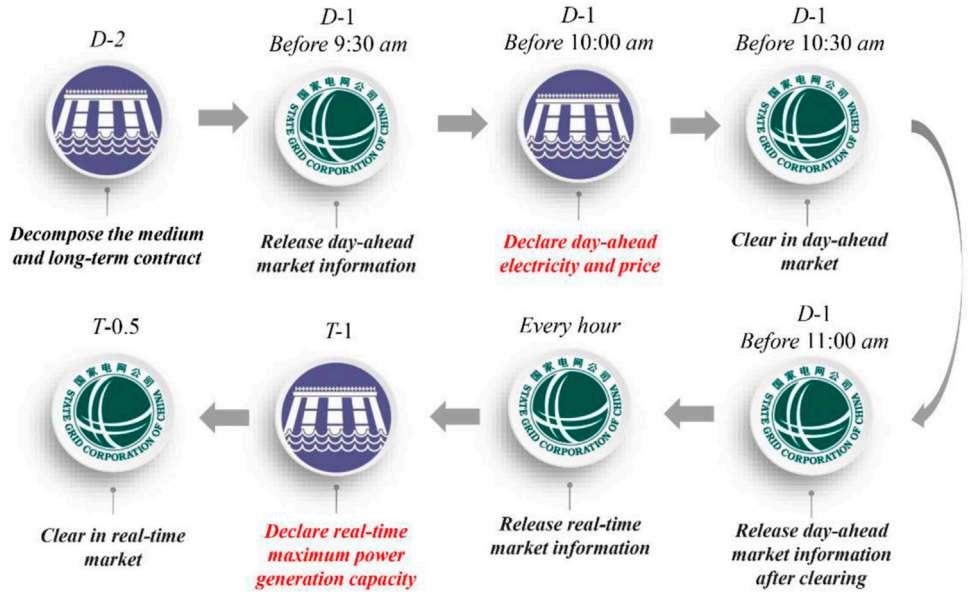

FIGURE 1
The time flow of spot trading in Sichuan.

carbon neutrality (Wang et al., 2022). Though measures have been taken, harvesting hydropower has not been uniform in all the regions for various reasons (Saini and Saini, 2019). When considering enrichment regions such as southwest Sichuan and Yunnan Province of China, harvesting hydropower remains challenging (Zhang et al., 2017). Sichuan is an important energy-producing area with 78 GW hydropower capacity to cover nearly 80% of the regional power supply (both reservoirs and runoff plants) (Luo et al., 2021). Under the constantly deepening electricity market reform, hydropower must be brought to market in Sichuan (Khorasany et al., 2020; Nunna et al., 2020). Unfortunately, a significant number of generators are unfamiliar with spot transactions; therefore, we attempt to build a bridge between the result of spot transactions and the operational process of cascade hydropower stations (CHSs), which shows the potential risks of the transactions more clearly and helps generators in bidding decision-making.

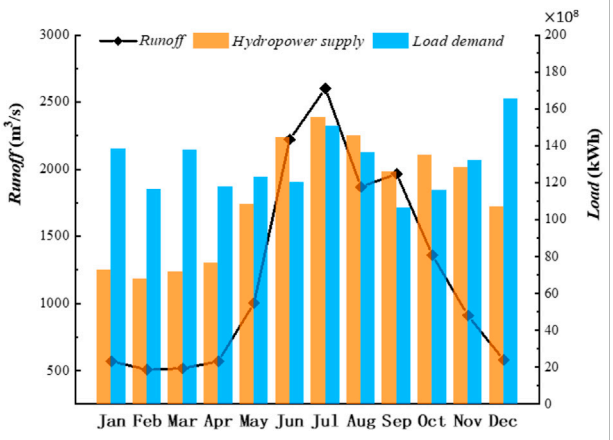

FIGURE 2
Annual runoff, generation, and load demand: Sichuan power grid.

1.1 Research problem and literature review

The power supply is surplus in the wet season but is slightly close-fitting during the rest of the periods in Sichuan, China (Tian et al., 2021). In 2016, the total energy loss of water spillage was 28.75 billion, equivalent to 8 billion CNY (approximately 1.18 billion USD) (Ye et al., 2018). As a result, interprovincial transmission is hindered by channel capacity and economic policies (Li et al., 2018). At the same time, internal absorption lacks low vitality under the current market and dispatching model (Liu et al., 2018). Therefore, there is an urgent need for a market-oriented transaction model which will guide the investment direction accurately, improve the initiative of generators, and reduce the waste of low-carbon and renewable energy (Zhang et al., 2018; Zhang Z. et al., 2021). But the power system reform that came in 2015 introduced more intense competition in the electricity market (Lei et al., 2018); since then, generators can complete medium and long-term contract transactions skillfully (Yu et al., 2019). However, since August 2017, Sichuan and the other seven provinces have been

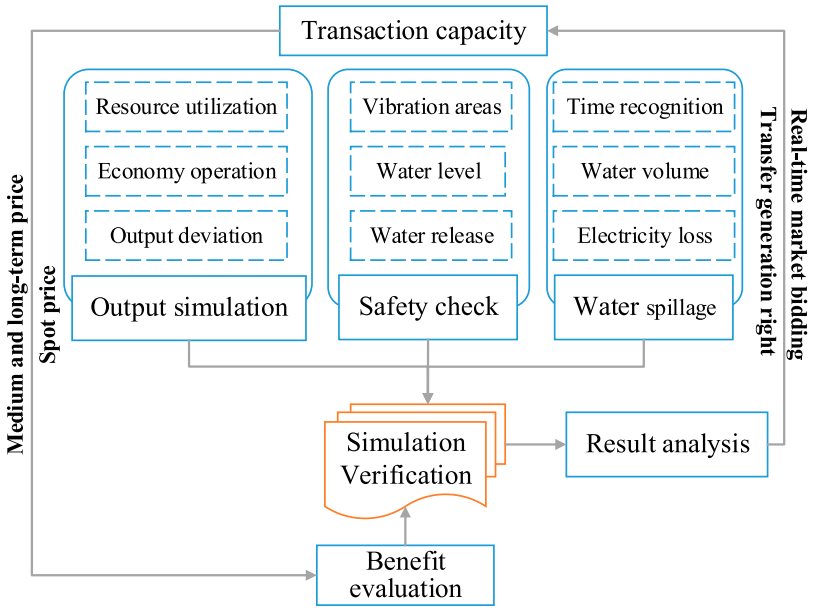

FIGURE 3
Technology roadmap.

encouraged to carry out pilot power spot transactions to provide the experience of full market development. By the end of 2022, each pilot would have been put into trial operation under the government's guidance, but the development process has been slow. As the only hydropower-dominated electricity spot pilot in China (Cai et al., 2021), both market organizers (MO) and generators are not fully prepared for the new market. System operators have habituated themselves in to generating electricity according to dispatching schedules and enjoying preferential pricing from the government (Wang J. et al., 2018; Ye et al., 2020). Subsequently, it has become a mandate to reveal the relationship between the results of spot transactions and the operational process of the reservoirs to expose risks, but research in this cognate area remains sparse. As a result, the day-ahead market has shortened the trading interval to 15 min for power generators. The traditional long-term economic dispatching strategy that aims to maximize generation capacity (Akbari-Dibavar et al., 2021; Lu et al., 2021) is being solved by large-scale optimization algorithms (Niu et al., 2018), which cannot satisfy demand.

Researchers in the literature have achieved some progress in the short-term optimization of CHSs (Sioshansi, 2015; Rasmussen et al., 2016; Apostolopoulou and McCulloch, 2019; Shafiekhani and Badri, 2019; Wang et al., 2019; Lu et al., 2020; Su et al., 2020; Zhang S. et al., 2021). However, there is significant deviation between the linearized solution and actual operation of the power stations (Sioshansi, 2015; Apostolopoulou and McCulloch, 2019). In addition, researchers have paid much attention to the bidding strategy, which directly affects the returns of the generating companies (Shafiekhani and Badri, 2019; Wang et al., 2019; Su et al., 2020). The comparison between the bidding and clearing results has been of less concern (Zhang S. et al., 2021), resulting in ignoring key factors such as unit and reservoir operating safety (Lu et al., 2020). So, turning to MOs could be a possible option, but the transition still lacks a distinct clearing model for the hydropower-dominated spot market. In some other hydropower systems, such as in Brazil and other countries, hydropower is purchased at a subsidized price to ensure adequate power supply (de Queiroz et al., 2016) where the generator can conduct self-dispatching as a pricemaker (Loschenbrand and Korpas, 2019).

On the contrary, in pool-based hydropower systems, such as in Norway and Sweden, the generation schedule and settlement price are determined with unified clearing (Pereira et al., 2017; Seljom and Tomasgard, 2017), similar to that in Sichuan, China. Meanwhile, when considering power line lock, the locational marginal price (LMP) from PJM, US market, is involved (Exizidis et al., 2019; Ali et al., 2021), and then a unique weighed clearing price is obtained. Due to the slow progress of clearing, MOs have to complete this task with security-constrained economic dispatch (SCED) in the day-ahead market (Xu et al., 2017). At the same time, real-time load balance and inflow uncertainty would be solved by bidding in a real-time market (Zhou et al., 2020). Finally, signed contracts in medium- and long-term markets are decomposed and then involved in a settlement-based "contract for difference (CFD)" to minimize bidding risk

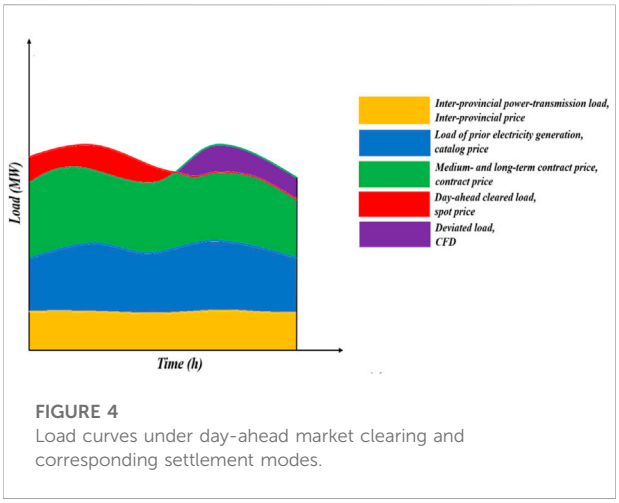

FIGURE 4
Load curves under day-ahead market clearing and corresponding settlement modes.

(Douglas Foster et al., 2019). The root cause of this issue is attributed to the complex, nonlinear coupling relationship between the CHSs, which is shown in the following aspects. Firstly, inflow is the primary factor of market supply capacity, resulting in different bidding strategies (Helseth et al., 2017; Li et al., 2019). Then, the water from the upstream power station will be used as the inflow of the downstream power station, which directly affects the power generation process (Wang X. et al., 2018). When multiple owners manage a cascade system, this information is unknown. A study attempted to divide the alliance according to the hydraulic connection to overcome owners' restrictions. The rationality of alliance with the symbiosis theory was proposed by Zhu et al. (2021) which later verified alliance's stability with the game theory (Liu et al., 2020). But here comes a new problem: when there are multiple nodes in the basin, as in the Dadu River, the alliance will collapse automatically and SCED must take the power station as the unit. Last but not the least, different from thermal power (Ye et al., 2017), it is impossible to forecast inflow accurately. However, in timely checking the transaction results according to the real-time parameters and rolling bidding in the real-time market can be a good choice. For this, simulation and verification in advance are essential measures to mine and avoid risks (Huang et al., 2019). The development of intelligent systems and software packages makes this simulation and verification more convenient. Ding Q et al. developed a spot transaction decision support system (Ding et al., 2018). Zakeri et al. (2016) simulated a multiregional electricity market, which made generators respond quickly to changes in market rules and environment. More recently, such simulations and decision-making in the electricity market have become more popular as the power generation systems became an integral part of the smart grid systems (Ringler et al., 2016). Whereas the previous research of Ivar Skjelbred and Kong (2018) made intraday replanning after simulating the actual operation process. The study by Aliabadi et al. (2017) concluded bidding decision-making by simulating the bidding behaviors of generators under different market modes, such as capacity and auxiliary market. Chen et al. (2017) applied the same method in another hydro-dominated environment for the power generation system in Yunnan Province of China.

1.2 Key contributions

Considering the research problem and gap stated in Section 1.1, we re-stored the results of spot transactions for CHSs to the operation process of reservoirs and stations by fully considering the hydroelectric coupling relationship between the CHSs. Some indicators are selected to describe the mismatch between the CHSs quantitatively. The Sichuan electricity spot market is considered as the case study. The meaning and discrimination methods of hydraulic power matching

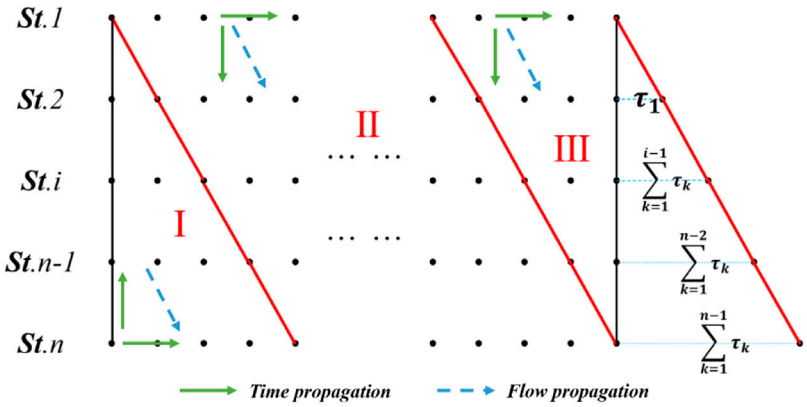

FIGURE 5
The effect of the propagation time of flows τ.

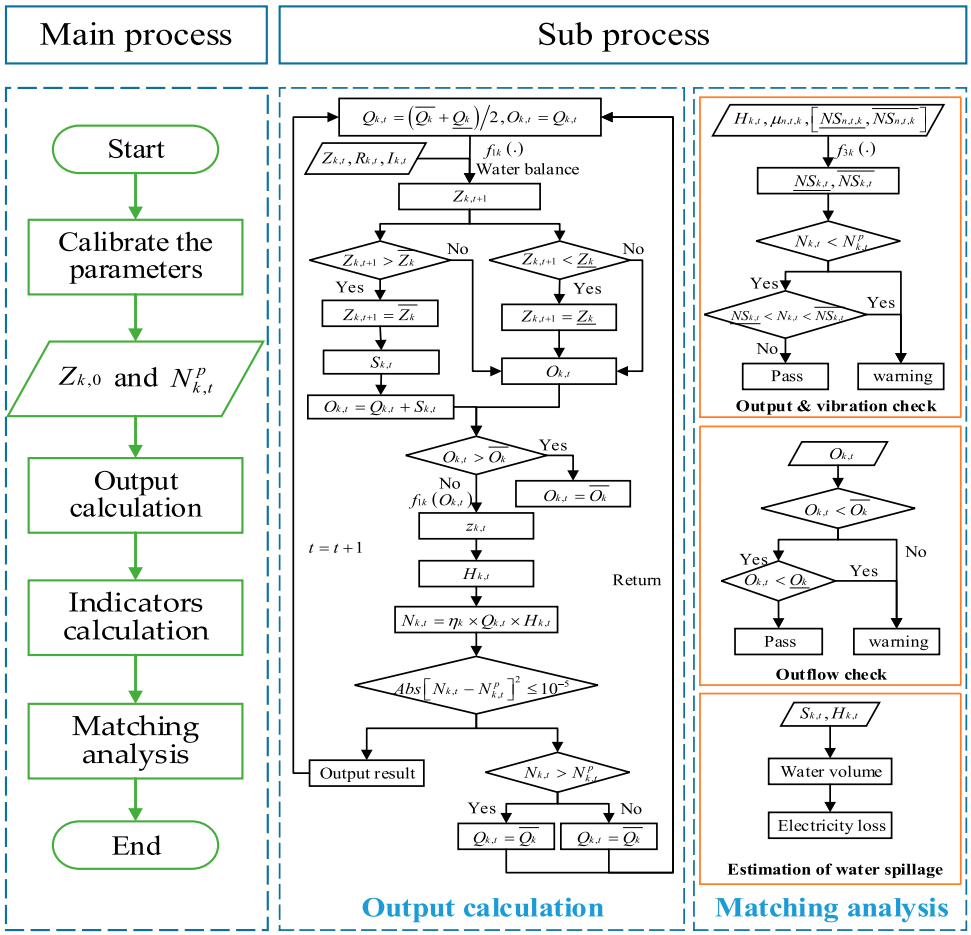

FIGURE 6
Algorithm for simulation and verification.

between the CHSs are described from four aspects with the help of multiple numerical indicators. We simulated the dispatching decision-making process of CHSs with a multi-objective optimization model followed by a fast search strategy for an equilibrium solution. The results provide the basis for load adjustment and bidding decision-making in the real-time market.

The key contributions of this study are as follows:

- In the transition period from the dispatching schedule to market transaction, this study puts forward a reliable risk identification and auxiliary decision-making approach that allows verification with the actual system.
- An efficient and accurate search strategy for multidimensional, nonlinear, and multi-objective problems is proposed, which expands the classical output calculation of hydrology from a single power station to the CHSs.
- The hydraulic power matching between the CHSs is quantified from multiple dimensions, providing a reference for subsequent transaction strategy decision-making and clearing improvement in the hydro-dominated market.

This study is organized into six sections. Section 2 presents the matching discrimination methods for the results of spot transactions. Section 3 demonstrates the model for simulating the dispatching decision-making of the CHSs in a market transaction and its calculation strategy. Section 4 presents the case study and test system used for an investigation, followed by results and discussion in Section 5. Lastly, the conclusions and drawbacks drawn from this study are presented in Section 6.

2 Matching discrimination methods

The spot electricity market is still immature in Sichuan, mainly reflected in the single type of transaction. Currently, only the day-ahead and real-time markets of electric energy have been open for

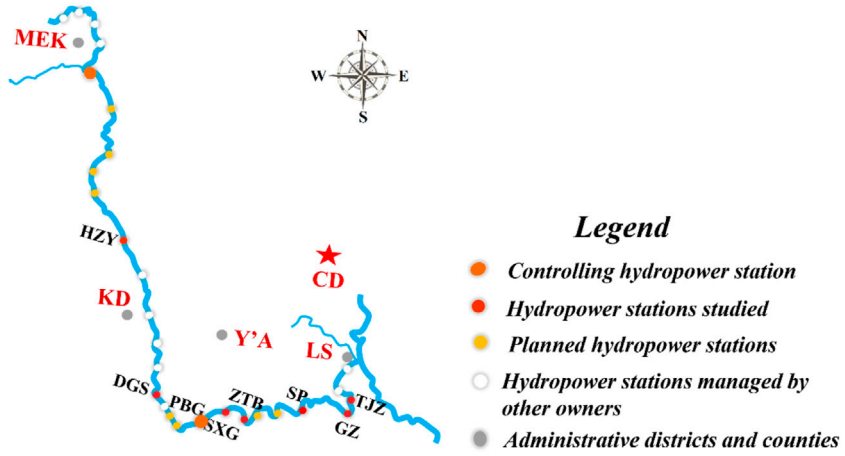

FIGURE 7
Distribution of the hydropower stations.

the time being. In the former, the generators submit each period's generation capacity and bidding price one day in advance (D-1). Turning to the latter, only the maximum generating capacity is submitted 1 hour in advance (T-1). The transaction results are distributed after the unified clearing of the MO. The complete process of spot transactions is illustrated in Figure 1.

Natural runoff significantly affects the supply and demand situation of the high-proportion hydroelectric power market. The supply exceeds demand during the wet season (June to October), resulting in a significant waste of hydropower resources. In the dry season, the supply is close-fitting due to the restrictions in coal supply. To promote hydropower absorption during the wet season, the waste of clean energy is reduced and sufficient power supply during the dry season is ensured, and hydropower plants only participate in spot market bidding during the wet season. The monthly hydropower generation, the power demand of Sichuan, and inflow runoff in the largest hydropower station are therein illustrated in Figure 2.

To maximize the utilization of hydropower resources in the basin, the same owner's CHSs adopt a unified method to optimize the volume and price combination process of each power station in the cascade according to the hydraulic connections therein, thereby forming a volume price and declaration plan for each power station in the cascade. However, the MO pursues minimization of expenditure during market clearing. Meanwhile, large-scale cascade hydropower clusters are often divided into multiple planning units during market clearing. Compared with the declared plan, both loads of a single power station at each time period or the load between the power stations in the same time period must have undergone significant changes. Therefore, it is necessary to simulate the load results according to the mode of organization and verify whether there is a mismatch between hydraulic and power in the cascade system.

The CHSs usually consist of one or two reservoirs connected with a series of runoff stations. The mismatch

TABLE 1 Hydropower station parameters.

Parameter	HZY	DGS	PBG	SXG	ZTB	SP	GZ	TJZ
Installed capacity (MW)	1700	2600	3600	660	720	345	770	700
Maximum water level (m)	1842	1130	850	660	624	554	528	474
Minimum water level (m)	1802	1120	790	655	618	550	520	469
Storage capacity (10^8 m^3)	37.06	7.62	51.22	0.31	0.41	0.15	1.38	1.00
Maximum water discharge (m^3/s)	1474	1834	2772	2619	2697	2825	1876	2536
Rated water head (m)	130	160	148	30	29.5	17.15	48	31
Output factor	8.5	8.5	8.29	8.38	8.34	8.5	8.5	8.5
Regulating performance	Season	Daily	Annual	Daily	Daily	Daily	Daily	Daily
Propagation time (15 min)	—	28	22	2	1	3	4	4

within the CHSs is described as follows: the upstream obtains less volume due to bidding failure, so they have to release less water. As for the downstream, the low running water head makes the power generation task impossible to complete when water is insufficient. This deviation may cause a loss of revenue. As the reservoir reaches the upper limit of storage capacity, all stations are forced to release water; a large amount of water spillage means clean energy wastage. Unfortunately, this mismatch occurs almost every day in the wet season.

The matching verification focuses on four aspects and has been quantified with many indicators. Firstly, output simulation ensures that the real-time output covers the transaction results and fully uses the water resources. Secondly, safety operations are checked to verify whether the hydraulic and electric constraints are damaged. Then, more attention is paid to the process of water spillage, the quantity of water, and generation of waste. Lastly, the benefit from the bidding is evaluated according to the settlement rules. When a mismatch occurs, it is advisable to strive for more capability in real-time bidding, which guarantees reservoir safety and benefits in market competition. The technology roadmap is displayed in Figure 3.

2.1 Output simulation

This part analyses the simulation results from the generation output. In addition to the apparent output deviation, the calculation results of the following four indicators can also show the effect on economic operation.

2.1.1 Water resource utilization

It is a numerical indicator reflecting the runoff conversion efficiency of a hydropower plant, which is recorded as E_{wu} (%):

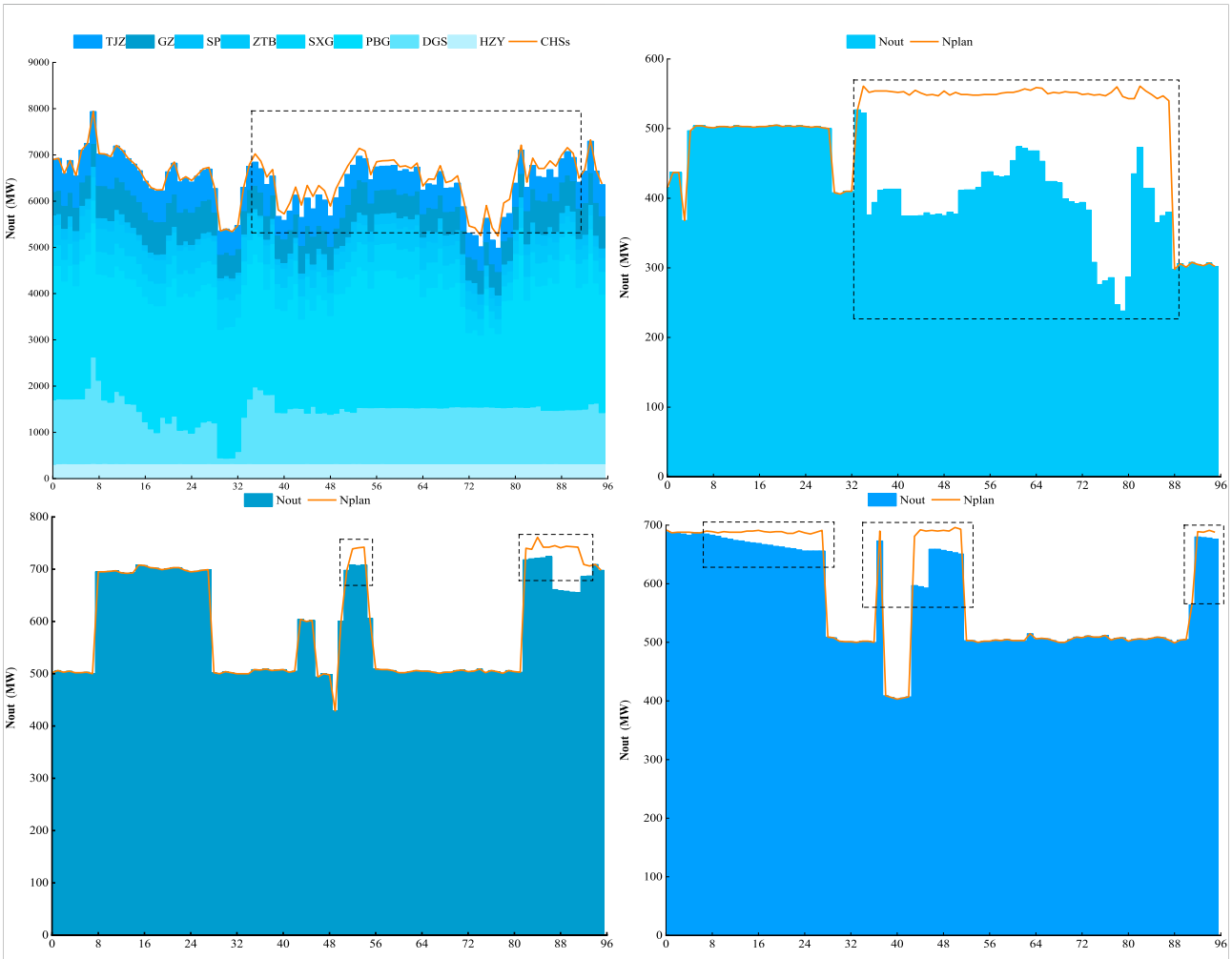

FIGURE 8
Completion results for the load transaction result, from left to right: ZTB, GZ, and TJZ.

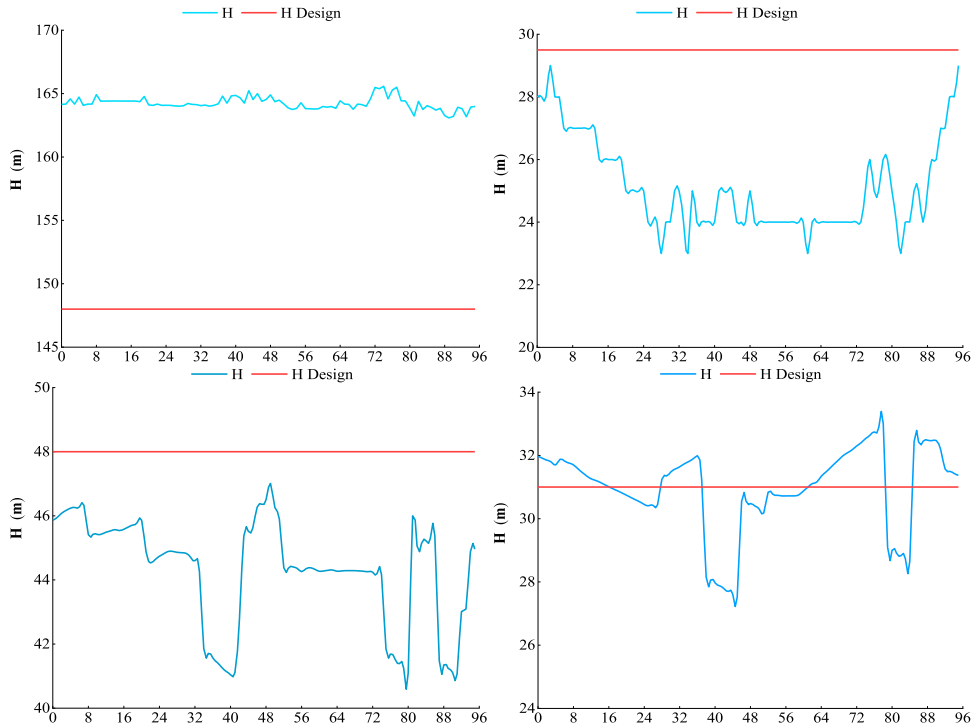

FIGURE 9
Changes in water head during operation, from left to right: PBG, ZTB, GZ, and TJZ.

$$E_{wu} = \sum_{t=1}^{T} N_{k,t} \Big/ \left(\eta_k \times \sum_{t=1}^{T} R_{k,t} \times H_k^D \right), \forall k \in K, \forall t \in T. \quad (1)$$

2.1.2 Load rate

It is an economic indicator to measure the utilization degree of units. It is recorded as E_p (%):

$$E_p = \left(\sum_{t=1}^{T} N_{k,t}/T \right) \Big/ \bar{N}, \forall k \in K, \forall t \in T. \quad (2)$$

2.1.3 Comprehensive water consumption rate

The water consumption per unit of power generation is recorded as $Hsl_{k,t}$:

$$Hsl_{k,t} = \left(Q_{k,t} \times M_t \times 60\right)/E_{k,t}, \forall k \in K, \forall t \in T. \quad (3)$$

2.1.4 Generating equipment availability hours

The operating hours of power generation equipment under full load operation are recorded as Tu_k (h):

$$Tu_k = \sum_{t=1}^{T} E_{k,t} \Big/ \bar{N}_k, \forall k \in K, \forall t \in T. \quad (4)$$

In the calculated results, if the load rate and availability hours are low for the stations with reservoirs, it results in low water resource utilization or high water consumption rate, or even the load transaction task cannot be completed for other stations. This result indicates that the transaction results exhibit the risk of mismatch between upstream and downstream operations.

TABLE 2 Calculated economic operation indices.

Indicator	HZY	DGS	PBG	SXG	ZTB	SP	GZ	TJZ
Water resource utilization (%)	30.5	62.2	131.7	88.9	72.7	42.6	44.7	71.5
Load rate (%)	19.0	44.7	74.0	77.3	58.1	52.4	75.9	81.5
Comprehensive water consumption rate	3.14	2.63	2.58	13.03	21.43	26.96	9.57	13.7
Availability hours (h)	4.6	10.7	17.8	18.6	13.9	12.6	18.2	19.6

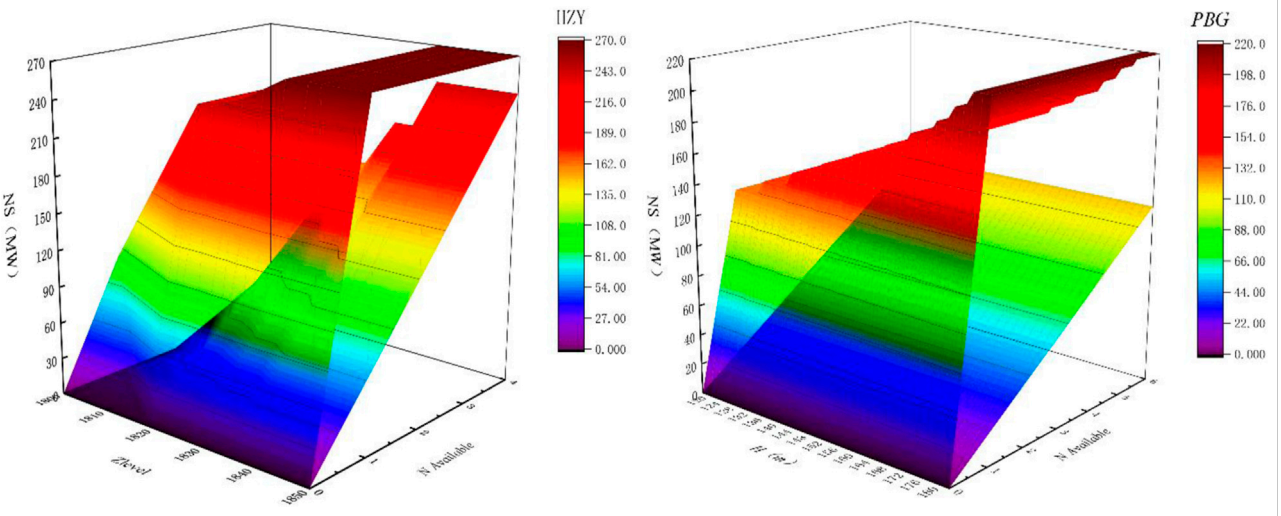

FIGURE 10
Range of fluctuation of hydropower stations HZY and PBG.

2.2 Safety risk identification

The safety of reservoirs and generating units is the basis and premise for successfully implementing transaction results. Therefore, it is necessary to reveal and warn the risks in advance when hydraulic power mismatch threatens the safe operation.

The vibration areas of each plant should be avoided as much as possible during power generation and this is determined by a ternary, implicit function containing the vibration area, real-time net head, and available status of each generation unit:

$$\left[\underline{NS_{k,t}}, \overline{NS_{k,t}}\right] = f_{3k}\left(H_{k,t}, \mu_{n,t,k}, \left[\underline{NS_{n,t,k}}, \overline{NS_{n,t,k}}\right]\right), \quad \forall k \in K, \forall t \in T, \forall n \in N. \tag{5}$$

The forebay elevations of reservoirs are usually limited to below the maximum in the wet season, which leaves surplus storage space for uncertain inflow. However, it is contradictory to the efficient production of electricity. It is insufficient to consider the upper and lower bounds of forebay elevations of reservoirs alone. The change speed of elevations during the dispatching period is also crucial to the safety of hydraulic structures. In particular, this constraint is indispensable for reservoirs.

Besides power generation, reservoirs usually play an important role in shipping, agricultural irrigation, and ecological landscapes. These functions put forward a series of constraints on the water release of the reservoirs.

2.3 Estimation of water spillage

When the forebay elevations of reservoirs gradually rise to the upper bound, the water spillage from the plants will naturally ensue, which implies a waste of renewable energy. The electricity loss with water spillage concerns generators, dispatching institutions, and government sectors.

This part pays attention to three aspects: firstly, time recognition to determine the time and distribution range of spillage water. Secondly, calculated natural water loss in the whole dispatching period. Finally, the conversion of water loss into generation wastage according to Eq. 6:

$$ES_k = \sum_{t=1}^{T} \eta_k \times S_{k,t} \times H_{k,t} \times 0.25, \forall k \in K, \forall t \in T. \tag{6}$$

where ES_k represents the generation wastage caused by water spillage (MW · h).

2.4 Benefit evaluation

In the current electricity market, spot transaction, including day-ahead and real-time markets, is only a supplement to medium- and long-term contracts. The load curves after day-ahead market clearing are formed by superimposing the following curves: interprovincial power-transmission curve, prior electricity generation curve, decomposition curve of medium- and long-term contracts, and the curve in the day-ahead market. Each part uses a different method for settlement, and the specific mode is shown in Figure 4. The first two parts represent fixed price, while the settlement mode based on CFD leads to bidding risk, which directly determines the benefits of the bidding.

CFD is a reasonable path to reduce the loss of bidding failure in the immature market environment. Medium- and long-term contracts can avoid economic risks as far as

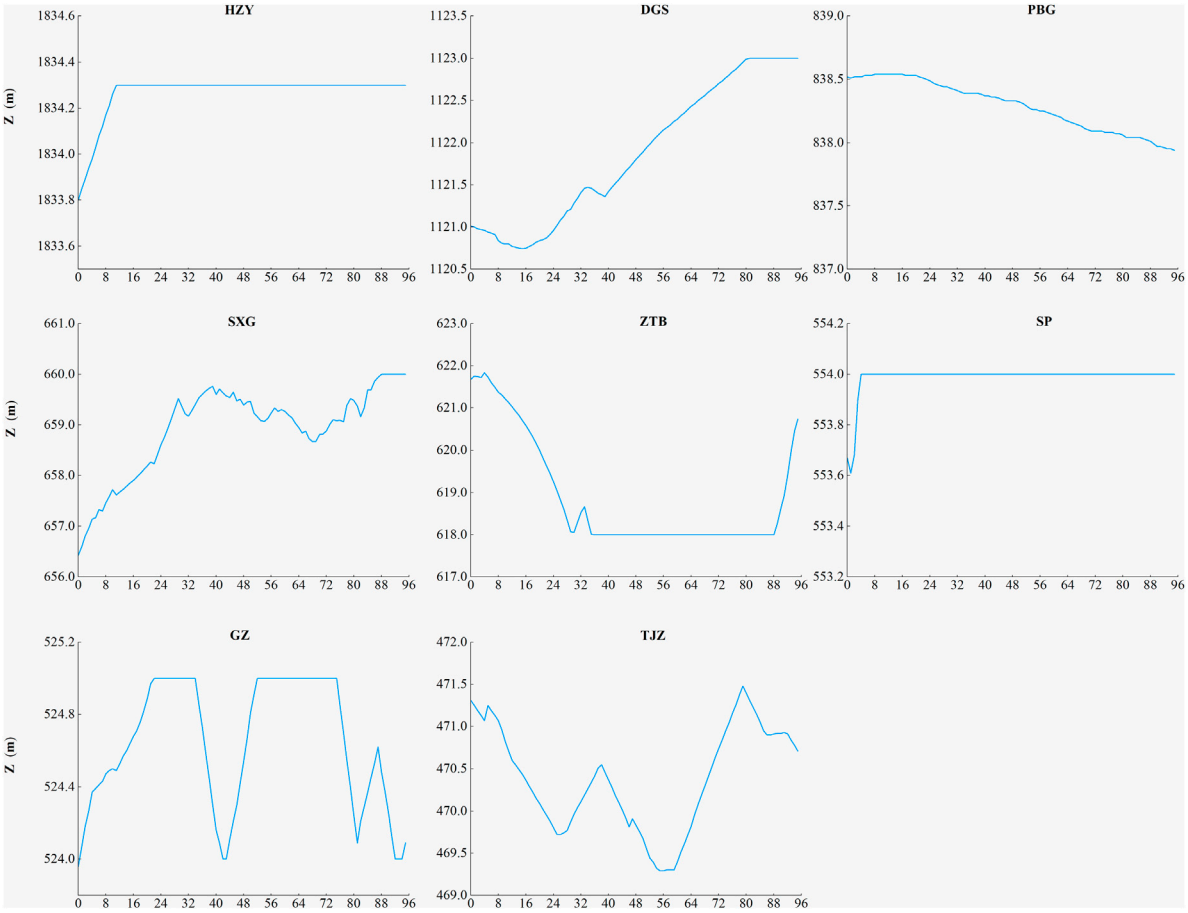

FIGURE 11
Changes in forebay elevations at CHSs.

possible. The profit is mainly from medium- and long-term contracts and day-ahead market, then reducing power deviation in real time. The benefits under the CFD settlement method are calculated as follows:

$$W_k = \sum_{t=1}^{T} E_{k,t} \times P_{k,t}^{d} + \left(E_{k,t} - E_{k,t}^{l}\right) \times \left(P_{k,t}^{d} - P_{k}^{l}\right), \forall k \in K, \forall t \in T, \tag{7}$$

where W_k represents the total benefit (CNY) of station k settled with CFD.

3 Model and algorithm

3.1 Model description

When receiving the transaction result, generators are willing to fully use reservoirs' regulation capacity to complete tasks with low water consumption. However, the failure of hydraulic power matching causes output deviation and water spillage, especially for runoff stations. Therefore, we describe the dispatching decision-making process of CHSs with an optimization model, whose results will reflect the real power generation operation process.

Objective 1: the output of each station shall be close to the transaction result as much as possible, that is, minimizing the deviation:

$$\min \sum_{t=1}^{T} \left(N_{k,t} - N_{k,t}^{p}\right)^2, \forall k \in K, \forall t \in T. \tag{8}$$

Objective 2: improve the utilization efficiency of water resources and reduce water consumption, especially water spillage:

$$\min \sum_{k=1}^{K} \sum_{t=1}^{T} S_{k,t}. \tag{9}$$

Constraint conditions:

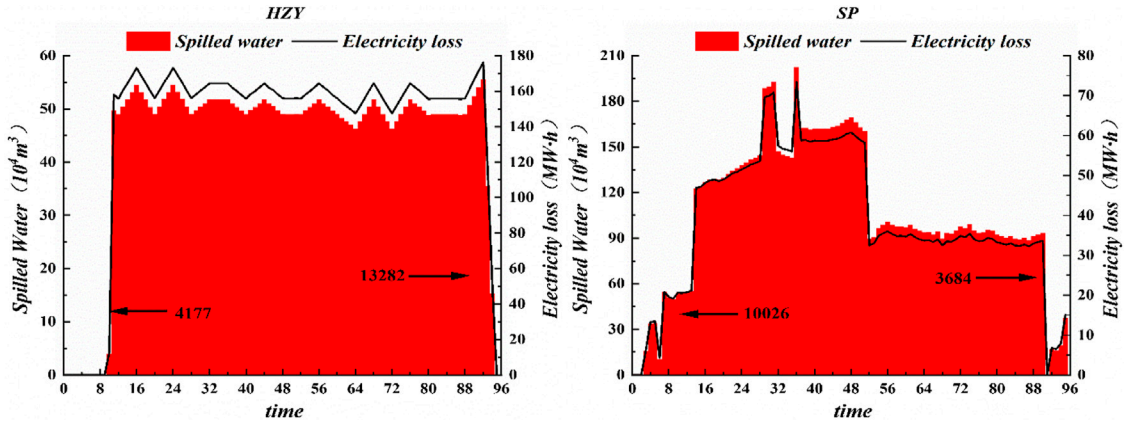

FIGURE 12
Calculated spilled water and generation wastage from HZY and SP.

(a) Water balance

$$V_{k,t+1} = V_{k,t} + \left(R_{k,t} + I_{k,t} - O_{k,t}\right) \times M_t \times 60, \forall k \in K, \forall t \in T, \tag{10}$$

$$I_{k,t} = \begin{cases} \sum_{w \in \Omega_k} O_{w,t-\tau_{k-1,k}}, & \text{if } t - \tau_{k-1,k} \geq 1 \\ 0, & \text{otherwise} \end{cases}, k \geq 2, \forall t \in T,$$
$$V_{1,t} = V_{1,0} + \left[R_{1,t} - O_{1,t}\right] \times M_t \times 60, \forall t \in T \tag{11}$$

$$O_{i,t} = Q_{i,t} + S_{i,t}, \forall k \in K, \forall t \in T. \tag{12}$$

(b) Forebay elevation of reservoirs

$$\underline{Z_{k,t}} \leq Z_{k,t} \leq \overline{Z_{k,t}}, \forall k \in K, \forall t \in T, \tag{13}$$

$$\overline{Z_{k,t}} - \underline{Z_{k,t}} \leq \Delta Z_k, \forall k \in K, \forall t \in T. \tag{14}$$

(c) Water discharge

$$\underline{Q_k} \leq Q_{k,t} \leq \overline{Q_k}, \forall k \in K, \forall t \in T. \tag{15}$$

(d) Water release

$$\underline{O_k} \leq O_{k,t} \leq \overline{O_k}, \forall k \in K, \forall t \in T. \tag{16}$$

(e) Vibration areas of plants

$$\left(N_{k,t} - \underline{NS_{k,t}}\right) \times \left(N_{k,t} - \overline{NS_{k,t}}\right) \geq 0, \forall k \in K, \forall t \in T. \tag{17}$$

(f) Relationship between forebay elevation and volume

$$Z_{k,t} = f_{1k}\left(V_{k,t}\right), \forall k \in K, \forall t \in T. \tag{18}$$

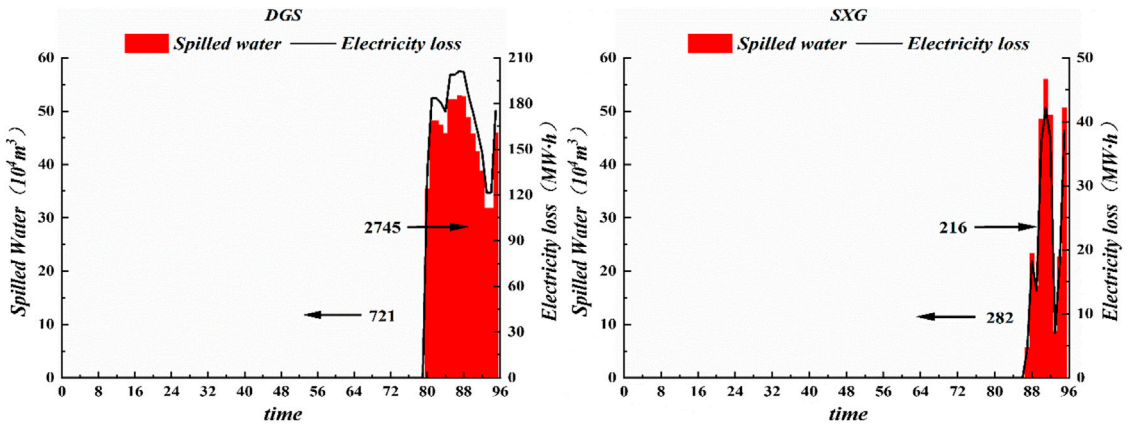

FIGURE 13
Calculated spilled water and generation wastage from DGS and SXG.

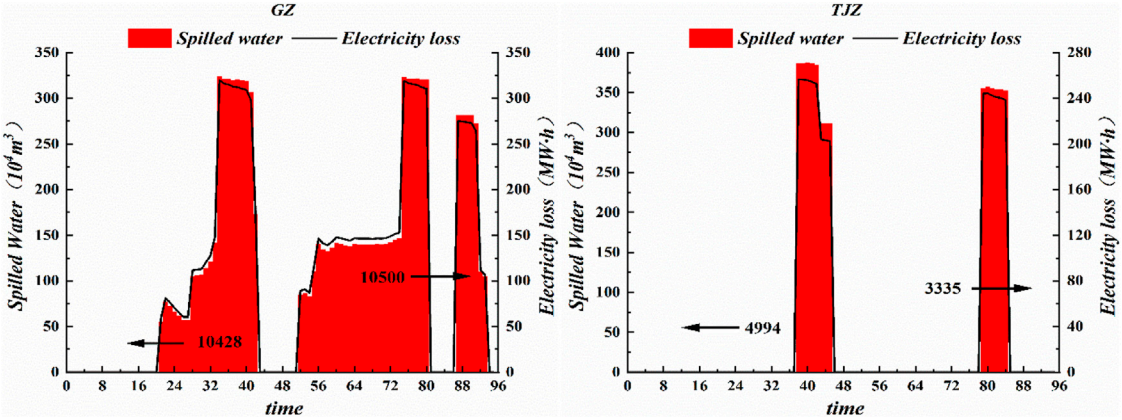

FIGURE 14
Calculated spilled water and generation wastage from GZ and TJZ.

(g) Relationship between tail-race elevation and water release

$$z_{k,t} = f_{2k}(O_{k,t}), \forall k \in K, \forall t \in T. \tag{19}$$

(h) Reservoir net head

$$H_{k,t} = (Z_{k,t} - z_{k.t}) \times (1 - L_k). \tag{20}$$

(j) Hydroelectric power generation function

$$N_{k,t} = \eta_k \times Q_{k,t} \times H_{k,t}, \forall k \in K, \forall t \in T, \tag{21}$$

$$\underline{N_k} \le N_{k,t} \le \overline{N_k}, \forall k \in K, \forall t \in T. \tag{22}$$

(k) Types of variables

$$\begin{aligned} &O_k(t) \ge 0, Q_k(t) \ge 0, S_k(t) \ge 0, \forall k \in K, \forall t \in T, \\ &V_k(t) \ge 0, Hu_k(t) \ge 0, Hd_k(t) \ge 0, \forall k \in K, \forall t \in T, \\ &H_k(t) \ge 0, \forall k \in K, \forall t \in T \end{aligned} \tag{23}$$

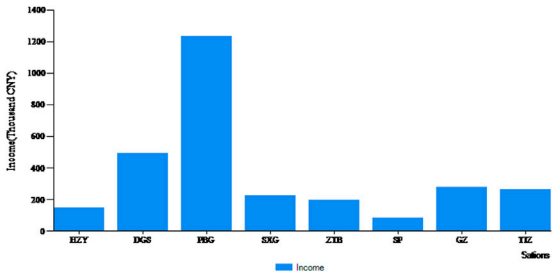

FIGURE 15
Comparison of profit and power generation among the test system.

3.2 Algorithm

The simulation model above is a complex optimization problem with multiple dimensions, stages, and objectives, whose Pareto front is almost impossible to be described thoroughly. Moreover, the time to search for the complete solution set is far more than 15 min, which is not conducive to rapid decision-making in the spot market. Decision makers determine whether there is a mismatch through a few equilibrium solutions in a short time and then formulate bidding strategies in a real-time market. Therefore, we redesigned the fast search algorithm for an equilibrium solution from the reality of decision-making.

The algorithm design considers the following principles: firstly, objective 1 is directly related to the benefits and deserves more attention. Then, minimizing the error during calculation restores the real operation process of the stations' reservoir and runoff. Last but not the least, reasonable time consumption spares enough time for marketing decision-making.

In order to maintain the balance and stability of the grid, generators organize power generation in strict conformity with the transaction results such that the actual output is not greater than the expected output. Suppose the hydraulic power matching relationship is destroyed, the transaction result will be regarded as the infeasible solution of the above optimization. Considering this, we fully use the solution's information and retain the original transaction result as much as possible to reduce the output deviation. The classical output calculation method in hydrology can quickly obtain the forebay elevation and water discharge process corresponding to each result. Especially after complete iteration using binary search, it will converge to the maximum generation capacity corresponding to the current water volume.

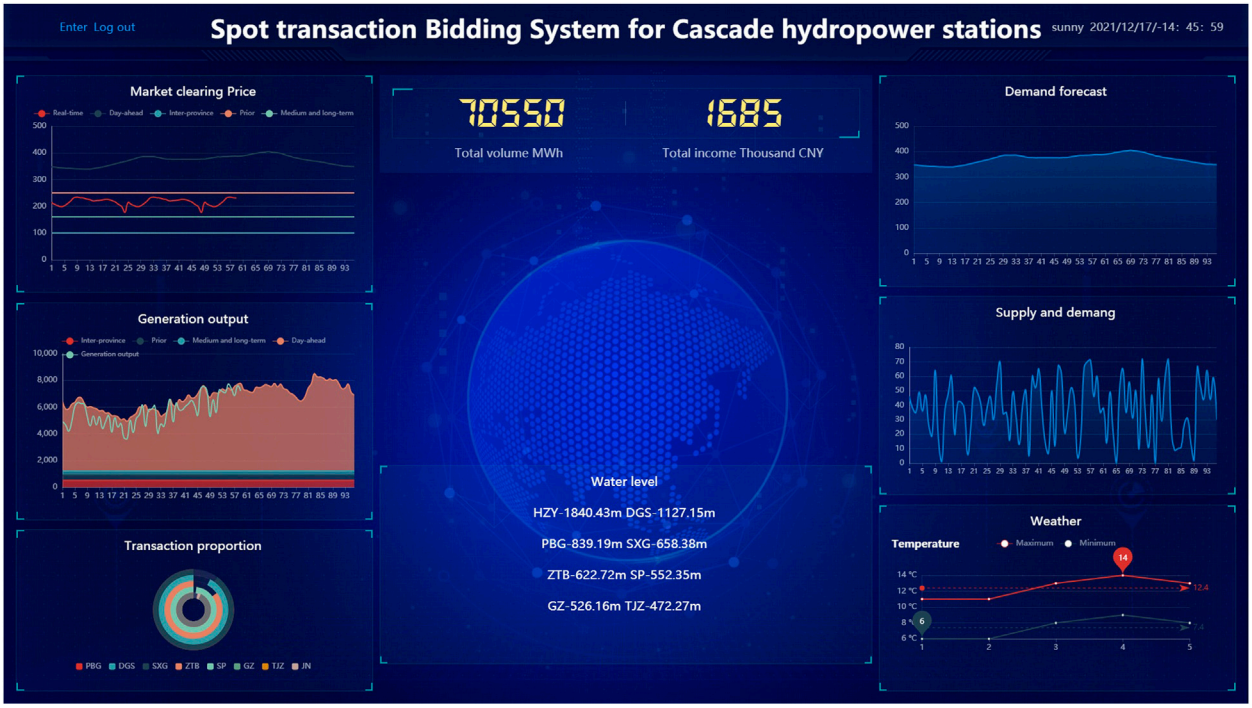

FIGURE 16
Login and home pages of spot transaction bidding system for CHSs of CHN Energy Co., Ltd.

The input of inflow in each period is the key to accurate calculation, and it is also an essential feature of CHSs. However, the propagation time of flows τ between the CHSs cannot be ignored in short-term scheduling operations. Thus, the asynchronous propagation of water energy divides the complete calculation process into three parts, as shown in Figure 5.

We discard the linearization of constraint (21) to maximize the accuracy of the calculation. Moreover, the binary search compresses the target space and ensures the stability of the solution. Finally, the solution set consists of some transaction results and the closest output. It is the dominant solution of objective 1, a Pareto equilibrium solution of the multi-objective problem. The specific steps are described as follows and shown in Figure 6.

Step 1: The initial forebay elevation $Z_{k,0}$ and load transaction result $N_{k,t}^{p}$ are recorded.

Step 2: The inflow information is unknown in both part 2 and 3; thus, the periods of each station in part 1 is first calculated with the output calculation method in hydrology and binary search. The result, including forebay elevation, water discharge, and release, is input to subsequent calculations according to time propagation as shown in Figure 5.

Step 3: The flow propagation in Figure 5 represents the propagation direction of inflow information: the inflow of each period is calculated one by one according to eq. 11, and the output calculation repeated until the operation results of all points are obtained successively.

Step 4: The safety risk and economic evaluation indicators are calculated with the results in Step 3 according to Section 2. Then, the matching among the CHSs is analyzed.

4 Case study: Cascade hydropower system in the Dadu River basin

This article uses an existing cascade system in the Dadu River basin, Southwestern China. The positions and configurations of the CHSs are illustrated in Figure 7, which comprise eight hydropower stations named HZY, DGS, PBG, SXG, ZTB, SP, GZ, and TJZ. Their total capacity reaches 11,095 MW, and the parameters of each station are listed in Table 1. The CHSs are all managed by Dadu River Hydropower Development Co., Ltd. and naturally adopt a consistent bidding strategy in the electricity market. In addition, the total capacity of the eight stations accounts for nearly 20% of the power supply in Sichuan,

Risk warning of safety operaion

Water level: m Generation output: MW Flow: m^3/s

Time	Initial water level	Final water level	Water level status	Transaction ouput	Actual ouput	Output status	Inflow	Water discharge	Water release	Flow status	Head	Vibration area
00:15	553.80	552.80		243	243		0	1733	1733		16.51	
00:30	552.80	551.65		244	244		0	1904	1904		15.08	
00:45	551.65	550.24	Lower	244	244		0	2161	2161		13.30	
01:00	550.24	550.00	Lower	245	223	Insufficient	1722	2825	2825		12.65	
01:15	550.00	550.00	Lower	243	195	Insufficient	1743	2825	2825		13.19	
01:30	550.00	550.00	Lower	246	195	Insufficient	1744	2825	2825		13.19	
01:45	550.00	550.00	Lower	243	191	Insufficient	1685	2825	2825		13.32	
02:00	550.00	550.00	Lower	244	190	Insufficient	1682	2825	2825		13.32	
02:15	550.00	550.00	Lower	214	205	Insufficient	1859	2825	2825		12.94	
02:30	550.00	550.00	Lower	210	205	Insufficient	1860	2825	2825		12.94	
02:45	550.00	550.00	Lower	216	205	Insufficient	1868	2825	2825		12.93	
03:00	550.00	550.00	Lower	219	206	Insufficient	1875	2825	2825		12.91	
03:15	550.00	550.00	Lower	212	206	Insufficient	1881	2825	2825		12.90	
03:30	550.00	550.00	Lower	217	207	Insufficient	1896	2825	2825		12.87	
03:45	550.00	550.00	Lower	215	207	Insufficient	1896	2825	2825		12.87	
04:00	550.00	550.00	Lower	236	200	Insufficient	1799	2825	2825		13.07	
04:15	550.00	550.00	Lower	243	200	Insufficient	1801	2825	2825		13.06	
04:30	550.00	550.00	Lower	242	200	Insufficient	1805	2825	2825		13.05	
04:45	550.00	550.00	Lower	241	201	Insufficient	1813	2825	2825		13.04	
05:00	550.00	550.00	Lower	235	189	Insufficient	1660	2825	2825		13.37	
05:15	550.00	550.00	Lower	236	189	Insufficient	1660	2825	2825		13.37	
05:30	550.00	550.00	Lower	235	189	Insufficient	1661	2825	2825		13.37	

FIGURE 17
Risk warning of safety operation results in the spot transaction bidding system.

China. Any deviation caused by hydraulic power mismatch among the CHSs will threaten the stability of the power grid.

5 Results and discussion

The total load transaction result of the test system mentioned above is 625 GW. However, the load deviation reached 10.1 GW due to mismatch, which accounts for 1.62% and almost covered all the middle and later schedule periods. Among them, the most significant deviation appears in ZTB (8433 MW), accounting for 17.4% of that station's total load transaction result. GZ and TJZ account for 1.2 and 1.8%, respectively. The load deviation time distribution is shown in Figure 8.

Changes in the water heads at some hydropower stations during the operation are plotted in Figure 9 to ascertain the reasons for failure to satisfy the transaction generation. The operating head of the power station is below the design head in ZTB, GZ, and TJZ (TJZ is lower in some periods), which can cause output attenuation among the hydropower stations.

The various economic indices of different CHSs mentioned in Section 4 are calculated and listed in Table 2. The water resource utilization and load rates of HZY, DGS, SP, and GZ are lower than those of the other four hydropower stations. The water consumption rate for ZTB and SP is higher than is for the others because there is a significant negative correlation between the rate of water consumption of hydropower stations and the head of water during the operation of such hydropower stations.

In summary, the hydraulic power mismatching among CHSs is hidden in spot transaction results; the abundant hydropower resources in the basin are not fully utilized in the wet season. HZY, DGS, ZTB, and SP should fully excavate their generation capacity and fully compete in the real-time market.

Figure 10 shows the combination and distribution of vibration zones in HZY and PBG, the two plants with reservoirs and a huge installed capacity in the test system. All CHS units were available on; the check shows that the transaction results of the various hydropower stations in all intraday time periods do not fall within the fluctuation range.

The initial forebay elevations of each station correspond to the forebay elevations at 00:15 on that day. Moreover, the daily rate of change in forebay elevations at hydropower station HZY is 0.5 m/d. In comparison, PBG presents a daily growth rate and reduced rates of 1.2 m/d and 1.5 m/d, respectively. The simulation results of the water level are shown in Figure 11.

The changes in water levels at various hydropower stations were obtained through simulation. Except for hydropower station SP, the highest water levels of the other hydropower stations do not reach the normal pool level. By contrast, the reservoir water levels satisfy the requirement of flood control safety in flood seasons. However, the hydropower station ZTB operates at a low water level for a long time and hydropower stations GZ and TJZ also operate at a low water level for some time periods. This causes the water

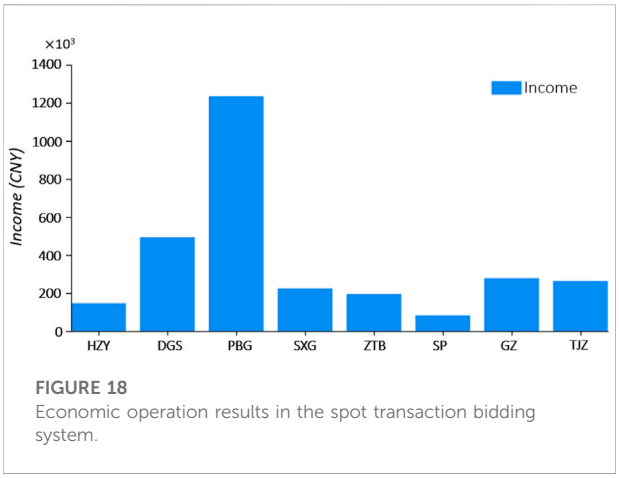

FIGURE 18
Economic operation results in the spot transaction bidding system.

head at these hydropower stations to be much lower than the design head of the generating units.

In summary, 3.38 TW · h of clean electricity is dissipated due to water spillage among the test CHSs, which is more than twice the actual power generation of 1.56 on the day. Nearly all power stations spill water, except PBG and ZTB. It is noticed that this situation happens in all periods in HZY and SP. The spilled water and generation wastage process of each station is illustrated in Figures 12–14. The numbers shown in Figures 12–14 denote the total intraday water loss and generation wastage caused by water spillage at various hydropower stations.

Same as the price bidding strategy, the average price transaction results among CHSs are observed to be the same. Nevertheless, the profits exhibit a noticeable difference (see Figure 15). As an objective economic law, there is a direct natural relationship between income and power generation. For example, the electricity generation at PBG is three to five times that at the other hydropower stations. However, HZY and SP separately account for 1/9 and 1/15 of the electricity generated at PBG.

Moreover, the CFD settlement method causes the loss of profits from power generation. DGS and SP do not satisfy the electrical energy generation required from medium- and long-term markets in many time periods during the bidding process. In this context, the profit margin is squeezed.

The model and technology proposed have been incorporated into the spot transaction bidding system for CHSs of CHN Energy Co., Ltd. (Figure 16). Relying on a comprehensive data collection and transmission cloud platform, the system can automatically capture inflow, water level, unit status, transaction information, and others. Adaptively rolling simulation and deduction can realize real-time transaction risk monitoring a day ahead and assist bid decision-making. Up to now, the system has been running stably for nearly 2 years. The actual risk warning of safety and economic operation results of the system on a certain day are illustrated in Figures 17, 18, respectively.

6 Conclusion

Considering the requirements of electricity market reform and reality in a hydro-dominated power system, a simulation approach to risk and economic evaluation among CHSs in spot transactions was proposed. Hydraulic power matching is the key, as well as a difficulty of the problem, so multiple numerical indicators from four aspects were selected to describe it. Furthermore, a model to simulate the decision-making process of hydropower generators was constructed and solved with an algorithm strategy that considers minimum error and reasonable time consumption. In this process, the classical output calculation of hydrology was expanded from a single power station to CHSs. Finally, a cascade system in Southwest China comprising eight hydropower stations with their real transaction results was used for verification. Through discussion, the security risks and economic damage hidden in the day-ahead market on a certain day were discovered and analyzed. The technique proposed provides support for bidding decisions in spot transactions and satisfies the reality during the transition period of electricity reform.

The proposed method's deficiency lies in regarding the propagation time of flows between the CHSs as a fixed value during calculation. However, the flow propagation time changes dynamically during a hydropower station's actual operation. Thus, the actual propagation time presents a certain difference relative to the fixed value used during calculation, which influences the calculation of the actual change of forebay elevations under corresponding outputs from hydropower stations to some extent. In subsequent research, the propagation time of flows will be introduced to calculations after being graded and calibrated to reduce the errors.

Data availability statement

The original contributions presented in the study are included in the article/supplementary material, and further inquiries can be directed to the corresponding author.

Author contributions

Conceptualization: SZ and GM; methodology: SZ; software: WH; validation: SZ, GM, and CT; formal analysis: BY and YX; resources: CT; writing—original draft preparation: SZ. All authors have read and agreed to the published version of the manuscript.

Funding

This research was funded by the National Natural Science Foundation of China, grant number 52039006; and National Key Research and Development Plans, grant number 2018YFB0905204.

Conflict of interest

Tao C-H was employed by the company Dadu River Hydropower Development Co., Ltd. and Yang B-Q and Xue Y-L were employed by the company Power China Hydropower Development Group Co., Ltd.

The remaining authors declare that the research was conducted in the absence of any commercial or financial relationships that could be construed as a potential conflict of interest.

Publisher's note

All claims expressed in this article are solely those of the authors and do not necessarily represent those of their affiliated organizations, or those of the publisher, the editors, and the reviewers. Any product that may be evaluated in this article, or claim that may be made by its manufacturer, is not guaranteed or endorsed by the publisher.

References

Akbari-Dibavar, A., Mohammadi-Ivatloo, B., Zare, K., Khalili, T., and Bidram, A. (2021). Economic-emission dispatch problem in power systems with carbon capture power plants. *IEEE Trans. Ind. Appl.* 57 (4), 3341–3351. doi:10.1109/tia.2021.3079329

Ali, H., Aslam, F., and Ferreira, P. (2021). Modeling dynamic multifractal efficiency of US electricity market. *Energies* 14 (19), 6145. doi:10.3390/en14196145

Aliabadi, D. E., Kaya, M., and Şahin, G. (2017). An agent-based simulation of power generation company behavior in electricity markets under different market-clearing mechanisms. *Energy Policy* 100, 191–205. doi:10.1016/j.enpol.2016.09.063

Apostolopoulou, D., and McCulloch, M. (2019). Optimal short-term operation of a cascaded hydro-solar hybrid system: a case study in Kenya. *IEEE Trans. Sustain. Energy* 10 (4), 1878–1889. doi:10.1109/tste.2018.2874810

Cai, Z., Li, Q., and Dai, S. (2021). "Discussion on key technologies and model for hydropower-dominated electricity spot market in sichuan," in 2021 China international conference on electricity distribution (CICED), Shanghai, China, 07-09 April 2021, 1074–1078.

Chen, F., Liu, B., Cheng, C., and Mirchi, A. (2017). Simulation and regulation of market operation in hydro-dominated environment: the yunnan case. *Water* 9 (8), 623. doi:10.3390/w9080623

de Queiroz, A. R., Lima, L. M. M., Lima, J. W. M., da Silva, B. C., and Scianni, L. A. (2016). Climate change impacts in the energy supply of the Brazilian hydro-dominant power system. *Renew. Energy* 99, 379–389. doi:10.1016/j.renene.2016.07.022

Ding, Q., Chang, L., and Tu, M. (2018). Key technologies of technical support system for electricity spot market. *Automation Electr. Power Syst.* 42 (23), 7–14. doi:10.7500/AEPS20180509006

Douglas Foster, F., Lee, A. D., and Liu, W.-M. (2019). CFDs, forwards, futures and the cost-of-carry. *Pacific-Basin Finance J.* 54, 183–198. doi:10.1016/j.pacfin.2018.05.004

Exizidis, L., Kazempour, J., Papakonstantinou, A., Pinson, P., De Greve, Z., and Vallee, F. (2019). Incentive-compatibility in a two-stage stochastic electricity market with high wind power penetration. *IEEE Trans. Power Syst.* 34 (4), 2846–2858. doi:10.1109/tpwrs.2019.2901249

Helseth, A., Fodstad, M., Askeland, M., Mo, B., Nilsen, O. B., Pérez-Díaz, J. I., et al. (2017). Assessing hydropower operational profitability considering energy and reserve markets. *IET Renew. Power Gener.* 11 (13), 1640–1647. doi:10.1049/iet-rpg.2017.0407

Huang, J., Lin, C., Zhou, H., Xu, Z., and Lin, C. (2019). Research on key technologies of deduction of multinational power trading in the context of Global Energy Interconnection. *Glob. Energy Interconnect.* 2 (6), 560–566. doi:10.1016/j.gloei.2020.01.010

Ivar Skjelbred, H., and Kong, J. (2018). "Operational hydropower simulation in cascaded river systems for intraday Re-planning," in 2018 power systems computation conference (PSCC), Dublin, Ireland, 11-15 June 2018, 1–7.

Khorasany, M., Mishra, Y., and Ledwich, G. (2020). A decentralized bilateral energy trading system for peer-to-peer electricity markets. *IEEE Trans. Ind. Electron.* 67 (6), 4646–4657. doi:10.1109/tie.2019.2931229

Lei, N., Chen, L., Sun, C., and Tao, Y. (2018). Electricity market creation in China: policy options from political economics perspective. *Sustainability* 10 (5), 1481. doi:10.3390/su10051481

Li, X. Z., Chen, Z. J., Fan, X. C., and Cheng, Z. J. (2018). Hydropower development situation and prospects in China. *Renew. Sustain. Energy Rev.* 82, 232–239. doi:10.1016/j.rser.2017.08.090

Li, Y., Zhao, T., Liu, C., Zhao, Y., Yu, Z., Li, K., et al. (2019). Day-ahead coordinated scheduling of hydro and wind power generation system considering uncertainties. *IEEE Trans. Ind. Appl.* 55 (3), 2368–2377. doi:10.1109/tia.2019.2893836

Liu, S., Bie, Z., Lin, J., and Wang, X. (2018). Curtailment of renewable energy in Northwest China and market-based solutions. *Energy Policy* 123, 494–502. doi:10.1016/j.enpol.2018.09.007

Liu, Y., Ma, G. W., Huang, W. B., Chen, S. J., and Zhang, S. (2020). Analyses of market alliance stability of hydropower stations. *Proc. Institution Civ. Eng. - Water Manag.* 173 (1), 31–45. doi:10.1680/jwama.18.00052

Loschenbrand, M., and Korpas, M. (2019). Multiple nash equilibria in electricity markets with price-making hydrothermal producers. *IEEE Trans. Power Syst.* 34 (1), 422–431. doi:10.1109/tpwrs.2018.2858574

Lu, J., Li, G., Cheng, C. T., and Liu, B. X. (2021). A long-term intelligent operation and management model of cascade hydropower stations based on chance constrained programming under multi-market coupling. *Environ. Res. Lett.* 16 (5), 055034. doi:10.1088/1748-9326/abef90

Lu, J., Li, G., Cheng, C., and Yu, H. (2020). Risk analysis method of cascade plants operation in medium term based on multi-scale market and settlement rules. *IEEE Access* 8, 90730–90740. doi:10.1109/access.2020.2994093

Luo, S., Hu, W., Liu, W., Xu, X., Huang, Q., Chen, Z., et al. (2021). Transition pathways towards a deep decarbonization energy system—a case study in sichuan, China. *Appl. Energy* 302, 117507. doi:10.1016/j.apenergy.2021.117507

Niu, W.-J., Feng, Z.-K., Cheng, C.-T., and Wu, X.-Y. (2018). A parallel multi-objective particle swarm optimization for cascade hydropower reservoir operation in southwest China. *Appl. Soft Comput.* 70, 562–575. doi:10.1016/j.asoc.2018.06.011

Nunna, H. S. V. S. K., Sesetti, A., Rathore, A. K., and Doolla, S. (2020). Multiagent-based energy trading platform for energy storage systems in distribution systems with interconnected microgrids. *IEEE Trans. Ind. Appl.* 56 (3), 3207–3217. doi:10.1109/tia.2020.2979782

Pereira, A. C., de Oliveira, A. Q., Baptista, E. C., Balbo, A. R., Soler, E. M., and Nepomuceno, L. (2017). Network-constrained multiperiod auction for pool-based electricity markets of hydrothermal systems. *IEEE Trans. Power Syst.* 32 (6), 4501–4514. doi:10.1109/tpwrs.2017.2685245

Rasmussen, C., Hansen, J. B. Ø., Korpås, M., and Fodstad, M. (2016). Profitability of a hydro power producer bidding in multiple power markets. *Energy Procedia* 87, 141–148. doi:10.1016/j.egypro.2015.12.344

Ringler, P., Keles, D., and Fichtner, W. (2016). Agent-based modelling and simulation of smart electricity grids and markets – a literature review. *Renew. Sustain. Energy Rev.* 57, 205–215. doi:10.1016/j.rser.2015.12.169

Saini, G., and Saini, R. P. (2019). A review on technology, configurations, and performance of cross-flow hydrokinetic turbines. *Int. J. Energy Res.* 43 (13), 6639–6679. doi:10.1002/er.4625

Seljom, P., and Tomasgard, A. (2017). The impact of policy actions and future energy prices on the cost-optimal development of the energy system in Norway and Sweden. *Energy Policy* 106, 85–102. doi:10.1016/j.enpol.2017.03.011

Shafiekhani, M., and Badri, A. (2019). A risk-based gaming framework for VPP bidding strategy in a joint energy and regulation market. *Iran. J. Sci. Technol. Trans. Electr. Eng.* 43 (3), 545–558. doi:10.1007/s40998-019-00179-6

Sioshansi, R. (2015). Optimized offers for cascaded hydroelectric generators in a market with centralized dispatch. *IEEE Trans. Power Syst.* 30 (2), 773–783. doi:10.1109/tpwrs.2014.2332501

Su, C., Yuan, W., Cheng, C., Wang, P., Sun, L., and Zhang, T. (2020). Short-term generation scheduling of cascade hydropower plants with strong hydraulic coupling and head-dependent prohibited operating zones. *J. Hydrol.* 591, 125556. doi:10.1016/j.jhydrol.2020.125556

Tian, C., Huang, G., and Xie, Y. (2021). Systematic evaluation for hydropower exploitation rationality in hydro-dominant area: a case study of sichuan province, China. *Renew. Energy* 168, 1096–1111. doi:10.1016/j.renene.2020.12.121

Wang, F., Ge, X., Li, K., and Mi, Z. (2019). Day-ahead market optimal bidding strategy and quantitative compensation mechanism design for load aggregator engaging demand response. *IEEE Trans. Ind. Appl.* 55 (6), 5564–5573. doi:10.1109/tia.2019.2936183

Wang, J., Chen, S., Ma, G., Huang, W., and Liu, Y. (2018). Competitiveness of hydropower price and preferential policies for hydropower development in Tibet and the Sichuan-Yunnan Tibetan area of China. *Water Policy* 20 (6), 1092–1111. doi:10.2166/wp.2018.122

Wang, X., Yang, K., and Zhou, X. (2018). Two-stage glowworm swarm optimisation for economical operation of hydropower station. *IET Renew. Power Gener.* 12 (9), 992–1003. doi:10.1049/iet-rpg.2017.0466

Wang, Y., Shi, R., Zhang, C., He, Y., Jiang, H., and Kubota, J. (2022). Structural changes and trends in China's renewable electricity production in the policy evolution process. *Renew. Energy* 182, 879–886. doi:10.1016/j.renene.2021.10.052

Xu, Z., Hu, Z., Song, Y., and Wang, J. (2017). Risk-averse optimal bidding strategy for demand-side resource aggregators in day-ahead electricity markets under uncertainty. *IEEE Trans. Smart Grid* 8 (1), 96–105. doi:10.1109/tsg.2015.2477101

Ye, H., Ge, Y., Shahidehpour, M., and Li, Z. (2017). Uncertainty marginal price, transmission reserve, and day-ahead market clearing with robust unit commitment. *IEEE Trans. Power Syst.* 32 (3), 1782–1795. doi:10.1109/tpwrs.2016.2595621

Ye, Y., Hu, Y., Ma, G., Huang, W., Chen, S., and Li, B. (2020). Pricing of grid electricity of reservoir power plants based on quantification of the values of positive externality factors. *Water Policy* 22 (3), 376–395. doi:10.2166/wp.2020.133

Ye, Y., Huang, W., Ma, G., Wang, J., Liu, Y., and Hu, Y. (2018). Cause analysis and policy options for the surplus hydropower in southwest China based on quantification. *J. Renew. Sustain. Energy* 10 (1), 015908. doi:10.1063/1.5024256

Yu, X., Li, G., Cheng, C., Sun, Y., and Chen, R. (2019). Research and application of continuous bidirectional trading mechanism in yunnan electricity market. *Energies* 12 (24), 4663. doi:10.3390/en12244663

Zakeri, B., Virasjoki, V., Syri, S., Connolly, D., Mathiesen, B. V., and Welsch, M. (2016). Impact of Germany's energy transition on the Nordic power market – a market-based multi-region energy system model. *Energy* 115, 1640–1662. doi:10.1016/j.energy.2016.07.083

Zhang, D., Wang, J., Lin, Y., Si, Y., Huang, C., Yang, J., et al. (2017). Present situation and future prospect of renewable energy in China. *Renew. Sustain. Energy Rev.* 76, 865–871. doi:10.1016/j.rser.2017.03.023

Zhang, S., Andrews-Speed, P., and Li, S. (2018). To what extent will China's ongoing electricity market reforms assist the integration of renewable energy? *Energy Policy* 114, 165–172. doi:10.1016/j.enpol.2017.12.002

Zhang, Z., Tang, H., Ren, J., Huang, Q., and Lee, W.-J. (2021). Strategic prosumers-based peer-to-peer energy market design for community microgrids. *IEEE Trans. Ind. Appl.* 57 (3), 2048–2057. doi:10.1109/tia.2021.3064523

Zhang, S., Chen, S., Ma, G., Zhu, Y., and Tao, C. (2021). Curve tracking and comparison during electricity spot trading based on judgment methods for curve similarity. *J. Phys. Conf. Ser.* 2005 (1), 012028. doi:10.1088/1742-6596/2005/1/012028

Zhou, N., Wu, D., Duan, P., Chen, L., Li, W., and Yang, Y. (2020). "Research and application of related settlement method considering price stabilization in yunnan power market," in 2020 IEEE sustainable power and energy conference (iSPEC), Chengdu, China, 23-25 November 2020, 1153–1158.

Zhu, Y., Huang, W., Chen, S., Zhang, S., Lai, C., and Ma, G. (2021). Spot quotation alliance modeling method of cascade hydropower based on symbiosis theory. *J. Hydrol.* 602, 126753. doi:10.1016/j.jhydrol.2021.126753

Nomenclature

η_k Average efficiency coefficient of station k

$\mu_{n,k,t}$ Binary constant indicating whether the unit n of the station k in period t is online, which is 1 when the unit is online; otherwise, it is 0.

$P_{k,t}^{d}$ Clearing price of the day-ahead spot market of station k in period t

H_k^D Design head of station k

Ω_k Downstream stations of CHSs

$E_{k,t}^{l}$ Electricity generation decomposed from medium- and long-term contracts of station k in period t

$E_{k,t}$ Electricity generation of station k in period t

N Generator units

K Hydroelectric stations/reservoirs

k Index for CHSs from 1 to K

w Index for downstream stations of CHSs from 2 to Ω_k

n Index for generator units from 1 to N

t Index for time periods from 1 to T

$R_{k,t}$ Inflow to station k in period t

M_t Length of the calculation period

ΔZ_k Limit of the rate of change in the water level at reservoir k

$N_{k,t}^{p}$ Load transaction result at station k in period t

L_k Loss constant of station k

$\underline{NS_{k,t}}$, $\overline{NS_{k,t}}$ Minimum/maximum fluctuations of the station k in period t

$\underline{N_k}$, $\overline{N_k}$ Minimum/maximum power output of station k

$\underline{NS_{k,t,n}}$, $\overline{NS_{k,t,n}}$ Minimum/maximum vibration areas of the generator unit n at station k in period t

$\underline{V_k}$, $\overline{V_k}$ Minimum/maximum volume of reservoir k

$\underline{Z_{k,t}}$, $\overline{Z_{k,t}}$ Minimum/maximum water level of station k in period t

$\underline{O_{k,t}}$, $\overline{O_{k,t}}$ Minimum/maximum water release from station k in period t

$H_{k,t}$ Net head of station k in period t

T Periods

$N_{k,t}$ Power output of station k in period t

P_k^l Price set by medium- and long-term contracts of station k in period t

$f_{1k}(\cdot)$ Relationship between forebay elevation and volume of reservoir k

$f_{2k}(\cdot)$ Relationship between tail-race elevation and water release from reservoir k

$f_{3k}(\cdot)$ Relationship between vibration areas of the generator unit n and station k

$z_{k,t}$ Tail level of reservoir k in period t

$V_{k,t}$ Volume of reservoir k in period t

$Q_{k,t}$ Water discharge from station k in period t

$Z_{k,t}$ Water level of reservoir k in period t

$O_{k,t}$ Water release from station k in period t

$S_{k,t}$ Water spillage from station k in period t

frontiers | Frontiers in Energy Research

TYPE Original Research
PUBLISHED 31 August 2022
DOI 10.3389/fenrg.2022.887946

OPEN ACCESS

EDITED BY
Nallapaneni Manoj Kumar,
City University of Hong Kong, Hong Kong SAR, China

REVIEWED BY
Mushan Jin,
Hong Kong University of Science and Technology, Hong Kong SAR, China
you Hai-Jiang,
Fujian Normal University, China

*CORRESPONDENCE
Guopeng Hu,
200411237@oamail.gdufs.edu.cn

SPECIALTY SECTION
This article was submitted to Sustainable Energy Systems and Policies, a section of the journal Frontiers in Energy Research

RECEIVED 02 March 2022
ACCEPTED 06 July 2022
PUBLISHED 31 August 2022

CITATION
Li L and Hu G (2022), Energy risk measurement and hedging analysis by nonparametric conditional value at risk model.
Front. Energy Res. 10:887946.
doi: 10.3389/fenrg.2022.887946

Energy risk measurement and hedging analysis by nonparametric conditional value at risk model

Ling Li[1] and Guopeng Hu[2]*

[1]Institute of Low Carbon and Sustainable Development, Jinan University, Guangzhou, China, [2]School of Public Administration, Guangdong University of Foreign Studies, Guangzhou, China

The accurate measurement and management of energy risk have become important issues of the economic development and energy security for all countries. The existing literature generally adopts the Value at Risk (VaR). However, VaR does not satisfy the subadditivity axiom to measure the energy risk, which makes the calculation defective. In this paper, we use the Conditional VaR (CVaR) with the characteristics of coherent and convex risk measurement to measure energy risk under nonparametric kernel (NPK) framework. We consider how to use the energy derivatives to hedge the price risk of energy so that the result is more reasonable and effective. The empirical results show that the NPK method that we propose is more effective to measure the actual energy risk and carry out more effective risk hedging.

KEYWORDS

energy price risk, price risk management, value-at-risk, conditional value, conditional value at risk

1 Introduction

Energy is an important driving force for the development of the world's economy. The development of any country cannot be separated from the contribution of energy. However, due to its non-renewability, the total energy consumption is decreasing while the demand is increasing, which will inevitably lead to the imbalance between supply and demand, and the sharp fluctuation of energy price. In addition, energy is dominated by a few countries, and for political and economic purposes, some energy-exporting countries often control energy-importing countries by reducing or expanding their energy supplies, which raises the risk of energy price fluctuation. Energy risk involves national and even global economic development in all aspects. In particular, in those countries with greater energy dependence, the impact of the international energy market is more obvious (Youssef et al., 2015). Therefore, how to measure the energy risk accurately and how to monitor and manage the risk have become important issues that need to urgently be solved.

The Value-at-Risk (VaR) method is an effective tool in energy risk measurement. The method was first proposed by the J.P. Morgan Group in 1994 to estimate the maximum possible loss to an asset or portfolio of assets for a given future period, at a given level of

confidence (Jorion, 2000). This concept not only covers the two risk characteristics of uncertainty and loss but also allows people to choose a specific subjective probability according to their own risk preferences, and its measurement of risk is very close to people's psychological feelings of risk. Therefore, once VaR was proposed, it was promptly promoted and was included in the supervisory indicators successively by the Basel Accord (1995) and EU Capital Adequacy Directive (1996). Driven by the Basel Degiannakis (2004) Committee on Banking Supervision and the International Organization of Securities Commissions, VaR has gradually developed into a common international risk measurement standard (Duffie and Pan, 1997; Engle and Manganelli, 2004). Since the diffusion of the Risk Metrics (RM), there is a dispute on how to do calculate VaR. Several approaches have been proposed and may be classified into three families: nonparametric historic simulation approaches, the parametric model approaches based on an econometric model for volatility dynamics, and the extreme value theory. However, these methods which have not reflected the current volatility (Youssef et al., 2015). Mcneil and Frey (2000) propose a combined approach to overcome the drawbacks. At present, there is a large body of literature that has studied financial assets using VaR (Angelidis et al., 2004; Tang and shieh, 2006; Kang and Yoon, 2007; Jinbo et al., 2020), and there are many studies that have focused on energy risk (Costello et al., 2008; Fan et al., 2008; Marimoutou et al., 2009; Krehbiel and Adkins, 2015). Aloui and Mabrouk (2010) use three long memory models (i.e., FLGARCH, HYGARCH, and FLAPARCH) to estimate the VaR of energy products basis on different hypotheses of error distribution; based on Aloui's study, Youssef et al. (2015) consider the extremum theory focusing on the tail distribution rather than on the entire distribution, and the results show that the FIAPARCH model with extreme value theory is more effective in prediction. In terms of energy risk management, Sadeghi and Shavvalpour (2006) believe that accurate price forecasting can help reduce portfolio risk. The existing literature is based on the principle that different kinds of products can be combined to invest and spread risk and propose that portfolio investment is applied to the field of energy risk management to avoid the risk brought by fluctuation of energy price. Wu et al. (2007) believe that the risk index model based on portfolio theory can guarantee the safety of China's oil imports. Muñoz et al. (2009) have established the linetype system model to calculate the cash flow to get the ROI at the lowest risk and study the portfolio risk of Spain's energy market. Vithayasrichareon and Macgill (2012, 2013) use the Monte Carlo method of portfolio analysis to setup Thailand's energy pricing.

The wide application of VaR has led to many in-depth studies, and researchers quickly began to compare VaR with other indicators. Artzner et al. (1997, 2010) proposed the theory of coherent risk measurement, which they believe should satisfy at least four axiomatic conditions: monotonicity, subadditivity, positive homogeneity, and translation invariance. Artzner et al. (1997, 2010) pointed out that VaR does not satisfy the subadditivity axiom in the theory of coherent risk measurement; that is, the combined risk measured by VaR may not be less than the sum of the single risks, thus breaking the risk diversification principle in portfolio theory. Meanwhile, many scholars pointed out that the VaR only reports one quantile of the distribution of returns (or losses) and does not focus on the risk distribution behind the quantiles. Because of the VaR deficiencies, Rockafellar and Uryasev (2000) proposed the concept of CVaR, which refers to the mathematical expectation of all losses exceeding the VaR level. Studies by Acerbi and Tasche (2002) show that CVaR is an index of coherent risk measurement that compensates for the shortcomings that VaR does not satisfy the subadditive axioms. It can be seen from the definition of CVaR that it focuses on the mean value of the distribution tail of the rate of return, and thus is more sensitive to changes in the tail than the VaR, making up for the defect that VaR is only one quantile and is not concerned with the losses beyond the quantile Hu et al. (2017). In addition, CVaR is a convex risk measurement. It is theoretically accepted as a more reasonable and effective risk measurement tool than VaR. CVaR is now written into Basel III as a risk measurement and monitoring tool. Zhang et al. (2018) added CVaR to model constraints, established a two-stage unit commitment model, and considered energy storage and demand side response in the model. Hu et al. (2017) considered CVaR in the objective function, conducted risk modeling of unit combination of power system based on CVaR theory, and considered the uncertainty of wind power in the model. Jin et al. (2019) considered CVaR theory can also be extended to the risk analysis of energy system to describe energy price risk.

The existing literature rarely analyzes the risk of energy system with CVaR theory. In contrast, we use the Conditional VaR (CVaR) with the characteristics of coherent and convex risk measurement to measure energy risk under nonparametric kernel (NPK) framework. Because we consider how to use the energy derivatives to hedge the price risk of energy, the result is more reasonable and effective.

The content of this paper is arranged as follows. Section 2 introduces the nonparametric CVaR model. Section 3 describes the empirical analysis on the basis of the energy market price data. The final section summarizes our study.

2 Models and methods

2.1 Model

There are many management methods and problems about energy risk. This paper focuses on how to use energy futures to hedge the risk of energy spots. It is assumed that the rates of return on energy futures and spots are r_1 and r_2, respectively; the

mean and standard deviation of r_1 are μ_1, σ_1; the mean and standard deviation of r_2 are μ_2, σ_2. The portfolio rate of return r_p formed by 1 unit of long energy spots and h units of short energy futures can be expressed as:

$$r_p = r_1 - hr_2 \tag{1}$$

The mean and variance of r_p are $\mu_p = \mu_1 - h\mu_2$ and $\sigma_p^2 = \sigma_1^2 + h^2\sigma_2^2 - 2h\rho\sigma_1\sigma_2$ respectively, in which ρ is the correlation coefficient of rates of return on energy spots and energy futures. Risk hedging strategy focuses on finding the best hedge ratio h to minimize the risk of the hedge portfolio. According to the different risk measurement indicators, risk hedging strategies of futures and spots are different. The classic and most commonly-used risk measurement is the variance proposed by Markowitz (1952). The minimum variance hedging strategy is to find the hedging ratio that minimizes the variance of the portfolio.

It is assumed the cumulative distribution function of the rate of return r_p on hedging portfolio is $F(x,h)$, and at a given confidence level of $1-\alpha$, the value-at-risk $VaR(h)$ of the hedging portfolio is expressed as (Jorion, 2000):

$$VaR(h) = -inf\{x \in R: F(x,h) \geq \alpha\} \tag{2}$$

The confidence level $1-\alpha$ is given in advance, usually by investors according to their own preferences or by regulatory agencies. In the condition that the distribution function $F(x,h)$ satisfies the continuity, $VaR(h)$ is the opposite of the lower α quantile of r_p. Although VaR is a widely-used risk measurement index, many scholars show the defect that VaR does not satisfy the subadditivity and it ignores the tail risk (Acerbi and Tasche, 2002). Therefore, Rockafellar and Uryasev (2000) proposed the concept of CVaR, which refers to the mathematical expectation of all losses exceeding the VaR level. The mathematical expression of the CVaR of the hedging portfolio is:

$$CVaR(h) = -E\left[r_p \middle| r_p \leq -VaR(h)\right] \tag{3}$$

Risk hedging strategy on the basis of CVaR focuses on finding the hedging rate h that minimizes the $CVaR(h)$ of the hedge portfolio. Under the assumption that r_p is subject to normal distribution, the corresponding $CVaR(h)$ can be expressed as the linear function of the mean value and standard deviation (Alexander and Baptista, 2004), namely:

$$CVaR(h) = \frac{\varphi(z_\alpha)}{\alpha}\sigma_p - \mu_p \tag{4}$$

where σ_p is the standard deviation of the combined rate of return. z_α is the lower α quantile of the standard normal distribution. φ is the density function of the standard normal distribution, The normal distribution assumption is not true in the real market. An equivalent definition of CVaR given by Rockafellar and Uryasev (2000) without any distribution setting is:

$$CVaR(h) = \min_{v \in R} F_\alpha(h,v) \tag{5}$$

where, $F_\alpha(h,v) = v + \alpha^{-1}E[(-r_p - v)^+]$, and $(x)^+ = max(x,0)$. Meanwhile, the authors pointed out that the minimum CVaR model is equivalent to the following optimization problem:

$$\min_{h \in R} CVaR(h) = \min_{(h,v) \in R \times R} F_\alpha(h,v) \tag{6}$$

2.2 Methodology

Given the distribution function or density function of r_p, $F_\alpha(h,v)$ can be obtained. However, we seldom know the specific form of distribution function or density function in real life and need to estimate it by using sample data. Supposing $\{r_{1,t}\}_{t=1}^T$ and $\{r_{2,t}\}_{t=1}^T$ are sample data of return rate on spots and futures, respectively, and $\{r_{p,t}\}_{t=1}^T$ is the sample data of portfolio rate of return in the period of T, and $r_{p,t} = r_{1,t} - hr_{2,t}$, thus the kernel estimator of the density function of the combined rate of return is:

$$\hat{f}(x,h) = \frac{1}{Tb}\sum_{t=1}^T g\left(\frac{x - r_{p,t}}{b}\right) \tag{7}$$

where $G(z) = \int_{-\infty}^z g(u)du$, and $g(z)$ is a kernel function selected by the researcher. According to the study by Li and Racine (2007), the Gauss kernel function is a good candidate if we intend to estimate the density function and distribution function of the univariate, that is, $g(z) = (\sqrt{2\pi})^{-1} exp(-z^2/2)$. b is bandwidth. According to the study by Li and Racine (2007), we set $b = 1.06 \times T^{-1/5} \times \hat{\sigma}_p = a\hat{\sigma}_p$, in which $a = 1.06 \times T^{-1/5}$, and $\hat{\sigma}_p$ is the sample covariance of the portfolio rate of return. Thus, under the kernel estimation framework, according to the kernel estimator (7) of density function, the kernel estimator of $F_\alpha(h,v)$ can be expressed as:

$$\begin{aligned}
\hat{F}_\alpha(h,v) &= v + \alpha^{-1}\hat{E}\left[\left(-r_p - v\right)^+\right] \\
&= v + \alpha^{-1}\int_{-\infty}^{+\infty}(-x-v)^+\hat{f}(x,h)dx \\
&= v + \alpha^{-1}\int_{-\infty}^{+\infty}(-x-v)^+\frac{1}{Tb}\sum_{t=1}^T g\left(\frac{x - r_{p,t}}{b}\right)dx \\
&= v + \frac{1}{Tb\alpha}\sum_{t=1}^T\int_{-\infty}^{-v}(-x-v)g\left(\frac{x - r_{p,t}}{b}\right)dx \\
&= v + \frac{1}{T\alpha}\sum_{t=1}^T\int_{-\infty}^{R_t}\left(-by - r_{p,t} - v\right)g(y)dy \\
&= v - \frac{1}{T\alpha}\sum_{t=1}^T\left(\left(r_{p,t} + v\right)G(R_t) + bH(R_t)\right)
\end{aligned} \tag{8}$$

where $y = (x - r_{p,t})/b$, $R_t = (-v - r_{p,t})/b$ and $H(x) = \int_{-\infty}^x yg(y)dy$. The minimum CVaR model under the kernel estimation framework can be expressed as:

$$\begin{aligned}&\min_{h\in R}\widehat{CVaR}(h)\\&=\min_{(h,v)\in R\times R}\hat{F}_\alpha(h,v)\\&=\min_{(h,v)\in R\times R}v-(T\alpha)^{-1}\sum_{t=1}^{T}\Big(\big(r_{p,t}+v\big)G(R_t)+bH(R_t)\Big)\end{aligned}\tag{9}$$

Similar to the study of Yao et al. (2013), the convexity theorem of optimization problem (9) is given as follows:

Theorem 1: Optimization Problem (9) is a convex optimization problem.

Proof: Because the constraint set of the optimization problem (9) is a nonempty convex set, we only need to prove that the Hessian matrix of the objective function $\hat{F}_\alpha(h,v)$ is a positive semi-definite matrix.

According to the function $\hat{F}_\alpha(h,v)$ and the formula $R_t=(-v-r_{p,t})/b$, we have:

$$\begin{aligned}&\frac{\partial\hat{F}_\alpha(h,v)}{\partial R_t}\\&=-\frac{1}{T\alpha}\sum_{t=1}^{T}\Big(\big(r_{p,t}+v\big)g(R_t)+bR_tg(R_t)\Big)=0\end{aligned}\tag{10}$$

$$\frac{\partial R_t}{\partial v}=-\frac{1}{b},\frac{\partial R_t}{\partial h}=\frac{r_{2,t}}{b}+\frac{v+r_{p,t}}{b^2}\frac{\partial b}{\partial h}\tag{11}$$

Furthermore, we take first order derivatives of v and h by the function $\hat{F}_\alpha(h,v)$. By simplifying the formula using the results of (10) and (11), we can obtain:

$$\frac{\partial\hat{F}_\alpha(h,v)}{\partial v}=1-\frac{1}{T\alpha}\sum_{t=1}^{T}G(R_t)\tag{12}$$

$$\frac{\partial\hat{F}_\alpha(h,v)}{\partial h}=\frac{1}{T\alpha}\sum_{t=1}^{T}\left[G(R_t)r_{2,t}-H(R_t)\frac{\partial b}{\partial h}\right]\tag{13}$$

Furthermore, by Formulas 12, 13, we have the second partial derivatives, as follows:

$$\frac{\partial^2\hat{F}_\alpha(h,v)}{\partial v^2}=\frac{1}{Tb\alpha}\sum_{t=1}^{T}g(R_t)\tag{14}$$

$$\frac{\partial^2\hat{F}_\alpha(h,v)}{\partial v\partial h}=-\frac{1}{T\alpha}\sum_{t=1}^{T}g(R_t)\frac{\partial R_t}{\partial h}\tag{15}$$

$$\begin{aligned}&\frac{\partial^2\hat{F}_\alpha(h,v)}{\partial h\partial v}\\&=\frac{1}{T\alpha}\sum_{t=1}^{T}\left[g(R_t)\frac{\partial R_t}{\partial v}r_{2,t}-R_tg(R_t)\frac{\partial R_t}{\partial v}\frac{\partial b}{\partial h}\right]\\&=-\frac{1}{T\alpha}\sum_{t=1}^{T}g(R_t)\left[\frac{r_{2,t}}{b}+\frac{v+r_{p,t}}{b^2}\frac{\partial b}{\partial h}\right]\\&=-\frac{1}{T\alpha}\sum_{t=1}^{T}g(R_t)\frac{\partial R_t}{\partial h}\end{aligned}\tag{16}$$

$$\begin{aligned}&\frac{\partial^2\hat{F}_\alpha(h,v)}{\partial h^2}\\&=\frac{1}{T\alpha}\sum_{t=1}^{T}\left(g(R_t)\frac{\partial R_t}{\partial h}r_{2,t}-R_tg(R_t)\frac{\partial R_t}{\partial h}\frac{\partial b}{\partial h}-H(R_t)\frac{\partial^2 b}{\partial^2 h}\right)\\&=\frac{1}{T\alpha}\sum_{t=1}^{T}\left(g(R_t)\frac{\partial R_t}{\partial h}\left(r_{2,t}-R_t\frac{\partial b}{\partial h}\right)\right)-\frac{1}{T\alpha}\sum_{t=1}^{T}\left(H(R_t)\frac{\partial^2 b}{\partial^2 h}\right)\\&=\frac{1}{T\alpha}\sum_{t=1}^{T}\left(g(R_t)\left(\frac{\partial R_t}{\partial h}\right)^2b\right)-\frac{1}{T\alpha}\sum_{t=1}^{T}\left(H(R_t)\frac{\partial^2 b}{\partial^2 h}\right)\end{aligned}\tag{17}$$

Then, the Hessian matrix of the objective function $\hat{F}_\alpha(h,v)$ can be expressed as:

$$\begin{aligned}\Theta&=\begin{pmatrix}\frac{\partial^2\hat{F}_\alpha(h,v)}{\partial v^2}&\frac{\partial^2\hat{F}_\alpha(h,v)}{\partial v\partial h}\\\frac{\partial^2\hat{F}_\alpha(h,v)}{\partial h\partial v}&\frac{\partial^2\hat{F}_\alpha(h,v)}{\partial h^2}\end{pmatrix}\\&=\frac{1}{T\alpha}\begin{pmatrix}\sum_{t=1}^{T}g(R_t)\frac{1}{b}&-\sum_{t=1}^{T}g(R_t)\frac{\partial R_t}{\partial h}\\-\sum_{t=1}^{T}g(R_t)\frac{\partial R_t}{\partial h}&\sum_{t=1}^{T}\left(g(R_t)\left(\frac{\partial R_t}{\partial h}\right)^2b\right)\end{pmatrix}\\&\quad-\frac{1}{T\alpha}\begin{pmatrix}0&0\\0&\sum_{t=1}^{T}\left(H(R_t)\frac{\partial^2 b}{\partial^2 h}\right)\end{pmatrix}\end{aligned}\tag{18}$$

$$\begin{aligned}\Theta_1&=\frac{1}{T\alpha}\begin{pmatrix}\sum_{t=1}^{T}g(R_t)\frac{1}{b}&-\sum_{t=1}^{T}g(R_t)\frac{\partial R_t}{\partial h}\\-\sum_{t=1}^{T}g(R_t)\frac{\partial R_t}{\partial h}&\sum_{t=1}^{T}\left(g(R_t)\left(\frac{\partial R_t}{\partial h}\right)^2b\right)\end{pmatrix}\\&=\frac{1}{T\alpha}\sum_{t=1}^{T}\left(g(R_t)\begin{pmatrix}\frac{1}{\sqrt{b}}\\-\frac{\partial R_t}{\partial h}\sqrt{b}\end{pmatrix}\begin{pmatrix}\frac{1}{\sqrt{b}}&-\frac{\partial R_t}{\partial h}\sqrt{b}\end{pmatrix}\right)\end{aligned}\tag{19}$$

Kernel function $g(\cdot)>0$, bandwidth $b>0$, and $\frac{1}{T\alpha}>0$. Therefore, Θ_1, the sum of T positive semi-definite matrixes, is still a positive semi-definite matrix.

$$\Theta_2=-\frac{1}{T\alpha}\begin{pmatrix}0&0\\0&\sum_{t=1}^{T}\left(H(R_t)\frac{\partial^2 b}{\partial^2 h}\right)\end{pmatrix}\tag{20}$$

For any $z\in R$, $H(z)=\int_{-\infty}^{z}yg(y)dy$, if $z<0$ then $yg(y)<0$ for any $y\in(-\infty,z)$, since $g(y)>0$. If $z\geq 0$, we have

TABLE 1 Descriptive statistics of daily rate of return.

	Mean	Median	Min	Max	Std	skewness	kurtosis	JB stat
Panel A crude oil								
Spots	−0.004	0.000	−13.065	21.277	2.446	0.286	8.603	3844.332
Future	−0.004	0.000	−13.065	16.410	2.392	0.168	7.752	2751.086
Panel B Gasoline								
Spots	−0.006	0.000	−22.485	22.240	2.749	0.073	10.631	7060.148
Future	−0.005	0.000	−16.162	21.655	2.420	0.015	8.940	4276.240

$$H(z) = \int_{-\infty}^{z} yg(y)dy = \int_{-\infty}^{-z} yg(\mathbf{y})dy + \int_{-z}^{z} yg(\mathbf{y})dy = \int_{-\infty}^{-z} yg(\mathbf{y})dy < 0 \quad (21)$$

Because $yg(y)$ is an odd function. Therefore $H(z) \le 0$ for any $z \in R$.

Because $-\frac{1}{T\alpha} < 0$, $\frac{\partial^2 b}{\partial^2 h} = \frac{a\sigma_1^2\sigma_2^2}{\sigma_p^3}(1-\hat{\rho}^2) \ge 0$ and $H(z) \le 0$, so we prove Θ_2 is a semi-positive definition matrix immediaely. Thus, optimization Problem (9) is a convex optimization problem. There are many algorithms to solve the convex optimization problem. In particular, for the one-dimensional optimization problem, we can obtain its global optimal solution easily.

3 Empirical analysis

This section uses the futures data and spots data of crude oil and gasoline for empirical analysis, and the sample data are ranged from 2 January 2006 to 24 February 2017, with a total of 2910 daily price data. The full sample data are used to measure the risk and are divided into training subsamples and testing subsamples to test the performance of risk hedging. The training subsamples range from 2 January 2006 to 30 December 2011, with a total number of 1565; the testing subsamples range from 2 January 2012 to 24 February 2017, with a total number of 1345. The price data comes from Datastream. The data of the daily rate of return is obtained using the first-order difference on the logarithm of the price. For convenience, all of the data of the rate of return are expanded by 100 times; that is, the data unit is %. Summary statistics for the spots and futures returns are reported in Table 1.

Table 1 shows that where the mean of the rate of return is less than zero, it indicates that both the crude oil price and the gasoline price are declining. Where the median of the rate of return is zero, it indicates that the number of days of rising prices and falling prices are roughly equal in the period of the sample. From the point of view of minimum, maximum, and standard deviation, the price of gasoline spots varies most, and the risk of fluctuations of the price of gasoline spots is the greatest. As for the daily rates of return on the four products, the skewness coefficients are all greater than zero, indicating a right shift in their distributions. The kurtosis coefficients are more than 3, indicating that the distributions of the rates of return on the four products are in "leptokurtosis and fat-tail". The JB statistics further confirm that the distributions of the rates of return on the four products are significantly different from the normal distribution, so the risk measurement and risk management on the basis of normal distribution are inaccurate. The last column shows the correlation coefficient of the rates of return on crude oil futures and spots is 0.908, while the correlation coefficient of the rates of return on gasoline futures and spots is 0.836. A higher correlation coefficient indicates that the corresponding futures are better risk hedging tools for spot assets.

3.1 Risk measurement

First, by using the nonparametric method, we measure the risks of the two products in the whole samples, with the result noted as NPK-CVaR. Meanwhile, the measurement result of CVaR under normal distribution is given as Norm-CVaR for comparison. In addition, because values of CVaR are related to the level of confidence, a series of different confidence levels are taken to test the measurement results. The results are shown in Table 2.

Table 2 shows that with all the four products and confidence levels $1-\alpha$, Norm-CVaR is less than NPK-CVaR, indicating that the normal distribution assumption always underestimates the risk of energy spots and futures in reality. In addition, according to the comparison between spots risk and futures risk, the measurement results of crude oil and gasoline show that no matter under nonparametric estimation method or normal distribution assumption, the risk value of futures are greater than that of the corresponding spots.

To see the differences of risks measured by the two different methods more directly, we use kernel estimation method and normal distribution to fit the sample distribution of the rates of return on the four products (Figure 1). Specifically, based on the sample data of the rates of return on the four products, the

TABLE 2 Risk measurement under different confidence level.

Panel A crude oil

	$1-\alpha$	99%	98%	97%	96%	95%	94%	93%	92%	91%	90%
Spots	Norm-CVaR	6.523	5.925	5.551	5.273	5.049	4.860	4.695	4.549	4.417	4.296
	NPK-CVaR	8.961	7.513	6.698	6.155	5.749	5.424	5.151	4.916	4.709	4.524
Future	Norm-CVaR	6.378	5.794	5.428	5.156	4.937	4.752	4.591	4.448	4.319	4.319
	NPK-CVaR	8.833	7.372	6.573	6.034	5.631	5.309	5.040	4.808	4.606	4.426

Panel B Gasoline

	$1-\alpha$	99%	98%	97%	96%	95%	94%	93%	92%	91%	90%
Spots	Norm-CVaR	7.332	6.660	6.240	5.927	5.675	5.463	5.278	5.114	4.965	4.830
	NPK-CVaR	10.495	8.684	7.723	7.083	6.598	6.205	5.874	5.590	5.341	5.121
Future	Norm-CVaR	6.455	5.864	5.494	5.219	4.997	4.810	4.647	4.502	4.372	4.252
	NPK-CVaR	9.168	7.690	6.847	6.285	5.865	5.528	5.245	5.000	4.785	4.592

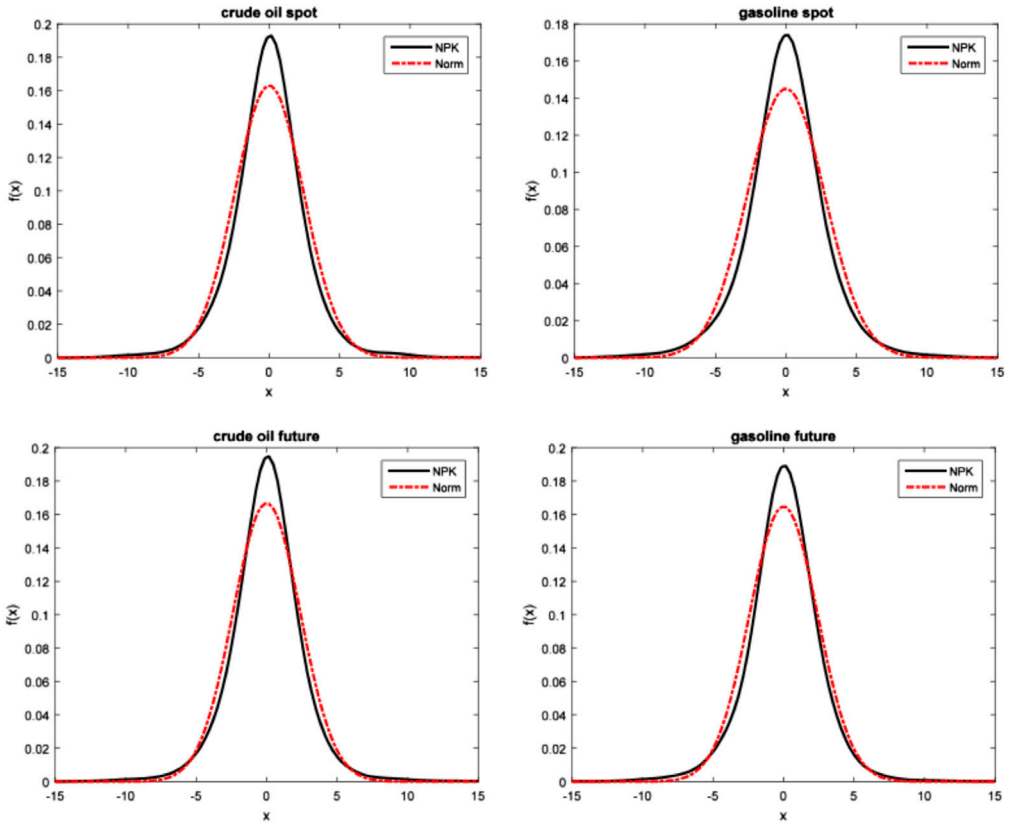

FIGURE 1
Sample distribution fitting of rates of return on futures and spots.

density function of the real data is estimated through kernel estimation, and the image is noted as NPK. As a comparison, the normally distributed density function is used to fit the density function of the sample data. That is to say, supposing that the real data are in normal distribution, we estimate the mean and the standard deviation through sample data, and the normally

TABLE 3 Comparison of the hedging effect of the three methods.

Commodity	NPK			Norm			CFM		
	Mean	%ΔStd	%ΔCVaR	Mean	%ΔStd	%ΔCVaR	Mean	%ΔStd	%ΔCVaR
Panel A: in sample									
Crude oil	0.007	54.310	42.712	0.003	56.703	39.338	0.027	11.332	9.695
Gasoline	0.008	39.720	28.645	0.000	44.693	26.488	0.022	12.027	10.695
Average	0.008	47.015	35.678	0.001	50.698	32.913	0.025	11.680	10.195
Panel B: out of sample (static hedging)									
Crude oil	-0.010	56.964	32.926	-0.004	60.620	28.809	-0.039	11.405	10.210
Gasoline	-0.014	42.083	27.328	-0.002	45.848	23.466	-0.036	12.935	11.381
Average	-0.012	49.523	30.127	-0.003	53.234	26.138	-0.038	12.170	10.796
Panel B: out of sample (dynamic hedging)									
Crude oil	-0.003	57.144	32.149	-0.003	60.525	26.742	-0.033	31.526	26.554
Gasoline	-0.015	40.668	25.829	-0.005	45.588	23.457	-0.026	11.086	9.967
Average	-0.009	48.906	28.989	-0.004	53.056	25.099	-0.029	21.306	18.260

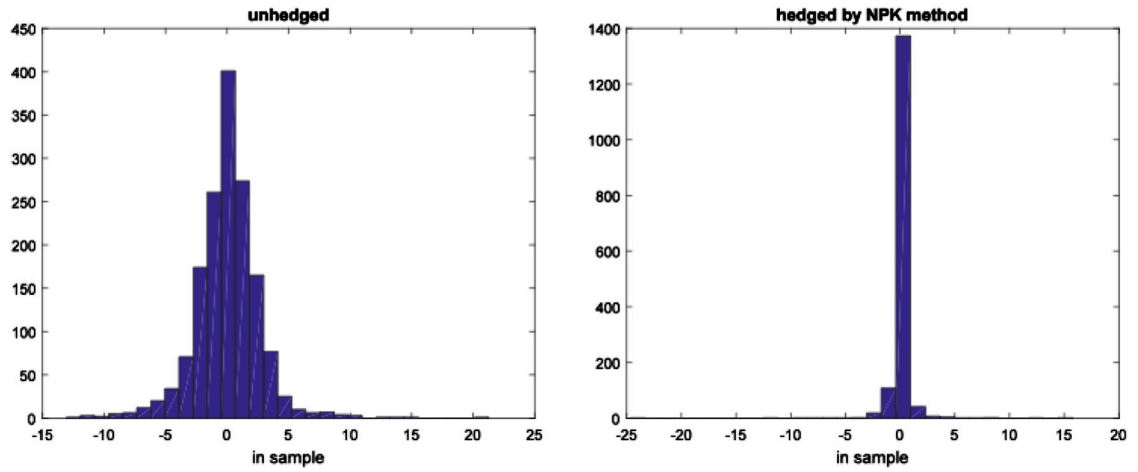

FIGURE 2
Histogram of crude oil (in sample).

distributed density function can be obtained and noted as Norm in the figure. It can be seen from the four figures that compared with the density function in normal distribution, density functions estimated by NPK have higher peaks and thicker left tail and right tail. This characteristic of "leptokurtosis and fat-tail" is vital for measurement and management of energy risk. For the long position (short position), the thicker left tail (right tail) indicates a greater probability of larger losses in the real energy market, which is seriously underestimated under normal distribution. This is consistent with the conclusion of Table 2; that is, the risk measurement under the normal distribution assumption tends to underestimate the risk.

3.2 Risk hedging

This section uses the futures data and spots data of crude oil and gasoline to study the risk hedging based on CVaR. Specially, we use the futures of the crude oil and gasoline to hedge the risk of the corresponding spots. As a comparison, we present the hedging performance under the NPK CVaR and the Norm CVaR. The previous analysis has shown that the Norm CVaR tends to underestimate the actual risk, and CVaR can be expressed as a linear function of the mean and standard deviation under normal distribution assumption, while only taking into account the information on the first two order moments. When the financial

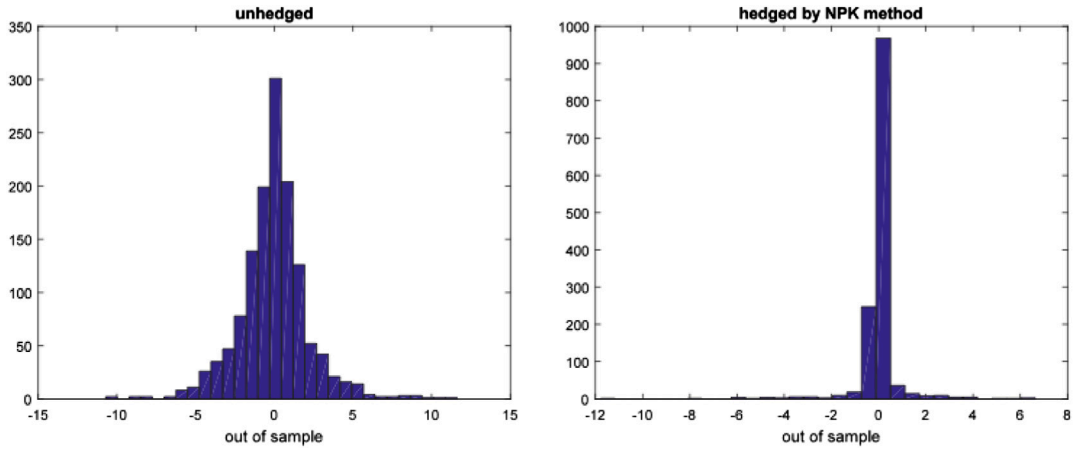

FIGURE 3
Histogram of crude oil (out of sample).

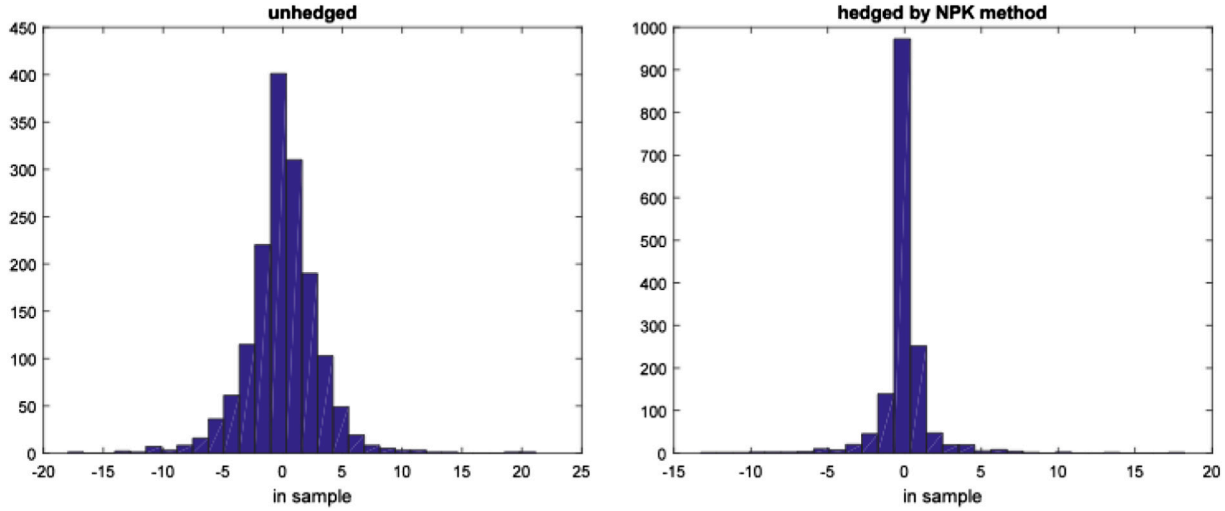

FIGURE 4
Histogram of gasoline (in sample).

market data are in non-normal distribution, investors will pay more attention to higher moments of market data in addition to the first two moments, such as mean and variance. Therefore, Cao et al. (2010) proposed a semi-parametric method to estimate CVaR. In fact, their method is the Cornish-Fisher expansion of CVaR (CFM CVaR), which includes the information on the third moment and fourth moment of the market data without any distribution assumption. This method is an improvement of normal method. Although CFM CVaR reflects the information on the first four moments of the risk factors, the information on higher order moments cannot be included because of the complexity of the formulas. The nonparametric kernel estimation method can get the sample distribution function of the market data exactly without any distribution setting, and therefore that the information on higher moments can be obtained. Theoretically, if the sample size is large enough, the nonparametric kernel estimation method can get the information on all moments of the risk factors. Therefore, we compare the performance of the three methods in the actual risk hedging. We consider both the static hedging strategy and the dynamic hedging strategy. Static hedging strategy, which is the

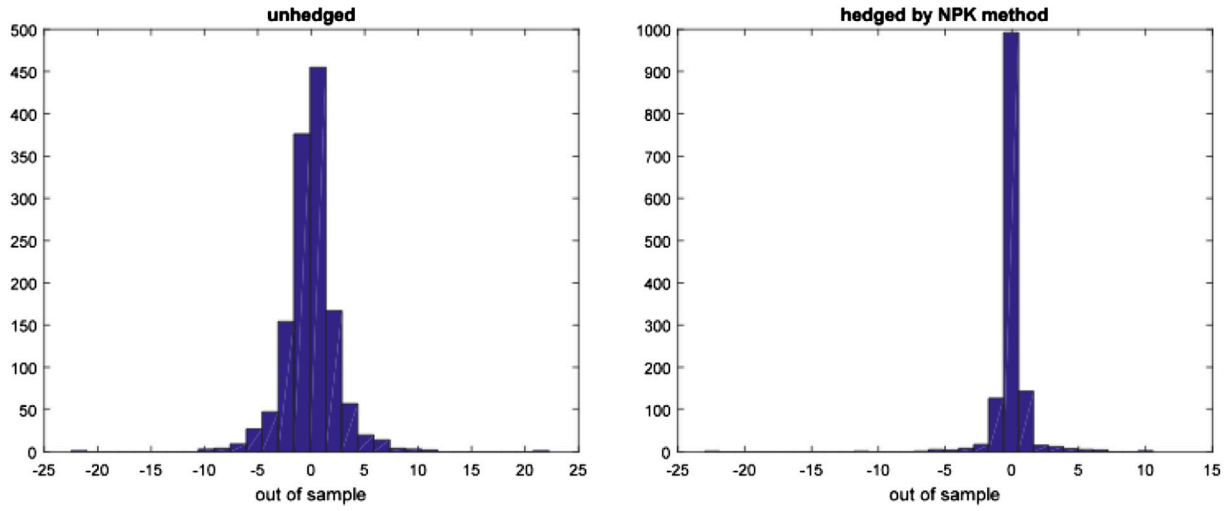

FIGURE 5
Histogram of gasoline (out of sample).

optimal hedging strategy obtained from the training subsamples, is applied to the training subsamples and testing subsamples to test the in sample and out of sample performances of the hedging strategies.

It is a defect that the static hedging assumes that the distribution of the sample data in the sample interval is unchanged, while the actual financial market environment is constantly changing. Therefore, if the sample interval is too long and the distribution of rate of return changes, then there may be deviation in the static hedging. In dynamic hedging, long intervals are divided into several short intervals, in which the distribution of rates of return is assumed to be unchanged. This avoids the problem in static hedging that the distribution of the rates of return is unchanged in a long interval. However, the defect in dynamic hedging is that the position of the futures needs to be constantly adjusted, which increases the cost of risk hedging. The dynamic hedging strategy is constructed as follows: the optimal hedge ratio is obtained from the initial 1565 training subsamples, and is applied to the next 10 trading days (2 weeks). The training subsamples are then updated by replacing the oldest 10 samples by the data of the 10 trading days, as mentioned earlier, while the training sample size of 1565 is unchanged. The new hedge ratio is obtained from the updated training subsamples, and is applied to the next 10 trading days, and so on until to the end of the sample period. This method reflects the latest transaction information by dynamically adjusting the training subsamples. Finally, based on the dynamic hedge ratio, the sequence of the portfolio rate of return is obtained and the out of sample performance (e.g., mean, standard deviation and CVaR) are calculated, see Table 3.

Table 3 shows the mean, the decline in the standard deviation (%ΔStd), and the decline in the CVaR (%ΔCVaR) of the portfolio rate of return after hedging based on the three methods. After being hedged by three methods, the CVaR and the standard deviation declined greatly. This shows whether the decline in the CVaR is the largest based on NPK CVaR from the point of view of a single asset or an average value. Specifically, NPK CVaR is superior to Norm CVaR, and Norm CVaR is superior to CFM CVaR. This indicates that as a modification to Norm, semi-parametric CFM is not satisfactory in practice. The decline in the standard deviation is the greatest in the Norm CVaR method, mainly because CVaR is the linear function of the standard deviation in the Norm method, and to minimize Norm CVaR is to minimize the standard deviation. The standard deviation is a symmetric index. Its decline may be caused by the decline, either in the left tail or in the right tail of the distribution. This shows that the decline in the standard deviation in Norm method is larger than that in NPK method, which is largely due to the decline in the right tail in the table because the left decline of CVaR in Norm is smaller than that in NPK. Similarly, the sequence of standard deviation declines from large to small is in the sequence of Norm, NPK, and CFM. Finally, the conclusion by the mean is mixed. The means in the three methods after hedging are all positive in sample, while they are negative out of sample. This happens because the mean of the rate of return on spots before hedging is positive in sample, while it is negative out of sample.

From Figures 2–5, the histograms of the pre-hedging and post-hedging rates of return on the two energies in and out of samples are shown, respectively. Only the hedging image in NPK CVaR is given, because the risk decline in it is the largest. It can be seen directly from the figures that after hedging, the histograms are more concentrated, and the tail samples at both ends are less with most of the samples distributed on the right side of zero. This shows that hedging significantly reduces the risk in the left

tail. The empirical results show that the NPK method that we proposed is more effective to measure the actual energy risk and carry out more effective risk hedging.

4 Conclusion

The accurate measurement of energy risk, and risk regulation and management have become important issues to be solved by academia and governments. However, VaR, which is the main tool for measuring risk, does not satisfy the subadditivity axiom and is defective in practical application. In this paper, we use a new nonparametric kernel estimation method to measure the price risk of energy. On this basis, we study how to hedge and manage the energy risk. Specifically, we use the CVaR to measure the downside risk of the energy, and obtain the NPK estimator of CVaR. Based on the estimation formula, we build the NPK CVaR risk hedging model and prove its convexity. The empirical results from crude oil and gasoline show that the NPK method that we propose is more effective to measure the actual energy risk and carry out more effective risk hedging.

Although CVaR is superior to VaR in nature, there are still some deficiencies in the practice of energy risk management and supervision. The effectiveness of CVaR depends on the accuracy of distribution tail estimation, but it is difficult to accurately estimate the tail of distribution. Under extreme market conditions, the original stable relationship between the influencing factors has been destroyed and the CVaR estimation may have a large deviation.

Data availability statement

The original contributions presented in the study are included in the article/supplementary material, and further inquiries can be directed to the corresponding author.

Author contributions

Conceptualization, LL; methodology, GH; software, GH; validation, GH and LL; formal analysis, GH; investigation LL; data curation, LL; writing—original draft preparation, LL; writing—review and editing, GH and LL; supervision, LL; funding acquisition, LL.

Funding

This paper is supported by the National Natural Science Foundation of China (No. 72003080), Southern Marine Science and Engineering Guangdong Laboratory (Zhuhai) (No. SML2021SP203), Carbon Emissions Accounting and Evaluation System of Marine Industry in Guangdong [No. GDNRC (2022)47] Doctor patient relationship model, form, governance, and conflict resolution in the context of big data (No. 299-gk19g051).

Conflict of interest

The authors declare that the research was conducted in the absence of any commercial or financial relationships that could be construed as a potential conflict of interest.

Publisher's note

All claims expressed in this article are solely those of the authors and do not necessarily represent those of their affiliated organizations, or those of the publisher, the editors and the reviewers. Any product that may be evaluated in this article, or claim that may be made by its manufacturer, is not guaranteed or endorsed by the publisher.

References

Acerbi, C., and Tasche, D. (2002). On the coherence of expected shortfall. *J. Bank. Finance* 26, 1487–1503. doi:10.1016/S0378-4266(02)00283-2

Alexander, G. J., and Baptista, A. M. (2004). A comparison of VaR and CVaR constraints on portfolio selection with the mean-variance model. *Manag. Sci.* 50 (9), 1261–1273. doi:10.1287/mnsc.1040.0201

Aloui, C., and Mabrouk, S. (2010). Value-at-risk estimations of energy commodities via long-memory, asymmetry and fat-tailed garch models. *Energy Policy* 38 (5), 2326–2339. doi:10.1016/j.enpol.2009.12.020

Angelidis, T., Benos, A., and Degiannakis, S. (2004). The use of GARCH models in VaR estimation. Statistical methodology *Stat. Methodol.* 1 (1–2), 105–128. doi:10.1016/j.stamet.2004.08.004

Artzner, P., Delbaen, F., Eber, J., and Heath, D. (2010). Coherent measures of risk. *Math. Finance* 9 (3), 203–228. doi:10.1111/1467-9965.00068

Artzner, P., Delbaen, F., Eber, J. M., and Heath, D. (1997). Thinking coherently. *Risk* 10 (11), 68–71.

Cao, Z., Harris, R. D., and Shen, J. (2010). Hedging and value at risk: a semi-parametric approach. *J. Fut. Mark.* 30, 780–794. doi:10.1002/fut.20440

Costello, A., Asem, E., and Gardner, E. (2008). Comparison of historically simulated var: evidence from oil prices. *Energy Econ.* 30 (5), 2154–2166. doi:10.1016/j.eneco.2008.01.011

Degiannakis, S. (2004). Volatility forecasting: evidence from a fractional integrated asymmetric power arch skewed-t model. *Appl. Financ. Econ.* 14 (18), 1333–1342. doi:10.1080/0960310042000285794

Duffie, D., and Pan, J. (1997). An overview of value at risk. *J. Deriv.* 4 (3), 7–49. doi:10.3905/jod.1997.407971

Engle, R. F., and Manganelli, S. (2004). Caviar: conditional autoregressive value at risk by regression quantiles. *J. Bus. Econ. Statistics* 22 (4), 367–381. doi:10.1198/073500104000000370

Fan, Y., Zhang, Y. J., Tsai, H. T., and Wei, Y. M. (2008). Estimating 'value at risk' of crude oil price and its spillover effect using the ged-garch approach. *Energy Econ.* 30 (6), 3156–3171. doi:10.1016/j.eneco.2008.04.002

Hu, H., Wang, Y., Zeng, B., Zhang, J., and Shi, J. (2017). Cvar-based economic optimal dispatch of integrated energy system. *Electr. Power Autom. Equip.* 37 (6), 209–219. doi:10.16081/j.issn.1006-6047.2017.06.028

Jinbo, H., Ding, A., Li, Y., and Lu, D. (2020). Increasing the risk management effectiveness from higher accuracy: A novel non-parametric method. *Pacific Basin Finance J.* 62, 101373. doi:10.1016/j.pacfin.2020.101373

Jin, H. Y., Sun, H. B., Niu, T., Guo, Q. L., and Wang, B. (2019). Coordinated dispatch method of energy-extensive load and wind power risk constraints. *Automation Electr. Power Syst.* 43 (16), 9–18. doi:10.7500/AEPS20180901001

Jorion, P. (2000). *Value at risk: the new benchmark for managing financial risk*. 2nd ed. New York, United States: McGraw-Hill.

Kang, S. H., and Yoon, S. M. (2007). Long memory properties in return and volatility: evidence from the korean stock market. *Phys. A Stat. Mech. its Appl.* 385 (2), 591–600. doi:10.1016/j.physa.2007.07.051

Krehbiel, T., and Adkins, L. C. (2015). Price risk in the nymex energy complex: an extreme value approach. *J. Fut. Mark.* 25 (4), 309–337. doi:10.1002/fut.20150

Li, Q., and Racine, J. S. (2007). *Nonparametric econometrics: theory and practice*. New Jersey, United States: Princeton University Press.

Marimoutou, V., Raggad, B., and Trabelsi, A. (2009). Extreme value theory and value at risk: application to oil market. *Energy Econ.* 31 (4), 519–530. doi:10.1016/j.eneco.2009.02.005

Markowitz, H. (1952). Portfolio selection. *J. Finance* 7 (1), 77–91. doi:10.1111/j.1540-6261.1952.tb01525.x

Mcneil, A. J., and Frey, R. (2000). Estimation of tail-related risk measures for heteroscedastic financial time series: an extreme value approach. *J. Empir. Finance* 7 (3), 271–300. doi:10.1016/S0927-5398(00)00012-8

Muñoz, J. I., Nieta, A. A. S. D. L., Contreras, J., and Bernal-Agustín, J. L. (2009). Optimal investment portfolio in renewable energy: the spanish case. *Energy Policy* 37 (12), 5273–5284. doi:10.1016/j.enpol.2009.07.050

Rockafellar, R. T., and Uryasev, S. (2000). Optimization of conditional value-at-risk. *Journal of risk* 2, 21–42. doi:10.21314/JOR.2000.038

Sadeghi, M., and Shavvalpour, S. (2006). Energy risk management and value at risk modeling. *Energy Policy* 34 (18), 3367–3373. doi:10.1016/j.enpol.2005.07.004

Tang, T. L., and Shieh, S. J. (2006). Long memory in stock index futures markets: a value-at-risk approach. *Phys. A Stat. Mech. its Appl.* 366 (1), 437–448. doi:10.1016/j.physa.2005.10.017

Vithayasrichareon, P., and Macgill, I. F. (2013). Assessing the value of wind generation in future carbon constrained electricity industries. *Energy Policy* 53 (1), 400–412. doi:10.1016/j.enpol.2012.11.002

Vithayasrichareon, P., and Macgill, I. F. (2012). Portfolio assessments for future generation investment in newly industrializing countries – a case study of Thailand. *Energy* 44 (1), 1044–1058. doi:10.1016/j.energy.2012.04.042

Wu, G., Wei, Y. M., Fan, Y., and Liu, L. C. (2007). An empirical analysis of the risk of crude oil imports in China using improved portfolio approach. *Energy Policy* 35 (8), 4190–4199. doi:10.1016/j.enpol.2007.02.009

Yao, H. X., Li, Z. F., and Lai, Y. Z. (2013). Mean–CVaR portfolio selection: a nonparametric estimation framework. *Comput. Operations Res.* 40 (4), 1014–1022. doi:10.1016/j.cor.2012.11.007

Youssef, M., Belkacem, L., and Mokni, K. (2015). Value-at-risk estimation of energy commodities: a long-memory garch–evt approach. *Energy Econ.* 51, 99–110. doi:10.1016/j.eneco.2015.06.010

Zhang, Y., Wang, J., Ding, T., and Wang, X. (2018). Conditional value at risk-based stochastic unit commitment considering the uncertainty of wind power generation. *IET Gener. Transm. &amp. Distrib.* 12 (2), 482–489. doi:10.1049/iet-gtd.2017.0509

frontiers | Frontiers in Energy Research

BRIEF RESEARCH REPORT
published: 02 May 2022
doi: 10.3389/fenrg.2022.880727

Rainwater Harvesting Systems That Reduce Water Consumption With Optimal Locations of Solar Concentration Power Plants

Pascual Eduardo Murillo-Alvarado and Marco Antonio Cárdenas Gil*

Department of Energy Engineering, Universidad de La Ciénega Del Estado de Michoacán de Ocampo, Sahuayo, Mexico

At present, the increase in population has caused an increase in the demand for electrical energy, which creates saturation in the national electrical system. In addition to this, the main source of energy for the generation of electricity is fossil fuels, which causes environmental pollution problems due to the increase in the concentration of greenhouse gases. To counteract the negative environmental impact, new energy sources that are friendlier to the environment have been sought, such as solar energy through power generation plants using solar concentrators. In this sense, this research proposes a mathematical optimization model to determine the feasibility of installing electric power generation plants through solar concentrators, to satisfy the energy demand in cities with the highest demand for electric power in the state of Michoacán. The proposed model considers the availability of water resources, the demand for energy, the costs involved for the installation of power generation plants, and the sizing of water collection systems to reduce the consumption of fresh water that is extracted from natural sources. It is a linear integer mixed programming model, where two scenarios are analyzed, considering variation in the operating time of the thermal storage system and the incorporation of the rainwater harvesting system to reduce freshwater consumption. The results show that 237,600 MW can be produced by installing three of the six power generation plants considered and considering a 19 h operation with thermal storage, generating a profit from the sales of the energy produced of 6,326,700 USD/year. Likewise, with the sizing of the rainwater harvesting system, it is possible to collect 1,678 m^3 for the operation of the three determined power generation plants.

Keywords: solar enegy, power energy, solar concentrator, rainwater harvesting system, optimization model

OPEN ACCESS

Edited by:
Nallapaneni Manoj Kumar, City University of Hong Kong, Hong Kong SAR, China

Reviewed by:
Ying Zhu, Xi'an University of Architecture and Technology, China
Daniel Tudor Cotfas, Transilvania University of Braşov, Romania

****Correspondence:***
Pascual Eduardo Murillo-Alvarado
pemurillo@ucemich.edu.mx

Specialty section:
This article was submitted to Sustainable Energy Systems and Policies, a section of the journal Frontiers in Energy Research

Received: *21 February 2022*
Accepted: *30 March 2022*
Published: *02 May 2022*

Citation:
Murillo-Alvarado PE and Cárdenas Gil MA (2022) Rainwater Harvesting Systems That Reduce Water Consumption With Optimal Locations of Solar Concentration Power Plants. Front. Energy Res. 10:880727. doi: 10.3389/fenrg.2022.880727

INTRODUCTION

Currently, fossil fuels are the main ones to produce most of the mechanical and electrical energy sources, which are consumed around the world. However, the mitigation of the environmental impact due to emissions from the use of these fuels is inevitable; greenhouse gas emissions due to the consumption of conventional fuels are increasing disproportionately, and it is also expected that the energy production using fossil fuels in Mexico will be limited by 60% by the year 2035 (Vidal-Amaro et al., 2015). In this sense, the renewable energy resources with the greatest application around the world are hydraulic, wind, biomass, marine, geothermal, and solar (Benedek et al., 2018). Solar

energy is the most abundant and available (Li et al., 2022) and can be harnessed in two ways: using heat (thermal conversion) or using light (in electrical–photovoltaic conversion or in natural lighting for buildings) (Kannan and Vakeesan, 2016). The first step for the use of solar energy is to process the radiation coming from the Sun, which can be carried out through two types of systems: passive systems or active systems (Sadhishkumar and Balusamy, 2014). The main active systems that are used are the thermal conversion elements, which comprise the heating harnessing sunlight, mainly the concentrators. In this sense, Ssemwanga et al., 2020, designed a hybrid solar dryer coupling an active solar photovoltaic obtaining higer efficiency in the drying process system. Ge et al., 2018 analyzed the future of solar applications in the heating and cooling system considering active solar systems. Kumar et al., 2019, realized a study of the solar application in the industrial process, and determined that the use of a solar energy system is an alternative to reduce fossil fuel sources. Joshi and Tiwari, 2018, considered the design of an active Solar System and heat exchanger for the water desalinization. Wu et al., 2019 designed an active Solar System considering parabolic concentrator and determined the thermal efficiency in the heat process from the Ssun's radiation. The concentrator technology is particularly distinguished by the shape and relationship of the concentrator and the receiver, such as parabolic trough concentrators, linear Fresnel concentrators, concentrators with a central tower receiver, and Stirling parabolic dishes. In the power energy generation, the most used are the central concentrator where the heat transfer fluid is in temperatures over 500°C (Guney, 2016). Beltagy et al., 2017, determined the parameters' design in the operation of the Fresnel solar concentrator and evaluated the possibility of power energy generation which can be carried out by increasing the area of the field. Santos et al., 2018, presented a study of the relevance of the solar concentrator systems in the power generation, considering that the parabolic Fresnel is a great alternative in the process for the conversion of the solar thermal energy. However, water is one of the main fluids used in both conventional and unconventional energy generation processes, added to this, not only is there currently little availability of energy resources but also a serious problem of water scarcity due to the increase in population (WWAP, 2017; Huang et al., 2021), which reduces the availability of freshwater resources. In this sense, multiple investigations have focused on finding new alternatives to reduce the consumption of water resources that is available for human consumption, considering alternatives of new sources to continue operating the energy process, analyzing problems such as water desalination (Panagopoulos, 2021) where the availability of water is related to the generation of energy. González-Bravo et al., 2016, proposed an optimization approach to define the optimal water distribution considering the overall sectors of water consumers. Ochoa-Barragán et al., 2021, determined an optimal distribution of water resources considering the natural sources of water available and the effect of incorporation of artificial sources to satisfy the demand in domestic and agricultural sectors. Considering that in the electrical power generation the main work fluid is water, the research are focused in reducing this water consumption. In this sense, Hamiche et al., 2016 analyzed the importance to identify the nexus with the water consumption and the industry mainly the power generation. Guo et al., 2021, proposed an optimization model to identify the optimal distribution of water sources in energy generation and water demand. Jamil et al., 2021, analyzed the freshwater reduction in the cooling process applied in thermal plants for power generation. The importance of minimize the water consumption in power energy generation represents a challenge to consider, in this sense, Tan et al., 2021 proposed a stochastic model to determine the optimal energy generation considering water conservation policy and the emission reduction of greenhouse gases. In this sense, the present research proposed the use of renewable energy sources that allow a self-sustaining increase in the generation of electrical energy. The solar active system is considering, with solar concentrator plants. Through a mixed-integer linear programing (MILP) optimization approach, we can identify the feasibility of installing solar thermal power plants to generate electricity and increase the coverage of the electrical system, the power energy generated will be fed into the national grid system, for these reasons, the mathematical model proposed maximizing the total annual profit considering the possible installation plants, the associated costs, and the possible electrical energy that can be generated, as well as satisfy the growing demand for electricity, incorporating fresh water sources available, and the effect of incorporating the rainwater harvesting system evaluating the potential and dimension of catchment systems. This research evaluated the potential for reducing the consumption of fresh water in the electric power generation. This proposal can be a sustainable solution to the generation of current energy, since the economic aspect is considered; reducing the costs involved in the installation of electric power generation plants. In the social aspect, a greater availability of electric energy is provided, which can bring better human development, and in the environmental aspect, it seeks to improve environmental conditions through the reduction of fossil resources in the generation of energy, in the same way reducing the consumption of resources can compromise the resources available for future generations, as in the case of water.

METHODOLOGY

The heliostat field captures solar radiation and reflects it onto an absorber or receiver that is located at the top of a tower located in the center of the heliostat field. A heat-conducting fluid circulates through this receiver, which, for the case of the plant analyzed in this work, is water. All the radiation reflected by the heliostats is transmitted to this fluid, thus converting solar energy into thermal energy, heating the fluid to more than 500°C. The already heated fluid is sent, either, if available, to the thermal store, which allows the plant to continue operating hours after sunset and on cloudy days, or directly to the turbine. The generation of electrical energy occurs through a steam or Rankine cycle, where there is a turbine coupled with an electric generator. The turbine rotates by

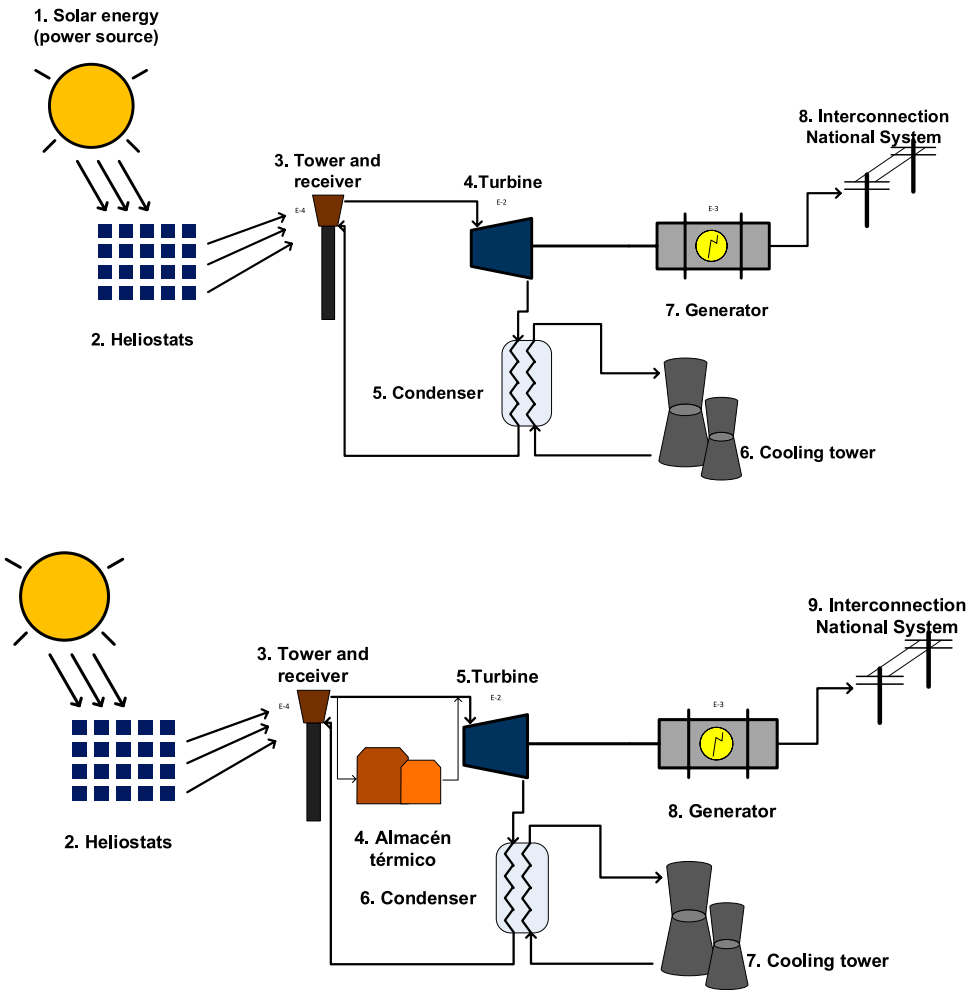

FIGURE 1 | Stages in the generation of electrical energy through solar concentrators, with and without thermal storage systems.

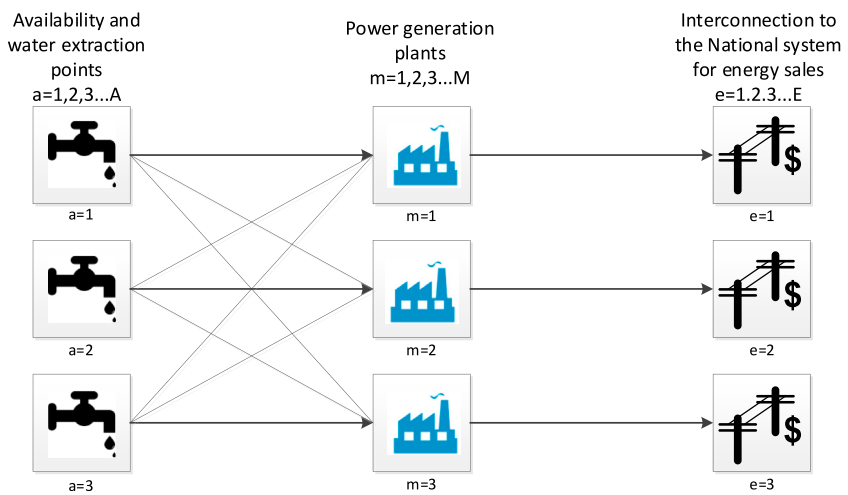

FIGURE 2 | Superstructure for the case study for the optimal location of power generation plants with solar concentrators.

means of the kinetic energy of the water vapor heated by solar radiation. When it rotates, this energy is transformed into electricity thanks to the generator. The electrical energy produced is conducted to a transformer that sends it to where it is demanded. The present work considers power plants of the type of central tower receiver with a circular heliostat field, as showed in **Figure 1**, due to the distance that exists between the location of the project and the line of the equator. **Figure 2** shows the superstructure to determine the optimal configuration for the optimal location of power generation plants with solar concentrators in the state of Michoacán, Mexico, the superstructure considering the extraction points of water for the steam generation in plants and the feasibility of supplying the energy generated to the network of the national electrical system.

Model Formulation

Figure 2 shows the proposed superstructure for the mathematical model, where we define the following sets: the set a represents the availability and extraction points of the water flow to feed the power generation plants, they are defined in set m, in which the flow of water through the action of the plant systems is converted into energy flow at the outlet to be marketed through interconnections to the national system network, this process is defined in set e, and finally, the set t represents the time intervals equivalent to the months of the year. For the mathematical formulation, the following systems are established: pretreatment system, tower system, turbine system, condenser system, and cooling tower system.

The balance to quantify the availability of water is determined through the following equation:

$$FTW_{a,t} = \sum_{m \in M} FTEP_{a,m,t}, \forall a \in A, t \in T. \quad (1)$$

In the previous balance (**Eq. 1**) the $FTW_{a,t}$ indicates the total flow of water from the extraction points a in a period t, this flow is sent to the plant m for the generation of electricity.

The following equation determines the flow of water that enters the pretreatment system within the plants:

$$FWPT_{m,t} = \sum_{a \in A} FTEP_{a,m,t}, \forall m \in M, t \in T. \quad (2)$$

To establish an input value for the input flow to the system, the following restriction is proposed, to establish a limit of water access to the electric power generation system.

$$FWPT_{m,t} \leq FMAXPT_{m,t}, \forall m \in M, t \in T. \quad (3)$$

Once the flow that enters in the pretreatment system is determined, the flow that enters the tower is established to the tower system, through the following balance:

$$FWTR_{m,t} = FWPT_{m,t} \cdot \alpha TR, \forall m \in M, t \in T. \quad (4)$$

In previous balance, αTR is a parameter that indicates the water loss factor during the process in the tower system.

The water flow in the turbine–generator system is represented by the following equation:

$$FWTU_{m,t} = FWTR_{m,t} \cdot \alpha TU, \forall m \in M, t \in T. \quad (5)$$

Additionally, a parameter is considered that indicates the water loss factor in the process of the turbine–generator system αTU.

In the following balance, the energy flow at the generator output is determined:

$$FETU_{m,t} = \frac{FWTU_{m,t}}{DU}, \forall m \in M, t \in T. \quad (6)$$

In the previous equation, DU is a parameter that indicates the quantity of fluid necessary to determine the energy that can be generated by the transfer of thermal energy that the fluid has.

The following balance determines the flow in the condenser system:

$$FWCO_{m,t} = FWTU_{m,t} \cdot \alpha CO, \forall m \in M, t \in T, \quad (7)$$

where αCO represents a parameter that indicates the water loss factor during the process in the condenser system.

The energy flow that enters the interconnection system to the national grid is established from the following equation:

$$FEMERC_{e,t} = \sum_{m \in M} FE_{m,e,t}, \forall e \in E, t \in T. \quad (8)$$

The following equation determines the benefit obtained from energy sales per plant:

$$SALES_{e,t} = FEMERC_{e,t} \left(0.98 \cdot \beta \cos tE_{e,t}\right), \forall e \in E, t \in T, \quad (9)$$

where $\beta \cos tE_{e,t}$ represents the unit price for each MWh injected into the network, which according to the National Interconnected System varies according to the proposed locations for the power plants and is multiplied by 0.98 because it is considered a system through a contract by the CRE, which establishes that only a supply of 98% of the total generation of the plant is approved.

The operation and maintenance costs of the various systems are determined considering a unitary operational cost $U\text{Costop}PT_{m,t}$ and the flow in each system, the cost is defined by the following equation:

$$CostopPT_m = \sum_{t \in T} FWTP_{m,t} \cdot U\text{Costop}PT_{m,t}, \forall m \in M. \quad (10)$$

In the following equation, a disjunction is proposed, considering the Boolean variable Y_{EN}, this variable is taken as the decision variable, since it can help us define when a solar concentration plant is installed. If the flow of fresh water and the costs associated with its installation exist, it means that these restrictions are true and the Boolean variable is true; otherwise, if there is no flow, no costs are associated with it and the Boolean variable is false. This disjunction takes into account the capital cost of each of the plant systems, which are given by the fixed costs and the variable part; the capital cost that refers only to the cost of the equipment used and a variable cost that refers to the cost of managing or adapting the flow that is being processed. In this sense the variable part is multiplied by the flow processed in each system.

$$\begin{bmatrix} Y_{EN} \\ FWTP_m^{CAP_{\min}} \le FWTP_m^{CAP} \le FWTP_m^{CAP_{\max}} \\ CostcapPT_m = CostFIX_m^{PT} + CostVAR_m^{PT} \cdot FWTP_m^{CAP} \\ CostcapTR_m = CostFIX_m^{TR} + CostVAR_m^{TR} \cdot FWTR_m^{CAP} \\ CostcapTU_m = CostFIX_m^{TU} + CostVAR_m^{TU} \cdot FWTU_m^{CAP} \\ CostcapCO_m = CostFIX_m^{CO} + CostVAR_m^{CO} \cdot FWCO_m^{CAP} \\ CostcapTE_m = CostFIX_m^{TE} + CostVAR_m^{TE} \cdot FWTE_m^{CAP} \end{bmatrix} \times \begin{bmatrix} \neg Y_{EN} \\ FWTP_m^{CAP} = 0 \\ CostcapPT_m = 0 \\ CostcapTR_m = 0 \\ CostcapTU_m = 0 \\ CostcapCO_m = 0 \\ CostcapTE_m = 0 \end{bmatrix} \forall m \in M. \tag{11}$$

However, for the encoding of the proposed model is considered to be an algebraic reformulation convex hull (Raman and Grossmann, 1994) to linearize the previous disjunction, the Boolean variable is reformulated by the binary variable y_{EN}. In this case when a flow of fresh water and cost associate with the installation of plants exist, the binary variable take a value of one, otherwise the binary variable is zero and the plant is not installed. This is obtained by the following equations:

$$FWTP_m^{CAP_{\min}} \cdot y_{EN} \le FWTP_m^{CAP} \le FWTP_m^{CAP_{\max}} \cdot y_{EN}, \forall m \in M, \tag{12}$$

$$CostcapPT_m = CostFIX_m^{PT} \cdot y_{EN} + CostVAR_m^{PT} \cdot FWTP_m^{CAP}, \forall m \in M. \tag{13}$$

Finally, is defined the transportation cost generated by the piping and pumping of water, from the extraction point to the power plants, is considering a unitary transport cost:

$$CostTransport = \sum_{a \in A} \sum_{m \in M} \sum_{t \in T} FWTP_{a,m,t} \cdot UnitTransp_{a,m} \cdot Dist_{a,m}. \tag{14}$$

The mathematical model proposed is defined to the maximization of the objective function. In this objective, the function is declared by the variable PROFIT, that, considering the sales of the energy supplied to the national grid and the total costs involved for power generation, the objective function is established by the following equation:

$$COSTOT = \sum_{m \in M} CostopPT_m + \sum_{m \in M} CostcapPT_m + CostTransport, \tag{15}$$

$$PROFIT = \sum_{e \in E} \sum_{t \in T} SALES_{e,t} - COSTOT. \tag{16}$$

The proposed mathematical model seeks to establish the feasibility of installing electric power generation plants through solar concentrator systems. The effect is determined by the use of water, which is the main working fluid for power generation.

RESULTS AND DISCUSSIONS

To show the applicability of the mathematical model proposed, the installation of solar thermal power plants is considering the case study, with a central tower receiver, and three possible locations for their installation in the state of Michoacán, Mexico. Michoacán is a state belonging to the central-western region of the country and one of the states that consumes the most electrical energy, with an approximate consumption of 6,794 GWh, however, the state only produces 2,779 GWh. Due to the exaggerated population growth, the state is therefore in the demand for electrical energy. For the possible installation of the plants, there is great interest in six locations in the regions of the Lerma–Chapala region, the Cuitzeo region, and the Sierra–Costa region. The criteria to establish a possible installation site for a power generation plant was that it would be close to a freshwater extraction point, since it is the main workflow for the operation of the plant, and that it would be close to the cities with the highest demand for electricity, in order to reduce losses in the process of distribution of electricity. The interest in these regions is because they are in the 3 municipalities that demand the most electricity in the state (Lazaro Cardenas, Morelia, and Zamora). Also, for purposes of analysis for the potential of usable solar radiation and the availability of water, necessary supplements for plant operation are to be given. The deterministic model MILP proposed is coded in the software GAMS through the solver CPLEX (Brooke et al., 2012), used to solve the mixed-integer linear programing (MILP) problem. The addressed case study has 517 continuous variables, 1 binary variable, and 525 constraints. The model was solved in a computer with the Intel® Core™ i7 processor at 2.80 GHz with 12.0 GB of Memory RAM with a 0.016 s of CPU time in each scenario. The proposed model seeks to find the optimal level of operation according to the thermal storage system, determine the optimal amount of installation of power generation plants according to the availability of water resources in the surroundings, the amount of profits obtained by the electrical energy generated and that is fed into the network of the national energy system, and determine what is the flow of rainwater that can be captured for the reduction of fresh water without harming the operation of the electric power generation plants through solar concentrators. Two scenarios are proposed. The first scenario contemplates the optimal energy generation considering several operational times in the thermal storage system, and in the second scenario, an economic benefit analysis is carried out to calculate the return on investment in the installation of power generation plants.

Scenario A: Optimal Power Generation Modified the Operation Times in the Thermal Storage System

This scenario presents the optimal solution of the installation of solar concentrator plants, considering the

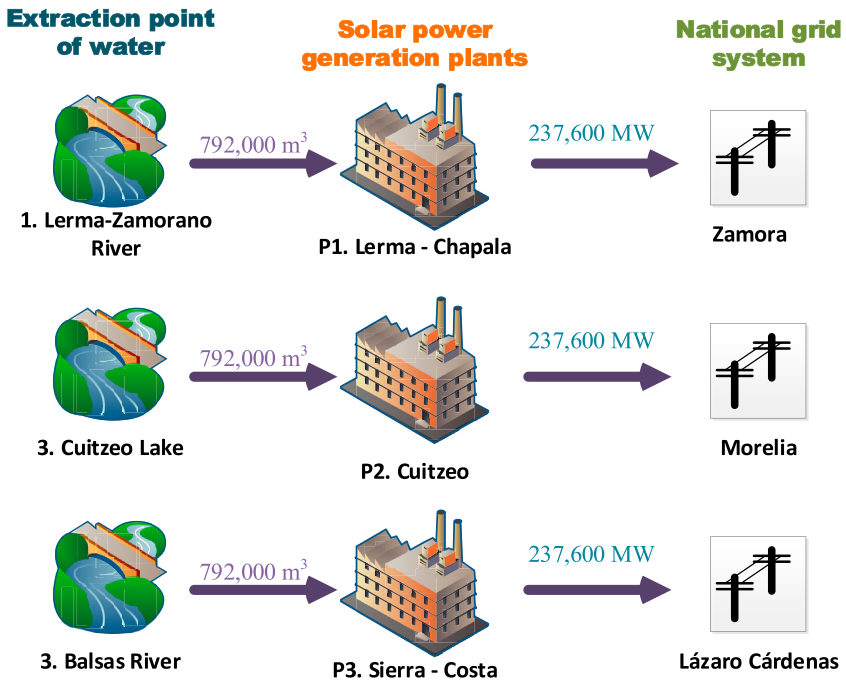

FIGURE 3 | Optimal distribution of scenario A, for the installation of solar concentration plants for electric power generation for case d (24 h of operation with 19 h of thermal storage).

TABLE 1 | Cost involved in the solar power generation plants.

Concept	Cost (US$)	% of total
Heliostats	46,200,000	25.895
Wiring and equipment	2,081,540	1.167
Ground	25,314,222	14.188
Civil work	21,335,508	11.958
Edging and adjustment	4,150,559	2.326

following operation times in the thermal storage system: 1) 5 h of operation without a thermal storage system, 2) 8 h of operation and contemplating 3 h of thermal storage, 3) 16 h of operation with 11 h of thermal storage, and 4) 24 h of operation with 19 h of thermal storage. The results show the feasibility of installation of three plants of the six considered for cases for the electric power generation (Plant 1. Lerma–Chapala, Plant 2. Cuitzeo, Plant 3. Sierra–Costa), the electric generation increase with the increase of the thermal storage system, the optimal distribution is showed in **Figure 3**. This figure shows the optimal distribution found for the case d, which represents the configuration with highest energy production; this configuration considers the extraction points of fresh water (1. Lerma–Zamorano River, 2. Cuitzeo Lake, and 3. Balsas River) that are fed to the plant for power generation. The plants involved take into account the same water extraction with a water flow of 792,000 m^3 and the same electricity generation of 237,600 MW because they have the same capacity, because the plants operate in the same way. Also, this configuration established the places where it is feasible to install three power generation plants through solar concentrators founded in the solution of the model proposed and finally the amount of energy that is generated in the installed plants that can be fed into the national energy network is calculated. For the economic analysis of the solar field, the first data to be considered are the cost of the heliostats, as well as the costs involved for their installation (Caminero Ocaña, 2014). For practical purposes, the total cost of the solar field, including heliostats, is broken down in the analysis of **Table 1**. According to previous information, the maximum energy generated is presented in the case with the highest thermal storage (case d) with a production of 237,600 MW, however, is the case with more use of water, as show in **Table 2**. The high production in case dpresents greater feasibility of energy production due to the incorporation of the thermal storage system, since without it, the generation process is not very feasible due to the low global efficiency in the system. However, despite being the solution with the highest energy generation, it is the one with the highest operating costs due to the implementation of the thermal storage system. In all cases, negative gains are presented until the first year of operation, however, in all cases, the energy generation is considerable, but a better effect is visualized considering the thermal storage system. The sales by the amount of energy supplied to the national grid is from 6′326,700 USD/year for the case a, to 30′368,000 USD/year for the case d. The profits for the three plants considered: 1.16×10^7 USD/year for plant 1, 2.19×10^7 USD/year for plant 2, and 3.19×10^7 USD/year for plant 3. These profits are obtained by operating with 19 h of thermal storage, which favors a greater

TABLE 2 | Total flow of new species used in biofuel production.

Case	Location plants	Electrical energy generated (MW)	Sales for electrical energy (USD/year)	Flow of water (m^3/year)
a	1. Lerma—Chapala 2. Cuitzeo 3. Sierra - Costa	49,500	6,326,700	165,000
b	1. Lerma—Chapala 2. Cuitzeo 3. Sierra - Costa	79,200	10,122,000	264,000
c	1. Lerma—Chapala 2. Cuitzeo 3. Sierra - Costa	158,400	20,245,000	528,000
d	1. Lerma—Chapala 2. Cuitzeo 3. Sierra - Costa	237,600	30,368,000	792,000

TABLE 3 | Monthly precipitation in the state of Morelia, Mexico.

Month	Precipitation (mm)
JAN	6.8
FEB	29.8
MAR	9
APR	5.1
MAY	9.8
JUN	92.5
JUL	155.9
AUG	201
SEP	167.6
OCT	20.2
NOV	2.9
DEC	2.4

generation of energy; however, due to the high feasibility of generating electricity, it is the case in which more water is processed in the system, processing approximately 792,000 m^3/year per plant.

Scenario B: Rainwater Harvesting System Incorporation

This scenario presents the rainwater harvesting system incorporation to reduce the consumption of fresh water in the process of generating electricity. Considering that the state of Michoacán is one of the states that has one of the highest rates of rainfall, the percentage of water that can be recovered is evaluated, as well as the feasible area for the implementation of the system. The solution of this scenario considering the recent values reported of precipitation indices evaluated in the year 2020 in the annual report by CONAGUA 2021, is shown in **Table 3**. Considering these values, the possibility of covering the demand for fresh water in the system through rainwater is established, so **Figure 4** shows the areas obtained from some scenarios to cover from 10 to 100% of the demand for fresh water. It is possible to observe that in the months with less precipitation, the necessary areas of the rain catchment system present very large areas, which is why it is infeasible, especially if it is required to cover 100% of the demand for fresh water. In order to determine a feasible

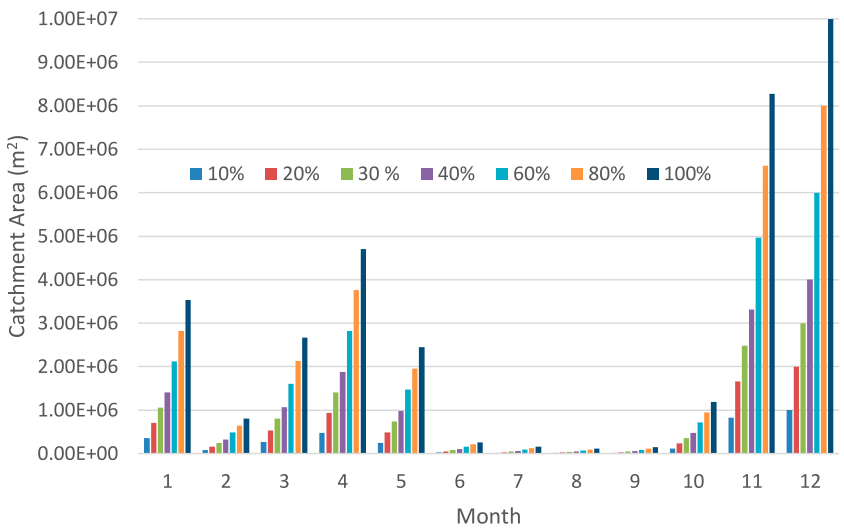

FIGURE 4 | Catchment area for the rainwater harvesting system considering the precipitation and demand covering of fresh water.

TABLE 4 | Length to the rainwater harvesting system considering variation in the percentage of demand for fresh water.

Month	Length (m)			
	10%	3%	2%	1%
1	11764.706	3529.412	2352.941	1176.471
2	2684.564	805.369	536.913	268.456
3	8888.889	2666.667	1777.778	888.889
4	15686.275	4705.882	3137.255	1568.627
5	8163.265	2448.98	1632.653	816.327
6	864.865	259.459	172.973	86.486
7	513.149	153.945	102.63	51.315
8	**398.01**	**119.403**	**79.602**	**39.801**
9	477.327	143.198	95.465	47.733
10	3960.396	1188.119	792.079	396.04
11	27586.207	8275.862	5517.241	2758.621
12	33333.333	10000	6666.667	3333.333

catchment area, various cases were resolved considering a lower demand for fresh water coverage. For these reasons, it was established to determine the area of a surface, considering a fix width of 30 m. **Table 4** shows the possible length of the rainwater harvesting system according to the monthly precipitation and percentage satisfaction of the demand for fresh water for the solar concentrator plants. Some areas are feasible as the case of 2% of coverage results in a catchment area of 2,388 m^2, this area represent the months with the highest precipitation. However, by establishing this system with a fixed area throughout the year, it would be possible to collect a volume of rainwater of 1,678 m^3.

CONCLUSION

In this article, an optimization methodology was presented to determine the optimal location of electric power generation plants from solar concentrator plants in the state of Michoacán. The results show that the generation of energy through solar concentrators is favored considering operation with a thermal storage system, since without this system, there is less operation time considering only the hours of available sunlight. The solution of the model proposed the installation of 3 of the 6 solar plants considered. The better value of energy generated was the option d with a thermal storage operation of 19 h. This configuration presented an energy production of 237,600 MW. The profits for the three plants considered was 1.16 $\times 10^7$ USD/year for plant 1, 2.19 $\times 10^7$ USD/year for plant 2, and 3.19 $\times 10^7$ USD/year for plant 3. In addition, the amount of freshwater flow supplied to the plant was determined and the dimensions of rainwater storage systems were identified to reduce freshwater consumption, showed in **Table 4**. According to the data on rainfall in the state, the optimal value rainwater recovery is 2% of coverage with a catchment area of 2,388 m^2. With this rainwater harvesting systems, it is possible to collect a volume of rainwater of 1,678 m^3 per year. For this reason, the result considered that it is feasible to install rainwater storage systems, allowing freshwater consumption to be reduced by 0.6% per year. Considering the installation of rainwater storage systems is feasible, the installation of power generation plants forms solar concentrator, the energy supply at the grid of the national system, will be significant in reducing the demand of electricity from conventional sources.

The model proposed is a deterministic optimization model, however, in future work uncertainty factors can be added. Two scenarios that are proposed could be considered an uncertainty in the price of MW, since in the Mexican electrical system, the price varies with respect to the daily hour. There are hours with high demand for electrical energy so the MW that is supplied to the network is valued at a better sale price. This could improve the economic results in terms of profit maximization since it could be determined at what times it is more convenient to generate energy and supply it to the national grid.

Similarly, uncertainty could be considered in the precipitation levels throughout the year, although in this model it only considers the precipitation values for the year 2020. A dataset could be implemented to predict which would be the values with the highest precipitation for the years subsequent and thus define what would be the volume of rainwater that could be captured. This leads to proposing a more robust mathematical optimization model. Two stages are established; in the first stage, a stochastic model is proposed, in which the uncertainty effect due to the variation in the price of MW in relation to the objective function is evaluated. This will generate multiple solutions, and through a pareto chart, you can visualize optimal solutions for the objective function. In the second stage, the solutions previously found are compared with the solutions for the deterministic model without the uncertainty effect in such a way that it is observed if it is possible to obtain better solutions under uncertainty. Finally, the same methodology applies to the uncertainty effect on precipitation levels but is related to the catchment area.

DATA AVAILABILITY STATEMENT

The original contributions presented in the study are included in the article/Supplementary Material, further inquiries can be directed to the corresponding author.

AUTHOR CONTRIBUTIONS

PE-MA proposed the idea, carried out the conceptualization, wrote the original draft, and conducted formal analysis. MA-CG was responsible for the coded model proposed, analysis of the data, and design of the case studies.

FUNDING

This work was supported by Universidad de la Ciénega del Estado de Michoacan de Ocampo.

REFERENCES

Beltagy, H., Semmar, D., Lehaut, C., and Said, N. (2017). Theoretical and Experimental Performance Analysis of a Fresnel Type Solar Concentrator. *Renew. Energ.* 101, 782–793. doi:10.1016/j.renene.2016.09.038

Benedek, J., Sebestyén, T.-T., and Bartók, B. (2018). Evaluation of Renewable Energy Sources in Peripheral Areas and Renewable Energy-Based Rural Development. *Renew. Sustain. Energ. Rev.* 90, 516–535. doi:10.1016/j.rser.2018.03.020

Brooke, A., Kendrick, D., Meeraus, A., and Raman, R. (2012). *GAMS A User's Guide*. Washington, D.C.: GAMS Development Corporation. Available in: http://www.gams.com/dd/docs/bigdocs/GAMSUsersGuide.pdf.

Caminero Ocaña, V. (2014). *Análisis Económico de Viabilidad de una planta termo-solarICAI - Proyectos Fin de Carrera*. Madrid, Spain: Repositorio de la Universidad Pontificia Comillas. https://repositorio.comillas.edu/xmlui/handle/11531/1297.

CONAGUA (2021). El Reporte del Clima en México, Reporte Anual 2020, Comisión Nacional del Agua 2021. Available: https://smn.conagua.gob.mx/tools/DATA/Climatolog%C3%ADa/Diagn%C3%B3stico%20Atmosf%C3%A9rico/Reporte%20del%20Clima%20en%20M%C3%A9xico/Anual2020.pdf (Accessed January 2022).

Ge, T. S., Wang, R. Z., Xu, Z. Y., Pan, Q. W., Du, S., Chen, X. M., et al. (2018). Solar Heating and Cooling: Present and Future Development. *Renew. Energ.* 126, 1126–1140. doi:10.1016/j.renene.2017.06.081

González-Bravo, R., Nápoles-Rivera, F., Ponce-Ortega, J. M., and El-Halwagi, M. M. (2016). Multiobjective Optimization of Dual-Purpose Power Plants and Water Distribution Networks. *ACS Sustain. Chem. Eng.* 4 (12), 6852–6866. doi:10.1021/acssuschemeng.6b01817

Guney, M. S. (2016). Solar Power and Application Methods. *Renew. Sustain. Energ. Rev.* 57, 776–785. doi:10.1016/j.rser.2015.12.055

Guo, Q., Guo, T., Tian, Q., and Nojavan, S. (2021). Optimal Robust Scheduling of Energy-Water Nexus System Using Robust Optimization Technique. *Comput. Chem. Eng.* 155, 107542. doi:10.1016/j.compchemeng.2021.107542

Hamiche, A. M., Stambouli, A. B., and Flazi, S. (2016). A Review of the Water-Energy Nexus. *Renew. Sustain. Energ. Rev.* 65, 319–331. doi:10.1016/j.rser.2016.07.020

Huang, Z., Liu, X., Sun, S., Tang, Y., Yuan, X., and Tang, Q. (2021). Global Assessment of Future Sectoral Water Scarcity under Adaptive Inner-basin Water Allocation Measures. *Sci. Total Environ.* 783, 146973. doi:10.1016/j.scitotenv.2021.146973

Jamil, A., Javed, A., Wajid, A., Zeb, M. O., Ali, M., Khoja, A. H., et al. (2021). Multiparametric Optimization for Reduced Condenser Cooling Water Consumption in a Degraded Combined Cycle Gas Turbine Power Plant from a Water-Energy Nexus Perspective. *Appl. Energ.* 304, 117764. doi:10.1016/j.apenergy.2021.117764

Joshi, P., and Tiwari, G. N. (2018). Energy Matrices, Exergo-Economic and Enviro-Economic Analysis of an Active Single Slope Solar Still Integrated with a Heat Exchanger: a Comparative Study. *Desalination* 443, 85–98. doi:10.1016/j.desal.2018.05.012

Kannan, N., and Vakeesan, D. (2016). Solar Energy for Future World: - A Review. *Renew. Sustain. Energ. Rev.* 62, 1092–1105. doi:10.1016/j.rser.2016.05.022

Kumar, L., Hasanuzzaman, M., and Rahim, N. A. (2019). Global Advancement of Solar thermal Energy Technologies for Industrial Process Heat and its Future Prospects: A Review. *Energ. Convers. Manage.* 195, 885–908. doi:10.1016/j.enconman.2019.05.081

Li, G., Li, M., Taylor, R., Hao, Y., Besagni, G., and Markides, C. N. (202211828). Solar Energy Utilisation: Current Status and Roll-Out Potential. *Appl. Therm. Eng.* 209, 118285. doi:10.1016/j.applthermaleng.2022.118285

Ochoa-Barragán, R., Nápoles-Rivera, F., and Ponce-Ortega, J. M. (2021). Optimal and Fair Distribution of Water under Water Scarcity Scenarios at a Macroscopic Level. *Int. J. Environ. Res.* 15 (1), 57–77. doi:10.1007/s41742-020-00297-8

Panagopoulos, A. (2021). Water-energy Nexus: Desalination Technologies and Renewable Energy Sources. *Environ. Sci. Pollut. Res.* 28 (17), 21009–21022. doi:10.1007/s11356-021-13332-8

Raman, R., and Grossmann, I. E. (1994). Modelling and Computational Techniques for Logic Based Integer Programming. *Comput. Chem. Eng.* 18 (7), 563–578. doi:10.1016/0098-1354(93)E0010-7

Sadhishkumar, S., and Balusamy, T. (2014). Performance Improvement in Solar Water Heating Systems-A Review. *Renew. Sustain. Energ. Rev.* 37, 191–198. doi:10.1016/j.rser.2014.04.072

Santos, J. J., Palacio, J. C., Reyes, A. M., Carvalho, M., Freire, A. J., and Barone, M. A. (2018). "Concentrating Solar Power," in *Advances in Renewable Energies and Power Technologies* (Elsevier), 373–402. doi:10.1016/B978-0-12-812959-3.00012-5

Ssemwanga, M., Makule, E., and Kayondo, S. I. (2020). Performance Analysis of an Improved Solar Dryer Integrated with Multiple Metallic Solar Concentrators for Drying Fruits. *Solar Energy* 204, 419–428. doi:10.1016/j.solener.2020.04.065

Tan, Q., Liu, Y., and Zhang, X. (2021). Stochastic Optimization Framework of the Energy-Water-Emissions Nexus for Regional Power System Planning Considering Multiple Uncertainty. *J. Clean. Prod.* 281, 124470. doi:10.1016/j.jclepro.2020.124470

Vidal-Amaro, J. J., Østergaard, P. A., and Sheinbaum-Pardo, C. (2015). Optimal Energy Mix for Transitioning from Fossil Fuels to Renewable Energy Sources - the Case of the Mexican Electricity System. *Appl. Energ.* 150, 80–96. doi:10.1016/j.apenergy.2015.03.133

Wu, G., Yang, Q., Fang, H., Zhang, Y., Zheng, H., Zhu, Z., et al. (2019). Photothermal/day Lighting Performance Analysis of a Multifunctional Solid Compound Parabolic Concentrator for an Active Solar Greenhouse Roof. *Solar Energy* 180, 92–103. doi:10.1016/j.solener.2019.01.007

WWAP (United Nations World Water Assessment Programme) (2017). *The United Nations World Water Development Report 2017. Wastewater: The Untapped Resource*. Paris: UNESCO.

Conflict of Interest: The authors declare that the research was conducted in the absence of any commercial or financial relationships that could be construed as a potential conflict of interest.

NOMENCLATURE

Indexes

a Index for extraction points of the water flow

m Index for power generation plants with solar concentrators

e Index for marketed in the national system network

t Index for time periods

Sets

A Set for extraction points of the water flow a

M Set for power generation plants with solar concentrators m

E Set for marketed in the national system network e

T Set for time periods t

Parameters

αCO Loss factor of water in the condenser system of the plant m

αTR Loss factor of water in the tower system of the plant m

αTU Loss factor of water in the turbine system of the plant m

$\beta \cos \mathbf{t} E_{e,t}$ Energy price (MWh) in energy cities e

DU Factor of energy generation in the plants m

$CostFIX_m^{CO}$ Fixed cost for the condenser system in the plants m

$CostFIX_m^{PT}$ Fixed cost for the pretreatment system in the plants m

$CostFIX_m^{TE}$ Fixed cost for the thermal storage system in the plants m

$CostFIX_m^{TR}$ Fixed cost for the tower system in the plants m

$CostFIX_m^{TU}$ Fixed cost for the turbine system in the plants m

$CostVAR_m^{CO}$ Unit variable cost for the condenser system in the plants m

$CostVAR_m^{PT}$ Unit variable cost for the pretreatment system in the plants m

$CostVAR_m^{TE}$ Unit variable cost for the thermal storage system in the plants m

$CostVAR_m^{TR}$ Unit variable cost for the tower system in the plants m

$CostVAR_m^{TU}$ Unit variable cost for the turbine system in the plants m

$FWTP_m^{CAP_{\max}}$ Maximum water flow in the plants m

$FWTP_m^{CAP_{\min}}$ Minimum water flow in the plants m

$Dist_{a,m}$ Distance from extraction points a to the plants m

$UnitTransp_{a,m}$ Unit transportation cost of water flow to the plants m

$U\mathbf{Costop}PT_{m,t}$ Unit operating cost for the plants m

Variables

$CostcapCO_m$ Capital cost for the condenser system in the plants m

$CostcapPT_m$ Capital cost for the pretreatment system in the plants m

$CostcapTE_m$ Capital cost for the thermal storage in the plants m

$CostcapTR_m$ Capital cost for the tower system in the plants m

$CostcapTU_m$ Capital cost for the turbine system in the plants m

$CostopPT_m$ Operational cost for the plants m

$COSTOT$ Total cost involved

$CostTransport$ Cost for transportation

$FE_{m,e,t}$ Energy flow supplied to the network e from the plants m

$FEMERC_{e,t}$ Energy flow supplied to the network e

$FETU_{m,t}$ Energy flow generated in the plants m

$FMAXPT_{m,t}$ Maximum input water flow in the plants m

$FTEP_{a,m,t}$ Water flow from each extraction point a to the plants m

$FTW_{a,t}$ Water flow considered in each extraction point a

$FWCO_{m,t}$ Water flow in the condenser system of the plants m

$FWCO_{m,t}$ Water flow in the pretreatment system of the plants m

$FWTP_m^{CAP}$ Water flow for the dimensions of the plants m

$FWTR_{m,t}$ Water flow in the tower system of the plants m

$FWTU_{m,t}$ Water flow in the turbine system of the plants m

$SALES_{e,t}$ Total sales for the energy flow supplied to the network e

PROFIT Total annual profit

y_{EN} Binary variable for the existence of the plants m

Y_{EN} Boolean variable for the existence of the plants m

frontiers | Frontiers in Energy Research

TYPE Original Research
PUBLISHED 18 January 2023
DOI 10.3389/fenrg.2022.1025564

OPEN ACCESS

EDITED BY
Anshu Priya,
City University of Hong Kong, Hong Kong SAR, China

REVIEWED BY
Sandhya Thotakura,
Gandhi Institute of Technology and Management (GITAM), India
Alpesh Desai,
Pandit Deendayal Petroleum University, India

*CORRESPONDENCE
Kim Chul-Soo,
kanjr@naver.com

SPECIALTY SECTION
This article was submitted to Sustainable Energy Systems and Policies, a section of the journal Frontiers in Energy Research

RECEIVED 23 August 2022
ACCEPTED 30 December 2022
PUBLISHED 18 January 2023

CITATION
Wu Z and Chul-Soo K (2023), A preliminary study understanding the possibility and benefits of solar photovoltaic collector integration with vertical green balconies in building facade reconstruction.
Front. Energy Res. 10:1025564.
doi: 10.3389/fenrg.2022.1025564

A preliminary study understanding the possibility and benefits of solar photovoltaic collector integration with vertical green balconies in building facade reconstruction

Zhang Wu and Kim Chul-Soo*

Pukyong National University, Busan, South Korea

The facades of buildings provide significant potential for photovoltaic panels integration, allowing renewable energy deployment within the built environment. In literature, various options, such as building-integrated photovoltaics, building-integrated photovoltaics-thermal collectors, building-attached photovoltaics, and rooftop photovoltaics, have already been explored. However, this study aimed to develop a new solar photovoltaic collectors' integration with vertical-green balconies in old high-rise buildings considering the façade reconstruction concepts mainly focusing on the water heating application. The objective of this study is to conduct a preliminary research study investigating such integration possibilities with old buildings considering the façade reconstruction concepts, followed by exploring various benefits. For this, an old high-rise building was rebuilt scientifically and rationally. PHOENICS tool was used to gauge and assess the building's wind environment first, followed by the solar photovoltaic collector-based facade installation and preliminary assessment. The results include the system design, economic analysis of the solar photovoltaic collector's application for water heating, calculation of the energy-saving rate, and functional analysis of the solar photovoltaic collectors combined with a vertical green balcony. The outcome of this study suggested that the process-specific rationalization plan can be applied in future urban architecture renovation.

KEYWORDS

building integrated photovoltaic (BIPV), photovoltaic panels, vertical greening, building facades, building retrofitting, wind environment, urban heat island effect

1 Introduction

The International Energy Agency (IEA) estimates that 50% of the world's population lives in cities, uses 73% of the world's energy, and emits 70% of its CO_2 emissions (Akram et al., 2021; IEA, 2021). The International Energy Outlook study also projects a 56% increase in global energy use between 2010 and 2040 (Akram et al., 2021). Additional forecasts show that the building industry will contribute significantly to overall energy usage when considering sectoral energy consumption assessments. Having said that, 50% of the population lives in urban areas, which is significantly increasing; more and more inner-city green spaces will need to be sacrificed to provide enough living space in urban centers in the future (Akram et al., 2021). As urbanization progresses, more and more high-rise residential structures are built; they typically have 10 to 15 stories. In this context, the quality of city life is affected by these places' significant impact on the microclimate, which impacts the thermal comfort of cities and their related recreational functions (Shih et al., 2019; Yu et al., 2020; Xue et al., 2017; Liu and Russo, 2021;

Puchol-Salort et al., 2020; Piselli et al., 2018). The option of creating green spaces in the city in locations that they previously believed impossible to create is provided by the vertical greening of buildings (Dunnett and Kingsbury, 2008). They provide significant potential for photovoltaic panels integration, allowing renewable energy deployment within the built environment. In literature, various options, such as building-integrated photovoltaics (BIPV), building-attached photovoltaics (BAPV), and rooftop photovoltaics (RTPV), have already been explored, but the most prominent option was BIPV. BIPV is one such popular way of integrating photovoltaics that enables both on-site green energy generation and vertical greening of buildings. Also, there is an increasing trend of BIPV adoption in the built environment to increase the proportion of renewable energy. The facades of buildings provide a significant amount of potential for BIPV deployment. Accurate external convective heat transfer coefficient modeling is necessary to evaluate BIPV facade performance. Moreover, a handful of studies (Ritzen et al., 2016; Yang and Zou, 2016; Goh et al., 2017; Prieto et al., 2017; Tabakovic et al., 2017) emphasize significant obstacles that prevent BIPV from being widely used. They vary from broad product concerns like functionality, aesthetics, and technological complexity (Prieto et al., 2017) to specialized regional concerns like the requirement for in-depth training at the professional and public levels (Ritzen et al., 2016; Goh et al., 2017; Tabakovic et al., 2017). The content of the current BIPV literature is summarized in Table 1, which highlights that there is only a limited amount of knowledge on customization as a possible driver for BIPV adoption. Building energy demand is influenced by several variables, some of which affect building energy usage. The terms "physical environmental elements" and "artificial designing parameters" are used to categorize these variables into two groups. While artificial designing parameters include building form factor and orientation, transparency ratio, optical and thermophysical properties of building material, and the distance between buildings, physical environmental factors include the amount of solar radiation, outdoor temperature, and wind speed, among others (Ekici and Aksoy, 2009).

In Table 2 design related summary, provides the benefits and drawbacks of each of the categories of photovoltaic integration for typical constructed example from literature is given.

More recently, application-specific design is becoming popular, and among the applications, water heating system is popular. Combining solar water heating technologies with building architecture involves two significant difficulties. One involves a solar water heating system consisting of a water pipeline, a water storage tank, and a solar collector (Ritzen et al., 2016; Prieto et al., 2017; Tabakovic et al., 2017). Evacuated tube Sun collectors are frequently used in buildings in China. However, Europe's flat plate solar collectors are more typical (Shi et al., 2013). The flat plate collectors are better suited for pressure and secondary circulation systems, are easier to install, have a longer service life, and go better with building aesthetics, even if these two types of solar collectors each have their own technical benefits and limitations. The solar energy system's performance is the subject of a lot of research. By conducting an experimental examination over a 1-year operating period, Zhai et al. (Wei et al., 2010) confirmed the real-world energy performance of a solar energy system capable of providing a hot water supply, natural ventilation, heating, and cooling in Shanghai. Building-integrated photovoltaic/thermal (BIPV/T) systems that use recovered heat for home heating were evaluated by Pantic et al. (Zhai et al., 2007) for their energy performance in three distinct open-loop air heating applications. Most vertical greening initiatives that have been put in place so far are showcases meant to create an impressive installation with a favorable reputation. The demand for vertical greening is growing, which is justified by the growing need for cities to be climate resilient and by the numerous benefits of green infrastructure in urban settings. This suggests that more and more cities are mandating the greening of buildings to some level, for instance, in the zoning plans.

Despite the greening mandates and various benefits of vertical greening that have been demonstrated, particularly in metropolitan settings, its use has thus far mostly been infrequent. On the one hand, many think installation, maintenance, and care are expensive for this type, but this could be dependent on many parameters (Hollands and Korjenic, 2021). So, the process of deciding on the greening system and choosing the photovoltaic application starts after the choice to design house greenery has been made. But so far, the available literature concerned it is mainly focused on facades and balconies are less explored for photovoltaics integration, nevertheless we see a great potential for photovoltaics integration with vertical green balconies by reconstructing facades in the buildings.

Therefore, this study aimed to develop a new photovoltaic panel's integration with vertical-green balconies in old high-rise buildings

TABLE 1 Content of current BIPV.

Study Area	Customized Content	Ref
PV products and high-quality architecture	Discussion of functions, examples, and difficulties	Scognamiglio et al. (2012)
The way to create the integrated PV of the future	A brief mention of potential product variety in the future	Jelle and Breivik, (2012)
BIPV products: an assessment of the current literature and potential for future research	The potential of commercially available bespoke goods	Jelle et al. (2012)
"State-of-the-art" integrated PV products construction	Information about market-available customized goods	Cerón et al. (2013)
Review, Potentials, Barriers, and Myths of Building Integrated Photovoltaics (BIPV)	Describe the need, options, and difficulties briefly	Heinstein et al. (2013)
Overview and analysis of existing BIPV products: new standards for promoting the use of new technologies in the construction industry	Opportunities, commercial alternatives, aesthetic levels; a design strategy using architectural layering	Bonomo et al. (2015)
A complete BIPV was an examination	An energy-conscious process design is mentioned	Shukla et al. (2016)

TABLE 2 Design impacts of façade types.

BIPV façade types	Advantage	Disadvantage	References
Advanced Envelope System Examples include façades with two skins, active skins, rotating or moving façade components*etc.*	• Integration with cutting-edge polymer aesthetic technology • Production of heat for room heating in the cold • BIPV panels are cooled by double-skinned facades • Potential integration with additional structural components for performance and appearance	• Likely to cost more than other varieties • The removal of heat in the summer may need energy through mechanical techniques or forced circulation	Montoro et al. (2011); Munari Probst et al. (2013); Nagy et al. (2016)
External Devices/Accessories Sunscreen and sunshades, parapets on balconies, spandrels, and other visual and auditory shielding components	• Possibility of reducing energy use and building heat loads • Sun shading provided above windows may be vertical or horizontal • Building shading structures can be used as mounts to reduce the stress placed on the façade • Possibility of becoming fixed or movable devices • Permits the use of PV modules in a variety of forms	• The distribution of light may need to be evened out by filtering the shadows that BIPV panels cast • If not clear or opaque, obstruction of vision	Montoro et al. (2011); Munari Probst et al. (2013)
Solar windows and glazing Depending on the transparency of solar cells, used as semi-transparent or translucent portions of the façade. They can be incorporated into glazing panels, windows, or windows for views or daylighting [59]	• Enabling energy production and restricted views • Useful applications involve transparent or opaque or semi-transparent glazing • Standard double or triple glazing components were combined with special PV elements that utilized thermal insulators • An excellent feature of sun shading • Through the day, the patterns created by the shade create a dynamic sensation of spatial variation	• lower potential efficiency • Increasing cell spacing results in fewer cells, which produces less energy	Montoro et al. 2011; Heinstein et al. (2013)
System for curtain walls or cladding As a standard cladding solution for curtain walls and single-layer façades, solar panels are included	• An innovative method of managing shade and sunshine • Architectural significance of legendary proportions • It is possible to use a variety of hues and visual effects • reduces sunlight gain throughout the summer to control the building's inside temperatures • The structure itself is illuminated by these panels, creating an ever-changing pattern of colors • Influence the overall perception of architecture • utilizes most of the façade wall to produce energy	• The price of installation may be substantial • less energy than on the roof, maybe • Advanced planning is necessary, as is adherence to a wide range of physical requirements • To avoid having electrical lines obscure your vision, handle them properly	(Montoro et al. (2011); Heinstein et al. (2013)

considering the façade reconstruction concepts mainly focusing on the water heating application. The objective of this study is to conduct a preliminary research study investigating such integration possibilities with old buildings considering the façade reconstruction concepts, followed by exploring various benefits.

2 System design and installation

2.1 Proposed integrated design photovoltaics integration with vertical green balconies in high-rise building

The proposed design considers the photovoltaics integration in the vertical green balconies where existing facades are replaced with photovoltaics facades. This arrangement can be seen in Figure 1. Also, in Figure 1, the design plan adopted for façade reconstruction considering a case of schematic representation of high-rise building is shown. While designing the system, it is crucial to consider the ambient temperature, the wind speed, the aperture area of the solar collector, the solar radiation on the collector's plane, and the amount of water in the water tank while designing a solar heat water system.

The total energy consumption by the solar water heating system is determined using Eq. 1

$$Q_z = \sum_{i=1}^{n} m_{zi}\rho_{\omega}C_{\omega}(t_{dzi} - t_{bzi})\Delta T_{zi} \times 10^{-6} \quad (1)$$

where, Q_z is the total energy consumption of the solar water heating system in MJ; n is the total number of records; mzi is the hot water flow rate recorded in *i*th test in m^3/s; ρw is the density of hot water in kg/m^3; c_w is the specific heat capacity of water in J/(kg,K); t_{dzi} is the hot water temperature recorded in *i*th test in C; t_{bzi} is the cold water temperature

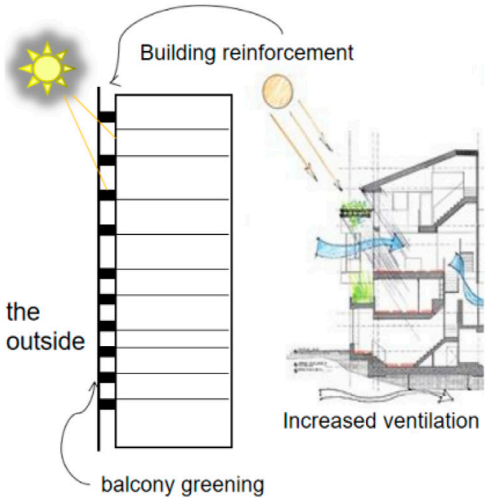

FIGURE 1
Concept design photovoltaics integration with vertical green balconies in high-rise building.

recorded in *i*th test in C; ΔT_{zi} is the time step in s, in this case, ΔT_{zi} = 10 s.

The total heat gain of solar collectors is expressed in Eq. 2.

$$Q_S = \sum_{i=1}^{n} m_{si}\rho_{s\omega}C_{s\omega}(t_{dsi} - t_{bsi})\Delta T_{si} \times 10^{-6} \quad (2)$$

where Q_s is the total heat gain of solar collectors in MJ; msi is the working fluid flow rate in the heat collection system recorded in *i*th test in m^3/s; ρsw is the density of collector fluid in kg/m^3; csw is the specific heat capacity of a collector fluid in J/(kg,K); tdsi is the collector fluid temperature at the outlet recorded in *i*th test in C; t_{bsi} is the collector fluid temperature at the inlet recorded in *i*th test in C; ΔT_{si} is the time step in s, in this case, ΔT_{si} = 10 s.

The solar fraction is expressed in Eq. 3.

$$f_j = \frac{Q_s}{Q_z} \quad (3)$$

where *fj* is solar fraction measured during short-term testing with certain Sun radiation circumstances, in %.

2.2 Solar photovoltaic collector installation designs

More of the urban buildings are multi-story buildings, whereas the roof heat collection area of urban buildings is generally regarded as sufficient to respond to the needs of the photovoltaic solar hot water systems. Therefore, currently, rooftop installations are the major form of photovoltaic board installation. On the other hand, in actuality, the building area is large, but the roof area is insufficient to meet the total heat demand of the building. To address the issue of insufficient heat collection area, balconies, walls between windows, and other parts of the east, south, and west building facades can be used. This study is aimed to transform the facade of high-rise buildings to achieve the best possible performance.

TABLE 3 Ecological area ratio.

Distinguish	Ecological area ratio	Increase value
Level 1	Ecological area ratio above 50%	1.0
Level 2	Ecological area ratio within 40%–50%	0.75
Level 3	Ecological area ratio within 25%–30%	0.5
Level 4	Ecological area ratio within 25%–30%	0.25

The quantitative evaluation of ecological function (natural circulation function) can improve the quality level of the target area environment by improving soil function, regulating microclimate and air quality, improving water circulation function, improving animal and plant habitat function, and leading to fundamentally solving urban ecological problems.

The ecological area ratio is given by Eq. 4 and levels are given in Table 3.

$$\text{Ecological area ratio} = \frac{\text{Natural circulation function area}}{\text{Overall floor area}} = \frac{\Sigma(\text{Space type area} \times \text{Weighted value})}{\text{Overall floor area}} \quad (4)$$

2.2.1 Facial installation method

In high-rise buildings, even if the entire roof is used, the problem of insufficient thermal collection area cannot always be solved. Therefore, the facade installation form can be adopted. The facade should be installed to receive as much sunlight as possible to avoid blocking, and safety should be prioritized. A balcony should be set up for older high-rise buildings and outdoor space for photovoltaic boards using thermal imaging analysis. In terms of integration with architecture, the heat collector can be combined with the building shading, and it should serve as shading and heat collector, simultaneously; for this purpose, arrange space can be arranged collector can be directly used as a balcony fence. Furthermore, the heat collector can be installed outside the air conditioner on the south side to serve the purpose of blocking the air conditioner. In Table 4, the business characteristics and local conditions that are a part of three-dimensional city greening plan are given.

2.2.2 Location of the balcony position and photovoltaic board

The exterior wall photovoltaic panel can be mounted directly from the building wall or on the walls of the construction to the south, west, southwest and east of the building. By reserving the tube and a heat collector on the wall, the water storage tank can be fixed to the wall, and the pipeline can be connected. The advantages of this scheme are as follows: i) the installation position of the heat collector is relatively flexible, and the size can be tailored according to the actual situation of the project; ii) the same layer can be used. Further, the pipeline gets shorter, and the heat loss becomes minimal. Also, the installation and maintenance are convenient; iii) a modeling element of architecture can be created when tightly combined with architecture. To achieve the ideal fusion of functionality and aesthetics, different color collecting pipes can be used to create heat collector arrays that have strong rhythmic senses based on the requirements of architectural shapes. The disadvantage of the exterior wall type is

TABLE 4 The three-dimensional city greening plan standards.

	Lowest standard	Proposed standard
Greening rate of artificial ground (Artificially caused green ratio within the foundation area)	About 30%	About 40%

that it is typically installed perpendicular to the ground and vertical to the wall surface. The efficiency of the thermal collection is consequently somewhat diminished. The underlying residents might also not be able to use it for other reasons. Therefore, installing solar heat collectors can be thought of as a courteous inclination in order to receive a lot of solar radiation. The association of the two types of window walls could be as follows: i) to fix the heat collector, the triangular frame is directly installed on the lower wall of the window. It is critical to note that it should be used as an oblique tilt collector to avoid obstruction for lower-level users; ii) to rectify the fixed heat collector, the triangle is installed directly on the window's wall, and used as an oblique tilt collector to avoid obstruction for lower-level users.

3 Results analysis and discussion

3.1 Thermal analysis of the building

It is an established fact that the heat island effect in cities worldwide is becoming increasingly severe, and heat energy in cities is disrupting human development activities. Basically, the heat energy was efficiently utilized by setting photovoltaic panels in the direction of concentrated heat energy and the facade of buildings to achieve the integration of solar energy systems and buildings can be expressed using Eq. 5.

$$\frac{U_z}{U_0} = \frac{Z^M}{Z_0} \tag{5}$$

where U_z is the horizontal direction wind speed at the height Z; U_o is the wind speed at the height of Z_o; M is the power index determined by the terrain roughness. Referring to the "Code for the load of the Architecture" (GB50009), the M-value was adopted to be .14 in this study.

The airflow around the building generally belongs to non-compressed low-speed turbulence as per the association assumptions. Owing to this, the contact formation restrictions of the airflow and the building have a beneficial effect. In general, the K model has minimal computation requirements and more accurate predictions.

Turbulent kinetic energy model given in Eq. 6.

$$\frac{\partial k}{\partial t} + u_j \frac{\partial k}{\partial x_j} = \frac{\partial}{\partial x_j}\left(\frac{v_t}{\ell_k}\frac{\partial k}{\partial x_j}\right) + P_k + G_k - \varepsilon \tag{6}$$

Dissipation rate model given in Eq. 7.

$$\frac{\partial \varepsilon}{\partial t} + u_j \frac{\partial \varepsilon}{\partial x_j} = \frac{\partial}{\partial x_j}\left(\frac{v_t}{\delta_\varepsilon}\frac{\partial \varepsilon}{\partial x_j}\right) + \frac{\varepsilon}{k}\left(C_1 P_k + C_3 C_k + C_2 \varepsilon\right) \tag{7}$$

For thermal analysis results, simulation on the outside natural ventilation of the buildings is conducted for a municipality first using PHOENICS software (PHOENICS, 2021). Figure 2A shows the simulated profile of the municipality. Figure 2B shows the profile of selected area for the computation reflected by the area's ventilation and heat energy. The outer field size of the model was chosen in PHOENICS software based on airflow at the building complex's boundary. The positive direction of the model was set to the north along the *y*-axis based on relevant engineering experience and simulation trial calculation.

3.2 Wind boundaries and wind speed

The non-compressed low-speed turbulence describes the airflow around the building according to the associated assumptions. Because of this, the airflow and building contact formation constraints are helpful. The K model generally requires less processing and produces more precise predictions. Figure 3 explains the wind boundaries and speed for the designed system.

3.3 Understanding the design efficiency by surface model

The following are essential steps to achieve the efficient integrated design of the solar heat water system and building: i) steel structure is set up on the outer facade of the original building to reinforce the building; ii) window is constructed between the floors and balcony space is created to facilitate the management of green plants, improve the ventilation of the building and reduce energy consumption; iii) a curved surface optical board device is set outside the balcony, which is convenient and easy to disassemble and maintain. The analysis shows that a curved surface is more conducive to alleviating urban wind pressure and protecting the buildings in comparison to a square surface, see Figures 4A, B. Further, for the aesthetic purpose, the outer balcony could be set up in a curved shape.

3.4 Annual energy savings potential

It is observed that the designed system can hold a total of 32 tons of hot water per day with a specific heat capacity of 5082880kj/per day. The conversion efficiency of electric heating is generally about 90%, and the total heat required to produce the same heat is Q = 5647644 kJ. While electrical energy used is 3,600 kJ and it needs 1568.7 kWh electricity/day. Table 5 shows the annual energy savings per solar photovoltaic collector technology.

3.5 Thermal efficiency

To illustrate how the thermal efficiency of a solar energy system was calculated, a centralized solar heat collection system with a circulating water pump was considered. Typically, under solar radiation, a solar heat collection system raises the temperature of hot water from its initial temperature to a preset level. In the solar heat collection system, only the water pump that circulates water uses electricity; no other equipment does. Using this system as an example, the circulating water pump's rated input power was estimated to be around .265 kW. It took .128 h and consumed .034 degrees of

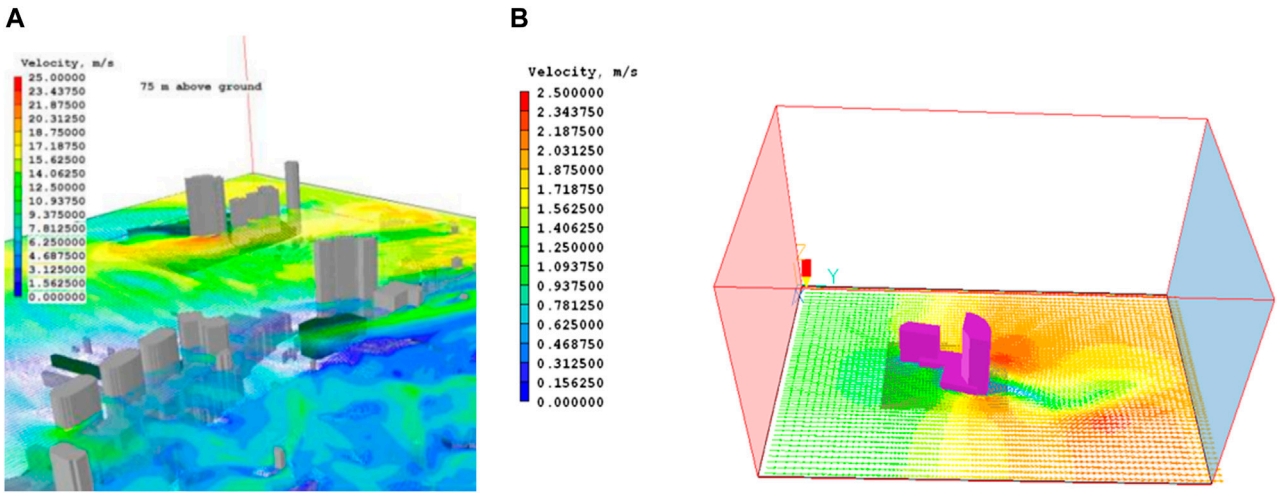

FIGURE 2
The thermal analysis of the buildings **(A).** Municipality with multiple buildings; **(B).** Selected areas with lower number of buildings.

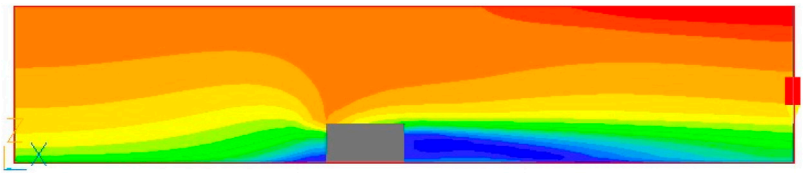

FIGURE 3
Building wind speed simulation diagram.

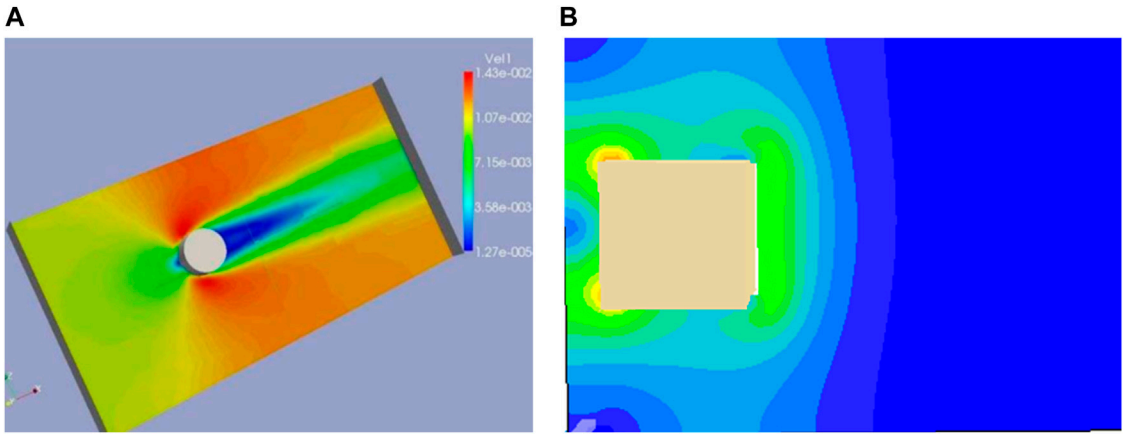

FIGURE 4
Surface model manifested by **(A).** Wind pressure; **(B).** Square model manifested.

electricity to circulate 1000 kg of water having 35° higher temperature. Therefore, the actual calorific value of the centralized solar heat collection system equipped with a circulating water pump is 1,029,411.76 kCal/degrees.

3.6 Wind load standard value detection

When there is no malfunction or damage from repeated pressure detection, the universal value of the wind load should be performed.

TABLE 5 Comparison of annual energy savings of photovoltaic systems.

System type		Festival energy/kW ha −1	Energy per unit area/kW h(m2 •a) −1
Solar photovoltaic system	Crystalline silicon	24,288.7	332.7
	Thin film	9715.3	133.1

Detection pressure increased by p_3', decreased to zero, then increased by p_3', again, and finally decreased to zero.′ When the first and last turns were made, the test parts were opened and closed at forward and negative pressure, respectively. Speed of lift and pressure was 300 p_a/s~500 p_a/s, and the pressure duration was not less than 3 s. The damage to the test element was noted.

3.6.1 Wind load design value detection

p_{max}' detection should be performed when the p_3' test does not become functionally disordered, and the angle displacement value does not exceed the allowable deflection. Detection pressure rose to p_{max}' (take $p_{max}' = 1.4\, p_3'$), then dropped to zero and to $-p_{max}'$, and then rose to zero in the end, with pressure duration not less than 3 s. The damage or dysfunction of the test piece was observed and noted.

3.6.2 Evaluation of the test results

The border support triangular glass surface plate method was calculated using Eq. 8

$$f_{max} = (d - d_0)\frac{(a - a_0) + (b - b_0) + c - c_0)}{3} \quad (8)$$

Where, f_{max} is the facial line deflection, mm; a_0, b_0, co, and d_o are the stable initial readings of each measuring point after preparing pressure, mm; b, c, and d are the readings of each measuring point at a certain level of detection, mm.

Other component face line deflection computation can be done using Eq. 9:

$$f_{max} = (b - b_0)\frac{(a - a_0) + c - c_0)}{3} \quad (9)$$

Where f_{max} is the facial line deflection, mm; a_0, b_0, co, and d_o are the stable initial readings of each measuring point after preparing pressure, mm; b, c, and d are the readings of each measuring point at a certain level of detection, mm.

3.6.3 Evaluation of deformed detection

The evaluation of the deformation detection should indicate the deflection of the opposite face line $f_0/2.5$ with a pressure difference of $\pm p_1$. The standard specimen used for wind load standard value detection is shown in Figure 5. According to Figure 5, the standard specimen has a thickness of 3.0 mm and .3 mm. The surface of the stainless-steel plate used for the balcony is processed to respond to leveling off, and cannot wait for scratches and burrs. The distance between the standard specimen's edge and the air vent's center is 100 + 1 mm. The air vent's diameter is 20 + .02 mm, and it needs to be neatly organized.

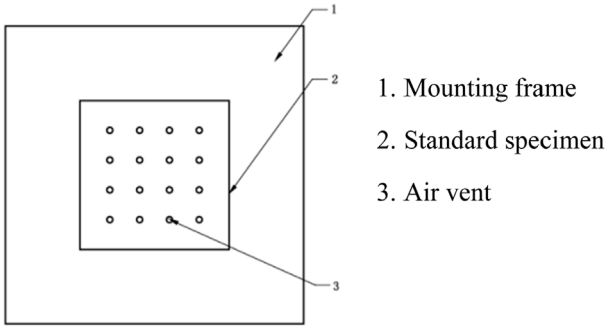

FIGURE 5
Standard specimen used for wind load standard value detection.

4 Discussion on functional benefits and conclusion

From the preliminary assessment carried out in this study, it is understood that façade reconstruction for integrating solar photovoltaic collectors with vertical green balconies is possible. The design and analysis, shows they could potentially offer two important functional benefits: 1). Ecological functions: Using their inherent ecological abilities, plants can purify indoor air, regulate temperature and humidity indoors, inhale carbon dioxide and exhale oxygen, maintain a balance of the two gases in the atmosphere, and keep the air fresh. They can also trap and filter airborne dust to clean the air. 2). Spatial function: By placing the balcony on the building's facade, it is important to organize, embellish, and beautify the interior space. However, in order to achieve the transition of indoor and outdoor space, the green color can be set up in the area where outdoor and indoor spaces meet. The technique of borrowing scenery, through the glass and through the window can also be used so that the inside and outside green scenery is connected into a single piece.

The scientific analysis of building construction could be carried out using the PHOENICS software model about the existing high-rise building facade, steel reinforcement of older buildings, installation of solar energy combined with balconies, installation of photovoltaic panels set out on the steel frame, and solution to the shortage of urban greening and internal user comfort. It also reduces construction costs and encourages the construction of green buildings, in addition to reducing air pollution. The plan discussed in this study contributes to the delivery of services that satisfy customers, the elimination of temporary conditions, the reduction of construction-related annoyance for locals, the opportunity for building owners to receive early rental income, and the creation of a comfortable workplace. Future renovations of urban architecture are predicted to apply the process-specific rationalization plan that was created as a consequence of this study, and numerous experiences will be gathered from this that will be used to carry out more type-specific research.

Data availability statement

The original contributions presented in the study are included in the article/supplementary material further inquiries can be directed to the corresponding author.

Author contributions

ZW is responsible for Conceptualization, Data Curation, Formal Analysis, Funding Acquisition, Investigation, Methodology, Project Administration, Resources, Software, Supervision, Visualization, and Writing. KC-S, as the corresponding author, is responsible for all communication related to the paper, regularly checks the progress of further studies, makes sure the IMRAD section of the manuscript meets the requirement both in content and format before submission, including Introduction, Research Methods, Results, Discussion, and Conclusions, uploads the paper to the relevant database as required, deal with all relevant procedures, and promotes the whole process.

Conflict of interest

The authors declare that the research was conducted in the absence of any commercial or financial relationships that could be construed as a potential conflict of interest.

Publisher's note

All claims expressed in this article are solely those of the authors and do not necessarily represent those of their affiliated organizations, or those of the publisher, the editors and the reviewers. Any product that may be evaluated in this article, or claim that may be made by its manufacturer, is not guaranteed or endorsed by the publisher.

References

Akram, M. W., Hasannuzaman, M., Cuce, E., and Cuce, P. M. (2021). Global technological advancement and challenges of glazed window, facade system and vertical greenery-based energy savings in buildings: A comprehensive review. *Energy Built Environ.* 4, 206–226. doi:10.1016/j.enbenv.2021.11.003

Bonomo, P., Chatzipanagi, A., and Frontini, F. (2015). Overview and analysis of current BIPV products: New criteria for supporting the technological transfer in the building sector. *Vitr. Int. J. Archit. Technol. Sustain.* 2015, 67–85. doi:10.4995/vitruvio-ijats.2015.4476

Cerón, I., Caamaño-Martín, E., and Neila, F. J. (2013). 'State-of-the-art' of building integrated photovoltaic products. *Renew. Energy* 58, 127–133. doi:10.1016/j.renene.2013.02.013

Dunnett, N., and Kingsbury, N. (2008). *Planting green roofs and living walls*. Portland, OR, USA: Timber Press.

Ekici, B. B., and Aksoy, U. T. (2009). Prediction of building energy consumption by using artificial neural networks. *Adv. Eng. Softw.* 40 (5), 356–362. doi:10.1016/j.advengsoft.2008.05.003

Goh, K. C., Goh, H. H., Yap, A. B. K., Masrom, M. A. N., and Mohamed, S. (2017). Barriers and drivers of Malaysian BIPV application: Perspective of developers. *Procedia Eng.* 180, 1585–1595. doi:10.1016/j.proeng.2017.04.321

Heinstein, P., Ballif, C., and Perret-Aebi, L. E. (2013). Building integrated photovoltaics (BIPV): Review, potentials, barriers and myths. *Green* 3, 125–156. doi:10.1515/green-2013-0020

Hollands, J., and Korjenic, A. (2021). Evaluation and planning decision on facade greening made easy—Integration in BIM and implementation of an automated design process. *Sustainability* 13 (16), 9387. doi:10.3390/su13169387

IEA (2021). Empowering "Smart Cities" toward net zero emissions. AvaliableAt: https://www.iea.org/news/empowering-smart-cities-toward-net-zero-emissions.

Jelle, B. P., Breivik, C., and Røkenes, H. D. (2012). Building integrated photovoltaic products: A state-of-the-art review and future research opportunities. *Sol. Energy Mat. Sol. Cells* 100, 69–96. doi:10.1016/j.solmat.2011.12.016

Jelle, B. P., and Breivik, C. (2012). The path to the building integrated photovoltaics of tomorrow. *Energy Procedia* 20, 78–87. doi:10.1016/j.egypro.2012.03.010

Liu, O. Y., and Russo, A. (2021). Assessing the contribution of urban green spaces in green infrastructure strategy planning for urban ecosystem conditions and services. *Sustain. Cities Soc.* 68, 102772. doi:10.1016/j.scs.2021.102772

Montoro, D. F., Vanbuggenhout, P., and Ciesielska, J. (2011). "Building Integrated Photovoltaics: An overview of the existing products and their fields of application," in *Report prepared in the framework of the European funded project* (Saskatoon, Canada: BIPV).

Munari Probst, M. C., Roecker, C., Frontini, F., Scognamiglio, A., Farkas, K., Maturi, L., et al. (2013). "Solar energy systems in architecture-integration criteria and guidelines," in *International energy agency solar heating and cooling programme*. Editors M. Probst, M. Cristina, and C. Roecker (Paris, France: International Energy Agency).

Nagy, Z., Svetozarevic, B., Jayathissa, P., Begle, M., Hofer, J., Lydon, G., et al. (2016). The adaptive solar facade: From concept to prototypes. *Front. Archit. Res.* 5, 143–156. doi:10.1016/j.foar.2016.03.002

PHOENICS (2021). Software. AvaliableAt: https://www.britannica.com.

Piselli, C., Castaldo, V., Pigliautile, I., Pisello, A., and Cotana, F. (2018). Outdoor comfort conditions in urban areas: On citizens' perspective about microclimate mitigation of urban transit areas. *Sustain. Cities Soc.* 39, 16–36. doi:10.1016/j.scs.2018.02.004

Prieto, A., Knaack, U., Auer, T., and Klein, T. (2017). Solar façades-Main barriers for widespread façade integration of solar technologies. *J. Façade Des. Eng.* 5, 51–62. https://sdgresources.relx.com/articles/urban-planning-sustainability-framework-systems-approach-blue-green-urban-design

Puchol-Salort, P., O'Keeffe, J., van Reeuwijk, M., and Mijic, A. (2020). An urban planning sustainability frame work: Systems approach to blue green urban design. *Sustain. Cities Soc.* 66, 102677.

Ritzen, M., Reijenga, T., El Gammal, A., Warneryd, M., Sprenger, W., Rose-Wilson, H., et al. (2016). "IEA-PVPS task 15: Enabling framework for BIPV acceleration. (IEA-PVPS)," in *Proceedings of the 48th IEA PVPS executive commitee meeting* (Vienna, Austria: IEA).

Scognamiglio, A., Farkas, K., Frontini, F., and Maturi, L. (2012). "Architectural quality and photovoltaic products," in *Proceedings of the 27th European photovoltaic solar energy conference and exhibition* (Frankfurt, Germany: EUPVSEC), 24–28.

Shi, J., Su, W., Zhu, M., Chen, H., Pan, Y., Wan, S., et al. (2013). Solar water heating system integrated design in high-rise apartment in China. *Energy Build.* 58, 19–26. doi:10.1016/j.enbuild.2012.10.018

Shih, W. Y., Ahmad, S., Chen, Y. C., Lin, T. P., and Mabon, L. (2019). Spatial relationship between land development pattern and intra-urban thermal variations in Taipei. *Sustain. Cities Soc.* 62, 102415. doi:10.1016/j.scs.2020.102415

Shukla, A. K., Sudhakar, K., and Baredar, P. (2016). A comprehensive review on design of building integrated photovoltaic system. *Energy Build.* 128, 99–110. doi:10.1016/j.enbuild.2016.06.077

Tabakovic, M., Fechner, H., Van Sark, W., Louwen, A., Georghiou, G., Makrides, G., et al. (2017). Status and outlook for building integrated photovoltaics (BIPV) in relation to educational needs in the BIPV sector. *Energy Procedia* 111, 993–999. doi:10.1016/j.egypro.2017.03.262

Wei, X., Ruicheng, Z., and Bin, L. (2010). *China Solar PV Industry Research Report*. Doudin.com 2010, 12–27. https://www.docin.com/p-111802404.html

Xue, F., Gou, Z., and Lau, S. S. Y. (2017). Green open space in high-dense Asian cities: Site configurations, microclimates and users' perceptions. *Sustain. Cities Soc.* 34, 114–125. doi:10.1016/j.scs.2017.06.014

Yang, R. J., and Zou, P. X. (2016). Building integrated photovoltaics (BIPV): Costs, benefits, risks, barriers and improvement strategy. *Int. J. Constr. Manag.* 16, 39–53. doi:10.1080/15623599.2015.1117709

Yu, Z., Chen, S., Wong, N. H., Ignatius, M., Deng, J., He, Y., et al. (2020). Dependence between urban morphology and outdoor air temperature: A tropical campus study using random forests algorithm. *Sustain. Cities Soc.* 61, 102200. doi:10.1016/j.scs.2020.102200

Zhai, X. Q., Wang, R. Z., Dai, Y. J., Wu, J. Y., Xu, Y. X., and Ma, Q. (2007). Solar integrated energy system for a green building. *Energy Build.* 39, 985–993. doi:10.1016/j.enbuild.2006.11.010

frontiers | Frontiers in Energy Research

REVIEW
published: 31 May 2022
doi: 10.3389/fenrg.2022.893475

Hydrogen Energy as Future of Sustainable Mobility

Suprava Chakraborty[1], Santanu Kumar Dash[1], Rajvikram Madurai Elavarasan[2]*, Arshdeep Kaur[3,4], Devaraj Elangovan[1]*, Sheikh Tanzim Meraj[5], Padmanathan Kasinathan[6] and Zafar Said[7,8]*

[1]TIFAC-CORE, Vellore Institute of Technology, Vellore, India, [2]Department of Electrical and Electronics Engineering, Thiagarajar College of Engineering, Madurai, India, [3]CPS Technologies, Brisbane, QLD, Australia, [4]Steering Committee (Hydrogen Society of Australia), Perth, WA, Australia, [5]Department of Electrical and Electronic Engineering, Universiti Teknologi PETRONAS, Seri Iskandar, Malaysia, [6]Department of Electrical and Electronics Engineering, Agni College of Technology, Chennai, India, [7]Sustainable and Renewable Energy Engineering Department, University of Sharjah, Sharjah, United Arab Emirates, [8]Research Institute for Sciences and Engineering, University of Sharjah, Sharjah, United Arab Emirates

Conventional fuels for vehicular applications generate hazardous pollutants which have an adverse effect on the environment. Therefore, there is a high demand to shift towards environment-friendly vehicles for the present mobility sector. This paper highlights sustainable mobility and specifically sustainable transportation as a solution to reduce GHG emissions. Thus, hydrogen fuel-based vehicular technologies have started blooming and have gained significance following the zero-emission policy, focusing on various types of sustainable motilities and their limitations. Serving an incredible deliverance of energy by hydrogen fuel combustion engines, hydrogen can revolution various transportation sectors. In this study, the aspects of hydrogen as a fuel for sustainable mobility sectors have been investigated. In order to reduce the GHG (Green House Gas) emission from fossil fuel vehicles, researchers have paid their focus for research and development on hydrogen fuel vehicles and proton exchange fuel cells. Also, its development and progress in all mobility sectors in various countries have been scrutinized to measure the feasibility of sustainable mobility as a future. This, paper is an inclusive review of hydrogen-based mobility in various sectors of transportation, in particular fuel cell cars, that provides information on various technologies adapted with time to add more towards perfection. When compared to electric vehicles with a 200-mile range, fuel cell cars have a lower driving cost in all of the 2035 and 2050 scenarios. To stimulate the use of hydrogen as a passenger automobile fuel, the cost of a hydrogen fuel cell vehicle (FCV) must be brought down to at least the same level as an electric vehicle. Compared to gasoline cars, fuel cell vehicles use 43% less energy and generate 40% less CO_2.

Keywords: climate change, sustainable mobility, hydrogen mobility, hydrogen fuel, GHG

OPEN ACCESS

Edited by:
Subrata Hait,
Indian Institute of Technology Patna, India

Reviewed by:
Muhammad Aziz,
The University of Tokyo, Japan
Sushant Kumar,
Indian Institute of Technology Patna, India

****Correspondence:***
Suprava Chakraborty
suprava@ee.ism.ac.in
Rajvikram Madurai Elavarasan
rajvikram787@gmail.com
Devaraj Elangovan
elangovan.devaraj@vit.ac.in

Specialty section:
This article was submitted to Sustainable Energy Systems and Policies, a section of the journal Frontiers in Energy Research

Received: *10 March 2022*
Accepted: *19 April 2022*
Published: *31 May 2022*

Citation:
Chakraborty S, Dash SK, Elavarasan RM, Kaur A, Elangovan D, Meraj ST, Kasinathan P and Said Z (2022) Hydrogen Energy as Future of Sustainable Mobility. Front. Energy Res. 10:893475. doi: 10.3389/fenrg.2022.893475

1 INTRODUCTION

Sustainable mobility is described as a transportation system that is ubiquitous, effective, clean, and ecologically beneficial. Whilst transportation is not having its own sustainable development goals (SDGs), it is critical for accomplishing other SDGs in order to reach desired growth and development. Top-scoring countries for the SDGs have more robust and long-term mobility

policies in place, whilst countries with the lowest scores are chastised for having inadequate transportation infrastructure (Sum4all.org, 2021). **Figure 1** depicts the SDGs that are directly or indirectly met by sustainable transportation.

The origin of "sustainable mobility" is from the broader definition of "Sustainable development". "Sustainable development" is "development that meets current needs without jeopardizing the ability of future generations to meet their own needs" (World Commission on Environment and Development, 1987). The infographic (**Figure 2**) depicts the broad benefits of sustainable mobility (Ransformative-Mobility, 2021), which include energy security, economic development, environmental sustainability, and social wellbeing.

The literature has a number of researches on sustainable mobility. The scope of technology in fostering a change in behaviour toward sustainable transportation has been investigated (Klecha and Gianni, 2018; Chng, 2021). Gonzales Green port strategies for reducing negative externalities in the countryside has been investigated (Gonzalez Aregall et al., 2018). **Table 1** lists the results of several studies on sustainable mobility.

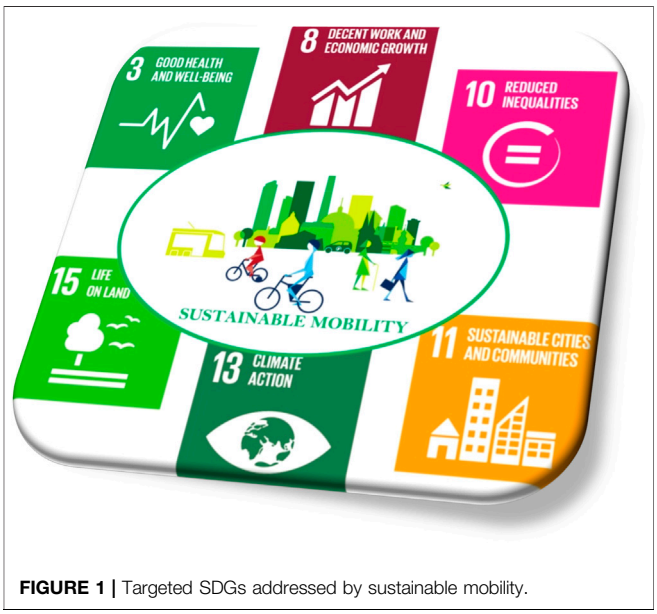

FIGURE 1 | Targeted SDGs addressed by sustainable mobility.

1.1 Hydrogen: The Most Reliable Form of Energy

The global need for energy has risen intensely with the growth of the world's population. This is because energy is required for all activities. The great majority of energy is imitative from fossil fuels, which are non-renewable resources that take longer to recharge or reoccurrence to their previous capacity. Energy imitative from fossil fuels is less costly; however, it has shortcomings when compared to renewable energy sources (Rohith et al., 2016).

Hydrogen is an emerging and almost established fuel source for cars (Apostolou and Xydis, 2019; Staffell et al., 2019; Falcone et al., 2021). The present state of the art and future possibilities of the burgeoning hydrogen-based market in road transportation, as well as an examination of existing hydrogen refuelling station technologies, have been explored (Apostolou and Xydis, 2019). The hydrogen economy offers a multi-sectoral view of low-cost clean energy and thorough decarbonization in process sectors. The ability to store hydrogen or derivatives is a game changer for the integration of high renewable energy source shares, resulting in beneficial effects on various SDGs through lower GHG and air pollution emissions (Falcone et al., 2021). Along with biofuels and electric cars, hydrogen is one of three key low-carbon transportation choices (EVs). Hydrogen avoids the negative effects of biofuels on land usage and air pollution, as well as the restricted range and long recharge periods associated with electric vehicles (Staffell et al., 2019). Hydrogen automobiles have been shown to have a threefold lower potential for global warming than other alternative technologies (Bicer and Dincer, 2017; Dincer, 2020; Apostolou and Welcher, 2021). In Denmark, variables that may influence public acceptability of hydrogen-powered cars have been explored. To that purpose, four primary hypotheses were proposed, assuming that variables such as technical and environmental knowledge, financial standing, and infrastructure have a direct impact on the societal acceptability of hydrogen-powered private road cars in the transportation sector. Most of the hypotheses, such as environmental awareness, limited refuelling infrastructure, and media backing for this sector, were supported by the findings (Apostolou and Welcher, 2021). To explore the effects of alternative cars on the environment and human health, a life cycle evaluation of methanol, hydrogen, and electric vehicles is done. The findings of this study demonstrate that owing to the manufacturing and maintenance phases, electric cars have higher human toxicity ratings. Because hydrogen has a higher energy density than methanol, hydrogen-powered cars are a more environmental sustainable alternative in terms of global warming and ozone layer depletion (Bicer and Dincer, 2017). The Covid-19 coronavirus has made it more important than ever for people to breathe cleaner air, drink cleaner water, eat cleaner food, and use cleaner energy. We were in a carbon age with hydrocarbon fuels until the coronavirus outbreak juncture in 2020, and now we must continue to change the driver to hydrogen, which is the start of the hydrogen age, in which the use of hydrocarbon fuels (fossil fuels) will decrease exponentially while the use of hydrogen energy will increase (Dincer, 2020). The Covid-19 has thrown the transition from the carbon (C) age to the emerging hydrogen (H_2) age into disarray (Apostolou et al., 2018).

As a result, renewable resources, particularly hydrogen energy, are the most promising choices for meeting energy demands. Hydrogen is found mainly in plant materials and is rare in nature. Hydrogen is a non-metallic, nontoxic fuel that can provide more energy per unit of mass than gasoline (Abdalla et al., 2018). However, a substantial study is required to investigate and design onboard applications in order to use hydrogen as a fuel.

FIGURE 2 | Benefits of sustainable mobility.

Hydrogen has lately emerged as a prospective energy carrier, and the organic chemical hydride approach offers significant advantages in terms of transportability and handling (Morel et al., 2015). The possibilities for combining stochastic power generation with hydrogen production, storage, and consumption is explained in (Korpas and Gjengedal, 2006).

1.2 Hydrogen as a Fuel in the Transportation Sector

"Centralized" production, where hydrogen is produced on a large scale and supplied to customers via truck or pipeline. "On-site" or "distributed" production, is where hydrogen is produced at the end-use site, generally through small-scale electrolysis or steam methane reforming (Meraj et al., 2020).

Hydrogen can also be converted to other energy carriers like electricity, methane, or liquid fuels, which incurs conversion costs and efficiency losses but allows access to existing energy distribution networks without requiring the construction of an extensive hydrogen distribution infrastructure. The relative cost of regional basic resources for hydrogen generation and policies is vital in determining the ideal hydrogen supply pathway. Transportation of hydrogen can be done using.

1) Pipelines (Weinmann, 1999).
2) Mobile by trucks, trains, vessels (Domashenko, 2002).

TABLE 1 | Investigating research on sustainable mobility.

Cited reference	Year of publication	Investigated on
Ren et al. (2019)	2020	Green and sustainable logistics
Kumar and Alok, (2020)	2020	Prospects for sustainability
López et al. (2019)	2019	The impact of technological advances in bus transportation on environmental and social sustainability
Tirachini, (2020)	2019	Travel behaviour and sustainable mobility
Holden et al. (2019)	2019	Aspects of sustainable mobility in 2030
Martínez-Díaz et al. (2019)	2019	Future of autonomous driving
Letnik et al. (2018)	2018	Sustainable and energy-efficient urban transportation policies and initiatives
Ranieri et al. (2018)	2018	Logistics innovations in cost reduction vision
Taiebat et al. (2018)	2018	Automated vehicles' energy, environmental, and sustainability consequences
(Ferrero et al., 2018; Santos, 2018)	2018	Shared mobility
Biresselioglu et al. (2018)	2018	Electric mobility
Pojani and Stead, (2018)	2018	Policy design for sustainable urban transport

The use of hydrogen in onboard vehicles has hurdles owing to the high weight, volume, and cost of hydrogen. Furthermore, as the refuelling process continues, the life cycle of hydrides shortens, reducing the vehicles' efficiency. Another disadvantage is the lack of adequate hydrogen storage system standards and protocols. The infrastructure to distribute hydrogen to the user requires entirely new infrastructure; the production and delivery systems must be integrated to reduce the cost of hydrogen delivery and distribution costs. At the moment, hydrogen transportation, storage, and delivery to the site of consumption are all related with inefficient energy use. Despite having some notable disadvantages, hydrogen is heavily used in several industries such as the transportation industry, power generation industry, and building industry instead of conventional fossil fuels (Reddy et al., 2020).

This paper aims to present the future of hydrogen energy as a solution to sustainable mobility. Existing literatures are mainly focusing on utilization of hydrogen for a particular sector of transportation; the overall transportation sector is not addressed. In detail analysis of techno-economic-environmental aspects of Hydrogen as sustainable mobility solution is missing in recent literature. The goal of this research is to evaluate the potential of hydrogen energy as a solution for sustainable transportation and to analyse its environmental and social consequences. This review aims to introduce the preparation processes, storage method, and critical technical issues of its application in vehicles and related mobility sectors in a systematic manner, providing exciting insights into hydrogen-based energy, the potential large-scale deployment process on a global scale including techno-economic aspects, selected implemented projects, policies and challenges. The paper helps the policymakers and industries decide on choosing hydrogen as the future of sustainable mobility.

This paper is structured as follows. **Section 2** provides an in-depth review of hydrogen as a fuel for transportation in many sectors and its environmental and technical elements. **Section 3** deals with the generation and storage of hydrogen energy. **Section 4** concludes the in-depth analysis to suggest the scope of hydrogen to be adopted as the future of sustainable mobility.

2 ENVIRONMENTAL ASPECTS

Considering the fact of depletion of energy resources and the rise in global warming, challenges are encountered with the combustion of energy due to the transportation sector in the present time. Green House Gas (GHG) emissions are caused by the dominant conventional road transportations, which have existed for more than a century and has reached its upper saturation level. As per the International Energy Agency regulations, global carbon dioxide emissions must be decreased to limit the consequences of climate change (Zhao et al., 2020). To enhance the technology that has zero pollutant discharge and zero climate change effect, hydrogen Fuel cell-based vehicles production is being promoted by automotive industries. The government of various countries like the United States, Japan and South Korea have encouraged the production of Hydrogen vehicles since 2018 (Meng et al., 2021). The upcoming subsections discuss the environmental and technical aspects of hydrogen in the mobility sector and its scope.

Transportation is the second-largest source of pollution in terms of GHG emissions, posing a serious threat to human health (Roadmap to a Single European Transport Area-Towards a competitive and resource efficient transport system, 2021). The transportation sector accounts for 23% of total CO_2 emissions. According to the report, the transportation sector would continue to rely on petroleum-based services for 90% of its fleet, with renewable energy sources accounting for only 10%. By 2050, carbon emissions from the transportation industry are predicted to be 33% more than they were in 1990 (Le Quéré et al., 2020).

2.1 Climatic Change and Greenhouse Gas Emissions

Climate change is the central point of focus in the present era due to the advancement of technologies in various sectors, including the transportation industries. The combustion of biofuels for transportation has captured the mobility sector for the last two centuries. Traditional combustion fuels by vehicles lead to the generation of pollutants and GHGs to the environment, which has various adverse effects (Engel, 2012; Zhongfu et al., 2015). Hydrogen is a carrier, like electricity, rather than an energy source, and the notion of "hydricity," or the inherent interchangeability of electricity and hydrogen, has been established (Engel, 2012). Anthropogenic GHG emissions are directly linked to the global warming trend. Climate change caused by GHG emissions is one of the most serious environmental issues confronting modern society (Ding et al., 2018). In order to stabilize the climate, it is the need of the time to reduce the emissions significantly (Liu et al., 2019). CO_2 is the major GHG contributor with a value of 76%, methane, while Nitrous Oxide and fluorinated gases together contributes the rest 24% (Global-Greenhouse-Gas-Emissions-Data, 2021). As illustrated in **Figure 3**, the global CO_2 concentration is growing rapidly.

The concentration of CO_2 in the atmosphere is currently at 414.00 ppm, the highest in the previous 800 k years, and it is closely connected to global temperature. The world has committed to keeping global warming below 2°C, and this goal can be met with a minimal carbon budget. According to researchers, mankind can only emit 565 Gt of CO_2 more and still meet the 2°C target—a limit that would be exhausted in 15 years if emissions continue at their current rate of 36.6 Gt CO_2 per year (Liu et al., 2019). It is also predicted that seven million people die each year as a result of illnesses caused by air pollution (Global-Energy-Related-Co2-Emissions, 2021).

During COVID-19, there is a temporary decline in daily global CO_2 emissions due to forced confinement. By early April 2020, daily global CO_2 emissions had decreased by 17% compared to the mean levels in 2019, with surface traffic accounting for half of the decline (Saleem et al., 2021). However, in the post-COVID-19 scenario, things will be different. As a result, adopting a sustainable transportation strategy is critical.

Although GHGs are released by a variety of sources, those produced by automobiles can be reduced by employing

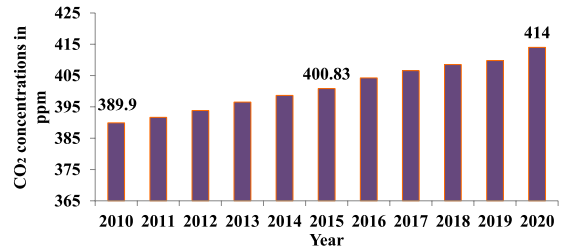

FIGURE 3 | Concentration of CO_2 in atmosphere in ppm (Climate-Change-Atmospheric-Carbon-Dioxide, 2021; Health-Topics, 2021)

alternative fuel vehicles (AFVs) or green vehicles. Advanced alternative fuel technologies have the potential to halve gasoline use while also cutting CO_2 emissions and their associated environmental consequences. Although fuel-efficient technologies help vehicles perform better in terms of environmental performance, they cannot assist cut overall emissions. This is ought to the fact that technology cannot change consumer habits on its own. So, framing a strategy that encourages consumers to choose energy-efficient vehicles over traditional one is critical, as is ensuring the use of AFVs that complies with environmental pollution-reduction measures like carpooling and using low-CO_2-emitting vehicles, public transportation, or bicycles to save fuel (Oliveira and Dias, 2020; García-Melero et al., 2021; Apostolou and Xydis, 2019).

2.2 Hydrogen as a Zero-Emission Source

Hydrogen energy follows a zero-emission policy towards the environment, making it a fundamental attraction for researchers and industries to study and develop hydrogen transport technologies. Additionally, hydrogen has become a truly sustainable energy resource because of the zero climate change effect, as hydrogen is a highly efficient, reliable, and soundless source of power.

The evaluation of hydrogen fuel transportation cannot be alone evaluated based upon the tailpipe gas emissions. The environmental aspects can be accounted for based on the vehicle's wheel to tank evaluation (Concawe and JRC, 2007; Yang and Ogden, 2007; Bethoux, 2020). Natural hydrogen may become a viable economic option, making fuel cell vehicles a viable and ecologically acceptable alternative to battery electric vehicles (Bethoux, 2020). The European Commission's Joint Research Centre, EUCAR, and CONCAWE have assessed the tank-to-wheels (TTW) energy usage and greenhouse gas emissions for a variety of future fuel and powertrain alternatives (Concawe and JRC, 2007). Moving our transportation sector away from petroleum-derived gasoline and diesel fuels and toward hydrogen derived from domestic primary energy resources can have a number of societal benefits, including lower well-to-wheels greenhouse gas emissions, zero point-of-use criteria air pollutant emissions, and less imported petroleum from politically sensitive areas (Yang and Ogden, 2007). Therefore, the accountability of hydrogen vehicles towards environmental effect has been studied and reported through one tool known as Ecoscore. The tool has been developed by the commission of the Flemish government (Sergeant. et al., 2009). This measurement is based upon the GHGs emissions, regulation of air quality and sound pollution. Apart from the three major aspects, two indirect aspects, including human lifecycle and ecosystem maintenance, are also included in the Ecoscore measurement scale (Van Mierlo et al., 2004). Environmental aspects of hydrogen vehicles are presented in **Figure 4**.

3 TECHNICAL ASPECTS

The study about hydrogen fuel vehicles has major issues related to high-pressure hydrogen storage. To tackle the problem of hydrogen storage, researchers have proposed the onboard hydrogen generation engines (Frenette and Forthoffer, 2009; Shusheng et al., 2020). The fuel cell electric vehicle is an onboard hydrogen-generation type in the design scheme that provides rapid hydrogen supply. Moreover, a self-heating reforming technology combining methanol vapour reforming and partial oxidation reforming being utilized (Özcan and Garip, 2020). The car is powered by a hybrid system that includes a lithium battery and a hydrogen fuel cell. The aforesaid approach is different from hydrogen storage fuel cell vehicles. It eliminates the hydrogenation process and the high-pressure hydrogen storage device, and drives the motor with the fuel cell as the primary power source, while the lithium battery as a backup. Based on the structure of the fuel cell electric vehicle designed in the literature (Li et al., 2016; Shusheng et al., 2020), the vehicle's critical components, such as a hydrogen production system, electric drive system, auxiliary power supply, and management system, were evaluated, and their management and control techniques were described.

3.1 Production of Hydrogen

Hydrogen may be produced using both renewable and fossil fuel technologies. Steam reforming, partial oxidation, auto thermal oxidation, and gasification are all methods for producing hydrogen from fossil fuels. By gasifying biomass/biofuels and

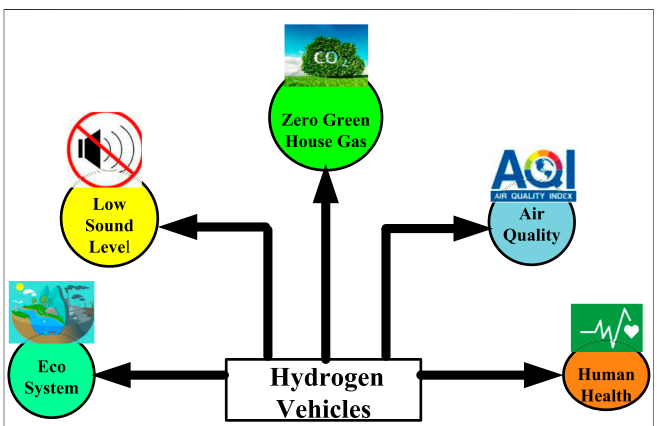

FIGURE 4 | Environmental aspect of hydrogen vehicle.

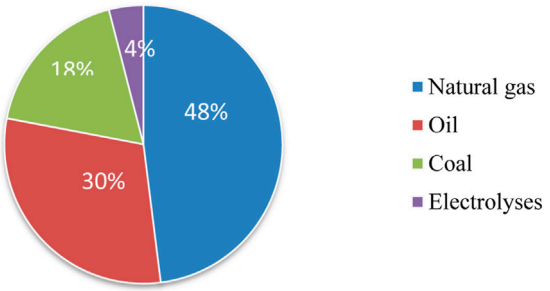

FIGURE 5 | Hydrogen production sources (Arat and Sürer, 2017)

splitting water with solar or wind energy, hydrogen can be synthesized from renewable energy sources (Apostolou, 2020). The Hydrogen production sources and technologies are shown in **Figure 5**.

The extraction of hydrogen from coal is the highest among all sources, approximately 21.5 billion tons/year, which need to be replaced by renewable resources.

3.1.1 Categorization of Hydrogen Based on the Source of Generation

By the adaptation of different technology and considered sources, hydrogen production has been categorized into three types according to the literature and study reports (von Döllen et al., 2021; Noussan et al., 2021). The utilization of major sources for the production of hydrogen has introduced the color conceptualization. By the application of fossil fuel for the generation of hydrogen leads to the emission of CO_2 and greenhouse gases. This technology of hydrogen production and its utilized source refers to grey hydrogen (Ivanenko, 2020). Blue hydrogen was introduced, while the grey hydrogen production approach was used to lower the quantity of greenhouse gas emissions in hydrogen production (Mari et al., 2016; Dickel, 2020). The utilization of fossil fuel, industrial gas, by-product gas, natural gas for hydrogen production for sustainable mobility as energy resources generally emit pollutants, and greenhouse gases to the environment (Jovan and Dolanc, 2020; Luo et al., 2020; Schiro et al., 2020). In a case study of a Slovenian hydro power plant, the possibility for green hydrogen generation was examined. If it is not burdened by different environmental fees, hydrogen can be competitive in the transportation sector (Jovan and Dolanc, 2020). Renewable hydrogen generation is a reliable alternative since this energy vector can be quickly created from electricity and injected into existing natural gas infrastructure, allowing for storage and transit (Schiro et al., 2020). The economic analysis of hydrogen was applied to hydrogen produced by natural gas, coal, and water electrolysis and conveyed in the form of high-pressure hydrogen gas or cryogenic liquid hydrogen. The cost of hydrogen produced from natural gas and coal is now cheaper, but it is heavily influenced by the cost of hydrogen purification and the price of carbon trading. Given the impact of future production technologies, raw material costs, and rising demands for sustainable energy development on hydrogen energy costs, it is suggested that renewable energy curtailment be used as a source of electricity and multi-stack system electrolyzers be used as large-scale electrolysis equipment, in combination with cryogenic liquid hydrogen transportation or on-site hydrogen production (Luo et al., 2020). To reduce these pollutants affecting the atmosphere, literature has reported various technological modifications for hydrogen generation. Therefore, the utilization of renewable energy resources for hydrogen generation has been reported in recent works of literature (Boretti, 2020; Manna et al., 2021; Rabiee et al., 2021). Green hydrogen is also resultants of electrolyzers produced by renewable energies. It has been also noticed that green hydrogen can be also produced from bioenergy such as biomethane and biomass combustion. As the green hydrogen generated from various methodologies has net-zero gas emission, researchers and industries have more attention towards its production advancement (Manna et al., 2021; Rabiee et al., 2021). Categories of Hydrogen generation is presented in **Figure 6**.

Hydrogen production from different sources and emission from it is tabulated in **Table 2**.

At present, coal is the primary source of hydrogen extraction, but the process emits GHGs. Hydrogen extraction through photocatalytic water decomposition with solar energy is the least popular process, with 1.8 billion tons of hydrogen annually. **Table 2**, concludes that the hydrogen production from photocatalytic water decomposition with solar energy is emission-free and the most sustainable path.

3.1.2 Water Electrolysis to Generate Hydrogen

Water as a feedstock is one of the most environmentally beneficial ways to produce hydrogen as it releases only oxygen as a by-product during processing. Green hydrogen is hydrogen produced by the breakdown of water using renewable energy sources. Electrolysis is currently the most established commercially accessible process for producing hydrogen from water. Water electrolysis is the process of breaking down water (H_2O) into its constituent's hydrogen (H_2) and oxygen (O_2) using electric current (Hydrogen-Production-Through-Electrolysis, 1927). Positive ions (H+) are drawn to the cathode, whereas negative ions (OH-) are drawn to the anode by the electric potential. Alkaline water electrolysis (AEL), proton exchange membrane (PEM) water electrolysis, solid oxide water electrolysis (SOE), and alkaline anion exchange membrane (AEM) water electrolysis are some of the water electrolysis procedures (Chi and Yu, 2018) as depicted in **Figure 7**.

Comparative analysis of different water electrolysis processes to generate hydrogen (Hydrogen-Production-By-Electrolysis-Ann-Cornell, 2017; Hydrogen-Production-Through-Electrolysis, 2017; Articlelanding, 2020) is tabulated in **Table 3**.

Use of AEM water electrolysis could allow low-cost transition metals to replace traditional noble metal electrocatalysts (Pt, Pd, Ru, and Ir). AEM electrolysis has garnered special interest due to its high power efficiency, membrane stability, durability, ease of handling, and low-cost hydrogen-production method (Vincent and Bessarabov, 2018), despite being a developing technology. Aside from the high energy consumption induced by the rise in

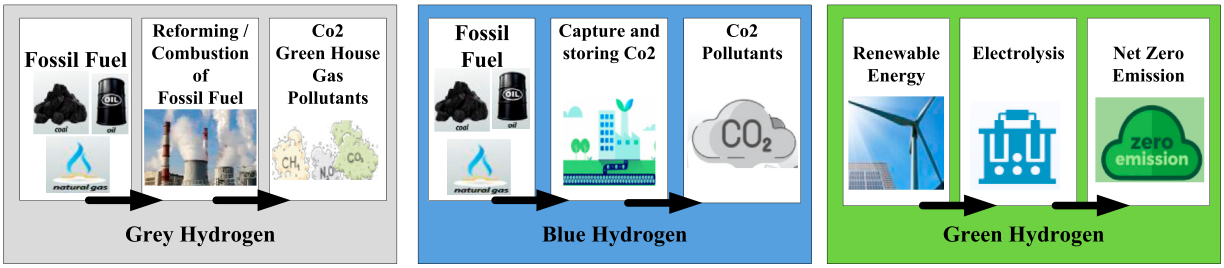

FIGURE 6 | Categories of hydrogen.

TABLE 2 | Hydrogen production from different sources and emissions.

Hydrogen extraction source	Quantity (billion tons/year)	Technical details	Emission	Ref no.
Coal	21.5	Homogeneous and high-speed reaction ought to its special physical and chemical process	GHG emission	(Li et al., 2010; Hui et al., 2017; Wang et al., 2020; Sun et al., 2021)
Industrial gas	12.5	Physical and chemical process	GHG emission with pollutants	(Vialetto et al., 2019; Ates and Ozcan, 2020; Okolie et al., 2021)
By product gas	7.07	Physical and chemical process	GHG emission	(Vialetto et al., 2019; Okolie et al., 2021)
Natural gas	4.6	Chemical process	Pollutants	(Perdikaris et al., 2010; Bicer and Khalid, 2020; Mayrhofer et al., 2021)
Electrolyzed water	2.1	Chemical process	Pollutants	(Mayrhofer et al., 2021; Sun et al., 2021)
Photocatalytic water decomposition with solar energy	1.8	Photocatalytic process	No GHG emission	(Jiang et al., 2013; Yan et al., 2013; Zhang et al., 2013; Tasleem and Tahir, 2020)
Biological H_2 production	2.05	Microorganisms and their metabolic mechanisms	Pollutants	(Bi et al., 2010; Cormos, 2012; Cao et al., 2020)

electrolysis voltage generated by the bubbles developed during the electrolysis process (Hu et al., 2019), high energy consumption is another barrier of hydrogen synthesis from water electrolysis. Hydrocarbons can be used in water electrolysis to reduce energy usage. Cheap metals or nonmetal composite materials, such as Ni, should be the electrodes' likely future direction.

The following are the major future directions to be investigated in the water electrolysis process of hydrogen generation:

- In-depth investigation of the reaction process in order to improve hydrogen generation efficiency and achieve conversion by combining chemical and electrical energy;
- Reduction in energy intake in the electrolysis process of water using renewable energy;
- In-depth investigation of the reaction process in order to improve the efficiency of hydrogen production;
- Improvements in electrode stability and corrosion resistance for increased longevity and lower electrode costs;
- Development of new catalytic electrodes and catalysts to improve reaction efficiency (Gao et al., 2019; Huang et al., 2019).

Hydrogen power is a promising technique for storing fluctuating Renewable Energy (RE) to establish a 100% renewable and sustainable hydrogen economy (Dawood et al., 2020). Hydrogen can be stored as gas or liquid form. High-pressure tanks (350.00–700.00 bar tank pressure) are primarily used to store hydrogen as a gas. Cryogenic temperatures are required to store hydrogen as a liquid (Hydrogen Storage, 2021). Sapru (2002) have given an summary on hydrogen storage systems, based on storage tanks integrated with fuel cells.

3.2 Hydrogen Storage

Hydrogen holds excellent potential to be an energy carrier, especially for fuel cell applications. With high calorific value, it is also termed as regenerative and environmentally friendly fuel. Additionally, it has energy density of 142 ML/kg, which is three times of petroleum (47 MJ/kg) (Kaur et al., 2016). This makes hydrogen as the most efficient fuel to replace petroleum-based vehicular. Thus, fossil fuel reliability can be reduced to fulfil all the global energy demands (Muir and Yao, 2011). Carbon and Hydrogen cycle are shown in **Figure 8**. The combustion process is shown below in blue arrows. The cycle shows how CO_2 released causes global warming (presented by black arrows). On the other hand, the hydrogen cycle is presented by green arrows and pointing towards renewable energy sources (Kaur et al., 2019).

Hydrogen energy has also been projected as a widespread resolution for a secure energy future to increase energy security and strengthen developing countries' economies (Marrero-Alfonso et al., 2009). Various technological, significant scientific, and economic challenges must be overcome before hydrogen can be used as a clean fuel source and the transition

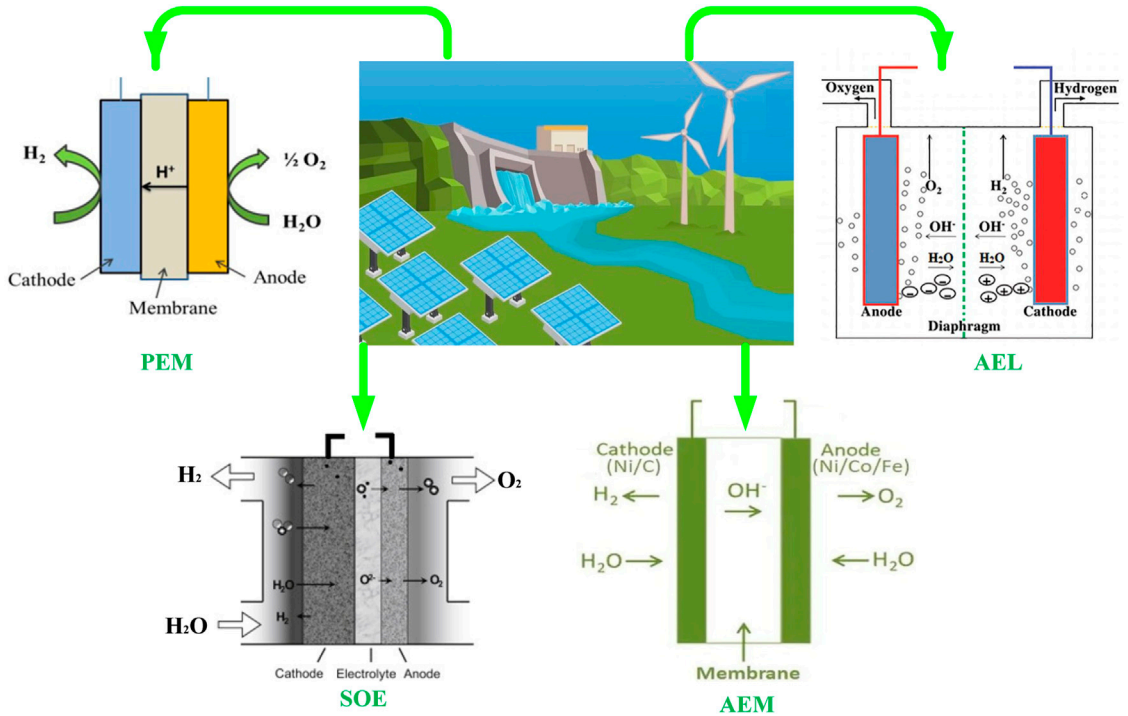

FIGURE 7 | Different types of water electrolysis processes to generate hydrogen.

TABLE 3 | Comparative analysis of different types of water electrolysis process to generate hydrogen.

Technology	AEL	PEM	SOE	AEM
Electrolyte	Aqueous KOH (20–40 wt%)	Proton exchange ionomer (e.g., Nafion)	solid-oxide	Anion exchange ionomer (e.g., AS-4) + optional dilute caustic solution
Cathode	Ni, Ni–Mo alloys	Pt, Pt–Pd	Ni-YSZ (yttria-stabilized zirconia)	Ni and Ni alloys
Anode	Ni, Ni–Co alloys	RuO_2, IrO_2	Lanthanum strontium manganate	Ni, Fe, Co oxides
Charge carriers	OH-, K+	H+	O2-	OH-
Operating temperature	100°–150°C	70°–90°C	700°C –800°C	50°C –60°C
Cell voltage (V)	1.8–2.4	1.8–2.2	1.6–1.8	1.8–2.2
Technology status	Mature	Commercial	Not yet commercial Pilot scale	R&D

from a carbon-based fossil fuel energy system to a hydrogen-based economy can be completed (Shashikala, 152012).

Additionally, in the transportation sector, hydrogen storage technologies are in consideration and gradually move towards designing highly efficient systems. For example, specific criteria are looked into, such as thermal stability of the system, gravimetric and volumetric densities and cost of the operating systems. Many of these sectors are being worked on, and improvements in hydrogen production and storage for various automotive applications have been made and deployed (Shang and Chen, 2006).

3.2.1 Hydrogen Storage Methods

Hydrogen storage methods can be categorized into three groups, as shown in **Figure 9**. Molecular hydrogen can be stored as (1) a gas or a liquid without any significant physical or chemical bonding to other materials; (2) molecular hydrogen can be adsorbed onto or into material and held in place by relatively weak physical van der Waals

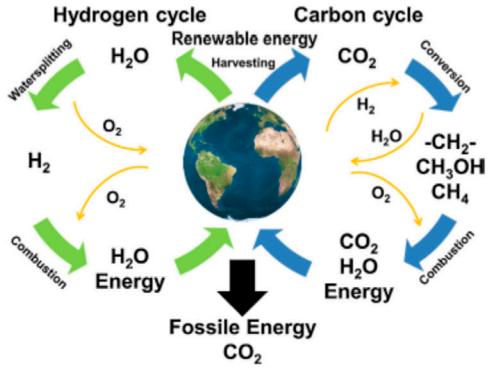

FIGURE 8 | Carbon and hydrogen cycle (Muir and Yao, 2011)

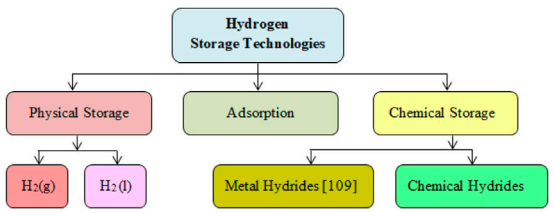

FIGURE 9 | Hydrogen storage technologies (Andersson and Grönkvist, 2019; Lototskyy et al., 2017)

bonds; (3) atomic hydrogen can be covalently bound (absorbed). The spread of hydrogen fueling stations across the transportation network, as well as investment in hydrogen fueling stations, can lead to increased profits (El-Taweel et al., 2019).

3.2.1.1 Compressed/Physical Hydrogen Storage

Hydrogen is stored at high pressure and in compressed form and specifically designed hydrogen cylinders reinforced by carbon fibre that can withstand very high pressure. Various concerns should be handled before using this technology, like high-pressure requirements, low volumetric density, energy required to compress hydrogen gas, and cylinder weight and to reduce the overall cost (Sakintuna et al., 2007).

Hydrogen can also be stored in cyro-compressed form by cooling hydrogen gas to −253°C; this process increases the volumetric storage capacity of hydrogen gas by 4 times. However, this process is highly energy intensive due to energy requirements for compressing and liquifying hydrogen gas. There are further limitations, such as liquid hydrogen being very volatile and potentially forming an explosive combination with air if evaporated. Thus, this system should be designed to cover all the safety concerns (Sakintuna et al., 2007). **Figure 10** shows hydrogen gas in the form of compressed gas and cryogenic liquid.

The weight, volume, cost, efficiency, codes, and standards are the primary problems in hydrogen storage. New materials, particularly polymers, must be developed as barrier materials to limit hydrogen leakage in storage tanks with high energy-to-weight ratios (Macher et al., 2021).

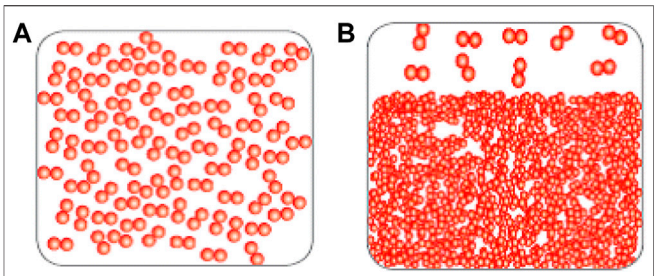

FIGURE 10 | (A) Compressed hydrogen gas storage and **(B)** cryo-compressed hydrogen gas storage (Sakintuna et al., 2007)

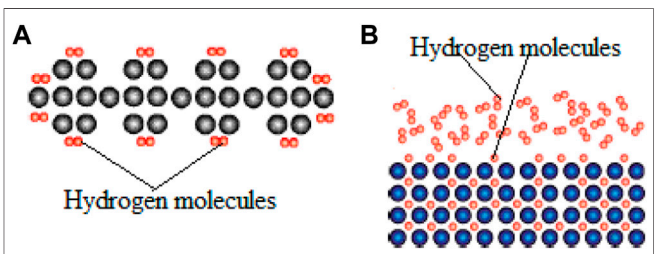

FIGURE 11 | (A) Surface adsorption and **(B)** Surface absorption (Klanchar et al., 2004)

3.2.1.2 Material Based Hydrogen Storage

In materials, hydrogen is generally stored as absorption, adsorption, and chemical reaction. If hydrogen is stored on the surface, then the phenomenon is called adsorption, and if it is stored within the solids, it is called absorption. The main difference is in the density as it increases from adsorption to absorption. Adsorption is further divided into chemisorption and physisorption based on their mechanism. Physiosorbed hydrogen is weakly bonded than chemisorbed hydrogen molecules. Also, it involves highly porous materials with high surface areas to efficiently uptake and release hydrogen molecules from the materials, such as metal hydride hydrogen storage.

However, absorption involves hydrogen atoms attached with strong bonds within the chemicals. Here, hydrogen is stored in large amounts with small quantities of materials also could be released at low temperature and pressure. For example, in complex and chemical hydrides, hydrogen is absorbed in the materials, as shown in **Figure 11** (Klanchar et al., 2004).

3.2.1.3 Chemical Hydrogen Storage Pathway

When hydrogen is generated and released through the chemical reaction, then the storage technology is defined as chemical hydrogen storage. The basic reactions involve the reaction of chemical hydrides with water and alcohols. However, this technology suffers lack of reversible onboard reactions and require spent fuel and by-products to be removed off-board. Here, hydrogen is strongly bonded as hydrogen atoms within the molecular structures of the chemical compounds, as presented in **Figure 12**. Therefore, for hydrogen generation and storage, a chemical reaction is required.

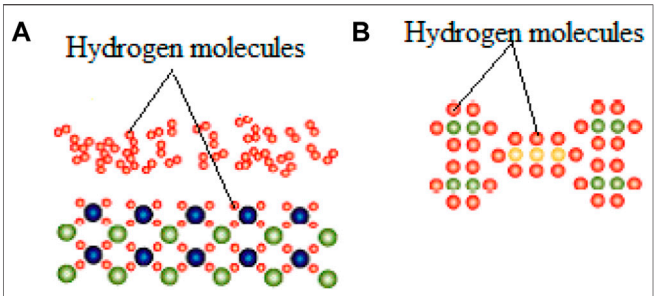

FIGURE 12 | (A,B): Absorption in complex chemical hydrides (Klanchar et al., 2004).

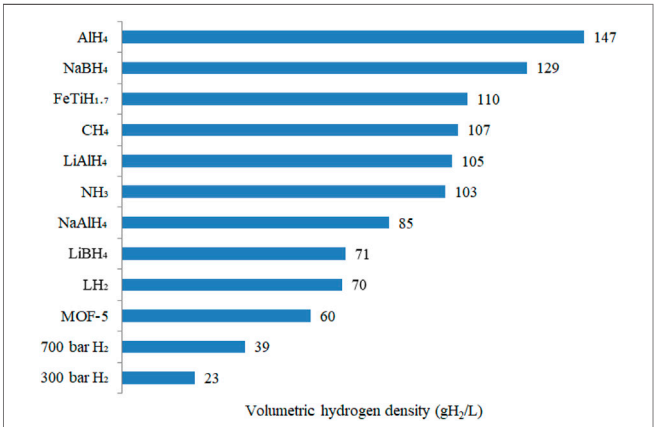

FIGURE 13 | Volumetric hydrogen density of various hydrogen storage methods (Graetz, 2012).

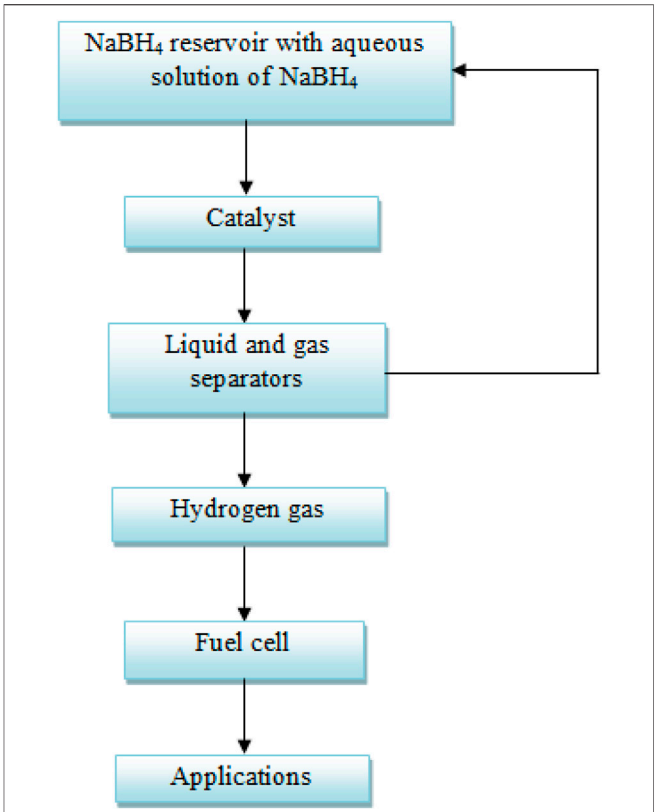

FIGURE 14 | Flow diagram of solid-state hydrogen generation system (Demirci and Miele, 2009).

As hydrogen is stored in chemical hydrides, these hydrides in the form of materials have high gravimetric and volumetric densities. Thus, hydrogen is released in the form of chemical reactions. There are two methods of hydrogen release; the first is hydrolysis, and the second is thermolysis. The former one requires low temperature and pressure, and the theoretical storage efficiency is very high. The latter one involves highly sophisticated technologies and energy requirements to break the hydrides by thermal pathways. Considering that few common chemical hydrides that release hydrogen by hydrolysis pathway are sodium, lithium, magnesium, calcium, titanium hydrides, and few of complex hydrides are sodium borohydride, lithium aluminium hydride and lithium borohydride (Klanchar et al., 2004).

Figure 13 presents various hydrides per their volumetric storage densities, with AlH3 having the highest value and pressurized tanks with the lowest values (Graetz, 2012). As shown in **Figure 14**.

The catalyst for the reaction is supplied in the form of an aqueous solution of $NaBH_4$ as a chemical hydride. This solution is run through a separator, which separates the pure hydrogen gas from the rest of the mixture. This pure hydrogen gas is then pumped into the fuel cell, where it can be used. After the recycling procedure, the by-products might be returned to the liquid reservoir and used again (Demirci and Miele, 2009).

As a clean resource, hydrogen energy might minimise energy savings and emissions caused by the use of fossil fuels, and it will likely play an increasingly important role in the future (Zhang et al., 2019a). In recent decades, the PEMFC (proton exchange membrane fuel cell or polymer electrolyte membrane fuel cell), which effectively transforms the chemical energy inherent in hydrogen into electricity without producing pollutants, has piqued interest in automotive applications (Ogungbemi et al., 2021).

3.3 Proton Exchange Fuel Cells

FCVs (fuel cell vehicles) powered by PEMFC have recently reached mass production, such as Toyota's Mirai, Honda's Clarity, and Hyundai's NEXO. Performance should be increased at a cheaper cost to improve its commercial uses.

The European Union and the US alone stand out alone in the majority to consume all petroleum products and energy demands. This has led to the development of alternative energy sources, with the best ones stated as hydrogen, synthetic fuels and biofuels. These energy sources are investigated for their suitability to sustain a clean form of energy (Ogungbemi et al., 2021). The source where hydrogen is produced from renewable energy to electricity by PEM fuel cells are under investigation. The PEM cells are capable of producing sufficient power to sustain commercial and residential usage under varying temperatures.

For example, a PEM fuel cell generator with Na metal and water chemical reaction generated hydrogen with minimum emissions and noise. This have extended its use to medium and high duty vehicular applications. Despite all such uses, PEM fuel cells face few disadvantages (Ijaodola et al., 2019) and studies are in progress based on economics, policy framework and advancements in electrolysis process to facilitate the use of PEM fuel cells for vehicular and general use. Due to myriads of advantages like low operating temperature, solid electrolyte and high power density, durability and reliability proton exchange, fuel cells can be used in several areas like on-site hydrogen generation, automotive, and portable electronic devices as discussed. The parameters of PEM fuel cells are based on operating conditions, and to accurately estimate its characteristics; research is also in progress with efficient mathematical modelling. It can disclose more about operating parameters linked with the PEM fuel cells (Rao et al., 2019a; Kandidayeni et al., 2019). Studies are also in progress to study the dynamic loading on the performance of PEMFC (Zhang et al., 2019b; Huang et al., 2020). The situation arises when unreasonable loading conditions increase and could even lead to failure (Mayyas et al., 2014) thus, adding to the disadvantages of the fuel cells. This could be explained as when PEM FC is used as a mechanical power source, it undergoes dynamic loading and response voltage becomes lower than the steady-state conditions; subsequently, the voltage increases gradually. This could lead to unfavourable operations of PEM fuel cells, and thus, dynamic performance needs to be studied.

Proton Exchange fuel cells have wide application in various sectors like power plants, transportation, digital devices etc. However, the short life span due to the degradation and reusability of fuel cells limits its applications in the commercial sector (Chen et al., 2019). Considering the lifespan of fuel cells in mobile applications, it is 3,000 h, but the demand rises to 5000 h to be used commercially. As per DOE (United States Department of Energy), the set future goals for transportation and stationary applications of PEM fuel cells as 5,000 h and 40000 h, respectively, by 2020 with performance degradation that should be less than 10% (Ren et al., 2020). The considerable difference between stationary and transportation can be attributed to different designs as fuel cells in vehicles encounters harsh conditions like the open-circuit voltage, dynamic load, startup and shutdown, overload and freezing thaw. Thus, the decay of fuel cells in vehicular applications is also thoroughly studied by developing various test protocols. With the performance of fuel cells, cost factors are also in consideration like The Strategic Analysis Inc. studied the most influencing factors on the cost of FC's in 2012 and 2017 (Li et al., 2020). The report (2012) concluded that the fuel cell stack and platinum loading are the most important factors which affect the cost of the fuel cells. Since then, the study has also focused on a low Pt-based catalyst that made significant development in Pt-M alloys, Pt-based core shell, and Pt-based nanostructure. Gradually this development led to Pt-free catalysts like carbon alloy catalysts in commercial markets in Japan. Thus, it can be stated that PEM fuel cells holds the potential to establish a hydrogen economy for a secure and sustainable future.

4 HYDROGEN BASED MOBILITY

Promotion of hydrogen vehicles as the future transportation platform has been chosen due to its zero-pollutant discharge characteristic. Hydrogen fuel cell vehicle technology has the scope to various categories of mobility sectors. This technology can replace lightweight vehicles, heavy goods vehicles, heavy passenger vehicles, trains, and unmanned vehicles. Adopting the concept of hydrogen fuel for heavy vehicles has attracted New Zealand and Paris to meet the zero climate change commitments. As reported in (MBIE, 2019), the proper examination of feasibility for adopting clean hydrogen for heavy vehicles exceeds 30 tons has been discussed in (Concept Consulting Group, 2021; Perez et al., 2021).

Apart from the development of hydrogen fuel, heavy and very heavy-duty vehicles, public lightweight vehicles, and passenger buses require a shift towards utilization of clean hydrogen (Topler and Lordache, 2017; Air Liquide Will Build the First High-pressure Hydrogen Refueling Station for Long-haul Trucks, 2021). Air Liquide has announced the opening of Europe's first high-pressure hydrogen filling station, which will support the first fleet of long-haul hydrogen vehicles (Air Liquide Will Build the First High-pressure Hydrogen Refueling Station for Long-haul Trucks, 2021). This investment is in line with the Group's objective of accelerating hydrogen energy adoption through large-scale initiatives, notably in the heavy vehicle category. Vulnerabilities of Hydrogen Energy in Emerging Markets describes strategies and developments for hydrogen civilization efforts implemented by various stakeholders in different countries and at different stages of the development cycle, including authorities, institutes, research, industry, and individuals (Topler and Lordache, 2017). Considering these facts, Germany has taken the lead in the global market for the commercialization of Hydrogen vehicles, along with the collaborators from Japan, Korea and the United States (Galich and Marz, 2012; Trencher and Edianto, 2021). Hydrogen and fuel cell technologies have the potential to help create a more environmentally friendly and emission-free transportation and energy system (Galich and Marz, 2012). Policymakers and automotive players throughout the world attempt to expedite the electrification of road transport using hydrogen (Trencher and Edianto, 2021). They examined and contrasted the factors impacting the production and market penetration of privately owned fuel cell electric passenger vehicles (FCEVs) and fuel cell electric buses (FCEBs) in public transportation fleets.

4.1 Hydrogen Vehicles

In the present time, railway is the most economical transportation preferred by the common citizen as well as it is also used for goods transportation. The conventional railway depends upon the fossil fuels leads to the emission of GHGs and the generation of sound pollution. In the line, to meet zero-emission and zero sound railway transportation, InnoTrans in 2016 of Berlin developed the Coradia iLint. This has been commercialized and launched in 2020 to run for 100 km between Cuxhaven, Bremerhaven, Bremervoerde and Buxtehude in northern Germany (Low et al., 2020). Understanding the requirement and need for replacing clean hydrogen fuel transportation with the second largest railway

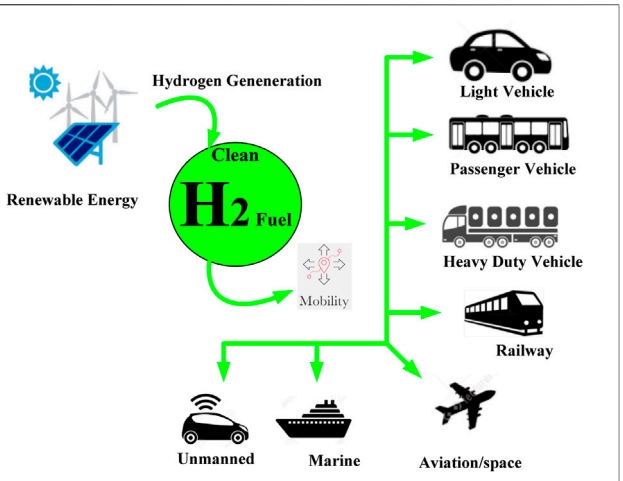

FIGURE 15 | Scope of hydrogen fuel in different mobility sectors.

network in the world, the Indian Railway has also started developing and testing passenger fuel cell train set (Jhunjhunwala et al., 2018).

Conventional fuel engines utilized in the shipping industries release the air pollutants and GHGs into the environment. In the regulation of these harmful gases, International Maritime Organization (IMO) has passed an article to prevent pollution from the ships under (World's First Hydrogen Train Runs Route in Germany, 2021; Traction: India to trial fuel cell trainset, 2021). Enhanced efficiency of the marine fuel cells for various applications of onboard ships has motivated the researchers to focus on hydrogen fuel-based marine engines. Electricity generation, emergency power supply and power propulsion are the major power requirement in an onboard ship, which can be generated through clean hydrogen fuel cells by replacing conventional fuels (Sattler, 2000; IMO, 2012a; IMO, 2012b). Fuel cells have a lot of potential for usage on ships. Fuel cells on merchant ships and naval surface ships can be used for a variety of purposes, including: (1) emergency power generation; (2) electric energy generation, particularly in waters and harbours with strict environmental regulations; (3) small power output for propulsion in special operating modes (e.g., very quiet run); and (4) electric power generation for the ship's network and, if necessary, the propulsion network on ships equipped with fuel cells (e.g., naval vessels as all-electric ships, AES) (Sattler, 2000). The actual requirement, replacement and advantage of combustion fuel engine by clean hydrogen fuel cell-based engine have been discussed in detail in (Leo et al., 2010; Tronstad et al., 2017). Submarines are now the most common marine use of fuel cells. In this industry, hydrogen/oxygen polymer electrolyte membrane (PEM) fuel cells are often utilized (Leo et al., 2010). The scope of hydrogen fuel in different mobility sectors is depicted in **Figure 15**.

The target to achieve limited emission fuel to protect the climate, world aviation industries have also focused on clean hydrogen as an efficient candidate for short and long-range aviation and space transportation (de-Troya et al., 2016). The research and development in aviation and space sector industries have reported continuous progress for choosing clean hydrogen fuel. The aviation and space industries of the United States (Committee on Air Force and Department of Defense Aerospace Propulsion Needs, 2006; Cecere et al., 2014; van Biert et al., 2016), Japan (Dawson, 2004; Dale Reed and Lister, 2011), Europe (Negoro, 2007), India (Sekigawa and Mecham, 1996; Chopinet et al., 2011), China (Rao et al., 2019b) and Russia (Lele, 2006) have already reported the developmental progress for hydrogen fuel technology adaptation.

The advancement of transportation in different segments and requirements has led to the development of unmanned vehicles. The most popular sector under this category is unmanned cars and unmanned Arial vehicles (UAV) (Tan, 2013). For UAV applications, various countries have focused the efficiency to cover longer distances and enhanced performance by replacing conventional fuel with clean hydrogen fuels (Sergienko, 1993; Wang et al., 2013). The development of Hydrogen mobility in different sectors are tabulated in **Table 4**.

It has been studied and reported that utilization of hydrogen fuel cell vehicles has been pointed in the United States and 5,899 hydrogen vehicles developed for commercialization (Bayrak et al., 2020). For the promotion of hydrogen utilized vehicles, companies like Toyota Mirai, Honda Clarity, Renault–Nissan, General Motors and Honda have formed alliances for the joint production (Giacoppo et al., 2017; Dudek et al., 2021).

4.2 Fuel Cells Electronic Vehicles

Vehicle manufacturers began producing hydrogen fuel passenger vehicles in 2002 (Tanç et al., 2018) due to an increase in the number of researchers interested in Fuel Cell Electronic Vehicles (FCEVs). They've been manufacturing a variety of models up to now. In addition to passenger automobiles (Lee et al., 2019; Tanç et al., 2020), these manufacturers are known to work with light commercial vehicles (Matulić et al., 2019), buses (de Miranda et al., 2017), and trucks (Lee et al., 2018). **Table 5**, lists all commercially available FCEVs, as well as their manufacturers and special features.

In recent years, the majority of passenger car manufacturers have started developing FCEVs. General Motors, Toyota, and Honda produce their own FC stacks, whereas Ford, Mazda, DaimlerChrysler, Mazda, Hyundai, Fiat, and Volkswagen purchase them from FC manufacturers. It is apparent from the specifications of available FCEVs that battery hybridization is currently favoured. Furthermore, automakers such as Honda, Hyundai, and Mercedes have recently developed plug-in FCEVs. Proton Exchange Membrane Fuel Cell is the most prevalent FC stack, and its efficiency for FCEVs is improving continuously. Detail specifications of the commercialized presently dominating FCEV for sale or leasing (Wasserstoffautos, 2021) are tabulated in **Table 6**.

For a shift from a carbon-based (fossil fuel) energy system to a hydrogen-based economy, three key technological hurdles (Chang et al., 2019) must be overcome that are as follows.

1) To compete with other options, the cost of efficient and sustainable hydrogen generation and transport must be considerably decreased.
2) In order to, offer an appropriate driving range, new generations of hydrogen storage technologies for vehicle applications must be created.

TABLE 4 | Development of Hydrogen Mobility in different sectors.

Mobility type	Country	Status	Ref no.
Heavy Duty Vehicles 	New Zealand	• Examination of feasibility • Energy strategy • Assessment of Potential	(MBIE, 2019; Concept Consulting Group, 2021; Perez et al., 2021)
	Paris	• Development of Vehicles	Air Liquide Will Build the First High-pressure Hydrogen Refueling Station for Long-haul Trucks, (2021)
• Fuel Station Light weight vehicles 	Germany	• Development • Commercialization	(Galich and Marz, 2012; Topler and Lordache, 2017; Trencher and Edianto, 2021)
	Japan	• Development of cars by 2030	Low et al. (2020)
	South Korea	• Development • Commercialization	Low et al. (2020)
	US	• Development • Commercialization	Low et al. (2020)
Railway transportation 	India	• Development • Research	Jhunjhunwala et al. (2018)
	Northern Germany	• Commercialized (Germany)	World's First Hydrogen Train Runs Route in Germany, (2021)
	India	• Developmental (India) • Commercialization Process	[137]
Shipping industries 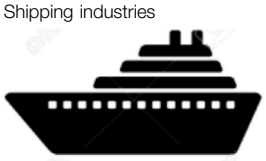	United Kingdom	• Developmental stage	(Sattler, 2000; IMO, 2012a; IMO, 2012b)
	Norway	• Risk & Safety aspects Analysis	(Tronstad et al., 2017; Leo et al., 2010; de-Troya et al., 2016; van Biert et al., 2016)
Aviation and Space 	United states	• Developmental Progress	(Dawson, 2004; Committee on Air Force and Department of Defense Aerospace Propulsion Needs, 2006; Dale Reed and Lister, 2011)
	Japan	• Progress, Testing and Safety Assessment	Negoro, (2007)
	India	• Developmental Progress	(Lele, 2006; Rao et al., 2019b)
	Europe	• Testing	Tan, (2013)
	China	• Testing	Wang et al. (2013)
	Russia	• Testing	Sergienko, (1993)
Unmanned Cars, Unmanned Arial vehicles 	Turkey	• Developmental Progress	(Sergienko, 1993; Tan, 2013; Wang et al., 2013)
	Italy	• Progress, Testing and Safety Assessment	(Giacoppo et al., 2017; Bayrak et al., 2020)
	China	• Developmental Progress	Chang et al. (2019)

3) Fuel-cell and other hydrogen-based technologies must be less expensive while having a longer useful life.

In this context, the future market of hydrogen transportation and distribution are determined mainly by four factors (Edwards et al., 2008; Olabi et al., 2021): (a) Cost of hydrogen in future, (b) the rate of advancement of various hydrogen-based technologies, (c) restriction in GHG emission, and (d) the cost of competing for alternative transportation systems. Hydrogen has the potential to be a long-term option for sustainable mobility with several social, economic, and environmental benefits (Forsberg, 2005). It can minimize reliance/dependency on fossil fuels and reduce carbon emissions from the transportation industry in the long run.

4.3 Techno Economic Aspects

The cost and performance competitiveness of fuel cell electric vehicles (FCEV) in the car industry will determine their future. FCEV adoption in the present transportation industry is still modest. Many governments have yet to take a firm stance on hydrogen for transportation. In this regard, comprehensive energy plans for the road transportation sector are required. The use of energy systems modelling (ESM) to support energy planning is frequently advised in

TABLE 5 | Commercially available FCEVs.

Model	Manufacturer	Appearance	Type	Range (km)	Top speed (km/h)	FC (type)	Interval (Year)	Leased/ Marked in	Ref no.
Gumpert Nathalie	Gumpert Aiways Automobile (RG)		FC and Battery hybridization	820	300	Direct Methanol Fuel Cell (DMFC)	2021	Germany, China	Rolandgumpert, (2021)
Hyundai Nexo	Hyundai		FC, Battery and UC hybridization	600	179	PEMFC	2018-Present	South Korea, California, and Europe	Hyundai, (2021)
Toyota Mirai	Toyota		FC and Battery hybridization	502	160	PEMFC	2015-Present	Japan, California, Europe, Québec and United Arab Emirates	Energy.Gov, (2021)
Honda Clarity	Honda		FC and Battery hybridization	590	178	PEMFC	2016–2021	Japan, Southern California, Europe	Automobiles.Honda, (2021)
Hyundai ix35 FCEV	Hyundai		FC and Battery hybridization	594	160	PEMFC	2014–2018	South Korea, California, Europe and Vancouver	Environment Hydrogen-Fuel-Cell, (2021)
Mercedes-Benz F-Cell (B class)	Daimler AG		FC and Battery hybridization	402	132	PEMFC	2010–14	southern California	Mercedes-Benz, (2021)
Honda FCX Clarity	Honda		FC and Battery hybridization	560	160	PEMFC	2008–2015	United States, Europe and Japan	Matsunaga et al. (2009)
Chevrolet Equinox FC	General Motors		FC and Battery hybridization	320	141	PEMFC	2007–2009	California and New York	Eberle et al. (2016)

(Continued on following page)

TABLE 5 | (*Continued*) Commercially available FCEVs.

Model	Manufacturer	Appearance	Type	Range (km)	Top speed (km/h)	FC (type)	Interval (Year)	Leased/ Marked in	Ref no.
Mercedes-Benz F-Cell (A-Class based)	Daimler AG		Full FCEV	160–180	132	PEMFC	2005–2007	United States, Europe, Singapore and Japan	Mercedes-Benz-Cars, (2021)
Nissan X-Trail FCV (2005 Model)	Nissan		FC, Battery and UC hybridization	500	150	PEFC	2003–2013	Japan and California	Nissan-Global, (2021)
2003 Model			FC and Battery hybridization	350	145	PEFC			
Ford Focus FCV	Ford		FC and Battery hybridization	320	129	PEMFC	2003–2006	California, Florida and Canada	Hydrogencarsnow, (2021)
Honda FCX-V4	Honda		FC and UC hybridization	315	140	PEMFC	2002–2007	America, Japan	Global.Honda, (2021)

this context, since it provides a scientific basis for the prospective evaluation of energy systems based on technical and economic factors across time (Bhattacharyya and Timilsina, 2010). Furthermore, by using life-cycle sustainability variables in the future evaluation, ESM studies might be improved (García-Gusano et al., 2016). A variety of pathways and important conversion technologies for biomass and organic solid waste to hydrogen have been investigated (Aziz, 2021). The potential for a techno-economic and environmental assessment of the hydrogen production mix that might meet the hydrogen demand for road transport under various scenarios for FCEV penetration in Spain has been addressed (Navas-Anguita et al., 2020). Due to the reasonable costs of natural gas and the maturity of the technology, the hydrogen demand associated with the eventual penetration of FCEV in the Spanish road transport system may be totally met by conventional steam reforming of natural gas. The worldwide view on hydrogen energy systems, on the other hand,

TABLE 6 | Technical specifications of FCEVs which are presently dominating the market.

Model	Type	Range (km)	Electric motor (kW)	Tank capacity (kg)	Fuel consumption (H_2) Kg/100 km
Toyota MIRAI II	Fuel cell vehicle	650	135	5.6	0.76
Hyundai NEXO	Fuel cell vehicle-5th generation	756	120	6.33	0.84
Mercedes-Benz GLC F-CELL	Electric vehicle with fuel cell and li-ion battery	478	141.557 (Li-ion battery 13.8 kWh)	4.4	0.97
Honda Clarity Fuel Cell	Fuel cell vehicle	589	130	5	
Hyundai ix35	4th generation Fuel cell vehicle	594	100	5.64	1

refers to a hydrogen economy based on environmentally friendly solutions. Lin et al. (Lin et al., 2013) used a cost-based consumer choice model to examine the market adoption and social advantages of FCEVs from 2015 to 2050. For the Indian urban driving cycle, Shakdwipee and Banerjee compared fuel cell cars against petrol and CNG automobiles (Manish Shakdwipee, 2006). Primary energy consumption (MJ/km), CO_2 emissions (kg CO_2/km), and cost (Rs./km) were used as comparison criteria. Fuel cell vehicles, they discovered, are more energy efficient and environmentally friendlier than gasoline automobiles. Fuel cell vehicles consume 43% less energy and emit 40% less CO_2 than gasoline automobiles. A techno-economic analysis is conducted to assess the feasibility of deploying Fuel Cell Electric Trucks (FCET) on the Oslo-Trondheim route in Norway (Diva-Portal, 2022). The output of the infrastructure's techno-economic model, which included various configurations and combinations of both hydrogen producing units (HPU) and hydrogen refuelling stations (HRS), was given in the form of a cost curve function based on the FCET's fleet size. The cheapest set-up was found, consisting of a 350-bar HRS for a type 3 onboard tank with hydrogen production connected directly to it. Future cost curves for FCETs and infrastructure that indicate development in 2030 were investigated. Chen and Melaina (Chen and Melaina, 2019) established a techno-economic analysis framework to analyse the cost and performance of main vehicle technologies (internal combustion, hybrid, plug-in hybrid, battery and fuel cell electric) under various advancement scenarios for the years 2035 and 2050. Based on a 5-years or 15-years ownership term, their findings suggest that the prices per mile for FCEVs are 36% or 22% more than those of regular gasoline automobiles in the 2035 scenarios. FCEVs have 15-years ownership costs that are equivalent to gasoline automobiles with comparable engineering performance in 2050 scenarios. Fuel cell cars have a cheaper driving cost in all of the 2035 and 2050 scenarios when compared to electric vehicles with a 200-mile range. To encourage the use of hydrogen as a passenger car fuel, the cost of an FCV must be reduced to at least the same level as that of an electric vehicle.

4.4 Selected Implemented Projects, Policies and Challenges

Throughout the world many demonstration projects are implemented on hydrogen mobility. Some important implemented projects are discussed here. Han (2014) investigated the hydrogen fuel cell car demonstration projects in China, as well as their marketing methods. Their research indicated that hydrogen fuel cells are the most promising technology for reducing urban air pollution, saving energy, achieving sustainable mobility, and promoting technical change in the automobile sector. The Chinese government has adopted an ambitious strategy and is providing significant financial assistance for the development of hydrogen and related technologies. Aditiya and Aziz examined the possibility of establishing an inter-state hydrogen energy system on selected countries in the Asia-Pacific region, based on individual evaluations from the nexus of technology, social, and economic perspectives, and utilising the respective strengths to identify an inter-state hydrogen network strategy in the Asia-Pacific region, dubbed the "Asia-Pacific Hydrogen Valley" (Aditiya and Aziz, 2021). Indonesia, Malaysia, Brunei Darussalam, the Philippines, Singapore, Vietnam, Thailand, Japan, South Korea, Australia, and New Zealand are among the countries assessed. According to the findings, countries with active hydrogen policies and high R&D capacity may lead the strategy, whilst countries with high primary energy supply capacity and an economic edge would aid the group in catering energy and commercial resources, respectively. The feasibility of using hydrogen cars in various modes of transportation, including personal automobiles, taxis, and shared mobility, was investigated (Turon., 2020). Hype is the first hydrogen-powered taxi fleet in the world. The first five cars were introduced to the system on 7 December 2015 at COP 21 by Société du Taxi Electrique Parisien ("STEP") (Hype, 2019). The fleet now consists of about 100 cars. Before the end of 2020, 600 cars are expected to be in use. The system's taxis have a range of more than 500 km. As a result, their charging time might be as long as 5 min (Hype, 2019). In 2016, the first attempts were made to develop a car-sharing system based on hydrogen-powered vehicles. The Linde Group commenced operations at that time by launching a service under the BeeZero brand in Munich, Germany. The system has a 50-vehicle fleet. Unfortunately, the system failed to work in June 2018 after 2 years of operation (Gas World Portal, 2018). The corporation claims that economic unprofitability was the cause for its demise. Unfortunately, one of the issues that car-sharing companies face is this type of issue (Gas World Portal, 2018). This is because car-sharing is a new type of urban transportation that is now being developed among today's communities that are accustomed to owning rather than renting a car (Turoń and Cokorilo, 2018). The introduction of hydrogen automobiles in the form of zero-emission buses is another alternative that allows the vehicle to reach the biggest number of people. A bus that uses electric energy generated by hydrogen in fuel cells or merely the engine whose cycle does not result in the production of greenhouse gases or other substances covered by the greenhouse gas emission management system (Polish Electromobility Act, 2018). An operator operating in Cologne or Wuppertal, Germany, is an example of how this type of bus may be implemented. Furthermore, this mode of transportation was so well received that a tender for the supply of a fleet of 40 cars was signed. Despite numerous dubious appraisals and public worries, primarily due to ignorance, hydrogen-powered cars appear to have a chance to becoming a viable alternative to conventional automobiles. The current condition of such vehicle use in various nations reflects a growing interest in green transportation technology and the hunt for diverse solutions that can assist transportation's long-term growth.

Many nations have strong hydrogen support policies, and hydrogen energy will become an essential element of the future global energy plan. Japan, the European Union, the United States, and South Korea all responded enthusiastically and pushed aggressively, with national policy support focusing on hydrogen energy fuel cell cars. Foreign subsidy programmes primarily targeted the consumption connection and were paid in the form of a purchase tax credit or a purchase subsidy. The United States is the first country to use hydrogen and fuel cells as an energy source. It first proposed the notion of "hydrogen

economy" in 1970, and in 1990, it passed the Hydrogen Research, Development, and Demonstration Act. The National Roadmap for Hydrogen Energy Development was announced by the US Department of Energy in November 2002, kicking off the methodical execution of the National Hydrogen Energy Plan (Wang et al., 2015). The United States of America designated October 8 as National Hydrogen and Fuel Cell Day of Remembrance in 2018. The total number of fuel-cell cars sold and leased in the United States as of 1 April 2020 was 8,285. Japan has implemented a variety of beneficial regulations aimed at speeding up the commercialization of hydrogen energy and fuel cells, with encouraging outcomes. Japan was the first country in the world to establish a comprehensive government strategy for the development of hydrogen and fuel cell technology, and the Basic Hydrogen Energy Strategy 2017 recommended that the government prepare for hydrogen and fuel cell development. Japan aims to build 320 hydrogen refuelling stations in 2025 and 900 in 2030, according to the Basic Hydrogen Energy Strategy issued in late 2017 (Wei and Chen, 2020). The Japanese government has spent hundreds of billions of yen on development and promotion of hydrogen and fuel cell technologies during the last 30 years. The EU sees hydrogen energy as a critical component of energy security and transformation. The EU Fuel Cell and Hydrogen Joint Action Plan (FCH JU) initiative offers major funding for the development and promotion of national energy and fuel cells across Europe. For the years 2014–2020, the entire budget was €665 million (European Commission, 2020). In Europe, there were 152 hydrogen refuelling stations in service by the end of 2018, with expectations to increase to 770 in 2025 and 1,500 in 2030, with roughly 1,080 fuel cell passenger cars being deployed. Since 2014, China has enacted a number of policies and measures reflecting the country's commitment to the growth of the hydrogen and fuel cell industries, as well as the obvious trend of Chinese policies supporting the hydrogen industry's development. According to the Ministry of Industry and Information Technology's (MIIT) 2018 fuel cell vehicle subsidy criteria, the state provides up to 200,000, 300,000, and 500,000 yuan in subsidies for fuel cell passenger cars, medium commercial vehicles, and large commercial vehicles, respectively (Liu and Zhong, 2019). As a first step toward the National Hydrogen Mission, the Indian government announced the first phase of its Green Hydrogen Policy in 2021. The mission's goal is to turn India into a green hydrogen centre that will assist the country reach its climate goals. It aims to produce five million metric tonnes per annum (MMTPA) of green hydrogen by 2030, as well as build renewable energy capacity in the process (Power-Technology, 2022).

Successful implementation of Hydrogen policy required extensive R&D to overcome the technical challenges to expedite the acceptance of hydrogen as future of sustainable mobility. The majority of hydrogen is now generated in a traditional manner, coming from the burning of fossil fuels, which emits a significant quantity of CO2. As a result, the primary difficulty is to create hydrogen utilising sustainable energy sources. This is a major step forward in the direction of green hydrogen. Only a few recharge stations exist across the world. Even though some governments are willing to invest in the building of hydrogen charging stations, demand remains low, and these terminals do not now make enough profit. Hydrogen produced from renewable sources is highly costly and inefficient when compared to hydrogen produced from natural gas. Furthermore, hydrogen is still exceedingly explosive. It must be kept and transported in big containers under pressure. This creates security, logistical, and financial issues that continue to obstruct its usage (Solarimpulse, 2022). According to hydrogen features and behaviour, hydrogen monitoring needs, including international partnerships and formal agreements, legislation, codes, and standards, Foorginezhad et al. (Foorginezhad, 2021) investigated the safety difficulties with hydrogen fuel cell cars. The detection performance of hydrogen sensor types relevant to fuel cell cars, such as catalytic hydrogen, electrochemical, semi-conductive metal-oxide, thermal conductivity, optical, palladium (alloy) film-based, and combination technology-based sensors, is also reviewed. Finally, future options for sensing and monitoring technologies, as well as obstacles ahead in the use of hydrogen fuel cells in automobiles as a replacement for traditional equivalents, are presented.

5 CONCLUSION

To reduce climate change and the adverse effect of pollutants from conventional fuel vehicles, sustainable transportation development and commercialization have evolved rapidly in the last few years. The purpose of this study is to draw attention towards the sustainable mobility and implementation of sustainable development since there is substantial potential for establishing convergence between climate change mitigation efforts and sustainable development goals in the transportation sector. Focusing on the rise in environmental concerns like greenhouse gas emissions and environmental sustainability, hydrogen energy-based technology is considered the potential for future transportation. Technical aspects presenting hydrogen generation and storage methods reveal that hydrogen is the only future fuel satisfying the criteria for sustainable mobility and designing hydrogen-based vehicles.

The review also presents exciting insights into hydrogen-based vehicles in the marine, railways and aerospace industry and concludes that hydrogen-based fuel cell vehicles should be commercialized worldwide. The review findings would also guide academia about various technical features of fuel cell electric vehicles, and they would benefit from recommending more advanced technologies for the coming future. However, the transportation and distribution of hydrogen is another significant challenge, and this is a crucial consideration while transitioning to a hydrogen economy. Investigation into hydrogen fuel vehicles and their utilization in different mobility sectors have been rigorously reviewed. Undeveloped hydrogen technologies have a high implementation cost for proper commercialization, discouraging vehicle manufacturers from adopting the technology.

Nevertheless, a potentially significant advantage in terms of zero-emission to climate has attracted the researchers for its

early development and progress to enhance more widespread. Different nations' governments must coordinate their energy requirements for the future to increase the use of hydrogen as a transportation fuel. Policy and regulatory measures and increased worldwide funding for research and commercialization initiatives would undoubtedly pave the way for taking the first steps toward a hydrogen economy, which guarantees energy security. Hydrogen holds much promise in the transportation industry if the appropriate steps and procedures are taken to make it safe, dependable, and robust.

AUTHOR CONTRIBUTIONS

Writing—Original draft, conceptualization, analysis, visualization and data curation, SC; writing—original draft, visualization, investigation, methodology, SD; resources, supervision and data curation, RE; Writing—original draft, visualization, validation and investigation, AK; Writing—Original draft, visualization, review and editing, DE; review and editing, SM; data curation, PK; review and editing, ZS. All authors have read and agreed to the published version of the manuscript.

REFERENCES

Abdalla, A. M., Hossain, S., Nisfindy, O. B., Azad, A. T., Dawood, M., and Azad, A. K. (2018). Hydrogen Production, Storage, Transportation and Key Challenges with Applications: A Review. *Energy Convers. Manag.* 165, 602–627. doi:10.1016/j.enconman.2018.03.088

Aditiya, H. B., and Aziz, M. (2021). Prospect of Hydrogen Energy in Asia-Pacific: A Perspective Review on Techno-Socio-Economy Nexus. *Int. J. Hydrogen Energy* 46 (Issue 71), 35027–35056. doi:10.1016/j.ijhydene.2021.08.070

Air Liquide Will Build the First High-pressure Hydrogen Refueling Station for Long-haul Trucks (2021). Air Liquide Will Build the First High-Pressure Hydrogen Refueling Station for Long-Haul Trucks in Europe-July 2020. Availableat: https://www.businesswire.com/news/home/20200630005806/en/Air-Liquide-Will-Build-the-First-High-pressure-Hydrogen-Refueling-Station-for-Long-haul-Trucks-in-Europe (Accessed on July 29, 2021).

Andersson, J., and Grönkvist, S. (2019). Large-scale Storage of Hydrogen. *Int. J. Hydrogen Energy* 44 (23), 11901–11919. doi:10.1016/j.ijhydene.2019.03.063

Apostolou, D., Enevoldsen, P., and Xydis, G. (2018). Supporting Green Urban Mobility – the Case of a Small-Scale Autonomous Hydrogen Refuelling Station. *Int. J. Hydrogen Energy* 44 (20), 9675–9689.

Apostolou, D. (2020). Optimization of a Hydrogen Production – Storage – Re-powering System Participating in Electricity and Transportation Markets. A Case Study for Denmark. *Appl. Energy* 265, 114800.

Apostolou, D., and Welcher, S. N. (2021). Prospects of the Hydrogen-Based Mobility in the Private Vehicle Market. A Social Perspective in Denmark. *Int. J. Hydrogen Energy* 46 (9), 6885–6900. doi:10.1016/j.ijhydene.2020.11.167

Apostolou, D., and Xydis, G. (2019). A Literature Review on Hydrogen Refuelling Stations and Infrastructure. Current Status and Future Prospects. *Renew. Sustain. Energy Rev.* 113, 109292. doi:10.1016/j.rser.2019.109292

Arat, H. T., and Sürer, M. G. (2017). State of Art of Hydrogen Usage as a Fuel on Aviation. *Eur. Mech. Sci.* 2 (1), 20–30. doi:10.26701/ems.364286

Articlelanding (2020). Articlelanding. Availableat: https://pubs.rsc.org/en/content/articlelanding/2020/se/c9se01240k.

Ates, F., and Ozcan, H. (2020). Turkey's Industrial Waste Heat Recovery Potential with Power and Hydrogen Conversion Technologies: A Techno-Economic Analysis. *Int. J. Hydrogen Energy*.

Automobiles.Honda (2021). Automobiles.Honda. Available at: https://automobiles.honda.com/clarity-plug-in-hybrid (Accessed on August 28, 2021).

Aziz, M. (2021). Hydrogen Production from Biomasses and Wastes: a Technological Review. *Int. J. Hydrogen Energy* 46, 33756–33781.

Bayrak, Z. U., Kaya, U., and Oksuztepe, E. (2020). Investigation of PEMFC Performance for Cruising Hybrid Powered Fixed-Wing Electric UAV in Different Temperatures. *Int. J. Hydrogen Energy* 45 (11), 7036–7045. doi:10.1016/j.ijhydene.2019.12.214

Bethoux, O. (2020). Hydrogen Fuel Cell Road Vehicles and Their Infrastructure: An Option towards an Environmentally Friendly Energy Transition. *Energies* 13 (22), 6132. doi:10.3390/en13226132

Bhattacharyya, S. C., and Timilsina, G. R. (2010). A Review of Energy System Models. *Int. J. Energy Sect. Manage* 4, 494–518. doi:10.1108/17506221011092742

Bi, Y., Hu, H., Li, Q., and Lu, G. (2010). Efficient Generation of Hydrogen from Biomass without Carbon Monoxide at Room Temperature - Formaldehyde to Hydrogen Catalyzed by Ag Nanocrystals. *Int. J. Hydrogen Energy* 35 (13), 7177–7182. doi:10.1016/j.ijhydene.2009.12.142

Bicer, Y., and Dincer, I. (2017). Comparative Life Cycle Assessment of Hydrogen, Methanol and Electric Vehicles from Well to Wheel. *Int. J. Hydrogen Energy* 42 (6), 3767–3777. doi:10.1016/j.ijhydene.2016.07.252

Bicer, Y., and Khalid, F. (2020). Life Cycle Environmental Impact Comparison of Solid Oxide Fuel Cells Fueled by Natural Gas, Hydrogen, Ammonia and Methanol for Combined Heat and Power Generation. *Int. J. Hydrogen Energy* 45 (5), 3670–3685. doi:10.1016/j.ijhydene.2018.11.122

Biresselioglu, M. E., Demirbag Kaplan, M., and Yilmaz, B. K. (2018). Electric Mobility in Europe: A Comprehensive Review of Motivators and Barriers in Decision Making Processes. *Transp. Res. Part A Policy Pract.* 109, 1–13. doi:10.1016/j.tra.2018.01.017

Boretti, A. (2020). Production of Hydrogen for Export from Wind and Solar Energy, Natural Gas, and Coal in Australia. *Int. J. Hydrogen Energy* 45, 3899–3904. doi:10.1016/j.ijhydene.2019.12.080

Cao, L., Yu, I. K. M., Xiong, X., Tsang, D. C. W., Zhang, S., Clark, J. H., et al. (2020). Biorenewable Hydrogen Production through Biomass Gasification: A Review and Future Prospects. *Environ. Res.* 186, 109547. doi:10.1016/j.envres.2020.109547

Cecere, D., Giacomazzi, E., and Ingenito, A. (2014). A Review on Hydrogen Industrial Aerospace Applications. *Int. J. Hydrogen Energy* 39 (20), 10731–10747. doi:10.1016/j.ijhydene.2014.04.126

Chang, X., Ma, T., and Wu, R. (2019). Impact of Urban Development on Residents' Public Transportation Travel Energy Consumption in China: An Analysis of Hydrogen Fuel Cell Vehicles Alternatives. *Int. J. Hydrogen Energy* 44 (30), 16015–16027. doi:10.1016/j.ijhydene.2018.09.099

Chen, K., Laghrouche, S., and Djerdir, A. (2019). Degradation Model of Proton Exchange Membrane Fuel Cell Based on a Novel Hybrid Method. *Appl. Energy* 252 (113439), 113439. doi:10.1016/j.apenergy.2019.113439

Chen, Y., and Melaina, M. (2019). Model-based Techno-Economic Evaluation of Fuel Cell Vehicles Considering Technology Uncertainties. *Transp. Res. Part D Transp. Environ.* 74, 234–244. doi:10.1016/j.trd.2019.08.002

Chi, J., and Yu, H. (2018). Water Electrolysis Based on Renewable Energy for Hydrogen Production. *Chin. J. Catal.* 39 (3Mar), 390–394. doi:10.1016/s1872-2067(17)62949-8

Chng, S. (2021). Advancing Behavioural Theories in Sustainable Mobility: A Research Agenda. *Urban Sci.* 5 (2), 43. doi:10.3390/urbansci5020043

Chopinet, J. N., Lassoudie` re, F., Fiorentino, C., Alliot, P., Guedron, S., Supie´, P., et al. (2011). Results of the Vulcain X Technological Demonstration. *62nd Int. Astronaut. Congr.* 8, 6289–6298.

Climate-Change-Atmospheric-Carbon-Dioxide (2021). Climate-Change-Atmospheric-Carbon-Dioxide. Available at: https://www.climate.gov/news-features/understanding-climate/climate-change-atmospheric-carbon-dioxidehttps://www.noaa.gov/ (Accessed on May 30, 2021).

Committee on Air Force and Department of Defense Aerospace Propulsion Needs (2006). *A Review of United States Air Force and Department of Defense Aerospace Propulsion Needs*. Washington, DC: The National Academies Press. 9780309102476. doi:10.17226/11780

Concawe and JRC (2007). *Well-to-Wheels Analysis of Future Automotive Fuels and Power Trains in the European Context, Well-To-Wheels Report*. Luxembourg: Publications Office of the European Union, 44.

Concept Consulting Group (2021). Hydrogen in New Zealand Report 2—Analysis. Availableat: http://www.concept.co.nz/uploads/2/5/5/4/25542442/h2_report2_analysis_v4.pdf (Accessed on July 28, 2021).

Cormos, C.-C. (2012). Hydrogen and Power Co-generation Based on Coal and Biomass/solid Wastes Co-gasification with Carbon Capture and Storage. *Int. J. Hydrogen Energy* 37 (7), 5637–5648. doi:10.1016/j.ijhydene.2011.12.132

Dale Reed, R., and Lister, D. (2011). *Wingless Flight: The Lifting Body storyNASA History Series SP-4220*. Washington, DC: Books Express Publishing.

Dawood, F., Anda, M., and Shafiullah, G. M. (2020). Hydrogen Production for Energy: An Overview. *Int. J. Hydrogen Energy* 45 (7), 3847–3869. doi:10.1016/j.ijhydene.2019.12.059

Dawson, V. P. (2004). *Taming Liquid Hydrogen: The Centaur Upper Stage Rocket1958-2002*. NASA-SP-2004-4230.

de Miranda, P. E. V., Carreira, E. S., Icardi, U. A., and Nunes, G. S. (2017). Brazilian Hybrid Electric-Hydrogen Fuel Cell Bus: Improved On-Board Energy Management System. *Int. J. Hydrogen Energy* 42 (19), 13949–13959. doi:10.1016/j.ijhydene.2016.12.155

de-Troya, J. J., Álvarez, C., Fernández-Garrido, C., and Carral, L. (2016). Analysing the Possibilities of Using Fuel Cells in Ships. *Int. J. Hydrogen Energy* 41 (4), 2853–2866. doi:10.1016/j.ijhydene.2015.11.145

Demirci, U. B., and Miele, P. (2009). Sodium Borohydride versus Ammonia Borane, in Hydrogen Storage and Direct Fuel Cell Applications. *Energy Environ. Sci.Energy Environ. Sci.* 2, 627. doi:10.1039/b900595a

Dickel, R. (2020). Blue Hydrogen As an Enabler Of Green Hydrogen: The Case Of Germany; *OIES Paper*. Oxford, UK: The Oxford Institute for Energy Studies.

Dincer, I. (2020). Covid-19 Coronavirus: Closing Carbon Age, but Opening Hydrogen Age. *Int. J. Energy Res.* 44 (8), 6093–6097. doi:10.1002/er.5569

Ding, Z., Jiang, X., Liu, Z., Long, R., Xu, Z., and Cao, Q. (2018). Factors Affecting Low-Carbon Consumption Behavior of Urban Residents: A Comprehensive Review. *Resour. Conservation Recycl.* 132, 3–15. doi:10.1016/j.resconrec.2018.01.013

Diva-Portal (2022). *Techno-economic Study of Hydrogen as a Heavy-Duty Truck Fuel A Case Study on the Transport, Corridor Oslo – Trondheim*. Available at: https://kth.diva-portal.org/smash/get/diva2:1372698/FULLTEXT01.pdf (Accessed on 04 03, 2022).

Domashenko, A. (2002). Production, Storage and Transportation of Liquid Hydrogen. Experience of Infrastructure Development and Operation. *Int. J. Hydrogen Energy* 27 (7–8), 753–755. doi:10.1016/s0360-3199(01)00152-5

Dudek, M., Lis, B., Raźniak, A., Krauz, M., and Kawalec, M. (2021). Selected Aspects of Designing Modular PEMFC Stacks as Power Sources for Unmanned Aerial Vehicles. *Appl. Sci.* 11 (2), 675. doi:10.3390/app11020675

Eberle, U., von Helmolt, R., Stolten, P. D., Samsun, D. R. C., and Garland, D. N. (2016). "GM HydroGen4 - A Fuel Cell Electric Vehicle Based on the Chevrolet Equinox," in *Fuel Cells : Data, Facts and Figures*, 75–86. doi:10.1002/9783527693924.ch08

Edwards, P. P., Kuznetsov, V. L., David, W. I. F., and Brandon, N. P. (2008). Hydrogen and Fuel Cells: Towards a Sustainable Energy Future. *Energy Policy* 36 (12), 4356–4362. doi:10.1016/j.enpol.2008.09.036

El-Taweel, N. A., Khani, H., and Farag, H. E. Z. (2019). Hydrogen Storage Optimal Scheduling for Fuel Supply and Capacity-Based Demand Response Program under Dynamic Hydrogen Pricing. *IEEE Trans. Smart Grid* 10 (4), 4531–4542. doi:10.1109/tsg.2018.2863247

Energy.Gov (2021). Energy.Gov. Available at: https://afdc.energy.gov/vehicles/fuel_cell.html (Accessed on August 29, 2021).

Engel, R. (2012). Tomorrow's Energy: Hydrogen, Fuel Cells, and the Prospects for a Cleaner Planet. *Int. J. Hydrogen Energy* 37 (21), 16264. doi:10.1016/j.ijhydene.2012.08.018

Environment Hydrogen-Fuel-Cell (2021). Environment Hydrogen-Fuel-Cell. Available at: https://www.hyundai.co.uk/about-us/environment/hydrogen-fuel-cell (Accessed on August 27, 2021).

European Commission (2020). *European Commission on Hydrogen Energy Strategy*. Paris: European Commission.

Falcone, P. M., Hiete, M., and Sapio, A. (2021). Hydrogen Economy and Sustainable Development Goals: Review and Policy Insights. *Curr. Opin. Green Sustain. Chem.* 31 (100506), 100506. doi:10.1016/j.cogsc.2021.100506

Ferrero, F., Perboli, G., Rosano, M., and Vesco, A. (2018). Car-sharing Services: An Annotated Review. *Sustain. Cities Soc.* 37, 501–518. doi:10.1016/j.scs.2017.09.020

Foorginezhad, .S. (2021). Sensing Advancement towards Safety Assessment of Hydrogen Fuel Cell Vehicles. *J. Power Sources* 489, 229450. doi:10.1016/j.jpowsour.2021.229450

Forsberg, C. W. (2005). *Hydrogen Markets: Implications for Hydrogen Production Technologies International Journal of Hydrogen Energy (DE-AC05-00OR22725)*. Oak Ridge, TN, United States: Oak Ridge National Laboratory. Available at: http://www.intpowertechcorp.com/122902.pdf (Accessed on August 29, 2021).

Frenette, G., and Forthoffer, D. (2009). Economic & Commercial Viability of Hydrogen Fuel Cell Vehicles from an Automotive Manufacturer Perspective. *Int. J. Hydrogen Energy* 34 (9), 3578–3588. doi:10.1016/j.ijhydene.2009.02.072

Galich, A., and Marz, L. (2012). Alternative Energy Technologies as a Cultural Endeavor: a Case Study of Hydrogen and Fuel Cell Development in Germany. *Energ Sustain Soc.* 2 (1), 2. doi:10.1186/2192-0567-2-2

Gao, Y., Xiong, T., Li, Y., Huang, Y., Li, Y., and Balogun, M.-S. J. T. (2019). A Simple and Scalable Approach to Remarkably Boost the Overall Water Splitting Activity of Stainless Steel Electrocatalysts. *ACS Omega* 4 (14), 16130–16138. doi:10.1021/acsomega.9b02315

García-Gusano, D., Martín-Gamboa, M., Iribarren, D., and Dufour, J. (2016). Prospective Analysis of Life-Cycle Indicators through Endogenous Integration into a National Power Generation Model. *Resources* 5, 39. doi:10.3390/resources5040039

García-Melero, G., Sainz-González, R., Coto-Millán, P., and Valencia-Vásquez, A. (2021). Sustainable Mobility Policy Analysis Using Hybrid Choice Models: Is it the Right Choice? *Sustainability* 13 (5), 2993. doi:10.3390/su13052993

Gas World Portal (2018). Hydrogen Car-Sharing System. Available at: https://www.gasworld.com/linde-to-close-worlds-first-fuel-cell-car-sharingservice/2014327.article (Accessed on 04 04, 2021).

Giacoppo, G., Barbera, O., Briguglio, N., Cipitì, F., Ferraro, M., Brunaccini, G., et al. (2017). Thermal Study of a SOFC System Integration in a Fuselage of a Hybrid Electric Mini UAV. *Int. J. Hydrogen Energy* 42 (46), 28022–28033. doi:10.1016/j.ijhydene.2017.09.063

Global-Energy-Related-Co2-Emissions (2021). Global-Energy-Related-Co2-Emissions. Availableat: https://www.iea.org/data-and-statistics/charts/global-energy-related-co2-emissions-by-sector (Accessed on June 15, 2021).

Global-Greenhouse-Gas-Emissions-Data (2021). Global-Greenhouse-Gas-Emissions-Data. Availableat: https://www.epa.gov/ghgemissions/global-greenhouse-gas-emissions-data (accessed on May 25, 2021).

Global.Honda (2021). Global.Honda. Available at: https://global.honda/heritage/timeline/product-history/automobiles/2001FCX-V4.html (accessed on August 28, 2021).

Gonzalez Aregall, M., Bergqvist, R., and Monios, J. (2018). A Global Review of the Hinterland Dimension of Green Port Strategies. *Transp. Res. Part D Transp. Environ.* 59, 23–34. doi:10.1016/j.trd.2017.12.013

Graetz, J. (2012). Metastable Metal Hydrides for Hydrogen Storage. *ISRN Mater. Sci.* 8. doi:10.5402/2012/863025

Han, W. (2014). Demonstrations and Marketing Strategies of Hydrogen Fuel Cell Vehicles in China. *Int. J. Hydrogen Energy* 39, 13859–13872.

Health-Topics (2021). Health-Topics. Availableat: https://www.who.int/health-topics/air-pollution#tab=tab_1 (Accessed on June 4, 2021).

Holden, E., Gilpin, G., and Banister, D. (2019). Sustainable Mobility at Thirty. *Sustainability* 11 (7), 1965.

Hu, Y., Huang, D., Zhang, J., Huang, Y., Balogun, M. S. J. T., and Tong, Y. (2019). Dual Doping Induced Interfacial Engineering of Fe 2 N/Fe 3 N Hybrids with Favorable d-Band towards Efficient Overall Water Splitting. *ChemCatChem* 11 (24), 6051–6060. doi:10.1002/cctc.201901224

Huang, Y., Hu, L., Liu, R., Hu, Y., Xiong, T., Qiu, W., et al. (2019). Nitrogen Treatment Generates Tunable Nanohybridization of Ni5P4 Nanosheets with Nickel Hydr(oxy)oxides for Efficient Hydrogen Production in Alkaline, Seawater and Acidic Media. *Appl. Catal. B Environ.* 251 (Aug), 181–194. doi:10.1016/j.apcatb.2019.03.037

Huang, Z., Shen, J., Chan, S. H., and Tu, Z. (2020). Transient Response of Performance in a Proton Exchange Membrane Fuel Cell under Dynamic Loading. *Energy Convers. Manag.* 226 (113492), 113492. doi:10.1016/j.enconman.2020.113492

Hui, J., Xiao, Z., Liejin, G., Chao, Z., Changqing, C., and Zhenqun, W. (2017). Experimental Investigation on Methanation Reaction Based on Coal Gasification in Supercritical Water. *Int. J. Hydrogen Energy* 42 (7), 4636–4641. doi:10.1016/j.ijhydene.2016.06.216

Hydrogen Storage (2021). Hydrogen and Fuel Cell Technologies Office. Availableat: https://www.energy.gov/e ere/fuecells/ hydro gen-storage (Accessed on August 20, 2021).

Hydrogen-Production-By-Electrolysis-Ann-Cornell (2017). Hydrogen-Production-By-Electrolysis-Ann-Cornell. Availableat: https://energiforskmedia.blob.core.windows.net/media/23562/5-hydrogen-production-by-electrolysis-ann-cornell-kth.pdf.

Hydrogen-Production-Through-Electrolysis (1927). Hydrogen-Production-Through-Electrolysis. Availableat: https://www.h2bulletin.com/knowledge/hydrogen-production-through-electrolysis/.

Hydrogen-Production-Through-Electrolysis (2017). Progress and Prospects of Hydrogen Production: Opportunities and Challenges. Availableat: https://www.h2bulletin.com/knowledge/hydrogen-production-through-electrolysis/.

Hydrogencarsnow (2021). Hydrogencarsnow. Available at: https://www.hydrogencarsnow.com/index.php/ford-focus-fcv/ (Accessed on August 28, 2021).

Hype (2019). Hydrogen Taxi Operator. available at: https://hype.taxi/ (accessed on 04 04, 2022).

Hyundai (2021). Hyundai. Availableat: https://www.hyundai.com/worldwide/en/eco/nexo/technology (Accessed on August 25, 2021).

Ijaodola, O. S., El- Hassan, Z., Ogungbemi, E., Khatib, F. N., Wilberforce, T., Thompson, J., et al. (2019). Energy Efficiency Improvements by Investigating the Water Flooding Management on Proton Exchange Membrane Fuel Cell (PEMFC). *Energy* 179, 246–267. doi:10.1016/j.energy.2019.04.074

IMO (2012b). *Guidelines for the Development of a Ship Energy Efficiency Management Plan (SEEMP); Resolution MEPC.213*. London, UK: IMO.

IMO (2012a). *Guidelines on the Method of Calculation of the Attained Energy Efficiency Design Index (EEDI) for New Ships; Resolution MEPC.212*. London, UK: IMO.

Ivanenko, A. (2020). A Look at the Colors of Hydrogen that Could Power Our Future. *Forbes*. Availableat: https://www.forbes.com/sites/forbestechcouncil/2020/08/31/a-look-at-the-colors-of-hydrogen-that-could-power-our-future/?sh=3edf9d6e5e91 (accessed on December 30, 2020).

Jhunjhunwala, A., Kaur, P., and Mutagekar, S. (2018). Electric Vehicles in India: A Novel Approach to Scale Electrification. *IEEE Electrific. Mag.* 6 (4), 40–47. doi:10.1109/mele.2018.2871278

Jiang, W., Jiao, X., and Chen, D. (2013). Photocatalytic Water Splitting of Surfactant-free Fabricated High Surface Area NaTaO3 Nanocrystals. *Int. J. Hydrogen Energy* 38 (29), 12739–12746. doi:10.1016/j.ijhydene.2013.07.072

Jovan, D. J., and Dolanc, G. (2020). Can Green Hydrogen Production Be Economically Viable under Current Market Conditions. *Energies* 13, 6599. doi:10.3390/en13246599

Kandidayeni, M., Macias, A., Khalatbarisoltani, A., Boulon, L., and Kelouwani, S. (2019). Benchmark of Proton Exchange Membrane Fuel Cell Parameters Extraction with Metaheuristic Optimization Algorithms. *Energy* 183, 912–925. doi:10.1016/j.energy.2019.06.152

Kaur, A., Gangacharyulu, D., and Bajpai, P. K. (2016). Catalytic Hydrogen Generation from $NaBH_4/H_2O$ System: Effects of Catalyst and Promoters. *Braz. J. Chem. Eng.* 35, 131.

Kaur, A., Gangacharyulu, d., and Bajpai, p. K. (2019). Kinetic Studies of Hydrolysis Reaction of Nabh4 with Γ-Al2o3 Nanoparticles as Catalyst Promoter and Cocl2 as Catalyst. *Braz. J. Chem. Eng.* 36, 929–939. doi:10.1590/0104-6632.20190362s20180290

Klanchar, M., Hughes, T. G., and Gruber, P. (2004). "Attaining DOE Hydrogen Storage Goals with Chemical Hydrides," in 15th Hydrogen Annual Conference (Washington D. C: National Hydrogen Association).

Klecha, L., and Gianni, F. (2018). "Designing for Sustainable Urban Mobility Behaviour: A Systematic Review of the Literature," in *Citizen, Territory and Technologies: Smart Learning Contexts and Practices* (Cham: Springer International Publishing), 137–149. doi:10.1007/978-3-319-61322-2_14

Korpas, M., and Gjengedal, T. (2006). "Opportunities for Hydrogen Storage in Connection with Stochastic Distributed Generation," in 2006 International Conference on Probabilistic Methods Applied to Power Systems. doi:10.1109/pmaps.2006.360255

Kumar, R. R., and Alok, K. (2020). Adoption of Electric Vehicle: A Literature Review and Prospects for Sustainability. *J. Clean. Prod.* 253, 119911.

Le Quéré, C., Jackson, R. B., Jones, M. W., Smith, A. J. P., Abernethy, S., Andrew, R. M., et al. (2020). Temporary Reduction in Daily Global CO2 Emissions during the COVID-19 Forced Confinement. *Nat. Clim. Chang.* 10 (7), 647–653. doi:10.1038/s41558-020-0797-x

Lee, D.-Y., Elgowainy, A., Kotz, A., Vijayagopal, R., and Marcinkoski, J. (2018). Life-cycle Implications of Hydrogen Fuel Cell Electric Vehicle Technology for Medium- and Heavy-Duty Trucks. *J. Power Sources* 393, 217–229. doi:10.1016/j.jpowsour.2018.05.012

Lee, D.-Y., Elgowainy, A., and Vijayagopal, R. (2019). Well-to-wheel Environmental Implications of Fuel Economy Targets for Hydrogen Fuel Cell Electric Buses in the United States. *Energy Policy* 128, 565–583. doi:10.1016/j.enpol.2019.01.021

Lele, A. (2006). *GSLV-D5 Success: A Major Booster to India's Space Program*. The space review. Available at: https://www.thespacereview.com/article/2428/1

Leo, T. J., Durango, J. A., and Navarro, E. (2010). Exergy Analysis of PEM Fuel Cells for Marine Applications. *Energy* 35 (2), 1164–1171. doi:10.1016/j.energy.2009.06.010

Letnik, T., Marksel, M., Luppino, G., Bardi, A., and Božičnik, S. (2018). Review of Policies and Measures for Sustainable and Energy Efficient Urban Transport. *Energy* 163, 245–257. doi:10.1016/j.energy.2018.08.096

Li, Q., Yang, H., Han, Y., Li, M., and Chen, W. (2016). A State Machine Strategy Based on Droop Control for an Energy Management System of PEMFC-Battery-Supercapacitor Hybrid Tramway. *Int. J. Hydrogen Energy* 41 (36), 16148–16159. doi:10.1016/j.ijhydene.2016.04.254

Li, Y., Guo, L., Zhang, X., Jin, H., and Lu, Y. (2010). Hydrogen Production from Coal Gasification in Supercritical Water with a Continuous Flowing System. *Int. J. Hydrogen Energy* 35 (7), 3036–3045. doi:10.1016/j.ijhydene.2009.07.023

Li, Y., Pei, P., Ma, Z., Ren, P., and Huang, H. (2020). Analysis of Air Compression, Progress of Compressor and Control for Optimal Energy Efficiency in Proton Exchange Membrane Fuel Cell. *Renew. Sustain. Energy Rev.* 133 (110304), 110304. doi:10.1016/j.rser.2020.110304

Lin, Z., Dong, J., and Greene, D. L. (2013). Hydrogen Vehicles: Impacts of DOE Technical Targets on Market Acceptance and Societal Benefits. *Int. J. Hydrogen Energy* 38 (19), 7973–7985. doi:10.1016/j.ijhydene.2013.04.120

Liu, J., and Zhong, F. (2019). Current Situation and Prospect of Hydrogen Energy Development in China. *China Energy* 41 (02), 32–36.

Liu, Y., Liu, R., and Jiang, X. (2019). What Drives Low-Carbon Consumption Behavior of Chinese College Students? the Regulation of Situational Factors. *Nat. Hazards (Dordr.)* 95 (1–2), 173–191. doi:10.1007/s11069-018-3497-3

López, C., Ruíz-Benítez, R., and Vargas-Machuca, C. (2019). On the Environmental and Social Sustainability of Technological Innovations in Urban Bus Transport: The EU Case. *Sustainability* 11 (5), 1413. doi:10.3390/su11051413

Lototskyy, M. V., Tolj, I., Pickering, L., Sita, C., Barbir, F., and Yartys, V. (2017). The Use of Metal Hydrides in Fuel Cell Applications. *Prog. Nat. Sci. Mater. Int.* 27 (1), 3–20. doi:10.1016/j.pnsc.2017.01.008

Low, J., Haszeldine, R. S., and Mouli-Castillo, J. (2020). *Comparative Evaluation of Battery Electric and Hydrogen Fuel Cell Electric Vehicles for Zero Carbon Emissions Road Vehicle Fuel in Scotland*. engrXiv.

Luo, Z., Hu, Y., Xu, H., Gao, D., and Li, W. (2020). Cost-Economic Analysis of Hydrogen for China's Fuel Cell Transportation Field. *Energies* 13, 6522. doi:10.3390/en13246522

Macher, J., Hausberger, A., Macher, A. E., Morak, M., and Schrittesser, B. (2021). Critical Review of Models for H2-Permeation through Polymers with Focus on the Differential Pressure Method. *Int. J. Hydrogen Energy* 46 (43), 22574–22590. doi:10.1016/j.ijhydene.2021.04.095

Manish Shakdwipee, R. B. (2006). *Techno-economic Assessment of Fuel Cell Vehicles for India WHEC 16 – Lyon France June*, 13–16.

Manna, J., Prakash, J., Sarkhel, R., Banerjee, C., Tripathi, A. K., and Nouni, M. R. (2021). Opportunities for Green Hydrogen Production in Petroleum Refining and Ammonia Synthesis Industries in India. *Int. J. Hydrogen Energy*. doi:10.1016/j.ijhydene.2021.09.064

Mari, V., Kristin, J., and Rahul, A. (2016). Hydrogen Production with CO_2 Capture. *Int. J. Hydrog. Energy* 41, 4969–4992.

Marrero-Alfonso, E. Y., Beaird, A. M., Davis, T. A., and Matthews, M. A. (2009). Hydrogen Generation from Chemical Hydrides. *Ind. Eng. Chem. Res.* 48, 3703–3712. doi:10.1021/ie8016225

Martínez-Díaz, M., Soriguera, F., and Pérez, I. (2019). Autonomous Driving: a Bird's Eye View. *IET Intell. Transp. Syst.* 13 (4), 563–579.

Matsunaga, M., Fukushima, T., and Ojima, K. (2009). Powertrain System of Honda FCX Clarity Fuel Cell Vehicle. *Wevj* 3 (4), 820–829. doi:10.3390/wevj3040820

Matulić, N., Radica, G., Barbir, F., and Nižetić, S. (2019). Commercial Vehicle Auxiliary Loads Powered by PEM Fuel Cell. *Int. J. Hydrogen Energy* 44 (20), 10082–10090.

Mayrhofer, M., Koller, M., Seemann, P., Prieler, R., and Hochenauer, C. (2021). Assessment of Natural Gas/hydrogen Blends as an Alternative Fuel for Industrial Heat Treatment Furnaces. *Int. J. Hydrogen Energy* 46 (41), 21672–21686. doi:10.1016/j.ijhydene.2021.03.228

Mayyas, A. R., Ramani, D., Kannan, A. M., Hsu, K., Mayyas, A., and Schwenn, T. (2014). Cooling Strategy for Effective Automotive Power Trains: 3D Thermal Modeling and Multi-Faceted Approach for Integrating Thermoelectric Modules into Proton Exchange Membrane Fuel Cell Stack. *Int. J. Hydrogen Energy* 39 (30), 17327–17335. doi:10.1016/j.ijhydene.2014.08.034

Mbie, A. (2019). Vision for Hydrogen in New Zealand. Energy Strategies for New Zealand. Availableat: https://www.mbie.govt.nz/building-and-energy/energy-and-natural-resources/energy-strategies-for-new-zealand/ (Accessed on August 19, 2021).

Meng, X., Gu, A., Wu, X., Zhou, L., Zhou, J., Liu, B., et al. (2021). Status Quo of China Hydrogen Strategy in the Field of Transportation and International Comparisons. *Int. J. Hydrogen Energy* 46 (57), 28887–28899. doi:10.1016/j.ijhydene.2020.11.049

Meraj, S. T., Yahaya, N. Z., Singh, B. S. M., and Kannan, R. (2020). Implementation of A Robust Hydrogen-Based Grid System to Enhance Power Quality. *Int. Conf. Power Energy Conf.*, 153–158. doi:10.1109/pecon48942.2020.9314536

Mercedes-Benz (2021). Mercedes-benz. Availableat: https://www.mercedes-benz.com/en/vehicles/passenger-cars/glc/the-new-glc-f-cell/ (Accessed on August 28, 2021).

Mercedes-Benz-Cars (2021). Mercedes-Benz-Cars. Availableat: https://www.mercedes-benz.co.in/passengercars/mercedes-benz-cars/models/a-class/sedan-v177/explore.html (Accessed on August 28, 2021).

Morel, J., Obara, S., Sato, K., Mikawa, D., Watanabe, H., and Tanaka, T. (2015). "Contribution of a Hydrogen Storage-Transportation System to the Frequency Regulation of a Microgrid," in 2015 International Conference on Renewable Energy Research and Applications (Palermo: ICRERA). doi:10.1109/icrera.2015.7418465

Muir, S. S., and Yao, X. (2011). Progress in Sodium Borohydride as a Hydrogen Storage Material: Development of Hydrolysis Catalysts and Reaction Systems. *Int. J. Hydrogen Energy* 36, 5983–5997. doi:10.1016/j.ijhydene.2011.02.032

Navas-Anguita, Z., García-Gusano, D., and Dufour, J. (2020). Diego Iribarren, Prospective Techno-Economic and Environmental Assessment of a National Hydrogen Production Mix for Road Transport. *Appl. Energy* 259, 114121. doi:10.1016/j.apenergy.2019.114121

Negoro, N. (2007). "Next Booster Engine LE-X in japan," in 43rd AIAA/ASME/SAE/ASEE Joint Propulsion (Conference & Exhibit), Cincinnati, OH. doi:10.2514/6.2007-5490

Nissan-Global (2021). Nissan-Global. Availableat: https://www.nissan-global.com/EN/TECHNOLOGY/OVERVIEW/fcv.html (Accessed on August 28, 2021).

Noussan, M., Raimondi, P. P., Scita, R., and Hafner, M. (2021). The Role of Green and Blue Hydrogen in the Energy Transition—A Technological and Geopolitical Perspective. *Sustainability* 13, 298. doi:10.3390/su13010298

Ogungbemi, E., Wilberforce, T., Ijaodola, O., Thompson, J., and Olabi, A. G. (2021). Selection of Proton Exchange Membrane Fuel Cell for Transportation. *Int. J. Hydrogen Energy* 46 (59), 30625–30640. doi:10.1016/j.ijhydene.2020.06.147

Okolie, J. A., Patra, B. R., Mukherjee, A., Nanda, S., Dalai, A. K., and Kozinski, J. A. (2021). Futuristic Applications of Hydrogen in Energy, Biorefining, Aerospace, Pharmaceuticals and Metallurgy. *Int. J. Hydrogen Energy* 46 (13), 8885–8905. doi:10.1016/j.ijhydene.2021.01.014

Olabi, A. G., Wilberforce, T., and Abdelkareem, M. A. (2021). Fuel Cell Application in the Automotive Industry and Future Perspective. *Energy* 214, 118955.

Oliveira, G. D., and Dias, L. C. (2020). The Potential Learning Effect of a MCDA Approach on Consumer Preferences for Alternative Fuel Vehicles. *Ann. Oper. Res.* 293 (2), 767–787. doi:10.1007/s10479-020-03584-x

Özcan, A., and Garip, M. T. (2020). Development of a Simple and Efficient Method to Prepare a Platinum-Loaded Carbon Electrode for Methanol Electrooxidation. *Int. J. Hydrogen Energy* 45 (35), 17858–17868. doi:10.1016/j.ijhydene.2020.04.230

Perdikaris, N., Panopoulos, K. D., Hofmann, P., Spyrakis, S., and Kakaras, E. (2010). Design and Exergetic Analysis of a Novel Carbon Free Tri-generation System for Hydrogen, Power and Heat Production from Natural Gas, Based on Combined Solid Oxide Fuel and Electrolyser Cells. *Int. J. Hydrogen Energy* 35 (6), 2446–2456. doi:10.1016/j.ijhydene.2009.07.084

Perez, R. J., Brent, A. C., and Hinkley, J. (2021). Assessment of the Potential for Green Hydrogen Fuelling of Very Heavy Vehicles in New Zealand. *Energies* 14 (9), 2636. doi:10.3390/en14092636

Pojani, D., and Stead, D. (2018). Policy Design for Sustainable Urban Transport in the Global South. *Policy Des. Pract.* 1 (2), 90–102. doi:10.1080/25741292.2018.1454291

Polish Electromobility Act (2018). Polish Electromobility Act. Available at: http://prawo.sejm.gov.pl/isap.nsf/download.xsp/WDU20180000317/T/D20180317L.pdf (Accessed on 04 04, 2022).

Power-Technology (2022). Power-Technology. Available at: https://www.power-technology.com/comment/green-hydrogen-india-energy-security/ (Accessed on 04 05, 2022).

Ren, P., Pei, P., Li, Y., Wu, Z., Chen, D., and Huang, S. (2020). Degradation Mechanisms of Proton Exchange Membrane Fuel Cell under Typical Automotive Operating Conditions, *Prog. Energy Combust. Sci.* 80, 100859.

Rabiee, A., Keane, A., and Soroudi, A. (2021). Green Hydrogen: A New Flexibility Source for Security Constrained Scheduling of Power Systems with Renewable Energies. *Int. J. Hydrogen Energy* 46. doi:10.1016/j.ijhydene.2021.03.080

Ranieri, L., Digiesi, S., Silvestri, B., and Roccotelli, M. (2018). A Review of Last Mile Logistics Innovations in an Externalities Cost Reduction Vision. *Sustainability* 10 (3), 782. doi:10.3390/su10030782

Ransformative-Mobility (2021). Ransformative-Mobility. Availableat: https://www.transformative-mobility.org/publications/benefits-of-sustainable-mobility (Accessed on August 15, 2021).

Rao, M. K., Sridhara Murthi, K. R., and Prasad, M. Y. S. (2019). The Decision for Indian Human Spaceflight Programme-Political Perspectives, National Relevance, and Technological Challenges. *New Space* 7 (2), 99–109. doi:10.1089/space.2018.0028

Rao, Y., Shao, Z., Ahangarnejad, A. H., Gholamalizadeh, E., and Sobhani, B. (2019). Shark Smell Optimizer Applied to Identify the Optimal Parameters of the Proton Exchange Membrane Fuel Cell Model. *Energy Convers. Manag.* 182, 1–8. doi:10.1016/j.enconman.2018.12.057

Reddy, S. N., Nanda, S., Vo, D.-V. N., Nguyen, T. D., Nguyen, V.-H., Abdullah, B., et al. (2020). "Hydrogen: Fuel of the Near Future," in *New Dimensions in Production and Utilization of Hydrogen* (Elsevier), 1–20. doi:10.1016/b978-0-12-819553-6.00001-5

Ren, R., Hu, W., Dong, J., Sun, B., Chen, Y., and Chen, Z. (2019). A Systematic Literature Review of Green and Sustainable Logistics: Bibliometric Analysis, Research Trend and Knowledge Taxonomy. *Ijerph* 17 (1), 261. doi:10.3390/ijerph17010261

Roadmap to a Single European Transport Area-Towards a competitive and resource efficient transport system (2021). Roadmap to a Single European Transport Area-Towards a Competitive and Resource Efficient Transport System. Available online: http://eur-lex.europa.eu/legal-content/EN/TXT/?uri=URISERV:tr0054 (Accessed on June 20, 2021).

Rohith, P. K., Priolkar, J., and Kunkolienkar, G. R. (2016). "Hydrogen: An Innovative and Alternative Energy for the Future," in 2016 World Conference on Futuristic Trends in Research and Innovation for Social Welfare(Coimbatore: Startup Conclave). doi:10.1109/startup.2016.7583905

Rolandgumpert (2021). Rolandgumpert. Available at: https://www.rolandgumpert.com/en/ (Accessed on August 28, 2021).

Sakintuna, B., Lamaridarkrim, F., and Hirscher, M. (2007). Metal Hydride Materials for Solid Hydrogen Storage: A Review☆. *Int. J. Hydrogen Energy* 32, 1121–1140. doi:10.1016/j.ijhydene.2006.11.022

Saleem, M. A., Eagle, L., and Low, D. (2021). Determinants of Eco-Socially Conscious Consumer Behavior toward Alternative Fuel Vehicles. *Jcm* 38 (2), 211–228. doi:10.1108/jcm-05-2019-3208

Santos, G. (2018). Sustainability and Shared Mobility Models. *Sustainability* 10 (9), 3194. doi:10.3390/su10093194

Sapru, K. (2002). "Development of a Small Scale Hydrogen Production-Storage System of Hydrogen Applications," in IECEC-97 Proceedings of the Thirty-Second Intersociety Energy Conversion Engineering Conference (Cat (No.97CH6203), Honolulu, HI.

Sattler, G. (2000). Fuel Cells Going Onboard. *J. Power Sources* 86 (1–2), 61–67. doi:10.1016/s0378-7753(99)00414-0

Schiro, F., Stoppato, A., and Benato, A. (2020). Modelling and Analyzing the Impact of Hydrogen Enriched Natural Gas on Domestic Gas Boilers in a Decarbonization Perspective. *Carbon Resour. Convers.* 3, 122–129. doi:10.1016/j.crcon.2020.08.001

Sekigawa, E., and Mecham, M. (1996). Mitsubishi Advances LE-5 Design as H2 Goes Commercial. *Aviat. Week Space Technol.* 145, 3.

Sergeant., N., Boureima., F.-S., Matheys., J., Timmermans., J.-M., and Van Mierlo., J. (2009). An Environmental Analysis of FCEV and H2-ICE Vehicles Using the Ecoscore Methodology. *World Electr. Veh. J.* 3 (3), 635–646.

Sergienko, A. (1993). Liquid Rocket Engines for Large Thrust: Present and Future. *Acta Astronaut.* 29 (12), 905–909. doi:10.1016/0094-5765(93)90011-k

Shang, Y., and Chen, R. (2006). Semiempirical Hydrogen Generation Model Using Concentrated Sodium Borohydride Solution. *Energy fuels.* 20, 2149–2154. doi:10.1021/ef050380f

Shashikala, K. (1520). Hydrogen Storage Materials. *Funct. Mater.*, 607.

Shusheng, X., Qiujie, S., Baosheng, G., Encong, Z., and Zhankuan, W. (2020). Research and Development of On-Board Hydrogen-Producing Fuel Cell Vehicles. *Int. J. Hydrogen Energy* 45 (35), 17844–17857. doi:10.1016/j.ijhydene.2020.04.236

Solarimpulse (2022). Solarimpulse. Availableat: https://solarimpulse.com/hydrogen-mobility-solutions (Accessed on 04 05, 2022).

Staffell, I., Scamman, D., Velazquez Abad, A., Balcombe, P., Dodds, P. E., Ekins, P., et al. (2019). The Role of Hydrogen and Fuel Cells in the Global Energy System. *Energy Environ. Sci.* 12 (2), 463–491. doi:10.1039/c8ee01157e

Sum4all.org (2021). Sum4all.org. Availableat: https://www.sum4all.org/implementing-sdgs (Accessed on July 28, 2021).

Sun, J., Feng, H., Xu, J., Jin, H., and Guo, L. (2021). Investigation of the Conversion Mechanism for Hydrogen Production by Coal Gasification in Supercritical Water. *Int. J. Hydrogen Energy* 46 (17), 10205–10215. doi:10.1016/j.ijhydene.2020.12.130

Taiebat, M., Brown, A. L., Safford, H. R., Qu, S., and Xu, M. (2018). A Review on Energy, Environmental, and Sustainability Implications of Connected and Automated Vehicles. *Environ. Sci. Technol.* 52 (20), 11449–11465. doi:10.1021/acs.est.8b00127

Tan, Y. H. (2013). Research on Large Thrust Liquid Rocket Engine. *Yuhang Xuebao/J Astronaut.* 34, 1303–1308.

Tanç, B., Arat, H. T., Baltacıoğlu, E., and Aydın, K. (2018). Overview of the Next Quarter Century Vision of Hydrogen Fuel Cell Electric Vehicles. *Int. J. Hydrogen Energy* 44 (20), 10120.

Tanç, B., Arat, H. T., Conker, Ç., Baltacioğlu, E., and Aydin, K. (2020). Energy Distribution Analyses of an Additional Traction Battery on Hydrogen Fuel Cell Hybrid Electric Vehicle. *Int. J. Hydrogen Energy* 45 (49), 26344–26356. doi:10.1016/j.ijhydene.2019.09.241

Tasleem, S., and Tahir, M. (2020). Current Trends in Strategies to Improve Photocatalytic Performance of Perovskites Materials for Solar to Hydrogen Production. *Renew. Sustain. Energy Rev.* 132 (110073), 110073. doi:10.1016/j.rser.2020.110073

Tirachini, A. (2020). Ride-hailing, Travel Behaviour and Sustainable Mobility: an International Review. *Transportation* 47 (4), 2011–2047. doi:10.1007/s11116-019-10070-2

Topler, J. (2017). "Hydrogen Technology and Economy in Germany-History and Present State," in *Hydrogen in an International Context: Vulnerabilities of Hydrogen Energy in Emerging Markets*. Editor I. Lordache (Gistrup, Denmark; Delft, Netherlands: River Publishers), 3–48.

Traction: India to trial fuel cell trainset (2021). Traction: India to Trial Fuel Cell Trainset. Available online: https://www.railwaygazette.com/in-depth/traction-india-to-trial-fuel-cell- trainset/57957.article#:~:text=India's%20hydrogen%20prototype,by%20the%20end%20of%202021 (Accessed on July 2, 2021).

Trencher, G., and Edianto, A. (2021). Drivers and Barriers to the Adoption of Fuel Cell Passenger Vehicles and Buses in Germany. *Energies* 14 (4), 833. doi:10.3390/en14040833

Tronstad, T., Åstrand, H. H., Haugom, G. P., and Langfeldt, L. (2017). *Study on the Use of Fuel Cells in Shipping*. Oslo, Norway. Report to European Maritime Safety Agency by DNV GL; DNV GL.

Turoń, K. (2018). "Car-sharing Problems - Multi-Criteria Overview," in *International Conference on Traffic and Transport Engineering*. Editor O. Cokorilo (Belgrade Serbia: City Net Scientific Research Center), 916–922. ICTTE, September 27-28th, 2018, Belgrade, Serbia.

Turon., K. (2020). Hydrogen-powered Vehicles in Urban Transport Systems – Current State and Development. *Transp. Res. Procedia* 45, 835–841. doi:10.1016/j.trpro.2020.02.086,

van Biert, L., Godjevac, M., Visser, K., and Aravind, P. V. (2016). A Review of Fuel Cell Systems for Maritime Applications. *J. Power Sources* 327, 345–364. doi:10.1016/j.jpowsour.2016.07.007

Van Mierlo, J., Timmermans, J.-M., Maggetto, G., Van den Bossche, P., Meyer, S., Hecq, W., et al. (2004). Environmental Rating of Vehicles with Different Alternative Fuels and Drive Trains: a Comparison of Two Approaches. *Transp. Res. Part D Transp. Environ.* 9 (5), 387–399. doi:10.1016/j.trd.2004.08.005

Vialetto, G., Noro, M., Colbertaldo, P., and Rokni, M. (2019). Enhancement of Energy Generation Efficiency in Industrial Facilities by SOFC - SOEC Systems with Additional Hydrogen Production. *Int. J. Hydrogen Energy* 44 (19), 9608–9620. doi:10.1016/j.ijhydene.2018.08.145

Vincent, I., and Bessarabov, D. (2018). Low Cost Hydrogen Production by Anion Exchange Membrane Electrolysis: a Review. *Renew. Sustain. Energy Rev.* 81 (Jan), 1690–1704. doi:10.1016/j.rser.2017.05.258

von Döllen, A., Hwang, Y., and Schlüter, S. (2021). The Future Is Colorful-An Analysis of the CO2 Bow Wave and Why Green Hydrogen Cannot Do it Alone. *Energies* 14, 5720. doi:10.3390/en14185720

Wang, H., Wang, Z., Sun, M., and Wu, H. (2013). Combustion Modes of Hydrogen Jet Combustion in a Cavity-Based Supersonic Combustor. *Int. J. Hydrogen Energy* 38 (27), 12078–12089.

Wang, Q., Xue, M., Lin, B.-L., Lei, Z., and Zhang, Z. (2020). Well-to-wheel Analysis of Energy Consumption, Greenhouse Gas and Air Pollutants Emissions of Hydrogen Fuel Cell Vehicle in China. *J. Clean. Prod.* 275 (123061), 123061. doi:10.1016/j.jclepro.2020.123061

Wang, Y., Gao, L., and Liu, Y. (2015). *America's National Hydrogen Energy Program and its Enlightenment*. U.S. Department of Energy, Office of Science, Office of Basic Energy Sciences, 22–29.

Wasserstoffautos (2021). Wasserstoffautos. Available at: https://h2.live/en/wasserstoffautos/ (Accessed on August 29, 2021).

Wei, W., and Chen, W. (2020). *Development Strategy and Enlightenment of Hydrogen Energy in Japan*. Globalization, 60–71+135.

Weinmann, O. (1999). Hydrogen - the Flexible Storage for Electrical Energy. *Power Eng. J.* 13 (3), 164–170. doi:10.1049/pe:19990311

World Commission on Environment and Development (1987). *Our Common Future*. Oxford, UK: Oxford University Press.

World's First Hydrogen Train Runs Route in Germany (2021). World's First Hydrogen Train Runs Route in Germany-Report 2020. Availableat: https://www.industryweek.com/technology-and-iiot/emerging-technologies/article/22026353/worlds-first-hydrogen-train-runs-route-in-germany (Accessed on August 5, 2021).

Yan, L., Zhang, J., Zhou, X., Wu, X., Lan, J., Wang, Y., et al. (2013). Crystalline Phase-dependent Photocatalytic Water Splitting for Hydrogen Generation on KNbO3 Submicro-Crystals. *Int. J. Hydrogen Energy* 38 (9), 3554–3561. doi:10.1016/j.ijhydene.2013.01.028

Yang, C., and Ogden, J. (2007). Determining the Lowest-Cost Hydrogen Delivery Mode. *Int. J. Hydrogen Energy* 32 (2), 268–286. doi:10.1016/j.ijhydene.2006.05.009

Zhang, G., Xie, X., Xuan, J., Jiao, K., and Wang, Y. (2019). "Three-dimensional Multi-Scale Simulation for Large-Scale Proton Exchange Membrane Fuel Cell," in *SAE Technical Paper Series*. doi:10.4271/2019-01-0381

Zhang, G., Yuan, H., Wang, Y., and Jiao, K. (2019). Three-dimensional Simulation of a New Cooling Strategy for Proton Exchange Membrane Fuel Cell Stack Using a Non-isothermal Multiphase Model. *Appl. Energy* 255 (113865), 113865. doi:10.1016/j.apenergy.2019.113865

Zhang, T., Zhao, K., Yu, J., Jin, J., Qi, Y., Li, H., et al. (2013). Photocatalytic Water Splitting for Hydrogen Generation on Cubic, Orthorhombic, and Tetragonal KNbO3 Microcubes. *Nanoscale* 5 (18), 8375–8383. doi:10.1039/c3nr02356g

Zhao, F., Mu, Z., Hao, H., Liu, Z., He, X., Victor Przesmitzki, S., et al. (2020). Hydrogen Fuel Cell Vehicle Development in China: An Industry Chain Perspective. *Energy Technol.* 8 (11), 2000179. doi:10.1002/ente.202000179

Zhongfu, T., Chen, Z., Pingkuo, L., Reed, B., and Jiayao, Z. (2015). Focus on Fuel Cell Systems in China. *Renew. Sustain. Energy Rev.* 47, 912–923. doi:10.1016/j.rser.2015.03.057

Conflict of Interest: Author AK was employed by the companies CPS Technologies and Steering Committee (Hydrogen Society of Australia).

The remaining authors declare that the research was conducted in the absence of any commercial or financial relationships that could be construed as a potential conflict of interest.

Publisher's Note: All claims expressed in this article are solely those of the authors and do not necessarily represent those of their affiliated organizations, or those of the publisher, the editors and the reviewers. Any product that may be evaluated in this article, or claim that may be made by its manufacturer, is not guaranteed or endorsed by the publisher.

frontiers | Frontiers in Energy Research

TYPE Original Research
PUBLISHED 20 September 2022
DOI 10.3389/fenrg.2022.965047

OPEN ACCESS

EDITED BY
Nallapaneni Manoj Kumar,
City University of Hong Kong, Hong Kong SAR, China

REVIEWED BY
Puranjan Mishra,
Hong Kong Baptist University, Hong Kong SAR, China
Anshu Priya,
City University of Hong Kong, Hong Kong SAR, China
Idiano D'Adamo,
Sapienza University of Rome, Italy

*CORRESPONDENCE
Bo Tian,
tianbo@synfuelschina.com.cn

SPECIALTY SECTION
This article was submitted to Sustainable Energy Systems and Policies, a section of the journal Frontiers in Energy Research

RECEIVED 09 June 2022
ACCEPTED 04 August 2022
PUBLISHED 20 September 2022

CITATION
Tian B, Gao J, Guo Q, Zhu X, Zhang H, Zhu W, Hao X, Yang C, Yang Y and Li Y-W (2022), Process study and CO_2 emission reduction analysis of coal liquefaction residue fluidized bed pyrolysis. *Front. Energy Res.* 10:965047. doi: 10.3389/fenrg.2022.965047

Process study and CO_2 emission reduction analysis of coal liquefaction residue fluidized bed pyrolysis

Bo Tian[1,2]*, Junhu Gao[2], Qiang Guo[2], Xiaoming Zhu[2], Hao Zhang[2], Wei Zhu[2], Xu Hao[2], Chaohe Yang[1], Yong Yang[2] and Yong-Wang Li[2]

[1]State Key Laboratory of Heavy Oil Processing, China University of Petroleum (East China), Shandong, China, [2]National Energy Center for Coal to Liquids, Synfuels China Technology Co., Ltd, Beijing, China

The direct coal liquefaction process usually produces a liquefaction residue of about 30% of its coal feed. The effective utilization of the coal liquefaction residue (CLR), which contains about 80% organic matter, is of great significance for improving the oil yield of the direct liquefaction process and reducing the amount of pollution emitted from this oil-containing organic solid waste. In this study, the CLR fluidized bed pyrolysis process was studied through a fluidized bed reactor pyrolysis experiment and steady-state thermal analysis. The characteristics of CLR were first analyzed, and then the pyrolysis experiment was conducted in a fluidized bed reactor system. The experiment results show that the oil yield is 34.81% at 540°C for an ash-free feedstock using a fluidized bed pyrolysis reactor. Based on the pyrolysis experimental data and the Aspen Plus software platform, the fluidized bed pyrolysis reactor, fractionation column, coke burner, gasifier, and other equipment were modeled to compare four different process schemes. CLR pyrolysis is an endothermic reaction, and its heat is usually supplied by coke combustion, which produces significant CO_2 emissions. Case studies of the pyrolysis process were performed in detail in order to reduce CO_2 emissions. Thermal efficiency, carbon efficiency, solid waste discharge, and CO_2 emissions of the different schemes were compared, and a flexible fluidized pyrolysis (FFP) process coupled with water electrolysis was proposed. The introduction of green hydrogen and green oxygen to the process can realize near-complete utilization of carbon and hydrogen elements in the CLR and produce high-quality liquid fuels and syngas (for further chemical synthesis), and this new process can achieve almost near-zero CO_2 emission in the entire unit. This process principle can also be applied to the CO_2 emission reduction of organic solid waste pyrolysis, catalytic fluid cracking, fluid coking, and so on.

KEYWORDS

direct coal liquefaction, coal liquefaction residue, fluidized bed pyrolysis, flexi-fluid pyrolysis, carbon emission reduction, energy analysis, process simulation

Introduction

China's energy situation of "rich in coal, less in oil, and poor in gas" determines the clean and efficient conversion and utilization of coal, which will remain the ballast of China's energy for a certain time in the future (Xiang et al., 2014), and the key coal conversion technologies are indirect coal liquefaction and direct coal liquefaction. Direct coal liquefaction (DCL) is a process for converting coal to liquid fuels by dissolving coal in an organic hydrogen donor solvent in the presence of hydrogen and a catalyst under high temperature and pressure. The typical pressure and temperature are 19–20MPa and 450°C, respectively, (Shu, 2009). It was reported that coal can also be liquefied at mild conditions of 5–8 MPa (Yang et al., 2020). Due to the existing ash content in coal, the coal liquefaction catalyst, and the incomplete reaction of organic matter in coal liquefaction, solids are always left in the effluent of the reactor. In discharging these solids from the separate unit, it is usually inevitable that some heavy oil accompanies them to ensure fluidity in the pipes out of the vacuum distillation unit. The direct coal liquefaction process usually produces a coal liquefaction residue (CLR) of about 30% of its coal feed (Xu et al., 2014), and there is more than 80% organic matter in the CLR. Therefore, effective utilization of the organic material in the coal liquefaction residue is of great significance for improving the oil yield of the direct liquefaction process and reducing the amount of pollution emissions from this oil-containing organic solid waste.

At present, the reported treatment technologies of the coal liquefaction residue include direct gasification, fuel for boiler combustion, coking, pyrolysis, carbon material preparation, etc. (Winschel and Burke, 1989; Cui et al., 1999; Zhou et al., 2007; Li et al., 2010; Liu, 2012; Chen et al., 2020; Tian et al., 2022) Among them, CLR pyrolysis technology, which can maximize the light oil yield from the oil containing feedstock, is considered the most promising and feasible path in the future. The reported pyrolysis studies of the coal liquefaction residue mainly focus on the use of a Thermal Gravimetric Analyzer (TGA) instrument or fixed-bed tube reactor (Li et al., 2010; Liu, 2012), which can only provide qualitative analysis results. Some groups used a continuous stirred coking unit (CSCU) to test the reaction performance of CLR fluid coking (Winschel and Burke, 1989). Unfortunately, no further study was reported. In this study, the fluidized bed pyrolysis experiments of the CLR were studied, and the fluidized bed reactor has the best temperature uniformity both in axial and radial directions, which is beneficial for the pyrolysis reaction in improving the oil yield and reducing the coking rate (Yang et al.,; Wang and Qi, 2012; kun et al., 2011; Yang et al., 2017).

Today, reducing carbon dioxide emissions has become an urgent global issue in order to delay global warming. Pyrolysis is an endothermic reaction, and its heat is usually supplied by coke combustion, which will result in CO_2 emissions. Based on the CLR pyrolysis experimental study results and Aspen Plus simulation software, the four different fluidized bed pyrolysis process schemes were modeled and the case studies of reducing CO_2 emissions from the pyrolysis process were performed. Eventually, solar water electrolysis for green hydrogen and green oxygen generation was also combined with the proposed fluidized bed pyrolysis process to optimize the carbon reduction effect (Xiang et al., 2022).

2 Experimental

2.1 Analysis of the coal liquefaction residue

2.1.1 Analysis method

1) Feed raw material and pretreatment

The coal liquefaction residue was taken from a coal direct liquefaction demonstration plant in China. 300-g samples were dried in an oven which was kept at a constant temperature at 105°C for 2–3 h for each experiment and crushed to about 200 mesh particles for raw material analysis, such as softening point, ash content, density, proximate analysis, ultimate analysis, and organic matter extraction (Li et al., 2010) (Liu, 2012).

2) Softening point test method

The softening point test method for the coal liquefaction residue is ASTMD3461-83, and the softening point analysis instrument is the WQD-1A drop point softening point tester.

3) Ash content test method

The ash content test method for the coal liquefaction residue is National Standard GB/T 29748-2013 (Li et al., 2010) (Liu, 2012).

4) Density analysis method

The density analysis of the coal liquefaction residues is tested with reference to GB/T 13377-2010 (Determination of Density or Relative Density of Crude Oil and Liquid or Solid Petroleum Products-Capillary Stopper Pycnometer and Double Capillary Pycnometer with Scale) and the HCR2000 petroleum density pycnometer (Li et al., 2010) (Liu, 2012).

5) Proximate analysis and ultimate analysis

The CLR proximate analysis and ultimate analysis use the national standard GB/T212-2001 and GB/T476-2001 analytical methods. The organic element analysis instrument model is the Elementar vario EL element analyzer. The sulfur measurement is made using the ZCS-1 type intelligent sulfur measuring

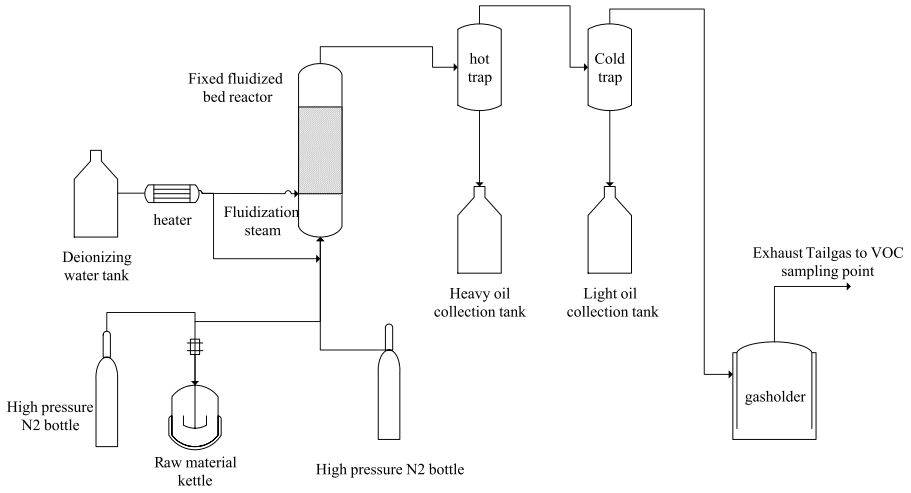

FIGURE 1
Flow diagram of the fluidized bed pyrolysis experimental apparatus. Bo Tian, female, (1981-), PhD, permanent resident of South Africa, Native place: Jiuquan, Gansu Province, Professoriate senior engineer, Technology development lead a n d senior Project technical leader, Fluidized bed process technical expert, 1. China University of Petroleum (East China), State Key Laboratory of Heavy Oil, 2. Synfuels China Technology Co., Ltd., National Energy Coal-based liquid fuel Research Center, Main research directions: coal-to-oil and chemicals, carbon-containing resource pyrolysis technology research and development, organic solid waste resource transformation, applied basic research, reaction process research, engineering technology development and design, process simulation and optimization, and engineering amplification, etc.

instrument of Xuzhou Analysis Instrument Factory (Li et al., 2010) (Liu, 2012).

6) Extraction analysis method

For the rapid solvent extraction analysis of coal liquefaction residues, the solvents of n-hexane toluene, and tetrahydrofuran (THF) were used as extraction agents. The extraction methods and procedures refer to the existing analysis standard NB/T-12005-2016 of the National Energy Administration (Li et al., 2010) (Liu, 2012).

2.2 Fluidized bed pyrolysis experiment

2.2.1 Experimental apparatus and method

The CLR pyrolysis experiment was performed in a fluidized bed reactor to investigate the influence of reaction temperature conditions on the product yield and distribution and provide detailed reaction data for further process simulation and optimization.

The experimental apparatus of the fluidized bed reactor is shown in Figure 1. 400 g of the coal liquefaction residue is added into the raw material kettle for each experiment and heated up to 150–250°C according to the experimental requirements before the pyrolysis experiment starts. The high-pressure N_2 is used to press the CLR into the reactor through the feed nozzle. Water vapor enters the reactor as a fluidized gas. The reaction temperature was tested in the range of 500–620°C. The product oil and gas vapor are discharged from the top of the reactor. The heavy oil and light oil are cooled stepwise and collected in the hot and cold traps. The tailgas enters the gas measurement and analysis system. After reaction, the liquid product and solid coke product from the reactor were collected for further analysis.

2.2.2 Product yield calculation method

The yield of fluidized bed pyrolysis products was calculated in two methods: water and ash-free feed basis or THF soluble feed basis. The yield calculated in THF soluble feed basis may be more accurate because the THF insoluble substances in the raw material are usually inert in the pyrolysis reaction and are directly converted into coke in the product. The dry gas and LPG of the product are calculated by the mass flow rate of each product in the actual exhaust gas. The amount of oil in different fraction sections is determined according to the simulated distillation process distribution of the actual received oil products, and the mass of the C_{5+} component in the exhaust gas is considered and added into the distillation of the naphtha fraction. For the coke yield calculation for water and ash-free feed basis, the total coke mass includes the coke produced by pyrolysis reaction and inert organic matter directly from the raw material, excluding the mass of inorganic ash brought into the raw material. For the coke yield calculation of the THF soluble basis, the coke yield is exactly the organic coke produced from the pyrolysis reaction.

TABLE 1 Analysis results of coal liquefaction residue properties.

Analyze the project	Analytic result
Proximate analysis/wt%	(As received basis)
Moisture	0.20
Ash content	12.05
Volatile matter	36.29
Fixed carbon	51.5
Elemental Analysis/wt%	
C	78.43
H	4.17
N	0.78
S	1.67
O	2.90
H/C	0.6336
Softening point/°C	182.5
THF soluble (THFS) wt%	51.27
Toluene soluble wt%	31.01
Average grain diameter/mm	<5
Density/g.ml^{-1}	1.4

2.2.2 Product analysis method

1) Tail gas analysis

For tail gas composition analysis, the Agilent 7890A gas chromatograph (GC) was used with the national standard GB/T 27885-2011.

2) Oil product analysis

For the simulated distillation analysis of the oil product, the Agilent 7890A gas chromatograph was used according to the national standard NB/SH/T 0879-2014 method.

3) Char ultimate analysis

The ultimate analysis of the char samples adopts the national standard of GB/T476-2001 analytical methods by the same analytical equipment as in Section 2.1.1.

2.3 Experimental results and discussion

2.3.1 Raw material analysis results and discussion

Property analysis of the coal liquefaction residue is of great significance to its utilization prospects and process scheme selection. The analysis results of the raw material properties of the coal liquefaction residue are shown in Table 1.

As can be seen from Table 1, the water content of the coal liquefaction residue is low, the ash content is 12.05%, the fixed carbon is 51.27%, and the volatile 36.29%. The ash in the coal liquefaction residue mainly comes from the ash in the raw coal and the catalyst added in the direct liquefaction reaction process. Because the water in the coal has been removed during the reaction process, a small amount of water may come from the water absorbed when the raw material is placed in the air. A large amount of ash will cause the calorific value of coke after pyrolysis to decline, and it is difficult to use it. Fixed carbon is mainly derived from unreacted coal and bituminous substances, and volatilization is the entrained heavy oil. It can be seen from the proximate analysis that if the volatile utilization of the raw material can be maximized to produce oil and the rational use of fixed carbon, it is very important for the high-value utilization of the coal liquefaction residue. It can be seen from the ultimate analysis that hydrocarbon elements account for more than 82% and the H/C element ratio is 0.6336, which has a very good utilization value. The softening point of the coal liquefaction residue is 180.2°C, which is closely related to the operating condition of the device, usually between 170 and 190°C. If the softening point is less than 170°C and the amount of heavy oil contained in the residue is large, it constantly affects the oil yield, and the residue is not easy to form. If the softening point is higher than 190°C, the liquidity is poor, making it easy to undergo coke formation and block the equipment pipeline, affecting the normal operation of the device. In addition, for the fluidized bed pyrolysis process, the softening point of the coal liquefaction residue directly affects the raw material feed and the flow condition in the fluidized pyrolysis reactor. It can be seen from the extraction results that the soluble matter content of tetrahydrofuran (THF) soluble is 51%, and it is the key index of pyrolysis of the coal liquefaction residue. Usually only THF Soluble matter undergoes pyrolysis or coke reaction, and the pyrolysis method makes the soluble matter crack into lighter oil and gas products, which is also the key benefit of pyrolysis. Therefore, the yield of pyrolysis oil is compared by using the Ash-free method and the THF soluble matter group method in Table 2.

2.3.2 Fluidized pyrolysis experimental results and discussion

Table 2 shows the experimental results of the pyrolysis of the coal liquefaction residue in a fixed fluidized bed reactor. In the table, the yields of dry gas, LPG, C_5^+ ~ 180°C naphtha fraction, 180–360°C diesel fraction, > 360°C wax oil fraction, and coke of the product are calculated according to the anhydrous ash free organic matter and tetrahydrofuran (THF) soluble organic matter of the raw material as reactants.

It can be seen that the oil yield is 34.81 wt% for the ash-free raw material base and 67.39 wt% for the THF-soluble raw material base, which shows that the fluidized bed pyrolysis process can effectively recover the oil in the raw material and convert some difficult heavy asphalt into light oil, which improves the yield of oil and realizes the light utilization of heavy oil. Compared with previous fixed-bed pyrolysis results

TABLE 2 Distribution of pyrolysis experimental data products of the coal liquefaction residue fluidized bed.

Product yield	Anhydrous and ash-free raw material base	THF-soluble raw material base
Dry gas/wt%	2.8	4.78
LPG/wt%	1.92	3.26
Naphtha fraction/wt%	6.54	11.15
Kerosene diesel fraction/wt%	18.19	30.99
Wax oil fractions/wt%	10.08	17.18
Coke/wt%	60.47	32.64
Gas yield rate/wt%	4.72	8.04
C_5^+ Oil yield/wt%	34.81	59.32
Coke yield,/wt%	60.47	32.64

Note: The reaction conditions are temperature 540°C, pressure 100 kPa, and fluidized medium water vapor 300 ml/h, with the generated coke solid as the heat carrier.

research, the best oil yield is around 16 wt% at 600°C (Xu et al., 2014) (Liu, 2012) and while in the TGA micro reactor in N_2 atmospheres, the total weight loss for oil and gas was reported to be 34.2 wt% and 33.74 wt% from two different researchers (Xu et al., 2014) (Li et al., 2010). This is mainly due to the fact that in a fluidized bed, the heat transfer efficiency is high, the temperature in the bed is easy to maintain uniform, and there is uniform gas–solid two-phase mixing of the reaction material. This is very important for the reaction process with large thermal effects and those sensitive to temperature, such as pyrolysis. The fluidized bed reactor has the best temperature uniformity both in axial and radial directions, which is beneficial for the pyrolysis reaction to improve the oil yield and reduce the coking rate. In addition, the coke product is less likely to agglomerate than in a fixed-bed reactor due to the high-speed uniform dispersion and flow of the coke inside a fluidized bed. In the fixed-bed reactor, 2~3 g of the raw coal residue was packed in the tube reactor during the pyrolysis reaction, and it had poorer heat transfer or uneven heat transfer, which could have impacted negatively on the pyrolysis reaction. In contrast, for the TG thermal reaction analysis, 20 mg of the raw coal residue was used in the TGA micro reactor. TGA is a thermal analysis technique that is usually used to study the thermal stability and composition of materials. It is not affected by mass and heat transfer effects; hence, the gas and oil yield is much higher than in fixed-bed and fluidized bed reactors.

Due to the high content of asphalt organic matter in the raw material and the unconverted coal, most or all of the feed organic substances will produce coke. The utilization of this coke will not only affect the economy of the process but also the disposal of inorganic materials and the coke, which also has a certain impact on the environment. If coke combustion provides energy for pyrolysis reaction, it will also lead to CO_2 emission problem. How to reduce CO_2 emissions is vital for the process; therefore, the process optimization of the coke heating part and coke usage is the focus of the next section of this study.

3 Fluidized pyrolysis process simulation and optimization

The complete process of the coal liquefaction residue not only includes the pyrolysis reaction part and the oil and gas fractionator part but also includes the combustion or gasification part that provides heat for the reaction. Moreover, the process setting of the coking and gasification parts will determine the thermal efficiency and carbon efficiency of the whole process, which is the second focus of this study. According to the two different schemes of coke burning heating and gasification heating, this technology is divided into two schemes: fluidized pyrolysis and flexible pyrolysis. In addition, according to the oxidant part of the process, using air or oxygen, it is also divided into four process schemes: fluidized pyrolysis air combustion, fluidized pyrolysis oxygen combustion, flexible pyrolysis air gasification, and flexible pyrolysis oxygen gasification. The four specific process schemes were simulated as below.

3.1 Process flow description

1) Fluidized pyrolysis air combustion process (Case 1)

Case 1: The fluidized pyrolysis air combustion coke process includes a fluidized pyrolysis reactor, coke air burner, oil and gas fractionator, and a fuel gas treatment system. The process requiring excess coke exhausts part of the coke.

The flow of the fluidized pyrolysis air combustion process is shown in Figure 2. The coal liquefaction residue and water vapor enter the reactor through the nozzle atomization, and the organic matter in the raw material undergoes thermal cracking reactions and condensation coke reactions. The generated oil and gas are discharged from the top of the reactor into the fractionation column, distilled, and cut into pyrolysis-rich gas, pyrolysis sewage, naphtha, kerosene and diesel distillate, wax oil

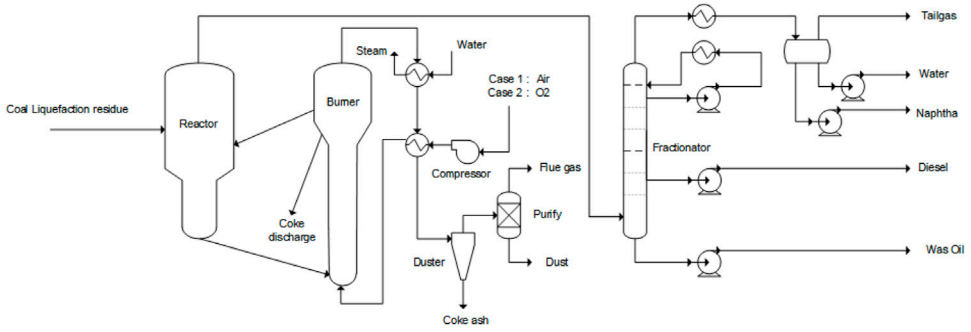

FIGURE 2
Fluidized pyrolysis process (case 1: fluidized pyrolysis with air combustion; Case 2 fluidized pyrolysis with oxygen air combustion).

distillate, and other products. The generated coke absorbs the water vapor and enters the coke burner. A certain amount of coke reacts with the air. The heat generated is for the heat balance of the whole system, and the excess coke is discharged from the system. The fuel gas generated by the combustion reaction enters the fuel gas treatment system, recovers heat, removes dust, and cleans it. The heat required by the pyrolysis reactor is provided by the circulation of hot focal particles. The pyrolysis reaction temperature was controlled at 500–620°C, and the coking reaction temperature was controlled at 650–750°C. Thermal cracking and condensation of all hydrocarbons occur in the fluidized bed pyrolysis reactor, which follows the free radical chain reaction mechanism. Complete combustion and partial combustion reactions of coke occur in the fluidized bed coke reactor, and the chemical reaction equation is as follows: R1 and R2. If the fuel gas contains CO, excess air needs to be further burned before heat exchange and cooling until all of it is converted into CO_2. The process oxidizer uses air because air contains a large amount of inert nitrogen, so it is required to consume additional coke and heat up the nitrogen, resulting in a decrease in thermal efficiency.

Full combustion of coke: $C + O_2 = CO_2$ -394.1 kJ/mol (R 1)

Incomplete combustion of coke: $C + 1/2\ O_2 = CO$ -110.4 kJ/mol (R2)

2) Fluidized pyrolysis oxygen combustion process (Case 2)

Case 2: The fluidized pyrolysis oxygen air combustion coke process includes a fluidized pyrolysis reactor, coke oxygen burner, oil and gas fractionator, and a fuel gas treatment system. The process requiring excess coke exhausts part of the coke.

Compared to the Case 1 air fluidization pyrolysis process, Case 2 uses pure oxygen for coke burning and combustion, and the rest of the equipment is the same as in Case 1, as shown in Figure 2. Using pure oxygen will hopefully reduce the size of the burner. The source of oxygen can be from an air separation unit in existing plants or from green oxygen from water electrolysis, a byproduct of the electrolysis of water hydrogen production plant.

3) Flexible fluidized pyrolysis air gasification process (Case 3)

Case 3: The flexible fluidized pyrolysis air gasification process includes a fluidized pyrolysis reactor, air coke gasifier, oil and gas fractionator, and a fuel gas treatment system. It is a process of complete coke gasification that discharges only inorganic solids and produces low calorific value fuel gas.

The flow diagram of the flexible fluidized pyrolysis process is shown in Figure 3. Compared with the fluidized pyrolysis process in Figure 2, the heat supply part of the flexible fluidized pyrolysis process utilizes the mode of coke gasification and coke heat exchange to produce fuel gas or syngas instead of the air coke combustion in Case 1, and the remaining pyrolysis reaction and fractionation part are the same as the fluidized pyrolysis of Case 1. The coke generated by the pyrolysis reaction is carried into the heat exchange room through effluent gas. After heat exchange with the high-temperature fuel gas generated after the gasification reaction, one part returns to the reactor to provide heat, and the rest enters the gasification device for gasification reaction. The remaining solid after the gasification reaction is discharged, or it is mixed with the cold coke particles from the pyrolysis reactor back into the heat transfer chamber. The temperature of the gasification reaction is at 900–1,200°C, and the temperature of the heat transfer chamber is controlled at 650–750°C. For the flexible fluidized pyrolysis air combustion process, the oxidant for the gasification reaction adopts air, and all coke undergoes gasification reaction. After gasification reaction, low calorific value fuel gas is generated, which can be supplied to other units as fuel gas in the whole plant. This unit, however, only discharges the inorganic solids after high-temperature treatment, which can achieve environmental protection emission standards. The fuel gas leaving the heater is heat exchanged by the built-in cyclone separator, external

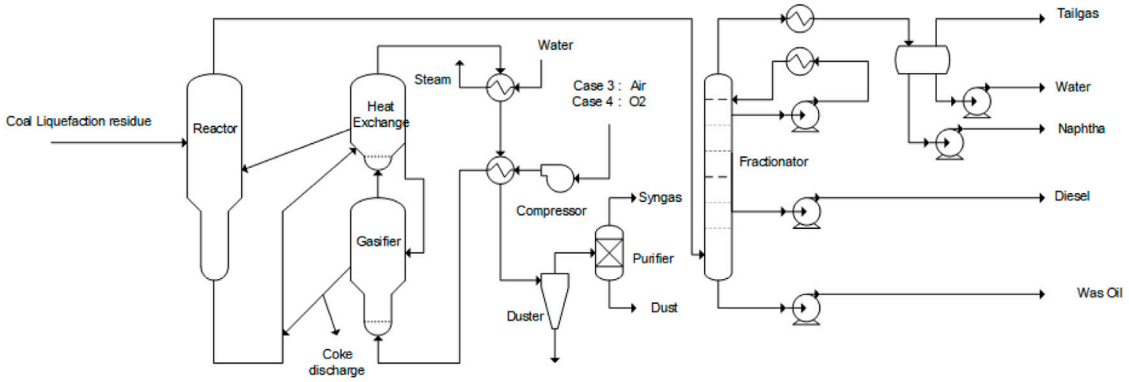

FIGURE 3
Flexible fluidized pyrolysis (case 3: flexible fluidized pyrolysis air gasification; case 4 flexible fluidized pyrolysis oxygen gasification).

high-pressure steam generator, oxygen water heater, and air heater, then enters the external high-efficiency gas-solid separator to remove the entrained dust, and is then sent to the desulfurization and purification device to produce low sulfur and low calorific value fuel gas.

4) Flexible fluidized pyrolysis oxygen gasification process (Case 4)

Case 4: The flexible fluidized pyrolysis oxygen gasification process includes a fluidized pyrolysis reactor, oxygen coke gasifier, oil and gas fractionator, and a syngas treatment system. This process of coke is complete gasification, and only discharged inorganic solids, with high calorific value syngas, can be used in the production of chemicals.

Based on the flexible fluidized pyrolysis process of Case 3, Case 4 introduces pure oxygen as an oxidant for the gasification reaction, which can reduce the heat loss of nitrogen heating and improve the calorific value of the generated gas and produce direct syngas (H_2 and CO) for downstream syngas production. This amount of syngas can be combined with green hydrogen to be used as feed gas for methanol or olefin production.

3.2 Process simulation assumptions and physical property selection

The simulation benchmark of the abovementioned four process schemes is the annual treatment capacity of the coal liquefaction residue of 700,000 tons, that is, 87,500 kg/h. The four fluidized pyrolysis reaction process parts are the same, while the effects of different coke combustion processes and gasification processes were compared. The ASPEN Plus simulation software platform is used to model these four process schemes. The mass balance, energy balance, thermal efficiency, and carbon efficiency, as well as CO_2 emission and solid discharge, were analyzed and compared.

The thermodynamic equation of the Soave–Redlich-Kwong (SRK) equation is used for pyrolysis and fractionation partial simulation, and the Peng–Robson equation of state is used to simulate the combustion and gasification part. The simulation of the reactions in the fluidized pyrolysis reactor was performed using the RYield yield reactor model to calculate the product distribution after the reactions based on the experimental results in Table 2. The fractionation tower uses the PetroFrac tower module combined with the design provisions to calculate the product distribution of different distillation processes. The coke combustion reactor was simulated by a RStoic reactor, considering two reactions, R1 and R2, and containing the CO/CO_2 in the tail gas according to the experimental coking reaction. The selectivity of the proportional adjustment reaction is carried out as follows: if the exhaust gas contains CO, the CO will be completely converted into CO_2 with the RStoic reactor module at the combustion reactor, thus calculating the carbon balance and the CO_2 emission reduction effect. According to the H content in coke, the reaction of H_2 and O_2 to generate water is adopted, and the combustion heat of H_2 is considered. For the coke gasification reaction, the RYield yield reactor and the RGibbs reactor were used to simulate the gasification process and adjust the proportion of key components in the product according to the reaction equilibrium temperature distance method to be close to the actual composition reported in the literature (Chen et al., 2020). The calculation method of the heat loss in the heat balance of the reactor, burner, and gasifier is obtained from the estimated heat exchange area of the estimated major equipment and the heat dissipation coefficient with reference to the fluidized catalytic cracking (FCC) process (Cao et al., 2000).

In this study, the thermal efficiency calculation adopts the ratio of the low calorific value of the whole process unit before and after the reaction, that is, the ratio of the low calorific value of

TABLE 3 Material balance of reaction part of the fluidized bed.

Content		Flow process of Case1-4: kg/h
Raw material		
	Coal liquefaction residue	87500
Products		
	Dry gas	2,152.48
	LPG	1,471.81
Oil	<180°C	5,026.63
	180–360°C	13962.89
	> 360°C	7,740.3
Solid waste	Total organic coke	46427.15
	Inorganic ash	10543.75
Water in raw materials	Water	175
	SUM	87500

all products to the low calorific value of all raw materials. The comparison of process schemes of the units only considers the difference in coke heating parts, and the other equipment is basically the same. Therefore, the change in energy consumption of the unit can be judged by the thermal efficiency. Carbon efficiency refers to the mass ratio of carbon elements in all products to carbon elements in raw materials, which can judge the transform direction of carbon in raw materials and the amount of CO_2 produced.

3.3 Process simulation/optimization results and discussion

1) Material balance of the fluidized pyrolysis reaction part

The abovementioned four coal liquefaction residue treatment process schemes have the same process of fluidized pyrolysis reaction parts, and the material balance of the reaction is shown in Table 3. For a direct coal liquefaction plant with an oil output of 1 million tons/year, the by-product coal liquefaction residue is about 700,000 tons/year. If the fluidization pyrolysis plant with a coal liquefaction residue treatment capacity of 700,000 tons/year is designed, the annual yield of C_3 + oil products is 225,600 tons/year, which is equivalent to an increase of 22% of the production capacity. At the same time, 17,200 tons/year of dry gas will be produced and processed in the downstream tail gas treatment unit. Fluidization pyrolysis produces about 371,400 tons/year of organic coke per year and 84,000 tons/year of inorganic ash at the same time. The organic coke produced by fluidized pyrolysis is attached to the inorganic ash, usually coke particles in the range of 10–100 microns. The granular coke with high ash content is difficult to be further processed and utilized. Only when the organic coke is burned or gasified can the inorganic ash be discharged up to the standard.

2) Heat balance analysis

The heat balance calculation results of two different coke burning/combustion methods of the fluidized pyrolysis process are shown in Table 4. For the pyrolysis reaction of the coal liquefaction residue, a raw material with a high coke generation rate, and because the condensation coke generation is an exothermic process, which will offset part of the heat absorbed by cracking, the total heat absorbed by the reaction is less, and the heating up energy of the raw material accounts for a large proportion, up to 72.67%, which is also related to the difficulty in heating solid raw materials and the low preheating temperature. The heat loss of the pyrolysis reactor is about 3.88%, which is equivalent to that of a traditional fluidized catalytic cracking reactor. The total heat required by the pyrolysis reactor is about 78264.37 MJ/h, which is provided by the circulating coke between the two reactors. For fluidized pyrolysis coke air combustion process Case 1, the combustion reaction between coke and oxygen in the air provides heat for circulating coke temperature

TABLE 4 Heat balance of the fluidized pyrolysis process of the coal liquefaction residue.

Content			Case 1 fluidized pyrolysis air combustion		Case 2 fluidized pyrolysis oxygen combustion	
			Quantity of heat MJ/h	Heat ratio%	Quantity of heat MJ/h	Heat ratio%
Reactor	Energy output	Heat of reaction	13571.25	17.34	13571.25	17.34
		Feed heating heat	56875	72.67	56875	72.67
		Steam heating heat	4,777.5	6.1	4,777.5	6.1
		Heat loss	3,040.52	3.88	3,040.52	3.88
	Energy import	Circulating coke provides the heat	78264.27	100	78264.27	100
Burner	Energy output	Circulating coke to heat up and heat	78264.27	66.81	78264.27	81.76
		The rest of the coke is hot	8,773.52	7.49	8,773.52	9.16
		Main wind/oxygen to heat up and heat	24777.21	21.15	4,368.83	4.56
		Heat loss	5,320.92	4.54	4,323.25	4.52
	Energy import	Combustion reaction exoheat	117135.92	100	95729.86	100

TABLE 5 Heat balance of the flexible fluidized pyrolysis process of the coal liquefaction residue.

Content			Case 3 flexible fluidized pyrolysis air gasification		Case 4 flexible fluidized pyrolysis oxygen gasification	
			Quantity of heat MJ/h	Heat ratio%	Quantity of heat MJ/h	Heat ratio%
Reactor	Energy output	Heat of reaction	13571.25	17.34	13571.25	17.34
		Feed heating heat	56875	72.67	56875	72.67
		Steam heating heat	4,777.5	6.1	4,777.5	6.1
		heat loss	3,040.52	3.88	3,040.52	3.88
	Energy import	Circulating coke provides the heat	78264.27	100.00	78264.27	100.00
Gasifier	Energy output	Circulating coke to heat up and heat	78264.27	32.28	78264.27	55.00
		Gasification coke heat up heating heat	13250.73	5.46	13250.73	9.31
		Steam heating heat	22475.65	9.27	22475.65	15.79
		Main wind/oxygen to heat up and heat	118999.17	49.07	22808.39	16.03
		heat loss	9,500	3.92	5,500	3.87
	Energy import	Gasification reaction to release heat	242489.82	100	142299.04	100

increase, combustion and exhaust coke temperature increase, main air temperature increase, and heat loss. For burners, in addition to the large proportion of circulating coke (66.81%), the temperature rise heat of the main air accounts for 21.15% because oxygen only accounts for 21% (volume ratio) in the air, and the remaining 79% is nitrogen. In order to obtain the oxygen required for the reaction, nitrogen is added to the system with air, which is about four times more to be heated up to the temperature of the coke burner (700 °C) and then discharged from the system, resulting in a large waste of energy and more CO_2 emissions.

For the fluidized pyrolysis coke oxygen combustion process Case 2, the coke and pure oxygen carry out the combustion reaction of carbon in the burner to provide heat for the temperature increase of circulating coke, the temperature increase of combustion and coke discharge, the temperature increase of main air, and the heat loss of the burner. Compared with Case 1, after coke is burned with oxygen in

Case 2, the total heat decreases to 95729.86 MJ/h, a decrease of 18.27%. At this time, the temperature rise heat of the main air (oxygen) only accounts for 4.56%, saving 21406.06 MJ/h of heat required for heating N_2. Thus, 91% of the heat generated by combustion reaction is used for the temperature increase of circulating coke and other coke, indicating that the heat utilization rate of the system is significantly improved.

The heat balance calculation results of two different flexible fluidized pyrolysis gasification methods are shown in Table 5. As with the fluidized pyrolysis conditions Case 1 & 2, the total heat required for the flexible fluidized pyrolysis reactor is about 78264.37 MJ/h, as provided by the circulating coke particles between the pyrolysis reactor and the heat transfer chamber. In the flexible fluidized pyrolysis process, all the organic coke generated by the pyrolysis is vaporized to produce fuel gas or syngas, while providing heat to the reactor. In order to control the temperature of the gasification device within the required range (the gasification temperature in this study is controlled at 950°C), it is often necessary to supplement a certain amount of steam. At this time, in addition to the gasification reaction between carbon and oxygen to generate CO, the reaction between water vapor and carbon will also occur in the gasification chamber to generate CO and H_2, the hydrogen element in coke will also generate H_2, C and H_2 may generate methane, and CO and water will also undergo a water vapor conversion reaction to generate CO_2, but the main reaction is the gasification reaction between carbon and oxygen and water to generate CO and H_2. For the flexible fluidized pyrolysis air gasification process Case 3, coke reacts with oxygen in the air, and the generated heat provides heat for circulating coke heating, gasification coke and discharged solid heating, main wind heating, and heat loss. As can be seen by the heat proportion, the gasification of heat consumption is the main wind heating, accounting for 49.07%, and has exceeded the circulating coke and gasification coke heat sum (37.74%), reaching 118999.17 MJ/h. While using air gasification, noble gas nitrogen heat has seriously affected the process of heat utilization, caused a larger energy waste, and produced more CO_2 discharge. At the same time, the presence of nitrogen causes the fuel gas produced by gasification to contain a large amount of nitrogen, and the volume and calorific value are reduced.

For the flexible fluidized pyrolysis oxygen gasification process Case 4, when the gasifying agent air in Case 3 is replaced with oxygen, it can be seen that the temperature rise heat of oxygen in the main air has decreased to 19.16% and its proportion has also decreased to 16.03%. At this time, the temperature rise heat of circulating coke and gasification coke accounts for 64.31% and returns to the dominant position. From the total heat release of the gasification reaction, it can be seen that the heat release required by oxygen gasification decreased by 41.32%, indicating that oxygen gasification has a very obvious effect on improving the heat utilization rate of the process.

3) Comparison of the main technical indexes of the four process schemes

The main technical indexes of the four process schemes for the coal liquefaction residue are shown in Table 6. From the amount of organic coke consumed in the reaction and the amount of remaining organic coke, it can be seen that for the fluidized pyrolysis scheme of partial combustion, the coke consumed in Case 1 and Case 2 reactions accounts for only 7.5% of the total amount of organic coke, which can meet the heat balance of the whole pyrolysis and coke burning system. Compared with Case 1, the coke consumption of Case 2 is reduced by 18% due to the use of oxygen coke burning. For the flexible fluidized pyrolysis schemes Case 3 and Case 4, the organic coke is completely gasified and only inorganic solids are discharged. After high-temperature heat treatment above 900°C, the discharged solid meets the requirements of environmental protection easily.

For oxidants and gasifiers, the amount of main air or oxygen required by a fluidized pyrolysis scheme is much less than that of a flexible fluidized pyrolysis scheme. For the fluidized pyrolysis scheme, oxygen coke burning is adopted, and the gas volume is far less than that of air coke burning. The size of the coke burner and main air and fuel gas systems can be greatly reduced, which can significantly reduce the equipment investment. Moreover, the actual amount of oxygen in oxygen coking is also less than that in air coking, indicating that the heat required in the process decreases and the thermal efficiency improves. For flexible fluidized pyrolysis, the amount of main air or oxygen is nearly five times higher than that of fluidized pyrolysis, indicating that the size of the equipment will increase significantly. However, the granular coke produced by fluidized pyrolysis needs further treatment, and the coke produced by flexible fluidized pyrolysis can be transformed *in situ*. Therefore, the increased investment is meaningful. Compared with Case 3, the amount of the gasification agent in Case 4 is significantly reduced to 18%, and the equipment size can be significantly reduced.

For the thermal efficiency of the process, if the product contains coke and fuel gas/syngas, the chemical thermal efficiency of the four process schemes is higher, at 93–99%. In contrast, the flexible fluidized pyrolysis scheme is higher than the fluidized pyrolysis scheme, and the utility of oxygen as an oxidant or gasifier is higher than that of air as an oxidant or gasifier.

For carbon efficiency, in addition to the carbon entering the pyrolysis products in the fluidized pyrolysis process, a small part of the carbon is used as fuel for coke burning and generates CO_2, and the rest of the carbon enters the coke products (granular coke is of little use and subsequent processing is difficult, so the direction of this part of carbon determines the total carbon efficiency). The total carbon efficiency is 93–94%. For the flexible fluidized pyrolysis process, if air is used as the gasification agent, coke gasification will make all the carbon in

TABLE 6 Main technical indexes of the four processing schemes of the coal liquefaction residue.

	Case 1 fluidized pyrolysis, air combustion	Case 2 fluidized pyrolysis, oxygen combustion	Case 3 flexible fluidized pyrolysis air gasification	Case 4 flexible fluidized pyrolysis of oxygen gasification
Reaction coke consumption/kg·h^{-1}	3,458.09	2,826.14	46427.15	46427.15
Remaining organic coke/kg·h^{-1}	42969.06	43601.01	0	0
Inorganic solid content/kg·h^{-1}	10543.75	10543.75	10543.75	10543.75
Air/Nm^3·h^{-1}	31488.31		152460.03	
Oxygen/Nm^3·h^{-1}		5,301.97		27815.77
Fuel gas/Nm^3·h^{-1}	31488.31	5,301.97		
Fuel gas/Nm^3·h^{-1}			238370.12	
Syngas/Nm3·h^{-1}				119573.65
Raw material thermal input flow/ MkJ h^{-1}	2,712.5	2,712.5	2,712.5	2,712.5
Oil and gas thermal output flow/MkJ h^{-1}	1,309.94	1,309.94	1,309.94	1,309.94
External coke thermal output flow/ MkJ h^{-1}	1,223.07	1,241.06	0	0
Fuel gas/syngas thermal output flow/ MkJ h^{-1}	0	0	1,297.88	1,397.79
Thermal efficiency/%	93.38	94.05	96.14	99.82
Carbon in raw material/kg·h^{-1}	68,626.25	68,626.25	68,626.25	68,626.25
Carbon in oil and gas/kg·h^{-1}	25,616.98	25,616.98	25,616.98	25616.98
Carbon in efflux coke/kg·h^{-1}	38,672.15	39240.91	0	0
Carbon in effective syngas/kg·h^{-1}	0	0	0	42676.73
Carbon Efficiency/%	93.68	94.51	37.33	99.52
Exhaust CO2/Nm^{3}h^{-1}	6,612.54	5,301.97	83,737.67	3,739.75

TABLE 7 Composition of fuel gas and syngas in the flexible fluidized pyrolysis process.

Process type	Case 3 flexible fluidized pyrolysis air gasification	Case 4 flexible fluidized pyrolysis of oxygen gasification
Dry-base composition, mol%		
N_2	50.62	0.21
O_2	0.00	0.00
CO	31.01	66.66
CO_2	4.11	3.13
H_2	14.14	29.54
H2S	0.11	0.21
CH4	0.01	0.24
sum	100.00	100.00
H_2/CO,mol/mol	0.4560	0.4432
Low heat, MJ/Nm^3	5.4448	11.6898

the coke generated by pyrolysis enter the fuel gas, which can only be burned as fuel and produce CO_2 in the heating furnace. Therefore, the carbon efficiency of the flexible fluidized pyrolysis air gasification process in the calculation is very low, only 37.33%, and produces a large amount of CO_2 emissions. In Case 4, because oxygen is used as a gasification agent, all the carbon

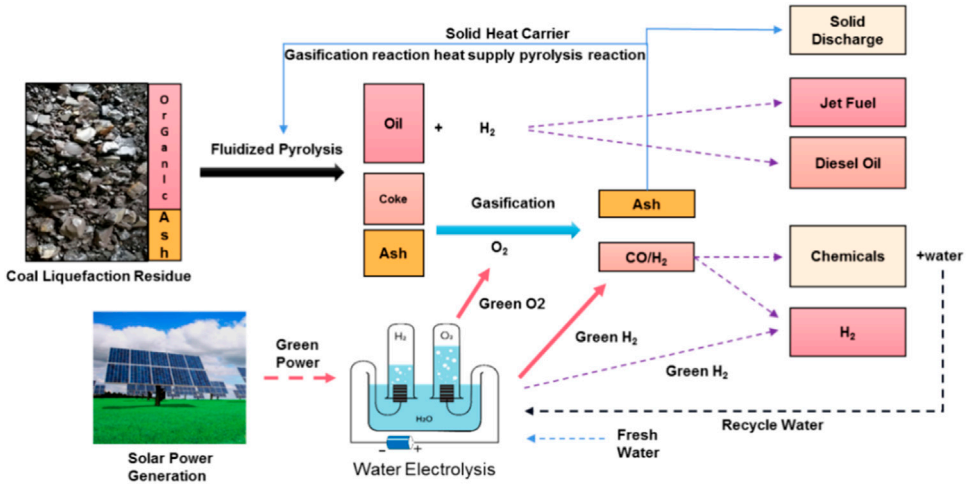

FIGURE 4
Coupling process of flexible fluidized pyrolysis of coal liquefaction residue with water electrolysis.

in coke can enter syngas and be used as raw material for downstream chemical production. Therefore, the total carbon efficiency of this process reaches 99.52%, which is the highest among all processes and the lowest CO_2 emissions. It can be seen that whether it is product scheme, thermal efficiency, or carbon efficiency, the flexible fluidized pyrolysis oxygen gasification scheme is the best scheme, which not only improves the process economy but also conforms to the China national environmental protection policy of energy conservation, emission reduction, and CO_2 emission reduction.

Table 7 shows the composition of fuel gas for Case3 and Case4. It can be seen that the nitrogen content of fuel gas produced by Case 3 by using air as a gasification agent reaches 50.62 mol%, the low calorific value is only 5.4448 MJ/Nm^3, and the molar ratio of H_2/CO is 0.4560. It can only be used as fuel gas for factory heating furnaces. However, when oxygen is used as the gasification agent, as in Case 4, the generated synthesis gas contains almost no nitrogen, the low calorific value reaches 11.6898 MJ/Nm^3, and the H_2/CO molar ratio is 0.4432. After a certain amount of hydrogen is proportioned, the H_2/CO is adjusted to the appropriate ratio, which can be used for syngas to methanol or syngas to olefin processes, which can produce high-value chemical products.

4) Flexible fluidized pyrolysis coupled with the water electrolysis process

The comparative study of the abovementioned four schemes shows that the flexible fluidized pyrolysis process using oxygen as a gasification agent is the best choice, which can not only realize the complete transformation and utilization of organic matter in raw materials but also meet the heat balance of the unit. The carbon efficiency and thermal efficiency are close to 100%. For the oxygen required by this process, if it is produced through the traditional air separation device, the cost is greater. The production of oxygen itself requires energy consumption, so it will lead to a reduction in the energy efficiency of the whole plant. The coupling process of the flexible fluidized pyrolysis process with the water electrolysis process by solar energy is presented as shown in Figure 4. The source problem of oxygen in this scheme can be well-solved, and the green hydrogen produced by water electrolysis can be used to regulate the H_2/CO of the syngas to meet the downstream chemical production requirements. This process scheme realizes the complete product utilization of organic matter in raw materials and the environmental protection standard discharge or comprehensive utilization of inorganic solids, and the heat required in the reaction is balanced by means of a small gasifier and its heat release. The oxygen required comes from the low-cost green oxygen byproduct of green hydrogen, and the syngas can be mixed with green hydrogen for chemical production. Syngas conversion into production chemicals, such as synthetic methanol in the process of water purification, can be used as a raw material for water electrolysis. Compared with the traditional fossil energy hydrogen production technology, hydrogen from water electrolysis production technology undergoes a simple process, no pollution, high hydrogen purity advantage, can be very good with renewable energy, and can also greatly reduce the cost of oxygen production from traditional air separation unit, so to become the final form of green hydrogen and green oxygen, the energy needed can come from solar or wind energy (Hu and Xu, 2022) (Yu et al., 2021) (dos Santos et al., 2017), which can realize the local coal conversion and utilization of solar energy.

4 Conclusion and future work

In this study, the feed material characterization and fluidized bed pyrolysis experiments of the coal liquefaction residue were conducted. Aspen modeling and analysis of four fluidized pyrolysis processes were performed. The experiment and simulation results lead to the following conclusions:

1) The fluidized bed pyrolysis can be an effective process for CLR treatment. A C_{5+} oil yield of 34.81 wt% was obtained in the experiment for water and ash-free raw material basis. The best temperature distribution both in axial and radial directions in the fluidized bed reactor for the heat sensitive pyrolysis reaction is favorable to improving its oil yield as reaction temperature is the most crucial parameter for the pyrolysis process. There is an optimal value of 540°C for pyrolysis reaction temperature since the higher or lower value will lead to reduction of oil yield. In addition, the product coke is less likely to agglomerate than in the fixed-bed reactor due to the high-speed uniform dispersion and flow of the coke inside a fluidized bed. Based on the outcome of the present experimental study, the coke formation mechanism of fluidized bed pyrolysis should be further investigated.

2) The comparison results of four fluidized bed pyrolysis process simulation schemes indicate that the coal liquefaction residue can be converted into a clean product with the highest carbon efficiency (99.52%) for the proposed flexible fluidized bed pyrolysis coupled with water electrolysis. In this scheme, green O_2 from water electrolysis is used for coke gasification for synthesis gas generation, and the green H_2 can be used for adjusting the H_2/CO ratio of the syngas, which can thus be used as feed gas for chemical production plants. This process can realize the energy balance between pyrolysis and gasification reactions, the complete organic matter utilization in raw materials, and nearly zero emission of CO_2. All the carbon elements in coke are converted into syngas, which can be further utilized for chemical production, such as methanol or olefins.
3) Since the proposed flexible fluidized bed pyrolysis coupled with the water electrolysis can realize nearly zero CO_2 emission in the CLR treatment process, it provides a new technical route for the CO_2 emission reduction in organic solid waste utilization and other organic conversion processes, for instance, solid containing coal tar pyrolysis, refinery vacuum residue fluidized catalytic cracking (FCC), and fluidized coking (FC) process.

Data availability statement

The original contributions presented in the study are included in the article/Supplementary Material; further inquiries can be directed to the corresponding author.

Author contributions

BT is the author of the article; leads project research and technology development, engineering development and scale up. Bo processed research data and analytical data and process flow design, and performed Aspen simulations; JG, has contributed in reviewing the final article; QG has contributed in reviewing the final article. XZ, contributed in assisting wit experimen ts and analytical work; HZ, has contributed by assisting with experimental and analytical work; WZ, has contributed by assisting with experimental and analytical work; XH, has contributed by guiding the work; CY, has contributed in guiding the work and article; YY, has contributed in guiding and supervising the work; Y-WL, has contributed to guiding the work.

Conflict of interest

Authors BT, JG, QG, XZ, HZ, WZ, XH, YY, Y-WL, were employed by Synfuels China Technology Co., Ltd.

The remaining author declares that the research was conducted in the absence of any commercial or financial relationships that could be construed as a potential conflict of interest.

Publisher's note

References

Cao, H., and Xiren, H. (2000). *Calculation and Technical Analysis of Catalytic Cracking Process*. Xi'an: Petroleum Industry Press, 10.

Chen, M., YaohuiWang, H., and Chang, H. (2020). Exploration and Research on the Preparation of High Value-Added Products from Direct Coal Liquefaction Residues [J]. *China coal.* 46 (05), 74–80. doi:10.19880/j.cnki.ccm.2020.05.014

Cui, H., Yang, J., and Liu, Z. (1999). Investigation on the Basic Properties and Gasification Activity of Coal Liquefaction Residual Coke [J]. *J. Fuel Chem.* (S1), 16–20.

dos Santos, K. G., Eckert, C. T., De Rossi, E., Bariccatti, R. A., Frigo, E. P., Lindino, C. A., et al. (2017). Hydrogen Production in the Electrolysis of Water in Brazil, a Review. *Renew. Sustain. Energy Rev.* 68, 563–571. doi:10.1016/j.rser.2016.09.128

Hu, B., and Xu, L. (2022). *Research Progress of PEM Electrolytic Water Hydrogen Production under Carbon Peak and Carbon Neutralization Target,* Chemical Progress, 1–15 [2022-09-02]. doi:10.16085/j.issn.1000-6613.2021-2464

kun, G., Tian, Y., Xia, D., et al. (2011). Research Progress of Heavy Oil Catalytic Cracking Technology. *Chem. Ind. Prog.* 30 (6), 1219–1223.

Li, J., Yang, J., and Liu, Z. (2010). Research on the Pyrolysis Characteristics of Coal Direct Liquefied Residue. *J. Fuel Chem.* 38, 4.

Liu, B. (2012). *Study on the Pyrolysis Characteristics of Direct Coal Liquefaction Residues*. Northwestern University.

Shu, Geping (2009). Development Process and Significance of Shenhua Direct Coal Liquefaction Process [J]. *Shenhua Sci. Technol.* 7 (01), 78–82.

Tian, B., Yang, C., and Yang, Y. (2022). Research Progress on the Treatment Process of Direct Coal Liquefaction Residues [J]. *Contemp. Chem. Industry Res.* (09), 144–149.

Wang, Y., and Qi, J. (2012). Research Progress in Fluidized Coking Technology in China. *Contemp. Chem. Ind.* 41.

Winschel, R. A., and Burke, F. P. (1989). Recycle Oils from Fluid Coking of Coal Liquefaction Bottoms. *Energy fuels.* 3 (4), 437–443. doi:10.1021/ef00016a002

Xiang, Hongwei, Yang, Yong, and Li, Yongwang (2014). Indirect Coal Liquefaction: From Basic to Industrialization [J]. *China Sci. Chem.* 44 (12), 1876–1892.

Xiang, H., Yang, Y., and Li, A. (2022). Coal Chemical Industry Reform and Development. *Chem. Prog.* 41, 2022.

Xu, Long, Tang, Mingchen, Duan, Line, Liu, Baolin, Ma, Xiaoxun, Zhang, Yulong, et al. (2014). Pyrolysis Characteristics and Kinetics of Residue from China Shenhua Industrial Direct Coal Liquefaction Plant. *Thermochim. Acta*, 1–10. doi:10.1016/j.tca.2014.05.005

Yang, C., Chen, X., Li, C., and Shan, H. (2017). Challenges and Opportunities for Catalytic Cracking Technology. *J. China Univ. Petroleum Nat. Sci. Ed.* 41 (6), 171177.

Yang, Y., Tian, B., Gao, J., Zhu, X., Guo, Q., and Li, Y. (2020). *A Continuous Treatment Method Containing Solid Slurry and a Device Used for the Implementation of This Method*, CN112048339A

Yang, Yong, Xu, Jian, Liu, Zhenyu, Guo, Qinghua, Ye, Mao, Wang, Gang, et al. (2020). Progress in Coal Chemical Technologies of China. *Rev. Chem. Eng.* 36 (1), 21–66. doi:10.1515/revce-2017-0026

Yu, H., Shao, Z., Hou, M., Yi, B., Duan, F., and Yang, Y. (2021). Hydrogen Production by Water Electrolysis: Progress and Suggestions. *Chin. J. Eng. Sci.* 23 (2), 146. doi:10.15302/j-sscae-2021.02.020

Zhou, Y., Zhang, Y., Li, Z., Yu, G., and Qiu, J. (2007). Preparation of Carbon Nanotubes from Direct Coal Liquefaction Residue as Raw Material[J]. *Coal Convers.* (03), 41–44.

frontiers | Frontiers in Energy Research

TYPE Brief Research Report
PUBLISHED 06 October 2022
DOI 10.3389/fenrg.2022.961734

OPEN ACCESS

EDITED BY
Nallapaneni Manoj Kumar,
City University of Hong Kong, Hong Kong SAR, China

REVIEWED BY
Sudhakar Babu Thanikanti,
Chaitanya Bharathi Institute of Technology, India
Niveditha Sivadanam,
National Institute of Technology Warangal, India

*CORRESPONDENCE
Sura Srinivasa Rao,
ssura@gitam.edu

SPECIALTY SECTION
This article was submitted to Sustainable Energy Systems and Policies, a section of the journal Frontiers in Energy Research

RECEIVED 05 June 2022
ACCEPTED 25 August 2022
PUBLISHED 06 October 2022

CITATION
Chowdary A and Rao SS (2022), Grid-connected photovoltaic-based microgrid as charging infrastructure for meeting electric vehicle load. *Front. Energy Res.* 10:961734. doi: 10.3389/fenrg.2022.961734

Grid-connected photovoltaic-based microgrid as charging infrastructure for meeting electric vehicle load

Appalanaidu Chowdary and Sura Srinivasa Rao*

Department of Electrical Electronics and Communication Engineering, Gandhi Institute of Technology and Management (Deemed to Be a University), Visakhapatnam, Andhra Pradesh, India

Concerns about charging Infrastructure have arisen as electric vehicles (EVs) gain popularity in the transportation sector. Like gas stations, the charging infrastructure is mainly used to power the EV batteries until they are fully charged. As a result, many alternative options for creating charging stations were explored in the literature. This study proposes a grid-connected photovoltaic-based microgrid for EV charging infrastructure. It has two objectives: to design and model a grid-connected photovoltaic-based microgrid and to analyze a hypothetical EV population charging. While modeling, the realistic EV loads are considered, and the simulation is carried out. Results of this study include the power generation potential from the solar power plant, the energy mix of the microgrid (i.e., grid shared energy and onsite solar generation), and supply and load mismatch relationships. The analysis results include the weather parameter influence on power produced, followed by sensitivity analysis quantifying the impact of scaled EV sessions over microgrid power balances. Overall, it is understood that grid-connected microgrids support the seamless charging of EVs even in the case of uncertainties observed with onsite solar energy generation.

KEYWORDS

electric vehicles, charging stations, solar for EVs, microgrid-based EV charging infrastructure, PV plant feasibility

1 Introduction

The growing climate change concerns for various reasons and the associated issues with fossil fuel-based energy have resulted in the decarbonization of the transportation sector. The transportation sector is still responsible for 24% of direct CO_2 emissions, mainly attributable to fossil fuel consumption, according to the International Energy Agency (IEA, 2021), suggesting the transition to the use of renewables for mobility. This pressing need sparked e-mobility leading to electric vehicle (EV) manufacturing and deployment in the market. Despite the growing EV adoption, it lags behind the sophisticated and long-term charging infrastructure needed for charging vehicles. As a result, charging stations were installed and powered mainly by the grid, which raised many critiques from technical aspects and contributions to sustainability (Boschmann

and Kwan, 2008). The technical aspects include many concerns, for instance, voltage stability, power losses, reliability, and an increase in peak load. These are the significant repercussions on the energy sector. The sustainability-related concerns mainly revolved around the grid energy mix; for instance, a country with a significant share of fossil fuel energy mix powering EVs may not be sustainable (Nallapaneni and Chopra, 2021). At the same time, their participation in energy management and power balancing services may also be not sustainable (Nallapaneni and Chopra, 2021). Considering these raised concerns (Boschmann and Kwan, 2008; Nallapaneni and Chopra, 2021), maintaining energy sustainability was prioritized, leading to the development of renewable-based EV charging infrastructure. As a result, experts started focusing on developing EV charging infrastructure with renewables as power sources.

We conducted a thorough literature review to better understand the progress in the charging station research. Sivadanam et al. (2020a) researched renewable energy sources and concluded that renewable energy could be used for EV charging as the power source in off-grid mode. Singh et al. (2020) used a single voltage source converter combined with the solar photovoltaic (PV) array, a storage battery, the grid, and a diesel generator as EV charging infrastructure power components. Later, with the rise of optimization-influenced decisions, researchers started applying optimization and heuristic methods to improve infrastructure sizing and performance further. For instance, a queuing model for a stochastic optimization issue that incorporates RESs and EV charging stations is investigated by Jin et al. (2014) to understand the viability of the EV charging system. Rezaeimozafar et al. (2017) showed the use of the genetic algorithm and particle swarm optimization to size renewable energy sources integrated EV charging stations. Commercial EV charging infrastructure is also created using an integrated power system approach (Deb et al., 2019). Sivadanam et al. (2020b) investigated the implications of large-scale EV integration into the power system. Later, Podder et al.(2021a) designed the solar plus biogas-based EV charging station to power on-road three-wheeler vehicles in developing nations. They mentioned that integrated renewable energy-based systems are more reliable in powering EVs (Podder et al., 2021b). Osório et al. (2018) proposed an EV charging model that examines the load profile effect on the power system for various EV adoption degrees using traditional. They considered solar PV and wind as the power system component, followed by power conversion devices. According to Osório et al. (2018), integrating 15 EVs raises the load by 2%, whereas integrating 50 EVs increases the load by 7%. The above literature covered the apparent transition of EV charging infrastructure research from planning to performance concerning EV fleet increase in the system. Based on the literature, it is understood that optimal modeling of charging stations considering the scaled averaged session of EVs for charging per day is more important.

Hence, this study's objectives align with the observed research gap (i.e., optimal modeling per EV fleet). Nevertheless, when we look further at the EV charging infrastructure, the reliable operation may be considered a critical issue. Researchers have proposed numerous options, for instance, energy storage and backup power generators (Das et al., 2020). Hence, in this study, we considered the grid as a support power option. The key contributions of this study include the formulation of a framework that aids in designing a reliable EV charging station and understanding the performance considering two objectives:

- To design and model the grid-connected photovoltaic-based microgrid considering the EV population while minimizing the peak load.
- To analyze the impact of the scaled average session of EV per day over the charging station power source sizing.

This study is structured in four sections. Section 2 presents the framework and methods adopted for modeling. Section 3 presents the discussion of the results, followed by the conclusion and future work in Section 4.

2 Framework and methods

This section presents the framework that aids in designing a reliable EV charging station for meeting the EV population's load demand without interruption, followed by the proposed system and methodology used for modeling.

2.1 Framework

In Figure 1A, the framework is shown, where a time *versus* load plot defines the reliable operation of charging Infrastructure, highlighting the need for disrupted load compensation by any power source. Therefore, considering the framework, a charging infrastructure system shown in Figure 1B is considered. This infrastructure has an onsite solar power plant that is used to power the EV charging station and the grid to support reliable operation. Additionally, an energy storage system (ESS) and a power converter unit are used. The PV array and ESS are connected on the direct current bus, the grid and EVs are connected on the alternating current bus side, and a power converter is placed between the direct current and alternating current bus.

In order to understand the reliable operation of the proposed charging infrastructure, a power governance function is used as follows:

$$P_{EVCS} = f\left(P_g, P_{pv}\right), \tag{1}$$

where P_{EVCS} is the power required by the EV charging station, P_g is the power from the grid, and P_{pv} is the power from photovoltaics.

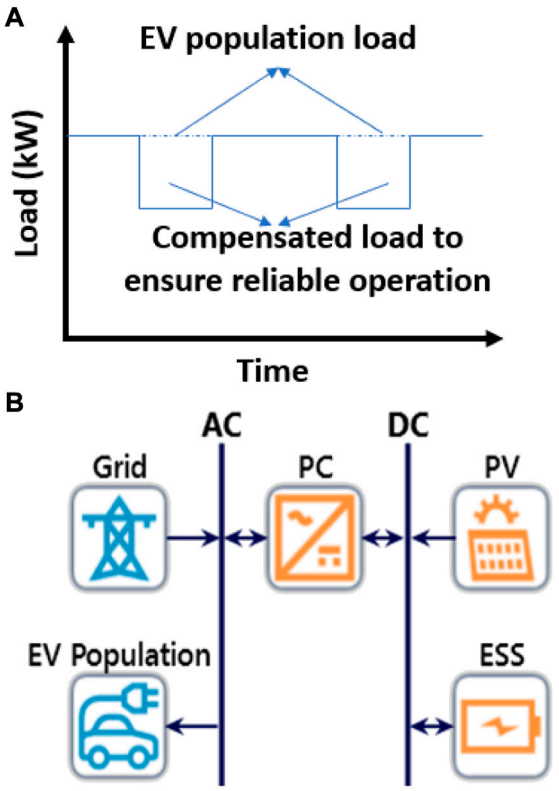

FIGURE 1
(A) Framework to ensure reliable operation of the EV charging station. **(B)** Schematic representation of proposed grid-connected photovoltaic-based microgrid as EV charging infrastructure.

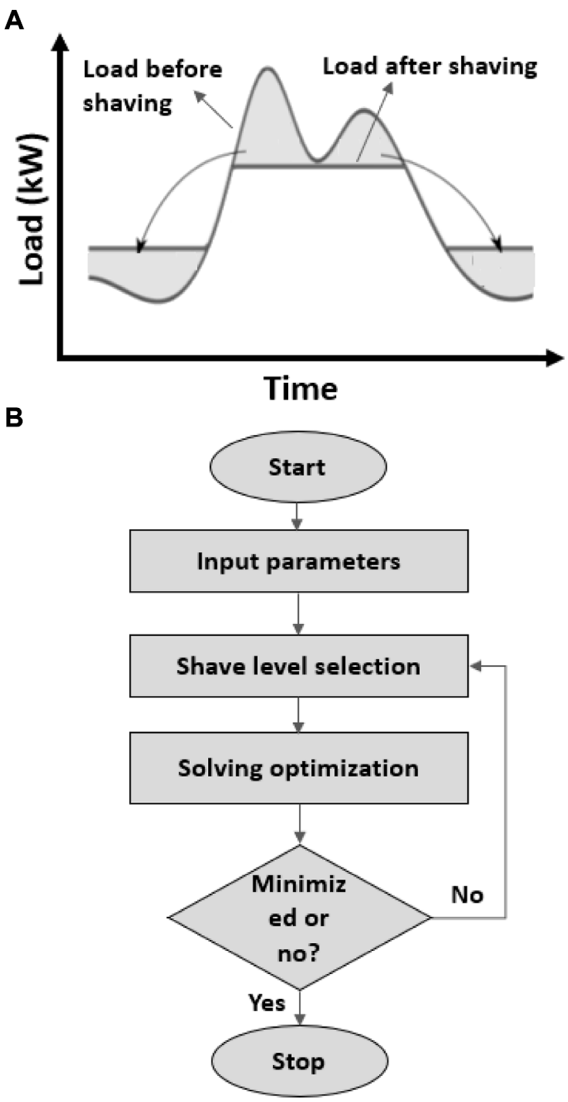

FIGURE 2
(A) Conceptual principle of peak shaving. **(B)** A simplified optimization approach for peak shaving in electric vehicle charging infrastructure.

As per Eq. 1, the power is maintained depending upon the reliable operating condition. For instance, the grid would provide support if there were disruptions on the solar PV array side. In all other cases, maximized use of solar PV energy is considered.

2.2 Grid-connected photovoltaic-based microgrid as charging infrastructure

In the below sections, the detailed modeling of individual components of the EV charging station is shown.

2.2.1 Electric vehicle load

An EV population of 100 is considered for this study, with 150 kW as the maximum power required to charge the vehicle, and the average duration of the vehicle charging is 50 min.

2.2.2 Modeling the power source

As shown in Figure 1B, the proposed system has two power sources: the grid and the onsite solar PV power plant. The PV plant's electric power output is given as follows (Chowdary et al., 2020, Podder et al. (2021b):

$$P_{pv} = \eta_{pv}.\eta_{pc}.A_{pv}.G_{pv}\left(1 + \gamma\left(T_c - T_{ref}\right)\right), \quad (2)$$

where P_{pv} is the power from photovoltaics, η_{pv} is the solar PV power conversion efficiency, η_{pc} is the power converter efficiency, A_{pv} is the surface area of the solar PV array, G_{pv} is the solar radiation incident on the solar PV array (see Supplementary Figure S1 for solar radiation profile), γ is the temperature coefficient, T_c is solar PV cell temperature, and T_{ref} is the reference temperature (i.e., 25°C).

In solar PV installations, temperature plays a crucial role in power performance. Hence, we considered temperature-influenced power. For evaluating the cell temperature, a model

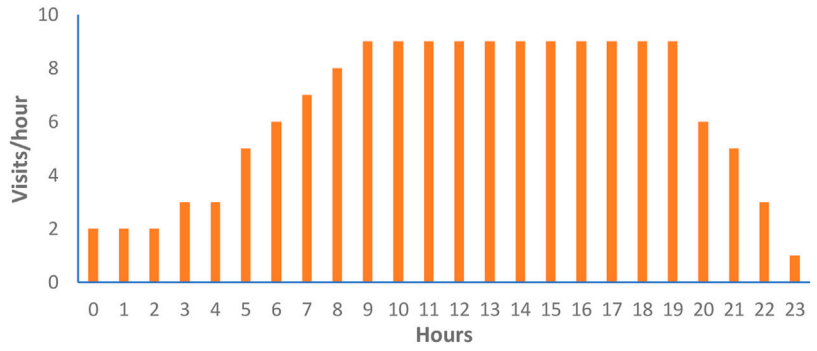

FIGURE 3
Electric vehicle visits profile at the charging station.

TABLE 1 Electric vehicle charging session summary.

Sessions per day	Sessions per year	Annual energy served (kWh)	Energy per session (kWh)	Peak power (kW)	Energy storage
10	3,609	450,845	125	350	6
20	7,312	912,965	125	600	11
30	11,058	1,382,360	125	700	17
40	14,466	1,808,302	125	840	19

shown in the following equation is used (Kumar et al., 2018; Kumar et al., 2019):

$$T_c = T_a + mc\left(\frac{0.32}{8.91 + 2W_s}\right).G_{pv}, \quad (3)$$

where T_a is the ambient temperature (see Supplementary Figure S2 for temperature profile), mc is the mounting coefficient for rooftop or building attached or integrated system, and W_s is the wind speed (see Supplementary Figure S3 for wind speed profile).

2.2.3 Modeling the power converter

A power converter is a device that helps convert the direct current produced by a solar PV array to alternating current and alternating current to direct current to charge the ESS with grid power. Thefollowing equation governs the power converter operation (Kumar et al., 2019; Chowdary et al., 2020).

$$P_{pc} = \eta_{pc}.P_{pv} \quad (4)$$

where P_{pc} is the power output from the power converter.

2.2.4 Energy storage system

We modeled the ESS as a charging station, where Eqs 5, 6 govern the charging and discharging patterns of the charging infrastructure based on the EV fleet (Kumar et al., 2018). Here, the number of chargers is 40, with each charger's capacity of 150 kW (Chowdary et al., 2020):

$$\sum_{t=1}^{n} ESS = \sum_{t=1}^{n}\left[\left(ESS(t-1).\left(1 - DR_{self}\right)\right) + \left(\left(P_g + P_{pv}\right) - P_{ev}\right).\eta_{pc}.\eta_{ess}\right], \quad (5)$$

$$\sum_{t=1}^{n} ESS = \sum_{t=1}^{n}\left[\left(ESS(t-1).\left(1 - DR_{self}\right)\right) + \left(P_{ev}.\eta_{pc} - \left(P_g + P_{pv}\right)\right)\right], \quad (6)$$

where DR_{self} is the self-discharge rate of the storage system, P_{ev} is the power profile of the EV, η_{ess} is the efficiency of the ESS, and t is the time starting from 1 to n.

2.3 Optimization method

The proposed system in this study is a grid-connected PV-based microgrid as EV charging infrastructure and is modeled considering Visakhapatnam city as the study location. The solar radiation, clearness index, temperature, and wind speed profiles are considered per the location; see Supplementary Figures S1–S3. Based on the discussed mathematical model in Section 2.2, the system is the preliminary model was modeled in the HOMER Grid tool (Grid, 2022). The peak-shaving

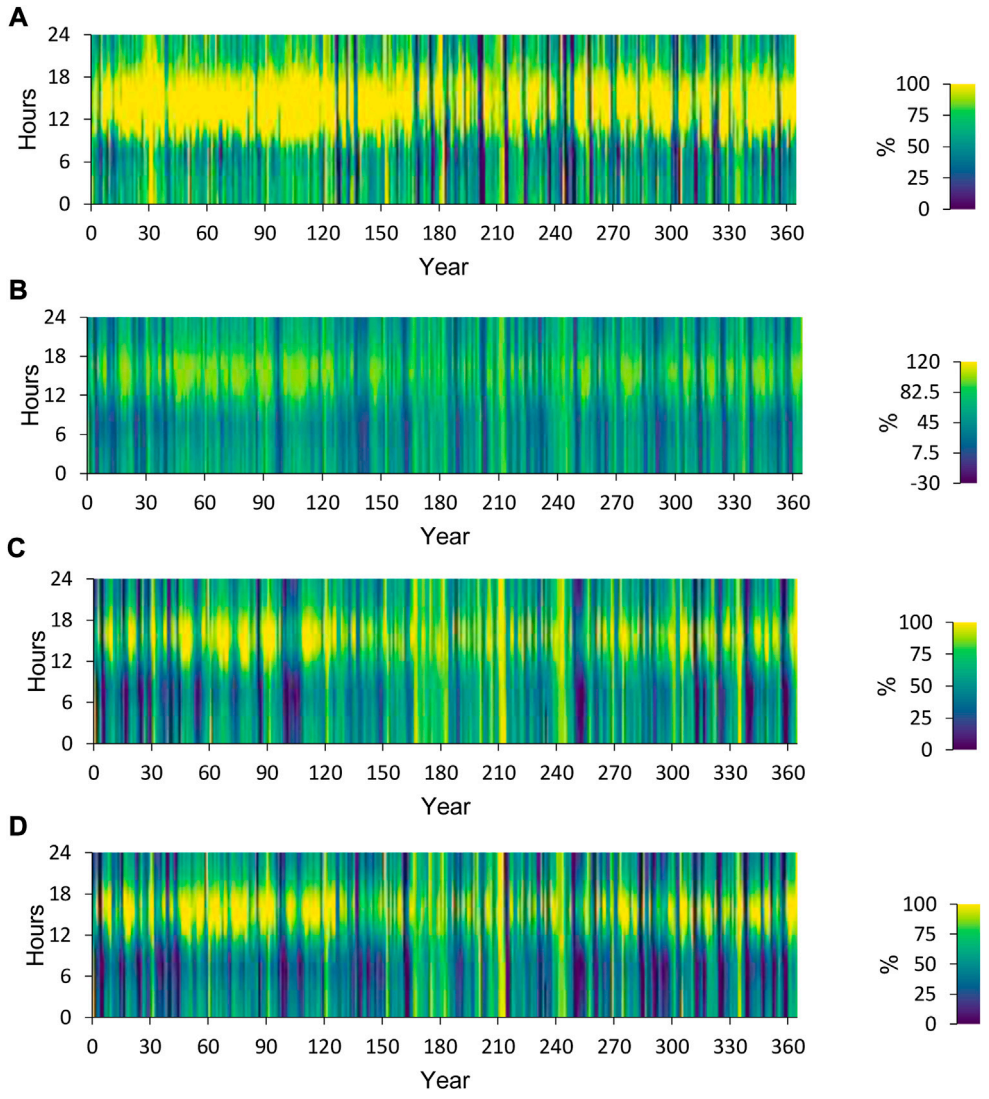

FIGURE 4
The energy storage state of charge in %. as per the scaled average daily sessions. **(A)** 10, **(B)** 20, **(C)** 30, and **(D)** 40.

strategy used for energy management was modeled in MATLAB 2019 (Mathworks, 2019), which was then coupled to the HOMER Grid optimization tool for further simulation and analysis.

2.3.1 Peak-shaving controller

A peak-shaving controller similar to the load leveling controller is used. The proposed controller proactively manages the EV overall load demand and, while managing it, eliminates the short-term demand spikes; see Figure 2A for a conceptual understanding of the peak-shaving strategy. To implement this strategy, we used the optimization approach that selects the shaving level governed by Eq. 8 while minimizing the optimization function below (Karmiris and Tengnér, 2013).

Objective function:

$$\min f(x) = \left| C_{ess} - \left(max \int_{t0}^{t} L(t).dt - min \int_{t0}^{t} (L(t) - x).dt \right) \right|, \tag{7}$$

Leveling constraints:

$$L(t)_{max} < x < L(t)_{min}, \tag{8}$$

Figure 2B shows the flowchart for solving the optimization problem, starting with input parameters selection followed by shave level selection and

TABLE 2 Energy storage system sizing and energy results.

Quantity	Value for each scenario of scaled sessions per day			
	10	20	30	40
Energy storage properties				
Batteries (qty)	6.00	11.0	17.0	19.0
String size (batteries)	1.00	1.00	1.00	1.00
Strings in parallel (strings)	6.00	11.0	17.0	19.0
Bus voltage (V)	380	380	380	380
Energy storage statistics				
Nominal capacity (kWh)	1,260	2,310	3,570	3,990
Lifetime throughput (kWh)	4,610,417	7,479,453	9,897,110	13,321,341
Expected life (yr)	10.0	10.0	10.0	10.0
Energy storage result data				
Annual throughput (kWh/yr)	461,042	747,945	989,711	133,213
Losses (kWh/yr)	28,228	45,529	59,732	81,214
Storage depletion (kWh/yr)	−1,260	−2,310	−3,570	−3,990

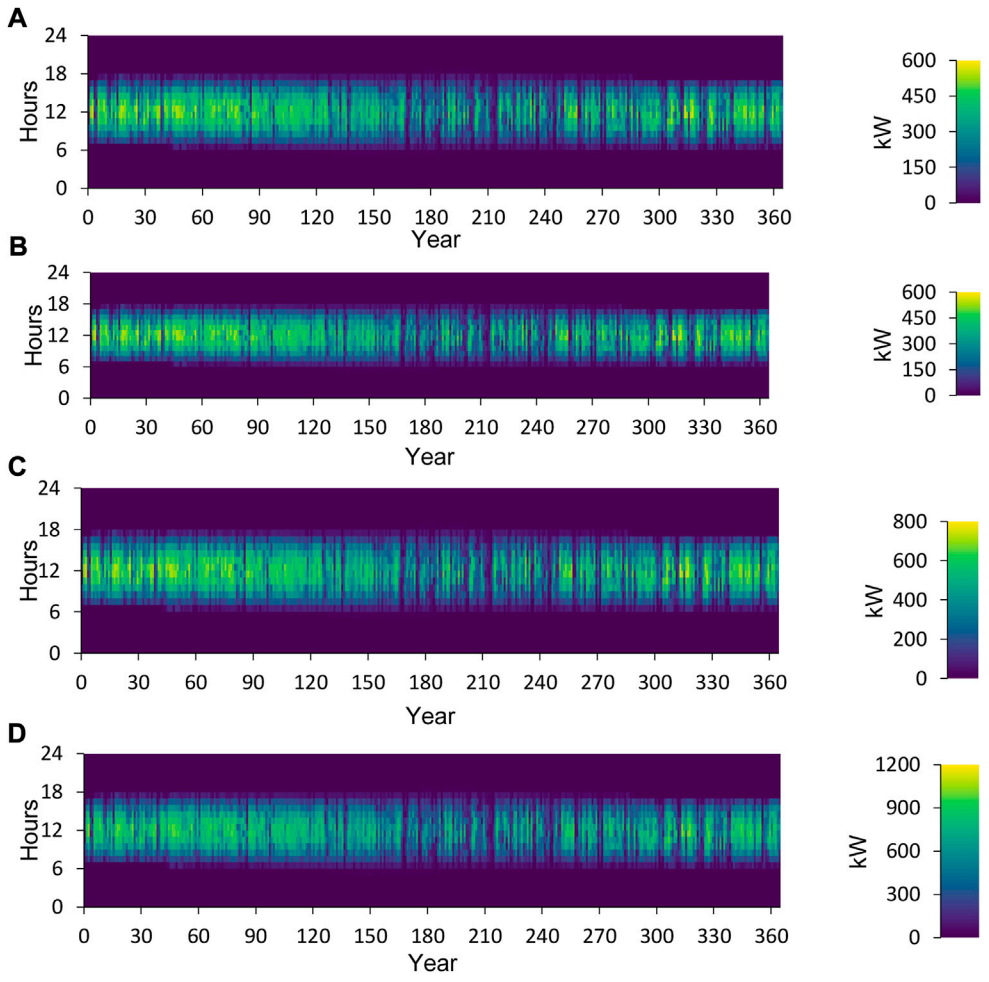

FIGURE 5
Power output from the solar photovoltaic plant as per the scaled average daily sessions. **(A)** 10, **(B)** 20, **(C)** 30, and **(D)** 40.

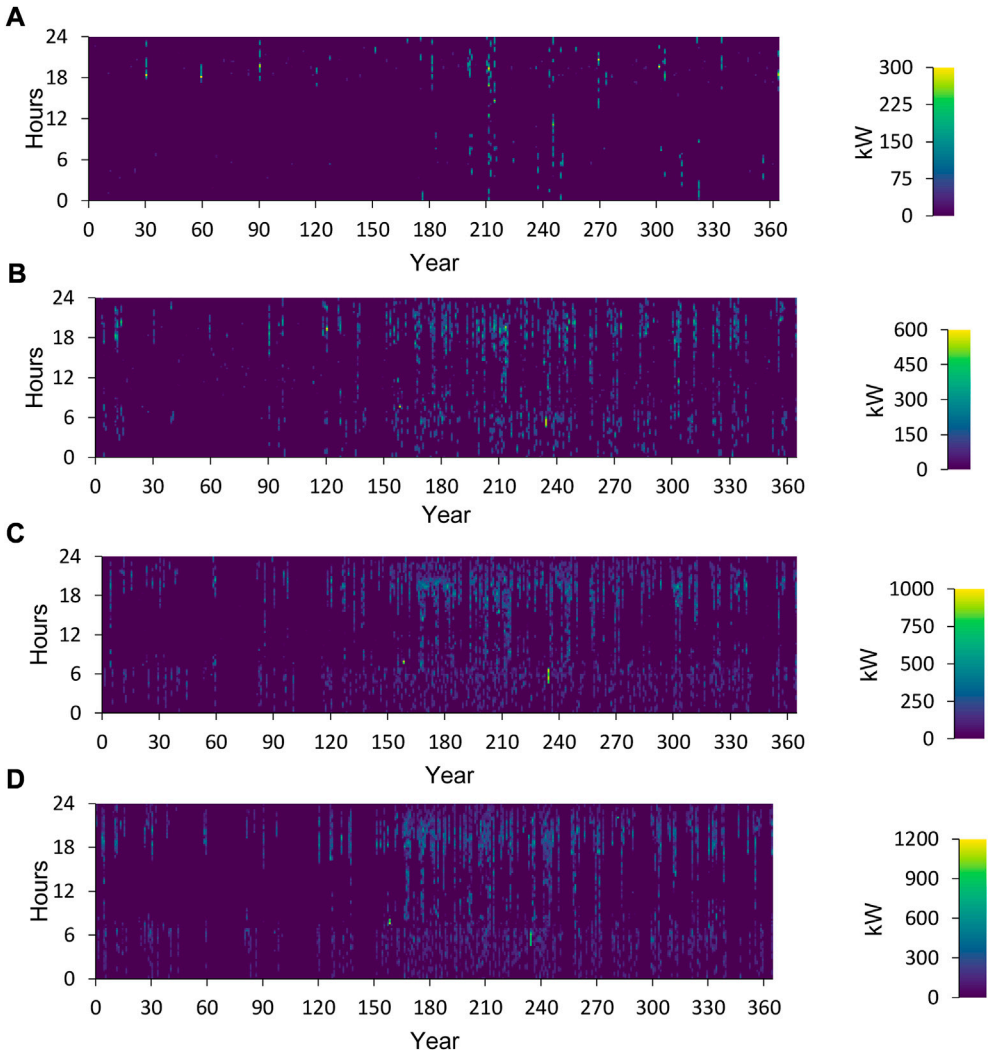

FIGURE 6
Power imports from the grid as per the scaled average daily sessions. **(A)** 10, **(B)** 20, **(C)** 30, and **(D)** 40.

optimization problem solving, then checking the decision whether the objective function error is minimized or not. If not minimized, it again checks by selecting different shave levels following Eq. 7.

2.3.2 Sensitivity analysis

For any EV charging station, the problem of the number of EVs connected could arise; hence, we considered the number of vehicles that could be connected to the charging station in a day as a sensitive parameter. Based on the visits/hour, the number of vehicles that can be connected to the charging station during the hour is calculated. For this, scaled average sessions/day is considered in the range of 10–40. Additionally, solar irradiation in the given location is considered a sensitive parameter.

3 Results and discussion

This section presents simulated results of the proposed grid-connected microgrid as an EV charging infrastructure. The results include the EV session per day's influence on the infrastructure design, powerful performance of microgrid, and the impact of scaled EV sessions over microgrid power balances.

3.1 Analysis of the charging station design

Figure 3 represents the EV average visits profile at the charging station on a 24 h time scale. Based on this, the applied sensitive cases of sessions per day varying from 10 to 40 resulted in a considerable impact on the energy served at the

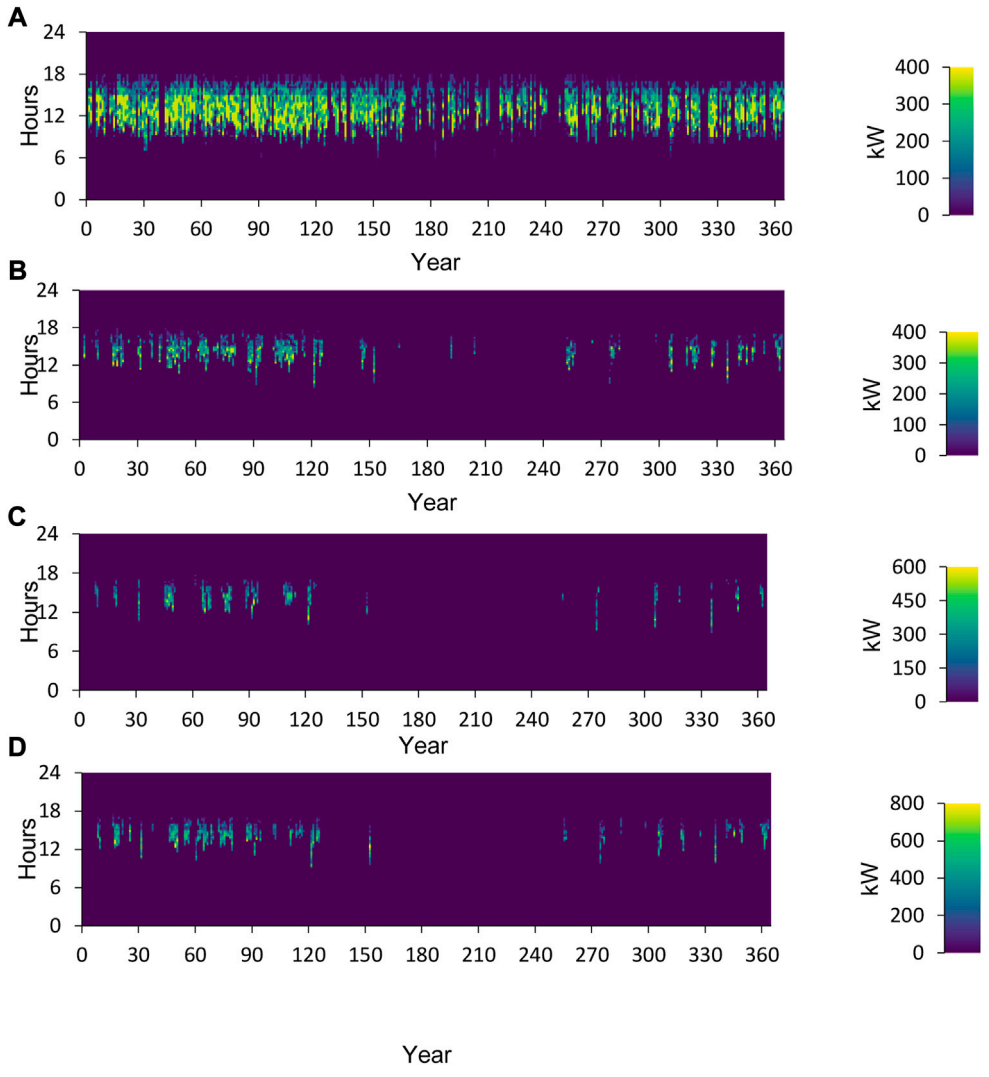

FIGURE 7
Power exports to the grid as per the scaled average daily sessions. **(A)** 10, **(B)** 20, **(C)** 30, and **(D)** 40.

charging station. The summary of the session profile and its impacts on energy served and peak demand are provided in Table 1.

Table 1 shows that the observed peak power demand varied from 350 to 840 kW. Furthermore, the energy storage strings required varied from 6 to 19. Table 2 presents the charging station's ESS properties and results. The nominal capacity is varied from 1,260 to 3,990 kWh. The observed annual throughput varies from 461,042 to 133,213 kWh/yr, whereas the energy losses range between 28,228 and 81,214 kWh/yr.

In Figure 4, the state of charge results is presented. The microgrid system design size also varied to power these varying energy needs. As a result, the component sizing of the microgrid that is believed to serve as a power source for a charging station is affected. Additionally, grid support was considered to ensure reliable operation.

3.2 Power performance results of microgrid

The proposed microgrid's primary power generation source is a solar PV power plant. The grid is a backup that provides and takes energy depending upon the situation of surplus and deficit based on the uncertain operation of solar and load. Figure 5 shows the DMap showing the solar PV power outputs for the whole year. This indicates that the PV plant supplies power to the charging station mostly between 06:10 and 18:00 h on a given day throughout the year with 2%–5% of the hourly variation. However, depending on the scaled session, the required peak capacity of the solar power plant varied; see Figures 5A–D. The observed mean power output from the solar power plant is varied between 2,592 and 4,753 kWh/day, depending on the peak installed capacities. The average capacity factor of the

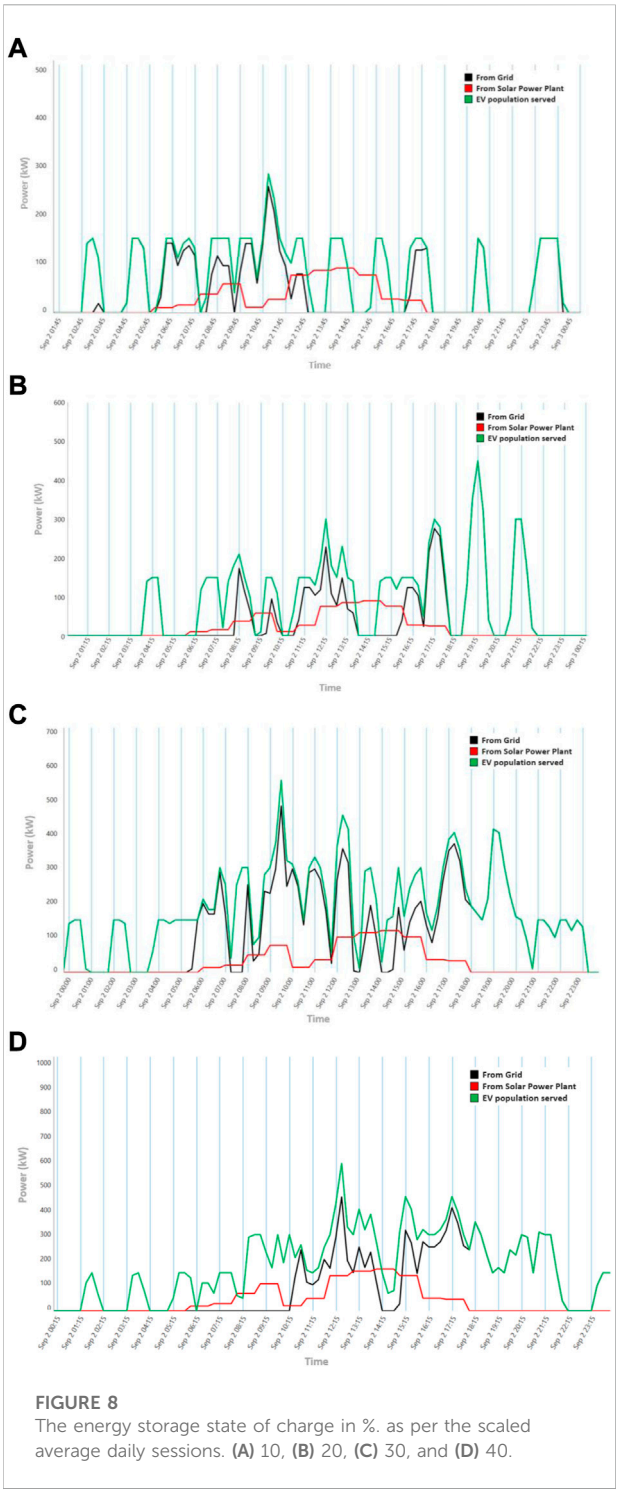

FIGURE 8
The energy storage state of charge in %. as per the scaled average daily sessions. **(A)** 10, **(B)** 20, **(C)** 30, and **(D)** 40.

photovoltaic plant is observed to be 18%. The total operating hours of the photovoltaic power plant is 4,343 h/y based on the incident solar radiation (i.e., 5.07 kWh/Sq.m/day) and the clearness index (i.e., 0.67). The total energy production under the four scaled sessions varied from 946,235 to 1,734,764 kWh/y. The observed solar power penetration was around 97%.

Figure 6 shows power imports from the grid to the charging station. Due to the solar PV plant's uncertain operation, gird support became obvious in meeting the EV charging station demand. The observed grid imports are 1.54% (i.e., 14,840 kWh/yr), 12.7% (i.e., 137,344 kWh/yr), 18.4% (i.e., 284,113 kWh/yr), and 15.7% (i.e., 322,092 kWh/yr) for 10, 20, 30, and 40 scaled averaged sessions per day, respectively.

Apart from imports, the proposed microgrid also exported some power share, as shown in Figure 7. The observed grid imports are 46.9% (i.e., 397,502 kWh/yr), 7.01% (i.e., 68,848 kWh/yr), 2.74% (i.e., 38,935 kWh/yr), and 4.13% (i.e., 77,973 kWh/yr) for 10, 20, 30, and 40 scaled averaged sessions per day, respectively.

3.3 Impact of scaled EV sessions over microgrid power balances

As discussed in Section 3.2, charging station interaction with solar PV plant and utility was evident, and this interaction varied dynamically. It is observed that the proposed peak-shaving control strategy proactively managed the EV overall load demand while eliminating the short-term demand spikes, as shown in Figure 8. To be more precise, a day's results (i.e., 2 September) are shown where the interactions are clearly shown. Figures 8A–Dshow that the power imported from the grid is varied both quantity-wise and consumption time-wise. It is also observed that the highest percentage of power is imported in the case where averaged sessions per day are more.

4 Conclusion and future work

This study proposed a grid-connected photovoltaic-based microgrid as an EV charging infrastructure. Its design and modeling are carried out, followed by an analysis. While modeling, realistic EV loads are considered and simulated in four scenarios based on the scaled averaged session per day. The analysis included the results mainly focusing on power generation potential from the solar power plant, energy mix of the microgrid (i.e., grid shared energy and onsite solar generation), and supply and load mismatch relationships for the EV charging station. Based on the observed results, the following conclusions were drawn:

- The proposed peak-shaving dispatch strategy eliminated short spikes, so incorporating this in the size optimization plays a crucial role.
- The proposed model showed a high solar fraction with a minor share of imports from and exports to the grid. This clearly showed that EV charging stations could be made grid-independent; however, keeping the uncertain renewable operation, it is suggested to have grid connectivity.
- Based on the scaled sessions per day, there is a possibility of increased peak capacity installation of the PV plant, which

might influence the overall cost of the charging infrastructure. This could be considered a research direction.

The future work includes placing the proposed microgrid-based EV charging station in the distribution system by identifying a suitable location, to understand the techno-economic feasibility of such integration.

Data availability statement

The original contributions presented in the study are included in the article/Supplementary Material. Further inquiries can be directed to the corresponding author.

Author contributions

Conceptualization and modeling are done by AC. Framework, design, and analysis are done by AC. SR guided and reviewed the work done.

Conflict of interest

The authors declare that the research was conducted in the absence of any commercial or financial relationships that could be construed as a potential conflict of interest.

Publisher's note

All claims expressed in this article are solely those of the authors and do not necessarily represent those of their affiliated organizations or those of the publisher, the editors, and the reviewers. Any product that may be evaluated in this article, or claim that may be made by its manufacturer, is not guaranteed or endorsed by the publisher.

Supplementary material

The Supplementary Material for this article can be found online at: https://www.frontiersin.org/articles/10.3389/fenrg.2022.961734/full#supplementary-material

References

Boschmann, E. E., and Kwan, M. P. (2008). Toward socially sustainable urban transportation: Progress and potentials. *Int. J. Sustain. Transp.* 2 (3), 138–157. doi:10.1080/15568310701517265

Chowdary, A., Sura, S., and Ra, O. (2020). Off-grid solar photovoltaics powered charging infrastructure for electric vehicles. *J. Green Eng.* 10, 12721–12728.

Das, S. R., Ray, P. K., Sahoo, A. K., Ramasubbareddy, S., Babu, T. S., Kumar, N. M., et al. (2020). Performance of hybrid filter in a microgrid integrated power system network using wavelet techniques. *Appl. Sci.* 10 (19), 6792. doi:10.3390/app10196792

Deb, S., Tammi, K., Kalita, K., and Mahanta, P. (2019). Charging station placement for electric vehicles: A case study of guwahati city, India. *IEEE Access* 7, 100270–100282. doi:10.1109/access.2019.2931055

Grid, H. (2022). Getting Started with HOMER Grid, March 5 2021. URL: https://homerenergy.force.com/supportcenter/s/article/getting-started-with-homer-grid (accessed August 18, 2022).

IEA (2021). Tracking Transport 2021 https://www.iea.org/reports/tracking-transport-2021.

Jin, C., Sheng, X., and Ghosh, P. (2014). Optimized electric vehicle charging with intermittent renewable energy sources. *IEEE J. Sel. Top. Signal Process.* 8, 1063–1072. doi:10.1109/jstsp.2014.2336624

Karmiris, G., and Tengnér, T. (2013). *Peak shaving control method for energy storage*. Vasterås, Sweden: Corporate Research Center.

Kumar, N. M., Gupta, R. P., Mathew, M., Jayakumar, A., and Singh, N. K. (2019). Performance, energy loss, and degradation prediction of roof-integrated crystalline solar PV system installed in Northern India. *Case Stud. Therm. Eng.* 13, 100409. doi:10.1016/j.csite.2019.100409

Kumar, N. M., Sudhakar, K., Samykano, M., and Jayaseelan, V., "BIPV market growth: SWOT analysis and favorable factors, " 2018 4th International Conference on Electrical Energy Systems (ICEES), 07-09 February 2018, Chennai, India, 2018, pp. 412–415.

Mathworks (2019). *R2019a at a glance*. URL: https://www.mathworks.com/products/new_products/release2019a.html (accessed August 19, 2022).

Nallapaneni, M. K., and Chopra, S. S. (2021). "Electric vehicles participation in load frequency control of an interconnected power system is not sustainable," in 6th AIEE Energy Symposium Current and Future Challenges to Energy Security: the energy transition, a pathway from low carbon to decarbonization, 14 - 17 December 2021, Milan, Italy.

Osório, G. J., Shafie-Khah, M., Coimbra, P. D. L., Lotfi, M., and Catalão, J. P. S. (2018). Distribution system operation with electric vehicle charging schedules and renewable energy resources. *Energies* 11, 3117. doi:10.3390/en11113117

Podder, A. K., Das, A. K., Hossain, E., Kumar, N. M., Roy, N. K., Alhelou, H. H., et al. (2021b). Integrated modeling and feasibility analysis of a rooftop photovoltaic systems for an academic building in Bangladesh. *Int. J. Low-Carbon Technol.* 16 (4), 1317–1327. doi:10.1093/ijlct/ctab056

Podder, A. K., Supti, S. A., Islam, S., Malvoni, M., Jayakumar, A., Deb, S., et al. (2021a). Feasibility assessment of hybrid solar photovoltaic-biogas generator based charging station: A case of easy bike and auto rickshaw scenario in a developing nation. *Sustainability* 14 (1), 166. doi:10.3390/su14010166

Rezaeimozafar, M., Moradi, M. H., and Amini, M. H. (2017). A simultaneous approach for optimal allocation of renewable energy sources and electric vehicle charging stations in smart grids based on improved GA-PSO algorithm. *Sustain. Cities Soc.* 32, 627–637. doi:10.1016/j.scs.2017.05.007

Singh, B., Verma, A., Chandra, A., and Al-Haddad, K. (2020). Implementation of solar PV-battery and diesel generator based electric vehicle charging station. *IEEE Trans. Ind. Appl.* 56, 4007–4016. doi:10.1109/TIA.2020.2989680

Sivadanam, N., Nagu, B., and Sydulu, M. (2020a). Inertial response and frequency control in electric vehicles integrated renewable and non-renewable power system. *J. Green Eng.* 10 (11), 10981–10993.

Sivadanam, N., Nagu, B., and Sydulu, M. (2020b). Performance optimization of an interconnected power system in the presence of plug-in hybrid electric vehicles. *J. Green Eng.* 10 (9), 4910–4925.

frontiers | Frontiers in Energy Research

TYPE Original Research
PUBLISHED 15 September 2022
DOI 10.3389/fenrg.2022.984003

OPEN ACCESS

EDITED BY
Nallapaneni Manoj Kumar,
City University of Hong Kong, Hong Kong SAR, China

REVIEWED BY
Idiano D'Adamo,
Sapienza University of Rome, Italy
Umar Muhammad Modibbo,
Modibbo Adama University of Technology, Nigeria
Sandhya Thotakura,
Gandhi Institute of Technology and Management (GITAM), India

*CORRESPONDENCE
Paul Weigel,
pweigel@uni-osnabrueck.de

SPECIALTY SECTION
This article was submitted to Sustainable Energy Systems and Policies, a section of the journal Frontiers in Energy Research

RECEIVED 01 July 2022
ACCEPTED 22 August 2022
PUBLISHED 15 September 2022

CITATION
Weigel P, Viebahn P and Fischedick M (2022), Holistic evaluation of aircraft detection lighting systems for wind turbines in Germany using a multi-method evaluation framework. *Front. Energy Res.* 10:984003. doi: 10.3389/fenrg.2022.984003

Holistic evaluation of aircraft detection lighting systems for wind turbines in Germany using a multi-method evaluation framework

Paul Weigel[1,2]*, Peter Viebahn[1] and Manfred Fischedick[1]

[1]Wuppertal Institute for Climate, Environment and Energy, Wuppertal, Germany, [2]Institute of Mathematics, Osnabrück University, Osnabrück, Germany

Transponder-based Aircraft Detection Lighting Systems (ADLS) are increasingly used in wind turbines to limit beacon operation times, reduce light emissions, and increase wind energy acceptance. The systems use digital technologies such as receivers of digital transponder signals, LTE/5G, and other information and communication technology. The use of ADLS will be mandatory in Germany both for new and existing wind turbines with a height of >100 m from 2023 (onshore) and 2024 (offshore), so a nationwide rollout is expected to start during 2022. To fully realize the benefits while avoiding risks and bottlenecks, a thorough and holistic understanding of the efforts required and the impacts caused along the life cycle of an ADLS is essential. Therefore, this study presents the first multi-aspect holistic evaluation of an ADLS. A framework for evaluating digital applications in the energy sector, previously developed by the authors, is refined and applied. The framework is based on multi-criteria analysis (MCA), life cycle assessment (LCA), and expert interviews. On an aggregated level, the MCA results show an overall positive impact from all stakeholders' perspectives. Most positive impacts are found in the society and politics category, while most negative impacts are of technical nature. The LCA of the ADLS reveals a slightly negative impact, but this impact is negligible when compared to the total life cycle impact of the wind turbines of which the ADLS is a part. Besides the aggregated evaluation, detailed information on potential implementation risks, bottlenecks, and levers for life cycle improvement are presented. In particular, the worldwide scarcity of the required semiconductors, in combination with the general lack of technicians in Germany, lead to the authors' recommendation for a limited prolongation of the planned rollout period. This period should be used by decision-makers to ensure the availability of technical components and installation capacities. A pooling of ADLS installations in larger regions could improve plannability for manufacturers and installers. Furthermore, an ADLS implementation in other countries could be supported by an early holistic evaluation using the presented framework.

KEYWORDS

digitalization, cyber-physical systems, wind energy, sustainability, holistic evaluation, multi-criteria analysis, life cycle assessment, aircraft detection lighting systems

1 Introduction

Wind turbines (WTs) are potential obstructions to air traffic and must therefore be equipped with obstruction lights (flashing red beacons) if their total height exceeds 100 m (outside of urban areas), as defined by the International Civil Aviation Organization (ICAO, 2018) and specified for Germany in the "General Administrative Regulation on the Marking of Aviation Obstructions" (BMDV, 2020). Obstruction lights can cause annoyance and thus reduce the acceptance of wind energy (Pohl et al., 2021). As modern turbines become taller and more turbines are installed, more people may be affected, leading to an increasing acceptance problem. Social acceptance of wind energy projects, however, is of great importance to avoid local opposition. Such opposition can delay or impede the construction of new WTs and even slow down the overall transition to renewable energies (Ellis and Ferraro, 2016).

In order to reduce the light emissions caused by the flashing red beacons and thereby increase the social acceptance of WTs, the German regulatory authority has specified in the Renewable Energy Act (German Federal Ministry for Economic Affairs and Energy, 2021) the obligation to equip WTs with Aircraft Detection Lighting Systems (ADLS). ADLS allow WTs' beacons to remain off during nighttime hours when no aircraft is detected in the vicinity. Under the aforementioned law, ADLS are mandatory for all onshore WTs that require aviation obstruction lighting and all offshore WTs located near the coast and in certain offshore areas. The obligation will take effect on 1 January 2023 for onshore and 1 January 2024 for offshore turbines. It is estimated that approximately 17,500 onshore turbines (Roscher, 2019) and all of the 1,500 offshore turbines (Deutsche WindGuard GmbH, 2021) will need to be retrofitted by the start of the obligation. However, due to a technological dispute that was not resolved until 2019, only a minority of turbines have already been equipped. Therefore, a large rollout is expected during the year 2022.

Given this nationwide rollout, a thorough understanding of its impacts is necessary for all stakeholders involved to be able to weigh positive and negative impacts against each other and to avoid otherwise unforeseen potential negative impacts or implementation bottlenecks. Several studies analyzed the impact of ADLS on WT acceptance. An early study (Hübner and Pohl, 2010; Pohl et al., 2012), funded by the German Federal Ministry for the Environment, Nature Conservation, Nuclear Safety, and Consumer Protection, found that nighttime obstruction lighting is less of a cause for annoyance compared to changes in the landscape and emitted noise, but is perceived as similarly annoying compared to shadow flicker. The authors recommend the use of ADLS as a measure to improve acceptance. Further, in (Rudolph et al., 2017), the authors confirmed previous studies and identified a perceived annoyance associated with obstruction lights from WTs. A comparison of annoyance between Europe and the United States (Hübner et al., 2019) shows that obstruction lights cause slightly higher annoyance among Europeans, but overall annoyance levels are relatively low. A more recent study found that annoyance from obstruction lighting is generally low but on average higher than noise annoyance and more geographically widespread. The authors again recommend the use of ADLS (Pohl et al., 2021). Overall, evidence suggests that ADLS will indeed have a positive impact on the social acceptance of wind turbines. In addition, a technical risk assessment focusing on aviation was conducted for the transponder-based technological options in comparison to radar-based options (Behrend, 2019). The author concludes that the risk of a system failure with consequences for aviation safety is very low and the same for all technological options.

According to the authors' knowledge, societal impacts beyond acceptance, non-aviation-risk-related technical impacts, and environmental as well as economic impacts have not yet been analyzed. In particular, neither a life cycle assessment nor an environmental study, or a holistic assessment incorporating multiple perspectives, involving relevant stakeholders, and considering all relevant impact areas has been conducted so far. In order to close this gap, in this paper, a multi-method framework for evaluating digital applications in the energy sector, previously developed by the authors (Weigel et al., 2021), is refined and applied to conduct a holistic evaluation of ADLS. The main novelty of the study is that it presents the first holistic evaluation of ADLS, in contrast to existing publications, which focus on single evaluation aspects. A secondary minor novelty is the refinement of the evaluation framework and its application.

The remainder of the article is organized as follows: the refinement of the evaluation framework and its adaption to ADLS is described in Section 2. While Section 3 shortly describes the ADLS technology and the chosen assumptions, Section 4 shows the results of the holistic evaluation. After discussing the results in Section 5, the conclusions and an outlook are given in Section 6.

2 Methodology

There are a variety of sustainability and multi-criteria evaluation methods and combinations of methods, many of which have recently been used for high-level assessments at

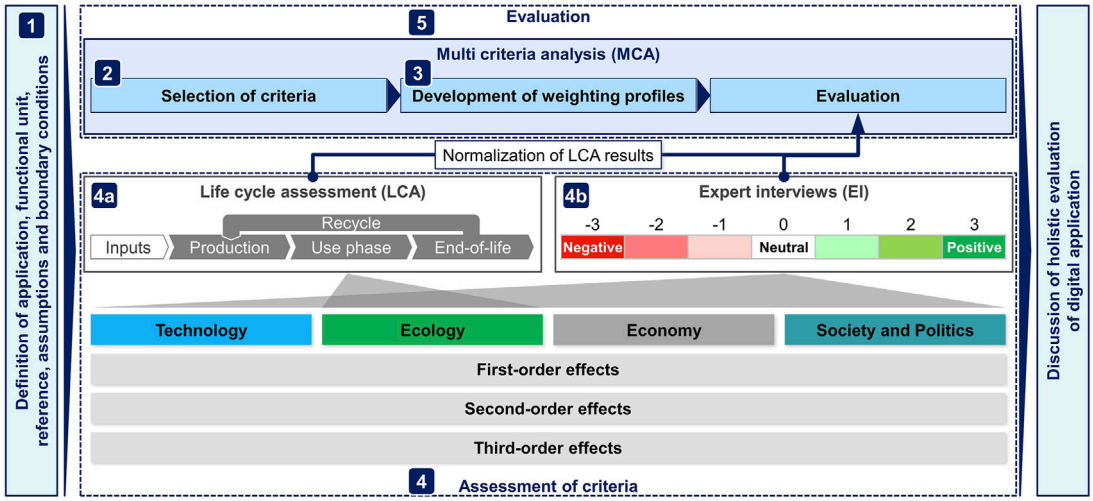

FIGURE 1
Modified multi-method framework for evaluating digital applications in the energy sector, based on (Weigel et al., 2021).

the country level, e.g. (Sun et al., 2022), (D'Adamo et al., 2022), for more specific assessments in the energy sector, e.g., (Kluczek and Gladysz, 2022), (Naegler et al., 2021), and for assessments of digital topics, e.g., (Gährs et al., 2021), (Zhang et al., 2021). A review of methods applied in the energy sector (energy planning) and each method's appropriateness in the decision problem's context is provided in (Cajot et al., 2017). In (Weigel et al., 2021) the authors thoroughly discuss a variety of current evaluation and assessment methods and identify a gap regarding an approach to transparently and holistically evaluate digital applications in the energy sector. To fill this gap, a combination of three well-established methods is suggested, and its use is demonstrated. The novelty of the framework consists of the specific combination of methods and its adaption to digital applications in the energy sector.

The objective of the framework is to provide a structured basis for the holistic evaluation of digital applications. To achieve this holistic view, multiple criteria covering the impact areas technology, ecology, economy and society and politics are evaluated in a multi-criteria analysis (MCA), and the perspectives of relevant stakeholders are considered in the form of weighting profiles. While most ecological criteria are assessed by performing a life cycle assessment (LCA), all other criteria are assessed by conducting expert interviews (EI) with relevant stakeholder representatives. Furthermore, due to the dynamic development of digital applications, a flexible approach is applied that can be adapted to the practitioner, the application, and the availability of information. In this way, a wide range of digital applications, including future developments, can be evaluated. Last but not least, the applied approach provides detailed insights as well as aggregated results with a high level of transparency on each step of the evaluation.

The framework applied in this study is a refined version of the framework originally presented by the authors in (Weigel et al., 2021) and consists of the following steps (Figure 1):

1) Definition of application, functional unit, reference, assumptions, and boundary conditions
2) Selection of criteria
3) Development of weighting profiles
4) Assessment of the criteria
   a) Environmental criteria based on LCA
   b) All other criteria based on EIs
5) Evaluation of application based on criteria assessments and weighting profiles within MCA

Generally, the first step is the definition of the application under investigation, the functional unit, the reference for the evaluation, and key assumptions. This step ensures a consistent and efficient assessment and evaluation process.

The selection of criteria (step 2) can be moved up and down in the sequence within certain limits. In this study, it is performed beforehand based on the general requirements for digital applications in the energy sector, following a thorough literature review and discussions with experts.

In step 3, weighting profiles are developed. To some extent, this could also be done beforehand, based on general requirements for digital applications. However, case-specific adaptations are likely to be required, as different applications may involve different stakeholder roles. The study-specific stakeholder profiles are derived from expert opinions following the expert interviews in step 4b. The point allocation method is applied. Experts are asked to assign 100 points sequentially to categories and then to criteria. The

100 points represent 100% importance, a concept that is intuitively understood by the interviewees.

The LCA approach (step 4a) is based on the standard defined in (ISO/TC 207/SC 5, 2006). It is carried out using the software openLCA (v1.10.1), the ecoinvent (v3.3) database, and the CML2001 impact calculation method, from which the environmental impact criteria global warming potential 100a (GWP), adiabatic resource depletion (ARD), human toxicity 100a (HT), and ecotoxicity 100a (ET—as the average of different ecotoxicity aspects) are selected, extended by the cumulative energy demand (CED). The LCA results are normalized to the MCA evaluation scale by comparison with a reference value. This reference value is a quantification of the reference defined in step 1.

The expert interviews (step 4b) are semi-standardized, which ensures comparable results across different EIs while providing the flexibility to capture additional detailed information. The list of criteria is used as the interview structure.

The MCA (step 5) uses a direct ordinal rating scale ranging from -3 (strongly negative impact) via 0 (no/neutral impact) to +3 (strongly positive impact). The scale is intuitive for experts, and the evaluation can be broken down into two questions: 1. Is the impact positive, negative or neutral (+ or—range); 2. how positive or negative is the impact (±1, 2, or 3). The simple additive weighting (SAW) method, also known as the weighted sum method (WSM) is used to aggregate the criteria evaluations into category and total results. The SAW method is commonly applied due to its popularity and simplicity (Cajot et al., 2017). It provides a high level of transparency on how results are aggregated from detailed criteria evaluations.

Compared to the originally provided version of the framework (Weigel et al., 2021), three main improvements to the method are made in this paper:

1) The list of criteria is modified in order to reduce the complexity and eliminate overlaps between criteria. In particular, the number of responses per criterion, the weighting of each criterion, as well as direct expert feedback were evaluated to identify required adaptions. Based on the findings, the former sub-criteria level is eliminated, the total number of criteria is reduced, and the number of criteria is more evenly distributed among the categories. Some sub-criteria are upgraded to criteria, and a few new criteria are added. The updated criteria used in this study can be found in the presentation of the results in Section 4.4.
2) In addition, the expert interview approach is adjusted. The weighting (formerly being the first part of each expert interview) is done independently by the experts after the interview. The adapted approach meets the experts' expectations to talk directly about the application itself, shortens the interview, and reduces the interviewer's influence on the weighting. However, a good explanation of how to perform the weighting is necessary, and not all experts provide (useful) weighting results on their own.
3) Last but not least, an indication of the uncertainty and data robustness of the expert interview results is assessed using the standard deviation and the number of received evaluations. The standard deviation s is calculated for the sample of each criterion as given in Formula 1

$$s = \sqrt{\frac{\sum_{i=1}^{n} [x_i - \bar{x}]}{n-1}} \quad (1)$$

where n is the number of evaluations per criterion provided by the experts in the expert interviews, x_i are the evaluations (between -3 and +3) per expert, and $\bar{x}$ is the average of the

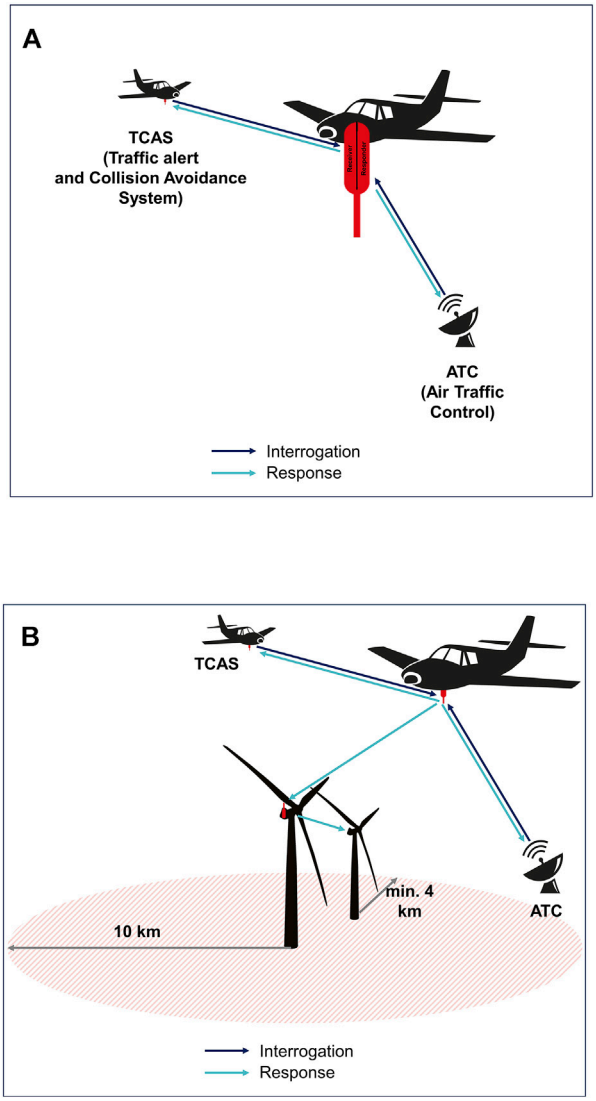

FIGURE 2
Illustrative functionality of **(A)** a transponder in aviation; **(B)** a transponder-based ADLS.

given evaluations. A margin of error for a specific confidence interval is not used because the data points do not necessarily follow a normal distribution shape. Furthermore, it should be noted that the deviation of the answers given in the expert interview is only one of many possible sources of error.

3 ADLS technology, system boundaries, and assumptions

3.1 Description of the technology

Different technologies to equip WTs with an ADLS are permitted. Three technological approaches can be distinguished based on active radar, passive radar, and transponders (secondary radar). Each technology may have its own use case due to its inherent advantages and disadvantages. There is evidence, however, that transponder-based ADLS technology will be predominantly deployed. Most of the consulted experts expected this trend, and two organizations are already in the process of covering two entire German states with this technology—North Rhine-Westphalia (Bode and Klümper, 2021) and Saarland (BNK, 2022). Therefore, this publication focuses on transponder-based ADLS.

Transponders have been widely used in commercial aviation for several decades. They are considered part of secondary surveillance radar (SSR). The term transponder is a hybrid of transmitter and responder. After receiving a signal from a secondary radar antenna on 1,030 MHz, the transponder actively sends a response signal on 1,090 MHz. The response signal contains a four-digit identity code as a minimum (Mode A) or a unique 24-bit aircraft identity number, altitude, speed, and flight path, as well as GPS coordinates for ADS-B (Automatic Dependent Surveillance - Broadcast) as a maximum (Mode S enhanced). Transponder responses are triggered by air traffic control (ATC) and other aircraft's traffic alert and collision avoidance systems (TCAS), see Figure 2A.

If airborne transponders are not triggered, they broadcast one signal per second by default (Mode S only, not Mode A). All aircraft flying at night within or outside of air traffic-controlled areas must use a Mode S transponder (BMDV, 2018). Some exceptions exist for military, police, and rescue aircrafts. The signals sent out by the aircrafts' transponders are used by the transponder-based ADLS. The ADLS passively receive the transponder signals without sending any interrogation signal themselves. The minimum information received is the aircraft identity code (from Mode A transponders). In this case, the distance is calculated based on the signal intensity. In most cases, more information such as altitude, speed, flight path, and GPS coordinates are received (Mode S and ADS-B), and the exact position can be determined. An ADLS receiver covers a minimum radius of 10 km. Based on the defined impact area of a horizontal 4 km radius around each WT (BMDV, 2020), all WTs within a 6 km radius can be covered by one ADLS, see Figure 2B. In practice, the ADLS receives transponder signals of well beyond 10 km, however, this does not change the evaluation since the technical setup (how many turbines are covered by one ADLS) is defined by the 10 km minimum radius.

3.2 Functional unit and system boundaries

The functional unit of the evaluation is one single transponder-based ADLS. The reference system used to evaluate the magnitude of the impact is the wind turbines covered by the ADLS. The selection of the reference is therefore aligned with the subjective perception of the relevance of ADLS's impact on the system they are part of. Since the number of covered turbines and the technical configuration of the ADLS may vary, a base case is defined, and sensitivity analysis for different setups are conducted. Theoretically, for modern wind farms, there is no limit to how many WTs can be covered by one single ADLS. In practice, however, there are technical, topological, and ownership structure limitations. In this paper, a setup with eight turbines is chosen as the base case based on the average number of turbines covered per ADLS in the German State of North Rhine-Westphalia (Bode and Klümper, 2021). If all covered turbines have a single central communication unit, which is usually the case for modern wind farms, the central ADLS can directly operate the obstruction lights of all turbines, as depicted in Figure 2B. However, if a central communication interface is not available, additional communication modules must be installed. For this study, the case of only one communication unit is chosen due to a lack of information on a realistic average number of communication units per ADLS. Therefore, the base case is defined as one ADLS with one signal receiver and one communication unit covering eight WTs.

3.3 Life cycle assessment key assumptions

For the life cycle inventory (LCI), the material and energy flows of one single ADLS are modeled. One analyzed base case ADLS consists of the following hardware components: one signal receiver, one communication module, mounting, cabling, antennas, and additional infrared (IR) beacons required per each of the eight turbines. As depicted in Figure 3, the model covers the production, the use, and the end-of-life phases. In addition to the directly attributable effects on the mass and energy flow, two effects caused by the reduced operating time of the beacons are additionally allocated to the LCI. Based on real-world data from a test site supplied by an ADLS supplier, it is assumed that the beacons remain off during 98% of the nighttime. Besides a reduced beacon electricity consumption, the reduced operating hours lead to an increased lifetime of the

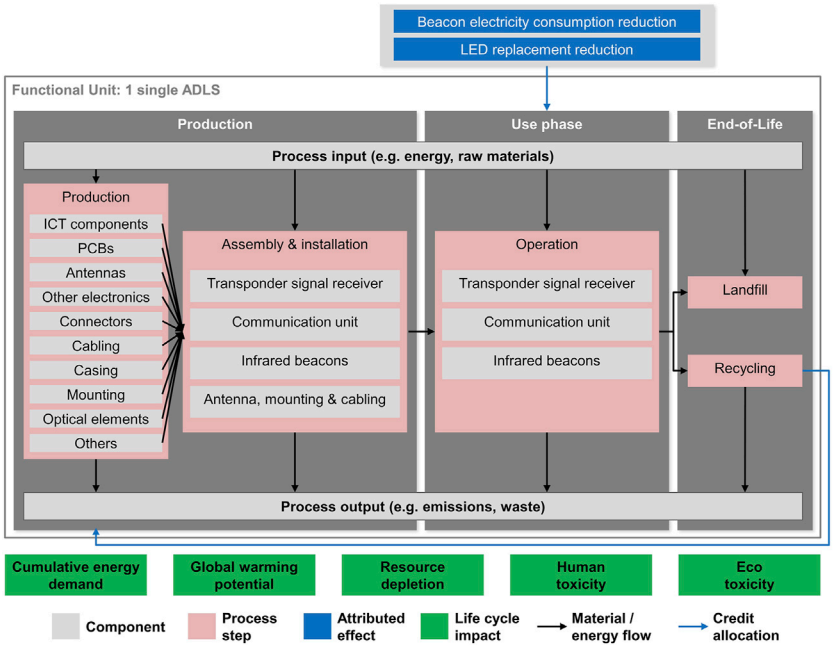

FIGURE 3
LCI model of ADLS.

beacons' LEDs and thus to a reduced need for replacement. A reduction in LED replacement of 1.29 units per beacon over the analysis period is calculated based on an expected LED operating life of 50,000 h and a correction factor based on manufacturers' knowledge of the probability of failure modes leading to replacement. It is assumed that the ADLS hardware has a technical lifetime of more than 25 years, but the hardware is decommissioned together with the turbine so that the effective ADLS lifetime depends on the lifetime of the turbine. Here, a turbine and ADLS lifetime of 20 years is assumed. Therefore, the analysis period is also set at 20 years.

Since the electricity consumption of digital applications with a long expected lifetime tends to have a great effect on the life cycle impact, special consideration is given to the electricity mix. Three different electricity mixes are defined for this study based on the expected development of greenhouse gas (GHG) intensity of the German electricity mix over time (measured in CO_2 equivalents, CO_2 eq.). The three mixes are defined as described in (Weigel et al., 2021), based on historical CO_2 emissions and energy consumption, reference prognosis, and trend scenarios for future energy generation and the 2019 developed coal exit path. Different shares of electricity generation technologies are modeled for each mix, however, the underlying unit processes for these technologies in the LCA database remain unchanged as no prospective datasets are available. The 2022 mix is used for the production phase, the expected 2032 mix for the use phase, and the expected 2042 mix for the end-of-life phase. The ADLS's energy self-consumption during the use phase is covered to 19% by electricity from the German electricity mix and to 81% by electricity from the wind turbine itself. The life cycle impact of the electricity generated by the wind turbine is based on a 3.25 MW turbine currently in operation. Effects that are not considered in the LCI are the need for maintenance and spare parts (no data available and the impact is likely to be very small), the server operation and data transmission (there is no data available), and the transport of materials for production, installation, and end-of-life steps (the impact is likely to be very small as most steps take place within Germany). Relevant assumptions and sources are listed in Appendix Table 2 in the Annex.

3.4 Expert interviews assumptions

The aim for the selection of experts is to cover all stakeholder roles and identify experts with a high level of expertise. In a first step governmental, scientific, business and journalistic publications were analyzed to identify relevant stakeholder roles and experts. Following the initial identification, further experts were identified by asking each expert at the end of the interview to identify further stakeholder roles and name experts.

The group of twelve interviewed experts includes: four representatives of wind farm operators or operator associations in charge of implementing ADLS, two

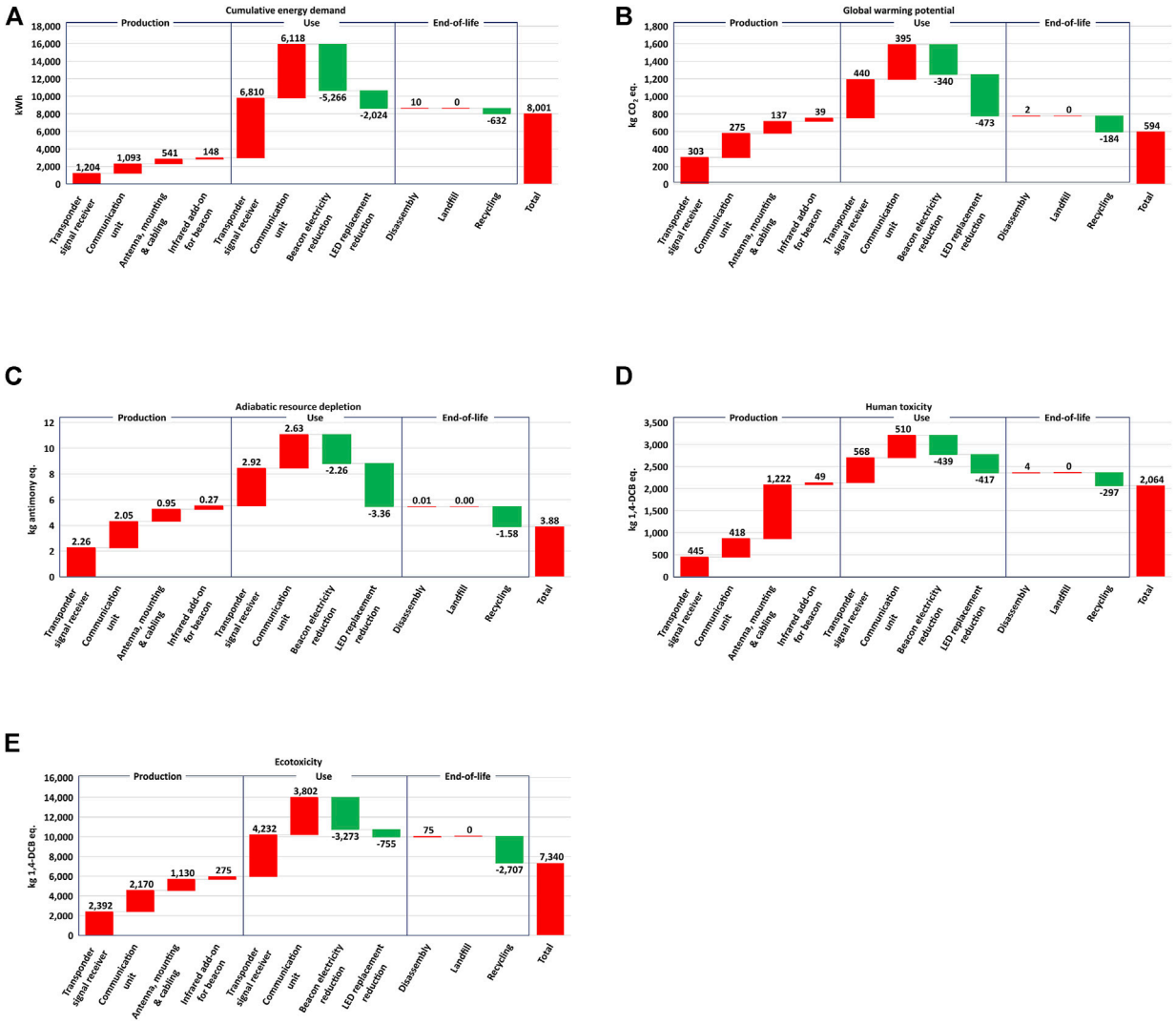

FIGURE 4
Life cycle impact assessment for the base case. Functional unit: one ADLS in the base case. **(A)** Cumulative energy demand; **(B)** Global warming potential; **(C)** Adiabatic resource depletion; **(D)** Human toxicity; **(E)** Ecotoxicity.

environmental NGO experts for wind energy, two ADLS-specific policy advisors to the involved German Federal Ministries, one employee of a wind turbine manufacturer tasked with equipping future turbines with ADLS, one ADLS manufacturer (from the same company that supplied the data for the LCA), and two scientists with expertise in social acceptance of WTs, including lighting induced stress. No affected neighbors of WTs were directly interviewed for this study, but rather the two mentioned scientists researching social acceptance were interviewed to present their insights of the perspective of this group. All experts are based in Germany and are native German speakers. Age and sex were not documented as deemed not relevant.

The individual online expert interviews were conducted between September 2021 and January 2022 and each took about 90 min. No material was sent out beforehand, the interviews were not recorded or transcribed, and the results were captured as the evaluation per criterion, including qualitative remarks. Furthermore, following the expert interviews, the experts were asked to assign weights to the criteria and to submit the weighting within 2 weeks. Based on the responses of nine experts (one wind farm operator, the turbine manufacturer, and the ADLS manufacturer did not submit weighting), five (non-representative) weighting profiles reflecting key stakeholders' perspectives were derived.

4 Results

In this section, the results of the LCA are presented first, followed by the results of the MCA, which integrates LCA and expert interviews. The LCA results are presented separately from the MCA results because detailed conclusions about life cycle impacts can be drawn.

4.1 LCA results

4.1.1 Impacts of the base case

In Figure 4, the breakdown of the calculated life cycle impacts over 20 years for the base case is depicted. In total, all five impacts increase with the application of an ADLS. The shares of the three life cycle phases on the total impact, however, are very different. Each step of the production phase leads to an increase in all five impacts. In the use phase, the energy consumption of the ADLS components leads to an increase, while the beacon electricity savings and the LED replacement reduction cause an impact decrease. Relative to the production and the use phase, the end-of-life phase causes a small impact decrease. The effort for disassembly and landfilling is more than compensated by credits given due to recycling.

The cumulative energy demand (CED) is depicted in Figure 4A. The ADLS use phase's energy consumption is 4.3 times higher than the production's energy consumption. The decisive impact on the CED during the 20-years use phase is caused in particular by the electricity consumption of the ADLS hardware (approx. 13,000 kWh) and the saved electricity consumption of the beacons (approx. -5,200 kWh).

Figure 4B shows the breakdown of the global warming potential (GWP). The ADLS operation's energy consumption emissions (835 kg CO_2 eq.) over 20 years are about 10% higher than the production-related emissions (754 kg CO_2 eq.). Similar to the CED, the GWP is mainly caused by the ADLS's electricity consumption. Since 81% of the consumed electricity is assumed to be generated by the turbine itself (with a low impact on GWP), the GWP is mainly driven by the remaining 19% taken from the grid (although an increasingly decarbonized future German electricity mix is assumed). During the production phase, the signal receiver is the largest GWP contributor with 303 kg CO_2 eq., followed by the communication unit with 275 kg CO_2 eq. The mounting, cabling, and antenna (137 kg CO_2 eq.) and the required infrared beacons (39 kg CO_2 eq.) cause a relatively small GWP. For these hardware units, the components with the highest GWP are the printed circuit boards, including the electronic components mounted on them such as integrated circuits, resistors and capacitors, other electronic components such as power supplies, heaters, surge suppressors, and circuit breakers, and the mounting material (mainly steel). The savings of -814 kg CO_2 eq. (caused by lower beacon energy consumption and reduced replacement of LEDs) offset 97% of the ADLS's

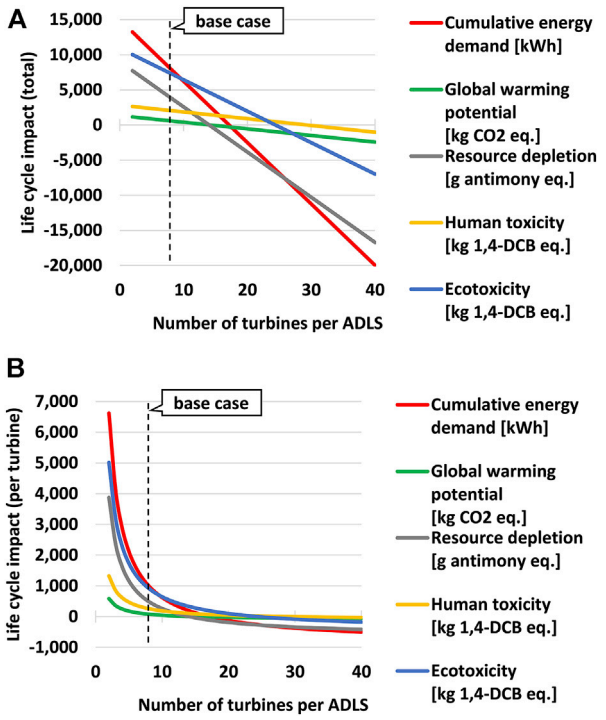

FIGURE 5
Life cycle impact of one ADLS for different numbers of covered WTs. Functional unit: one ADLS in the base case with varying numbers of WT. **(A)** per ADLS; **(B)** per turbine.

electricity consumption emissions. The reduction in LED replacement causes a larger GWP effect (-473 kg CO_2 eq.) than the reduced beacon electricity consumption (-340 kg CO_2 eq.). The main driver for the LED replacement reduction's GWP effect is the saved energy consumption of the avoided production of diodes and PCBs. Again, the beacon energy consumption reduction's GWP effect is driven by the 19% CO_2 intensive electricity taken from the German energy mix. The end-of-life steps, especially disassembly and landfilling of the non-recyclable parts, do not cause significant GWP impacts. Recycling, however, can avoid emissions of -184 kg CO_2 eq.

The breakdown of adiabatic resource depletion (ARD) impacts given in Figure 4C shows a high correlation with the GWP. The main driver in both cases is the use of fossil fuels for energy (electricity and heat) generation during production, use, and end-of-life. However, compared to GWP, production and recycling have a slightly higher proportional impact on ARD, as physical production materials contribute directly to ARD, while only their CO_2 eq. footprint contributes to GWP.

The main difference in the breakdown of human toxicity (HT) impacts in Figure 4D compared to GWP and ARD is the high impact of the antenna, mounting, and cabling component production. With 1,222 kg 1,4-DCB eq., these parts cause more than half of the total HT production impact, compared to only

17–18% of the production impact for GWP and ARD. This high impact is driven by the exploration of copper, which is mainly used for cabling. The HT production impact is significantly higher than the impact caused by the ADLS's electricity consumption during the use phase. Furthermore, it is evident that both savings in the use phase have a similar impact on the HT, while for GWP and ARD, the saving due to the reduction of LED replacement is larger.

The ecotoxicity (ET) impact in Figure 4E shows a relatively high impact of the ADLS energy consumption compared to the production. Moreover, the saved electricity consumption of the beacons causes a much higher ET impact than the reduction of the LED replacement. It is evident that ET is also driven by energy consumption. However, unlike GWP and ARD, it is not driven by the use of fossil fuels but rather by the production of the required power infrastructure such as power plants, wind turbines, and grids. Therefore, the advantage of using wind energy over fossil fuel energy is smaller for ET than for GWP/ARD. During production, ET is driven by the use of gold, brass, silver, and other precious metals.

In the following, the sensitivity of the results regarding the most relevant factors is presented. These factors are, in particular, the number of turbines covered by one ADLS, the required number of communication units, and the achieved beacon operation reduction rate.

4.1.2 Variation in the number of wind turbines

Figure 5A depicts the life cycle impact depending on the number of WTs covered by the ADLS. The technical setup of the base case is applied, i.e., the ADLS contains one signal receiver and one communication unit independently of the number of covered turbines. On the one hand, the required efforts for the production and operation of the ADLS hardware remain the same regardless of the number of turbines. In theory, there is no limit to how many turbines can be covered by one ADLS as long as they are within the defined spatial range of the system. On the other hand, the savings, i.e., the reduction of the beacon energy consumption and the LED replacements, occur per turbine. Therefore, the life cycle impacts decrease linearly the more turbines are covered by one ADLS. Depending on the impact criteria, the break-even point (BEP), i.e., the number of turbines, for which the savings outweigh the impacts of ADLS production and operation, is different. While for less than 15 turbines, all indicators show an increased impact (as also analyzed above for the base case with 8 WT), they all decrease if more than 30 turbines are covered. The BEP for both the GWP and the ARD, appears at about 15 WTs. In the case of CED, ET, and HT, it occurs only at larger numbers of turbines of about 18, 27, and 30, respectively. The setup of one single turbine covered by one ADLS is not displayed in Figure 5 since, in this case, the ADLS hardware can be reduced, making this a special case with a non-linear effect, which, however, in reality, is rather rare.

If the results are normalized to one turbine, the impact per turbine decreases and follows a hyperbola (Figure 5B). The family of curves can be described by

$$f_{a,b}(x,i) = a_i + \frac{b_i}{x} \tag{2}$$

where x describes the number of WTs, a the horizontal asymptote, b the shape of the hyperbola and i denotes the five different impact criteria. The factor b depends on the life cycle impact of the central parts of the ADLS, i.e., the signal receiver, communication units, and antenna, mounting and cabling. In this study, the impact of these parts is always a positive value (increased impact) since no saving effects are generated. The horizontal asymptote a depends on the life cycle impact of all turbine-dependent parts and effects, i.e., infrared beacons, reduced beacon operation, and reduced LED replacement. In this study, the impact of these parts and effects is a negative value (decreased impact) because for each additional turbine, the credited saving effects outweigh the impact of the additional infrared beacon. Therefore, for a large number of turbines, the impact curves converge to the horizontal asymptote $\lim_{x \longrightarrow \infty} a_i$. The curves cross the zero line at the break-even points BEP_i (see Figure 5A) when the sum of the savings per turbine outweighs the increased impact.

In order to understand the different BEP per impact criteria, the findings of Figure 5 and Figure 4 need to be combined. GWP and ARD are both driven by the use of fossil fuels. Both savings, beacon electricity consumption reduction and LED replacement reduction, increase directly with the number of turbines and have a proportionally large effect on fossil fuel use and thus on GWP and ARD, causing a BEP at already 15 turbines. The CED is directly driven by energy demand, regardless of its source. Therefore, while the reduction in LED replacement has a proportionally large impact (compared to the energy consumption of the ADLS and the saved energy consumption of the beacons) on GWP and ARD, it does not have a strong impact on CED. Consequently, the CED savings achieved per turbine are proportionally smaller than for GWP and ARD, so more turbines are required to achieve a net-zero balance. The HT has the same proportional reduction impact per turbine as the GWP (the lines are close to parallel), but because of the higher production effect, mainly driven by the use of copper, more turbines are needed to balance the production impact, i.e., the BEP shifts to the right. The ET has a rather similar BEP as the HT. However, the main reason why more turbines are needed to offset the ET impact of the production is that the reduction in LED replacement has a proportionally small impact on ET since, for the given quantity of LEDs, neither the total energy consumption for production nor the demand for precious metals is exceptionally high.

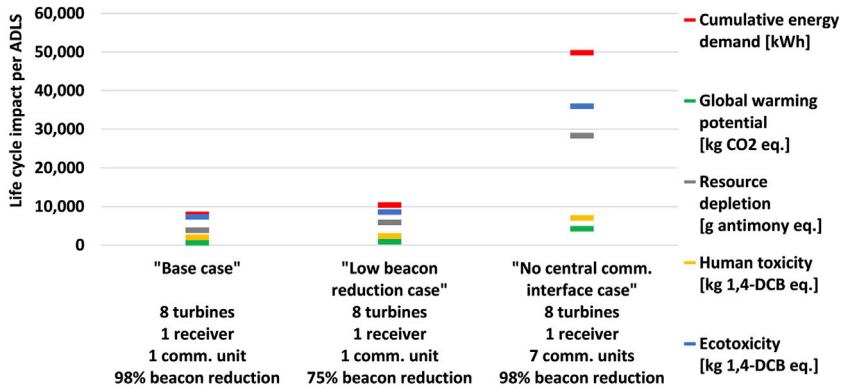

FIGURE 6
LCIA for different ADLS cases. Functional unit: one ADLS.

4.1.3 Variation of the required number of communication units

The base case contains one communication unit. Depending on the technical and legal setup of the wind farm, however, between one communication unit for all turbines and one unit for each turbine may be necessary. The additional communication units cause impacts both through their production and their energy consumption during the use phase. The results for different numbers of communication units are depicted in Figure 6: One unit as the base case (all turbines are part of the same wind farm with one central communication infrastructure) and seven units as the worst case (each turbine is a single wind farm, and/or no central communication infrastructure exists). It is evident that the requirement to install more than one communication unit could drastically increase all analyzed life cycle impacts. Between the best and the worst case, the identified impacts increase by a factor of about 3–7, depending on the impact criterion. The highest increase is observed for ARD, GWP, and CED.

4.1.4 Variation of the beacon operation reduction rate

Furthermore, the life cycle impact depends on the beacon operation reduction rate, i.e., the percentage of nighttime that the lights remain off. The beacons are assumed to remain off during 98% of the nighttime in the base case. The reduction rate could realistically be as low as 75% near airports with more nighttime air traffic. Figure 6 shows the impact of a low reduction rate, leading to a smaller reduction in beacon power consumption as well as a smaller reduction in LED replacement. The impact on the outcome compared to the base case is an increase of 50% on GWP and ARD, 30% on CED, and approximately 15% on human and ecotoxicity.

4.2 LCA result normalization

Since the MCA evaluation scale ranges from -3 to +3, the LCA results must be normalized to this scale in order to include them in the MCA. The reference chosen in Section 3.2 for this study are the WTs, which are covered by the ADLS, thus, the reference value is the life cycle impact of these WTs. By comparing the ADLS's impact to the reference value, the normalized evaluation E_i can be calculated for each impact criterion i. If the ADLS has the same life cycle impact as the group of turbines, i.e., the total impact is doubled, this is considered strongly negative (-3). If the life cycle impact of the ADLS is zero, i.e., total impact does not change, this is considered neutral (0). If the ADLS reduces the life cycle impact by the absolute value that the turbines increase it, i.e., the total impact is neutralized to zero, this is considered strongly positive (+3). Within this range, the evaluation E_i for each criteria can be calculated using

$$E_i = \frac{I_{ADLSi}}{I_{WTs\,i}} \times E_{max} \tag{3}$$

based on the ratio between the assessed ADLS's and WTs' life cycle impact, I_{ADLSi} and $I_{WTs\,i}$ respectively and the maximum evaluation E_{max}, i.e. -3 or +3. If $I_{WTs\,i}$ is an increased impact E_{max}, i.e., -3 is used and vice versa. This approach leads to the evaluation calculated in Table 1.

It can be seen that all criteria are evaluated very close to zero, i.e., with a negligible or neutral impact. In the context of the life cycle impact of the WTs covered by the ADLS, the ADLS life cycle impact is less than 0.006% and thus negligible. This finding also holds true for the technical scenarios with the highest increase in life cycle impact (two turbines, one receiver, one communication unit) and the highest (realistic) decrease in life cycle impact (40 turbines, one receiver, one communication

TABLE 1 Normalization of LCA results to MCA evaluation scale.

Life cycle impacts	1 ADLS	8 WTs	1 ADLS/8 WTs (%)	Evaluation
Cumulative energy demand	8,001 [kWh]	1,299,030,015 [kWh]	0.0006	- 0.00002
Global warming potential	594 [kg CO_2 eq.]	20,039,960 [kg CO_2 eq.]	0.0030	- 0.00009
Resource depletion	4 [kg antimony eq.]	132,273 [kg antimony eq.]	0.0029	- 0.00009
Human toxicity	2,064 [kg 1,4-DCB eq.]	60,690,800 [kg 1,4-DCB eq.]	0.0034	- 0.00010
Ecotoxicity	7,340 [kg 1,4-DCB eq.]	383,844,537 [kg 1,4-DCB eq.]	0.0019	- 0.00006

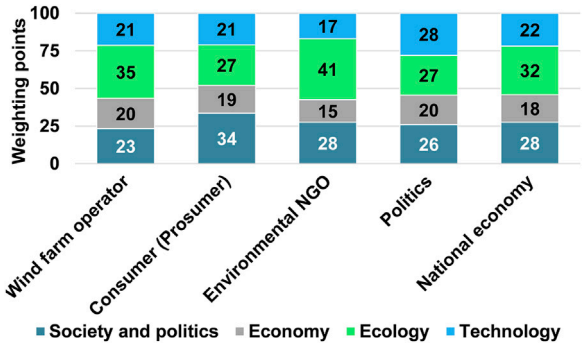

FIGURE 7
MCA weighting profiles.

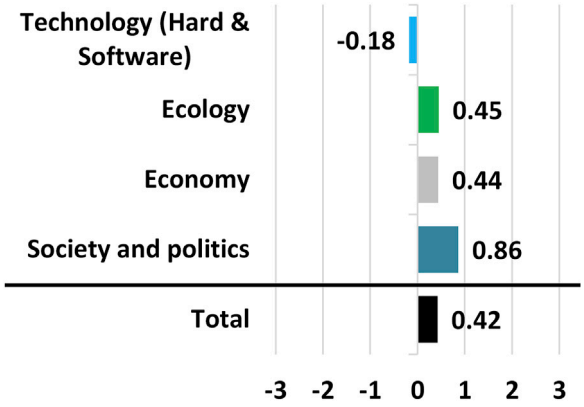

FIGURE 8
Aggregated MCA result from a national economy perspective.

unit). It can be concluded that environmental life cycle impacts do not play a significant role in the holistic evaluation of the application in this case.

4.3 MCA weighting profiles

Before combining the LCA and the EI assessment results in the MCA, weighting profiles for the criteria must be defined. As described earlier, the responses of nine experts are used to derive five weighting profiles, as depicted in Figure 7. The wind farm operator perspective is based on the three wind farm operator representatives, the consumer perspective on the two scientists with wind energy acceptance expertise, the environmental NGO perspective on the two NGO members, and the political perspective on the two political advisors. The national economy perspective is calculated as the average of the preceding weighting profiles.

For wind farm operators, i.e., the users of ADLS, the ecological impact is the most important impact, followed by societal, technical, and economic aspects, all of which are about equally important. From the consumers' point of view, technical and economic aspects have low relevance, while aspects concerning society and politics have the highest importance. From the environmental NGO's perspective, ecological aspects are by far the most important ones. The political perspective is the most balanced weighting profile, and the national economy represents the average view across all interviewed experts. Overall, ecological aspects are considered as most important, while the economic aspects are considered the least relevant.

4.4 MCA results integrating LCA and EIs

Subsequently, the normalized LCA and the EI results are combined in the MCA and aggregated based on the weighting profiles. First, the results calculated based on the "national economy" weighting profile are presented (Figure 8 and highlighted lines in Figure 9), followed by an overview of the results based on the different weighting profiles (Figure 10).

Figure 8 illustrates the aggregated results at the MCA category level. The overall evaluation is slightly positive. The largest positive impacts are in the society and politics category. The technology category is evaluated slightly negatively. The ecology and economy categories are both slightly positive.

The next level of detail, i.e., the results per criterion, is depicted in Figure 9. Together with each result, the standard deviation of the EI responses and the number of responses

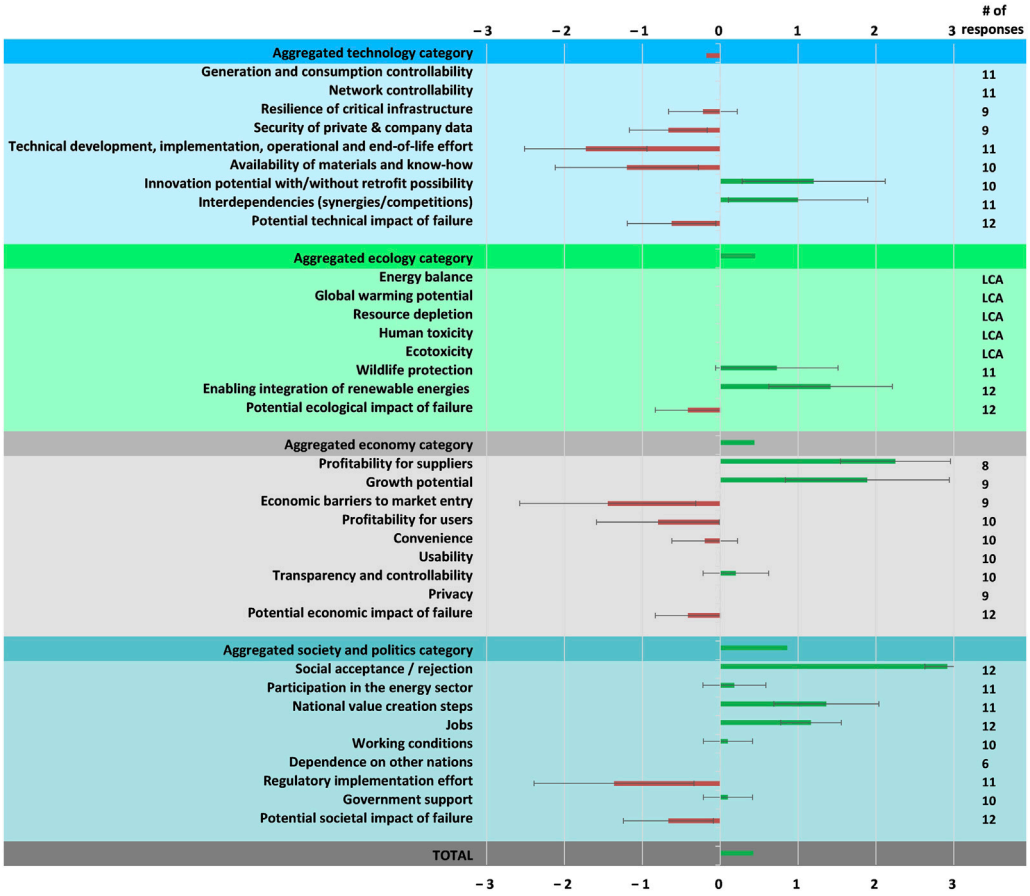

FIGURE 9
Criteria level MCA results from a national economy perspective, including standard deviation and number of data points.

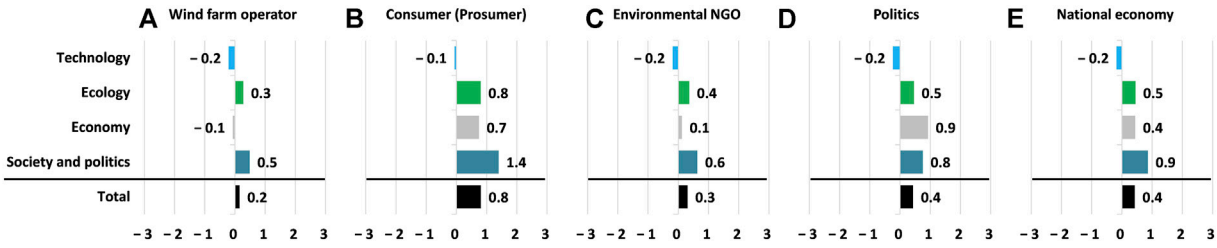

FIGURE 10
Aggregated MCA results from different stakeholders' perspectives: **(A)** Wind farm operator; **(B)** Consumer (Prosumer); **(C)** Environmental NGO; **(D)** Politics; **(E)** National economy.

received are given as an indication of the reliability of the data per criterion. Since the values of the five LCA-based criteria are derived from the normalization in Section 4.2, no standard deviation is provided. Further sources of uncertainty are qualitatively discussed in Section 5.3.

Within the slightly negatively evaluated technology category, the main negative drivers are the required technical effort and the availability of materials and know-how. The greatest technical effort is required for development and implementation, while operation does not cause any relevant additional effort. In

particular, the implementation effort for existing turbines is high, especially for old turbines without appropriate communication infrastructure. For newly built turbines, the additional implementation effort will be low. Regarding the availability of materials and know-how, a major bottleneck for the rollout is identified. In particular, the production bottleneck is a shortage of ICT equipment on the world market, especially semiconductor-based integrated circuits. A bottleneck for the implementation is a shortage of technicians with the necessary know-how due to a general shortage of technicians in Germany. Although these shortages are generally expected to persist for several years, they are most likely no long-term barrier to further ADLS deployment after the initial rollout due to the small quantities needed in comparison to the total capacities of semiconductors and trained technicians. Minor negative effects are expected on the resilience of the critical infrastructure and data security, as there are additional potential points of attack, especially for systems with internet access. However, since the information processed is not critical, the risk of cyberattacks is low. Nevertheless, there is an additional dependency on the availability of correct data. The main positive factors are seen in the potential for innovation, such as improved accuracy of aviation data, integration of other data sources, improved monitoring of beacons, and synergies with other applications. These synergies could include, for example, more effective management of increasing air traffic and control of, for example, unmanned aerial vehicles (UAVs) based on detailed traffic data over lower airspace. Others are the identification of noise sources by matching air traffic data with sound pressure levels and the application of ADLS to other obstacles such as buildings. No impacts on generation, consumption, and grid controllability are identified.

Although the five normalized LCA results do not show significant impacts on the ecology category, the overall category reveals a positive result due to the anticipated positive impacts on enabling more renewable energies and protecting wildlife. The integration of more renewable energies could be positively influenced as approval processes could proceed more quickly due to a reduced number of arguments of lawsuits against new WTs, and neighbors could accept more turbines in their vicinity because they are perceived as less stressful. Although a positive impact on wildlife protection is expected by most experts, the standard deviation of responses is very high. On the one hand, the impact on wildlife could be reduced as nighttime light emissions are reduced. On the other hand, IR light could have a new impact, possibly on other species. Plants will most likely not be affected.

In the economy category, high profits and growth potential are seen for ADLS providers. After an initial spike during the rollout, long-term demand to equip new turbines and offer operational services is likely. Since Germany is the first country to introduce a nationwide ADLS obligation that also allows the use of transponder technology, there could be significant export potential, giving German providers a first-mover advantage. In addition, as mentioned, further growth potential exists through the application of the technology to other obstacles such as buildings, bridges, chimneys, etc. However, the standard deviation of responses regarding growth potential is high, indicating significantly divergent views. Furthermore, market entry barriers are estimated to be relatively high. The main obstacles for new suppliers are patents and the complex type examination certification procedure. For the user's side, the profitability is evaluated slightly negatively, with a high standard deviation in responses. No significant impact on non-monetary user benefits, such as transparency, controllability, usability, etc., is found. Monitoring and control of beacons could be slightly improved, which would lead to more transparency.

The most positively evaluated category, society and politics, is primarily driven by the very strong positive evaluation of the impact of ADLS on social acceptance. Reduced lighting reduces lighting-related stress and thus increases acceptability. The acceptance evaluation shows a very low standard deviation and a maximum number of responses, indicating low uncertainty. In addition, positive effects on the value creation steps in Germany and on the number of jobs are also expected. New value creation steps for the production, installation, and opertion of ADLS will be implemented, creating some jobs in the medium to high qualification range. No significant impacts are seen on participation in the energy sector, labor conditions, dependence on other nations, or need for government support. However, the regulatory implementation effort is evaluated relatively strongly negatively. The effort required to create the necessary regulatory framework in advance of the ADLS obligation was quite high, several laws and regulations had to be amended. Some final procedural clarifications are still needed, in particular, a definition of who is authorized to test and certify the proper installation and operation of ADLS.

The potential impact of a failure is a cross-category set of criteria. These criteria are therefore analyzed jointly. The impact of a failure is a combination of its probability and its potential magnitude. The overall potential impact of a failure is found to be low. The probability of a failure, such as a collision between an aircraft and a turbine, is judged to be virtually zero. Systems must be designed with an engineered fallback option to ensure that beacons remain on if the system fails to operate properly. In addition, always-on IR lights will be added for pilots conducting low-level night flights without transponders, e.g., military and police. The technical and social/political impacts if a failure (collision) actually occurs are somewhat higher compared to the environmental and economic impacts. The technical impact of such a failure could, in the worst case, be the loss of the aircraft, the turbine, and even loss of life. Socially/politically, such a failure could lead to a reduction in the acceptance of wind energy in general.

While the weighting profile "national economy" was analyzed above, the MCA results can also be analyzed with weighting profiles representing the perspectives of the different stakeholders. The aggregated results for different weighting profiles are displayed in Figure 10. The evaluations with all weighting profiles show a positive total result. Overall, the result of the consumer perspective (B) is the most positive, which is mainly due to the high weighting of the society and politics category and in particular the social acceptance criterion. Wind farm operators (A), on the other hand, evaluate the application almost neutrally overall, which is mainly due to the high weighting of profitability for the user. The technology category is evaluated slightly negatively and very similarly across all weighting profiles. The ecology category is evaluated the most positively from the consumer perspective (B), even more positively than from the environmental NGO perspective (C). This is due to the high importance consumers place on enabling renewable energies, while environmental NGOs distribute the weighting more evenly across all ecology criteria. The evaluations for the economics category range from very slightly negative for wind farm operators (A) to positive from a political perspective (D). This evaluation range is based on the different prioritization of economic impacts on the provider side compared to the user side. All weighting profiles lead to a positive evaluation of the category society and politics. From a political perspective (D), not only positive impacts in the society and politics category but also economic benefits are expected. However, from a national economy perspective (E), these are less relevant.

5 Discussion

Following the structure of the result section, the LCA results are discussed first, followed by the MCA results, which integrate LCA and EI results. The section concludes with a discussion of the possible sources of error.

5.1 LCA result discussion

Based on the LCA results given in Figure 4, it is evident that the five considered impact criteria increase by the use of ADLS in the base case. The analysis of the breakdown of each of the impact criteria reveals the impact drivers and thus aspects with potentially high improvement levers. ADLS hardware energy consumption emerges as one of the most important impact drivers for CED, GWP, ARD, and ET. This underscores the importance of paying attention to energy-efficient design in engineering development. The impact of GWP and ARD can be further reduced by decreasing the CO_2 intensity of the energy mix used for production. To reduce the HT and ET impact, the design of the hardware needs to be analyzed regarding the presence and possible substitution of certain materials such as copper, gold, silver, brass, and other precious metals. The finding that GWP and ARD are driven by the CO_2 intensity of the energy mix, while HT and ET are driven by the underlying infrastructure, is consistent with other LCAs on energy systems, e.g., (Baumgärtner et al., 2021). Recycling, as modeled in the presented study, results in only a small reduction in all impact criteria (compared to the production impacts). However, an improved recycling process could improve the overall result.

Given the results shown in Figure 5 and Figure 6, it is evident that the ADLS life cycle impacts depend heavily on the number of turbines covered by one ADLS and the number of communication units required per ADLS. Although it may be difficult to influence the layout for existing wind farms, both of these issues can be considered for newly built WTs. Based on the experience from the ADLS planning in North Rhine-Westphalia, the realistic range of onshore turbines covered by one ADLS is between 1 and 33. Therefore, in some cases, the ADLS may lead to an impact reduction of some or all of the analyzed ecological criteria, at least if only one communication unit is required. Since offshore wind farms typically consist of significantly more turbines (currently 12–80 turbines per operational German offshore wind farm) with a central communication unit and are less likely to be located in high air traffic zones, a decreased life cycle impact of using ADLS can be expected here.

5.2 MCA result discussion

The MCA provides a holistic overview of all relevant criteria from relevant stakeholders' perspectives. The main objective of the ADLS obligation, to increase social acceptance of wind energy, is likely to be achieved. The evaluation from the consumers' point of view is the most positive, with the highest evaluation in the society and politics category. No fundamental opposition to the obligation needs to be expected, as all stakeholders come to an overall positive evaluation. The stakeholders most affected by the obligation, the wind farm operators, are the ones with the least positive evaluation. Compensation, i.e., a lower regulatory burden, could improve their perception of the application. From a political perspective, not only the positive impact on the society but also on the economy is relevant. Furthermore, it is evident that due to the identified bottlenecks for the rollout (global scarcity of semiconductors and lack of technicians in Germany) and the regulatory process clarifications still needed, the feasibility of a full rollout by the end of 2022 is questionable. The authors recommend a limited extension of the rollout period until these challenges are likely to be mitigated to an acceptable degree. With a very similar argumentation, the German authorities intend to postpone the deadline by 1 year, according to the first draft of a future version of the German Renewable Energy Law (BMWK, 2022).

Such a limited extension of the rollout period would also allow for analyzing the pre- and post-implementation situation of two important aspects, which still require investigation:

1) No studies have yet been conducted on the effects of ADLS on wildlife. Therefore, the uncertainty of expert responses for this criterion is very high (reflected in the high standard deviation shown in Figure 9). Further studies are recommended, e.g., by monitoring finds of dead birds in the area.
2) Several studies demonstrate the relevance of WT lighting on stress and acceptance. Even though lighting is a less relevant cause of stress than noise and shadows flicker, it is visible in a larger surrounding and thus affects more people (Rudolph et al., 2017). However, no study has been conducted that directly measured the change in acceptance in the vicinity of a wind farm before and after the implementation of an ADLS. Therefore, such a study is recommended.

5.3 Validity of the results

The evaluation shown here is valid for currently installed ADLS. It is assumed that changing conditions within a short time frame of a few years will not significantly change the evaluation, but changes occurring after more than a decade might do so. Although LCA results, particularly the GWP and ARD impact, might become more positive due to reductions in GHG intensity of the energy used and advances in recycling, the LCA impact as part of the MCA will still be insignificant. However, as the size and number of WTs increase, more people might be affected by lighting-related stress without ADLS. Therefore, it is likely that more and more countries will approve the application of transponder-based ADLS, which will increase the market size and growth potential. At the same time, this will lead to more international competition, which will likely reduce profitability for the first movers.

Furthermore, a critical look at potential sources of error and uncertainty is needed. Some sources of error are inherent to the design and methodology of the framework, while others depend on the evaluation practitioner, the availability of data, and the functionality of the application being evaluated. The most important source of error in MCA is the selection of evaluation criteria. If the criteria do not cover the relevant impacts, the evaluation cannot produce a meaningful result. Therefore, considerable effort has been put into the development of the criteria, which have been updated for this study based on a previous study (Weigel et al., 2021). Furthermore, the MCA and weighting methods may have an impact on the result. The simple additive weighting method (SAW, also known as the weighted sum method), which is commonly applied due to its popularity and simplicity (Cajot et al., 2017), makes it intuitive for decision makers and thereby reduces the probability of user error. Furthermore, the aggregation method allows for a high level of transparency on how aggregated results are derived from criteria evaluations (Wilkens, 2012). The downside of the simplicity is that the compensatory aggregation might reduce the clarity of specific effects for complex problems (Marler and Arora, 2010), (Chu et al., 2007). This disadvantage is mitigated in this study by discussing results on aggregated levels as well as on the detailed criteria level. In (Terrapon-Pfaff, 2014) and (Daugavietis et al., 2022) the authors compare results obtained with different methods, including SAW, and conclude that results using the SAW method do not differ significantly from the results obtained with more complex methods. Furthermore, the SAW method is suitable to be applied with fuzzy numbers for uncertain input data such as subjective expert evaluations. The use of fuzzy sets is described in (Greco et al., 2016, 637), and an application is presented, for example, in (Ziemba, 2021). The integration of fuzzy SAW presents a future improvement possibility for the evaluation framework.

Further uncertainties may arise from the criteria assessment in the LCA and the EIs. The accuracy of the LCA result depends largely on the life cycle model created, including system boundaries, assumptions, input data, databases used, and the inclusion or exclusion of effects. A structured approach to assessing LCA data quality is the pedigree matrix (Weidema, 1998). Since the quality of the data used in this study varies significantly by data point, an overall evaluation of data quality according to the pedigree matrix does not appear feasible. Therefore, rather than assessing the quality of the input information, the effect of uncertainties on the results is estimated using sensitivity analysis. In this study, the sensitivity of the results is shown regarding several parameters, namely the number of turbines per ADLS, the number of communication units per ADLS, and the beacon reduction rate. No other parameters are identified as having a significant impact on the ADLS result. It should be noted that some ADLS use cloud data management, but the required data transfer and server operation are not included in the LCA due to a lack of information (Malmodin et al., 2014). find that the end-user applications cause a significantly higher GHG impact than the data transfer and servers. Therefore, it is unlikely that including both aspects would drastically change the outcome. Yet, a more accurate assessment could increase certainty. Furthermore, the LCA impact method used may have an influence on the results. Within the limited options of methods which include the required impact criteria (CML2001 and ReCiPe) the (midpoint) methods provide largely consistent results for the analyzed impacts (Bueno et al., 2016).

The choice of the reference for normalizing the LCA might have the greatest impact on how the LCA result affects the MCA result. In this study, the life cycle impact of the WTs, which are covered by the ADLS, is used as the reference. The WTs' life cycle

impacts assessed with the Ecoinvent database (data source from 2001) result in a GHG intensity of 17.6 g CO_2 eq./kWh, while (Hengstler et al., 2021) finds a lower intensity of 10.6 g CO_2 eq./kWh for modern onshore low wind turbines. However, even a very large deviation of ±50% from the reference values would not significantly change the impact of the LCA on the MCA outcome.

The EIs are mainly influenced by the selection of experts, i.e., the number of experts, the area and level of their expertise, and their self-perception of knowledgeability to evaluate criteria. Unless a large number of interviews are conducted, which would require a great effort, the interview results cannot be considered representative. Nevertheless, expert knowledge can provide very valuable insights into the subject. Therefore, even a smaller number of experts is acceptable as long as their expertise covers the perspectives of the relevant stakeholders. A practical approach used in this study to ensure that the relevant stakeholder representatives are included is to ask each expert to identify relevant stakeholders. It is highly unlikely that a relevant stakeholder role would not be identified by any of the 12 experts interviewed, so good coverage of the relevant perspectives can be expected. However, as mentioned, no affected neighbors of WTs are directly included in the EIs of this study, but the insights of the two scientists researching the social acceptance of WTs is seen as a good proxy for the perspective of this group. The level of expertise of the experts can be difficult to assess for a non-expert, but information about professional positions, publications, or involvements in reputable organizations can be used as quality control. In addition, each expert is explicitly advised to evaluate only criteria regarding which he or she feels sufficiently knowledgeable. Thus, it can be expected that most answers are based on sound expertise and that different answers are mainly an indication of uncertainty due to the range of possible impacts. As an improvement of the framework in this study, the standard deviation of the EI results is used in combination with the number of responses as an indicator of uncertainty, which revealed high uncertainties in particular for the criteria innovation potential, growth potential, economic barriers, availability of materials and know-how and regulatory implementation effort. Last but not least, the EI result may also be influenced by the interviewer during the interview. Here, a minimal intervention approach was applied, i.e., besides an initial introduction and some necessary criteria clarifications, the interviewer only passively documented the experts' evaluation.

5.4 Suitability of the framework

Since, in this study, an adapted version of the previously developed framework is applied, the adapted version's suitability is reviewed. The intended characteristics of the framework are that meaningful and useful results can be obtained, that it is easily usable for researchers and representatives of companies and organizations, and that it can be applied to the variety of current and future digital applications. Therefore, the suitability should be evaluated based on the conclusiveness of results, the feasibility of use, and the adaptability of the framework. The conclusiveness of the results includes both correctness and potential for deriving action. Feasibility of use is based on the effort required for each evaluation as well as the inherent complexity and thus the level of expertise required by the practitioner. Adaptability of the framework is required regarding different types of digital applications, the level of data availability, and practitioners' preferences. These suitability criteria are specific to the evaluation of this framework and can only be evaluated qualitatively.

The correctness of the results is difficult to assess due to the lack of other studies on ADLS. However, based on the possible comparisons of specific aspects with other publications and the relatively high consistency of expert opinions, the results are likely to be very realistic. Sources for uncertainties are identified and, where possible, analyzed via sensitivity analysis or statistical means. Furthermore, the potential to derive actions is high as direct measures and recommendations for further studies, life cycle improvement initiatives, as well as regulatory adjustments are identified. The overall conclusiveness of the result is therefore considered to be high.

The effort required to collect the necessary data for the LCA and to conduct the twelve expert interviews is relatively high. However, the framework improvement implemented in this study to let experts independently conduct the weighting after the interview decreased the interview effort and time requirement for the research team significantly. Due to the methods chosen, the complexity of the MCA and the EIs is rather low, such that this part of the framework can also be carried out by practitioners without a deep theoretical understanding of the methodology. The LCA, however, requires in-depth expertise. Therefore, the feasibility of use is evaluated as medium. This drawback could be mitigated if existing life cycle results could be integrated instead of conducting a separate LCA. In addition, the effort could be further reduced by decreasing the number of expert interviews. However, this could affect the correctness of the result.

The adaptability of the framework regarding different types of applications can be assessed by looking at the difference between the application evaluated in this study and the smart meter rollout evaluated in (Weigel et al., 2021). The two applications differ greatly in terms of the energy value stream step in which they are deployed, their function, and their effects. Furthermore, in this study, a single application is evaluated, while in (Weigel et al., 2021), a nationwide rollout of an application is evaluated. The adaptability regarding the type of application is therefore considered to be very high. The availability of information differs considerably between criteria, e.g., there are several studies on the social acceptance of ADLS, but none

on the impact on wildlife. Nevertheless, all criteria can be evaluated in the expert interviews and discussed, including the standard deviation and the number of responses as a measure of the robustness of the result. This demonstrates the very high adaptability of the framework to different levels of data availability. Finally, the adaptability to practitioners' preferences can only be evaluated once the framework has been applied by different practitioners, which is not the case at this stage. Therefore, the overall adaptability is considered to be very high, but the unevaluated adaptability to practitioners' preferences has to be taken into account.

Considering the high conclusiveness of the results, the medium feasibility of use, and the very high adaptability, it is concluded that the evaluation framework is well suited for its purpose.

6 Conclusion and outlook

In this study, an updated version of a holistic evaluation framework previously developed by the authors was applied to evaluate the application of aircraft detection lighting systems for wind turbines. The framework is specifically designed for the holistic evaluation of digital applications in the energy sector. To achieve a holistic view, multiple criteria covering all relevant impact areas were evaluated, relevant stakeholders' perspectives were considered as weighting profiles, and representatives of relevant stakeholders were involved in the process. A life cycle assessment was performed to assess several environmental criteria. The required data and information were provided by both an ADLS and a beacon manufacturer. Furthermore, twelve expert interviews were conducted to assess all other criteria that were not part of the LCA. The experts also weighted the criteria, and five weighting profiles were created. The study presents the first holistic evaluation of ADLS, in contrast to previous studies, which focus on single evaluation aspects such as aviation risks or social acceptance as well as a refined version of the evaluation framework.

The results of the LCA show a likely increase in the life cycle impact of all analyzed criteria if a realistic design of the system is assumed. The magnitude of the increase depends mainly on the number of WTs covered per ADLS and the need to install additional communication units. Due to the size of offshore wind farms, the ADLS could lead to a reduction in life cycle impacts here. The LCA results of this study can be used by ADLS manufacturers as a starting point for life cycle improvement activities. However, in the context of the life cycle impacts of the turbines covered by the ADLS, the impact of the ADLS is negligible, whether it is increased or decreased. The MCA based on LCA and EI results shows an overall slightly positive evaluation from all stakeholders' perspectives. Therefore, a rollout is expected to be beneficial. The most significant benefits are seen in the increased social acceptance of wind turbines as well as the economic (international) growth potential for the providers of the technology and the resulting impact on the national economy. Two further studies are recommended with respect to 1) wildlife impacts to ensure that potential adverse impacts are identified and addressed and 2) social acceptance impacts to validate and measure wind energy acceptance before and after installing ADLS. Three main bottlenecks for the rollout were identified: the shortage of global semiconductor supply needed for production, the lack of trained technicians for installation, and remaining regulatory uncertainties regarding the approval process. Given these bottlenecks, an extension of the rollout period is recommended. The remaining time until the obligation becomes effective should be used by decision-makers to address the identified bottlenecks. Political decision-makers should drive the administrative process to eliminate the regulatory uncertainties. The issues of global semiconductor scarcity and lack of technicians in Germany go well beyond affecting only ADLS but hinder major developments, such as the transition towards renewable energies, and therefore, need to be counteracted on a broader economic-political level by, e.g., researching material substitutions, investing in new production capacities and supporting continuing professional development. However, smaller measures to mitigate the impact of these bottlenecks on the ADLS rollout can be taken by business decision-makers. For example, the pooling of ADLS installations for an entire region, as done by the association for renewable energies in the state of North Rhine-Westphalia, could improve the plannability for both ADLS manufacturers and installers. Furthermore, the implementation of ADLS in other countries could benefit from an early holistic evaluation using the presented framework.

Potential sources of uncertainty were identified, and, where possible, sensitivity analyses were performed. Given the limitations and uncertainties, the study provides a robust evaluation result with an aggregated overview and valuable insights into bottlenecks and potential for improvements at the criteria level.

The suitability of the updated framework was assessed based on three criteria: conclusiveness of results, feasibility of use, and adaptability of the framework. Overall, the framework was found to be highly suitable for its purpose. Two measures are suggested to further improve the feasibility of use. In addition, the possibility of applying fuzzy sets for the SAW aggregation method was pointed out to improve the handling of uncertainties.

A prospective future direction of the research might be for the framework to be applied to different digital applications in the energy sector by different practitioners. Additionally, the framework could be adapted for the evaluation of digital

applications in other sectors. With increasing numbers of performed evaluations, the comparability of results becomes increasingly interesting and should be analyzed. The proposed integration of fuzzy logic may improve the comparability of applications with varying uncertainties. Another interesting future aspect could be the retrospective analysis of previous evaluations regarding the accuracy of results and conclusions.

Data availability statement

The datasets presented in this article are not readily available because due to confidentiality restrictions of the information supplying company, data on the technical setup of the application can only be shared on an aggregated level upon request to the corresponding author. Raw and anonymized expert interview results can be shared upon request. Requests to access the datasets should be directed to pweigel@uni-osnabrueck.de.

Ethics statement

Ethical review and approval was not required for the study on human participants in accordance with the local legislation and institutional requirements. Written informed consent from the (patients/participants OR patients/participants legal guardian/next of kin) was not required to participate in this study in accordance with the national legislation and the institutional requirements.

Author contributions

All authors contributed to the conception and design of the study. PW gathered and analyzed the data and conducted the assessments. The manuscript was prepared by PW, with frequent input and revisions from PV. All authors carefully read and approved the submitted manuscript.

Conflict of interest

The authors declare that the research was conducted in the absence of any commercial or financial relationships that could be construed as a potential conflict of interest.

Publisher's note

All claims expressed in this article are solely those of the authors and do not necessarily represent those of their affiliated organizations, or those of the publisher, the editors and the reviewers. Any product that may be evaluated in this article, or claim that may be made by its manufacturer, is not guaranteed or endorsed by the publisher.

Acknowledgments

We acknowledge financial support by Wuppertal Institut für Klima, Umwelt, Energie gGmbH within the funding programme Open Access Publishing.

References

Baumgärtner, N., Deutz, S., Reinert, C., Nolzen, N., Kuepper, L. E., Hennen, M., et al. (2021). Life-cycle assessment of sector-coupled national energy systems: Environmental impacts of electricity, heat, and transportation in Germany till 2050. *Front. Energy Res.* 9. Available at: https://www.frontiersin.org/article/10.3389/fenrg.2021.621502 (Accessed April 26, 2022).

Behrend, F. (2019). *Identifizierung und Bewertung der durch die Einführung der transponderbasierten bedarfsgesteuerten Nachtkennzeichnung (BNK) entstehenden flugbetrieblichen Risiken und Beschreibung von Risikominimierungsmaßnahmen*. Rosengarten, Germany: German Federal Ministry for Economic Affairs and Energy (BMWi).

BMDV (2020). *Allgemeine Verwaltungsvorschrift zur Kennzeichnung von Luftfahrthindernissen*. Offenbach, Germany: German Federal Ministry for Digital and Transport (BMDV).

BMDV (2018). *Verordnung über die Flugsicherungsausrüstung der Luftfahrzeuge*. Berlin, Germany: German Federal Ministry for Digital and Transport (BMDV).

BMDV (2022). *Wetter und Klima - deutscher Wetterdienst - EDDE Erfurt*. Berlin, Germany: German Federal Ministry for Digital and Transport. Available at: https://www.dwd.de/DE/fachnutzer/luftfahrt/teaser/luftsportberichte/edde/node.html (Accessed May 2, 2022).

BMWK (2022). *Entwurf eines Gesetzes zu Sofortmaßnahmen für einen beschleunigten Ausbau der erneuerbaren Energien und weiteren Maßnahmen im Stromsektor*. Berlin, Germany: German Federal Ministry for Economic Affairs and Climate Action. Available at: https://www.bmwk.de/Redaktion/DE/Artikel/Service/Gesetzesvorhaben/referentenentwurf-erneuerbaren-energien-und-weiteren-massnahmen-im-stromsektor.html (Accessed April 27, 2022).

BNK (2022). Saar GmbH BNK saar. Available at: https://bnk-saar.de/(Accessed May 25, 2022).

Bode, M., and Klümper, L. (2021). *Das BNK Gemeinschaftsprojekt für NRW*. Düsseldorf, Germany: Association for renewable energies in the state of North Rhine-Westphalia (LEE NRW GmbH).

Bueno, C., Hauschild, M. Z., Rossignolo, J. A., Ometto, A. R., and Mendes, N. C. (2016). Sensitivity analysis of the use of life cycle impact assessment methods: A case study on building materials. *J. Clean. Prod.* 112, 2208–2220. doi:10.1016/j.jclepro.2015.10.006

Cajot, S., Mirakyan, A., Koch, A., and Maréchal, F. (2017). Multicriteria decisions in urban energy system planning: A review. *Front. Energy Res.* 5, 10. doi:10.3389/fenrg.2017.00010

Chu, M.-T., Shyu, J., Tzeng, G.-H., and Khosla, R. (2007). Comparison among three analytical methods for knowledge communities group-decision analysis. *Expert Syst. Appl.* 33, 1011–1024. doi:10.1016/j.eswa.2006.08.026

D'Adamo, I., Gastaldi, M., and Morone, P. (2022). Economic sustainable development goals: Assessments and perspectives in Europe. *J. Clean. Prod.* 354, 131730. doi:10.1016/j.jclepro.2022.131730

Daugavietis, J. E., Soloha, R., Dace, E., and Ziemele, J. (2022). A comparison of multi-criteria decision analysis methods for sustainability assessment of district heating systems. *Energies* 15, 2411. doi:10.3390/en15072411

Deutsche WindGuard GmbH (2021). *Status des Offshore-Windenergieausbaus in Deutschland*. Varel, Germany: Deutsche WindGuarad GmbH.

Ellis, G., and Ferraro, G. (2016). The social acceptance of wind energy. LU: European commission. Joint research centre. Available at: https://data.europa.eu/doi/10.2789/696070 (Accessed April 28, 2022).

Gährs, S., Bluhm, H., Dunkelberg, E., Katner, J., Weiß, J., Henning, P., et al. (2021). Potenziale der Digitalisierung für die Minderung von Treibhausgasemissionen im Energiebereich. Umweltbundesamt. Available at: https://www.umweltbundesamt.de/publikationen/potenziale-der-digitalisierung-fuer-die-minderung (Accessed April 26, 2022).

German Corporation for International Cooperation GmbH (GIZ) (2022). Extractive industries transparency initiative - report 2019 for Germany. Available at: https://d-eiti.de/en/(Accessed May 4, 2022).

German Federal Ministry for Economic Affairs and Energy (2021). *Gesetz für den Ausbau erneuerbarer Energien*. Berlin, Germany: German Federal Ministry for Economic Affairs and Energy (BMWi).

S. Greco, M. Ehrgott, and J. R. Figueira (Editors) (2016). *Multiple criteria decision analysis* (New York, NY: Springer New York). doi:10.1007/978-1-4939-3094-4

Hengstler, J., Russ, M., Stoffregen, A., Hendrich, A., Weidner, S., Held, M., et al. (2021). Aktualisierung und Bewertung der Ökobilanzen von Windenergie- und Photovoltaikanlagen unter Berücksichtigung aktueller Technologieentwicklungen. Umweltbundesamt. Available at: https://www.umweltbundesamt.de/publikationen/aktualisierung-bewertung-der-oekobilanzen-von (Accessed April 28, 2022).

Hübner, G., and Pohl, J. (2010). *Akzeptanz und Umweltverträglichkeit der Hinderniskennzeichnung von Windenergieanlagen*. Halle (Saale): Martin-Luther-Universität Halle–Wittenberg Institut für Psychologie.

Hübner, G., Pohl, J., Hoen, B., Firestone, J., Rand, J., Elliott, D., et al. (2019). Monitoring annoyance and stress effects of wind turbines on nearby residents: A comparison of U.S. And European samples. *Environ. Int.* 132, 105090. doi:10.1016/j.envint.2019.105090

ICAO (2018). Aerodromes: International standards and recommended practices. *Int. Civ. Aviat. Organ*. Available at: https://store.icao.int/en/annex-14-aerodromes (Accessed March 22, 2022).

Kluczek, A., and Gladysz, B. (2022). Frontiers in energy research *10*. Available at: https://www.frontiersin.org/article/10.3389/fenrg.2022.848584 (Accessed April 26, 2022).Energy sustainability performance index of biodigester using energy LCA-based indicators

Malmodin, J., Lundén, D., Moberg, Å., Andersson, G., and Nilsson, M. (2014). Life cycle assessment of ICT. *J. Industrial Ecol.* 18, 829–845. doi:10.1111/jiec.12145

Marler, R. T., and Arora, J. S. (2010). The weighted sum method for multi-objective optimization: New insights. *Struct. Multidiscipl. Optim.* 41, 853–862. doi:10.1007/s00158-009-0460-7

Naegler, T., Becker, L., Buchgeister, J., Hauser, W., Hottenroth, H., Junne, T., et al. (2021). Integrated multidimensional sustainability assessment of energy system transformation pathways. *Sustainability* 13, 5217. doi:10.3390/su13095217

Pohl, J., Hübner, G., and Mohs, A. (2012). Acceptance and stress effects of aircraft obstruction markings of wind turbines. *Energy Policy* 50, 592–600. doi:10.1016/j.enpol.2012.07.062

Pohl, J., Rudolph, D., Lyhne, I., Clausen, N.-E., Aaen, S. B., Hübner, G., et al. (2021). Annoyance of residents induced by wind turbine obstruction lights: A cross-country comparison of impact factors. *Energy Policy* 156, 112437. doi:10.1016/j.enpol.2021.112437

Roscher, M. (2019). *BNK – Genehmigt!*. Berlin: Fachagentur Windenergie an Land e.V..

Rudolph, D., Kirkegaard, J., Lyhne, I., Clausen, N.-E., and Kørnøv, L. (2017). Spoiled darkness? Sense of place and annoyance over obstruction lights from the world's largest wind turbine test centre in Denmark. *Energy Res. Soc. Sci.* 25, 80–90. doi:10.1016/j.erss.2016.12.024

Sun, J., Jin, H., Tsai, F.-S., and Jakovljevic, M. (2022). A global assessment of sustainable development: Integrating socioeconomic, resource and environmental dimensions. *Front. Energy Res.* 10, 816714. doi:10.3389/fenrg.2022.816714

Terrapon-Pfaff, J. (2014). *Nachhaltige Bioenergieoptionen für Afrika: energetische Nutzung von Agrarreststoffen als Teil einer Transformationsstrategie hin zur nachhaltigeren Energieversorgung in Tansania: Potentialanalyse und multikriterielle Bewertung*. Hamburg: Dr. Kovač GmbH.

Weidema, B. P. (1998). Multi-user test of the data quality matrix for product life cycle inventory data. *Int. J. Life Cycle Assess.* 3, 259–265. doi:10.1007/BF02979832

Weigel, P., Fischedick, M., and Viebahn, P. (2021). Holistic evaluation of digital applications in the energy sector—evaluation framework development and application to the use case smart meter roll-out. *Sustainability* 13, 6834. doi:10.3390/su13126834

Wilkens, I. (2012). Multikriterielle Analyse zur Nachhaltigkeitsbewertung von Energiesystemen - von der Theorie zur praktischen Anwendung. Available at: https://depositonce.tu-berlin.de//handle/11303/3682 (Accessed May 29, 2018).

Zhang, S., Ma, X., and Cui, Q. (2021). Assessing the impact of the digital economy on green total factor energy efficiency in the post-COVID-19 era. *Front. Energy Res.* 9, 798922. doi:10.3389/fenrg.2021.798922

Ziemba, P. (2021). Selection of electric vehicles for the needs of sustainable transport under conditions of uncertainty—a comparative study on fuzzy MCDA methods. *Energies* 14, 7786. doi:10.3390/en14227786

10.3389/fenrg.2022.984003

Appendix: Relevant assumptions for the LCA of the ADLS

Assumption	Value	Unit	Source
Turbine lifetime	20	Years	Industry standard
ADLS lifetime	20	Years	ADLS manufacturer
Analysis period	20	Years	Turbine lifetime
Reduction of beacon operational hours during night	98	%	ADLS manufacturer
Reduction of LED replacements	1.29	Replacements/ 20 years	Beacon manufacturer
ADLS receiver electric capacity	31	W (average per day)	ADLS manufacturer
ADLS communication electric capacity	28	W (average per day)	ADLS manufacturer
Infrared (IR) beacon electric capacity	1.3	W (during operation)	Beacon manufacturer
Beacon W red electric capacity	5	W (during operation)	Beacon manufacturer
Beacon W red + IR electric capacity	6	W (during operation)	Beacon manufacturer
Share of on-site electricity of consumption	81	%	ADLS manufacturer
GWP 100 of German electricity mix in 2022/ 32/42	460/330/257	kg CO_2 eq./kWh	Weigel et al. (2021)
Location (Erfurt Germany)	51°13′55 N 6°48′42 O	GPS coordinates	
Yearly average night hours	10.48	h/d	BMDV (2022)
Yearly average twilight hours	1.25	h/d	BMDV (2022)
Recycling shares		%	
Aluminum	90[1]		
Cables	84[2]		
Electronics	84[1]		1) (German Corporation for International Cooperation GmbH (GIZ), 2022)
PCBs	84[2]		2) assumed to be same as electronics
Plastics	47[1]		
Steel	95[1]		
Component weights	Kg		
Receiver	21.5		ADLS manufacturer
Communication module	22.1		ADLS manufacturer
Mounting/Antenna/Cabling	43.2		ADLS manufacturer
Infrared beacon components	0.16		Beacon manufacturer
LED beacon components	0.57		Beacon manufacturer
LED Lifetime	50,000	h	Beacon manufacturer

frontiers | Frontiers in Energy Research

TYPE Original Research
PUBLISHED 23 August 2022
DOI 10.3389/fenrg.2022.974747

OPEN ACCESS

EDITED BY
Massimo Gastaldi,
University of L'Aquila, Italy

REVIEWED BY
Brenno Menezes,
Hamad bin Khalifa University, Qatar
Idiano D'Adamo,
Sapienza University of Rome, Italy

*CORRESPONDENCE
Lijie Feng,
ljfeng@shmtu.edu.cn

SPECIALTY SECTION
This article was submitted to Sustainable Energy Systems and Policies, a section of the journal Frontiers in Energy Research

RECEIVED 21 June 2022
ACCEPTED 29 July 2022
PUBLISHED 23 August 2022

CITATION
Wang J, Li K and Feng L (2022), Tracing the technological trajectory of coal slurry pipeline transportation technology: An HMM-based topic modeling approach.
Front. Energy Res. 10:974747.
doi: 10.3389/fenrg.2022.974747

Tracing the technological trajectory of coal slurry pipeline transportation technology: An HMM-based topic modeling approach

Jinfeng Wang[1], Kang Li[2] and Lijie Feng[1]*

[1]China Institute of FTZ Supply Chain, Shanghai Maritime University, Shanghai, China, [2]Institute of Logistics Science and Engineering, Shanghai Maritime University, Shanghai, China

Coal slurry pipeline transportation is an important way to realize green coal logistics. However, there are still challenges in understanding the cognitive aspects of coal slurry pipeline transportation technology development trajectory. This study attempts to trace and predict the technology trend from patent texts through the stochastic process analysis of topic evolution. It helps understand the challenges in the development process of coal slurry pipeline transportation technology. And capture trends and development characteristics of the technology to improve research and development (R&D) efficiency and sustainability. As a result, this study extracts potential technology topics from patent text by using the Latent Dirichlet Distribution method. Then, a Word2vec-based topic word vector model is applied to calculate the cosine similarity between topics. And the HMM-based topic evolution trend model is constructed by introducing the Hidden Markov Model (HMM) which can portray a dual stochastic process. Finally, it is used to analyze and predict trends in the technological evolution of this field. It was found that the advancement of technology related to pulping is fundamental to promoting the development of coal slurry pipeline transportation technology, which is also a common research topic. Finally, technologies related to pipeline transportation capacity enhancement and the industrial application of coal slurry will be the focus of future R&D in this field with broad research and application prospects. This study is intended to provide directions for sustainable R&D activities in coal slurry pipeline transportation technology, facilitate interdisciplinary discussions, and provide objective data for future decisions making for scientists and R&D managers in this field.

KEYWORDS

coal slurry, pipeline transportation, trend analysis, patent analysis, topic modeling

1 Introduction

As China's basic energy source, coal causes staggering pollution and waste during transportation (Li et al., 2021). China issued the Energy Technology Revolution Innovation Action Plan (2016–2030) and the 13th 5-year plan for the development of the coal industry, which emphasizes efforts to build an efficient, green, and modern coal industry system. Coal logistics is a key link between coal production and consumption, and its green transformation and development are crucial to building a modern coal industry system (Li et al., 2020). Currently, the research and development (R&D) of closed transportation technology, such as coal slurry pipeline transportation, has become a major research focus of green coal logistics. In recent years, the pipeline transportation technology has been applied widely in engineering fields, such as pipeline long-distance transportation of iron ore concentrate or nickel-cobalt ore, reservoir dredging, etc. With the development of pipeline transportation technology, it has gradually become one of the important ways for the coal logistics industry to achieve green transformation and sustainable development (Prasad et al., 2020; Das et al., 2021). However, countries with coal-dominated energy use have not fully adopted and promoted coal slurry pipeline transportation, much less achieved real commercial application. For example, in China, 80% of coal is transported by train, 13% by ship, and 7% by truck (Oberschelp et al., 2019). Thus, the development of pipeline transportation of coal is still limited.

Technological advancement is an important factor in promoting the diffusion of environmentally friendly technologies (Rao and Kishore, 2010; Tabrizian, 2019; Markard, 2020). Currently, the immaturity of technology is the key factor restricting coal transportation by pipeline projects for large-scale operation and promotion. From a historical development perspective, the trajectory of coal slurry pipeline transportation technology is also full of high uncertainty. In this case, it becomes extremely challenging to identify and analyze the evolution characteristics and the development trends of coal pipeline transportation technology. In other words, the overall development trend of coal slurry pipeline transportation technology is still unclear. This does not help policy-makers introduce targeted policies or develop more competitive R&D strategies to drive technological advancement (Lai et al., 2020; Yuan and Cai, 2021). Therefore, it is necessary to identify and analyze the evolutionary characteristics and the development trends of coal pipeline transportation technology.

However, relatively little attention has been paid to tracking the evolving trends and characteristics of coal slurry pipeline transportation technology based on objective data. Until now, most research concerning coal slurry pipeline transportation technology has focused on modeling (Das et al., 2020; Singh et al., 2020; Yin et al., 2021), method optimization (Singh et al., 2018; Yang et al., 2019; Singh et al., 2022), and literature review (Mishra et al., 2019; Nunes, 2020; Das et al., 2021). And the research methods are usually based on experiments, surveys, case studies or expert reviews. The resulting lack of research concerning technology trend analysis based on scientific systematic analysis is a fact in this field. Tracking the trend of coal slurry pipeline transportation technology could help scientists and R&D managers understand the technology development characteristics in time to improve the sustainability of future R&D activities. Recently, the increasing number of patents has provided an opportunity to investigate technology trends in specific fields. Patents are reliable data for the quantitative analysis of technology trends, which contain complete and valuable information about a specific product or technology (Yoon et al., 2017). Therefore, this study tracks the development trend and characteristics of coal slurry pipeline transportation technology based on the analysis of patent information.

There are various patent analysis methods, such as patent number analysis (Chen and Lin, 2020), technology classification code analysis (Aaldering et al., 2019a), social network analysis (Aaldering et al., 2019b), and patent map analysis (Renaldi et al., 2021). However, these previous studies often ignore the stochastic process characteristic of technological innovation, which may lead to biased analysis results (Pan et al., 2017; Wei et al., 2020). Since this field is characterized by highly uncertain technological developments, it may be more appropriate to trace technology trends from a stochastic process perspective. A Hidden Markov Model (HMM) includes a double stochastic process, which has outstanding advantages in portraying the dynamic stochastic evolution process. Therefore, we adopt an approach that integrates patent semantic analysis with the HMM. It can better portray the stochastic evolution process of technological topics based on patent semantic information, which provides effective data for the quantitative analysis and prediction of technology trends.

Therefore, this study has the following objectives: ① identifying the potential different categories of technological information by extracting technology topics from patent data about coal slurry pipeline transportation technology; ② tracing the development path of coal slurry pipeline transportation technology based on the HMM modeling of the topic evolution stochastic process; and ③ quantitatively predicting the development trend of coal slurry pipeline transportation technology by using the HMM backward algorithm.

This study has two contributions. First, we are the first to explore the development path of coal slurry pipeline transportation technology from the perspective of patent text mining, and we predict possible development trends. Second, semantic mining techniques are applied to the topic stochastic evolution process analysis, which makes us not only rely on the existing term co-occurrence methods for the measurement of the topic evolution stochastic process.

TABLE 1 Comparison of key features of coal transportation ways.

Type	Advantages	Disadvantage
#0000FF	Short and medium distance transportation	Highest operating costs and low labor productivity (relative to pipelines)
Truck	High flexibility	The most serious environmental pollution
#0000FF	High reliability and long transportation distance	High occupancy rate of land resources (25 acres per kilometer of railway)
Rail	Large volume of coal transportation	Serious pollution along the way
	Strong continuity of operation	High coal loss rate (0.8%–1%)
	Low operating costs (relative to pipelines)	Vulnerable to topographic conditions
#0000FF	Low occupancy rate of land resources	Strict concentration requirements (fluidity and stability effects)
Coal slurry Pipeline	Long transportation distance and large coal slurry transportation volume	Strict flow rate requirements (critical flow rate greater than 1.1 m/s)
	Low degree of environmental pollution (closed transportation)	Limited laying slope (up to 16%)
	Low coal loss rate (below 0.1%)	Easily blocked (settlement characteristics)
	Low cost (long distance or relatively short distance)	Waste of water and high-power consumption
	Strong continuous operation characteristics	

The rest of this study is organized as follows: Section 2 provides a literature review of coal slurry pipeline transportation technologies, text mining, and a technology trend analysis. Section 3 describes the research framework and the research process. Section 4 analyzes the technology's stochastic evolutionary trends and the predicted results. Section 5 provides a discussion. Section 6 summarizes this study.

2 Literature review

2.1 Coal slurry pipeline transportation technology

Coal slurry pipeline transportation refers to the process of using high-pressure pumps to continuously transport coal slurry through closed pipes to end-users (Lahiri and Ghanta, 2008). The United States built the first long-distance coal slurry pipeline in 1957 to transport large quantities of coal over long distances (Kania, 1984). Over the years, many countries have been attracted to exploring this technology. We summarized the major advantages and disadvantages of the existing discussed coal slurry pipeline transportation ways in a compact manner, as shown in Table 1. Subsequently, we will briefly summarize the existing research directions and characteristics in the field of coal slurry pipeline transportation.

From Table 1, it is not difficult to find that pipeline transportation technology has a potentially disruptive impact on the future development of the traditional coal logistics system (Zahed et al., 2018). At present, truck and rail transportation are the main ways of coal transportation. The environmental pollution and economic loss caused by the coal dust emission problem during their transportation is huge (Bao et al., 2020). In contrast, the pipeline transportation method is an important way to achieve environmentally friendly, clean, and economical transportation of coal (Jati et al., 2021). Coal slurry pipelines can effectively reduce NOx emissions and energy consumption during the transportation process of coal compared to railroads and highways (Rao et al., 2020). In addition, coal slurry pipeline transportation has the advantage of low maintenance cost, transportation cost and high safety (Kumar et al., 2014). One of the main challenges lies in the high requirement for laying slope of the pipeline since the limitation of the hydraulic properties of slurry. Thus, several scholars have researched specific sub-technologies to tackle such challenges, such as coal slurry rheological properties (Singh et al., 2017), pipeline detection techniques (Zhang et al., 2019), and coal slurry particle composition (Prasad et al., 2020).

Additionally, there are studies on the cost and economic feasibility of constructing a coal slurry pipeline transportation system by reviewing the previous literature. Strogen et al. (2016) discusses the advantages and the disadvantages of pipeline transportation and proposes an evaluation framework for the economic feasibility and the nonmarket benefits of different means of transportation. Jati et al. (2021) analyzed the economic and environmental benefits of using a coal slurry pipeline, aiming to evaluate its feasibility to replace truck transportation of coal. In addition, some scholars provided solutions to specific technical problems in this field by reviewing the literature. Sinha et al. (2017) investigated the best way to reduce the wear rate by reviewing the research on the pipeline wear rate prediction model. Zaman et al. (2020) classified existing research on pipeline leak detection methods and discussed innovations in existing methods. Some scholars also systematically reviewed the development history of long-distance pipeline transportation technology and discussed the

future development trend of long-distance pipelines in Australia (Cowper and Thomas, 2009).

Most research methods in this field were experimental, and contained simulation and method optimization, a literature review, etc. Some studies analyzed the progress of sub-technologies, which were only done by literature review or expert judgment (Khan et al., 2019; Das et al., 2021). In particular, a rapidly increasing number of papers and patents on coal slurry pipeline transportation technology have been published in the last few years. It was difficult for academics to accurately analyze potential technology trends from a large number of papers and patents. Thus, this study attempts to explore the development trend of coal slurry pipeline transportation technology based on patent text mining. In the process, a suitable quantitative method was used for the development characteristics of this technology with high uncertainty.

2.2 Patent semantic analysis

Patent documents are an important carrier of technological information and an up-to-date and reliable data resource to study the development trend of specific technology (Yoon and Song, 2014). In fact, the vast amount of patent data makes it difficult to effectively analyze technology trends by relying only on expert knowledge (Park et al., 2016). With the advancement of text mining technology, various patent semantic analysis methods are emerging, such as topic analysis and vector space modeling. Many scholars use patent semantic analysis methods to mine potential technological information, which is widely used for quantitative analysis of technology trends.

Among them, topic analysis is a popular text mining method that identifies hidden topics in documents based on semantic clustering. Latent Dirichlet allocation (LDA) has become a mature topic modeling method that is widely used in text processing, such as in patent text classification (Kim et al., 2019) and topic identification (Chehal et al., 2021), etc. It provides an effective tool for accurately identifying technology trends from a large number of patent documents.

To be clear, LDA is a typical bag of words model that only extracts relationships between words and documents, without considering the relationships between words. However, word context information is often the most important aspect in text semantic mining (Blei et al., 2003; Li et al., 2018). Word2vec provides a modeling method that extracts feature vectors of words from their contexts to express deep semantic information about the words (Mikolov et al., 2013). Word2vec is also an effective tool to obtain semantic similarity (Zhao et al., 2020). Therefore, to better quantitatively analyze technology trends, we combine the LDA and Word2vec to capture technical information about potential topics in patent texts at the semantic level.

2.3 Technological trend analysis

We analyze and forecast the development trends of specific technologies to reveal their development paths (Liu et al., 2020). However, it is difficult to accurately analyze technology trends due to the stochastic nature of the innovation process and the complexity of technology relationships (Frenken, 2006; Pan et al., 2017). Several studies have found that simulation can portray the potential logical relationships among complex systems (Davis et al., 2007). It can be an effective tool for capturing the potential evolutionary relationships between technologies. Some attempts have been made to use simulation methods to capture potential evolutionary relationships among technology topics. Wu et al. (2014) first proposed a topic evolution trend prediction that integrated the LDA and HMM to predict stem cell topic research trends. Later, some studies analyzed and predicted marine diesel engine and 3D printing technology trends by adopting an approach that integrated the LDA and HMM (Wei et al., 2018; Wei et al., 2020). They tended to calculate stochastic evolutionary relationships among topics by the HMM to quantify the development process of technology trends.

HMM is an application of Markov chain, which is an effective method to solve problems such as inferring future states from known states. It has become a simulation method for quantitatively portraying technology trends. Existing studies have provided important insights for us to accurately identify the technology trends of specific technologies. However, we found that the initial parameters of the HMM in these studies were similar results between topics obtained based on term co-occurrence. Compared with citation analysis, the topic co-occurrence results based on term frequency can better reveal the similarity between topics (Feng et al., 2017). However, the term co-occurrence method is still limited in measuring the semantic similarity between topics (Wang et al., 2012). Therefore, it is necessary to explore the HMM-based approach to explore technology trends at the semantic level.

3 Data and methods

3.1 Analysis framework

This study proposes an analysis framework, as shown in Figure 1. The framework consists of four main components: collection and preprocessing of patent data, extraction of technology topics, identification of topic evolution processes, and prediction of topic evolution trends. It explores the technology trends of coal slurry pipeline transportation technology by mining topic information on their patent data. It is of strategic importance for countries to promote clean transportation technologies by tracking their development trends and predicting their future trends.

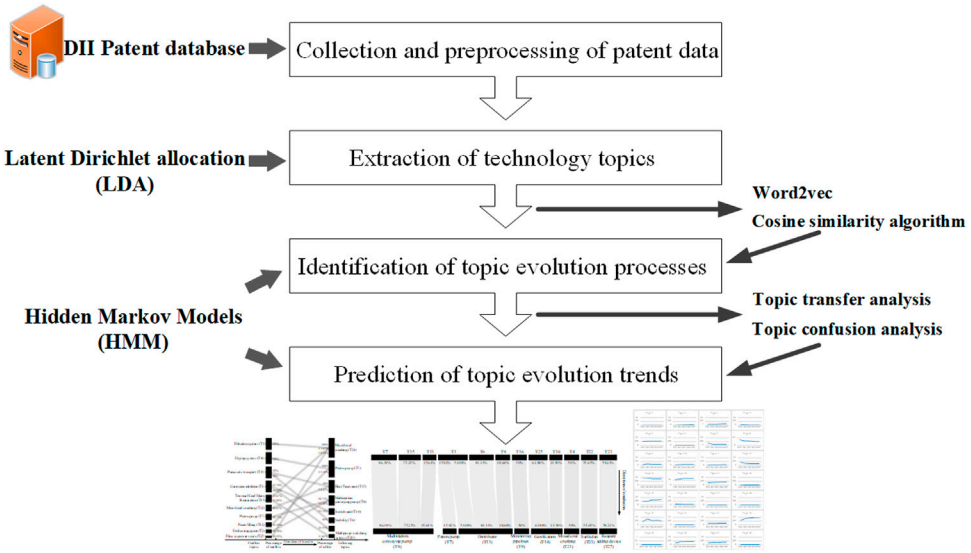

FIGURE 1
Framework for analyzing and forecasting technology trends.

After collecting patent data from Derwent Innovations Index (DII) database and preprocessing them, we first extract technology topics by the LDA. This step involves determining topic numbers to obtain valid topic information. Additionally, we obtain the temporal distribution of topics and classify them. In the subsequent analysis step, an HMM is constructed to portray the dual stochastic evolution process of technology topics, which aim to identify technology evolution trends. To portray the technology topic evolution process from the semantic level, the HMM modeling method based on Word2Vec and cosine similarity is proposed. Then, the technology topic evolution trends are analyzed and predicted by the calculation results of the optimal parameters of this HMM. Finally, based on the above results, we systematically analyze the technology trends of coal slurry pipeline transportation technology.

3.2 Collection and preprocessing of patent data

We use Derwent Innovations Index (DII) database as the patent data source. After repeated screening and testing, this paper uses the term " ((pipeline OR pipe*) AND coal AND (slurry OR slime) AND transport*)" as the retrieval formula to collect patent data. The search was performed in December 2021, and 672 issued patents were retrieved. We further excluded 90 patent records not related to coal slurry pipeline transportation technology.

A patent record consists of many parts, such as a title, abstract, and description. The title and abstract include some key terms that briefly summarize technological innovations. For analysis, we select titles and abstracts from 582 patent records. Then, we remove several meaningless words such as "text", "easy", "user", etc., based on the frequency of each word in the document. In addition, we construct a list of new stop words to remove those words that do not provide useful information for subsequent analysis.

3.3 Extraction of technology topics

This study uses the LDA to extract valid technology topics from acquired patent data. The LDA is a typical bag of words model approach that treats documents as collections of topics and words. This method assumes that each word in the document is drawn from a potential topic. For each document, a topic is drawn from the topic distribution. Then, a word is drawn from the distribution of words corresponding to that topic. Finally, the above process is repeated until all words in the documents are traversed. It generates document-topic distribution and topic-word distribution by sampling regardless of the order that the words appear in. In other words, this process can be understood as extracting multiple sets of words from documents with a certain probability to achieve topic extraction. The number of topics generated by the LDA model needs to be set manually. Here, we can determine the final number of topics based on the perplexity value.

Furthermore, hierarchies can be used for the in-depth analysis of specific technology areas (Li et al., 2019). It can represent the relationship between product components or

technical functions in a specific technical field (Choi et al., 2012). Therefore, to analyze the technology trends of coal slurry pipeline transportation technology more systematically and comprehensively, this study is divided into topic categories. We name the topic extraction results and divided the into three categories: "pulping", "pumping " and "end-processing".

3.4 Identification of topic evolution processes

With the rapid development of topic modeling techniques, it is worth considering how to identify technology trends from the extracted results of topics. Actually, the topic evolution process is characterized by double stochasticity, which reflects technology trends. Technical ideas are constantly generating new ideas in the process of updating, and this process is unobservable. This process is observable where these innovative ideas may be documented as patents or literature. Thus, patents can be mined to extract topics to identify technology trends.

Therefore, we construct a discrete HMM to portray the topic evolution process to quantitatively analyze coal slurry pipeline transportation technology trends. The HMM is an observation model with a dual stochastic process, containing a stochastic transfer process of hidden states and a process of hidden states to generate observable sequences. In the HMM, the stochastic transfer process of the hidden states is unobservable, and it can be regarded as a historical change in technology research. The process of generating observable sequences from hidden states can reflect the independent degree of technical research content evolution. The observable states are also patent records. With the HMM modeling of the technology topic evolution process, we can identify technology trends, determine technology directions, and discover technology hotspots and difficulties.

Based on the above idea, we need to clarify the parameters that are used to describe the HMM, which are $\lambda = (Q, V, \pi, A, B)$. Their contents are set as follows.

1) Q is the state set of all possible technology topics. $Q = \{q_1, q_2, \cdots q_N\}$, where N represents the number of technology topics. These states can be transformed with each other, which are unobservable. It is also denoted as the hidden state.
2) V is the set of all possible observable states. $V = \{v_1, v_2, \cdots v_M\}$, where M represents the number of possible observations.
3) π is the probability distribution of the initial state. $\pi_i = P(i_1 = q_i)$, $1 \le i \le N$, where π_i represents the probability of being in state q_i at time $t = 1$. In this study, the similarity matrix between technology topics is used as the initial iteration variable of π_i.
4) A is the transition probability distribution of the hidden state. $A = [a_{ij}]_{N\times M}$, $a_{ij} = P(i_{t+1} = q_j | i_t = q_i)$, $1 \le i, j \le M$. It represents the probability that a topic is transferred from a state q_i to state q_j during the R&D process, where the state sequence I with length T is generated by transferring the hidden state. $I = \{i_1, i_2, \cdots i_T\}$, $i_t \in Q$. i_t is the hidden state at time t.
5) B is the probability distribution of the observable state. $B = [b_j(k)]_{N\times M}$, where $b_j(k) = P(O_t = v_k | i_t = q_j)$, $1 \le k \le M, 1 \le i$. It represents the probability of generating an observable state v_k under hidden state q_j at time t, where O_t represents the observable state variable at time t, which is the observation sequence O. $O = \{o_1, o_2, \cdots o_T\}$ with length T. It represents the annual statistical results of technology topics in this study.

In this study, the topic stochastic evolution process is used to find the optimal parameters A and B for the HMM to achieve $P(O|\lambda)$ maximization. Based on the calculation results of the parameters, thresholds are set to identify the topic evolution process and draw trend graphs, as shown in Figures 2, 3. The *Baum–Welch* algorithm is used in the calculation of the optimal parameters, which is essentially a method for maximum likelihood estimation. In other words, the computational process is a process of stepwise approximation to the lower bound of the maximized likelihood function. However, it only converges to the local extreme points of the log-likelihood function sequence, not the global extreme points. It has been claimed that only suitable initial parameters can obtain local maxima close to the global optimum (Xining et al., 2018). In other words, the setting of the initial parameters is crucial to the calculation results of the optimal parameters of the HMM.

In contrast from previous studies, this study considers optimizing the initial parameters of the HMM from a semantic perspective. Some studies have selected the results of word co-occurrence between topics as the initial parameters to obtain the optimal parameters of the HMM. With the rapid development of text mining technology, it is no longer limited to mining the internal relationship between topics from external features, such as word frequency statistics or word co-occurrence. In contrast, it is of great concern to consider mining key information from lexical contexts to measure inter-topic relationships. Higher similarity between topics implies a stronger possible evolutionary relationship between them. Thus, this study uses the semantic similarity results among topics as initial parameters to calculate the optimal parameters of the HMM.

In this case, this study uses the semantic similarity results between topics as the initial parameters of the HMM. The topic semantic similarity is obtained by using Word2vec and cosine similarity. Word2vec is a vector computation tool that includes the Continuous Bag of Words (CBOW) model and the Skip-gram model. The skip-gram learning model can generate word

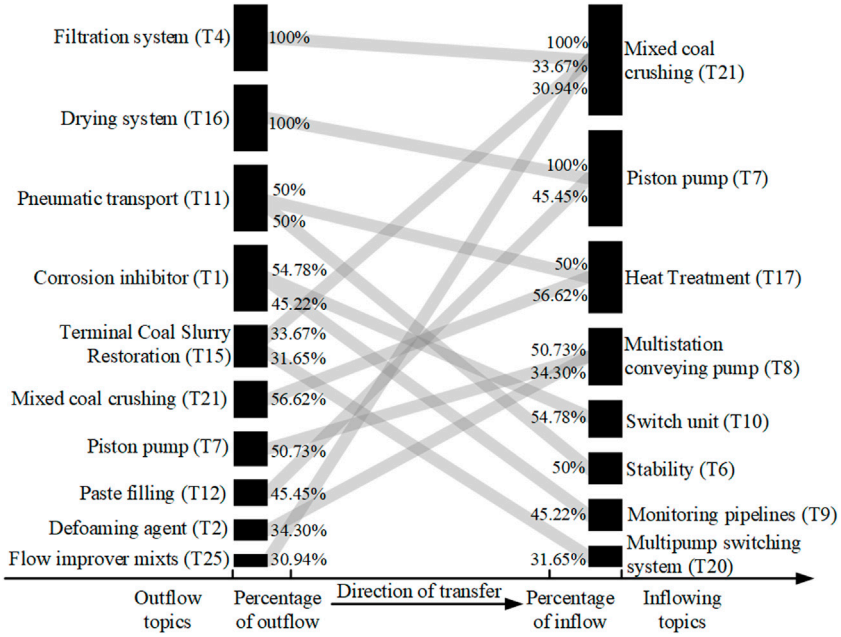

FIGURE 2
The transfer process between technology topics.

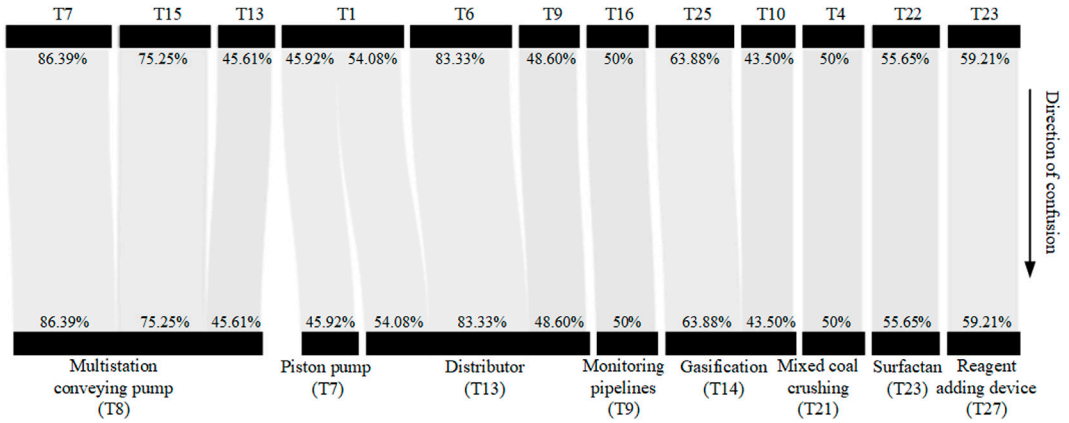

FIGURE 3
The confusion process between technology topics.

vectors from the context of a word. In other words, it can express words as vectors with real values by training the model. These vectors reflect the contextual semantic information of the target words. For this, we use extracted topic terms as objects and apply the skip-gram learning model in Word2vce to obtain the word vectors of these terms. Then, the cosine similarity algorithm is used to calculate semantic similarity between topics. The calculation formula is as follows:

$$\text{similarity} = \cos(\theta)\frac{V_A V_B}{||A| \times |B||} = \frac{\sum_{i=1}^{n} V_{Ai} V_{Bi}}{\sqrt{\sum_{i=1}^{n} (V_{Ai})^2} \times \sqrt{\sum_{i=1}^{n} (V_{Bi})^2}}$$

where V_{Ai} and V_{Bi} represent the components of topic vectors V_{Ai} and V_{Bi}, respectively.

TABLE 2 The results of topic extraction.

Topic	Meaning	Words
1	Corrosion inhibitor	Fluid, equipment, solvent, surface, pipeline, inhibitor, composition, condensate, polymer, aliphatic
2	Defoaming agent	Carbon, catalyst, density, slurry, hydrogen, dry, reduction, pulp, pressure, nitrogen
3	Pulping	Slurry, processing, liquid, pulp, separator, pipeline, settling, pump, transport, connected
4	Filtration system	Water, Vibration, coal, reduce, discharging, slurry, filtering, drying, environment, extracting
5	Dispersant	Acid, salt, slurry, coal, sulphonic, metal, stabilizer, dispersion, copolymer, viscosity
6	Stability	Plate, rod, connected, shaft, fixedly, rotate, support, mounting, coal, block
7	Piston pump	Layer, shell, material, grain, pump, facility, pressure, transportation, motor
8	Multi-station conveying pump	Slurry, coal, pump, connect, pipeline, inlet, pressure, outlet, transmitter, distance
9	Monitoring pipelines	Coal, fluid, portion, pipeline, flow, rate, wall, data, continue, real
10	Switch unit	Valve, control, pressure, drilling, electric, closed, gate, pipeline, station, ball
11	Pneumatic transport	Stir, pneumatic, flotation, tank, spray, pulp, cake, overflow, filter, spray
12	Paste filling	Grout, fill, gangue, coal, underground, slurry, transportation, ground, lift, hydraulic
13	Distributor	Coal, slurry, connected, pipeline, mill, conveying, sieve, screen, pump, tank
14	Gasification	Coal, slurry, tank, powder, mixing, storage, gasification, pipeline, pump, grind
15	Terminal Coal Slurry Restoration	Tank, filter, pump, coal, slurry, concentration, dehydration, sedimentation, thickener, distance
16	Drying system	Chamber, wall, temperature, steam, sludge, centrifugal, treat, wastewater, coal, efficiency
17	Heat Treatment	Boiler, coal, drying, air, tower, heat, furnace, combustion, steam, temperature
18	Cleaning cabin machine	Machine, hopper, cylinder, driving, collecting, cleaning, spiral, power, slime, lifting
19	Concentration and pressure filtration	Waste, transport, filter, coal, thickener, slurry, chute, scraper, clean, grain
20	Multi-pump switching system	Liquid, pump, air, station, pipeline, mechanism, diaphragm, pressure, power, supply
21	Mixed coal crushing	Crusher, Material, ash, cement, mortar, powder, mixing, raw, stirring, construction
22	Annexing agent	Polymer, sulphonated, aliphatic, monomer, vinyl, additive, acid, copolymer, surfactant, lignin
23	Surfactant	Additive, surfactant, oxide, Coal, slurry, powder, water, alcohol, salt, acid
24	Coal particles	Solid, slurry, form, liquid, particulate, coal, mixing, dispersion, compound, produce
25	Flow improver mixts	Tower, layer, stabilizer, sulphonate, bottom, low, tank, concentration, formaldehyde, solid
26	Anti-corrosion coating	Surface, corrosion, polymer, compound, uveous, solution, alkyl, apparatus, mixture, contact
27	Reagent adding device	Coal, slurry, particle, water, pipeline, size, viscosity, conic, coarse, suspension
28	Polymer	Dispersant, monomer, alkyl, water, slurry, ammonium, metal, coal, conic, organic

3.5 Prediction of topic evolution trends

In this study, we predict technology topic evolution trends to identify potential technology growth or decline points. It is important for governments and companies to anticipate potential technological development opportunities and conduct R&D activities strategically. From the above analysis, it was found that the key to achieving the goal is to predict the trend of topic changes over the future years. This belongs to the calculation of the backward probability of the observed sequence in the HMM.

Thus, we first provide the HMM. Then, $\beta_t(i)$ is calculated in the hidden state q_i at time t, which represents the probability that the partial observation sequence from $t+1$ to T is $o_{t+1}, o_{t+2}, \cdots, o_T$. Finally, the observation sequence probability $P(O|\lambda)$ is calculated by continuous recursion, which is calculated as follows:

$$P(O|\lambda) = \sum_{j=1}^{N} a_{ij} b_j(o_{t+1}) \beta_{t+1}(j),\ t = 1, 2, \cdots T-1$$

where, in the step of providing the HMM model λ, the optimal parameters A and B obtained in the previous step are used as the initial values of the HMM input parameters in this study.

Moreover, in a given HMM step, this study uses the optimal parameters A and B obtained in the previous step as the initial values of the HMM input parameters. Additionally, in the input step of the observation sequence O, the proportion of technology topics in the known year t is given. Then, after continuous recursion, the structure of the technology topics in the forecast period is obtained.

4 Results

4.1 Results of technology topic identification

We determine that the number of topics is 28 based on the perplexity score of the LDA model, and the results are shown

TABLE 3 The classification results of topics.

Category	Topic and number
pulping	Defoaming agent (T2), Pulping (T3), Dispersant (T5), Distributor (T13), Cleaning cabin machine (T18), Mixed coal crushing (T21), Annexing agent (T22), Surfactant (T23), Coal particles (T24), Flow improver mixts (T25)
pumping	Corrosion inhibitor (T1), Stability (T6), Piston pump (T7), Multi-station conveying pump (T8), Monitoring pipelines (T9), Switch unit (T10), Pneumatic transport (T11), Multi-pump switching system (T20), Anti-corrosion coating (T26), Polymer (T28)
end-processing	Filtration system (T4), Paste filling (T12), Gasification (T14), Terminal Coal Slurry Restoration (T15), Drying system (T16), Heat Treatment (T17), Concentration and pressure filtration (T19), Reagent adding device (T27)

TABLE 4 The annual distribution results of topics based on categories.

1967–1980			1980–2010			2010–2021		
PUL	**PUM**	**END**	**PUL**	**PUM**	**END**	**PUL**	**PUM**	**END**
T13	**T26**	**T4**	T13	T26	**T27**	T13	T7	T16
T23	**T1**	**T16**	T22	**T6**	T4	T23	T20	T12
T18	**T10**		T23	T7	**T12**	T25	T10	T14
T24	**T7**		T18	**T8**	T16	**T3**	T26	**T17**
T22			**T21**	**T20**	**T14**	T2	**T9**	**T15**
			T2	T1		**T5**	T6	
			T25	**T11**			T1	
							T8	
							T11	

Note: PUL, pulping; PUM, pumping; END, end-processing. The topic number in bold font represents the first appearance of the technical topic.

in Table 2. After obtaining the technology topics, we divide the results of the topics into three categories based on the composition of the coal slurry pipeline transportation systems.

The three technology categories are considered as the "pulping", "pumping" and "end-processing". The "pulping" category addresses technologies related to the production process of coal-water slurry. The "pumping" category addresses technologies related to the transport of coal slurry along a pipeline to its destination. The "end-processing " category addresses technologies involved in the reprocessing or utilization of coal slurry after it reaches the end terminal. Identifying technological categories of technology topics is very useful for the systematic analysis of technology trends. Then, we divide all topics into categories with the help of domain experts, and the results are shown in Table 3.

In addition, we also obtain the annual distribution of technology topics based on the results of category classification; the results are shown in Table 4. In Table 4, the topic number in bold font represents the first appearance of the technical topic.

4.2 Analysis of the topic evolution processes

After obtaining the results of technology topics, we obtain the word vectors of all topics by Word2vec. Based on this, the semantic similarity between topics is calculated by using the cosine similarity method, and the results are shown in Table 5. Then, we calculate the optimal parameters A and B, which are the transfer process and the confusion process in the optimal state, and the results are shown in Tables 6, 7. They present the stochastic evolution processes of topics in a quantified way. From Tables 6, 7, it was found that the self-transfer rate of most topics is above 40%, and the self-confusion rate is above 50%. These topics are concentrated in the "pulping" category and the "end-processing" category. Furthermore, we use the calculation results from Tables 6, 7 to set thresholds to present the topic evolution process. We draw the relationship chains with the optimal transfer probability above 0.3 and the optimal confusion probability above 0.4 as trend graphs, and the results are shown in Figures 2, 3.

Figure 2 shows that T1 (corrosion inhibitor) and T11 (pneumatic transport) have the highest outflow rates.

TABLE 5 The semantic similarity results of topics.

	Topic 1	Topic 2	Topic 3	Topic 4	Topic 5	Topic 6	Topic 7	Topic 8	...	Topic 28
Topic 1	1	0.132	0.077	0.021	0.198	0.059	0.103	0.206	...	0.114
Topic 2	0.132	1	0.015	0.006	0.050	0.007	0.019	0.121	...	0.033
Topic 3	0.077	0.015	1	0.021	0.011	0.047	0.074	0.180	...	0.028
Topic 4	0.021	0.006	0.021	1	0.022	0.005	0.010	0.047	...	0.016
Topic 5	0.198	0.050	0.011	0.022	1	0.015	0.027	0.189	...	0.186
Topic 6	0.059	0.007	0.047	0.005	0.015	1	0.025	0.125	...	0.010
Topic 7	0.103	0.019	0.074	0.010	0.027	0.025	1	0.166	...	0.027
Topic 8	0.206	0.121	0.180	0.047	0.189	0.125	0.166	1	...	0.159
...	...	...	...	...	...	...	...	...	1	...
Topic 28	0.114	0.033	0.028	0.016	0.186	0.010	0.027	0.159	...	1

TABLE 6 Matrix of optimal transfer relations between topics.

	Topic 1	Topic 2	Topic 3	Topic 4	Topic 5	Topic 6	Topic 7	Topic 8	...	Topic 28
Topic 1									...	
Topic 2		0.657						0.343	...	
Topic 3							0.126	0.269	...	
Topic 4									...	
Topic 5					0.844				...	0.363
Topic 6						0.667			...	
Topic 7							0.176	0.507	...	
Topic 8	0.137							0.188	...	
...	...	...	...	...	...	...	...	...	...	...
Topic 28									...	0.9

T1 moves to T9 (monitoring pipelines) and T10 (switch unit). T11 is transferred to T6 (stability) and T17 (heat treatment). This reflects the growing maturity of corrosion protection and the dense-phase transport technologies, which are the basis for the research in other technologies. Next, T15 (terminal coal slurry restoration) is transferred to T21 (mixed coal crushing) and T20 (multi-pump switching system). Due to the development of terminal coal slurry reprocessing technology, fine grinding technology and multi-pump switching control technology are gradually becoming common research topics. This trend can also be found in the transfer process from T4 (filtration system), T15 (terminal coal slurry restoration), and T25 (flow improver mixts) to T21 (mixed coal crushing), where T21 has the highest inflow percentage. Additionally, with the development of pipeline transportation technology, T7 (piston pump), T8 (multi-station conveying pump), and T17 (heat treatment) have become targets for technology transfer. This means that many studies are gradually turning to the technical research direction of improving the transportation efficiency of coal slurry.

From Figure 3, T8 (multi-station conveying pump), T13 (distributor), T14 (gasification), and T27 (reagent adding device) are the terminals of multiple confusion relationship chains. This shows that the technical research related to these topics is trending and appealing. Among them, T8 has four chains of confusing relationships from T7 (piston pump), T15 (terminal coal slurry restoration), T13 (distributor), and T19 (concentration and pressure filtration). This means that pump-related technology is a popular research direction, with more technical results. The pump is the core equipment in the transportation process, which is directly related to transportation safety and stability. In addition, there are some topics with few or even no confusion relationship chains, but they have a high rate of self-transfer. This means that the technology R&D associated with them is difficult. However, they attract much attention from academics and practitioners. These include T5 (dispersant) and T24 (coal particles). Coal water slurry is a fluid fuel with coarse particle suspension characteristics. Additives, as an effective method to control the properties of coal slurry, such as concentration, stability, and flowability, are highly researched. However, the molecular structure of additives varies with the quality of different coal types,

TABLE 7 Matrix of optimal confusion relations between topics.

	Topic 1	Topic 2	Topic 3	Topic 4	Topic 5	Topic 6	Topic 7	Topic 8	...	Topic 28
Topic 1							0.459		...	
Topic 2		0.224							...	
Topic 3			1						...	
Topic 4				0.5					...	
Topic 5					0.668			0.034	...	
Topic 6								0.166	...	
Topic 7								0.864	...	
Topic 8								0.591	...	
...	...	...	...	...	...	...	...	...	...	...
Topic 28					0.143		0.082	0.077	...	0.118

resulting in limited versatility. Consequently, technical research related to these topics has been difficult.

4.3 Prediction of topic evolution trends

The relationship matrix in the optimal state is calculated in the previous step and it is applied to the topic prediction step. We verify the effect of the prediction model. Using topics from 2010 as the prediction base period, the topic share prediction results in 2011–2015 were obtained by the backward algorithm, and the RMSE was calculated as 0.036. The HMM-based prediction model was determined by experts to have effective prediction performance. Then, we chose the patent data from 2020 as the prediction base period. The predicted percentage results of technology topics generated over 2021–2025 are shown in Figure 4.

In Figure 4, we can see that the trends of some topics trend higher considerably over the prediction period. These topics are T24 (coal particles), T14 (gasification), and T17 (heat treatment). They are related to the industrial application of coal slurries. For example, particle control technology can meet the different requirements of end-users for coal slurry concentration and particle size, which is beneficial to the industrial application of coal slurry. Hence, technical research that facilitates the improvement of industrial applications on coal slurry deserves attention in the future. Additionally, some topics have a slightly increased percentage of growth over the next 5 years. Although the growth is not substantial, it can continue to focus on these technologies. For example, technologies related to T26 (anti-corrosion coating), T15 (terminal coal slurry restoration), and T27 (reagent addition devices). Their research heat is gradually stabilizing and has certain application prospects.

Additionally, T8 (multi-station conveying pump) shows a rapid downward trend over the prediction period, indicating that it will not be a future research focus. Multiple pump operation transport technology has gradually matured in long-distance pipeline transportation. It has the characteristics of a simple structure and easy installation and is already widely used in the mineral industry. Additionally, technology development related to T21 (mixed coal crushing) has moved in other directions as surface coal supply technology has improved. The predicted results show that the development trend of this topic has declined after a short-term rise. The current large-scale production of high-quality coal slurry is no longer a technical challenge. There is also a decreasing trend in T12 (paste filling), T7 (piston pump), and T13 (distributor) over the prediction period. This indicates that the technology development related to it is moving toward specialization and has wide application in other fields. Their research and application in the field of coal slurry pipeline transportation will gradually lose attention.

5 Discussion

We discuss the findings and contributions of this study in more detail below and provide arguments for their practical value.

As the first key finding, the results show that topics in the “pulping” category have a high self-transferability probability. They are the starting of many transfer relationship chains, which can easily be transferred to other categories. This indicates that technologies related to the “pulping” category are the basis for technological development, such as defoamers, flow improvers, and coal blending and crushing. This result responds to Das et al. (2021) call for research on coal pulping technology. The development of pulping technology is the premise of increasing pipeline transport capacity and industrial applications (Hu et al., 2021). With the development of technology, technical research has gradually focused on the direction related to the “pumping”. That development trajectory is also reflected in the transfer results of the topics.

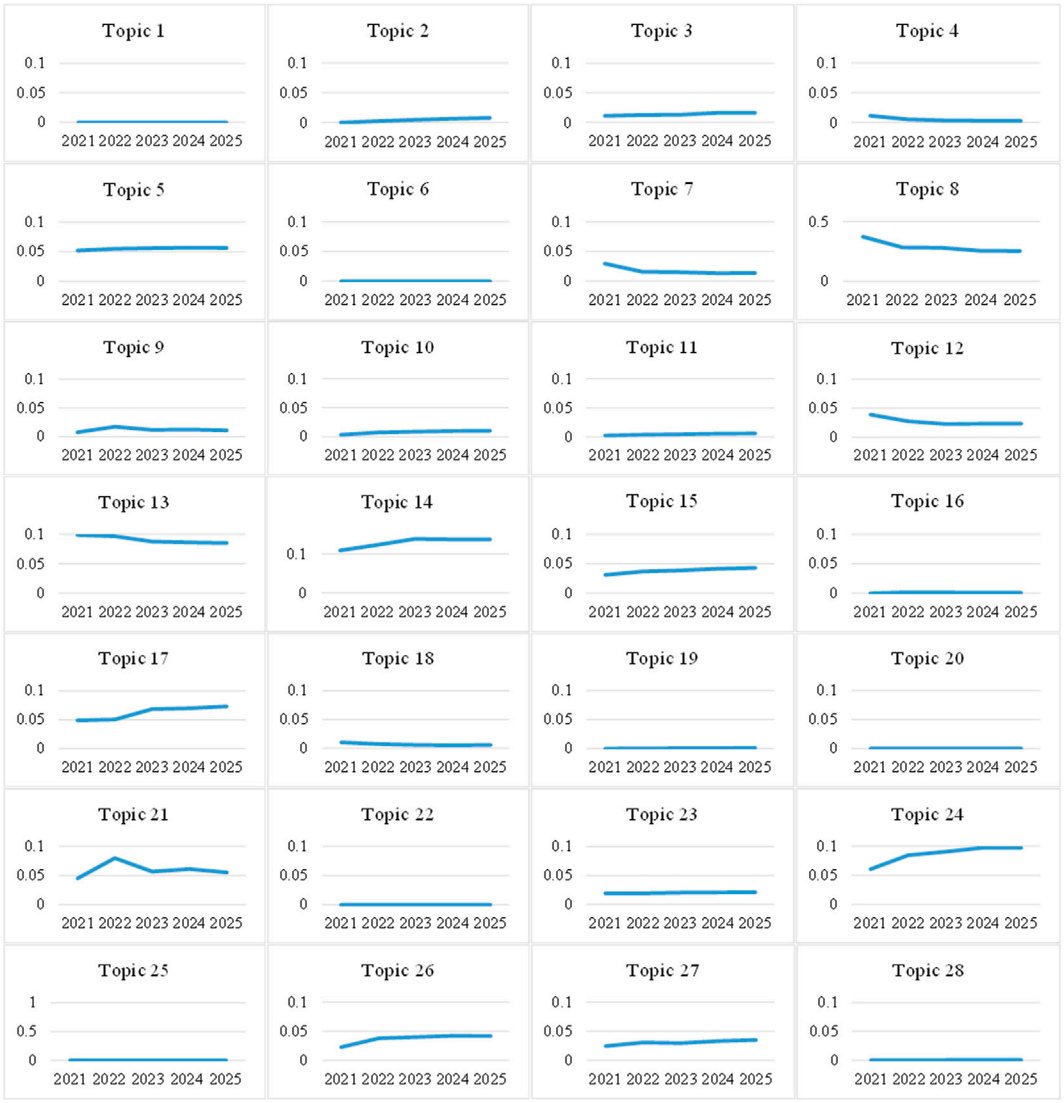

FIGURE 4
The prediction results of the evolutionary trend of technology topics.

Domain experts consider that the transport capacity in coal slurry transport processes has been a long-standing research concern for scholars (Rogovyi et al., 2021). Our data also shows that many topics are diverted to the "pumping" category. Most topics in this category have a low self-transfer probability and are less likely to transfer to other topics, such as plunger pumps, multiple pumping, and stability. It reflects the high degree of independence and stability of technical research in this category.

The second key finding is that the technology hotspots in the field of coal slurry pipeline transportation are concentrated in the "pulping" category. Most topics in this category are confusing targets for other topics, such as separators, coal blending crushing, and surfactants. This indicates that there are numerous theoretical and experimental studies in the "pulping" category, which produce a wealth of patented results (Glushkov et al., 2016). Furthermore, our results show that most technical topics in the "pumping" category have low self-confusion probabilities and are not confusion targets of other topics. This means that the technology in this category is difficult to develop and patent. Interestingly, most of the topics in the "end-processing" category have high self-confusion probability while not being the confusion target of other topics. Topics in this category are mainly related to coal chemical technology. This shows that coal chemical technology has a high technological barrier, although it has high research stability and heat. These findings agree with Xie et al. (2010) who concluded that although

coal chemical technology has attracted attention from many countries and scholars, it is very complex and requires multiple inputs with high technical barriers.

The third key finding is that our prediction data shows less potential for technology development in the "pulping" categories, such as mixed coal crushing, separators, and scrubbers. In addition, topics with a rising trend in the future belong to the "pumping" and the "end-processing" categories. This means that technologies in these two categories have promising research and applications. These may also be the frontiers of technologies that need attention, such as technologies related to pipeline corrosion protection and coal gasification. It is worth noting that in our prediction result, only pump-related topics in the "pumping" category have a declining trend in the future and with high rates. This may be due to the limited transport efficiency improvements by the coal slurry quality, the performance of the main pump, and the auxiliary facilities to a large extent (Das et al., 2021). Furthermore, other technologies in the "pumping" category have been developed. Such a trend also confirms the result that many technical topics in the "pumping" category will show an upward trend in the future.

Finally, the innovative HMM-based technology trend research methodology of this study extends the research of Wei et al. (2020). Their research is limited to using co-occurrence features of keywords as a medium to analyze the evolutionary relationships between topics alone, with applications in the fields of 3D printing and marine diesel engines. They emphasize calculating the similarity between topics from the word frequency and the co-occurrence results of topic words. It provides a reference for us to investigate the topic stochastic evolutionary process from the semantic level. Based on the topic results extracted by the LDA, we combine the Word2Vec and the cosine similarity to obtain the semantic similarity results between the topics. The semantic similarity results among the topics are used as the initial variables of the HMM to infer the stochastic evolutionary relationships and the trends among the topics. Therefore, this study can supplement previous studies that analyze technical information from the semantic level of patent texts. Furthermore, in the field of coal slurry pipeline transportation, more insightful information can be identified from patent data *via* text mining and machine learning methods.

6 Conclusion

This study aims to comprehensively understand the development trend of coal slurry pipeline transportation technology through the mining of patent texts. After extracting technology topics from patents, a dual topic stochastic process modeling approach based on semantic similarity is used to quantitatively analyze and predict technology trends. From a methodological perspective, we consider the influence of the term context on measuring thematic similarity. Moreover, this study is also the first to explore the current state of technological development in this field through patent analysis. It helps decision-makers and researchers comprehensively and systematically understand this field to facilitate scientific R&D management and decision-making.

Our results show that the technological evolution of the "pumping" and the "end-processing" category are the main technological development paths with a substantial impact on the coal slurry pipeline transportation industry. In particular, technologies aimed at improving transport efficiency and the coal chemical industry are major areas of technological development. With the maturity of coal slurry preparation technology, the "pumping" and the "end-processing" categories will become popular for research, and the corresponding patent output will also increase. Their development benefits from the technological development of the "pulping" category. However, limited by distance, equipment, end-users, and other objective reasons, the development of coal pipeline transportation technology is relatively slow. It also reflects the difficulty of developing technology in the categories of the "pumping" and the "end-processing". For example, pumps, valves, and other equipment design and manufacturing requirements are complex and difficult. This may be due to the strong corrosive influence of coal slurry on pipes and various parts. Moreover, the development of coal slurry dewatering technology is not ideal. Currently, even with the dewatered slurry, it still has a higher moisture content than raw coal. It has serious influences on the subsequent use of coal slurry. There are many other technical difficulties such as this. Thus, scholars and researchers need to focus on technological innovation in these two areas.

Despite the contributions, there are still some limitations in this study. First, this study is only based on the analysis of patent texts to trace the development of coal slurry pipeline transportation technology. But not all technical information exists only in patents. Future studies can extend the data analysis to literature and commercial reports to better analyze the comprehensive technical landscape of pipeline coal transport systems. In addition, future studies can also include the application cases of pipeline transportation technology in other fields in the analysis, such as iron concentrate slurry transportation pipeline, phosphorus concentrate slurry transportation pipeline or nickel-cobalt slurry transportation pipeline, etc. Mutual learning from technology experience can promote the sustainable development of coal pipeline transportation technology. Finally, this study only considers the use of first order HMM to build a technology theme trend analysis model. However, the current state of technology is indirectly related to the past state. Then, the higher order HMM can be adopted for future studies to analyze and predict the evolution of technology trends more accurately.

Data availability statement

The original contributions presented in the study are included in the article/Supplementary Material, further inquiries can be directed to the corresponding author.

Author contributions

Conceptualization, JW and KL; methodology, KL; software, KL; validation, JW and LF; formal analysis, LF; investigation LF; data curation, LF; writing-original draft preparation, KL; writing-review and editing, KL; supervision, LF; funding acquisition, JW.

Funding

This work was supported by Innovation Method Fund of China [grant number 2018IM020300]; Shanghai Science and Technology Program [grant number 20040501300]; Innovation Method Fund of China [grant number 2019IM020200].

Acknowledgments

The authors gratefully acknowledge funding from the Innovation Method Fund of China [grant number 2018IM020300; 2019IM020200], and Shanghai Science and Technology Program [Project No. 20040501300].

Conflict of interest

The authors declare that the research was conducted in the absence of any commercial or financial relationships that could be construed as a potential conflict of interest.

Publisher's note

All claims expressed in this article are solely those of the authors and do not necessarily represent those of their affiliated organizations, or those of the publisher, the editors and the reviewers. Any product that may be evaluated in this article, or claim that may be made by its manufacturer, is not guaranteed or endorsed by the publisher.

References

Aaldering, L. J., Leker, J., and Song, C. H. (2019a). Analysis of technological knowledge stock and prediction of its future development potential: The case of lithium-ion batteries. *J. Clean. Prod.* 223, 301–311. doi:10.1016/j.jclepro.2019.03.174

Aaldering, L. J., Leker, J., and Song, C. H. (2019b). Competition or collaboration? – analysis of technological knowledge ecosystem within the field of alternative powertrain systems: A patent-based approach. *J. Clean. Prod.* 212, 362–371. doi:10.1016/j.jclepro.2018.12.047

Bao, Q., Nie, W., Liu, C., Zhang, H., Wang, H., Jin, H., et al. (2020). The preparation of a novel hydrogel based on crosslinked polymers for suppressing coal dusts. *J. Clean. Prod.* 249, 119343. doi:10.1016/j.jclepro.2019.119343

Blei, D. M., Ng, A. Y., and Jordan, M. I. (2003). Latent Dirichlet allocation. *J. Mach. Learn. Res.* 3, 993–1022.

Chehal, D., Gupta, P., and Gulati, P. (2021). Retracted article: Implementation and comparison of topic modeling techniques based on user reviews in e-commerce recommendations. *J. Ambient. Intell. Humaniz. Comput.* 12 (5), 5055–5070. doi:10.1007/s12652-020-01956-6

Chen, Y., and Lin, B. (2020). Decomposition analysis of patenting in renewable energy technologies: From an extended LMDI approach perspective based on three Five-Year Plan periods in China. *J. Clean. Prod.* 269, 122402. doi:10.1016/j.jclepro.2020.122402

Choi, S., Park, H., Kang, D., Lee, J. Y., and Kim, K. (2012). An SAO-based text mining approach to building a technology tree for technology planning. *Expert Syst. Appl.* 39 (13), 11443–11455. doi:10.1016/j.eswa.2012.04.014

Cowper, N. T., and Thomas, A. D. (2009). Slurry pipelines: Past, present and future. *Aust. J. Multi-disciplinary Eng.* 7 (2), 189–196. doi:10.1080/14488388.2009.11464813

Das, D., Das, S. K., Parhi, P. K., Dan, A. K., Mishra, S., and Misra, P. K. (2021). Green strategies in formulating, stabilizing and pipeline transportation of coal water slurry in the framework of WATER-ENERGY nexus: A state of the art review. *Energy Nexus* 4, 100025. doi:10.1016/j.nexus.2021.100025

Das, D., Mohapatra, R. K., Belbsir, H., Routray, A., Parhi, P. K., and El-Hami, K. (2020). Combined effect of natural dispersant and a stabilizer in formulation of high concentration coal water slurry: Experimental and rheological modeling. *J. Mol. Liq.* 320, 114441. doi:10.1016/j.molliq.2020.114441

Davis, J. P., Eisenhardt, K. M., and Bingham, C. B. (2007). Developing theory through simulation methods. *Acad. Manage. Rev.* 32 (2), 480–499. doi:10.5465/amr.2007.24351453

Feng, J., Zhang, Y. Q., and Zhang, H. (2017). Improving the co-word analysis method based on semantic distance. *Scientometrics* 111 (3), 1521–1531. doi:10.1007/s11192-017-2286-1

Frenken, K. (2006). Technological innovation and complexity theory. *Econ. Innovation New Technol.* 15 (2), 137–155. doi:10.1080/10438590500141453

Glushkov, D., Strizhak, P., and Chernetskii, M. Y. (2016). Organic coal-water fuel: Problems and advances (Review). *Therm. Eng.* 63 (10), 707–717. doi:10.1134/S0040601516100037

Hu, S., Jiang, F., Zhao, B., Chen, Y., Wu, C., Li, J., et al. (2021). The enhancement on rheology, flowability, and stability of coal water slurry prepared by multipeak gradation technology. *Energy fuels.* 35 (3), 2006–2015. doi:10.1021/acs.energyfuels.0c03032

Jati, H. A., Monei, N., Barakos, G., Tost, M., and Hitch, M. (2021). Coal slurry pipelines: A coal transportation method in kalimantan, Indonesia. *Int. J. Min. Reclam. Environ.* 35, 638–655. doi:10.1080/17480930.2021.1949857

Kania, J. J. (1984). Economics of coal transport by slurry pipeline versus unit train: A case study. *Energy Econ.* 6 (2), 131–138. doi:10.1016/0140-9883(84)90028-8

Khan, N., Dilshad, S., Khalid, R., Kalair, A. R., and Abas, N. (2019). Review of energy storage and transportation of energy. *Energy Storage* 1 (3), e49. doi:10.1002/est2.49

Kim, D., Seo, D., Cho, S., and Kang, P. (2019). Multi-co-training for document classification using various document representations: TF–IDF, LDA, and Doc2Vec. *Inf. Sci.* 477, 15–29. doi:10.1016/j.ins.2018.10.006

Kumar, S., Gandhi, B. K., and Mohapatra, S. (2014). Performance characteristics of centrifugal slurry pump with multi-sized particulate bottom and fly ash mixtures. *Part. Sci. Technol.* 32 (5), 466–476. doi:10.1080/02726351.2014.894163

Lahiri, S., and Ghanta, K. (2008). Development of an artificial neural network correlation for prediction of hold-up of slurry transport in pipelines. *Chem. Eng. Sci.* 63 (6), 1497–1509. doi:10.1016/j.ces.2007.11.030

Lai, C., Xu, L., and Shang, J. (2020). Optimal planning of technology roadmap under uncertainty. *J. Operational Res. Soc.* 71 (4), 673–686. doi:10.1080/01605682.2019.1581406

Li, A., Chen, Y., and Wang, D. (2020). An empirical study of the factors influencing the willingness to implement green coal logistics in China. *J. Clean. Prod.* 245, 118932. doi:10.1016/j.jclepro.2019.118932

Li, C., Lu, Y., Wu, J., Zhang, Y., Xia, Z., Wang, T., et al. "(2018). "LDA meets Word2Vec: A novel model for academic abstract clustering," in Companion proceedings of the the web conference 2018), 1699–1706.

Li, P., Yu, H., Zhang, J., Du, M., and Xiong, J. (2021). Coal supply sustainability in China: A new comprehensive evaluation methodology. *Front. Energy Res.* 9. doi:10.3389/fenrg.2021.701719

Li, X., Xie, Q., Daim, T., and Huang, L. (2019). Forecasting technology trends using text mining of the gaps between science and technology: The case of perovskite solar cell technology. *Technol. Forecast. Soc. Change* 146, 432–449. doi:10.1016/j.techfore.2019.01.012

Liu, H., Chen, Z., Tang, J., Zhou, Y., and Liu, S. (2020). Mapping the technology evolution path: A novel model for dynamic topic detection and tracking. *Scientometrics* 125 (3), 2043–2090. doi:10.1007/s11192-020-03700-5

Markard, J. (2020). The life cycle of technological innovation systems. *Technol. Forecast. Soc. Change* 153, 119407. doi:10.1016/j.techfore.2018.07.045

Mikolov, T., Chen, K., Corrado, G., and Dean, J. (2013). Efficient estimation of word representations in vector space. arXiv preprint arXiv 1301, 3781. doi:10.48550/arXiv.1301.3781

Mishra, R., Ghanta, K., Mullick, A. N., and Sinha, S. L. (2019). Experimental and numerical prediction of slurry flow in pipe: A review. *Inter. J. Fluid Mech. Res.* 46 (2), 167–185. doi:10.1615/InterJFluidMechRes.2018021915

Nunes, L. J. (2020). Potential of coal–water slurries as an alternative fuel source during the transition period for the decarbonization of energy production: A review. *Appl. Sci.* 10 (7), 2470. doi:10.3390/app10072470

Oberschelp, C., Pfister, S., Raptis, C. E., and Hellweg, S. (2019). Global emission hotspots of coal power generation. *Nat. Sustain.* 2 (2), 113–121. doi:10.1038/s41893-019-0221-6

Pan, J., Jiang, X., Wan, X., and Ding, W. (2017). A filtering based multi-innovation extended stochastic gradient algorithm for multivariable control systems. *Int. J. Control Autom. Syst.* 15 (3), 1189–1197. doi:10.1007/s12555-016-0081-z

Park, S., Kim, J., Lee, H., Jang, D., and Jun, S. (2016). Methodology of technological evolution for three-dimensional printing. *Industrial Manag. Data Syst.* 116 (1), 122–146. doi:10.1108/imds-05-2015-0206

Prasad, V., Thareja, P., and Mehrotra, S. P. (2020). Role of rheology on the hydraulic transportation of lignite coal and coal ash slurries in the pipeline. *Int. J. Coal Prep. Util.* 42, 1263–1277. doi:10.1080/19392699.2020.1721482

Rao, K. U., and Kishore, V. (2010). A review of technology diffusion models with special reference to renewable energy technologies. *Renew. Sustain. energy Rev.* 14 (3), 1070–1078. doi:10.1016/j.rser.2009.11.007

Rao, N. D., Thatoi, D. N., and Biswal, S. K. (2020). Rheological study and numerical analysis of high concentration iron ore slurry pipeline transportation. *Mater. Today Proc.* 22, 3197–3202. doi:10.1016/j.matpr.2020.03.457

Renaldi, R., Miranda, N. D., Khosla, R., and McCulloch, M. D. (2021). Patent landscape of not-in-kind active cooling technologies between 1998 and 2017. *J. Clean. Prod.* 296, 126507. doi:10.1016/j.jclepro.2021.126507

Rogovyi, A., Korohodskyi, V., and Medvediev, Y. (2021). Influence of Bingham fluid viscosity on energy performances of a vortex chamber pump. *Energy* 218, 119432. doi:10.1016/j.energy.2020.119432

Singh, J., Kumar, S., and Mohapatra, S. (2018). Optimization of erosion wear influencing parameters of HVOF sprayed pumping material for coal-water slurry. *Mater. Today Proc.* 5 (11), 23789–23795. doi:10.1016/j.matpr.2018.10.170

Singh, M. K., Kumar, S., and Ratha, D. (2020). Computational analysis on disposal of coal slurry at high solid concentrations through slurry pipeline. *Int. J. Coal Prep. Util.* 40 (2), 116–130. doi:10.1080/19392699.2017.1346632

Singh, M. K., Kumar, S., Ratha, D., and Kaur, H. (2017). Design of slurry transportation pipeline for the flow of muti-particulate coal ash suspension. *Int. J. hydrogen energy* 42 (30), 19135–19138. doi:10.1016/j.ijhydene.2017.04.259

Singh, M. K., Rathore, S. S., Kumar, S., and Sandhu, H. (2022). Taguchi approach for optimization of pressure drop characteristics for fly ash with bottom ash addition in slurry pipeline. *Mater. Today Proc.* 48 (5), 1305–1309. doi:10.1016/j.matpr.2021.09.002

Sinha, S. L., Dewangan, S. K., and Sharma, A. (2017). A review on particulate slurry erosive wear of industrial materials: In context with pipeline transportation of mineral– slurry. *Part. Sci. Technol.* 35 (1), 103–118. doi:10.1080/02726351.2015.1131792

Strogen, B., Bell, K., Breunig, H., and Zilberman, D. (2016). Environmental, public health, and safety assessment of fuel pipelines and other freight transportation modes. *Appl. Energy* 171, 266–276. doi:10.1016/j.apenergy.2016.02.059

Tabrizian, S. (2019). Technological innovation to achieve sustainable development—renewable energy technologies diffusion in developing countries. *Sustain. Dev.* 27 (3), 537–544. doi:10.1002/sd.1918

Wang, Z.-Y., Li, G., Li, C.-Y., and Li, A. (2012). Research on the semantic-based co-word analysis. *Scientometrics* 90 (3), 855–875. doi:10.1007/s11192-011-0563-y

Wei, C., Chaoran, L., Chuanyun, L., Lingkai, K., and Zaoli, Y. (2020). Tracing the evolution of 3-D printing technology in China using LDA-based patent abstract mining. *IEEE Trans. Eng. Manag.* 69, 1135–1145. doi:10.1109/tem.2020.2975988

Wei, C., Chaoran, L., and Jinqiu, L. (2018). Analysis of the evolutionary trend of technical topics in patents based on LDA and HMM—taking marine diesel engine technology as an example. *J. China Soc. Sci. Tech. Inf.* 37 (7), 732–741. doi:10.3772/j.issn.1000-0135.2018.07.009

Wu, Q., Zhang, C., Hong, Q., and Chen, L. (2014). Topic evolution based on LDA and HMM and its application in stem cell research. *J. Inf. Sci.* 40 (5), 611–620. doi:10.1177/0165551514540565

Xie, K., Li, W., and Zhao, W. (2010). Coal chemical industry and its sustainable development in China. *Energy* 35 (11), 4349–4355. doi:10.1016/j.energy.2009.05.029

Xining, Z., Wei, L., and Yuwei, Y. (2018). Adaptive genetic particle swarm algorithm for optimization hidden Markov models with applications. *J. Xi'an Jiaot. Univ.* 52 (8), 1–8. doi:10.7652/xjtuxb201808001

Yang, J., Yang, B., and Yu, M. (2019). Pressure study on pipe transportation associated with cemented coal gangue fly-ash backfill slurry. *Appl. Sci.* 9 (3), 512. doi:10.3390/app9030512

Yin, J., Wang, J., You, J., Chen, H., and Shi, W. (2021). Integrated energy system optimal operation in coal district with hydrogen heavy trucks. *Front. Energy Res.* 9. doi:10.3389/fenrg.2021.748673

Yoon, B., and Song, B. (2014). A systematic approach of partner selection for open innovation. *Industrial Manag. Data Syst.* 114 (7), 1068–1093. doi:10.1108/imds-03-2014-0086

Yoon, J., Seo, W., Coh, B.-Y., Song, I., and Lee, J.-M. (2017). Identifying product opportunities using collaborative filtering-based patent analysis. *Comput. Industrial Eng.* 107, 376–387. doi:10.1016/j.cie.2016.04.009

Yuan, X., and Cai, Y. (2021). Forecasting the development trend of low emission vehicle technologies: Based on patent data. *Technol. Forecast. Soc. Change* 166, 120651. doi:10.1016/j.techfore.2021.120651

Zahed, S. E., Shahandashti, S., and Najafi, M. (2018). Lifecycle benefit-cost analysis of underground freight transportation systems. *J. Pipeline Syst. Eng. Pract.* 9 (2), 04018003. doi:10.1061/(ASCE)PS.1949-1204.0000313

Zaman, D., Tiwari, M. K., Gupta, A. K., and Sen, D. (2020). A review of leakage detection strategies for pressurised pipeline in steady-state. *Eng. Fail. Anal.* 109, 104264. doi:10.1016/j.engfailanal.2019.104264

Zhang, J., Cheng, L., Yuan, H., Mei, N., and Yan, Z. (2019). Identification of viscosity and solid fraction in slurry pipeline transportation based on the inverse heat transfer theory. *Appl. Therm. Eng.* 163, 114328. doi:10.1016/j.applthermaleng.2019.114328

Zhao, F., Yao, Z., Luan, J., and Liu, H. (2020). Inducing stock market lexicons from disparate Chinese texts. *Industrial Manag. Data Syst.* 120 (3), 508–525. doi:10.1108/IMDS-04-2019-0254

frontiers | Frontiers in Energy Research

TYPE Original Research
PUBLISHED 24 January 2023
DOI 10.3389/fenrg.2022.1029077

OPEN ACCESS

EDITED BY
Massimo Gastaldi,
University of L'Aquila, Italy

REVIEWED BY
Idiano D'Adamo,
Sapienza University of Rome, Italy
Nallapaneni Manoj Kumar,
City University of Hong Kong, Hong Kong SAR, China
Claudio Sassanelli,
Politecnico di Bari, Italy

*CORRESPONDENCE
Xianfeng Zhang,
tobyzhang@163.com
Xiangping Hu,
Xiangping.Hu@ntnu.no

†These authors share first authorship

SPECIALTY SECTION
This article was submitted to Sustainable Energy Systems and Policies, a section of the journal Frontiers in Energy Research

RECEIVED 26 August 2022
ACCEPTED 05 December 2022
PUBLISHED 24 January 2023

CITATION
Wang X, Lu X, Zhang X, Zeng W, Liu Z and Hu X (2023), Identifying the critical factors of transmission efficiency loss in China's natural gas network. *Front. Energy Res.* 10:1029077. doi: 10.3389/fenrg.2022.1029077

Identifying the critical factors of transmission efficiency loss in China's natural gas network

Xiaolin Wang[1,2†], Xiangyi Lu[1†], Xianfeng Zhang[1*], Weijing Zeng[1], Zhankun Liu[1] and Xiangping Hu[3*]

[1]School of Economics and Management, China University of Geosciences (Wuhan), Wuhan, China, [2]China University of Geosciences (Wuhan) Resource & Environment Center, Wuhan, China, [3]Department of Energy and Process Engineering, Industrial Ecology Programme, Norwegian University of Science and Technology, Trondheim, Norway

China's market-oriented reform supports the sustainable development of energy mix and the low-carbon target, and natural gas has bridged the transition from traditional fossil energy to clean and renewable energies. The third-party access policy, launched recently by China's natural gas market, drives the decouple between gas trade and transport. The decouple might lead to the transmission resources of physical network not optimally used, which is caused by the contractual arrangement between entry and exit capacities in commercial network. Aiming at this issue, we established a mathematical programming with equilibrium constraints (MPEC) to integrate the allocations of commercial capacity and physical flows, based on a minimum cost maximum flow problem (MCMF) abstracted from China's existing gas network. The MPEC model was then used to strategically evaluate the transmission efficiency, and identify the critical factors of its loss. Our results show that there is transmission efficiency loss of China's gas network from the shortage of geospatial gas supply and the invisible segmentation of gas network due to interdicted cost of pipeline, bottleneck of pipeline capacity and economic radius of gas supply chains to transport gas. Therefore, the critical factor of the loss to be identified will be helpful for strategically reducing the cost of decoupling gas trade and transport.

KEYWORDS

natural gas network, transmission efficiency loss, minimum cost maximum flow problem, mathematical program with equilibrium constraints, market segmentation

Highlights

1) The spatial mismatch of entry/exit capacities causes network transmission efficiency loss.
2) MPEC integrates the commercial capacity allocation and physical flows allocation.
3) The interdicted costs lead to the segmentation of local network.
4) The elasticity of pipeline capacity is spatially heterogeneous.
5) The economic radius of gas supply chains hinders network integration.

1 Introduction

As a clean and efficient energy, natural gas has been bridging the energy transition security from traditional fossils to renewable energies for coping with climate change and energy sustainable development in countries all over the world (Ogden et al., 2018; Gillessen et al., 2019; Holz, 2020). Chinese government has been committed to the development and utilization of natural gas, meeting with the goal of carbon emission reduction (Qin et al., 2019; Xu & Lin, 2019). At present, market-oriented reform of natural gas is an important guarantee for the sustainable development and supply security of China's natural gas market, which is very critical for supporting the energy transition.

Recently, China has promulgated the directive of the third-party access and established National Oil and Gas Pipeline Company (SONGPC) to accelerate natural gas market from monopoly to perfect competition (DNRC & NEA, 2018; DNRC, 2019). The directive encourages gas traders to enter natural gas network without discriminatory, resulting in gradual decoupling between natural gas trade and transport (Wang and Cheng, 2017; Xu, et al., 2017; Dong et al., 2019). Consequently, gas traders shift the competition for pipeline capacity to for entry and exit capacity of nodes in gas network. The SONGPC acts as a transmission system operator (TSO) to deliver gas from entry nodes to exit nodes. However, the entry-exit capacities booked by traders will hinder physical network not optimally used. It produces the transmission efficiency loss of gas network from the decoupling. Thereby, how to identify the critical factors of transmission efficiency loss is crucial for SONGPC to explore the strategies for reducing the efficiency loss by rationally allocating the entry and exit capacities for gas traders.

Analysing the transmission efficiency loss was firstly conducted in traffic network research (Roughgarden, 2002) by the cost of travellers in user equilibrium exceeding the optimal cost of the traffic network (Huang et al., 2006; Lindseya et al., 2019). The mathematical program with equilibrium constraints (MPEC) is employed to evaluate the losses between the leader TSO and the follower users (Patriksson and Rockafell, 2002). There were existing literatures focusing on either the minimum transport cost or the maximum profits of TSO, but little attention on the transmission efficiency losses of natural gas network.

The transport cost was involved in the allocation of gas flows. It is generally affected by the controls of compressors, valves and gas velocity, and usually optimized by mixed integer or linear programming models (Richard et al., 1979; Wolf & Smeers, 2000; Rose et al., 2016). In addition, the profit drives the TSO to arbitrage between transportation charge and transmission cost in liberalized gas market (Golombek et al., 1995; Gabriel, 2005). It may lead to the pipeline capacity to be allocated inefficiently. In market equilibrium modelling, many researchers have tried to explore the impacts of monopoly, transportation fee, long-term contract, and pipeline bottleneck on the efficiency losses (Cremer and Laffont, 2003; Egging et al., 2008; Gabriel and Smeer, 2006). However, these studies focused on the allocation of pipeline capacity rather than the entry/exit capacities of nodes.

Entry-exit regime was implemented in European gas market to allocate the entry-exit capacity around a virtual hub (Hunt, 2008). However, the regime faces a challenge of the transmission capacity not efficiently used because of the line-pack flexibility not commercially covered and the congestion from the contractual arrangement between one entry node and one exit node (Keyaerts et al., 2011; Hallack and Vazquez, 2013). Vazquez and Hallack (2013) developed a clearing algorithm for the combinational auctions of entry/exit capacity with the aim to discover the entry and exit nodal prices for guiding the efficient allocation of network resources. However, their studies still regarded physical network as a black box. These researchers expected that the hands of free market can allocate transmission resources efficiently. However, there are still market failures from the lack of TSO's intervention through unified scheduling of gas flows.

Therefore, there is a necessary for the TSO to transform the allocation of entry and exit capacities into gas flows through physical gas network. Hiller and his colleagues have developed a bi-level programming for the TSO to improve the transformation with a two-stage model (Hiller et al., 2018). However, this programming is difficult to mathematically find a feasible solution since it is challenged by the uncertainty of capacity contracts and the transported feasibility of a given gas flow. Series of optimalization models (MINLP, NLP, and MPEC etc.) have been developed to overcome the drawbacks (Koch et al., 2015). Furthermore, based on the assumption of linear gas flow, Böttger et al. (2022) developed an exact single-level reformulation for a four-level programming to reduce the difficulty (Grimm et al., 2019).

To make it simpler, Hennig and Schwarz (2016) transferred the bi-level programming to an incapacitated maximum-minimum cost flow problem (UMMCF). In this programming, gas traders as a leader tried to pay the maximum transmission cost while TSO as a follower hoped to balance the injected and withdrawn gas at all nodes with the minimum cost. Furthermore, Hoppmann and Schwarz (2016) reformulated this problem by applying Karush-Kuhn-Tucker condition (KKT) to the follower, and then the UMMCF is substituted to the MPEC which is easy to solve with the software CPLEX. The above models, however, do not solve the spatial mismatch caused by the contractual arrangement between entry and exit capacities, which leads to gas flow inefficiently allocated in the physical network.

If all entry nodes are aggregated into one virtual entry node and all exit nodes into one virtual exit node, the UMMCF could be transformed into a classic minimum cost maximum flow problem (MCMF) with the objective at the upper level changed to the maximum entry-exit capacity (Boykov and

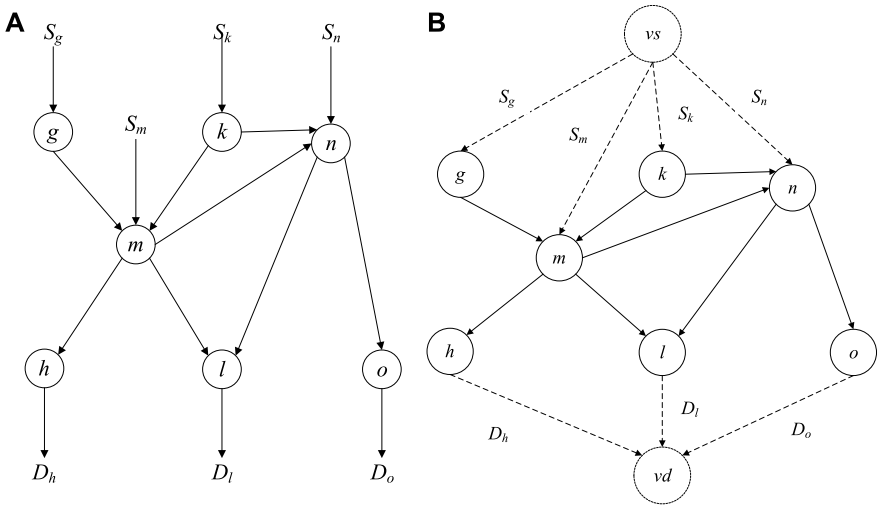

the pipeline network with gas injected and withdrawn (Wolf and Smeers, 2000)

the pipeline network with one virtual origin and virtual destination

FIGURE 1
A transportation network is generalized into a network with a pair of O-D **(A)** the pipeline network with gas injected and withdrawn (Wolf and Smeers, 2000) **(B)** the pipeline network with one virtual origin and virtual destination.

Kolmogorov,2004; Benda et al., 2019; Moolman, 2020). Actually, gas traders are willing to pay the maximum transmission cost to book the entry or exit capacity at the node in advance as much as possible. Therefore, the entry and exit capacities can be optimally allocated to reduce the spatial mismatch between one entry node and one exit node without restriction from the contractual arrangement. The MCMF is also a combinatorial graph problem which is characterized by bipartite matching (Chen et al., 2022). It was usually solved by the primal-dual algorithm, but not efficient and robust (Moolman, 2020). In the early research literatures, Bollobás et al. (1998) and Russell et al. (1998) implied that MCMF was a bi-level optimization problem that could be easily solved by the MEPC model (Xie et al., 2012). Unfortunately, it has not been further reformulated into a MPEC problem.

In this paper, the transmission cost of gas network is taken as the efficiency index, and further a MPEC model was established to integrate the allocation of commercial capacity and that of physical flows, based on a MCMF problem abstracted from existing gas network with only one virtual entry node and one virtual exit node in Section 2. This model was a coarse-grained bi-level programming without considering gas pressure, velocity, and line-pack. Subsequently, the model was used to evaluate the transmission efficiency of China's existing gas network in Section 3, and to identify the critical factors of its loss in Sections 4. Finally, some conclusions and suggestions were given in Section 5.

This paper has two contributions: Firstly, the MPEC model is established to integrate the allocation of commercial capacity and that of physical flows, based on a MCMF problem abstracted from existing gas network with only one virtual node and one exit node. It provides the direction for reducing the transmission efficiency loss of gas network from the spatial mismatch between the entry and exit capacity in the context of decoupling between gas trade and transport. Secondly, the transmission efficiency loss of China's existing gas network is identified from two aspects: one from the spatial mismatch between the entry and exit capacities caused by the shortage of natural gas supply and another from invisible segmentation in gas network, which is caused by interdicted cost of pipeline, bottleneck of pipeline capacity and economic radius of gas supply chains to transport gas.

2 Methodologies

2.1 Multiple entry-exit network generalized into an *O-D* network

A natural gas network with multiple entry and exit nodes, illustrated by Wolf and Smeers (2000), was introduced in this paper with nodal pressure not considered, as shown in Figure 1A. In this network, S_g, S_m, S_k and S_n are the entry capacities. Similarly, D_h, D_l and D_o are the exit capacities. Considering the entry and exit capacities, a transportation problem model (TP) could be employed to dispatch gas flows through physical network. As mentioned in Section 1, there might be a spatial mismatch from the contractual arrangement between entry capacity and exit capacity. TSO needs to reallocate the

capacity booked by gas traders on the maximum carrying capacity of physical network to rebalance the booked entry/exit capacities through the gas flows.

All entry nodes g, m, k, and n are connected to a virtual original node vs, as shown in Figure 1B and the entry capacities S_g, S_m, S_k and S_n are also converted into the capacities of the directed arcs of (vs, g), correspondingly (vs, m), (vs, k) and (vs, n) are denoted by dotted lines. Similarly, a virtual destination node vd is linked to the node h, l and o, and D_h, D_l and D_o are the capacities of the directed arcs in Figure 1B. Thereby, the gas network can be abstracted into a transmission network with an O-D pair. Consequently, the TP is generalized into a MCMF. And then, The MCMF is reformulated by the MPEC model in the framework of bi-level programming. Finally, the MPEC model is used to obtain the maximum flow at the optimal cost, as well as the optimal gas-injected flows on the directed arcs of (vs, g), (vs, m), (vs, k) and (vs, n). Meanwhile, the optimal gas-withdrawn flows on the arcs of (h, vd), (l, vd) and (o, vd) are also obtained.

2.2 MPEC model reformulating to MCMF

Suppose there is a gas network G (V, A, C, B), where $V = (v_1, v_2, ..., v_n)$ is a set with the elements v_j ($j = 1, 2, ..., n$). There is a virtual original node v_{vs} and a virtual destination node v_{vd} in this network as shown in Figure 1B. A is a directed arc set with the elements $(v_i, v_j) \in A$, and C is a set of arcs' capacities with the elements $c(v_i, v_j)$ which denoted briefly as c_{ij}. B is a transport fee set for arcs with the elements $b(v_i, v_j) \in B$ which is denoted as b_{ij}. In addition, $f(v_i, v_j)$ is denoted as the flow through the arc (v_i, v_j) and expressed as f_{ij}. The gas flows through the network is expressed as $v(f)$. Therefore, the MCMF is formulated to a bi-level programming as follows (Xie et al., 2012):

The upper level:

$$min \sum_{(v_i,v_j)\in A} b_{ij} f_{ij} \quad (B-1)$$

and the lower level:

$$max \quad v(f) \quad (B-2)$$

The objective function in the lower level, as seen the Eq B-2, should comply with the constraint equations as follows from B-3 to B-6, where p_{vs} p_i, p_{vd} is the shadow price of the nodes which are related to eqs B-3–5. Additionally, λ_{ij} are congestion rents of the capacity of the arc (v_i, v_j) related to the equation B-6.

$$\sum_{(v_{vs},v_j)\in A} f_{vs,j} - \sum_{(v_j,v_{vs})\in A} f_{j,vs} = v(f) \ \perp \ p_{vs} \geq 0, \forall j \quad (B-3)$$

$$\sum_{(v_i,v_j)\in A} f_{ij} - \sum_{(v_j,v_i)\in A} f_{ji} = 0 \ \perp \ p_i \geq 0, \forall i \quad (B-4)$$

$$\sum_{(v_{vd},v_j)\in A} f_{vd,j} - \sum_{(v_j,v_{vd})\in A} f_{j,vd} = -v(f) \perp p_{vd} \geq 0, \forall j \quad (B-5)$$

$$0 \leq f_{ij} \leq c_{ij} \perp \lambda_{ij} \geq 0, \forall i, j \quad (B-6)$$

Applying the KKT to the eqs B-2–6, we could obtain the dual conditions as given in Equations M-2 to M-7. If these conditions are combined with the objective function in the upper level, and then the MCMF would be reformulated into a MPEC model. This MPEC model could be solved by the software GAMS.

$$min \sum_{(v_i,v_j)\in A} b_{ij} f_{ij} \quad (M-1)$$

$$s.t. 1 + p_{vs} - p_{vd} = 0 \quad (M-2)$$

$$p_j - \lambda_{ij} - p_i \leq 0 \quad (M-3)$$

$$c_{ij} - f_{ij} \geq 0 \quad (M-4)$$

$$v - \sum_{(v_{vs},v_j)\in A} f_{vs,j} + \sum_{(v_j,v_{vs})\in A} f_{j,vs} \geq 0 \quad (M-5)$$

$$-\sum_j f_{ij} + \sum_j f_{ji} \geq 0 \ \ i \neq vs, vd \quad (M-6)$$

$$v - \sum_{(v_{vd},v_j)\in A} f_{vd,j} + \sum_{(v_j,v_{vd})\in A} f_{j,vd} \geq 0 \quad (M-7)$$

2.3 MCP for solving the TP model

The MPEC model can obtain the optimal flows $f_{vs,j}$ and $f_{j,vd}$ from the virtual nodes to the actual entry and exit nodes as shown in Figure 1A. If they are assigned to the gas injected or withdrawn volumes s_j or d_j, respectively, and then a transportation problem under a given natural gas supply and demand can be constructed, as shown in equations T-1, T-2 and T-3. In these equations, the node set VR does not include the virtual nodes vs and vd, and can be expressed as $VR = V - \{vs, vd\}$ Accordingly, the arc set AR is represented as $A - \{(vs, j), (j, vd)\}$.

$$min \sum_{(v_i,v_j)\in AR} b_{ij} f_{ij} \quad (T-1)$$

$$s.t. s_i + \sum_{(v_j,v_i)\in AR} f_{ji} = \sum_{(v_i,v_j)\in AR} f_{ij} + d_i \ \perp \ p_i, \forall i \quad (T-2)$$

$$0 \leq f_{ij} \leq c_{ij} \ \perp \lambda_{ij}, \forall i, j \quad (T-3)$$

The KKTs of the TP are:

$$0 \leq (\lambda_{ij} + b_{ij}) - (p_j - p_i) \ \perp f_{ij} \geq 0 \quad (T-4)$$

$$0 \leq -\sum_j f_{ij} + \sum_j f_{ji} - d_i + s_i \ \perp \ p_i \geq 0 \quad (T-5)$$

$$0 \leq c_{ij} - f_{ij} \ \perp \lambda_{ij} \geq 0 \quad (T-6)$$

The above three equations T-4, T-5 and T-6 constitute the MCP model of transportation programming (TP). The GAMS solver can be used to solve the MCP model to obtain the optimal flow distribution of the given gas-injected and withdrawn flows

in gas network, as well as the entry/exit nodal price of each node. In addition, we can track the nodal prices along the arcs in gas network from equations T-4 and T-6 to get insight into the transmission efficiency loss. The right item of the equation T-4 can be denoted as $\xi_{ij} \geq 0$, namely $\xi_{ij} = (b_{ij} + \lambda_{ij}) - (p_j - p_i)$. Three phenomena will take place between gas flows and nodal prices along one directed arc.

1) if $\xi_{ij} > 0$ then $f_{ij} = 0$ and $\lambda_{ij} = 0$. This means the transportation cost b_{ij} is greater than the arbitrage profit $(p_j - p_i)$ when p_j is greater than p_i. It leads to the pipeline capacity of arc (v_i, v_j) being not occupied because the transportation cost is not covered by the arbitrage profit. Therefore, the cost $\xi_{ij} = b_{ij} - (p_j - p_i)$ interdicts the possibility of TSO transporting natural gas from v_i to v_j, which is called the interdicted cost (Wood, 1993; Smith and Song, 2020). It is necessary for TSO to reduce the transportation cost to make it possible for traders to arbitrage, aiming to make full use of the pipeline capacities
2) However, when p_j is less than p_i , the interdict cost ξ_{ij} will always be greater than 0. This indicates that the flow direction of natural gas potentially restricts traders' arbitrage between these two nodes. Therefore, TSO needs to reverse the flow direction of natural gas pipeline to alleviate the mismatch between local supply and demand.
3) Conversely, in equation T-4 if $0 < f_{ij} \leq c_{ij}$, then $\xi_{ij} = 0$, which resulting in the transmission cost $(b_{ij} + \lambda_{ij})$ equals to the arbitrage $(p_j - p_i)$. Therefore, the $(p_j - p_i)$ drives the flow from node v_i to v_j, and is regarded as the critical cost to arbitrage.

3 The transmission efficiency loss of China's existing gas network

3.1 Natural gas pipeline network in China

The length of China's long-distance natural gas pipelines has reached 7.8 × 104 km by the end of 2018, constructing a gas network that runs from the north to the south, and crosses from the east to the west (see Appendix 1). This network is mainly composed of the West-East Gas Transmission Lines, Shaanxi-Beijing Line, Sichuan-East Gas Transmission Line, Zhong-Wu Line and China-Myanmar Line. These pipelines are gradually linked by the branch pipelines, such as Ji-Qing-Ning line, Lan-Yin Line, Zhong-Gui Line and Zhong-Jing Line. Chinese government is planning to build China-Russian East Line, Sakhalin Line, Ordos-Anping-Cangzhou Line and Xinjiang-Guangdong-Zhejiang Line. These four trunk lines will make up for the gas shortage of five gas supply chains of Tarim Basin, Ordos Basin, Sichuan Basin, Songliao Basin and import LNG in southeast coast, as shown in Appendix 2 (Wang et al., 2022).

In this paper, gas sources and cities located at the main pipelines are selected as entry and exit nodes, respectively. According to their latitude and longitude, China's exiting gas network is generalized as shown in Appendix 3. Therefore, there are 264 nodes and 309 pipelines in the generalized gas network.

1) Supply and demand nodes. There are 29 supply nodes and 235 demand nodes. The supply nodes include domestic gas, imported pipeline gas and LNG receiving stations as shown in Appendix 2. The imported LNG is converted to gas volume under the standard state by the conversion factor published in BP World Energy Statistical Yearbook (2022). The demand is the gas volumes consumed by a city or aggregated cities around a central city. Data resource are from the CNPC Yearbook, Sinopec Yearbook, China Energy Statistics Yearbook, provincial statistical yearbooks, and EPS database (CNOOC Yearbook, 2018; CNPC Yearbook, 2018; Sinopec Yearbook, 2018).
2) Pipelines and pipeline capacity. Pipelines in the generalized gas network include existing gas trunk lines and long-distance pipelines under construction. The pipeline capacity is based on the design transmission capacity. The data is from the CNPC Yearbook and Sinopec Yearbook.
3) Transportation cost. Pipeline transportation charge is determined by both unit transportation fee and distance. For simplicity, the distance between nodes is calculated by latitude and longitude, and the unit freight rate is regulated by National Development and Reform Commission in 2017. For examples, the unit freight rate of Sichuan-East Gas Transmission Line is 0.3894 RMB/1000 m^3 km, and of Shaanxi-Beijing Line is 0.2857 RMB/1000 m^3 km. In addition, the coastal LNG is transported according to the average transportation cost of CNPC, CNOOC and Sinopec pipelines.

3.2 The transmission efficiency loss

The TP model is used to obtain the minimum transmission cost under existing gas supply and demand in 2017. And then, the MPEC model is carried out to obtain the minimum cost and maximum flow without supply and demand restrictions. In Table 1, the transmission cost of the former is reduced to about 80 × 10^8 m^3/a, compared with the latter. It indicates that there is a transmission efficiency loss of 17.9% in the existing gas network. Moreover, the max flows optimized by the MEPC model is about 2914 × 10^8 m^3/a, much larger than that by TP (2128 × 10^8 m^3/a). These results show that existing gas network can provide entry and exit capacity of 2914 × 108 m3/a for gas traders, but it doesn't happen. It implies that the allocation of entry and exit capacities depends on whether the gas physical network is optimally used through gas flows.

TABLE 1 Transmission efficiency of China's natural gas network.

	TP model	MPEC model	Efficiency loss
Transmission cost (10^8 Yuan/a)	579.48	491.42	17.9%
Maximum flow (bcm)	2128.34	2914.53	——

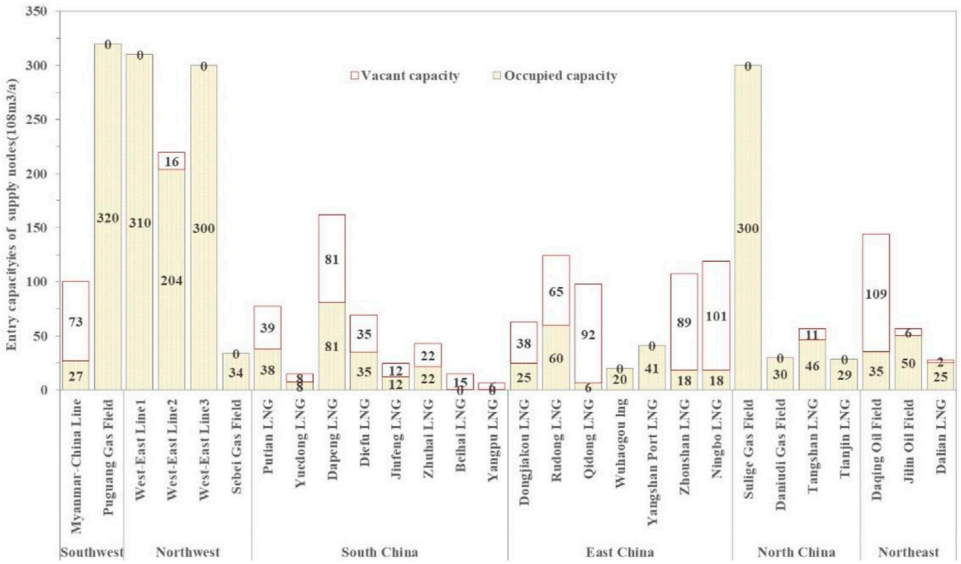

FIGURE 2
The occupied entry capacity obtained by TP model in existing gas network and the vacant capacity is the difference between the entry capacities obtained by MPEC and by TP.

If the entry capacities obtained by MPEC and TP models are further deconstructed spatially as shown in Figure 2, we could observe that there are many nodes with vacant entry capacities. In particular, the entry capacities of LNG receiving stations along the coast of East China and South China have not been fully utilized, with the vacant capacity of about 21 bcm in South China and 38.5 bcm in East China, respectively. There is the insufficient LNG supplies in these two regions. Thereby, the shortage of gas supply in these two regions have to drive gas sources in Xinjiang and Sichuan Basin to be transported to these two areas over a long distance to make up for the shortage of LNG supply. The same reason is also applied to the vacant entry capacities of China-Myanmar pipeline and Daqing gas field. Therefore, the mismatch of capacities between the entry nodes and the exit nodes comes from the spatial insufficiency of gas supply. Moreover, MEPC model could be used to globally allocate these capacities, benefiting from the setting of virtual entry and extraction nodes in MCMF.

The congestion degree of the pipeline and the nodal prices are obtained by TP model and MPEC model, respectively, as shown in Figure 3A, B. Comparing these two figures, we could get such an understanding that much more gas supply can improve spatially the reallocation of entry/exit capacities, leading to the pipeline capacities to be more optimally used with the lower nodal prices in Figure 3B. Concretely, the pipeline congestion degree obtained by MPEC model gradually decreases from west to east, compared with that obtained by TP model. However, the nodal prices show a concave distribution with high price in the middle and low price in the west and east. This is the capacities of entry nodes located at the southwest and east China to receive more natural gas, thus mitigating the pressure of long-distance transportation of natural gas in the west to supply the demands in the east.

In addition, the MPEC model could be validated by the actual gas consumptions in 2017, 2018, and 2019 (BP, 2022). 212.8 bcm/a of natural gas could be transported by existing gas network, including PNG of 160.1 bcm and LNG of 537 bcm, as shown in Figure 2, which are close to the actual consumption 241.3 bcm in 2017. The optimal transportation capacity is 2911.4 bcm, which can cover the consumptions in 2018 and even 2019 with 283.9 bcm and 308.4 bcm, respectively.

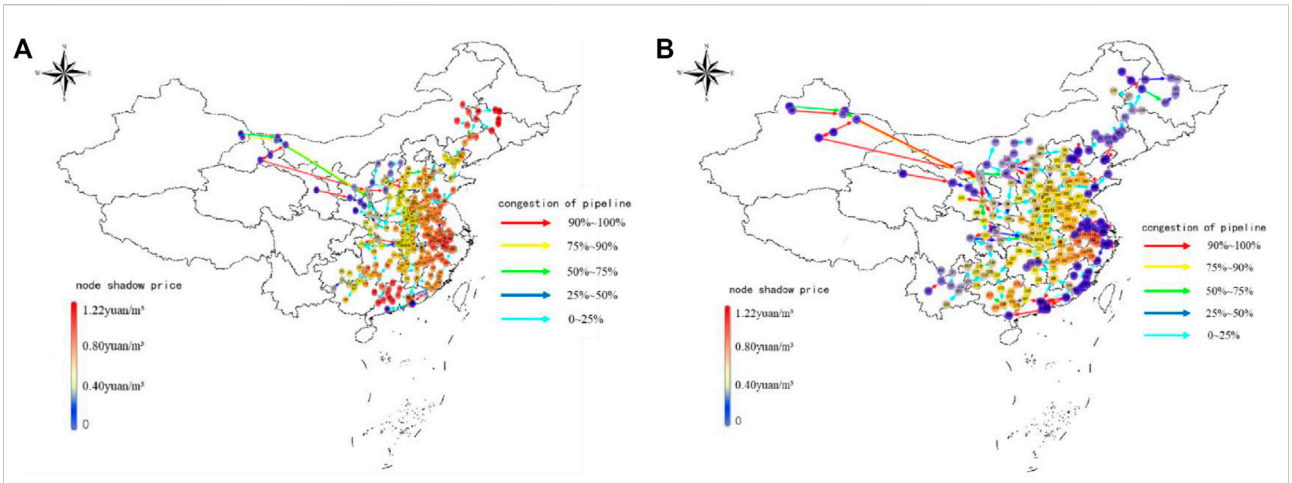

the flow distribution in exiting natural gas network by TP model

the optimal flow distribution in existing natural gas network by MEPC model

FIGURE 3
Spatial distribution of nodal prices and pipeline congestion in gas network (the pipeline congestion is expressed by the ratio of flow to capacity **(A)** the flow distribution in exiting natural gas network by TP model **(B)** the optimal flow distribution in existing natural gas network by MEPC model.

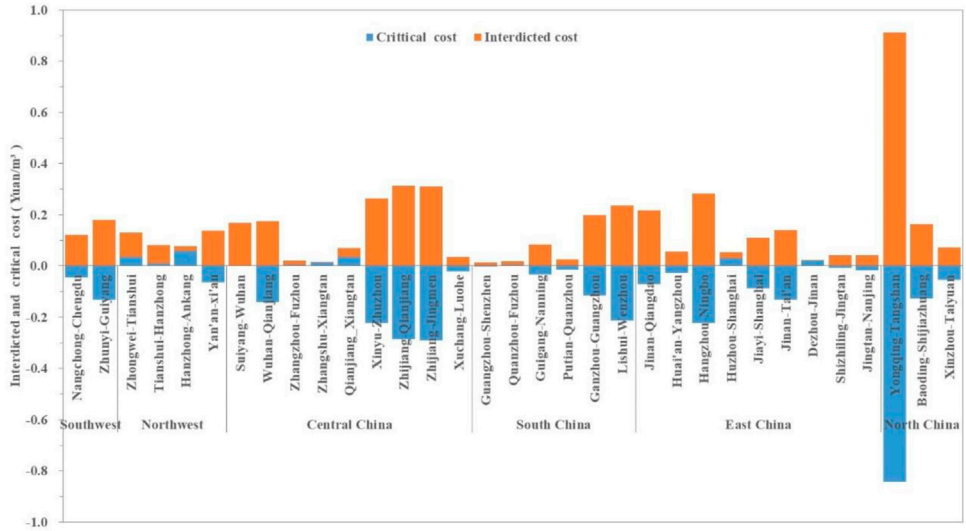

FIGURE 4
Spatial distribution of critical costs and interdicted costs of unoccupied gas pipelines.

In Figure 4A, The color of natural gas pipeline in northwest China is yellow, while that in central China, southeast China and south China is red. The color of the nodes in Figure 4A gradually changes from pale yellow to red and from the northwest to the southeast coast, except that the color of the gas supply node is blue. However, in Figure 4B, the color of nodes in central China, north China and south China is yellow, while the color of nodes in other regions is blue.

4 Results and discussion

We further investigate how the reallocation of entry and exit capacity affects the pipeline resources to be optimally used because the reallocation depends on whether gas physical network is optimally used, as stated in Section 3.2. It can also be asked that how the pipeline resources affect the spatial rebalancing of the entry and exit capacities. Therefore, we

TABLE 2 Impacts of reducing interdicted cost on transmission cost, max flow, and transmission efficiency loss.

	North China	East China	Central China	Yongqing-Tangshan pipeline
The reduction of transmission cost (10^8 Yuan/a)	1.6892	0.1592	0.0012	5.9237
The increment of max flow (bcm/a)	0	0	0	20.6569
The decrease of transmission efficiency loss	0.29%	0.02%	0%	1.02%

explore the mechanism of transmission efficiency loss from three aspects of network segmentation: the interdicted cost, the elasticity of pipeline capacity and the deployment of gas trunk lines in China's natural gas market.

4.1 The spatial distributions of interdicted cost

Looking back at the congestion degrees of pipelines and nodal prices in Figure 3A, there are 29 pipelines with their interdicted costs greater than zero under existing supplies and demands, as shown in Figure 4. It means that the gas flows through these pipelines are equal to zero, and the pipeline capacities is not occupied according to the complementary relationship between gas flows and the prices in eq. T-4.

It can be further observed that there are a few pipelines with critical cost greater than zero, which indicates that the transportation fee builds the cost barrier of gas flows through the pipelines. In addition, the critical cost of most pipelines is less than zero, that is, the regulated direction of gas flows through the pipeline produces the technical barrier of gas flow. Especially, the transportation channel between North China gas network with Northeast China gas network is interdicted by the regulated direction of Yongqing-Tangshan pipeline. Therefore, the interdicted cost hinders the fluidity of gas flows in the local network and then segments regionally the gas network, which potentially increasing the radius of gas supply chain to transport gas flows from Xingjiang, Erodes basin to gas network of Northeast China.

It is possible to decrease the interdicted cost of the above-mentioned 29 pipelines by reducing the transportation fee or reversing the direction of gas flows through pipelines for improving the transmission efficiency of exiting gas network. Therefore, among the 29 pipelines, the interdicted costs of pipelines in East China, North China and Southeast China are reduced respectively. Considering the segmentation between North China and Northeast China gas network from the Yongqing-Tangshan pipeline, it is necessary to independently observe the transmission efficiency by reversing its gas flow direction. The results are shown in Table 2.

The results in Table 2 illustrate that the reduction of pipelines' interdicted cost in North China, East China and Central China would heterogeneously affect the transmission cost and transmission efficiency loss of existing gas network. However, the maximum transmission capacity could be not affected, and the change would be close to 0. The reason is that these interdicted pipelines in these three regions only improve the transportation path of gas flow through the local gas network, but can't cause the reallocation of entry and exit capacities.

Compared with the three regions, reversing the gas flow direction of Yongqing-Tangshan pipeline would not only increase the transportation capacity by 20.657 × 108 m/a, but also reduce the transportation cost by 5.924 × 108 yuan/a, resulting in a 1.02% reduction in transmission efficiency loss. This implies that once the channel barriers between gas network in North China and Northeast China are removed, natural gas from North China will flow to Northeast China through this key channel. At the same time, coastal LNG will supplement the natural gas demand in North China, East China and Central China. Although the nodal prices in Northeast China has increased by about 0.8 yuan/m3, compared with those before the gas flow direction change, the clearing prices of nodes in North China, Central China and Southeast China have decreased, as shown in Figure 2A and Figure 5. Therefore, the reversal of gas flow direction in this critical channel will cause the reallocation between the entry and exit capacities to move towards the optimization direction.

4.2 The heterogenous elasticities of the pipeline capacity

There are 11 arcs congested by gas flows which obtained by MPEC model in exiting supply and demand. They are mainly located in Shaanxi-Beijing First line, Shaanxi-Beijing Second and Third lines, Yu-Ji line, and other eight branch lines, as shown in Fig. 6. One-unit capacity 1 × 108 m3/a is added to these pipelines, respectively, to observe the changes of transmission efficiency and network maximum gas flow.

Once the capacities of these pipelines are expanded, the transportation cost will be correspondingly increased. In addition, the increase of the maximum gas flow is equal to the capacity expansion of Lunnan-Korla pipeline, Yulin-Taiyuan pipeline, Yulin-Shenchi pipeline and Puyang-Jinan pipeline respectively, as the dotted lines shown in Figure 6. It indicates that these four pipelines are still congested by gas flow,

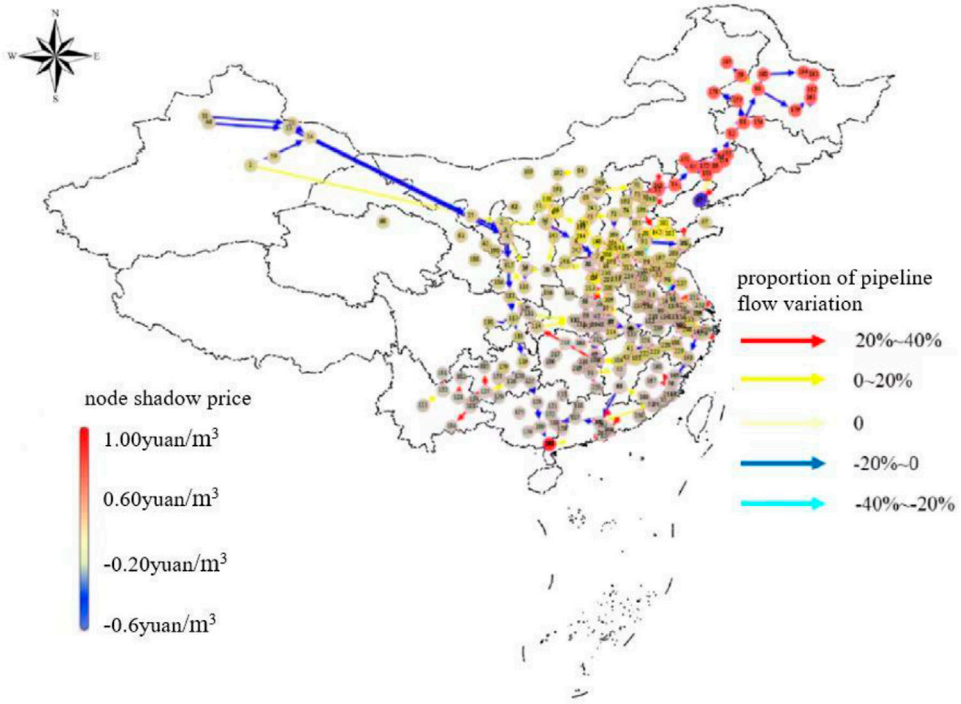

FIGURE 5
Nodal prices and flow distribution in gas network when reversing the gas flow direction through Yongqing-Tangshan pipeline.

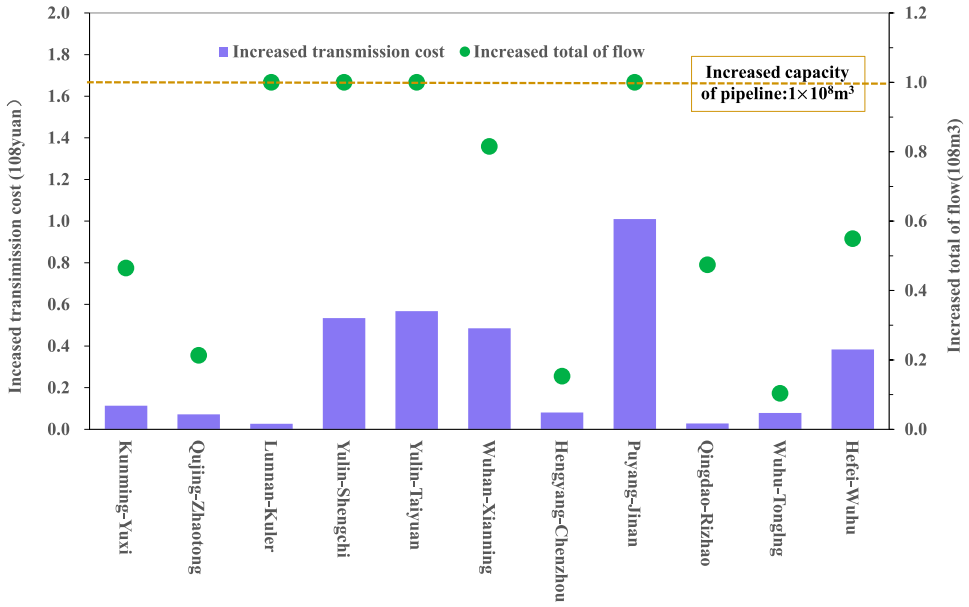

FIGURE 6
Impact of pipe capacity changes on the marginal cost and marginal flow of distribution network.

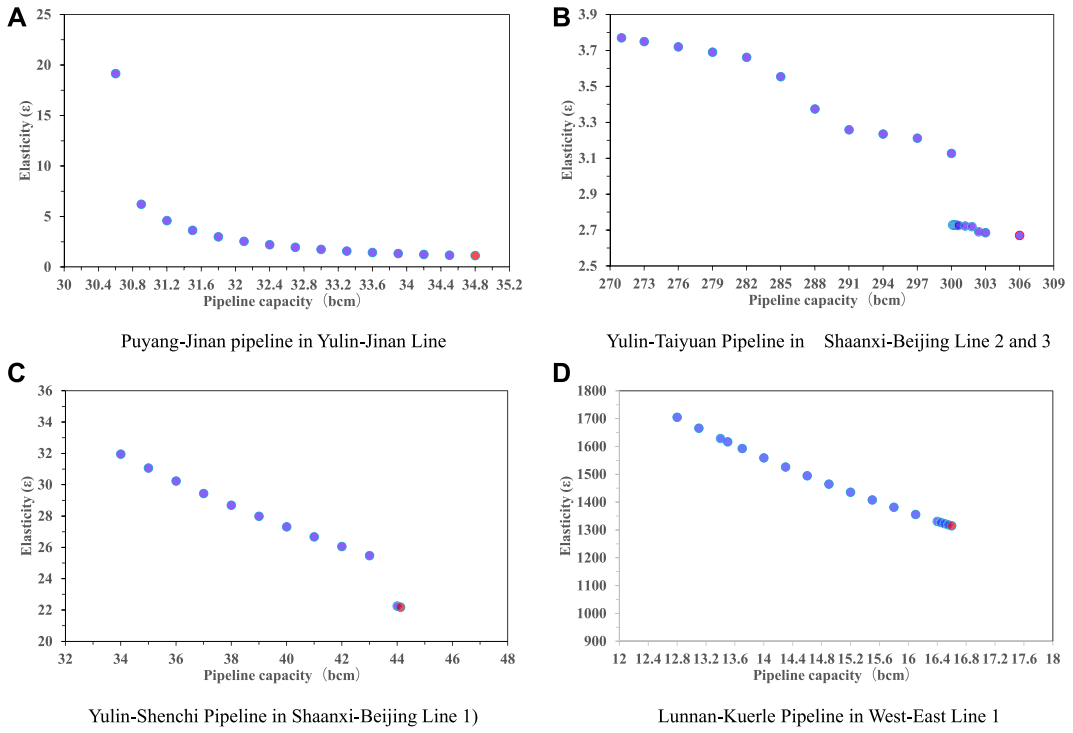

FIGURE 7
The heterogeneous elasticity of capacity-cost in China's exiting gas network **(A)** Puyang-Jinan pipeline in Yulin-Jinan Line **(B)** Yulin-Taiyuan Pipeline in Shaanxi-Beijing Line 2 and 3 **(C)** Yulin-Shenchi Pipeline in Shaanxi-Beijing Line 1) **(D)** Lunnan-Kuerle Pipeline in West-East Line 1

so they are still the bottleneck of gas network. However, for the residual seven pipelines, the increase of maximum gas flow is less than the increase of pipeline capacity, so these seven pipelines are no longer congested. Therefore, the expansion of pipeline capacity has certain elasticity, which will inevitably lead to the transmission efficiency loss.

To measure the elasticity of pipeline capacity, we introduce the elasticity of "capacity-cost" by referring to price-demand elasticity in economics. The elasticity is expressed as $\varepsilon_{ij} = (\Delta c_{ij}/c_{ij})/(\Delta tc/tc)$, where ε_{ij} is the capacity cost elasticity of pipeline (i, j), Δc_{ij} is the change of pipeline capacity, tc is the transmission cost of gas network and Δtc is the change of the transmission cost.

Four pipelines are selected for experiments and the elasticity curves of these four pipelines are obtained by simulation, as shown in Figure 7. It can be seen that the elastic curves of the four pipelines have different shapes. The curve of Puyang-Jinan pipeline is close to an "L" shape, that of Yulin-Taiyuan pipeline is close to an "S" shape. However, the curves of Yulin-Shenchi pipeline and Lunnan-Korla pipeline are close to a straight line. These different shapes imply that pipeline elasticity is spatially heterogeneous. In addition, we can observe that the elastic coefficient of Lunnan-Korla pipeline is much higher than that of the other three pipelines, while the coefficient of Puyang-Jinan pipeline is the smallest. The above two phenomena can be attributed to the fact that these two pipelines are located at different positions in gas network. Puyang-Jinan pipeline is located in the trunk of Yulin-Jinan line. There are many entry-exit nodes on this trunk line, and then the expansion of the capacity of Puyang-Jinan pipeline will reallocate increased gas flow among entry and exits nodes along this line. Thereby, the transportation cost by the expansion will be diluted. On the contrary, Lunnan-Korla pipeline is located on the West-East pipeline, and there are no more entry and exit nodes to dilute the transportation cost. Therefore, the location of the pipeline in gas network determines its' elasticity, and then the transmission cost is robust to the expansion of the pipeline capacity of the trunk line, whereas it is rigid.

4.3 The deployment of gas pipelines

Chinese government plans to build the China-Russia East Line and Sakhalin Line with the capacity of 380×10^8 m^3/a, respectively. Moreover, Xinjiang- Guangdong-Zhejiang Line and Ordos-Anping-Cangzhou Line are planned to be built with the capacity of 300×10^8 m^3/a. Their planned paths are shown in

TABLE 3 The results of the three Scenario I, II, and III

	Scenario I	Scenario II	Scenario III
Transmission cost (10^8 Yuan)	597.15	613.50	1010.99
Transmission capacity (bcm)	2182.35	2203.36	4094.53
Efficiency loss	21.51%	24.84%	——

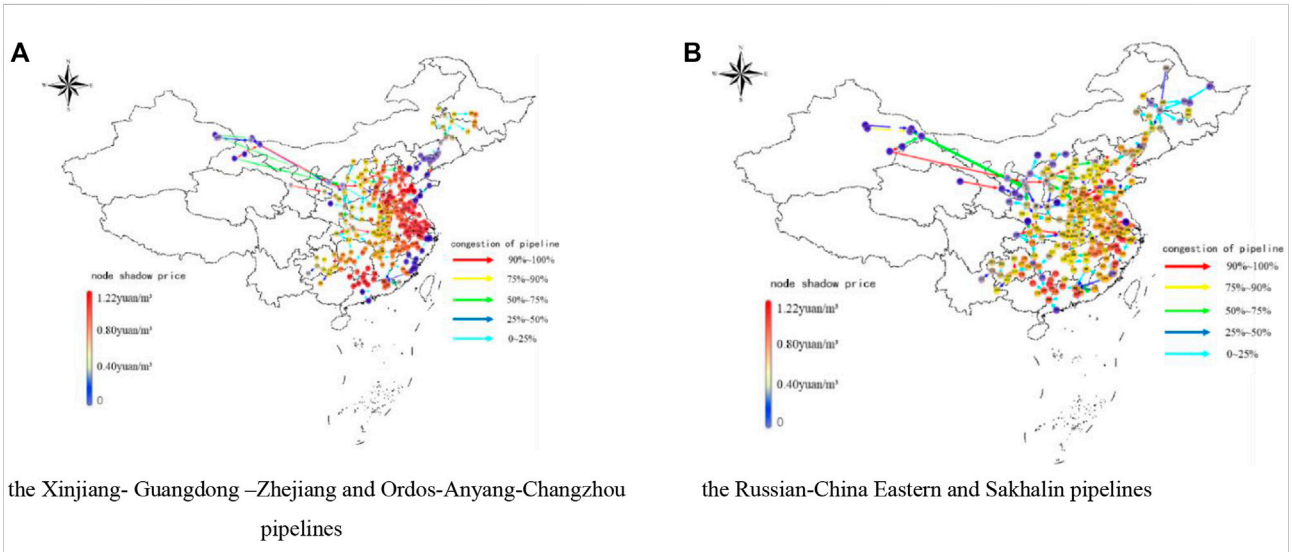

FIGURE 8
Distributions of nodal prices and pipeline congestions in scenario I and II **(A)** the Xinjiang- Guangdong–Zhejiang and Ordos-Anyang-Changzhou pipelines **(B)** the Russian-China Eastern and Sakhalin pipelines.

dotted lines in Appendix 1. Undoubtedly, these four trunk lines will expand the capacities of the two supply chains of Ordos Basin gas source and Russian imported natural gas. Therefore, we analyze the transmission efficiency of gas network in three scenarios, as follows:

1) Scenario I: Xinjiang- Guangdong-Zhejiang Line and Ordos-Anping-Cangzhou Line are added to the existing gas network;
2) Scenario II: China-Russia East Line and Sakhalin Line are added to the existing gas network;
3) Scenario III: These four lines are added to the existing gas network, taking account into the requirement of China's natural gas supply for gas network in 2030.

It could be found that the transmission efficiency losses in Scenario I and Scenario II are 21.51% and 24.84%, respectively. As shown in Table 3. Both of them are higher than 17.92% in MEPC model as seen in Table 1. Differently, the maximum flows in these two scenarios are only increases by 54.01 × 108m3/a and 75.02 × 108m3/a, compared with the result of MPEC model (see Table 1). Actually, the trunk lines to be built in these two scenarios only extend the gas supply chain radius of transporting gas flows from gas sources in Xingjiang, Erodes basin and imported gas from Russia to North China, East China and South China.

In Scenario I, these two trunk lines to be built not only expand the entry capacities of gas sources from Xinjiang and Erodes basin, but also reduce the pressure of the supply chain of Xinjiang gas source on the gas supply in Southeast and South China. These two supply chains coordinate with each other and optimally reallocate entry and exit capacities, thus reducing the congestions and nodal prices, as shown in Figure 8A. Similarly, In ScenarioII, natural gas imported from Russia also alleviates the gas supply pressure of the above two supply chains to Central, East and South China. Therefore, the congestion degrees and node prices in Scenario II are lower than those in Scenario I, as shown in Figure 8B.

In Scenario III, the maximum transportation capacity of China natural gas network will reach 4094.53 × 108 m3/a, although more transportation costs will have to be paid. That is to say, these four pipelines will greatly improve the spatial distribution of entry and exit capacities. It will also increase the fluidity of gas flows among the five gas supply chains, as shown in Appendix 2. Therefore, more gas supply chains will improve the spatial distribution of entry/exit capacity, thus reducing the gas

supply shortage caused by the mismatch between entry and exit capacities.

4.4 Discussion

The results need to be further discussed, even including the verification of the model in Section 3. Inspired by Acerbi et al. (2022), we triangulated this discussion from model, data, and information.

In MPEC, the transaction process of capacity (booking and nominating entry-exit capacity) is simplified, as well as technical constraints, such as gas pressure and compressibility which addressed by Hiller (2018) and Böttger et al. (2022). Thereby, our model is suitable for strategically evaluating the supports of existing physical network to commercial network, but not for real-time scheduling (hourly or daily) of entry-exit capacity. In addition, the spatial mismatch of deterministic entry-exit capacities is the focused of our model, rather than the capacities to be randomly booked in realistic and severe transport situations which were studied by Hiller (2018), Böttger et al., 2022 (2018) and Hennig and Schwarz (2016). From this point of view, we extended their research work.

The visualized results give three strategies of gas flow management: reducing the interdicted cost (reducing transportation cost and reversing gas flow direction), increasing the pipeline capacity and building new trans-regional pipelines. A high degree of physical gas market integration is of great importance to enhance competition under the Third-Access Party policy implemented recently in China. Therefore, the obtained gas flow data provides visual observation for TSO to improve gas flow andto decrease pipeline congestions for more gas market integration (Dieckhöner,et al., 2013). For example, the variation of natural gas flow direction and pipeline capacity can be realized practically by node pressure controls which normally optimized in technical and economic models (Wolf and Smeers, 2000; Rose et al., 2016).

Nodal prices are transmitted on gas network with gas flows. When pipeline congestion occurs, the congestion rent will be transmitted on the network along with nodal prices, and be recovered by TSO. Therefore, the nodal prices obtained by our model is similar to the nodal capacity price obtained by market auction (Vazquez and Hallack, 2013). This implies that the nodal price provides a reference for regionally pricing the entry/exit capacity. Moreover, congestion rents of pipelines could be fed back to the virtual origin and destination (as shown in Figure 1) to guide the total of entry/exit flows to be redistributed among all of entry and exit nodes. Hence, it implicitly suggests the sharing and distributing of nodal price signal is realized on the virtual origin and destination nodes, although our model design is more closely relate to UMMCF (Hennig and Schwarz, 2016; Hoppmann and Schwarz,2016).

5 Conclusion and implications

In this paper, The MPEC model was established to evaluate the transmission efficiency and identified the critical factors of its loss. Some conclusions are made as follows.

The third-party access policy will drive the decoupling between gas trade and transport, leading to the transmission resources of the physical network cannot be optimally used to meet with the contractual arrangement between entry and exit capacities in commercial network. The MPEC model could integrate the allocation of commercial capacity and that of physical flows, based on a MCMF problem abstracted from existing gas network with only one virtual entry node and one virtual exit node. Moreover, this model cloud be used to spatially reallocate entry and exit capacities through the optimal scheduling of gas flow. It can reduce the transmission efficiency loss from the gap between commercial network and physical network, and delivers a feasible solution for the large-scale scheduling operation of natural gas network.

There is a transmission efficiency loss of 17.9% in China's existing natural gas network and the loss mainly comes from the spatial mismatch between the entry and exit capacities caused by the shortage of natural gas supply in the South, East and Northeast China. However, the entry and exit capacities offered by TSO still depends on the optimal allocation of pipeline capacity. Specifically, the interdicted cost of pipeline, capacity-cost elasticity of pipeline and economic radius of gas supply chain to transport gas flows will produce the invisible segmentation of local networks, networks along trunk lines and regional networks, respectively. These invisible allocations will indeed extend the distance to transport gas, thus distorting the efficiency of pipeline capacity allocation. Thereby, the three segmentations are the critical factors of transmission efficiency loss in China's natural gas network.

Some implications are given to improve the transmission efficiency.

Firstly, the allocation of entry-exit capacity should be dominated by TSO, not by traders. Otherwise, the contractual arrangement of entry-exit capacity will distort the allocation of pipeline capacity. China's gas network could not be managed by absolutely copying the entry-exit regime in European natural market. The reason is that gas supply shortage and imperfect pipeline network layout will lead to supply security, which is the priority of TSO scheduling objectives.

Secondly, China government has formulated diversified import strategies to meet the market demand, but a large number of natural gas imports come from East Asian countries adjacent to Xinjiang. These imported natural gas are far away from the three high-demand areas of East China, South China and Northeast China. This means that China's natural gas import should pay more attention to the LNG import volume of these two regions, so as to improve the mismatch between entry and exit capacities caused geographically by import gas shortage.

Thirdly, although China government promulgated the supervision and examination of pipeline transportation cost to regulate TSO's abuse of market power, the transportation price

may block gas flow in local network, resulting in local network segmentation. Therefore, a flexible transportation price system is needed for the fluidly of gas flow. Up to now, Chinese government has not issued regulations on pipeline capacity management. The spatial heterogeneity of pipeline capacity-cost elasticity is an important way to improve the transmission efficiency. But the detailed design is a challenge. In addition, it is necessary to complete the construction of planning pipeline as soon as possible to establish a multi-supply chain system, so as to improve the transmission efficiency.

Data availability statement

The original contributions presented in the study are included in the article/supplementary material, further inquiries can be directed to the corresponding authors.

Author contributions

XW and XL conceptualized the idea of the study design and wrote the manuscript; XW, XZ, and XH designed the discussion. XW, XL, and XH revised the article; XW provided fund support. WZ and ZL collected the data and performed statistical analysis. All authors have read and agreed to the published version of the manuscript.

Funding

This research is financially supported by the National Natural Science Foundation of China (No. 71874166) and the Ministry of education of Humanities and Social Science project (No. 11YJC630211).

Acknowledgments

The authors appreciate the editors' and reviewers' help for improving the manuscript.

Conflict of interest

The authors declare that the research was conducted in the absence of any commercial or financial relationships that could be construed as a potential conflict of interest.

Publisher's note

All claims expressed in this article are solely those of the authors and do not necessarily represent those of their affiliated organizations, or those of the publisher, the editors and the reviewers. Any product that may be evaluated in this article, or claim that may be made by its manufacturer, is not guaranteed or endorsed by the publisher.

Supplementary material

The Supplementary Material for this article can be found online at: https://www.frontiersin.org/articles/10.3389/fenrg.2022.1029077/full#supplementary-material

References

Acerbi, F., Sassanelli, C., and Taisch, M. (2022). A conceptual data model promoting data driven circular manufacturing. *Oper. Manag. Res.* 15, 838–857. doi:10.1007/s12063-022-00271-x

Benda, D., Chu, X., Sun, S., Quek, T., and Buckley, A. (2019). Renewable energy sharing among base stations as a min-cost-max-flow optimization problem. *IEEE Trans. Green Commun. Netw.* 3 (1), 67–78. doi:10.1109/tgcn.2018.2876005

Bollobás, B. (1998). *Modern graph theory*. Springer Science & Business Media. Heidelberg, Germany, Vol. 184.

Böttger, T., Grimm, V., Kleinert, T., and Schmidt, M. (2022). The cost of decoupling trade and transport in the European entry-exit gas market with linear physics modeling. *Eur. J. Operational Res.* 297 (3), 1095–1111. doi:10.1016/j.ejor.2021.06.034

Boykov, Y., and Kolmogorov, V. (2004). An experimental comparison of min-cut/max-flow algorithms for energy minimization in vision. *IEEE Trans. Pattern Anal. Mach. Intell.* 26, 1124–1137. doi:10.1109/tpami.2004.60

BP (2022). Statistical Review of World Energy [EB/OL]. Available at: http://www.bp.com/statisticalreview.

Chen, L., Kyng, R., Liu, Y. P., Peng, R., Gutenberg, M. P., and Sachdeva, S. (2022). Maximum flow and minimum-cost flow in almost-linear time. https://arxiv.org/abs/2203.00671.

Cnooc (2018). The yearbook of CNOOC. https://www.cnoocltd.com/col/col3881/index.html.

Cnpc (2018). The yearbook of CNPC. http://www.cnpc.com.cn/cnpc/ndbg/201905/7e0bac0d766f4b43af8a29c86cc0a3d2/files/4f804543315143a28058814d5af95392.pdf.

Cremer, H., Gasmi, F., and Laffont, J. J. (2003). Access to pipelines in competitive gas markets. *J. Regul. Econ.* 24 (1), 5–33. doi:10.1023/a:1023943613605

Dieckhöner, Caroline, Lochner, Stefan, and Lindenberger, Dietmar (2013). European natural gas infrastructure: The impact of market developments on gas flows and physical market integration. *Appl. Energy* 102, 994–1003.

DNRC & NEA (2018). Notice on issuing opinions on accelerating the construction of gas storage facilities and perfecting the market mechanism of auxiliary services for gas storage and peak-shaving Regulation. https://www.ndrc.gov.cn/xxgk/zcfb/ghxwj/201905/t20190531_960966.html?code=&state=123.

DNRC (2019). Notice on the regulation measures for fair and open oil and gas pipeline network facilities. https://www.ndrc.gov.cn/xxgk/zcfb/ghxwj/201905/t20190531_960966.html?code=&state=123.

Dong, J., Sha, S., Li, X., Xu, J., Dai, W., and Duan, H. (2018). Ownership unbundling of natural gas transmission networks in China. *J. Clean. Prod.* 195, 145–153. doi:10.1016/j.jclepro.2018.05.173

Egging, R., Gabriel, S. A., Holz, F., and Zhuang, J. (2008). A complementarity model for the European natural gas market. *Energy policy* 36 (7), 2385–2414. doi:10.1016/j.enpol.2008.01.044

Gabriel, S. A., Zhuang, J., and Kiet, S. (2005). A large-scale linear complementarity model of the North American natural gas market. *Energy Econ.* 27 (4), 639–665. doi:10.1016/j.eneco.2005.03.007

Gabriel, S., and Smeers, Y. (2006). Complementarity problems in restructured natural gas markets. *Recent Adv. Optim.*, 343–373.

Gillessen, B., Heinrichs, H., Hake, J. F., and Allelein, H. J. (2019). Natural gas as a bridge to sustainability: Infrastructure expansion regarding energy security and system transition. *Appl. Energy* 251, 113377.

Golombek, R., Gjelsvik, E., and Rosendahl, K. E. (1995). Effects of liberalizing the natural gas markets in Western Europe. *Energy J.* 16 (1). doi:10.5547/issn0195-6574-ej-vol16-no1-6

Hallack, M., and Vazquez, M. (2013). European Union regulation of gas transmission services: Challenges in the allocation of network resources through entry/exit schemes. *Util. Policy* 25, 23–32. doi:10.1016/j.jup.2013.01.003

Hennig, K., and Schwarz, R. (2016). Using bilevel optimization to find severe transport situations in gas transmission networks. *ZIB-Report*, 16–68.

Hiller, B., Koch, T., Schewe, L., Schwarz, R., and Schweiger, J. (2018). A system to evaluate gas network capacities: Concepts and implementation. *Eur. J. Operational Res.* 270 (3), 797–808. doi:10.1016/j.ejor.2018.02.035

Holz, F., Von Hirschhausen, C., and Kemfert, C. (2008). A strategic model of European gas supply (GASMOD). *Energy Econ.* 30 (3), 766–788. doi:10.1016/j.eneco.2007.01.018

Hoppmann, K., and Schwarz, R. (2018). "Finding maximum minimum cost flows to evaluate gas network capacities," in *Operations research proceedings 2017* (Heidelberg, Germany: Springer), 339–345.

Huang, H., Ouyang, L., and Liu, T. (2006). Upper bounds of efficiency loss for user equilibrium behavior in traffic networks. *J. Beijing Univ. Aeronautics Astronautics* 32 (10), 1215.

Keyaerts, N., Hallack, M., Glachant, J. M., and D'haeseleer, W. (2011). Gas market distorting effects of imbalanced gas balancing rules: Inefficient regulation of pipeline flexibility. *Energy Policy* 39 (2), 865–876. doi:10.1016/j.enpol.2010.11.006

Koch, T., Hiller, B., Pfetsch, M. E., and Schewe, L. (2015). *Evaluating gas network capacities*. Society for Industrial and Applied Mathematics. Philadelphia, PA, USA

Lindsey, R., De Palma, A., and Silva, H. E. (2019). Equilibrium in a dynamic model of congestion with large and small users. *Transp. Res. Part B Methodol.* 124, 82–107. doi:10.1016/j.trb.2019.04.005

Moolman, W. (2020). The maximum flow and minimum cost–maximum flow problems: Computing and applications. *Asian J. Probab. Statistics*, 28–57. doi:10.9734/ajpas/2020/v7i330185

Ogden, J., Jaffe, A. M., Scheitrum, D., McDonald, Z., and Miller, M. (2018). Natural gas as a bridge to hydrogen transportation fuel: Insights from the literature. *Energy Policy* 115, 317–329.

Patriksson, M., and Rockafellar, R. T. (2002). A mathematical model and descent algorithm for bilevel traffic management. *Transp. Sci.* 36 (3), 271–291. doi:10.1287/trsc.36.3.271.7826

Qin, Y., Tong, F., Yang, G., and Mauzerall, D. L. (2018). Challenges of using natural gas as a carbon mitigation option in China. *Energy Policy* 117, 457–462.

Richard, P., O'Neill, R. P., Williard, M., Wilkins, B., and Pike, R. (1979). A mathematical programming model for allocation of natural gas. *Operations Res.* 27 (5), 857–873. doi:10.1287/opre.27.5.857

Rose, D., Schmidt, M., Steinbach, M. C., and Willert, B. M. (2016). Computational optimization of gas compressor stations: MINLP models versus continuous reformulations. *Math. Methods Oper. Res. (Heidelb).* 83 (3), 409–444. doi:10.1007/s00186-016-0533-5

Roughgarden, T., and Tardos, É. (2002). How bad is selfish routing? *J. ACM (JACM)* 49 (2), 236–259. doi:10.1145/506147.506153

Russel, R. S., and Taylor, B. W. (1998). *Operations management: Focusing on quality and competitiveness*. Prentice-Hall. Hoboken, NJ, USA,

Sinopec (2018). The yearbook of Sinopec. http://www.sinopecgroup.com/group/xxgk/jtnb/20210914/news_20210914_406264092787.shtml.

Smith, J. C., and Song, Y. (2020). A survey of network interdiction models and algorithms. *Eur. J. Operational Res.* 283 (3), 797–811. doi:10.1016/j.ejor.2019.06.024

Wang, J. H., and Cheng, X. J. (2017). Network bottleneck, strategic behaviorbehaviour and pipeline open fair A research based on the oil and gas industry. *China Ind. Econ.* 1, 117.

Wang, X., Qiu, Y., Chen, J., and Hu, X. (2022). Evaluating natural gas supply security in China: An exhaustible resource market equilibrium model. *Resour. Policy* 76, 102562. doi:10.1016/j.resourpol.2022.102562

Wolf, D., and Smeers, Y. (2000). The gas transmission problem solved by an extension of the simplex algorithm. *Manag. Sci.* 46 (11), 1454–1465. doi:10.1287/mnsc.46.11.1454.12087

Wood, R. K. (1993). Deterministic network interdiction. *Math. Comput. Model.* 17 (2), 1–18. doi:10.1016/0895-7177(93)90236-r

Xie, F., Jia, Y., and Jia, R. (2012). Algorithm for minimum cost maximum flow in transportation network. *J. Converg. Inf. Technol.* 7 (7), 165–173. doi:10.4156/jcit.vol7.issue7.21

Xu, J., Hallack, M., and Vazquez, M. (2017). Applying a third party access model for China's gas pipeline network: An independent pipeline operator and congestion rent transfer. *J. Regul. Econ.* 51 (1), 72–97. doi:10.1007/s11149-017-9316-z

Xu, B., and Lin, B. (2019). Can expanding natural gas consumption reduce China's CO_2 emissions?. *Energy Economics*, 81, 393–407. doi:10.1007/s11149-017-9316-z

frontiers | Frontiers in Energy Research

TYPE Original Research
PUBLISHED 05 September 2022
DOI 10.3389/fenrg.2022.918425

OPEN ACCESS

EDITED BY
Nallapaneni Manoj Kumar,
City University of Hong Kong, Hong Kong SAR, China

REVIEWED BY
Alberto-Jesus Perea-Moreno,
University of Cordoba, Spain
Mohieddine Rahmouni,
King Faisal University, Saudi Arabia

*CORRESPONDENCE
Tze San Ong,
tzesan033@hotmail.com
Boon Heng Teh,
bhteh@mmu.edu.my

SPECIALTY SECTION
This article was submitted to Sustainable Energy Systems and Policies, a section of the journal Frontiers in Energy Research

RECEIVED 12 April 2022
ACCEPTED 03 August 2022
PUBLISHED 05 September 2022

CITATION
Ao X, Teh BH, Ong TS, Muhammad H, Selamat AI and Chen A (2022), Does the utilisation of new energy and waste gas resources contribute to product innovation from the perspective of a circular economy? Evidence from China.
Front. Energy Res. 10:918425.
doi: 10.3389/fenrg.2022.918425

Does the utilisation of new energy and waste gas resources contribute to product innovation from the perspective of a circular economy? Evidence from China

Xiangyuan Ao[1], Boon Heng Teh[2]*, Tze San Ong [3]*, Haslinah Muhammad[1], Aslam Izah Selamat[1] and Anqi Chen[1,4]

[1]School of Business and Economics, Universiti Putra Malaysia, Seri Kembangan, Malaysia, [2]Faculty of Management, Multimedia University Malaysia, Cyberjaya, Malaysia, [3]Department of Business Administration, Daffodil International University, Dhaka, Bangladesh, [4]School of Economics and Management, East China Jiaotong University, Jiangxi, China

These days energy-related enterprises started using a fancy terminology called circular economy (CE) to display their progress in opting for innovative approaches to mitigate carbon emissions and waste gas released in the enterprise during the operation. Hence, this paper examines whether there is any mediating role of innovation from a CE point of view or not in managing the waste resources and minimising the carbon emission on the innovation and quality of new energy products. For this, secondary data with a sample observation of 608 was selected from Chinese listed enterprises from 2015–2020. The empirical results revealed that the waste resource utilisation by firms is helpful to the quality of their products but does not significantly affect the innovation of their new energy products. In addition, the evidence from developing countries shows that companies' carbon reduction behaviour benefits their new energy product innovation. However, it does not significantly impact the quality of their products. Model validation analyses the existence of corporate waste resource utilisation through corporate new energy product innovation, thereby contributing to corporate product quality. Overall, this paper facilitates enterprises' new energy product development activities and fills the research gap between companies' waste gas resource utilisation and new energy product innovation.

KEYWORDS

carbon emission 1, waste gas resources2, new energy3, reduction4, circular economy5

1 Introduction

With the increase in human and economic activity, the global climate is getting deteriorated, resulting in land and sea warming, rising sea levels, degradation of glaciers, frequent extreme weather events and other acute events that cause disasters. Even the economic downturn associated with the COVID-19 outbreak has failed to

contain the drivers of climate change (The Global Climate Status Report, 2020). As a result, the year 2020 remained as one of the three hottest years on record, with a global average temperature of around 1.2°C higher than temperatures observed in the pre-industrial era (1850–1900). Not only the rise in temperatures but climate change-related disasters are frequently happening in developed and developing countries. Such disasters have become the main concern for governments in developed and developing countries (Del Giudice et al., 2021). So, understanding the environmental impacts due to various initiatives have become mandatory, and at the same time, economic stability should be achieved (Bag et al., 2022).

The circular economy is a concept that has become popular in the last decade and can potentially promote economic stability and sustainable development. However, it has to be implemented only through corporate strategies; only then the true potential can be realised. Considering the energy sector, the circular economy is being promoted widely, especially in the content of waste to energy. More recently, new energy sources such as solar photovoltaics, wind energy, biomass, fuel cells and others have also gained importance in the circular economy context. At the same, new processes and technologies and integrated approaches have also evolved, focusing on net zero or near zero emissions. Such developments attracted energy and other energy-dependent sectors, for instance, iron and steel, paper, and cement. As a result, the captive power plants in the industries started expanding from an innovation point of view.

So, promoting new energy sources is one of the essential options for decarbonising and increasing fuel diversity. Furthermore, with the development of energy saving and emission reduction technologies, the advantages of new energy sources, such as low consumption and low exhaust emissions, are gaining increasing attention. Meeting environmental issues and resource efficiency requirements in manufacturing has become necessary to achieve effective production management. The circular economy aims to reduce resource consumption by slowing, closing and shrinking resource cycles (Geissdoerfer et al., 2017). Through the use of new energy sources and recycled materials, a circular economy can help reduce lifecycle greenhouse gas emissions and resource consumption (Aguilar Esteva et al., 2021). Thus, while the circular economy is inextricably linked to carbon reduction in enterprises, it also promotes product innovation for environmental protection.

The circular economy is a series of abstract concepts (Ripanti & Tjahjono, 2019), and past research has found that the circular economy can provide innovation in environmentally friendly products (Hopkinson et al., 2018) or processes that transform environmentally friendly resources into a variety of usable products and services and ultimately manifest in products or

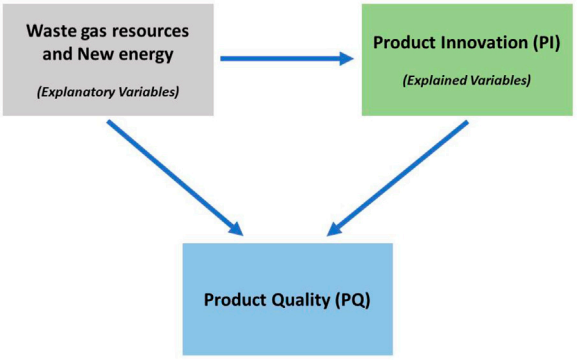

FIGURE 1
Framework highlighting the explanatory and explained variables in waste to energy.

consumers (Lloret 2016). As the evolution of CE shows its multidisciplinary background, Pizzi et al., 2020 argue that approaches from various disciplines such as engineering, economics and ecology have contributed to its development. As a theoretical basis, the circular economy provides a favourable research perspective. There are many perspectives on new energy sources at this stage of research and study, often focusing on new energy products and corporate financing models and the impact of crude oil prices on new energy product innovation (He et al., 2022; Fu & Yang's 2021). Some scholars have focused on recycling within the production cycle of products and the recycling of industrial solid waste (Richa et al., 2017; Martínez-Martínez et al., 2020). However, there is less research on the study of carbon reduction and corporate waste gas resource use in new energy product innovation. So, this study seeks to explore the impact of corporate carbon reduction behaviour and waste body resource use on corporate new energy product innovation and quality. So, we formulated the following research questions; 1). Does carbon emission reduction by enterprises improve new energy product innovation and product quality?; 2). Does waste gas emission utilisation promote environmental innovation by enterprises; and 3). Does waste gas resource utilisation improve product quality through green innovation?

Hence, to answer the above-raised research questions, this study aims to explore whether the enterprises' carbon and greenhouse gas emission reduction promotion is conducive to their product innovation and quality improvement. This study also attempts to analyse the mediating effect of new energy product innovation between product quality as well as waste gas emission utilisation. The past literature has suggested a higher expected return on investment for new energy products and technology innovation (He et al., 2022). This study also considers the relationship between innovation and quality of new energy products and whether there are potential

TABLE 1 Descriptive statistics.

Variable	Obs	Mean	Std. Dev	Min	Max
PI	608	6.862	19.11	0	139
CE	608	116648.8	3679198	0	3.23e + 08
GHG	608	123028.3	591434.6	1.86	3724022
Size	608	22.213	1.289	19.939	26.063
TQ	608	2.992	10.717	0.219	983.491
FirmAge	608	2.939	0.230	2.080	3.555
indep	608	0.377	0.0538	0.308	0.6
PQ	608	0.246	1.315	0	9

Note: PI, product innovation; CE, carbon emission; GHG, greenhouse gas emission; PQ, product quality; FirmAge, firm's age; Indep, independent director; TQ, tobin's Q.

channels for more linkages between new energy product innovation and the quality of products using waste gas resources. The impact of the endogeneity problem of the variables on the regression results is quite often raised in the literature, which is also addressed in this study by proposing a firm fixed effects model.

The manuscript is structured in three sections. Section 2 presents the framework and data sources. Section 3 presents the sample selection and models used for the analysis. In Section 4, the observed results are presented with a brief discussion, followed by conclusions and future work in Section 4.

2 Framework and data collection

Based on the objective, we have formulated the research framework shown in Figure 1. The framework consists of two main variables: Explanatory and explained. The explanatory variables are the waste gas resources, exhausts and any other energy type in the firm (that includes renewables too). The explained variables are the product innovation approaches used in the firm. In the below subsections, these two variables are clearly explained along with control variables, which collectively would affect the product quality in the firm.

2.1 Explanatory variables

According to Fu & Yang's (2021) research on product measures for a new energy firm, most enterprises reuse waste gas resources for industrial production. So, a firm's waste gas resource utilisation and carbon emission reductions can be the core explanatory variables. These can be measured or collected from the greenhouse gas emissions and the firm's carbon emission reduction reports. Cheng et al. (2021) also state that greenhouse gas emission reduction of enterprises can be a good standard to measure waste gas resource utilisation. The data source for greenhouse gas and carbon emission reduction is the China Industrial Enterprises Database (2015–2020).

2.2 Explained variables

The explained variable is considered to be the firm's new energy product innovation, which is measured by the firm's product-related new energy patents (Bag et al., 2022; He et al., 2022). The firm's product innovation data is obtained from the China Research Data Service (CNRDS). In addition, information on product quality is extracted from Corporate Social Responsibility (CSR) and financial data, and the Production Quality (PQ) variable is measured by the product quality score disclosed in the CSR.

2.3 Control variables

Control variables are chosen to assess the impact of carbon emission reduction and exhaust gas resources on new energy products' innovation and product quality and exclude other confounding factors. The control variables, the firm's age, size and Tobin's Q are represented by Indep, FirmAge, Size, and TQ, respectively. These variables are obtained from the firms' annual financial reports, and the firm's financial information is obtained from the China Stock Market Accounting Research Database (CSMAR).

3 Sample selection and methodology

3.1 Sample selection

The selected sample for this study is the panel data of listed enterprises in mainland China. An adequate sample size of 608 enterprises listed between 2015–2020 was obtained. For all these 608 enterprises or firms, the data related to three variables (explanatory, explained, and control) is collected using the resources mentioned in Section 2.

3.2 Model setting

For every enterprise or firm, our focus is mainly on understanding the impact of carbon emission reduction and exhaust pollutants on the innovation of new energy products from a circular economy perspective. For this, we developed the fixed effects models briefly presented below:

Model 1: Aims to explore the impact of corporate carbon emission reduction on new energy product innovation, as given in Eq. 1.

$$PI = a_0 + a_1 * GHG + FirmSize + TQ + Indep + Firmage + e_1 \quad (1)$$

where PI is the product innovation, a_0 is the intercept, a_1 is the co-efficient for GHG, GHG is the greenhouse gas emission, e_1 is the residual variance.

Model 2: Aims to explore whether greenhouse gas emission reduction promotes enterprise environmental protection innovation, as given in Eq. 2.

$$PI = a_0 + a_2 * CE + Size + TQ + Indep + Firmage + e_2 \quad (2)$$

where PI is the product innovation, a_0 is the intercept, a_2 is the co-efficient for CE, CE is the carbon emission reduction, e_2 is the residual variance.

Model 3: investigate the influence of enterprise carbon emission reduction on product quality, as given in Eq. 3.

$$PQ = a_0 + a_3 * GHG + Size + TQ + Indep + Firmage + e_3 \quad (3)$$

where PQ is the product quality, a_0 is the intercept, a_3 is the co-efficient for GHG, GHG is the greenhouse gas emission, e_3 is the residual variance.

Model 4: analyses whether greenhouse gas emission reduction can improve product quality through green innovation, as given in Eq. 4.

$$PQ = a_0 + a_4 * CR + Size + TQ + Indep + Firmage + e_4 \quad (4)$$

where PQ is the product quality, a_0 is the intercept, a_4 is the co-efficient for CE, CE is the carbon emission reduction, e_4 is the residual variance.

4 Results and discussion

This section presents the data analysis results as well as the main empirical results and the discussion. The descriptive

TABLE 2 Correlation matrix.

Variable	PQ	PI	CE	GHG	Size	TQ	FirmAge	Indep
PQ	1.000							
PI	0.041***	1.000						
CE	0.354	−0.080	1.000					
GHG	0.006	0.128***	0.994***	1.000				
Size	0.136***	0.399***	−0.015	0.072***	1.000			
TQ	−0.010	−0.047***	−0.016	-0.004	−0.400***	1.000		
Firmage	−0.006***	0.029***	−0.004***	−0.015***	−0.018	0.056***	1.000	
indep	−0.011	−0.014***	−0.021	−0.007	0.165***	−0.112***	−0.030***	1.000

Note: PI: product innovation; CE: carbon emission; GHG: greenhouse gas emission; PQ: product quality; FirmAge: firm's age; Indep: independent director; TQ: Tobin's Q.

TABLE 3 Regression results of enterprise carbon emission and greenhouse gas emission reduction on products.

Variable	(1)	(2)	Variable	(3)	(4)
PI	GHG	CE		GHG	CE
	−0.00000572	0.000000353***	PQ	0.00000198*	−1.99E-09
	(−0.57)	(11.04)		(2.34)	(−0.75)
Indep	69.56	11.80***	Indep	−21.83	−0.269
	(0.35)	(4.32)		(−1.29)	(−1.18)
FirmAge	−74.37	−4.801***	FirmAge	1.599	−0.102*
	(−1.62)	(−9.64)		(0.41)	(−2.43)
Size	17.30*	6.674***	Size	−0.947	0.200***
	(2.35)	(52.82)		(−1.51)	(18.96)
TQ	−6.949	0.304***	TQ	0.414	0.0229***
	(−0.87)	(6.06)		(0.61)	(5.46)
_cons	−177.1	−132.2***	_cons	26.94	−3.791***
	(−0.77)	(−41.10)		(1.38)	(−14.08)
N	30	15,266	N	30	14924

Note: t statistics in parentheses; *p < 0.05, **p < 0.01, ***p < 0.001.
Note: PI, product innovation; CE, carbon emission; GHG, greenhouse gas emission; PQ, product quality; FirmAge, firm's age; Indep, independent director; TQ, Tobin's Q.

TABLE 4 Sobel-goodman mediation tests.

	Coef	Std. Err	Z	P>|Z|
Sobel	−A5.826e-10	2.440e-10	−2.388	0.0169
Goodman-1 (Aroian)	−5.826e-10	2.449e-10	−2.379	0.0174
Goodman-2	−5.826e-10	2.430e-10	−2.398	0.0165
	Coef	Std Err	Z	P>|Z|
A coefficient	3.5e-07	3.2e-08	10.965	0
B coefficient	−0.001651	0.000675	−2.447	0.014
Indirect effect	−5.8e-10	2.4e-10	−2.388	0.017
Direct effect	−1.4e-09	2.7e-09	−0.530	0.596
Total effect	−2.0e-09	2.7e-09	−0.752	0.452

Note: The proportion of total effect that is mediated: 0.2922; The ratio of indirect to direct effect: 0.4128; The ratio of total to direct effect: 1.4128.

statistical analysis of the collected 608 enterprises' sample data is shown in Table 1. The observed correlations between variables are listed in Table 2.

Table 3 reveals the regression results for Models 1–4. Model 1 reported the impact of corporate GHG emission reduction on corporate new energy product innovation. The results reflect that the use of waste gas resources does not have a direct positive impact on the innovation of new energy products, with a correlation coefficient of −0,57. However, for the reduction of carbon emissions (Model 2), the adoption of carbon reduction behaviour by companies has a significant positive relationship with the innovation of new energy products, with a p-value = 0 (<0.05) and a positive correlation. Furthermore, Model 3 reveals that the use of waste resources significantly affects the quality of a company's products, with a p = 0.028 (<0.05) and a positive correlation coefficient. The results of model 4 show that carbon reduction behaviour does not effectively stimulate product quality and has a negative correlation.

The use of exhaust gas resources in enterprises' new energy innovations is insignificant because new energy product innovations generally use new energy power such as photovoltaics, wind, fuel cells and others. While the use of exhaust gas resources is generally reflected in the innovation process but the technology and systems are mainly considered old or relatively conventional. Therefore, from a technical point of view, there is limited scope to improve the number of patents granted for the use of waste gas resources. In addition, the reason why carbon reduction does not directly improve the quality of a company's products in this study is considered to be that carbon emission reduction behaviour in the production process is not related to the product quality of enterprises. So it will not have a direct impact. However, coming to the economic benefits, the past study by Xue et al. (2019) showed that carbon reductions in the circular model could generate additional revenue. Therefore, carbon reductions from this mode can have significant environmental and economic benefits. Shan et al. (2021) found that green innovation and renewable energy reduce carbon emissions when put under this approach in a given enterprise or firm, depending upon the industrial operations they perform. Thus, the model proposed in this study is further analysed to understand the relationship between corporate waste resource utilisation and corporate new energy product innovation, thereby contributing to corporate product quality. For this, a Sobel test is performed, and the results can be seen in Table 4.

Although in the previous model, corporate waste resource utilisation did not have a positive impact on new energy product innovation, the results of the Sobel test show that there is a partial mediating pathway existing for corporate waste resource utilisation through new energy innovations and thus have an impact on the quality of the firm's products. The mediating effect accounted for 29.22% of the total effect, and the ratio of indirect to direct effect was 41.28%.

5 Conclusion and future work

The circular economy is a concept promoted by policymakers and businesses worldwide (Iaquaniello et al., 2018), emphasising waste as a way to close the cycle and minimise resource use (Hollins et al., 2017). Therefore in a circular economy, in addition to using and reducing waste, there needs to be an incentive to make products that do not become waste, which is product innovation (Iaquaniello et al., 2018). The empirical results of this paper show a model of the impact of carbon emission reduction and waste resource utilisation on the innovation and quality of new energy products for Chinese listed enterprises with a total sample observation of 608. It also analyses the impact of carbon emission reduction and waste resource utilisation of enterprises on new energy product innovation and quality based on a circular economy perspective, as well as the mediating role of new energy innovation. The model results of this paper show that the use of waste gas resources by companies is an important factor in improving the quality of their products. However, it does not positively affect the innovation of new energy products. In addition, the model results reveal that companies' carbon reduction behaviour is beneficial to their new energy product innovation but has a negative impact on their product quality that warrants our attention. The results of this paper are beneficial to the company's internal governance, such as the R&D and innovation activities of new energy products and

the control of product quality. At the same time, the findings of this study will fill the research gap between companies' waste gas resource utilisation and new energy product innovation. However, this paper only focuses on Chinese companies from 2015 to 2020. Future research could consider other long-term results or markets in other countries or regions.

Data availability statement

The original contributions presented in the study are included in the article/Supplementary Material, further inquiries can be directed to the corresponding authors.

Author contributions

All authors listed have made a substantial, direct, and intellectual contribution to the work and approved it for publication.

Funding

The authors extend their gratitude to Universiti Putra Malaysia for this research opportunity. This work was supported by Grant number FRGS/1/2020/SS01/MMU/02/4.

Conflict of interest

The authors declare that the research was conducted in the absence of any commercial or financial relationships that could be construed as a potential conflict of interest.

Publisher's note

References

Aguilar Esteva, L. C., Kasliwal, A., Kinzler, M. S., Kim, H. C., and Keoleian, G. A. (2021). Circular economy framework for automobiles: Closing energy and material loops. *J. Ind. Ecol.* 25 (4), 877–889. doi:10.1111/jiec.13088

Bag, S., Dhamija, P., Bryde, D. J., and Singh, R. K. (2022). Effect of eco-innovation on green supply chain management, circular. economy capability, and performance of small and medium enterprises. *J. Bus. Res.*, 141, 60–72. doi:10.1016/j.jbusres.2021.12.011

Cheng, L., Liu, Y., Lou, X., Chen, Z., and Yang, Y. (2021). Does technology conglomeration promote innovative outcomes of new energy vehicle enterprises? The moderating effect of divisive faultlines. *J. Clean. Prod.*, 324, 129232. doi:10.1016/j.jclepro.2021.129232

Del Giudice, M., Chierici, R., Mazzucchelli, A., and Fiano, F. (2021). Supply chain management in the era of circular economy: The moderating effect of big data. *Int. J. Logist. Manag.* 32 (2), 337–356. doi:10.1108/IJLM-03-2020-0119

Fu, Q., and Yang, Z. (2021). Mode selection and risk estimation of financing in new energy automobile enterprises. *Energy Rep.*, 7, 330–337. doi:10.1016/j.egyr.2021.06.053

Geissdoerfer, M., Savaget, P., Bocken, N. M. P., and Hultink, E. J. (2017). The Circular Economy – a new sustainability paradigm? *J. Clean. Prod.* 143, 757–768. doi:10.1016/j.jclepro.2016.12.048

The Global Climate Status Report (2020). NOAA national centers for environmental information, state of the climate: Monthly global climate report for annual 2020. Available at: https://www.ncei.noaa.gov/access/monitoring/monthly-report/global/202013.

He, J., Li, J., Zhao, D., and Chen, X. (2022). Does oil price affect corporate innovation? Evidence from new energy vehicle enterprises in China. *Renew. Sustain. Energy Rev.*, 156, 111964. doi:10.1016/j.rser.2021.111964

Hollins, O., Lee, P., Sims, E., Bertham, O., Symington, H., Bell, N., et al. (2017). *Towards a circular economy–Waste management in the EU*. STOA–EU. 978-92-846-1548-3. Available at: https://www.europarl.europa.eu/at-your-service/en/stay-informed/research-and-analysis.

Hopkinson, P., Zils, M., Hawkins, P., and Roper, S. (2018). Managing a complex global circular economy business model: Opportunities and challenges. *Calif. Manag. Rev.* 60 (3), 71–94. doi:10.1177/0008125618764692

Iaquaniello, G., Centi, G., Salladini, A., Palo, E., and Perathoner, S. (2018). Waste to chemicals for a circular economy. *Chem. Eur. J.* 24, 11831–11839. doi:10.1002/chem.201802903

Lloret, A. (2016). Modeling corporate sustainability strategy. *J. Bus. Res.* 69 (2), 418–425. doi:10.1016/j.jbusres.2015.06.047

Martínez-Martínez, S., Pérez-Villarejo, L., Eliche-Quesada, D., Sánchez-Soto, P. J., Christogerou, A., Kanellopoulou, D. G., et al. (2020). New waste-based clinkers for the preparation of low-energy cements. A step forward toward circular economy. *Int. J. Appl. Ceram. Technol.* 17 (1), 12–21. doi:10.1111/ijac.13390

Pizzi, S., Caputo, A., Corvino, A., and Venturelli, A. (2020). Management research and the UN sustainable development goals (SDGs): A bibliometric investigation and systematic review. *J. Clean. Prod.* 276, 124033. doi:10.1016/j.jclepro.2020.124033

Richa, K., Babbitt, C. W., and Gaustad, G. (2017). Eco-efficiency analysis of a lithium-ion battery waste hierarchy inspired by circular economy. *J. Industrial Ecol.* 21 (3), 715–730. doi:10.1111/jiec.12607

Ripanti, E. F., and Tjahjono, B. (2019). Unveiling the potentials of circular economy values in logistics and supply chain. management. *Int. J. Logist. Manag.* 30 (3), 723–742. doi:10.1108/IJLM-04-2018-0109

Shan, S., Genç, S. Y., Kamran, H. W., and Dinca, G. (2021). Role of green technology innovation and renewable energy in. Carbon neutrality: A sustainable investigation from Turkey. *J. Environ. Manag.* 294, 113004. doi:10.1016/j.jenvman.2021.113004

Yu-nan, X., Wei-xin, L., Wang, H., and Yu-jie, Y. (2019). Environmental and economic benefits of carbon emission. reduction in animal husbandry via the circular economy: Case study of pig farming in Liaoning, China. *J. Clean. Prod.* 238, 117968. doi:10.1016/j.jclepro.2019.117968

frontiers | Frontiers in Energy Research

ORIGINAL RESEARCH
published: 08 July 2022
doi: 10.3389/fenrg.2022.910565

Analysis of Regional Carbon Emission Decoupling Coupling in China Based on ArcGIS Analysis-Empirical Evidence From Urban-Rural Integration in Fujian Province

Renshan Xie[1], *Dongye Yu*[1], *Xingyuan Zhang*[1], *Ze Yang*[1], *Jianzhou Yang*[1]* *and Jie Ye*[2]*

[1]School of Economics and Management, Fujian Agriculture and Forestry University, Fuzhou, China, [2]Business School, Quanzhou Normal University, Quanzhou, China

OPEN ACCESS

Edited by:
Idiano D'Adamo,
Sapienza University of Rome, Italy

Reviewed by:
Mohammad Haseeb,
Wuhan University, China
Meena Kumari Kolli,
Indian Institute of Technology Bombay, India

***Correspondence:**
Jianzhou Yang
yjzfafu@163.com
Jie Ye
yejie0126@126.com

Specialty section:
This article was submitted to Sustainable Energy Systems and Policies, a section of the journal Frontiers in Energy Research

Received: *01 April 2022*
Accepted: *17 June 2022*
Published: *08 July 2022*

Citation:
Xie R, Yu D, Zhang X, Yang Z, Yang J and Ye J (2022) Analysis of Regional Carbon Emission Decoupling Coupling in China Based on ArcGIS Analysis-Empirical Evidence From Urban-Rural Integration in Fujian Province. Front. Energy Res. 10:910565. doi: 10.3389/fenrg.2022.910565

China's ambitious measures for developing a low-carbon economy led to the "double carbon" target initiation. Under this national goal, reaching peak carbon emissions by 2030 is desired. This should not come at the cost of economic growth; which means carbon emissions can be reduced while economic growth can be achieved simultaneously. To realise this strategic reform, the first pilot ecological civilisation zone in Fujian Province of China was initiated; its outcome is set to be the responsible case for such initiations aiming at increased low-carbon economy development. Therefore, it is essential to investigate the relationship between carbon emissions and economic growth based on the evidence. Hence, we applied a model that combines the Tapio and Coupled coordination. Combining the Tapio and the coupled coordination models allows us to analyse carbon emissions and economic growth in Fujian Province over 20 years, i.e., 2001–2020. First, we divided the urban-rural integration process into four stages following China's Five-Year Plan (FYP): T1 (2001–2005), T2 (2006–2010), T3 (2011–2015), and T4 (2016–2020). Second, ArcGIS mapping was used to represent the spatial evolution pattern of low-carbon economic development in Fujian Province. We observed that the low-carbon economy in Fujian Province had reached a point where the economic growth rate has already exceeded its carbon emission growth rate and is currently in a weak decoupling state. In addition, there observed a bifurcation pattern between carbon emissions and economic growth, especially in the coastal cities that are out of balance, whereas the inland cities are being coordinated. Overall, it is observed that the concept of ecological civilisation is crucial for China to achieve the "double carbon goal," and it is high time to create accelerating measures that guide the integration of urban and rural areas in the future with appropriate infrastructure.

Keywords: China, Fujian; carbon emissions, urban-rural integration, decoupling model, coupled coordination model

1 INTRODUCTION

1.1 Background

In the ninth meeting of the 2021s Central Finance and Economics Commission, China proposed incorporating "carbon neutrality and carbon peaking" measures as part of the overarching design of ecological civilisation (Wang et al., 2021). This incorporation insists on reducing carbon emissions and following a path of low-carbon sustainable development (Wang et al., 2021). But there lies the biggest macroscopic challenge as China's economy continues to develop at high speed. On the other side, the energy demand for the "high carbon" structure has not yet reached saturation. On top of it, the phenomenon of industrial and urban-rural incoordination in economic development is highly seen. So, all these issues collectively made the carbon emission reduction task a more challenging one. The concept of urban-rural integration has been around since the last century. China released the Blue Book on Urban-Rural Integration, in which the achievements of the integration process have been summarised and discussed from the perspective of urban-rural planning, industrial layout, infrastructure development (primarily the critical services like energy, healthcare, road etc.) and public services (Baoxin et al., 2019). Also, the new development path of "four synchronisations" (industrialisation, informatisation, urbanisation, and agricultural modernisation) heavily dependent on energy is discussed. So, the aim was to integrate the urban and rural areas to promote economic, environmental, and urban-rural development in coordination. However, in such complex approaches, understanding the synergies would be better. Therefore, the critical issue is the relationship between carbon emissions and economic growth as well as urban-rural integration. At the same time, exploring synergistic ways to promote high-level economic development and an ecological environment are also crucial, especially when implementing the new development concept in line with sustainable economic principles.

1.2 Literature Review

To understand the problem's complex nature, we conducted a literature survey on the four aspects that are deemed necessary for the investigated concept. These four include the relationship between carbon emissions and economic growth, decoupling analysis, the impact of energy infrastructure on carbon emissions, and urbanisation on carbon emissions.

1.2.1 The Relationship Between Carbon Emissions and Economic Growth

When we looked at the literature exploring the relationship between carbon emissions and economic growth, there has been considerable research on China's and China's contiguous regions, such as the Jin-Shaan-Menggu region 2), the Yellow River basin region 3), and the Yangtze River economic belt 4). All the studies by (Wu et al., 2019; Mo and Wang., 2021; Tian and Lin., 2021) have concluded that the relationship between the two gradually tends toward low-carbon economic development, providing a scientific theoretical basis for adopting emission reduction measures to reach the peak in each region. In another study, Zhao et al. (2022) argued that carbon emissions and economic growth are closely related and generally do not cross over in the long run; this view was also supported by (Myszczyszyn and Suproń, 2021) study of carbon emissions and economic growth in V4 countries (namely Czech Republic, Hungary, Poland, and Slovakia). However, there is still a degree of dependence of economic growth on carbon emissions.

1.2.2 Decoupling Analysis of Carbon Emissions

Peng et al. (2011) looked at the spatial and temporal decoupling of China's economic growth and carbon emissions at the national and regional levels. They concluded that China would remain in a weak state of decoupling for a long time, and low-carbon emission reduction technology has yet to impact the economy as a whole practically (Peng et al., 2011). Wang B et al. (2021) used the Mann-Kendall (MK) trend test to identify the characteristics of China's provincial carbon emissions from 2000 to 2018 and classified them into high and low types. Also, their empirical study showed that China's carbon emissions generally showed a spatial pattern of "high in the east, low in the west, high in the north and low in the south" (Wang et al., 2021). From the perspective of counties, Ji and Xue., 2022 investigated the decoupling of carbon emissions in Jiangsu Province, China, and concluded that economic growth and carbon emission reduction did not always happen at the same time. However, the decoupling effect of carbon emissions in counties gradually increased over time Ji and Xue., 2022. Liu et al. (2021), enriched Energy-Economy-Environment (3E) system theory. They then analysed the coupling relationship of carbon emission reduction and economic growth and environmental protection with China's national conditions after clarifying the coupling mechanism of carbon emission reduction-economic growth-environmental protection in provincial areas. Based on clarifying the coupling mechanism, Liu et al. (2021) assessed the degree to which carbon emission reduction, economic growth, and environmental protection are coupled and coordinated in the Chinese provinces. Also, the coupling and coordinated comprehensive evaluation index system of "provincial carbon emission-economic growth-environmental protection" was constructed and found that the degree of coupling and coordination of the 3E system is "high in the southeast and low in the middle and west" (Liu et al., 2021).

1.2.3 Impact of Energy Infrastructure on Carbon Emissions

Usman et al. (2021) looked at the 15 highest carbon-emitting countries from the context of economic inclusion over renewable and non-renewable energy projects. In the analysis, Usman et al. (2021) observed a strong dependency on the cross-sectors; then, only such projects will help in reducing environmental degradation and boost economic growth. Usman and Makhdum., 2021, in another study, investigated taking the data from the year 1990–2018 and observed a dynamic linkage between ecological footprint, agriculture value-added, forest area, non-renewable and renewable energy use, and financial development in BRICS-T countries (Brazil, Russia, India,

China, South Africa, and Turkey). Likewise, Balsalobre-Lorente et al. (2022) investigated the relationship between economic complexity and environmental degradation in the countries of the PIIGS (Portugal, Ireland, Italy, Greece, and Spain). They found a unidirectional causality link between the energy infrastructure and the amount of emission mitigated. Huang et al., 2022 investigated the moderating effect of ICT and renewable energy and human capital in E-7 (developing countries) and G-7 (developed countries). The observed effect was significantly positive, highlighting a high chance of reducing ecological footprint levels in E-7 and G-7 countries due to this moderating effect.

1.2.4 Impact of Urbanisation on Carbon Emissions

The urbanisation process will inevitably have an impact on increasing the use of energy, resulting in the emission of large amounts of greenhouse gases such as CO_2 (Haouraji et al., 2021; Mata et al., 2021; Pang et al., 2021). Ding et al. (2021) analysed the impact of 182 prefecture-level cities in China on carbon emissions during rapid urbanisation. They found that urban construction increases the growth of carbon emissions (Ding et al., 2021). Liu et al. (2022) found that under China's new urbanisation scenario, the population-land-economic urbanisation (PLEU) coupling coordination degree has an inverted U-shaped effect on carbon emissions and gradually tends to decrease as the PLEU coupling coordination degree is high to a certain degree (Liu et al., 2022). In their study of 283 cities in China, Zhou et al. (2021) evaluated the impact of multidimensional urbanisation on carbon emissions efficiency, finding that multidimensional urbanisation exhibits spatial heterogeneity characteristics for carbon emissions efficiency and carbon emission efficiency is gradually enhanced through the process of multidimensional urbanization. Xiao, (2012) used factor analysis to measure rural carbon emissions in Hubei Province in the process of urban-rural integration and concluded that urban-rural integration is positively related to rural carbon emissions. Shi et al. (2021) used the Epsilon Based Measure (EBM) super-efficiency model, kernel density estimation, and Global Malmquist-Luenberge (GML) index analysis to study the efficiency of urban-rural integration development in the Yangtze River Delta and its dynamic evolution characteristics. They concluded that economically developed areas of the Yangtze River Delta have lower efficiency of urban-rural integration than economically less developed areas, the polarisation of urban-rural integration development has serious consequences, and redundancy of carbon emissions negatively affect urban-rural integration development (Shi et al., 2021).

Based on the literature review carried out in the above paragraphs, it can be understood that the current studies on the Spatio-temporal coupling relationship between carbon emissions and economic growth are mostly focused on large regions such as national provinces or regional integration. In contrast, the studies on the relationship between urban-rural integration and carbon emissions and economic development, the impact of "four synchronisations," and energy infrastructure are diverse. Their general laws and policy inspirations on carbon emissions and economic growth are more macroscopic, which may not lead to an effective decision. For the diversified characteristics of economic development in provincial areas, especially in distinct regions at the prefecture level, further research is needed on micro-level comparisons.

Therefore, this paper pays special attention to integrating low-carbon transition into the whole process of national economic development requirements, followed by analysing the changes in carbon emissions during different economic development stages in the urban-rural integration process. To realise this strategic reform, the first pilot ecological civilisation zone in Fujian Province of China was analysed as the responsible case aiming to increase low-carbon economy development. We applied the Tapio decoupling model and the coupled coordination model to study the data of Fujian Province and nine prefectures in Fujian Province. ArcGIS method was used to describe the decoupling relationship and spatial-temporal coupling evolution characteristics between carbon emissions and economic growth in Fujian Province to provide a scientific basis and policy inspiration for the smooth promotion of carbon emission reduction in Fujian Province.

The manuscript is structured in five sections; **Section 2** discusses the data collection and methods considered for the analysis. In **section 3**, results are presented and discussed. **Section 4** presented the policy insights, followed by conclusions in **section 5**.

2 DATA COLLECTION AND METHODS

2.1 Data Collection

Carbon emissions and gross domestic product (GDP) are the two key data needed for the investigation. The required data on carbon emissions is collected using the China Carbon Accounting Database (https://www.ceads.net.cn). However, we noticed some missing data; for which we used an approach to estimate the reduction target of carbon emissions intensity based on the 13th 5-year plan of Fujian Province. As we all know, the economic growth is expressed by the GDP; hence the GDP values of prefecture-level cities in Fujian Province over the years. The GDP data are all from the 2002 to 2021 Fujian Statistical Yearbook and the statistical yearbooks of prefecture-level cities to avoid the impact of inflation caused by price fluctuations. The real GDP of each region is converted from the nominal GDP of 2001–2020 to the constant price GDP of 2020, with 2001 as the base period. At the same time, given the lag between carbon emissions and economic growth, ensuring authenticity was critical (Wu et al., 2019). To ensure the authenticity of the Spatio-temporal coupling relationship, this paper took 5 years as a stage [divided into four periods: $T_{1\ (2001–2005}$, $T_{2\ (2006–2010}$, $T_{3\ (2011–2015)}$, and $T_{4\ (2016–2020)}$].

Each period also coincides with the national 5-year plan period. This model enables us to examine the decoupling relationship between greenhouse gas emissions and economic growth at different stages of economic development, both by examining the decoupling relationship and the Spatio-temporal relationship.

TABLE 1 | Decoupling elasticity and degree.

Category	Degree of decoupling	△C	△G	Unhooking elasticity
Decoupling	Strong decoupling	<0	>0	E < 0
	Weak decoupling	>0	>0	0 ≤ E < 0.8
	Decline decoupling	<0	<0	E > 1.2
Connect	Expansion link	>0	>0	0.8 ≤ E ≤ 1.2
	Recession link	<0	<0	0.8 ≤ E ≤ 1.2
Negative decoupling	Dilated negative decoupling	>0	>0	E > 1.2
	Weak negative decoupling	<0	<0	0 ≤ E < 0.8
	Strong negative decoupling	>0	<0	E < 0

TABLE 2 | Coupling coordination value and grade division.

Coupling coordination value interval	Level	Degree of coupling coordination
(0.0~0.1)	1	Extremely maladjusted
[0.1~0.2)	2	Severe maladjustment
[0.2~0.3)	3	Moderate disorder
[0.3~0.4)	4	Mild disorder
[0.4~0.5)	5	On the verge of disorder
[0.5~0.6)	6	Barely coordinated
[0.6~0.7)	7	Primary coordination
[0.7~0.8)	8	Intermediate coordination
[0.8~0.9)	9	Good coordination
[0.9~1.0)	10	Quality coordination

2.2 Research Methods

2.2.1 Tapio Decoupling Model

Tapio decoupling elasticity model considered in this study is a further supplement and improvement to the decoupling index model of the Organization for Economic Cooperation and Development (OECD). This model effectively alleviates the calculation deviation caused by the highly sensitive or extreme selection of the initial and final values of the OECD index model and exceedingly improves the objectivity and accuracy of decoupling relationship measurement and analysis (Chen et al., 2022).

The economic growth and carbon dioxide emissions can be calculated using **Eq. 1**.

$$E(c_i, g_i) = \frac{\triangle C_i / C_{iBase}}{\triangle G_i / G_{iBase}} = \frac{(C_{iEnd} - C_{iBase})/C_{iBase}}{(G_{iEnd} - G_{iBase})/G_{iBase}} \tag{1}$$

where, $E(c_i, g_i)$ represents the decoupling elasticity of economic growth and carbon emissions in the i^{th} period; $\triangle C_i$ and $\triangle G_i$ respectively represent the changes in carbon emissions and economic growth in the period i; C_{iEnd} and G_{iEnd} represents the end of C_i and the end of G_i respectively represent the carbon emission and the economic growth value at the end of the i^{th} period; C_{iBase} and G_{iBase} represents respectively represent the carbon emissions and economic growth values of the base period in the i^{th} period.

Generally, the decoupling elasticity state is divided into three categories and eight degrees (see **Table 1**). When the decoupling elasticity E is less than 0, that is, when the rate of change in carbon emissions is negative while the rate of economic expansion is positive, this is an ideal condition for sustainable development of a low-carbon economy, namely, maximised economic benefits while minimising resource consumption (Zhang, 2016).

2.2.2 Coupled Coordination Model

The coupling coordination model can reflect the overall "efficacy" and "synergy" of multiple systems and determine whether the multiple systems are mutually reinforcing at a high level of mutually restricting at a low level. **Table 2** provides a breakdown of the reference coupling coordination degree.

While establishing the coupling and coordination model, it is essential to acknowledge that both positive and negative effects of carbon emissions and economic growth exist in developing a low-carbon economy. Additionally, all original data should be normalised to make the research results more scientific and objective. After eliminating the difference, the data is changed into the same dimensional value, so the variable x_{ijt} is set to represent the sample value of the index j of district i in the period t; The maximum value is a_{ijt}; while the minimum value is b_{ijt} of the index j in the region i at the time period t (Jiang et al., 2017). The processing formula is as follows:

$$\text{GDP has a positive effect}: u_{ijt} = \frac{x_{ijt} - b_{ijt}}{a_{ijt} - b_{ijt}} \tag{2}$$

$$\text{CO}_2 \text{ has a negative effect}: u_{ijt} = \frac{a_{ij} - x_{ijt}}{a_{ijt} - b_{ijt}} \tag{3}$$

where, u_{ij} is represented as the degree of contribution to the efficiency of low-carbon economic construction, and the value range is [0,1]. When $u_{ij} = 0$ means that the system has the worst effect on the construction of a low-carbon economy; When $u_{ij} = 1$ means that the system has the best effect on low-carbon economy development.

In light of this, **Eq. 4** represents the coupling coordination model of carbon emissions and economic growth:

$$D = \sqrt{C * S} \overset{Among}{\Rightarrow} \begin{cases} c = \sqrt[2]{\dfrac{U_1 U_2}{(U_1 + U_2)^2}} \\ s = aU_1 + bU_2 \end{cases} \tag{4}$$

where the notations D, C, and S, represent the degree of coupling coordination, the degree of coupling, and the measure of economic growth system-wide. a and b are the weight

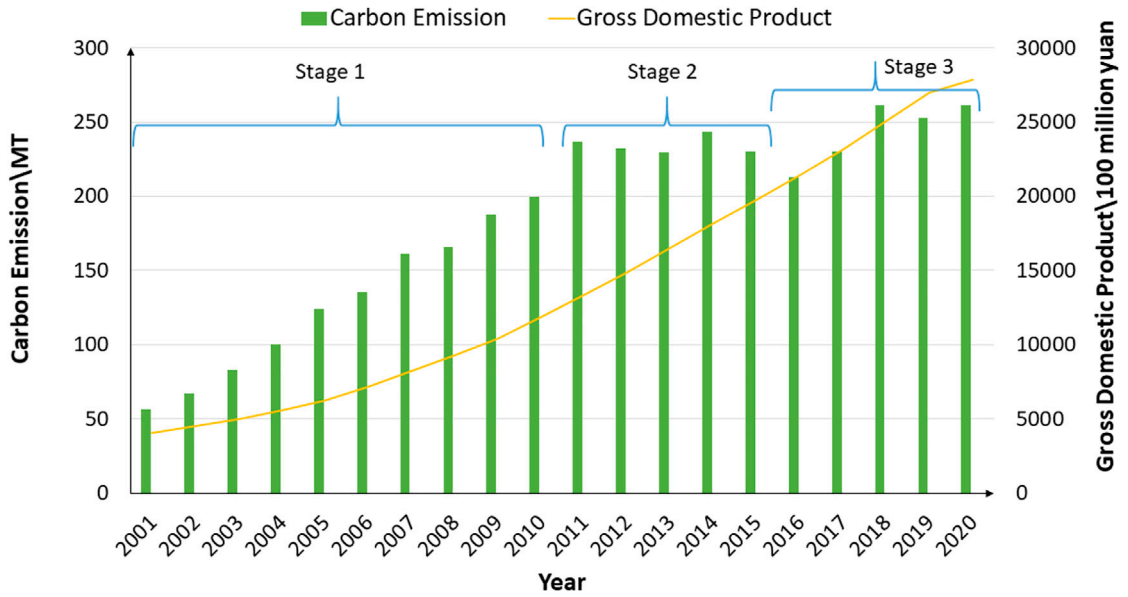

FIGURE 1 | The trend of Carbon Emissions and GDP of Fujian Province from 2001 to 2020.

coefficients of carbon emissions and economic growth. Referring to the existing literature document by (Tian and Lin, 2021), the importance of carbon emissions and economic growth is usually placed in the same position, so the values of *a* and *b* are 0.5.

3 RESULTS AND DISCUSSION

3.1 Analysis of the Trend of Total Carbon Emissions and Gross Domestic Product Changes

The trend of carbon emissions and GDP of Fujian Province from 2001 to 2020 is shown in **Figure 1**. From this, it can be understood that the total carbon emissions show a fluctuating upward trend.

Combined with the Fujian Province's development characteristics, it can roughly be divided into three stages: 2001–2010 is the first stage, carbon emissions continue to rise, the overall layout of China in this period is still the core of GDP growth, urbanisation rate is faster. The same is true for Fujian Province, where the influx of labour from the countryside to the cities accelerated the development of the industry. Industrial development at this time was relatively rough. Agriculture also used a lot of machinery, chemical fertilisers, pesticides, plastic films, etc., resulting in significant carbon emissions at this stage. 2011–2015 is the second stage, where carbon emissions fluctuated and slightly decreased in total. In 2011, Fujian Province issued the "Fujian Urban System Plan (2010–2030)," which set the near, medium, and long term planning period and formulated a complete development strategy for urban-rural integration. During this period, the ecological construction in Fujian Province has continued to increase, with joint efforts to control carbon emissions and absorb and transform carbon pollution. At the same time, the urbanisation rate of Fujian Province reaches 62.7%, the mileage of highways and railroads increases rapidly, and the construction and formation of a modern transportation network increase the total carbon emissions. In contrast, the pilot work of county-level urbanisation is focused on Fujian Province in 2014, accelerating the development of urban-rural integration ideas, thus making the industry more coordinated. Hence, the carbon emissions show a fluctuating trend of first decreasing, then increasing and then decreasing. The third stage is from 2016 to 2020, in which the economic strength of Fujian Province has achieved more remarkable development and the high quality of economic development while focusing on ecological and environmental management and carbon emission control has slowed down the growth rate of carbon emissions. In this stage, Fujian Province is gradually realising a more comprehensive policy system of urban-rural combination and has also made certain efforts in social security, compulsory education, urban-rural water supply integration, etc. The development of urban-rural integration makes urban-rural industries more coordinated, urban-rural residents' lives happier, and economic development more efficient, which reduces the waste of resources and slows down the growth rate of carbon emissions.

3.2 Analysis of How Carbon Emission is Decoupled From Economic Growth

The decoupling elasticity between carbon emission and economic increase of nine prefecture-level cities in Fujian Province from 2001 to 2020 is calculated according to **Eq. 1** and shown in **Table 3**.

TABLE 3 | Decoupling elasticity index of prefecture-level cities in Fujian Province from 2001 to 2020.

	T_1			T_2			T_3			T_4		
	C_1	G_1	E_1	C_2	G_2	E_2	C_3	G_3	E_3	C_4	G_4	E_4
Fuzhou	0.624	0.564	1.105	0.392	0.678	0.578	–0.010	0.508	–0.020	0.124	0.339	0.366
Xiamen	0.694	0.820	0.847	0.440	0.610	0.722	–0.065	0.436	–0.149	0.116	0.322	0.362
Putian	0.553	0.637	0.867	0.470	0.769	0.612	0.125	0.558	0.224	0.097	0.293	0.331
Sanming	0.626	0.449	1.393	0.422	0.701	0.602	–0.096	0.484	–0.199	0.112	0.305	0.368
Quanzhou	0.650	0.629	1.034	0.371	0.678	0.547	–0.063	0.501	–0.126	0.117	0.312	0.374
Zhangzhou	0.572	0.495	1.156	0.398	0.702	0.567	0.073	0.551	0.132	0.030	0.215	0.138
Nanping	0.613	0.514	1.193	0.373	0.669	0.557	–0.116	0.476	–0.245	0.025	0.219	0.114
Longyan	0.633	0.495	1.279	0.420	0.722	0.581	–0.092	0.488	–0.188	0.103	0.313	0.328
Ningde	0.586	0.480	1.220	0.398	0.741	0.537	–0.034	0.526	–0.065	0.082	0.318	0.258

After analysing the results from **Table 3**, it is evident that in the period of $T_{1\ (2001–2005)}$, the prefecture-level cities in Fujian Province show two decoupling states of expansion, i.e., negative decoupling and expansion connection. However, the observed growth rate of carbon emissions was too fast, except for Xiamen. The decoupling elasticity of Xiamen and Putian is 0.847 and 0.867, respectively. The decoupling elasticity of the other seven prefecture-level cities is greater than 1, and the growth rate of carbon emissions exceeds the growth rate of economic growth. During this period, Fujian Province, as a coastal port province, grasped the improvement opportunity of Chinese accession to WTO. Also, a large number of rural population flocked to cities, which accelerated the urbanisation rate, which led to industrial emissions and waste generated by heavy industries such as petrochemicals and metallurgy and steel making a pronounced increase. As a result, the overall carbon emissions increased.

In the period of $T_{2\ (2006–2010)}$, the decoupling status of Fujian prefecture-level cities has been significantly better than that of $T_{1\ (2001–2005)}$. The decoupling elasticity of all prefecture-level cities has exceeded the critical value of 0.8, reaching the weak decoupling status. It can be seen that the task of optimising the quality of ecological protection and environment launched in Fujian Province in the 11th Five-Year Plan has been quite effective. The growth rate of carbon emissions has slowed down. In contrast, the economy has grown at a high rate, and all prefecture-level cities have achieved the provincial targets for saving energy and reducing carbon emissions. In Fujian Province, urbanisation has accelerated since this period. However, the government has also been conducting waste and sewage treatment, which to a certain extent reduced the problem of the rapid increase in carbon emissions brought about by rapid urbanisation. Fujian Province has also been committed to agricultural forestry issues during this period, improving rural productivity and promoting the coordinated development of urban and rural areas.

In the period $T_{3\ (2011–2015)}$, Putian City and Zhangzhou City are in a highly weak decoupling; in the short term, seven prefecture-level cities are in a strong decoupling state and have reached the most desirable state of low-carbon economic development by maintaining positive economic development while the growth rate of carbon emissions is in a negative value. Ningde, Sanming, and Longyan have the most obvious improvement in decoupling elasticity, from negative decoupling in $T_{1\ (2001–2005)}$ to strong decoupling in $T_{3\ (2011–2015)}$. It is mainly due to the "12th Five-Year Plan" period that Fujian Province accelerated the construction of ecological provinces, strengthened the development and application of new technologies, new equipment, new products for energy conservation and emission reduction, and effectively controlled the total emissions of sulfur dioxide and other major pollutants. During this period, Fujian Province has put forward a clear vision of urban-rural integration, so it has carried out environmental construction and protection, public service facilities construction, etc. During this time, the concept of urban-rural integration has gradually taken root in people's hearts. Also, the domestic waste has been reasonably disposed of, energy-saving and emission reduction in industry, and more collaborative development among industries, further reducing carbon emissions. It is noteworthy that in this development stage, Fujian Province specifies that the carbon emission intensity should be reduced by 17.5% (Lin, 2012), resulting in a significant decrease in the GDP growth rate of each prefecture-level city in the $T_{3\ (2011–2015)}$ period compared with the $T_{2\ (2006–2010)}$ period. Accordingly, the concept of sustainable and green development has begun to take shape in the 12th Five-Year Plan period. The concept of green and high-quality, sustainable development took shape during the 12th Five-Year Plan period, avoiding the pursuit of high economic increase at the expense of the ecological environment.

In the $T_{4\ (2016–2020)}$ period, China has transitioned from a fast-growing to a high-quality development stage, emphasising the organic combination of ecological civilisation construction and economic development to achieve sustainable economic and social improvement (Ma, 2019). "During the 13th Five-Year Plan period, the decoupling elasticity index of Fujian Province has rebounded in all prefecture-level cities, with an average increase of 0.36 units compared with the $T_{3\ (2011–2015)}$ period, but it is still in a fragile decoupling state, and the low-carbon economic development trend is relatively stable. The increase in urbanisation rate and the increase in domestic waste, etc., in Fujian Province during this period, together with its promotion of the whole industrial chain of the petrochemical industry, are the main reasons for the rebound in carbon emissions. However, the urban-rural integration in Fujian Province has progressed during this period. The policy system of urban-rural integration is gradually improved, the concept of coordinated urban-rural

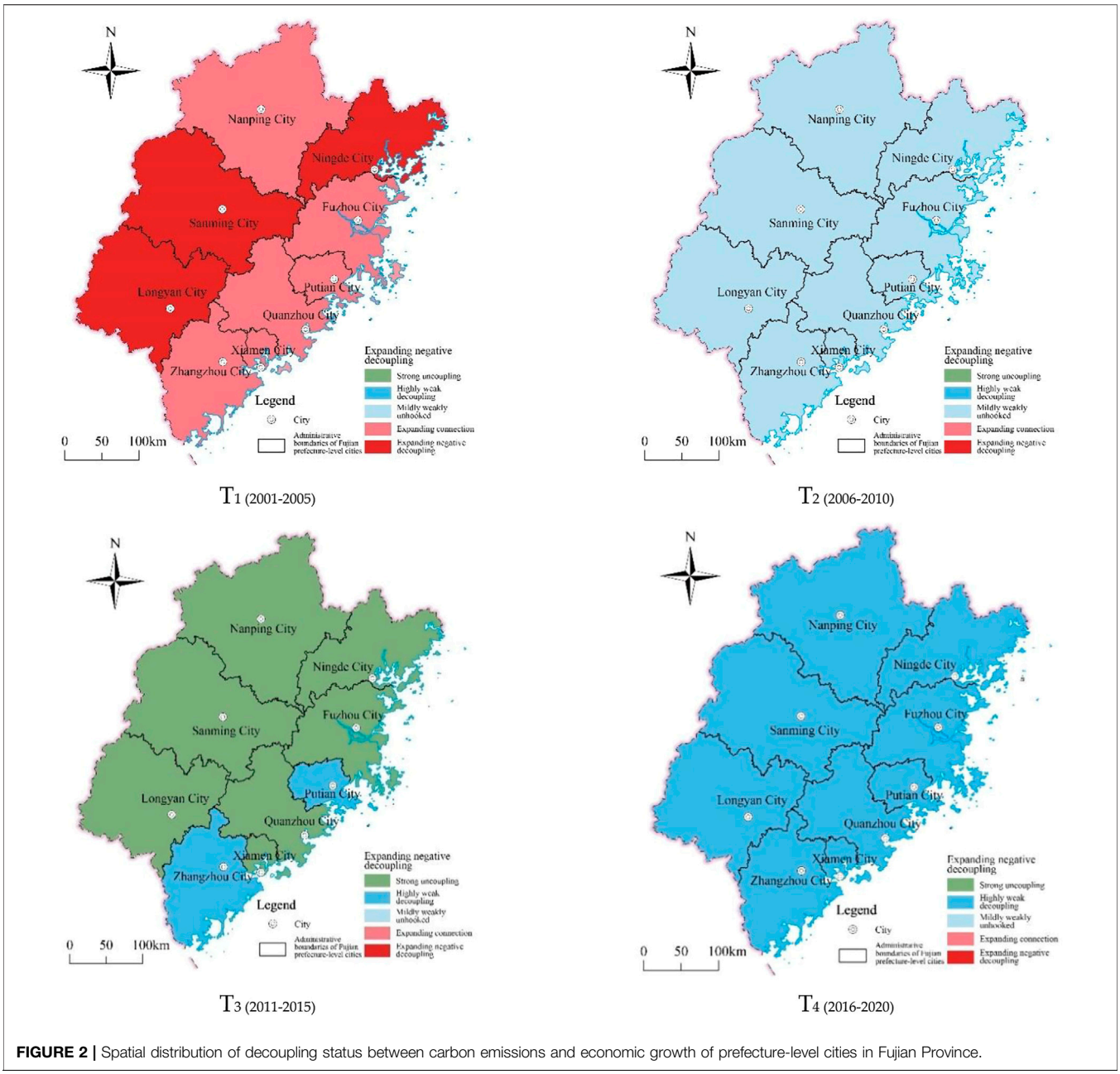

FIGURE 2 | Spatial distribution of decoupling status between carbon emissions and economic growth of prefecture-level cities in Fujian Province.

development is gradually popularised, and the industrial and agricultural increasing urban-rural integration is more coordinated. In addition, the government is committed to environmental construction and reasonable treatment of domestic waste while strengthening other areas. These include the total energy consumption and intensity constraints and supporting the optimisation of the development of the regional carbon emission rate to prioritise reaching the peak. As a result, from a comprehensive view of Fujian Province's decoupling seem still in a better state. Also, the optimisation and integration of industry make the GDP growth rate more than twice the growth rate of carbon emissions. From the spatial perspective, the decoupling index of prefecture-level cities in Fujian Province gradually tends to be in an overall good state through the polarisation between the east and west with an expanding negative decoupling state and the north and south with an expanding connected state. The differences between regions gradually decrease, see **Figure 2**.

3.3 The Coupling and Coordination Degree of Economic Growth and Carbon Emissions: A Correlation Analysis

The coupling and coordination degree of carbon emission and economic growth in Fujian Province from 2001 to 2020 is mainly on the verge of dissonance and barely coordinated. In general, the

TABLE 4 | The degree of coupling and coordination between carbon emissions and economic growth in Fujian Province between 2001 and 2020.

Prefecture-level city	$T_{1\ (2001–2005)}$	$T_{2\ (2006–2010)}$	$T_{3\ (2011–2015)}$	$T_{4\ (2016–2020)}$
Fuzhou city	◆	○	○	△
Xiamen city	△	○	△	△
Putian city	◆	○	○	△
Sanming city	◆	○	◆	◇
Quanzhou city	◆	○	△	△
Zhangzhou city	◆	○	○	△
Nanping city	△	○	△	◇
Longyan city	◆	○	◆	○
Ningde city	◆	○	△	△

Note: Mild disorder ◆, Impending disorder △, Reluctant coordination ○, Primary coordination ◇.

coupling and coordination degree of carbon emissions and economic growth in Fujian Province has experienced a change from mostly dissonance to mostly coordination in the past 20 years, reflecting that most regions in Fujian Province have controlled carbon emissions to a certain extent while promoting economic growth. **Table 4** takes 5 years as an observation period and divides the coupling coordination degree of each prefecture-level city in Fujian into four observation periods over 20 years. This explains the differentiated characteristics of the coupling coordination degree of each prefecture-level city in Fujian Province in different observation periods.

In the first observation period, the degree of coupling coordination in Fujian Province was out of balance, among which seven cities reached a mild level of dissonance, while Xiamen and Nanping did not reach a mild level of dissonance but were on the verge of dissonance; the possible reason was that the economic development of Fujian Province was still dominated by rough and labour-intensive manufacturing industries. The greenhouse gases produced in the production process were not effectively controlled. In the second observation period, Fujian Province changed its development concept and focused on developing environmental industries while upgrading traditional manufacturing industries so that the coupling and coordination between carbon emissions and economic growth in the whole Fujian Province reached a barely coordinated level in this period. In the third observation period, the degree of coupling and coordination decreases in most regions of Fujian Province, and the degree of coupling in Sanming and Longyan even reaches a slight disorder. During this period, the economic strength of Fujian Province continues to increase, and the regional GDP grows rapidly. However, high energy-consuming industries still dominate, and high-tech new industries are not yet mature. Each prefecture-level city's coupling and coordination degree in Fujian Province is steadily increasing in the fourth observation period. Compared with other regions, the coupling and coordination degree of Sanming City, Nanping City, and Longyan City, located in the mountainous area of northwestern Fujian Province, increases, and the coupling and coordination degree of Sanming City and Nanping City reaches the primary coordination.

To show the coupling and coordination between carbon emissions and economic growth in Fujian Province and the regional differentiation characteristics, the results are plotted based on each of the coupling and coordination degrees in the four observation periods and the natural interruption point method as shown in **Figure 3**. The prospect of the regional differentiation characteristics presents the state of polarised distribution, "coastal-inland". The degree of coupling and coordination between carbon emissions and economic growth of inland cities in Fujian Province is better than that of coastal cities. Specifically, the coupling degree of Xiamen and Nanping does not reach the disorder degree in the period 2001-2020. Compared with the other eight regions, the development process of the coupling and coordination degree of Sanming City, although it has experienced two decreases to the mild disorder level, is now located at the top of Fujian Province.

3.4 Discussion

Based on the analysed results in **sections 3.1–3.3**, a discussion was carried out to clearly understand the relationship between carbon emission and economic growth in different stages of urban-rural integration. In addition, the discussion is extended to shred some views on green economy rebound possible.

3.4.1 Relationship Between Carbon Emission and Economic Growth

In the $T_{1\ (2001–2005)}$ period, there was no urban-rural integration planning in Fujian Province during the 10th Five-Year Plan period. The ecological construction planning focused on agricultural production pollution control, domestic waste treatment, water resources protection, soil erosion control, etc. At the same time, more attention was paid to urbanisation during this period. Even though the transformation of traditional industries was proposed, it mainly focused on improving technology and machinery and equipment levels without focusing on the coordination between urban and rural industries. So, the transformation measures could not do a good job in controlling the carbon emissions of heavy industries and manufacturing industries in the industrialisation process. Therefore, during the 10th Five-Year Plan, the rapid economic development was accompanied by a significant increase in carbon emissions. The decoupling between regional carbon emissions and economic growth in nine prefecture-level cities in Fujian Province was mainly an expansionary link, and the coupling coordination was mainly in a mild disorder.

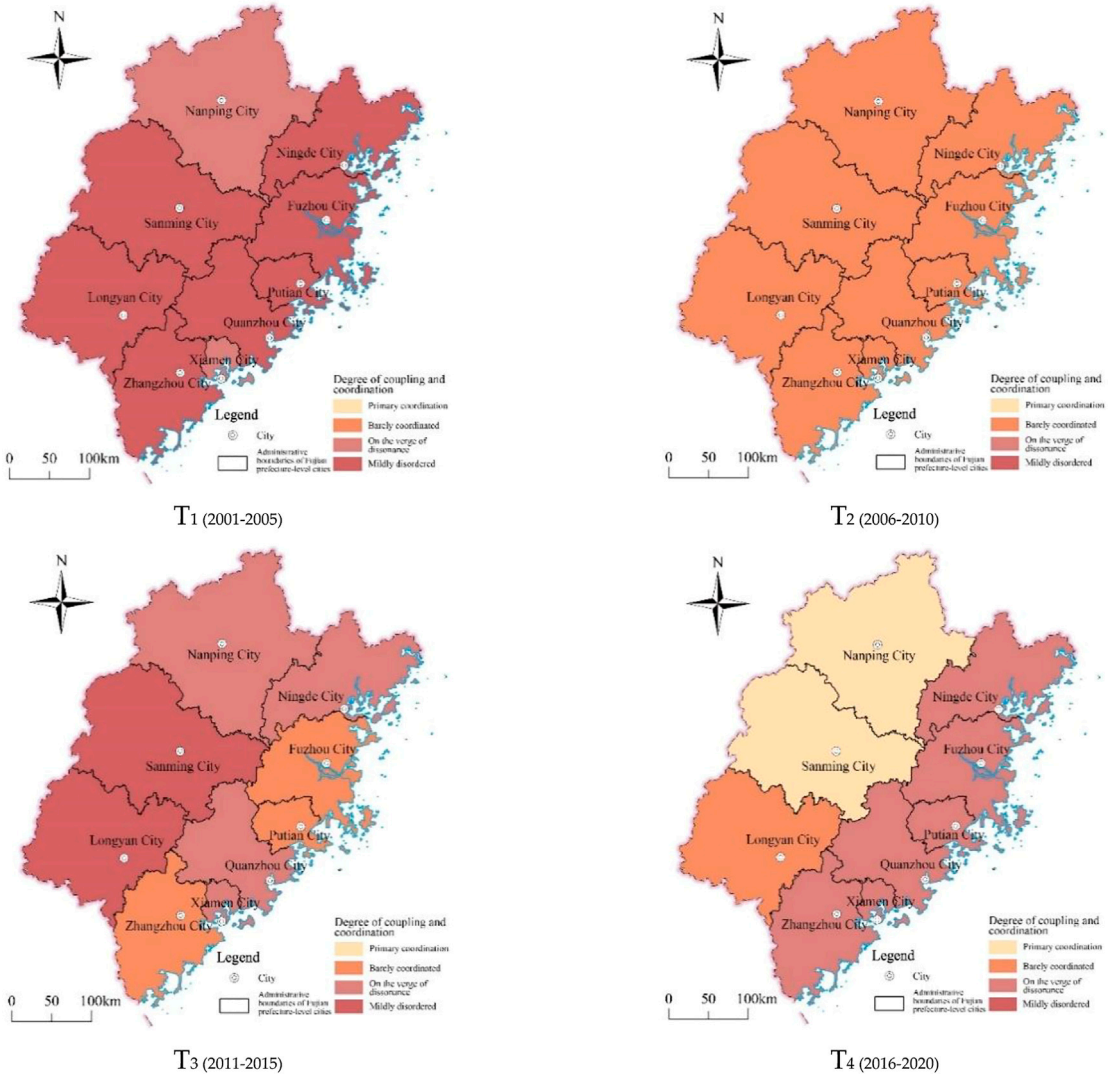

FIGURE 3 | Spatial distribution of coupling coordination degree between carbon emissions and economic growth in prefecture-level cities of Fujian Province.

During the $T_{2\ (2006–2010)}$ period, Fujian Province changed its development concept and focused on the development of environmental industries while upgrading traditional industries. "During the 11th Five-Year Plan period, Fujian Province accelerated the development of urbanisation and industrialisation, focusing on the industrialisation process and strengthening transportation construction, and on the other hand, made special plans for the environmental protection industry, built environmental protection industry bases, and developed purification devices and other projects in terms of solid, liquid and gas pollution control. The agricultural and forestry land reform has been carried out, promoting environmental protection. According to the result, the economy develops while the carbon emission is barely taken control. The decoupling between regional carbon emissions and economic growth in nine prefecture-level cities in Fujian Province is mildly decoupled. The coupling coordination is mainly barely coordinated.

In $T_{3\ (2011–2015)}$, Fujian Province accelerated the construction of an ecological province, strengthened the development and application of new technologies, equipment, and products for energy conservation and emission reduction, and effectively controlled the total emissions of major pollutants such as sulfur dioxide. During this period, Fujian Province began to plan the blending of urban and rural development, and promote the coordinated construction of cities, so that the industry in Fujian Province could be better optimised and upgraded; during the "12th Five-Year Plan" period, Fujian Province continued to optimise the energy structure, providing energy security for the further development of the low-carbon economy. "In the 12th Five-Year Plan, when planning the development of the three leading industries and manufacturing industries, more attention is paid to upgrading low energy consumption and low pollution technology and equipment transformation, controlling the layout of carbon-

intensive industries, and improving the coordination between industries. Meantime, the investment in scientific and technological study and development of low-carbon industries is increased, and low-carbon industries are vigorously developed. In addition, while focusing on the integrated improvement of urban and rural areas, the concept of green low-carbon consumption is vigorously promoted to reduce the consumption of high-carbon products and stimulate the production and consumption of low-carbon products.

$T_{4\ (2016–2020)}$ period, during the 13th Five-Year Plan period in Fujian Province, the policy system of urban-rural integration will be gradually improved. The planning of ecological and environmental governance and low-carbon development will be further refined in terms of environmental protection and carbon emission reduction, proposing to take the initiative to control carbon emissions, increase the carbon emissions control of key industries such as petrochemicals and manufacturing, and implement demonstration projects of near-zero carbon emission zones. In the high-quality, coordinated development of the economy, while focusing on ecological and environmental governance and carbon emission control, higher demand for carbon emission intensity reduction has been put forward. The carbon emission intensity in Fujian Province in 2020 has decreased by nearly 20% compared with that in 2015. The low-carbon development in Nanping and Sanming cities, in particular, has been effective. Agriculture and forestry in Fujian Province have also been reformed in this stage. The application of pesticides and fertilisers has been reduced. The development of urban-rural integration has been more effective in dealing with domestic waste, social security, and environmental protection concepts. The growth rate of carbon emissions has gradually slowed down while the overall economic development.

3.4.2 Green Economy Rebound Effects

Green economy rebound effects may occur when the firms aim for greater efficiency. As a result, resources might become cheaper especially in the economic terms. Such progress may affect the demand having a direct influence on the brown products. Such effects are known as macro-level rebound effects. In our study, there is a possibility for variety of rebound effects. The one could be related to investments. For instance, the difference in the projected investment's composition from the capital stock's initial composition may have unexpected indirect consequence on the green growth. As a result, the economic outcomes would vary. In the four stages of urban-rural integration, such effect is mildly observed if we look at it theoretically. The other could be related to employment that is created during and after urban and rural integration. Generally, green growth is assumed to provide more employment opportunity than the conventional due to the involved operations in the value chain. However, if the governing body can be able to provide or not by satisfying the employment regulations will be a big question and can be considered as a potential rebound. On the other side, the improvements in energy efficiency for the related energy infrastructure may have influence on the resource consumption (e.g., patterns, type, technology and others). So, by conducting a macroeconomic relationship between resource consumption and investment for urban-rural integration and the outcome may be analyzed to exactly quantify the possible rebound effects.

4 POLICY INSIGHTS

Based on the observed results, it is clear that China needs immediate measures to build a low carbon economy. So, the following six policy inspirations are proposed to accelerate the development of China's regional low-carbon economy.

First, promote the integration of urban and rural areas to reduce the wastefulness caused by the uneven development of urban and rural areas through coordinated development of urban and rural areas and strengthen the carbon sequestration capacity of ecosystems. We should make full use of the natural ecological pattern of "eight mountains, one water, and one field" in Fujian Province, promote the integrated protection of mountains, water, forests, fields, lakes, grasses, and sands, improve forest quality, continuously increase forest area and storage volume, and give full play to the carbon absorption and sequestration capacity of the forest system (Fan, 2021).

Second, adhere to the reduction principle and deepen the reform of energy structure. Rapid technological progress has promoted the development of renewable energy and renewable power generation as well as energy technology efficiency (Chen, 2022), strengthening technological innovation and effective energy use (Lu et al., 2021), shorting energy demand, and increasing renewable energy applications on the demand side and supply side, respectively (Xu et al., 2022), giving full play to the leading role of scientific and technological innovation, implementing green low-carbon cycle technological innovation and technology research and development actions, improving the research and development of demand-side and production-side technological innovation. Promote the development and application of clean energy, green energy, renewable energy, and other related low-carbon technologies, control fossil energy consumption, gradually realise the replacement of low-carbon energy for high-carbon, and realise resource conservation and carbon emission reduction from the source. Also, focus on developing the remanufacturing industry and strengthening the comprehensive utilisation of resources. While expanding the supply and consumption of green, low-carbon products, it should also uphold the concept of waste recycling and reuse to realise the saving and replacement of primary resources and form a green production and lifestyle, which can reduce carbon emissions generated by primary resources mining, smelting, processing, and other links.

Third, promote the development of industrial integration and innovation of green, low-carbon industries. On the one hand, we can construct smart cities and smart industries through the application of technological innovation to promote energy saving and emission reduction in industrial production and build a more green and efficient industrial chain; on the other hand, the development of green finance is a driving force to achieve carbon neutrality (Wang et al., 2022). Fujian Province should focus on its geographical advantages and policy orientation to build forest banks, establish carbon trading markets, develop green industries, and optimise forestry industries to coordinate economic development and environmental protection.

Fourth, we should strengthen the coordinated development between industries and between urban and rural areas. The integrated development of urban and rural areas is for our country's overall planning and coordinated development. In its process, we should build a good social and market environment through policy politics, etc., so that urban and rural populations, resources, technology, etc. can be integrated, and in the market can take each other's needs, so that urban and rural areas can develop in a coordinated manner. In terms of environmental coordination, the amount of carbon sequestered by forests and crops can be increased through better construction of villages. The amount of carbon emitted in the process of agro-industrial production can be reduced through research on energy-saving and emission reduction technologies.

Fifth, the "two mountains" concept of "green water and green mountains are the silver and golden mountain" should be fully implemented in urban-rural integration. We should strengthen the promotion of the concept of ecological construction, resource conservation, and environmental protection, reduce pollution in all areas when ensuring the combined development of urban and rural areas, reduce the use of chemical fertilisers, pesticides, and mulch in agriculture, and accelerate the integration of modern scientific and technological achievements with the whole process of ecological resource development, promote the ecologicalization of science and technology, explore potential ecological, economic resources, stimulate the internal driving force of green development, and form new green development methods such as carbon sink economy, forestry, forest recreation, etc. Forest recreation and other new green development methods continuously promote ecological restoration and treatment. At the same time, they accelerate the realisation of ecological resources' value and make us realise the outcome of coordinated development of economic, social, and ecological benefits.

Sixth, build a city cluster system to build urban integration better. The urban cluster relationship between coastal cities and inland cities is constructed through regional relationships, transportation networks, policy measures, and industrial chains. Thus, the urban economy can be developed in a more coordinated way, and the process can promote the high-quality development of the overall economy of Fujian Province by reasonably optimising the market and industry, etc. At the same time, due to the difference in geographical conditions, through the coordination between cities, we can improve the local economic development; for example, more hilly and mountainous areas can pay more attention to the protection of mountains and forests to improve the carbon sequestration capacity. In contrast, coastal ports and economically developed areas can optimise industries to improve the quality of economic development, increase the employment rate, etc.

5 CONCLUSION

In conclusion, this study revealed that carbon emissions and regional GDP in Fujian Province show an upward trend. The carbon emissions are observed to have slight fluctuations. The economic development pattern, industrial structure (that includes energy), industrialisation process, urbanisation development, and other factors can affect the rate of increase in carbon emissions. The decoupling state and the degree of coupling and coordination between carbon emissions and economic growth in each prefecture-level city of Fujian Province have different characteristics at different times, resulting from the combined effect of economic development pattern, industrial structure, and technology development level. At the present stage, the carbon emission and economic growth in Fujian Province have reached a high degree of weak decoupling. The coupling and coordination degrees are more obviously different between coastal and inland, with inland cities reaching the coupling and coordination state and coastal cities relatively poor. We believe that proposed policy insights could help China develop a low carbon economy.

DATA AVAILABILITY STATEMENT

The original contributions presented in the study are included in the article/supplementary material, further inquiries can be directed to the corresponding author.

AUTHOR CONTRIBUTIONS

All the authors have made a substantial, direct, and intellectual contribution to the work and approved it for publication.

FUNDING

This research was supported by the National Natural Science Foundation of China under Grant 71773016; Natural Science Foundation of Fujian Province Program Projects, grant number 2021J01230662.

REFERENCES

Balsalobre-Lorente, D., Ibáñez-Luzón, L., Usman, M., and Shahbaz, M. (2022). The Environmental Kuznets Curve, Based on the Economic Complexity, and the Pollution Haven Hypothesis in PIIGS Countries. *Renew. Energy* 185, 1441–1455. doi:10.1016/j.renene.2021.10.059

Baoxin, W., Baoxiu, Z., Xu, H., Yinghong, Z., Jingqiu, Z., and Bin, M. (2019). *Beijing Urban and Rural Blue Book: Beijing Urban-Rural Integration Development Report*. Beijing: Social Sciences Literature Press.

Chen, F., Zhao, T., and Wang, D. (2022). Research on China Cities' Total Factor Productivity of Carbon Emission: Based on Decoupling Effect. *Ijerph* 19, 2007. doi:10.3390/ijerph19042007

Chen, W.-J. (2022). Toward Sustainability: Dynamics of Total Carbon Dioxide Emissions, Aggregate Income, Non-renewable Energy, and Renewable Power. *Sustainability* 14, 2712. doi:10.3390/su14052712

Ding, Y., Yang, Q., and Cao, L. (2021). Examining the Impacts of Economic, Social, and Environmental Factors on the Relationship between Urbanization and CO2 Emissions. *Energies* 14, 7430. doi:10.3390/en14217430

Fan, Q. (2021). The Development Logic and Revelation of the Idea of "Mountain, Water, Forest, Lake, Grass and Sand" System Management in the Past 100 Years since the Founding of the Chinese Communist Party. *J. Poyang Lake* (02), 5–17.

Haouraji, C., Mounir, B., Mounir, I., and Farchi, A. (2021). Exploring the Relationship between Residential CO2 Emissions, Urbanization, Economic Growth, and Residential Energy Consumption: Evidence from the North Africa Region. *Energies* 14, 5849. doi:10.3390/en14185849

Huang, Y., Haseeb, M., Usman, M., and Ozturk, I. (2022). Dynamic Association between ICT, Renewable Energy, Economic Complexity and Ecological Footprint: Is There Any Difference between E-7 (Developing) and G-7 (Developed) Countries? *Technol. Soc.* 68, 101853. doi:10.1016/j.techsoc.2021.101853

Ji, Y., and Xue, J. (2022). Decoupling Effect of County Carbon Emissions and Economic Growth in China: Empirical Evidence from Jiangsu Province. *Ijerph* 19, 3275. doi:10.3390/ijerph19063275

Jiang, L., Bai, L., and Wu, Y. (2017). Analysis of the Coordination of Economy, Resources, and Environment in Chinese Provinces-Aand on the Three-System Coupling Formula and its Extended Form. *J. Nat. Resour.* 32 (05), 788–799.

Lin, J. (2012). An Overview of the Clean Development Mechanism in Southeast Asia. *Dev. Res.* (08), 99–126. doi:10.1142/9789814277532_0004

Liu, K., Wang, J., Kang, X., Liu, J., Xia, Z., Du, K., et al. (2022). Spatio-Temporal Analysis of Population-Land-Economic Urbanization and its Impact on Urban Carbon Emissions in Shandong Province, China. *Land* 11, 266. doi:10.3390/land11020266

Liu, Z. H., Xu, J. W., and Zhang, C. H. (2021). Spatial and Temporal Divergence and Driving Mechanism of the Coordinated Development of Carbon Emission Reduction-Economic Growth-Environmental Protection in Provincial Areas [J]. *J. Hainan Univ. Humanit. Soc. Sci. Ed.* 39 (05), 63–72.

Lu, C., Wang, D., Li, H., Cheng, W., Tang, X., and Liu, W. (2021). Measurement of the Degree of Coordination in Regard to Carbon Emissions, Economic Development, and Environmental Protection in China. *Appl. Sci.* 11, 1750. doi:10.3390/app11041750

Ma, Y. (2019). Thirteenth Five-Year Plan": High Growth to High-Quality Development-An Interview with Zhang Junxuan, Deputy Director and Researcher of the Development Research Center of the State Council. *China Dev. Watch* (20), 5–10.

Mata, M. N., Oladipupo, S. D., Husam, R., Ferrão, J. A., Altuntaş, M., Martins, J. N., et al. (2021). Another Look into the Relationship between Economic Growth, Carbon Emissions, Agriculture and Urbanization in Thailand: A Frequency Domain Analysis. *Energies* 14, 5132. doi:10.3390/en14165132

Mo, H., and Wang, S. (2021). Spatial and Temporal Pattern Evolution and Spatial Effect Mechanism of Carbon Emissions in Counties of the Yellow River Basin. *Geoscience* 41 (08), 1324–1335.

Myszczyszyn, J., and Suproń, B. (2021). Relationship Among Economic Growth (GDP), Energy Consumption and Carbon Dioxide Emission: Evidence from V4 Countries. *Energies* 14, 7734. doi:10.3390/en14227734

Pang, Q., Zhou, W., Zhao, T., and Zhang, L. (2021). Impact of Urbanization and Industrial Structure on Carbon Emissions: Evidence from Huaihe River Eco-Economic Zone. *Land* 10, 1130. doi:10.3390/land10111130

Peng, J., Huang, X., Zhong, T., and Zhao, Y. (2011). Decoupling of Economic Growth and Energy Carbon Emissions in China. *Resour. Sci.* 33 (04), 626–633.

Shi, J., Duan, K., Wu, G., Li, J., and Xu, K. (2021). Efficiency of Urban-Rural Integration Development in the Yangtze River Delta Region under Carbon Emission Constraints. *Econ. Geogr.* 41 (06), 57–67. doi:10.15957/j.cnki.jjdl.2021.06.007

Tian, Y., and Lin, Z. J. (2021). Spatial and Temporal Coupling of Agricultural Carbon Emissions and Economic Growth in the Yangtze River Economic Zone. *J. China Agric. Univ.* 26 (01), 208–218.

Usman, M., Makhdum, M. S. A., and Kousar, R. (2021). Does Financial Inclusion, Renewable and Non-renewable Energy Utilization Accelerate Ecological Footprints and Economic Growth? Fresh Evidence from 15 Highest Emitting Countries. *Sustain. cities Soc.* 65, 102590. doi:10.1016/j.scs.2020.102590

Usman, M., and Makhdum, M. S. A. (2021). What Abates Ecological Footprint in BRICS-T Region? Exploring the Influence of Renewable Energy, Non-renewable Energy, Agriculture, Forest Area and Financial Development. *Renew. Energy* 179, 12–28. doi:10.1016/j.renene.2021.07.014

Wang, B., Zheng, Q., Sun, A., Bao, J., and Wu, D. (2021). Spatio-Temporal Patterns of CO2 Emissions and Influencing Factors in China Using ESDA and PLS-SEM. *Mathematics* 9, 2711. doi:10.3390/math9212711

Wang, G., Li, S., and Yang, L. (2022). Research on the Pathway of Green Financial System to Implement the Realization of China's Carbon Neutrality Target. *Ijerph* 19, 2451. doi:10.3390/ijerph19042451

Wang, P., Feng, X., Wang, M., An, Q., Yang, R., and Zhao, M. (2021). Identification and Typology of Provincial Carbon Emission Characteristics in China. *Environ. Sustain. Dev.* 46 (03), 31–36.

Wu, N., Shen, L., Zhong, S., and Zhang, C. (2019). Spatio-temporal Coupling Relationship between Economic Growth and Carbon Emissions in Jin-Shaanxi-Mongolia Region. *Econ. Geogr.* 39 (09), 17–23.

Xiao, E. (2012). An Empirical Study on the Measurement of Rural Carbon Emissions in the Process of Urban-Rural Integration: Hubei as an Example. *Jiangsu Commer. Forum* (08), 138–141. doi:10.13395/j.cnki.issn.1009-0061.2012.08.016

Xu, X., Wang, Y., Ruan, Y., Wang, J., Ge, K., Zhang, Y., et al. (2022). Integrated Energy Planning for Near-Zero Carbon Emission Demonstration District in Urban Areas: A Case Study of Meishan District in Ningbo, China. *Energies* 15, 874. doi:10.3390/en15030874

Zhang, Y. (2016). *Study on the Factors Influencing Carbon Emissions of Planting Industry in Fujian Province*. Fuzhou: Fujian Normal University.

Zhao, X., Jiang, M., and Zhang, W. (2022). Decoupling between Economic Development and Carbon Emissions and its Driving Factors: Evidence from China. *Ijerph* 19, 2893. doi:10.3390/ijerph19052893

Zhou, Z., Cao, L., Zhao, K., Li, D., and Ding, C. (2021). Spatio-Temporal Effects of Multi-Dimensional Urbanization on Carbon Emission Efficiency: Analysis Based on Panel Data of 283 Cities in China. *Ijerph* 18, 12712. doi:10.3390/ijerph182312712

Conflict of Interest: The authors declare that the research was conducted in the absence of any commercial or financial relationships that could be construed as a potential conflict of interest.

Publisher's Note: All claims expressed in this article are solely those of the authors and do not necessarily represent those of their affiliated organizations, or those of the publisher, the editors and the reviewers. Any product that may be evaluated in this article, or claim that may be made by its manufacturer, is not guaranteed or endorsed by the publisher.

frontiers | Frontiers in Energy Research

ORIGINAL RESEARCH
published: 08 July 2022
doi: 10.3389/fenrg.2022.896529

Decoupling Re-Analysis of CO_2 Emissions and Economic Growth From Two Dimensions

Yuling Han[1,2]*, *Yiping Liu*[1] *and Xiao Liu*[3]

[1]College of Economics and Management, Nanjing University of Aeronautics and Astronautics, Nanjing, China, [2]College of Management, Nanjing University of Posts and Telecommunications, Nanjing, China, [3]School of Economics and Management, Huaiyin Normal University, Huai'an, China

The 21st Conference of the Parties (COP 21) was a significant attempt by governments to make and monitor commitments to limit global warming. However, COP 23 "sought to continue the global momentum to decouple output from greenhouse gas (GHG) emissions." Among the GHGs, carbon dioxide (CO_2) is the major one most countries worry about. This paper examines the decoupling situations of China's CO_2 emissions and economic growth, considering the country's progress situation from the year 2000 to 2019. For this, we employed two models: the environmental Kuznets curve (EKC) model for exploring the long-run decoupling status and the influence factors of CO_2 emissions and the Tapio model for the short-run decoupling status. Later, the Tapio model was extended to analyze the influence of industrial structure, energy structure, and population structure. The long-term results suggest that China's CO_2 emissions have not decoupled yet, but the emission's intensity has decoupled in mid-2006. The short-term decoupling results revealed that the degree of decoupling changed to weak from strong in the last five years. According to the influencing structure's results, the industrial and energy structures inhibited CO_2 emissions, but their influence was not strong enough to offset the impact of economic growth; however, the population structure indorsed CO_2 emissions. Lastly, we found an unusual verdict that is the change of EKC into a U-shape from an inverted U-shape, and the observed reason is the control variable introduction. We also observed that the turning point became greater after introducing the industrial structure separately. Overall, from the perspective of the observed decoupling trends, it is suggested that China should strengthen and further optimize its energy structure to match the industrial structure.

Keywords: carbon dioxide emissions, decoupling analysis, economic growth, EKC, Tapio decoupling model

OPEN ACCESS

Edited by:
Anshu Priya,
City University of Hong Kong, Hong Kong SAR, China

Reviewed by:
Kittisak Jermsittiparsert,
University of City Island, Cyprus
Syed Ale Raza Shah,
Xi'an Jiaotong University, China

***Correspondence:**
Yuling Han
hannjupt@163.com

Specialty section:
This article was submitted to Sustainable Energy Systems and Policies, a section of the journal Frontiers in Energy Research

Received: *15 March 2022*
Accepted: *31 May 2022*
Published: *08 July 2022*

Citation:
Han Y, Liu Y and Liu X (2022) Decoupling Re-Analysis of CO_2 Emissions and Economic Growth From Two Dimensions. Front. Energy Res. 10:896529. doi: 10.3389/fenrg.2022.896529

1 INTRODUCTION

The pledge to tackle global warming potential was a significant attempt by nations in the 21st Conference of the Parties (COP 21) (De Moor (2018). The follow-up COP summits have maintained the same pledge; however, in COP 23, there was a global momentum on decoupling the country's outcome from greenhouse gas emissions (Gough, 2017). Carbon dioxide (CO_2) is the most significant GHG that most countries are concerned about. The recent report "State of the Global Climate 2020" (WMO, 2021) from the World Meteorological Organization (WMO) suggests that

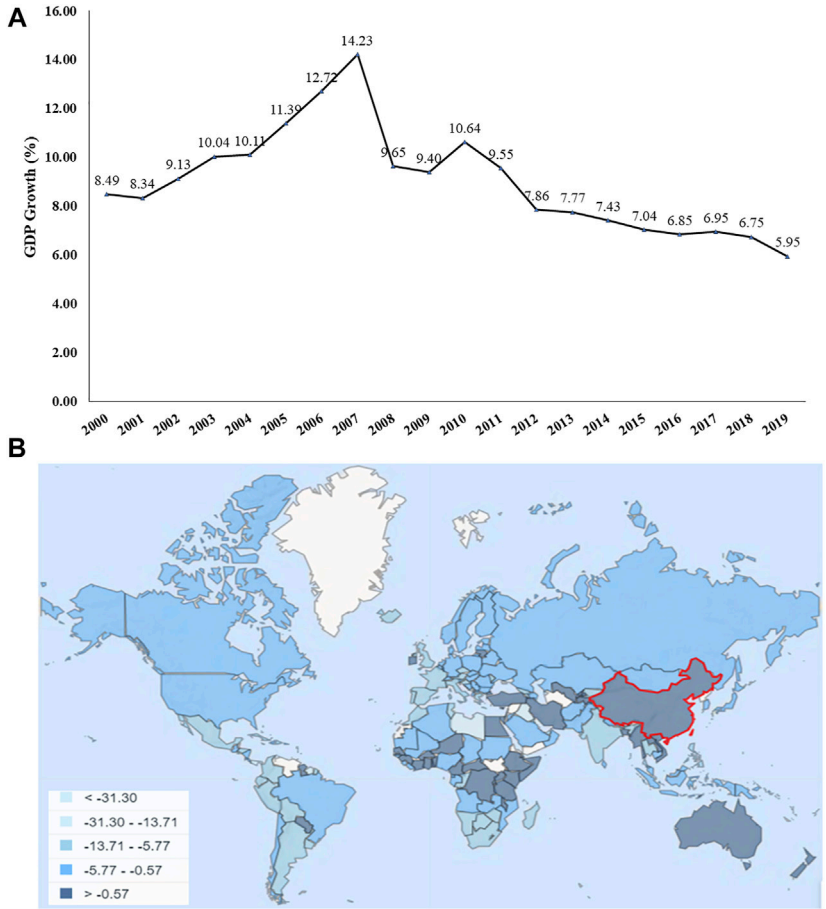

FIGURE 1 | (A) China's annual GDP growth % from 2000 to 2019; **(B)** comparison of China's annual GDP growth % with those of other nations. Data source: World Bank national accounts data and OECD National Accounts data files (World Bank, 2020).

even though the global economy is declined and the emissions of new GHG were only reduced temporarily, the positive effect of the COVID-19 pandemic is significant here. Also, it did not inhibit the increase in atmospheric GHG concentration and temperature (WMO, 2021). Though this mere effect on decreasing GHG is seen, the theories and proven facts clearly leave the signs of increasing global warming and global climate change, which are the most considerable environmental problems of the present. They pose a greater threat to both developed and developing countries, especially those aiming to achieve sustainable economic growth and development (Alege et al., 2016). As a result, the extent to which decoupling is occurring is still seen as a point of contention. China is one leading nation aiming to achieve sustainable economic growth and development. If we look at China's historical gross domestic product (GDP) data, as shown in **Figure 1A** (World Bank, 2020), the trend can be observed clearly. As per the 2020 reports, the annual GDP growth % was maintained at 2.3% (World Bank, 2020). However, if we compare the % of annual GDP growth rates with those of other nations, China's performance is notable (see **Figure 1B**) (World Bank, 2020). More recently, in 2020, President Xi Jinping said that China's CO_2 emissions should reach their peak by 2030, and China would strive to achieve net neutrality by 2060. Given China's current position as one of the largest CO_2 emitters, its emission reduction targets are significant in achieving the global target of 2°C in this century.

In this context, it is imperative to understand the upshot of COP 23's momentum of decoupling the country's outcome from GHG. The environmental Kuznets curve (EKC) hypothesis holds that economic growth leads to increased environmental pollution at the beginning of the economic development process. However, when economic growth reaches a turning point, the economic growth will decrease the environmental pollution. The EKC hypothesis has been widely used, and many researchers hope to predict the turning point to help policymakers predict the peak time (Jin et al., 2017; Dong et al., 2018; He et al., 2021). Dong et al. (2018) estimated that the per capita gross domestic product (GDP) at the inflection point is 96,680.47 yuan, which will be reached by 2028. While Jin et al. (2017) suggested that the inflection point would be reached at least five years later in the period from 1995 to 2012, yet the peak did not appear now. This is affected by energy conservation, emission reduction, and related policies; as a result, the growth rate of China's CO_2 emissions has gradually slowed since 2012 (He et al.,

2021). Almost at the same time, the speed of China's economic development has slowed, entering a new development stage. This new development stage triggered numerous questions. For instance, do the CO_2 emissions decouple from the economic growth in the new stage? Are there any new changes? What factors affect CO_2 emissions by the view of structure change?

Considering the above-raised questions, this study aims to compare the decoupling of economic growth and CO_2 emissions from different points. A key focus was made on exploring the potential new changes in this new development stage in China, followed by finding the reasons for such changes.

2 LITERATURE REVIEW

As mentioned earlier in **Section 1**, many governments and researchers always focus on the relationship between economic growth and environmental pollution. Some even focus on specific sectors or specific technology in a specific sector, as discussed by Shah et al. (2020a), Shah et al. (2020b), and Naqvi et al. (2020). To explain such a relationship, numerous methods are being used in the literature. For the decoupling analysis, there are two main types. One is judging whether CO_2 emissions decrease with the growth of economy from the view of absolute quantity.

The popularly used method is the EKC model. Many researchers have verified it in different countries or regions. Shah et al. (2021) tested the EKC model to identify the drivers of environmental degradation with economic development for Western Asia and North African regions and reported that the U-shaped and inverted U-shaped EKC hypotheses are valid. Naqvi et al. (2021) verified EKC and renewable energy environment Kuznets curve (RKC) hypotheses considering the renewable energy, economic development, and ecological footprint nexus for 155 countries. Ali et al. (2021) tested the EKC in Nigeria from 1981 to 2014; their results supported the EKC hypothesis. In Pata (2018) research, the EKC in Turkey from 1974 to 2013 existed in the long term and short term. Prastiyo et al. (2020) found the EKC in Indonesia was in existence, Haseeb et al. (2018) found that BRICS economies supported the EKC hypothesis, and Zaidi et al. (2019) discussed the EKC of Asia-Pacific Economic Cooperation (APEC) member countries; the results supported the EKC too. Gokmenoglu and Taspinar (2018) explored the EKC hypothesis that also existed in the agricultural sector in Pakistan from 1971 to 2014. For China, Li et al. (2020) found the EKC hypothesis held by the province panel data of China from 1997 to 2016. Sun et al. (2021) got similar results in the research period of 2000–2012. In the research by Hao et al. (2019), they found that the EKC was in existence, but the turning point would not appear soon. Furthermore, Xia and Wang (2020) and Liu and Xiao (2018) verified the existence of the CO_2 EKC hypothesis in China. However, some studies did not verify the EKC hypothesis. For instance, Jin and Kim (2020) studied 34 Annex I countries and found that only 5 countries supported the EKC. Other researchers found the curves instead showed linear (Hu et al., 2013), U-type (Ajmi and Inglesi-Lotz, 2021; Hasanov et al., 2019), N-type (Allard et al., 2018; Shah et al., 2020a], and inverted N-type (Ameyaw et al., 2020) relationships.

The other type is judged by the growth rate, in other words, whether the CO_2 emission growth speed declines or even reaches negative growth as the economic growth rate increases. The commonly used method is the Tapio decoupling model. Some studies showed that the decoupling level of developed countries or regions is more robust than that of developing countries or regions. Li and Jiang (2020) compared the decoupling of the six highest global CO_2-emitting countries by using the Tapio decoupling model; their results showed that the decoupling situation of the developing countries was more unstable and weaker than that of the developed countries. The verification results of Ozturk et al. (2021) in China, India, and Pakistan show that all three countries have a decoupling trend. However, Pakistan is the most expensive, followed by India and China. Researchers also produced similar findings in China; the decoupling degree of developed regions or provinces is more robust than that of underdeveloped regions or provinces. Cohen et al. (2018) found that the decoupling of more prosperous provinces is more robust than that of poorer provinces in China. Peng et al. (2011) found that although the degree of decoupling in the eastern region was more robust than that in other regions in China, the regional differences had a noticeable narrowing trend with the improvement of the economy. As China's per capita income grows continually, our study wants to find whether the degree of carbon emission decoupling is more substantial than before or not. Numerous other approaches are applied in the literature to different countries to understand the relationships between economic growth and CO_2 emissions, for instance, the unexplored nexus in ASEAN countries (Haseeb et al., 2019), bootstrap ARDL approach for Singapore (Meirun et al., 2021), fixed asset model for ASEAN countries (Krisada et al., 2021), and Markov switching equilibrium correction model (MS-ECM) for Pakistan (Shah et al., 2022). Additionally, there is some instance of understanding carbon footprint implications due to outward foreign direct investment (OFDI), human well-being, and the public sector's macro indicators based on the cross-country analysis (Zhang et al., 2021).

In summary, the theoretical and empirical research on the decoupling of CO_2 emissions has obtained many essential conclusions. However, most of the existing literature was based on only one decoupling method, and there were fewer studies with two or more methods. Coming to the research on China, the study period was mostly 2016; the conclusions were optimistic and did not lead to a strategic conclusion. In addition, the literature evidence suggests that most studies believe CO_2 emissions are affected by exogenous factors, such as energy consumption, urbanization development, transportation, and OFDI.

Hence, this paper will explain the influence factors of CO_2 emissions from a new point. For this, we claim that the characteristics of CO_2 emissions were affected by the industrial structure. The endowment structure affected the industrial structure (including energy and population structures) (Lin 2011). So, the structure of the CO_2 emission was endogenously determined by the endowment structure. The EKC and Tapio models were used to analyze the decoupling in terms of quantity and speed separately. Furthermore, we

selected 2000–2019 as the research period, including the latest data after 2016. Firstly, we analyzed the long-term decoupling trend of China's CO_2 emissions based on the EKC hypothesis model. Then, we discussed the short-term CO_2 decoupling based on the Tapio model. Finally, we introduced three control variables (including the industrial structure, energy structure, and population structure) into the model to explore the influence on decoupling.

3 METHODS AND DATA COLLECTION

3.1 Decoupling Models

3.1.1 EKC Model

Kuznets originally used the EKC hypothesis to describe the inverted U-shaped curve relationship between economic growth and income inequality. Grossman and Krueger found that an inverted U-shaped curve was also valid in economic growth and environmental pollution. Later, environmental economists extended Kuznets's hypothesis theory. The inverted U-shaped curve was called the environmental Kuznets curve (EKC) (Lin 2011).

The general formula for the EKC hypothesis is given as follows (Bhattarai and Hammig, 2001):

$$Y = \alpha + \beta_1 G + \beta_2 G^2 + \beta_3 G^3 + \gamma X + \varepsilon, \quad (1)$$

where Y represents environmental pollution, G represents economic growth, X represents other control variables that significantly impact Y, *a* is the intercept term, the β's are the estimation parameters, and ε represents the random error term.

The natural pair of variables is generally used for numerical modeling in practical applications. The advantage of this is that it can change the relationship between variables and reduce the fluctuation of variables and reduce the value of sample heteroscedasticity. Thus, the regression coefficient is transformed into the elasticity coefficient of independent variables to dependent variables. Therefore, **Eq. 1** is changed into the following equation:

$$\ln Y = \alpha + \beta_1 \ln G + \beta_2 \ln G^2 + \beta_3 \ln G^3 + \gamma \ln X + \varepsilon. \quad (2)$$

The curvilinear relationship between G and Y is as follows:

If $\beta1 = \beta2 = \beta3 = 0$, then G and Y are not related;
If $\beta1 > 0$ and $\beta2 = \beta3 = 0$, then G and Y are monotonically increasing;
If $\beta1 < 0$ and $\beta2 = \beta3 = 0$, then G and Y are monotonically decreasing;
If $\beta1 > 0$, $\beta2 < 0$, and $\beta3 = 0$, then G and Y show an inverted U-shaped curve;
If $\beta1 < 0$, $\beta2 > 0$, and $\beta3 = 0$, then G and Y show a U-shaped curve;
If $\beta1 > 0$, $\beta2 < 0$, and $\beta3 > 0$, then G and Y show an N-shaped curve;
If $\beta1 < 0$, $\beta2 > 0$, and $\beta3 < 0$, then G and Y are in an inverted N-shaped curve.

Among the above seven relationships, only the fourth relationship is the EKC relationship.

Figure 2A shows the decoupling states of the inverted U-shaped curve. As shown in **Figure 2A**, G_0 is the turning point. When $G < G_0$, Y increases with the growth of G, but the change rate of Y becomes increasingly smaller, i.e., the same difference of G brings a smaller difference of Y, so Y and G are in a relative decoupling state. When $G > G_0$, Y decreases with the increase of G, and Y and G are in an absolute decoupling state. In contrast, in the U-shaped curve shown in **Figure 2B**, when $G < G_0$, Y decreases with the increase of G, and Y and G are in an absolute decoupling state. When $G > G_0$, Y increases with the increase of G, and the change rate of Y becomes larger and larger, so Y and G are in an expansive coupling state. Similarly, the N-shaped curve is just like a U-shaped curve following an inverted U-shaped curve. When G reaches the first turning point, Y and G are in an absolute decoupling state from a relative decoupling state. Then, with the uncontrolled economic development, the capacity of the environment regarding pollution exceeds the limit, and the decrease of Y becomes smaller; when G reaches the second turning point, Y and G are in the coupling state again, also called re-linking (Grossman and Krueger, 1995). In contrast, the inverted N-shaped curve is a U-shaped curve in the first half and an inverted U-shaped curve in the second half. When G reaches the first turning point, it will experience a more expansive coupling process and then gradually improve to a relative decoupling state. When G reaches the second turning point, Y and G are again in the absolute decoupling state.

As discussed in **Section 1** and **Section 2**, there were some different research results regarding the EKC, and the results showed that the EKC is sensitive to research years and research indicators. When the economic growth of an economy achieves a high level, the "CO_2 emissions per unit GDP" will first reach an inflection point that displays a downward trend. However, the "CO_2 emissions per capita" peak will lag behind. However, they achieved a real turning point only when per capita CO_2 emissions began to decline continuously (Mikayilov et al., 2018). Hence, this study selected per capita CO_2 emissions (PC) and CO_2 emission intensity (CI) to represent the variable Y and used total CO_2 emissions (TC) to test the stability. The economic growth variable G was the per capita gross domestic product (PGDP) (Bhattarai and Hammig, 2001). So, **Eq. 2** is changed and represented as follows:

$$\ln TC = \alpha + \beta_1 \ln PGDP + \beta_2 \ln PGDP^2 + \beta_3 \ln PGDP^3 + \varepsilon, \quad (3)$$

$$\ln PC = \alpha + \beta_1 \ln PGDP + \beta_2 \ln PGDP^2 + \beta_3 \ln PGDP^3 + \varepsilon, \quad (4)$$

$$\ln CI = \alpha + \beta_1 \ln PGDP + \beta_2 \ln PGDP^2 + \beta_3 \ln PGDP^3 + \varepsilon. \quad (5)$$

According to Lin (2011), the factor endowment structure of an economy determines its production structure, including the industrial structure and technological structure, and the characteristics of the production structure determine its environmental structure. Energy is the major force of motive in the industry. Fossil energy consumption, especially coal, is the major leading source of CO_2 emissions. Therefore, we selected the energy structure (ES) and population structure (PS) in factor

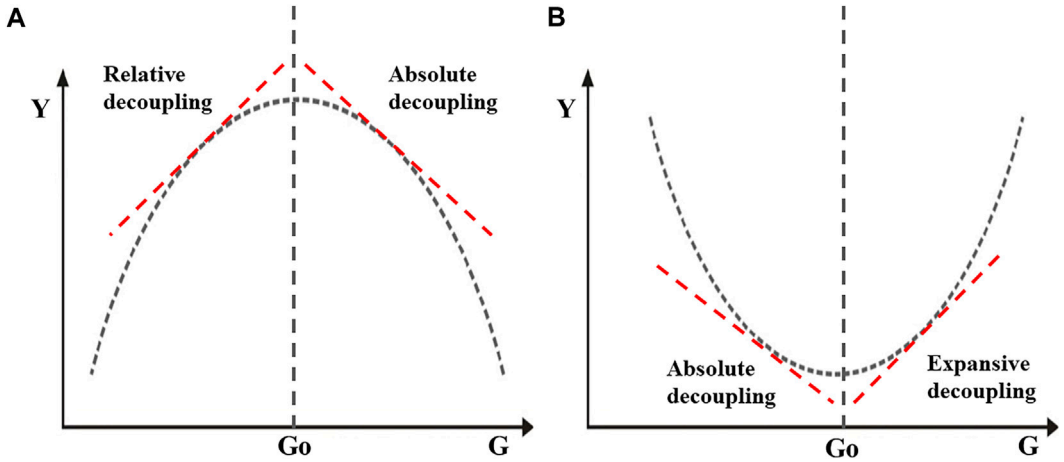

FIGURE 2 | Decoupling states: **(A)** inverted U-shaped and **(B)** U-shaped curves.

TABLE 1 | Judgment rules of the Tapio decoupling index.

Economic growth	Decoupling state	ΔC	ΔGDP	Decoupling index (DI)
Economic expansive	Expansive negative decoupling (END)	>0	>0	DI > 1.2
	Expansive coupling (EC)	>0	>0	0.8 ≤ DI ≤ 1.2
	Weak decoupling (WD)	>0	>0	0 ≤ DI < 0.8
	Strong decoupling (SD)	<0	>0	DI < 0
Economic recessive	Recessive decoupling (RD)	<0	<0	DI > 1.2
	Recessive coupling (RC)	<0	<0	0.8 ≤ DI ≤ 1.2
	Weak negative decoupling (WND)	<0	<0	0 ≤ DI < 0.8
	Strong negative decoupling (SND)	>0	<0	DI < 0

endowment and industrial structure (IS) as control variables; then, **Eq. 2** is changed into the following equation:

$$\ln PC = \alpha + \beta_1 \ln PGDP + \beta_2 \ln PGDP.^2 + \beta_3 \ln PGDP.^3 + \gamma_1 \ln ES + \gamma_2 \ln IS + \gamma_3 \ln PS + \varepsilon. \quad (6)$$

3.1.2 Tapio Decoupling Model

The Organisation for Economic Co-operation and Development (OECD) developed the Tapio decoupling model. While Tapio studied the correlation between the transportation CO_2 emissions and the GDP of EU 15 countries, taking the elastic value of environmental pressure on driving factors as the division basis, he improved the OECD. Decoupling theory extended the decoupling situations into eight types, usually called them decoupling states. The following equation represents the GDP elasticity of CO_2 emissions (Tapio 2005):

$$DI_{(C,GDP)} = \frac{\%\Delta C}{\%\Delta GDP} = \frac{\Delta CO_2/CO_2}{\Delta GDP/GDP}, \quad (7)$$

where $DI_{(C,\ GDP)}$ represents the GDP elasticity of CO_2 emissions, ΔCO_2 represents the growth of CO_2, and ΔGDP is the growth of the economy.

The judgment rules of Tapio decoupling were divided into two categories according to economic expansion and economic recession. **Table 1** shows the judgment rules' details.

As the decoupling index constructed by Tapio is not affected by the base period year, the division is detailed, making it more objective and accurate than the OECD index. According to **Table 1**, due to China's stable economic growth, %ΔGDP is always greater than 0, and the decoupling state is in four states in the stage of economic expansion. For different CO_2 emission variables, if %ΔGDP is constant, then the smaller %ΔC is, the smaller the decoupling coefficient DI is and the stronger the decoupling degree is. Conversely, %ΔC is more significant, the decoupling coefficient DI is greater, and the degree is weaker.

We extended the Tapio model to analyze the role of different driving factors, where the driving factor decoupling model is given as

$$DI_{(C,GDP)} = \frac{\%\Delta C}{\%\Delta X} = \frac{\Delta CO_2/CO_2}{\Delta X/X}, \quad (8)$$

where ΔCO_2 implies the difference in CO_2 emission growth and X implies the growth of three different driving factors (energy structure, industrial structure, and population structure). According to **Eq. 8**, if %ΔC is constant, then the smaller %ΔX is, the greater the decoupling coefficient DI is and the greater the

TABLE 2 | Carbon emission factors and standard coal conversion factors of energy types.

Energy type	Carbon emission factors (kgC/kg)	Standard coal conversion factors (coal/kg)	Energy type	Carbon emission factors (kgC/kg)	Standard coal conversion factors (coal/kg)
Coal	0.7559	0.7143	Kerosene	0.5714	1.4714
Coke	0.8550	0.9714	Diesel oil	0.5912	1.4571
Crude oil	0.5857	1.4286	Fuel oil	0.6185	1.4286
Gasoline	0.5538	1.4714	Natural gas	0.4226	1.3300

The unit of natural gas is kgC/m^3 and coal/m^3. Data source: The 2006 IPCC national greenhouse gas guide (33).

TABLE 3 | Definitions of variables.

Variable	Definition	Unit
TC	Total CO_2 emissions	10^8 tons
PC	Per capita CO_2 emissions	ton
CI	CO_2 emissions per unit gross regional product	ton/10^4 yuan
PGDP	Per capita GDP	yuan
PS	The urban population divided by the total population	%
IS	The output of secondary industry divided by GDP	%
ES	Coal consumption divided by total energy consumption	%

effect of the corresponding driving factors on CO_2 emissions is. Conversely, the larger %ΔX is, the smaller DI is and the smaller the effect of the corresponding driving factors on CO_2 emissions is.

3.2 Data Sources

3.2.1 CO_2 Emission Estimation Model

The standard method used to estimate CO_2 emissions is the emission factor by the IPCC, and it has been the most widely used method even at present. This method estimates carbon emissions based on the greenhouse gas inventory, such as "the 2006 IPCC national GHG guide" prepared by the IPCC (The Intergovernmental Panel on Climate Change, 2006) and "the provincial GHG inventory preparation guide" prepared by China (NDRC, 2011). We used the following specified formula for estimation:

$$CO_2 = \sum CO_{2,i} = \sum ED_i \times EF_i \times 44/12, \quad (9)$$

where CO_2 is total CO_2 emissions related to energy consumption, ED represents the energy consumption, EF represents the carbon emission factors (**Table 2**), and the subscript I represents the energy type; here, we selected eight types that include coal, coke, crude oil, gasoline, kerosene, diesel, fuel oil, and natural gas.

3.2.2 Variables and Data Sources

Table 3 indicates the selected variables for this study, along with definitions. The energy consumption data were collected from the China Energy Statistical Yearbook (2001–2020) (NBS, 2001–2020). The GDP was calculated at the constant price of 2000. The population was counted at the end of the year. Total urban population, total population, GDP, and GDP index (last year = 100) were accumulated from China Statistical Yearbook 2020 (NBS, 2020).

As shown in **Table 4**, the maximum amount of total CO_2 emissions and the per capita CO_2 emissions were about three times the minimum over the whole study period separately. The average annual growth rate was 6.05% from 2000 to 2019, slightly higher than the per capita CO_2 emissions, which were 5.49% of the average annual growth rate. The CO_2 emission intensity was 4.49 tons/10^4 yuan in 2000, but only 2.44 tons/10^4 yuan in 2019, i.e., nearly half in 20 years. The average per capita income was 20,417 yuan, and the highest was 37,000 yuan, about four times the minimum. The value of the industrial structure decreased from 47.56 to 38.97%, which showed that some achievements were made, but there is still much room for improvement. The mean of the energy structure was as high as 67.51%, but the minimum value was 57.7%. Although it was still more than half and was the primary energy consumption category, the gap between the proportion of non-coal energy and coal was narrowing. The maximum population structure was 60.6%, the minimum was 36.22%, and the average annual growth rate was 9.8%. It seemed that China's urbanization was developing rapidly.

TABLE 4 | Description statistics of the variables.

Variable	TC	PC	CI	PGDP	IS	ES	PS
Mean	93.04	6.90	3.64	20417	44.27	67.51	48.91
St. Dev	30.56	2.11	0.64	9429	2.87	4.56	7.67
Min	41.45	3.27	2.44	7912	38.97	57.70	36.22
Max	126.50	9.07	4.49	37021	47.56	72.50	60.60

4 RESULTS

4.1 EKC Model Results

Using **Eqs. 3–5**, the EKC model was tested. We first selected the square term for regression, if the results were significant, and then added the cubic term for regression. Rs.(1) and Rs.(2) showed the

TABLE 5 | Results of the EKC model.

Variables	Rs.(1)	Rs.(2)	Rs.(3)	Rs.(4)	Rs.(5)	Rs.(6)
lnPGDP	9.9037***	−15.6132	9.9865***	−21.3665	8.9778***	−22.2694
$(lnPGDP)^2$	−0.4697***	2.1489	−0.4770***	2.7404	−0.4766***	2.7300
$(lnPGDP)^3$	—	−0.08944	—	−0.1099	—	−0.1095
_cons	−47.3748***	35.3914	−50.0699***	51.6261	−40.8162***	60.5366
R2	0.9920	0.9924	0.9904	0.9909	0.9665	0.9687
Turning point	10.5432	—	10.4674	—	9.4187	—
Per capita GDP	37,919	—	35,151	—	12,317	—

Note: *p < *0.1,* **p < *0.05, and* ***p < *0.01.*

TABLE 6 | Results of Tapio decoupling.

Time period	%ΔTC	%ΔPGDP	Dltc	State	%ΔPC	Dlpc	State	%ΔCI	Dlci	State
2000–2001	4.80	7.55	0.64	WD	4.07	0.54	WD	−3.26	−0.43	SD
2001–2002	6.85	8.40	0.81	EC	6.16	0.73	WD	−2.09	−0.25	SD
2002–2003	17.75	9.35	1.90	END	17.04	1.82	END	7.01	0.75	WD
2003–2004	15.30	9.46	1.62	END	14.62	1.55	END	4.71	0.50	WD
2004–2005	13.92	10.74	1.30	END	13.25	1.23	END	2.26	0.21	WD
2005–2006	10.44	12.09	0.86	EC	9.86	0.82	EC	−2.02	−0.17	SD
2006–2007	7.09	13.64	0.52	WD	6.54	0.48	WD	−6.25	−0.46	SD
2007–2008	3.56	9.09	0.39	WD	3.03	0.33	WD	−5.56	−0.61	SD
2008–2009	7.81	8.86	0.88	EC	7.28	0.82	EC	−1.45	−0.16	SD
2009–2010	8.40	10.10	0.83	EC	7.88	0.78	WD	−2.02	−0.20	SD
2010–2011	9.53	9.03	1.06	EC	9.01	1.00	EC	−0.02	0.00	SD
2011–2012	6.08	7.34	0.83	EC	5.56	0.76	WD	−1.65	−0.22	SD
2012–2013	3.39	7.24	0.47	WD	2.88	0.40	WD	−4.06	−0.56	SD
2013–2014	−0.47	6.88	−0.07	SD	−0.98	−0.14	SD	−7.35	−1.07	SD
2014–2015	−1.52	6.50	−0.23	SD	−2.00	−0.31	SD	−7.99	−1.23	SD
2015–2016	−0.77	6.27	−0.12	SD	−1.36	−0.22	SD	−7.13	−1.14	SD
2016–2017	0.91	6.35	0.14	WD	0.38	0.06	WD	−5.64	−0.89	SD
2017–2018	2.01	6.26	0.32	WD	1.62	0.26	WD	−4.44	−0.71	SD
2018–2019	2.35	5.73	0.41	WD	2.01	0.35	WD	−3.54	−0.62	SD
2000–2005	65.24	43.78	1.49	END	61.29	1.40	END	12.18	0.28	WD
2005–2010	29.60	48.61	0.61	WD	27.05	0.56	WD	−14.51	−0.30	SD
2010–2015	7.52	31.01	0.24	WD	5.38	0.17	WD	−19.56	−0.63	SD
2015–2019	5.36	19.64	0.27	WD	4.06	0.21	WD	−13.02	−0.66	SD

results of **Eq. 3**, Rs.(3) and Rs.(4) were for **Eq. 4**, and Rs.(5) and Rs.(6) were from **Eq. 5**.

As can be seen from **Table 5**, for Rs.(1), Rs.(3), and Rs.(5), each coefficient of the PGDP was positive, and each quadratic term coefficient was negative at the 1% level suggesting that China's CO_2 emission and per capita GDP follow an inverted U-shape. Meanwhile, for Rs.(2), Rs.(4), and Rs.(6), each of the coefficients of the PGDP was negative, each square term coefficient was positive, and each of the cubic term coefficients was negative. The results indicated that the relationship between CO_2 emissions and PGDP was an inverted N curve, but none of the coefficients was significant. Therefore, it could be considered that the relationship supported the EKC hypothesis, that is, CO_2 emissions enhanced first and then fell down with economic development. The turning point was 10.5432 for total CO_2 emissions, 10.4674 for per capita CO_2 emissions, and 9.4187 for CO_2 emission intensity. The corresponding PGDP was CNY 37,919, CNY 35,151, and CNY 12,317, respectively. In 2006, the per capita GDP was CNY 13,722, more significant than the turning point of CO_2 emission intensity, so it was obviously found that the CO_2 emission intensity absolutely decoupled from the PGDP in 2006. The per capita GDP in 2019 was CNY 37,021, which was greater than the turning point of per capita CO_2 emissions and smaller than the point of total CO_2 emissions. Therefore, the per capita CO_2 emissions were absolute decoupling too. However, the total CO_2 emissions were relative decoupling.

4.2 Tapio Decoupling Model Results

Equation 7 was used for Tapio decoupling, and the results are revealed in **Table 6**. First, the decoupling index was calculated year by year, and then the decoupling coefficient was calculated per five years.

As shown in **Table 7**, the decoupling results corresponding to different CO_2 emission variables were considerably different. From 2000 to 2019, the per capita CO_2 emission decoupling index rose and fell. It did not achieve decoupling except in 2013–2016. The decoupling index of total CO_2 emissions showed similar results, while the CO_2 emission intensity

TABLE 7 | Results of the influence factors.

Variables	Rs.(1)	Rs.(2)	Rs.(3)	Rs.(4)
lnPGDP	5.5215***	0.3844	10.2552***	-6.6466*
$(lnPGDP)^2$	−0.2432**	0.0254	−0.4910***	0.3444*
lnIS	1.0625**			0.8779**
lnES		2.0654***		2.5048***
lnPS			−0.6019	2.9108**
_cons	−27.9608***	−3.5249	−52.7648***	37.6761*
R2	0.9936	0.9941	0.9905	0.9968
Turning point	11.3518		10.4432	
Per capita GDP	85,116		34,309	

*Note: *p < 0.1, **p < 0.05, and ***p < 0.01.*

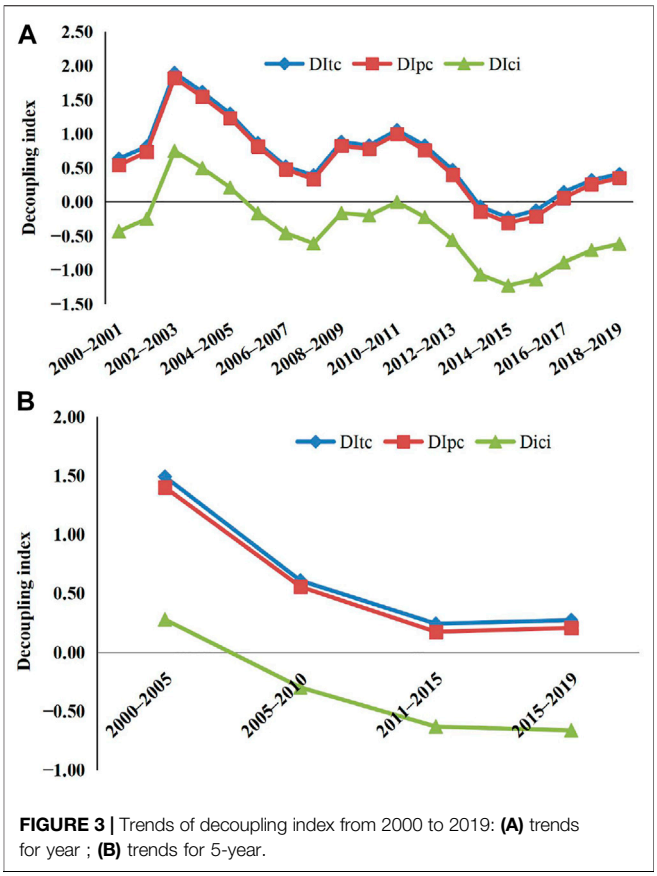

FIGURE 3 | Trends of decoupling index from 2000 to 2019: **(A)** trends for year ; **(B)** trends for 5-year.

showed strong decoupling except 2002–2005 with a state of weak decoupling. **Figure 3A** shows that the earliest decoupling time was CO_2 emission intensity, followed by per capita CO_2 emissions and total CO_2 emissions. It was obviously confirmed that the decoupling index was periodic, but the peak decoupling coefficient gradually decreased; that is to say, the decoupling state was periodically enhanced.

For the Five-Year Plan results, the decoupling index of the total CO_2 emissions and the per capita CO_2 emissions was weak decoupling except for the first five years. The decoupling for the CO_2 emission intensity was weak decoupling only during the 10th Five-Year Plan period and was strong decoupling in the rest period. However, **Figure 3B** seems to show a U-shaped trend of each variable's decoupling index.

4.3 Regression Results Showing the Influence Factors

As stated earlier, we used **Eq. 6** to observe the effects of influence factors. As **Table 5** already exhibited no complex N-shaped or inverted N-shaped curves, we removed the cubic term when adding the control variables. The regression results are exhibited in **Table 7**. Results (1)–(3) show the results of a single control variable; result (4) shows all control variables.

The industrial structure presented a significant and co-directional influence on the per capita CO_2 emissions. The inverted U-shaped curve still existed, but the turning point was 11.3518, which changed a lot, and the corresponding per capita income was CNY 85,116, which was more greater than above. The per capita GDP and per capita CO_2 had relative decoupling. The energy structure positively influenced the per capita CO_2 emissions at the 1% level. However, the linear and quadratic coefficients of per capita GDP were positive and were not statistically significant. The EKC hypothesis was not valid. Therefore, the decoupling state was indeterminate. The population structure had a negative but non-significant impact. However, the EKC hypothesis still existed, and the threshold point was CNY 34,309, which was consistent with CNY 35,151 above.

When added, all three control variables, the industrial structure, energy structure, and population structure, all significantly presented a positive influence on the per capita CO_2 emissions. While the relationship displayed a U-shaped curve, the EKC hypothesis did not exist.

Equation 8 was used to explore the influence of factors further. **Table 8** shows the decoupling results between the influence factors, industrial structure, energy structure, and population structure, and per capita CO_2 emissions.

Table 8 indicates the impact factors' decoupling results. Overall, the expansive negative decoupling was mainly shown for the industrial structure from 2000 to 2011, and strong negative decoupling was mostly exhibited from 2011 to 2019. The decoupling results were roughly divided into two stages for the energy structure too. They were mostly expansive negative decoupling in 2000–2011 and strong negative decoupling in 2011–2019. During the sample period 2000–2019, the decoupling of the population structure was mainly expansive negative decoupling, and the decoupling elasticity coefficient changed little.

From the Five-Year Plan results, it can be seen the decoupling between the industrial structure and per capita CO_2 emissions manifested expansive negative decoupling only in 2000–2005 and showed strong negative decoupling in 2006–2019. The energy structure displayed similar results to the industrial structure. During the first two "Five-Year Plans," the population structure showed expansive negative decoupling and then turned to weak decoupling during the following two "Five-Year Plans." As displayed in **Figure 4**, the increment of CO_2 emissions was positive, but the change rate strongly decreased

TABLE 8 | Influence factors' decoupling results.

Time period	ΔPC	ΔIS	DI_{IS}	State	ΔES	DI_{ES}	State	ΔPS	DI_{PS}	State
2000–2001	4.07	−1.63	−2.50	SND	−0.73	−5.58	SND	3.98	1.02	EC
2001–2002	6.16	−0.77	−8.05	SND	0.74	8.38	END	3.80	1.62	END
2002–2003	17.04	2.64	6.46	END	2.48	6.87	END	3.68	4.62	END
2003–2004	14.62	0.61	24.04	END	0.00	+∞	END	3.03	4.82	END
2004–2005	13.25	2.45	5.42	END	3.13	4.23	END	2.95	4.50	END
2005–2006	9.86	1.14	8.67	END	0.00	+∞	END	3.15	3.13	END
2006–2007	6.54	−1.42	−4.62	SND	0.14	47.35	END	3.49	1.88	END
2007–2008	3.03	0.19	16.35	END	−1.38	−2.20	SND	2.40	1.27	END
2008–2009	7.28	−2.16	−3.37	SND	0.14	52.09	END	2.88	2.53	END
2009–2010	7.88	1.18	6.70	END	−3.35	−2.35	SND	3.33	2.37	END
2010–2011	9.01	0.07	133.15	END	1.45	6.23	END	2.64	3.41	END
2011–2012	5.56	−2.38	−2.34	SND	−2.42	−2.30	SND	2.54	2.19	END
2012–2013	2.88	−2.74	−1.05	SND	−1.61	−1.80	SND	2.21	1.31	END
2013–2014	−0.98	−2.47	0.40	WND	−2.37	0.41	WND	1.94	−0.51	SD
2014–2015	−2.00	−5.21	0.38	WND	−3.04	0.66	WND	2.43	−0.83	SD
2015–2016	−1.36	−3.09	0.44	WND	−2.51	0.54	WND	2.23	−0.61	SD
2016–2017	0.38	0.68	0.55	WD	−2.57	−0.15	SND	2.04	0.19	WD
2017–2018	1.62	−0.41	−3.93	SND	−2.64	−0.61	SND	1.81	0.90	EC
2018–2019	2.01	−2.74	−0.73	SND	−2.20	−0.91	SND	1.71	1.18	EC
2000–2005	61.29	4.98	12.32	END	6.47	9.47	END	14.15	4.33	END
2005–2010	27.05	−2.23	−12.14	SND	−4.42	−6.12	SND	12.64	2.14	END
2010–2015	5.38	−12.22	−0.44	SND	−9.12	−0.59	SND	9.42	0.57	WD
2015–2019	4.06	−2.48	−1.64	SND	−7.23	−0.56	SND	5.67	0.72	WD

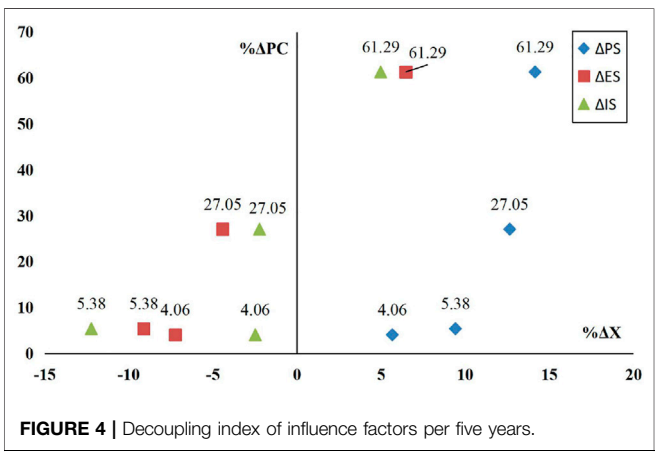

FIGURE 4 | Decoupling index of influence factors per five years.

from 61.29% in 2000–2005 to 4.06% in 2015–2019. Industrial and energy structures were negative with CO_2 emissions, unlike the population structure that positively impacted CO_2 emissions.

5 DISCUSSION AND CONCLUSION

5.1 Discussion of the EKC Results

From the EKC results shown in **Section 4.1**, the order for decoupling was CO_2 emission intensity, per capita CO_2 emissions, and total CO_2 emissions. This was in support of the literature results by Wu et al. (2018) and Shuai et al. (2018). However, a new insight was that the per capita CO_2 emissions in 2019 were greater than those in 2018, i.e., $\Delta C > 0$, which is inconsistent with the result above. In other words, the change in per capita CO_2 emissions did not decrease with economic growth. The probable reason was that other factors impacted the relationship between CO_2 emissions and economic growth. Actually, after adding the control variable of industrial structure, the turning point has swollen significantly. The use of fossil fuels may lead to endogeneity, which distorts EKC results (Jin and Kim, 2020). As a result, the EKC was invalid after adding the control variable of energy structure.

The sign of the industrial structure matched expectations. The proportion of China's secondary industry decreased from 47.56% in 2006 to 38.97% in 2019, so the industrial structure positively influenced CO_2 emission reduction; a similar conclusion was found by Simbi et al. (2021), when they studied the CO_2 emission patterns in Africa. However, the industrial structure led to a severe lag of the turning point; in other words, the absolute decoupling state could not be achieved in a short time. In the early stage of industrialization, there was an inhibitory influence on decoupling because of the scale effect (Wang and Su, 2019). The advantages of industrial structure upgrading seemed to be limited to reducing CO_2 emissions. Liu et al. (2021) found the tertiary industry beginning to become a new growth point of China's CO_2 emissions, which supported our finding.

The elasticity coefficient of energy structure was positive and significant. This showed that upgrading the energy structure made an essential reduction effect on CO_2 emissions. The elasticity coefficient of population structure was not significant in Rs.(3) but positive and significant in Rs.(4). The influence of the population structure was different on CO_2 emissions of the economic structure and the technical structure (Liu and Han, 2021).

However, after introducing control variables, the U-shaped curve was unexpected. From the perspective of factor endowment

structure, the growth of population structure fueled the shift of labor from agriculture to industry and service industry, and population has a negative impact on CO_2 emissions (Roy et al., 2017; Shahbaz et al., 2017). The energy structure has declined, but the proportion of coal was still as high as 57.7% in 2019. Although some studies declared that clean energy could effectively reduce CO_2 emissions (Pilatowska et al., 2020; Moutinho et al., 2018), other studies had found that the energy structure had little contribution to CO_2 emissions (Ghazali and Ali, 2019; Han and Liu, 2018; Wang and Feng, 2017). For China, the power structure was heavily dependent on coal-fired power generation. Although the proportion of renewable energy has increased significantly, the utilization rate of new energy power generation is low, and the average wind and light rejection rate is high (Liu et al., 2021). Isik et al. (2019) found that renewable energy consumption was much higher than that of fossil energy in Texas, but they did not find the CO_2 emissions reduced because of the swollen renewable energy consumption. Therefore, the inhibitory effect of energy structure optimization temporarily cannot offset the advancement effect of economic growth on CO_2 emissions. To reduce the CO_2 emissions and to develop the economy, we not only need to enhance the proportion of renewable energy and reduce the proportion of coal but also need to make technological breakthroughs, improve new energy power generation and energy storage technology (Liu et al., 2021), stabilize grid connection technology, and improve the utilization rate of renewable energy.

5.2 Discussion of the Tapio Decoupling Results

The periodicity of decoupling results was synchronized with the change cycle of economic growth. In 2000, the primary industry accounted for 14.7%. Due to the low consumption of fossil energy by agriculture, the CO_2 emissions were also relatively low. However, the output of agriculture was low; to pursue higher economic growth, the proportion of industry increased, from 44.5% in 2002 to 47% in 2008 (NBS, 2020). According to China's previous strong environmental pollution absorption capacity and the limit of science and technology development, many industrial projects with high energy consumption and high emissions were implemented in the climax of economic growth from 2002 to 2008. Consequently, an extensive economic growth model would lead to a doubling of environmental pressure (Li et al., 2021).

The US subprime mortgage crisis in 2008 triggered the global economic crisis, which affected China's economic growth. Subsequently, with the efforts of the government, China's economy recovered rapidly, triggering another wave of growth in CO_2 emissions. China's leading power's economic development was still a secondary industry at that time (Li et al., 2021). Even though technology progressed, and carbon emission intensity was declining, the positive effect of technological progress on CO_2 emissions was even offset by the negative effect of economic burgeoning growth (Wang and Feng, 2017) Since 2012, the industrial structure adjustment has achieved a part and positive effect in controlling CO_2 emissions. In 2012, the output of the tertiary industry accounted for 45.5% of GDP, surpassed that of the secondary industry for the first time, and rose to 53.9% by 2019 (NBS, 2020). As a result, the decoupling index gradually decreased and even reached negative decoupling from 2013 to 2016.

However, the re-link phenomenon from 2016 to 2019 might be caused by the low level of scientific and technological innovation and slow structural adjustment in the high-carbon industry (Liu, et al., 2021). The high-carbon industries were energy-intensive industries and highly depended on fossil energy. The emission reduction effect of industrial structure optimization had not reached the expectation, and the impact of technological progress and technological efficiency of the manufacturing industry on decoupling was still relatively small (Hang et al., 2019). However, from the long-term trend, the peak value of the decoupling index future will not exceed the decoupling index in 2010–2011.

The CO_2 intensity had been decoupled, but the decoupled index also increased slightly from 2016 to 2019. Although China's CO_2 intensity had decreased significantly by 40.96% from 2000 to 2019 (NBS, 2020), there is still a considerable difference between developed and developing countries. At present, China's carbon intensity is 2.8 times that of the United States and Japan, 3.6 times that of Germany, 5.5 times that of Britain, and 6 times that of France (Mikayilov et al., 2018).

5.3 Discussion of the Influence Factors

The industrial structure greatly impacted CO_2 emissions from the decoupling index of the three influencing factors. Different industrial structures have different characteristics of carbon dioxide emission density and energy consumption intensity (Zhou, 2022). During the course of an industrial structure optimization, the proportion of agriculture continues to decline, and the proportion of industry first rises and then falls. The proportion of the service industry continues to rise. The emission density of the service industry is lower than that of industry, and the economic output is higher than that of agriculture. It can be convinced that upgrading the industrial structure can not only reduce energy consumption (Qu and Li, 2019) but also ensure economic growth. However, the decoupling results from 2016 to 2019 showed that the advantages of industrial structure did not seem significant at this stage. For this reason, on the one hand, we need to increase investment in clean technology and vigorously develop clean technology in the tertiary industry. On the other hand, energy-intensive industries need to transfer to capital-intensive industries as soon as possible to satiate the advantages of energy structural updating.

The energy structure impacted little CO_2 emissions, which was distinct from the EKC conclusion. From 2000 to 2011, the proportion of coal in energy consumption was almost unchanged, while CO_2 emissions continued to proliferate. From 2011 to 2019, the proportion of coal continued to decline, but in **Figure 4**, the growth rate of carbon dioxide did not decline much from 2010 to 2019. On the changes in CO_2 emissions, energy-intensive industries mainly depended on the impact of industrial structure and energy structure (Moreau et al., 2018). Therefore, on the one side, our enterprises should strive to

raise energy efficiency and innovative technologies to enhance the utilization of renewable energy and reduce carbon dioxide emission intensity; on the other side, it is more important for the government to push for industrial structure transformation.

With the transfer of population structure to cities and towns, the rapid urbanization process affected the increase in CO_2 emissions (Ali et al., 2019; Abbasi et al., 2020). The proportion of CO_2 emissions from residents' life, transportation, storage, and postal industries increased. In 2018, the CO_2 emissions from these two industries accounted for 72.6% of the total emissions of the tertiary industry (Liu et al., 2021). Wang et al. (2018) also found that the population limits the decoupling of China and the United States. Therefore, in the urbanization process, the government should improve residents' low-carbon awareness and advocate a low-carbon lifestyle, such as reducing takeout and reducing fuel vehicles.

5.4 Conclusions, Executive Suggestions, and Research Direction

The purpose of our work was to compare the decoupling of China with two different decoupling models from 2000 to 2019, mainly to investigate the changes in the new economic growth between 2012 and 2019. Investigation using both methods found the CO_2 emission intensity had decoupled since 2006, but the CO_2 emissions had not decoupled. The results of the EKC model showed that the PGDP had not spanned the turning point. Moreover, the results of the Tapio model displayed that CO_2 emissions strongly decoupled from 2013 to 2016 but retreated to weak decoupling after 2016. In terms of influencing factors, energy and industrial structures positively impacted CO_2 emission reduction. However, the advantages were not significant at the new stage because the decoupling situation was weaker in 2015–2019 than in 2010–2015, and the growth of CO_2 emission rebounded after 2016. The population structure had a negative impact on CO_2 emissions. Then, there was a new finding in the results of the EKC model; the EKC was not valid after the introduction of control variables and showed a U-shape. When the control variables were introduced one by one, only the energy structure caused the EKC hypothesis to be invalid. After adding the industrial structure, the turning point more than doubled from 37,919 yuan to 85,116 yuan.

We provided the following executive suggestions along with future research directions based on the above-drawn conclusions:

1) First, from the perspective of the decoupling trend, it is suggested that China should strengthen and further optimize its energy structure to match the industrial structure. Also, at the new stage of China's economic development, the mismatch between the energy structure that is heavily dominated by coal and the industrial structure is the primary reason leading to the CO_2 emission increase. Clean energy and circular economy strategies could possibly be the main driving force for achieving "carbon peak and carbon neutralization." Under clean energy, the government should encourage the energy structure that of renewables, power to hydrogen-based. At the same time, research and innovation in the listed areas be considered.
2) Second, the government should strengthen low-carbon education for the public and let people change the traditional high-carbon lifestyle into a low-carbon lifestyle. The continuous growth of the population structure has become the main influencing factor for CO_2 emission growth in recent years. Although the expansion of the urban population has promoted economic development, the lifestyles of many rural people remain traditional when they transfer to cities and towns. Publicity and guidance should be strengthened to enhance people's low-carbon awareness.
3) Third, the government should strengthen and encourage technological innovation and encourage the synergistic effects of technological innovation, the industrial structure, and the energy structure on emission reduction. In addition to providing full support for low-carbon, energy-saving technologies, improving energy efficiency, and replacing coal with clean energy, China also needs to vigorously promote carbon capture and storage technologies to reduce carbon dioxide content in the atmosphere directly.
4) In addition, we need to strengthen institutional innovation, for example, using the carbon emission market to promote the establishment and improvement of the carbon financial system, implementing an individual carbon credit system, and encouraging the participation of everyone. China needs to seize the opportunities and challenges and strive to achieve the "carbon peak and carbon neutralization" goal as soon as possible.

Overall, the findings of this study can be helpful for China to take measures to manage carbon emissions. Given the data availability, the same models can be leveraged in other nations (Department of energy statistics, National Bureau of Statistics, 2001-2020).

DATA AVAILABILITY STATEMENT

The original contributions presented in the study are included in the article/Supplementary Material, and further inquiries can be directed to the corresponding author.

AUTHOR CONTRIBUTIONS

YH conceptualized the research idea, performed the methodology and formal analysis, administrated the project, supervised the work, validated the data, and wrote the original draft. YL curated and investigated the data. XL was involved in funding acquisition and reviewing and editing the paper.

FUNDING

This research was funded by the National Science Fund for Distinguished Young Scholars (Grant No. 71904059), Natural

Science Research of Jiangsu Higher Education Institutions of China (Grant No. 19KJB580007), and Humanities and Social Science Research of Nanjing University of Posts and Telecommunications (Grant No. NYS217021).

REFERENCES

Abbasi, M. A., Parveen, S., Khan, S., and Kamal, M. A. (2020). Urbanization and Energy Consumption Effects on Carbon Dioxide Emissions: Evidence from Asian-8 Countries Using Panel Data Analysis. *Environ. Sci. Pollut. Res.* 27 (15), 18029–18043. doi:10.1007/s11356-020-08262-w

Ajmi, A. N., and Inglesi-Lotz, R. (2021). Revisiting the Kuznets Curve Hypothesis for Tunisia: Carbon Dioxide vs. Ecological Footprint. *Energy Sources, Part B Econ. Plan. Policy* 16 (5), 1–14. doi:10.1080/15567249.2020.1850923

Alege, O. P., Adediran, S. O., and Ogundipe, A. A. (2016). Pollutant Emissions, Energy Consumption and Economic Growth in Nigeria. *Int. J. Energy Econ. Policy* 6 (2), 202–207.

Ali, R., Bakhsh, K., and Yasin, M. A. (2019). Impact of Urbanization on CO2 Emissions in Emerging Economy: Evidence from Pakistan. *Sustain. Cities Soc.* 48, 101553. doi:10.1016/j.scs.2019.101553

Ali, A., Usman, M., Usman, O., and Sarkodie, S. A. (2021). Modeling the Effects of Agricultural Innovation and Biocapacity on Carbon Dioxide Emissions in an Agrarian-Based Economy: Evidence from the Dynamic ARDL Simulations. *Front. Energy Res.* 8, 592061. doi:10.3389/fenrg.2020.592061

Allard, A., Takman, J., Uddin, G. S., and Ahmed, A. (2018). The N-Shaped Environmental Kuznets Curve: an Empirical Evaluation Using a Panel Quantile Regression Approach. *Environ. Sci. Pollut. Res.* 25 (6), 5848–5861. doi:10.1007/s11356-017-0907-0

Ameyaw, B., Li, Y., Annan, A., and Agyeman, J. K. (2020). West Africa's CO2 Emissions: Investigating the Economic Indicators, Forecasting, and Proposing Pathways to Reduce Carbon Emission Levels. *Environ. Sci. Pollut. Res.* 27 (12), 13276–13300. doi:10.1007/s11356-020-07849-7

Bhattarai, M., and Hammig, M. (2001). Institutions and the Environmental Kuznets Curve for Deforestation: A Crosscountry Analysis for Latin America, Africa and Asia. *World Dev.* 29 (6), 995–1010. doi:10.1016/s0305-750x(01)00019-5

Cohen, G., Jalles, J. T., Loungani, P., Marto, R., and Wang, G. (2019). Decoupling of Emissions and GDP: Evidence from Aggregate and Provincial Chinese Data. *Energy Econ.* 77, 105–118. doi:10.1016/j.eneco.2018.03.030

De Moor, J. (2018). The 'efficacy Dilemma' of Transnational Climate Activism: the Case of COP21. *Environ. Polit.* 27 (6), 1079–1100. doi:10.1080/09644016.2017.1410315

Department of energy statistics, National Bureau of Statistics (2001-2020). *China Energy Statistical Yearbook*. Beijing: Chinese Statistics Press.

Dong, K., Sun, R., Jiang, H., and Zeng, X. (2018). CO2 Emissions, Economic Growth, and the Environmental Kuznets Curve in China: What Roles Can Nuclear Energy and Renewable Energy Play? *J. Clean. Prod.* 196, 51–63. doi:10.1016/j.jclepro.2018.05.271

Ghazali, A., and Ali, G. (2019). Investigation of Key Contributors of CO2 Emissions in Extended STIRPAT Model for Newly Industrialized Countries: A Dynamic Common Correlated Estimator (DCCE) Approach. *Energy Rep.* 5, 242–252. doi:10.1016/j.egyr.2019.02.006

Gokmenoglu, K. K., and Taspinar, N. (2018). Testing the Agriculture-Induced EKC Hypothesis: the Case of Pakistan. *Environ. Sci. Pollut. Res.* 25 (23), 22829–22841. doi:10.1007/s11356-018-2330-6

Gough, I. (2017). *Beyond Bonn: Eco-Social Policies for Social Justice and Environmental Sustainability", Social Europe*.

Grossman, G. M., and Krueger, A. B. (1995). Economic Growth and the Environment. *Q. J. Econ.* 110, 353–377. doi:10.2307/2118443

Han, Y. L., and Liu, Y. P. (2018). Study on Influencing Factors of Industrial in Jiangsu Based on LMDI Model. *Environ. Sci. Technol.* 41 (12), 278–284.

Hang, Y., Wang, Q., Zhou, D., and Zhang, L. (2019). Factors Influencing the Progress in Decoupling Economic Growth from Carbon Dioxide Emissions in China's Manufacturing Industry. *Resour. Conservation Recycl.* 146, 77–88. doi:10.1016/j.resconrec.2019.03.034

Hao, Y., Huang, Z., and Wu, H. (2019). Do Carbon Emissions and Economic Growth Decouple in China? an Empirical Analysis Based on Provincial Panel Data. *Energies* 12 (12), 2411. doi:10.3390/en12122411

Hasanov, F. J., Mikayilov, J. I., Mukhtarov, S., and Suleymanov, E. (2019). Does CO2 Emissions-Economic Growth Relationship Reveal EKC in Developing Countries? Evidence from Kazakhstan. *Environ. Sci. Pollut. Res.* 26 (34), 30229–30241. doi:10.1007/s11356-019-06166-y

Haseeb, A., Xia, E., DanishBaloch, M. A., and Baloch, M. A. (2018). Financial Development, Globalization, and CO2 Emission in the Presence of EKC: Evidence from BRICS Countries. *Environ. Sci. Pollut. Res.* 25 (31), 31283–31296. doi:10.1007/s11356-018-3034-7

Haseeb, M., Wattanapongphasuk, S., and Jermsittiparsert, K. (2019). Financial Development, Market Freedom, Political Stability, Economic Growth and C [O. Sub. 2] Emissions: An Unexplored Nexus in ASEAN Countries. *Contemp. Econ.* 13 (3), 363–375. doi:10.5709/ce.1897-9254.319

Hu, Z. Y., Liu, Y. W., and Tang, L. W. (2013). The Study on EKC Curve of Carbon Dioxide Emissions in China at the Background of Lower-Carbon Economy. *Stat. Res.* 30 (02), 73–79.

He, Y. D., Wen, H., and Sun, C. W. (2021). Forecasting China's Total Carbon Emission and its Structure in the 14th Five-Year Plan: Based on Mixed-Frequency ADL-MIDAS Model. *Econ. Prob.* 4, 31–40.

Isik, C., Ongan, S., and Özdemir, D.(2019). The Economic Growth/development and Environmental Degradation: Evidence from the US State-Level EKC Hypothesis. *Environ. Sci. Pollut. Res.* 26, 30772–30781. doi:10.1007/s11356-019-06276-7

Jin, L., Duan, K. R., Shi, C. M., and Ju, X. W. (2017). The Impact of Technological Progress in the Energy Sector on Carbon Emissions: An Empirical Analysis from China. *Int. J. Environ. Res. Public Health* 14 (12), 1505. doi:10.3390/ijerph14121505

Jin, T., and Kim, J. (2020). Investigating the Environmental Kuznets Curve for Annex I Countries Using Heterogeneous Panel Data Analysis. *Environ. Sci. Pollut. Res.* 27 (9), 10039–10054. doi:10.1007/s11356-020-07668-w

Krisada, C., Chanakan, C., Nutnapha, L., and Kittisak, J. (2021). The Impact of Economic Growth, Globalization, and Financial Development on Co2 Emissions in ASEAN Countries. *Acad. Strategic Manag. J.* 20, 1–14.

Li, R. R., and Jiang, R. (2020). Investigating Effect of R&D Investment on Decoupling Environmental Pressure from Economic Growth in the Global Top Six Carbon Dioxide Emitters. *Sci. Total Environ.* 740, 140053. doi:10.1016/j.scitotenv.2020.140053

Li, Z., Sun, R. J., Qin, M. M., and Hu, D. O. (2020). Gasoline to Diesel Consumption Ratio: A New Socioeconomic Indicator of Carbon Dioxide Emissions in China. *Sustainability* 12 (14), 5608. doi:10.3390/su12145608

Li, M. Y., Zhang, S. H., Wang, C., and Cai, B. F. (2021). The Carbon Emission Status and Emission Reduction Positioning of Key Industrial Sectors. *Chin. J. Environ. Manage.* 3, 28–39.

Lin, J. Y. F. (2011). New Structural Economics: A Framework for Rethinking Development. *World Bank Res. Observer* 26 (2), 193–221. doi:10.1093/wbro/lkr007

Liu, D. N., and Xiao, B. W. (2018). Can China Achieve its Carbon Emission Peaking? A Scenario Analysis Based on STIRPAT and System Dynamics Model. *Ecol. Indic.* 93, 647–657. doi:10.1016/j.ecolind.2018.05.049

Liu, R. H., Wang, G., Huang, N., and Ding, M. L. (2021). Research on the Path of China's Scientific and Technological Innovation Supporting Carbon Peak and Carbon Neutralization. *Soc. Sci. Guangxi.* 8, 1–7.

Liu, Y. P., and Han, Y. L. (2021). Impacts of Urbanization and Technology on Carbon Dioxide Emissions of Yangtze River Economic Belt at Two Stages: Based on an Extended STIRPAT Model. *Sustainability* 13, 7022. doi:10.3390/su13137022

Meirun, T., Mihardjo, L. W., Haseeb, M., Khan, S. A. R., and Jermsittiparsert, K. (2021). The Dynamics Effect of Green Technology Innovation on Economic Growth and CO2 Emission in Singapore: New Evidence from Bootstrap ARDL Approach. *Environ. Sci. Pollut. Res.* 28 (4), 4184–4194. doi:10.1007/s11356-020-10760-w

Mikayilov, J. I., Hasanov, F. J., and Galeotti, M. (2018). Decoupling of CO2 Emissions and GDP: A Time-Varying Cointegration Approach. *Ecol. Indic.* 95, 615–628. doi:10.1016/j.ecolind.2018.07.051

Moreau, V., Neves, C. A. De. O., and Vuille, F. (2018). Is Decoupling a Red Herring? the Role of Structural Effects and Energy Policies in Europe. *Energy Policy* 128, 243–252. doi:10.1016/j.enpol.2018.12.028

Moutinho, V., Madaleno, M., Inglesi-Lotz, R., and Dogan, E. (2018). Factors Affecting CO 2 Emissions in Top Countries on Renewable Energies: A LMDI Decomposition Application. *Renew. Sust. Energy Rev.* 90, 605–622. doi:10.1016/j.rser.2018.02.009

Naqvi, S. A. A., Shah, S. A. R., and Mehdi, M. A. (2020). Revealing Empirical Association Among Ecological Footprints, Renewable Energy Consumption, Real Income, and Financial Development: a Global Perspective. *Environ. Sci. Pollut. Res.* 27 (34), 42830–42849. doi:10.1007/s11356-020-09958-9

Naqvi, S. A. A., Shah, S. A. R., Anwar, S., and Raza, H. (2021). Renewable Energy, Economic Development, and Ecological Footprint Nexus: Fresh Evidence of Renewable Energy Environment Kuznets Curve (RKC) from Income Groups. *Environ. Sci. Pollut. Res.* 28 (2), 2031–2051. doi:10.1007/s11356-020-10485-w

National Bureau of Statistics (2020). *China Statistical Yearbook*. Beijing: China Statistics Press.

National Development and Reform Commission (2011). *The Provincial Greenhouse Gas Inventory Preparation Guide*. Beijing: China Statistics Press.

Ozturk, I., Majeed, M. T., and Khan, S. (2021). Decoupling and Decomposition Analysis of Environmental Impact from Economic Growth: a Comparative Analysis of Pakistan, India, and China. *Environ. Ecol. Stat.* 28, 793–820. doi:10.1007/s10651-021-00495-3

Pata, U. K. (2018). The Effect of Urbanization and Industrialization on Carbon Emissions in Turkey: Evidence from ARDL Bounds Testing Procedure. *Environ. Sci. Pollut. Res.* 25 (8), 7740–7747. doi:10.1007/s11356-017-1088-6

Peng, J. W., Huang, X. J., Zhong, T. Y., and Zhao, Y. T. (2011). Decoupling Analysis of Economic Growth and Energy Carbon Emissions in China. *Res. Sci.* 33 (4), 626–633.

Pilatowska, M., Geise, A., and Wlodarczyk, A. (2020). The Effect of Renewable and Nuclear Energy Consumption on Decoupling Economic Growth from CO2 Emissions in Spain. *Energies* 13 (9), 2124. doi:10.3390/en13092124

Prastiyo, S. E., Irham, Hardyastuti, S., and Jamhari. (2020). How Agriculture, Manufacture, and Urbanization Induced Carbon Emission? the Case of Indonesia. *Environ. Sci. Pollut. Res.* 27 (33), 42092–42103. doi:10.1007/s11356-020-10148-w

Qu, J. Y., and Li, K. (2019). Measurement and Analysis of "Decoupling" between Industrial Growth and Carbon Dioxide Emissions in China. *J. Xi'an Jiaot. Univers.* 39 (5), 92–104.

Roy, M., Basu, S., and Pal, P. (2017). Examining the Driving Forces in Moving toward a Low Carbon Society: an Extended STIRPAT Analysis for a Fast Growing Vast Economy. *Clean. Technol. Environ. Policy* 19 (9), 2265–2276. doi:10.1007/s10098-017-1416-z

Shah, S. A. R., Naqvi, S. A. A., and Anwar, S. (2020a). Exploring the Linkage Among Energy Intensity, Carbon Emission and Urbanization in Pakistan: Fresh Evidence from Ecological Modernization and Environment Transition Theories. *Environ. Sci. Pollut. Res.* 27 (32), 40907–40929. doi:10.1007/s11356-020-09227-9

Shah, S. A. R., Naqvi, S. A. A., Riaz, S., Anwar, S., and Abbas, N. (2020b). Nexus of Biomass Energy, Key Determinants of Economic Development and Environment: A Fresh Evidence from Asia. *Renew. Sustain. Energy Rev.* 133, 110244. doi:10.1016/j.rser.2020.110244

Shah, S. A. R., Naqvi, S. A. A., Nasreen, S., and Abbas, N. (2021). Associating Drivers of Economic Development with Environmental Degradation: Fresh Evidence from Western Asia and North African Region. *Ecol. Indic.* 126, 107638. doi:10.1016/j.ecolind.2021.107638

Shah, S. A. R., Naqvi, S. A. A., Anwar, S., Shah, A. A., and Nadeem, A. M. (2022). Socio-economic Impact Assessment of Environmental Degradation in Pakistan: Fresh Evidence from the Markov Switching Equilibrium Correction Model. *Environ. Dev. Sustain.*. doi:10.1007/s10668-021-02013-8

Shahbaz, M., Chaudhary, A. R., and Ozturk, I. (2017). Does Urbanization Cause Increasing Energy Demand in Pakistan? Empirical Evidence from STIRPAT Model. *Energy* 122, 83–93. doi:10.1016/j.energy.2017.01.080

Shuai, C. Y., Chen, X., Wu, Y., Zhang, Y., and Tan, Y. T. (2018). A Three-step Strategy for Decoupling Economic Growth from Carbon Emission: Empirical Evidences from 133 Countries. *Sci. Total Environ.* 646, 524–543. doi:10.1016/j.scitotenv.2018.07.045

Simbi, C. H., Lin, J. Y., Yang, D. W., Ndayishimiye, J. C., Liu, Y., Li, H. M., et al. (2021). Decomposition and Decoupling Analysis of Carbon Dioxide Emissions in African Countries during 1984-2014. *J. Ecviron. Sci.* 102, 85–98. doi:10.1016/j.jes.2020.09.006

Sun, Y., Li, M. X., Zhang, M. J., Khan, H. S. U. D., Li, J. Q., Li, Z. Y., et al. (2021). A Study on China's Economic Growth, Green Energy Technology, and Carbon Emissions Based on the Kuznets Curve (EKC). *Environ. Sci. Pollut. Res.* 28 (6), 7200–7211. doi:10.1007/s11356-020-11019-0

Tapio, P. (2005). Towards a Theory of Decoupling: Degrees of Decoupling in the EU and the Case of Road Traffic in Finland between 1970 and 2001. *Transp. Pol.* 12 (2), 137–151. doi:10.1016/j.tranpol.2005.01.001

The Intergovernmental Panel on Climate Change (IPCC) (2006). *IPCC Guidelines for National Greenhouse Gas Inventories*. Hayama, Kanagawa, Japan: Institute for Global Environmental Strategies.

Wang, M., and Feng, C. (2017). Decomposition of Energy-Related CO2 Emissions in China: An Empirical Analysis Based on Provincial Panel Data of Three Sectors. *Appl. Energy* 190, 772–787. doi:10.1016/j.apenergy.2017.01.007

Wang, Q., and Su, M. (2019). The Effects of Urbanization and Industrialization on Decoupling Economic Growth from Carbon Emission - A Case Study of China. *Sustain. Cities Soc.* 51, 101758. doi:10.1016/j.scs.2019.101758

Wang, Q., Zhao, M. M., Li, R. R., and Su, M. (2018). Decomposition and Decoupling Analysis of Carbon Emissions from Economic Growth: A Comparative Study of China and the United States. *J. Clean. Prod.* 197, 178–184. doi:10.1016/j.jclepro.2018.05.285

WMO (2021). *The State of the Global Climate 2020 (WMO-No.1264)*. Switzerland: World Meteorological Organization.

GDP Growth Annual (%)-China (2020). Available on: https://data.worldbank.org/indicator/NY.GDP.MKTP.KD.ZG?end=2020&locations=CN&start=1961&view=map&year=2020.

Wu, Y., Tam, V. W. Y., Shuai, C. Y., Shen, L. Y., Zhang, Y., and Liao, S. J. (2018). Decoupling China's Economic Growth from Carbon Emissions: Empirical Studies from 30 Chinese Provinces (2001-2015). *Sci. Total Environ.* 656, 576–588. doi:10.1016/j.scitotenv.2018.11.384

Xia, C. X., and Wang, Z. L. (2020). The Effect of Fossil Fuel and Hydropower on Carbon Dioxide Emissions: EKC Validation with Structural Breaks. *J. Environ. Eng. Landsc.* 28 (1), 36–47. doi:10.3846/jeelm.2020.11832

Zaidi, S. A. H., Zafar, M. W., Shahbaz, M., and Hou, F. J. (2019). Dynamic Linkages between Globalization, Financial Development and Carbon Emissions: Evidence from Asia Pacific Economic Cooperation Countries. *J. Clean. Prod.* 228, 533–543. doi:10.1016/j.jclepro.2019.04.210

Zhang, Q., Naqvi, S. A. A., and Shah, S. A. R. (2021). The Contribution of Outward Foreign Direct Investment, Human Well-Being, and Technology toward a Sustainable Environment. *Sustainability* 13 (20), 11430. doi:10.3390/su132011430

Zhou, M. Z. (2022). Global Carbon Emission Pattern and China's Challenges. Available at: https://baijiahao.baidu.com/s?id=1698066633643641593&wfr=spider&for=pc (Accessed February 15, 2022).

Conflict of Interest: The authors declare that the research was conducted in the absence of any commercial or financial relationships that could be construed as a potential conflict of interest.

Publisher's Note: All claims expressed in this article are solely those of the authors and do not necessarily represent those of their affiliated organizations, or those of the publisher, the editors, and the reviewers. Any product that may be evaluated in this article, or claim that may be made by its manufacturer, is not guaranteed or endorsed by the publisher.

frontiers | Frontiers in Energy Research

TYPE Original Research
PUBLISHED 05 September 2022
DOI 10.3389/fenrg.2022.987495

OPEN ACCESS

EDITED BY
Nallapaneni Manoj Kumar,
City University of Hong Kong, Hong Kong SAR, China

REVIEWED BY
Amit Kumer Podder,
Khulna University of Engineering & Technology, Bangladesh
Aneesh A. Chand,
University of the South Pacific, Fiji
Gautam Raina,
Malaviya National Institute of Technology, Jaipur, India

*CORRESPONDENCE
Jeung-Soo Huh,
jshuh@knu.ac.kr

SPECIALTY SECTION
This article was submitted to Sustainable Energy Systems and Policies, a section of the journal Frontiers in Energy Research

RECEIVED 06 July 2022
ACCEPTED 25 July 2022
PUBLISHED 05 September 2022

CITATION
Same NN, Yakub AO, Kigha Nsafon BE, Owolabi AB, Mih TA, Suh D and Huh J-S (2022), Performance evaluation of renewable-based sustainable micro-grid under predictive management control strategy: A case study of Gado refugee camp in Cameroon. *Front. Energy Res.* 10:987495. doi: 10.3389/fenrg.2022.987495

Performance evaluation of renewable-based sustainable micro-grid under predictive management control strategy: A case study of Gado refugee camp in Cameroon

Noel Ngando Same[1], Abdulfatai Olatunji Yakub[1], Benyoh Emmanuel Kigha Nsafon[1], Abdulhameed Babatunde Owolabi[1], Thomas Attia Mih[2], Dongjun Suh[1] and Jeung-Soo Huh[1]*

[1]Department of Energy Convergence and Climate Change, Department of Convergence and Fusion System Engineering, Institute for Global Climate Change and Energy, Kyungpook National University, Daegu, South Korea, [2]Department of Computer Engineering, College of Technology, University of Buea, Buea, Cameroon

The recent use of hybrid renewable energy systems (HRESs) is considered one of the most reliable ways to improve energy access to decentralized communities because of their techno-economic and environmental benefits. Many distant locales, such as camps in war-torn nations, lack basic necessities like power. This study proposes a remedy for power outages in these areas; by designing an HRES and a control system for monitoring, distributing, and managing the electrical power from sustainable energy sources to supply the load. Hence, providing affordable, reliable, and clean energy for all (Sustainable Development Goal 7). In this study, the feasibility and techno-economic performance of an HRES for a refugee camp was evaluated under load following (LF), cycle charging (CC), and predictive control strategy (PS). The optimization results revealed that the PS was the most suitable, as it had the lowest cost and was more eco-friendly and energy-efficient. The predictive control strategy had a 48-h foresight of the load demand and resource potential and hence could effectively manage the HRES. The total net present cost (NPC) for the electrification of this refugee camp was $3,809,822.54, and the cost of electricity generated for every kWh is $0.2018. Additionally, 991,240.32 kg of emissions can be avoided annually through the hybridization of the diesel generator under the PS.

KEYWORDS

hybrid renewable energy systems, predictive control strategy, techno-economic modelling, energy management, refugee camp

1 Introduction

Energy is one of the main elements required for the development and growth of a country. The global population and the emergence of new technologies are on an ever-increasing trend, creating a vast gap in energy demand and supply. Due to this gap and the overexploitation of currently available resources, primary energy resources, such as fossil fuels, are reaching a state of depletion. It is worth noting that the primary source of energy in the world is fossil fuels, which constitute approximately 84% of the total global energy system (Mubaarak et al., 2021). Power generation is unsustainable because of the overexploitation of fossil fuels and their adverse effects on the environment. With this in mind, the development and deployment of sustainable energy technologies are on the rise (Chowdhury et al., 2020). In this context, renewable energy is considered an effective means of providing sustainable energy generation that is affordable, accessible, and reliable (Mubaarak et al., 2021) and supported by the United Nations (UN) Sustainable Development Goals (SDGs) (Manoj Kumar et al., 2020). The IEA forecasts that Africa's total energy consumption and power demand will increase at average annual rates of 1.4% and 2.6%, respectively. Unfortunately, as of 2019, approximately 770 million people still do not have access to electricity, with 75% of this population in the sub-Saharan region of Africa, the majority of which live in rural areas (Jahangiri et al., 2019; IEA, 2020).

Furthermore, according to the United Nations High Commissioner for Refugees (UNHCR), 9.2% of the 770 million people are displaced individuals and refugees who have been forced away from their homes by natural disasters or wars (I. Renewable Energy Agency, 2019). These individuals rely solely on unsustainable polluting energy, which sometimes poses a significant risk to their security, health, and well-being (Aste et al., 2017). Usually, on the scale of preference of humanitarian organization actions in response to refugee needs, access to clean and reliable energy is considered a low priority (van Hove and Johnson, 2021). This is a result of inadequate funding and limited policies and practices within the humanitarian organization concerning the provision of reliable and sustainable clean energy (van Hove and Johnson, 2021). In contrast, access to reliable and sustainable energy in a refugee camp can quickly boost the social, economic, productivity, safety, and health aspects of refugees and displaced persons, the host country, and humanitarian organizations (I. Renewable Energy Agency, 2019). According to the UNHCR, Cameroon has 1.9 million persons of concern (PoC) and 460,317 refugees and asylum seekers (spread across eight camps). A total of 1,052,591 internally displaced persons (IDPs) and 466,578 returned IDPs (Septembre, 2014; UNHCR, 2021). The provision of necessities for sustenance and productivity for these PoCs is mainly by the local government, with support from the humanitarian organization, and other benevolent individuals (van Hove and Johnson, 2021).

In addition, studies have shown that most refugee camps rely on diesel generators and other conventional sources, such as fuelwood, kerosene lamps, and candles, for their daily needs and other settlement services. Aside from the environmental and health detriments, fuel prices usually fluctuate, making them unreliable (Grafham and Lahn, 2018; Solar Energy, 2022). The transition from these conventional sources to renewable energy is required to bridge the gap in energy access to these camps. Thus, this study aimed to design an optimal hybrid renewable energy system (HRES) for the Gado Badzarre refugee camp in the eastern region of Cameroon using the hybrid optimization of multiple energy resources (HOMER). This HRES will go a long way to improve the livelihood of PoCs within the camp, contribute to the reduction of greenhouse gas (GHG) emissions and also act as a means of ensuring reliable, affordable, sustainable and clean energy for all.

Many researchers have worked on HRESs using HOMER for off-grid and grid electrification. Table 1 summarizes some recent studies. While the technologies used in each study differ, most of the HRESs in Table 1 are clean energy-based. The optimal component sizing of an HRES was investigated in (Chand et al., 2019; Kumar et al., 2020; Abada et al., 2021; Aditya et al., 2021). Their research concluded that to size the components of HRESs properly, effective control management strategies need to be implemented because of dispatchable components, such as batteries and diesel generators. Various studies have proposed dispatch strategies (such as load following and cycle charging) to control the operation of generators and batteries in HRESs. (Ansong et al., 2017; Halabi et al., 2017) used the load following strategy (LF) to analyze the performance of their proposed HRES to obtain the optimal size of the components. The size of each component differed across both studies. Similarly, Rajbongshi et al. (2017) and Murugaperumal and Ajay D Vimal Raj (2019) investigated the optimum HRES design with variation in the state of charge under the cycle charging (CC) strategy. Other studies employed both strategies to determine the best strategy for the proposed HRES. Singh et al. (2017) designed a standalone wind/diesel/battery HRES under LF and CC dispatch strategies. Their results indicate that LF produced the best performance based on the renewable fraction. Nsafon et al. (2020) carried out an optimization and sustainability analysis of a PV-wind-diesel hybrid energy system for decentralized energy generation using HOMER. They varied the PV slope and wind turbine hub height under the LF and CC dispatch strategies to supply the load. The results showed that for this residential estate, the best option was PV-wind-diesel with a PV slope and hub height of 3° and 75 m, respectively, under the LF strategy. A comparative study was conducted by Shoeb and Shafiullah (2018) for the PV/diesel HRES under the FL and CC strategies. They concluded that CC was the most suitable based on net present cost (NPC), cost of

TABLE 1 Summary of some recent studies on different HRES.

Configuration	System type	Evaluation criteria	Methodology	Location	Year
Biogas/grid (Karmaker et al., 2020)	Off-grid	NPC, GHG	HOMER	Bangladesh	2020
PV/battery/diesel (Soudan and Masoud Darya, 2021)	Off-grid	LCOE	HOMER	Western Asia	2021
PV/wind/fuel-cell/electrolyzer (Rezaei et al., 2021)	Grid	NPC, LCOE, OP	HOMER	Iran	2021
PV/wind/battery/diesel (Chowdhury et al., 2020)	Off-grid	LCOE, NPC, GHG, RF	HOMER	Bangladesh	2020
Wind/diesel/fuel cell/battery/electrolyzer (Seedahmed et al., 2022)	Off-grid	GPC, LCOE, O&M	HOMER	Saudi Arabia	2022
PV/wind/diesel/battery (Babaei et al., 2022)	Off-grid	LCOE, NPC	HOMER	Canada	2022
PV/wind/fuel cell/battery (Zhang et al., 2022)	Off-grid	NPC, LCOE	HOMER	South Korea	2022
PV/wind/hydro/battery (Sharma et al., 2022)	Grid	NPC, LCOE, GHG, BL, RF	HOMER	India	2022
PV/wind/diesel/run-river-hydro/battery (Ma et al., 2022)	Off-grid	NPC, LCOE, RF	HOMER	Iran and Kuwait	2021
PV/wind/diesel (Mubaarak et al., 2021)	Off-grid	GHG, NPC, LCOE	HOMER	Yemen	2020
PV/wind/diesel/fuel-cell/ battery (Jegadeesan et al., 2020)	Off-grid	LCOE, NPC	HOMER	India	2021
PV/diesel (Baranda Alonso et al., 2021)	Off-grid	GHG, PP, NPC	HOMER	Rwanda	2021
PV/diesel/biomass/wind/battery (Neves et al., 2021)	Off-grid	PP, LCOE, NPC	HOMER	Zambia	2021
PV/wind/fuel-cell/diesel/electrolyzer/battery/tank (Ur Rashid et al., 2022)	Grid	NPC, LCOE, IC, OC	HOMER	Pakistan	2022
PV/fuel-cell (Pal and Mukherjee, 2021)	Off-grid	LCOE, RF, NPC	HOMER	India	2021

Keywords: LCOE, levelized cost of energy; GHG, greenhouse gas; GPC, gross present cost; NPC, net present cost; RF, renewable fraction; RP, renewable penetration; O&M, operation and maintenance cost; PP, payback period; BL, battery life; TC, total cost; CR, connection rate; IC, initial cost; OC, operating cost.

electricity (COE), and GHG emissions. Aziz et al. (2019) proposed a combined dispatch strategy (CD) for the energy management and optimization of PV/diesel/battery HRES. In their study, they evaluated the performance of the HRES under LF, CC, and CD. They concluded that the CD showed the best economic and environmental results. Das and Zaman (2019) carried out performance analysis of dispatch strategies, batteries, and generator selection on a PV/diesel HRES. The results showed that CD outperformed LF and CC.

Based on the above literature, HOMER has been used to design various HRESs for refugee camps and other settlements using different control strategies. Still, none has employed a predictive control strategy. Furthermore, no study has adopted a predictive control strategy as an energy management technique for modeling an HRES. In this context, we propose the design of an optimal HRES with HOMER, primarily focusing on refugee camps in Cameroon, with the principal aim of modeling and designing an affordable, reliable and sustainable HRES that combines alternative sources using a predictive control strategy. To achieve the stated objective, the scope of this study is as follows:

- Perform a techno-economic and environmental design and modeling of an HRES.
- Carry out a comprehensive performance analysis of the different control strategies employed in hybrid PV/diesel/battery systems.
- Evaluate the predictive control strategy as an energy management technique.
- Finally, perform a sensitivity analysis of the HRES under the predictive control strategy.

2 Materials and methods

The proposed schematic diagram of the hybrid system, comprising a solar PV, diesel generator, Li-ion battery, bidirectional converter, and the load as its components, is shown in Figure 1. The DC bus had a solar PV and battery system, whereas the AC bus had a diesel generator. The battery and generator acted as backups for the proposed micro-grid system.

The system algorithm for the optimization process of the refugee camp by HOMER is shown in Figure 2. This section details the study area, load profile, resource data, component specifications, mathematical modelling, and control strategies.

2.1 Study area

The Gado refugee camp (Table 2) is located in eastern Cameroon. It is the largest of the four camps in this region and the second-largest in Cameroon (Kehdinga and Zacharie, 2020). The camp covers approximately 55 ha and is located in Lom–et–Djerem, approximately 78 km^2 from the border between Cameroon and the Central African Republic (CAR). The total camp population is 28,181 inhabitants, most of whom are refugees from the CAR (SEPTEMBRE, 2021).

Two seasons exist in this region: the wet and dry seasons, with an annual average temperature of 23°C. In the evenings, the primary light sources used in the camp households include oil and solar lamps, candles, and fuelwood. The location of the refugee camp is shown in Figure 3.

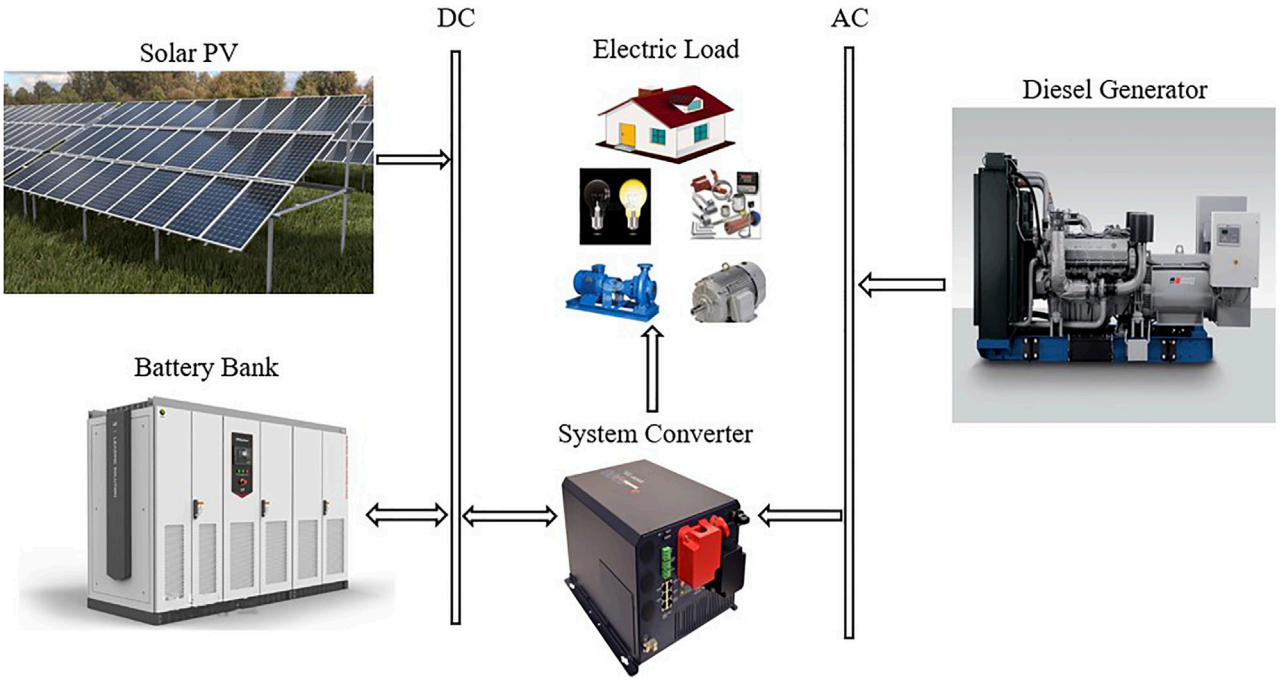

FIGURE 1
Schematics of the proposed hybrid system.

2.2 Load profile and resource data

Electricity is a crucial factor in improving the living standards and well-being of citizens, as it is used for lighting, communication, and motor applications. The potential needs of the location were assessed, and different loads were identified, such as the domestic load, which mainly comprised compact fluorescent lamps (CFLs) for lighting; commercial loads, which include refrigerators, computers, and CFLs; and community loads arising from the healthcare centre, kindergarten, and primary school located in the area (SEPTEMBRE, 2021). The ratings of all electrical appliances, their time of use, and the corresponding number of appliances are listed in Table 3. From the information gathered in this study, the total daily load demand (kWh) of the camp was calculated using Eq. 1 (Ramesh and Prasad Saini, 2020):

$$E_{Demand} = \frac{\sum_{j=1}^{Type} n_{user} \times \left(\sum_{i}^{Load} n_{Load_i,j} \times r_{rating_i,j} \times T_{duration_i,j}\right)}{1000} \quad (1)$$

From the calculations, the daily average load was estimated to be 3,830.805 kWh, with a peak load of 365.645 kW between 6 p.m. and 8 p.m. HOMER software generated the load profile for the refugee camp, as shown in Figure 4. The renewable resource potential for this region is solar, wind, and river-run type hydropower (on the river Lom). The renewable power source considered in this study is solar, with an estimated average annual solar radiance of 5.3 kWh m^{-2}/day in this region (Figure 5). This selection was made due to a lack of accurate information on the other sources, such as a river or headstream velocity. Furthermore, the average wind speed in this area is 2.23 m s^{-1}, which is too low to harness the power.

2.3 Component specification and economic modelling

2.3.1 Component modelling

The solar PV performance is affected by various operating and environmental conditions. The power output of the module varies according to solar irradiation, ambient temperature, and wind velocity (Mandal et al., 2018). Eq. 2 was used to calculate the hourly power output of the PV module (Mandal et al., 2018), where P_{PV} (kW) is the power output, Y_{PV} (kW) is the rated capacity of the PV array, F_{PV} (%) is the derating factor, GT (kW·m^{-2}) is the solar radiation incident on the PV array, $G_{T,\,STC}$ (1 kW/m^2) is the incident radiation under standard test conditions (STC), α_p (%/°C) is the temperature coefficient of power, and Tc (°C) is the PV cell temperature at the current time step. Table 4 presents the technical and economic data for the components (Ramesh and Prasad Saini, 2020), (Owolabi et al., 2019; Diesel Generators, 2021; Richardvigilantebooks, 2021). A mono–Si–CSUN200–72M solar PV system was used in this study with an efficiency of 15.67%, a temperature coefficient of 0.4%,

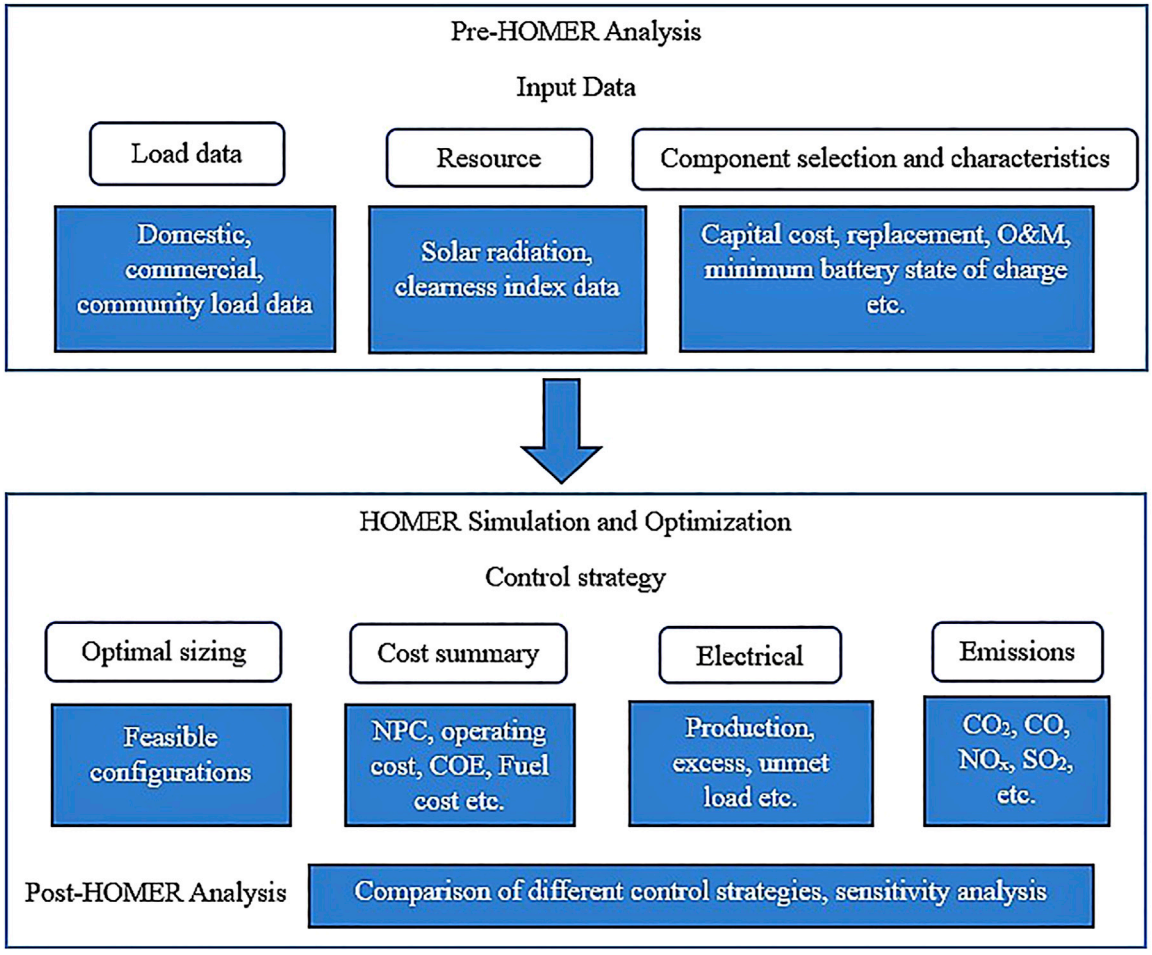

FIGURE 2
Adopted HOMER methodology algorithm.

TABLE 2 Summarized information about the study area.

Particulars	Details
Country	Cameroon
Region/division	East/Lom—et—Djerem
Surface area	55 Hectares
Principal religion	Muslims (98.8%), christians (0.8%), others (0.4%)
GPS coordinates	5°45′15.9114″N, 14°26′0.6″E
Total population	28,181
Average number of households size	8,937
Number of persons with specific needs	4,102 (14.88%)
Opening date of site	01 March 2014
Education level	Adults: 50.4% without education, 37,4% informal education, 0.80% university education

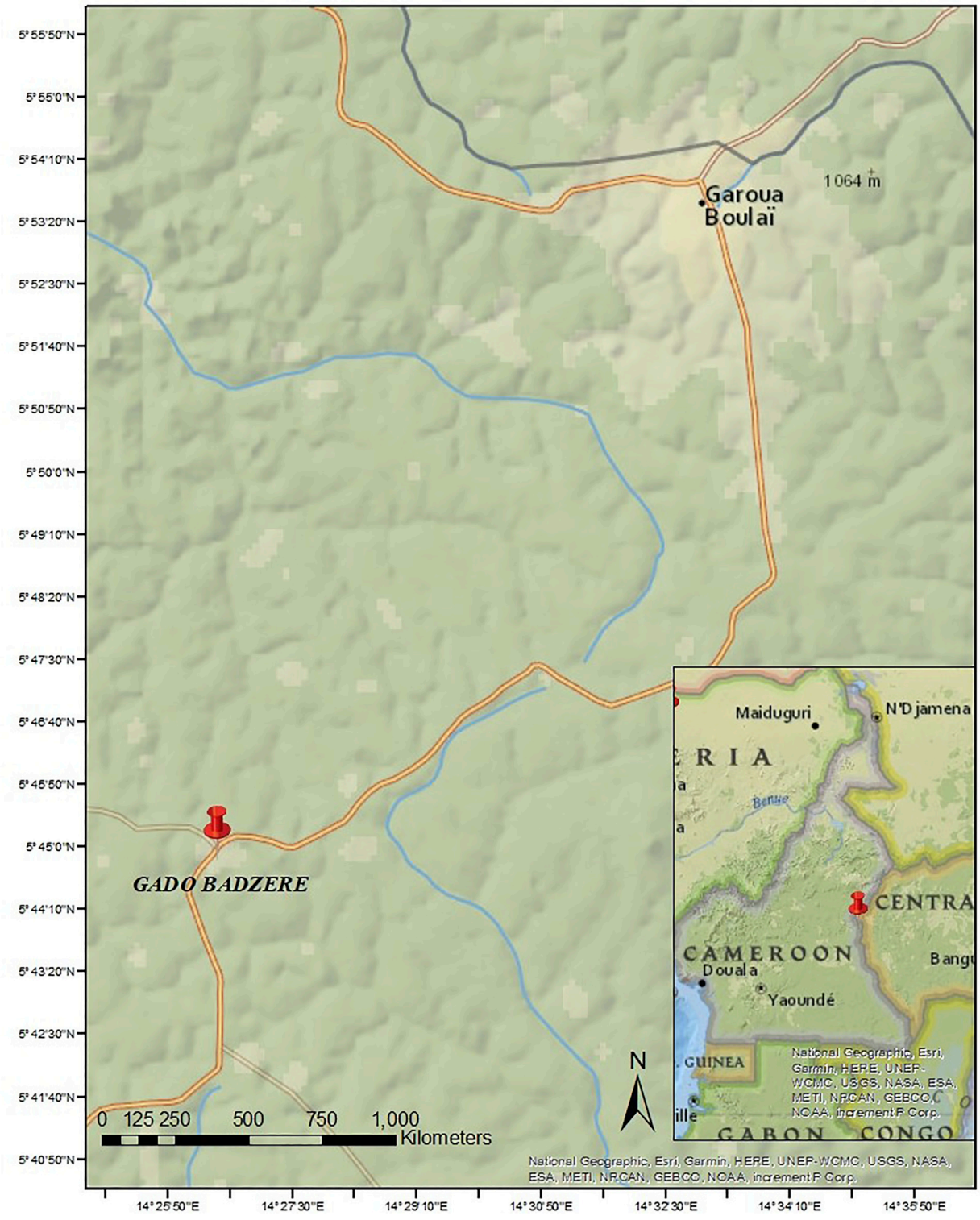

FIGURE 3
Location of the study area.

TABLE 3 Electrical load at the camp site.

Type	No. of households	Appliance type	Rating (W)	No of appliance	Run time h/day
Residential load					
Household	7,045	CF lamp	15	2	5
Type	No. of facilities	Appliance type	Rating (W)	No of Appliance	Run time h/day
School load					
Kindergarten	1	CF lamp	15	1	3
Primary school	4	CF lamp	15	2	6
		Computer	120	1	3
Secondary school	1	CF lamp	15	7	6
		Computer	120	3	6
		Fan	80	1	3
		Refrigerator	200	1	6
Health loads					
Health posts	1	CF lamp	15	25	8
		Computer	120	5	7
		Fan	80	12	7
		Refrigerator	200	4	24
		Lab equipment	1,000	2	8
Other loads					
Workshop	1	Hydra form machine	7,500	1	9
		Crushing mill	12,500	2	2
		Broiler heater	17,000	9	17
Total refugee camp load		3,830.805			

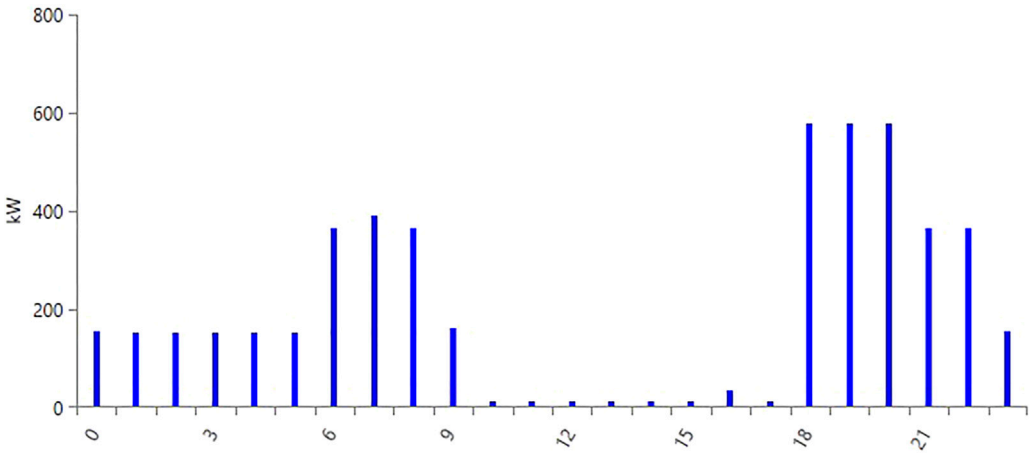

FIGURE 4
Daily hourly load profile of the refugee camp.

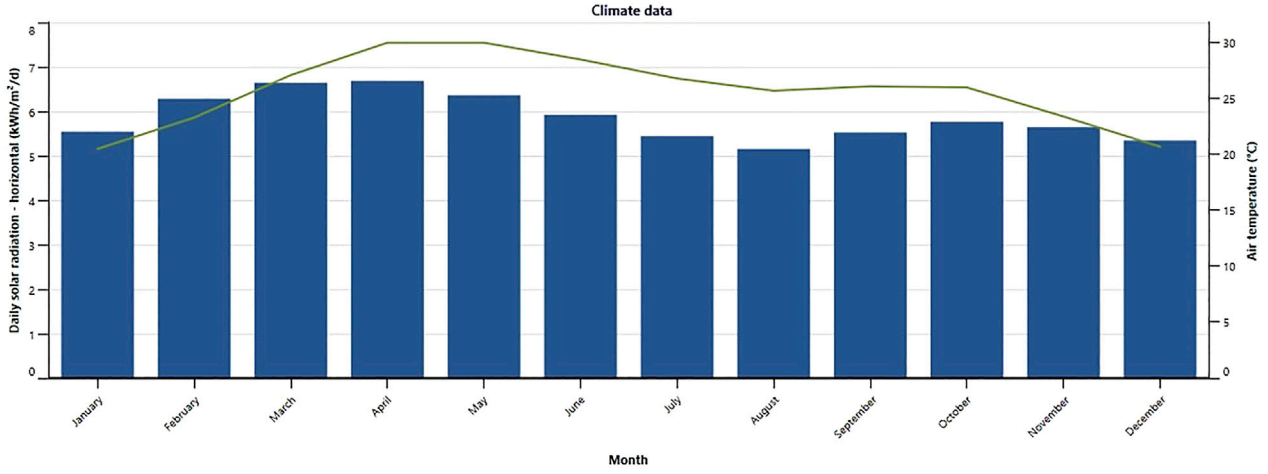

FIGURE 5
Average annual solar radiation in the study area.

TABLE 4 Techno-economic data for system components.

Component	Technical description	Cost ($)	Replacement cost ($)	O&M cost ($)	Lifetime (years)
Flat plate, PV module	mono—Si—CSUN200—72 M PV	1,800/kW	1,800	18/yr	25
Diesel generator	420 kW	300/kW	300	0.030/hr	26
Lithium-ion battery	100 kW Li-ion	13,700	10,960	10/yr	15
System converter	Generic	300/kW	300	-NA-	15

and a nominal operating temperature of 45°C. This PV module was chosen because it is relatively cheap and available in the African market (Owolabi et al., 2019).

$$P_{PV} = Y_{pv} f_{pv} \left(\frac{G_T}{G_{T,STC}} \right) \left[1 + \propto_P (T_c - T_{c,STC}) \right] \quad (2)$$

Owing to the intermittent nature of solar resources, an energy storage system (ESS) was required to increase the reliability and resilience of the designed microgrid. In this case, a 100 kW Lithium-ion battery was used as the energy storage system. When excess electricity was produced, the battery stored this excess electricity and discharged it when the demand was more significant than the supply. The state of charge (SOC) of the battery was calculated by HOMER using Eq. 3 (Toopshekan et al., 2020):

$$P_{Bat}(t) = P_{Bat}(t-1) \times (1-\sigma) + \left[generated\ power - \frac{consumed\ power}{\eta_{INV}} \right] \quad (3)$$

where $P_{Bat}(t)$ is the battery SOC at time t, $P_{Bat}(t-1)$ is the SOC at time t-1, σ is the battery's self-discharge rate, and finally, η_{INV} is the efficiency of the converter.

In addition, a diesel generator was included in the system design because renewable sources and the ESS are sometimes unable to meet the demand. Eq. 4 determined the quantity of fuel required by the diesel generator (Mandal et al., 2018):

$$F_G = \left(B_G \times P_{G\_rated} \right) + \left(A_G \times P_{G\_out} \right) \quad (4)$$

where F_G is the diesel generators' fuel consumption, P_{G_rated}, is the nominal power of the diesel generator, P_{G_out} is the output power, B_G and A_G are the coefficients of the fuel consumption curve defined by the user (1 kWh^{-1}). The operating range should be between 70 and 89% (Mandal et al., 2018) for efficient diesel generator operation while avoiding partial loading and excessive operation.

Since we have both AC and DC bus bars, power conversion is needed. In this study, a power converter acted as an inverter (DC-AC) and a rectifier (AC-DC). It maintains the electrical connection between the AC bus and DC bus components.

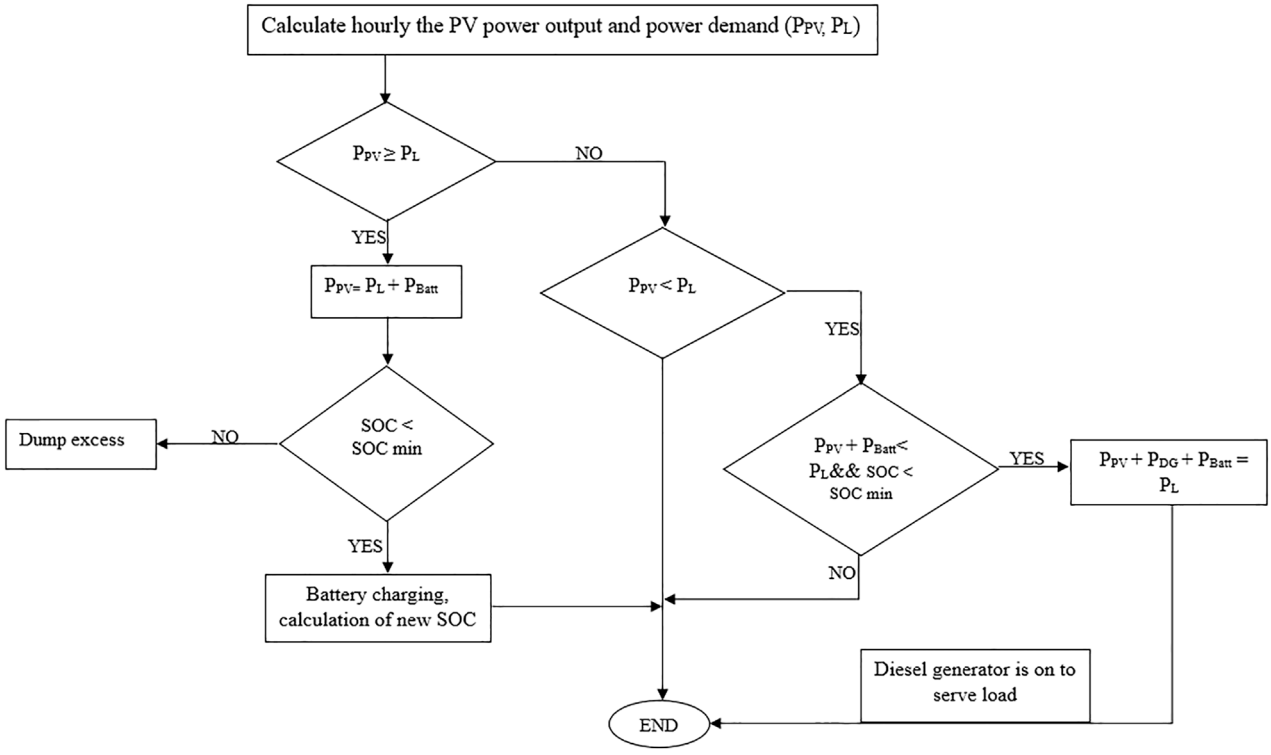

FIGURE 6
Flow chart for LF strategy.

Table 4 provides the converter's cost factors. The inverter input had lifetime and efficiency specifications of 15 years and 95%, but the rectifier input has a relative capacity of 100% and an efficiency of 85% (Owolabi et al., 2019). Eq. 5 calculates the converter power capacity levels where Li and Lr stand for inductive and resistive loads, respectively.

$$C = (3 \times L_i) + L_r \tag{5}$$

2.3.2 Optimization modelling

HOMER presents its results according to the lowest net present cost (NPC), which indicates the total life cycle cost of the system. The NPC comprises the initial, replacement, O&M, and fuel costs (Olatomiwa et al., 2018). Eq. 6 provided the formula for calculating the NPC:

$$NPC = \frac{C_{ann,Tot}}{CRF} \tag{6}$$

Where CRF is the capital recovery factor and is determined as (Olatomiwa et al., 2018):

$$CRF = \frac{i(1+i)^n}{(1+i)^n - 1} \tag{7}$$

Where i and n are interest rate and project lifetime, respectively.

Moreover, the total annual cost of the proposed hybrid system is expressed as (Toopshekan et al., 2020):

$$C_{ann,Tot} = \sum_{N=1}^{N_{pv}} C_{ann,pv} + \sum_{N=1}^{N_{DG}} C_{ann,DG} + \sum_{N=1}^{N_{batt}} C_{ann,batt} + \sum_{N=1}^{N_{conv}} C_{ann.conv} \tag{8}$$

Where $C_{ann,pv}$, $C_{ann,DG}$, $C_{ann,batt}$, $C_{ann.conv}$, are the annualized costs of the solar PV, DG, battery, and system converter, respectively, and N_{pv}, N_{DG}, N_{batt}, N_{conv} are the numbers of solar PV, DG, batteries, and converters, respectively.

In addition, the cost of electricity (COE), which is the average cost of power (kWh) delivered by the system, is considered an essential factor in this study. The COE was calculated as follows (Olatomiwa et al., 2018; Toopshekan et al., 2020):

$$COE = \frac{C_{ann,\,Tot}}{E_{served}} \tag{9}$$

$$C_{ann} = C_{ann,cap} + C_{ann,rep} + C_{ann,O\&M} \tag{10}$$

2.4 Constraints

This study set some constraints to obtain an optimal, resilient, and reliable micro-grid design. The total capacity

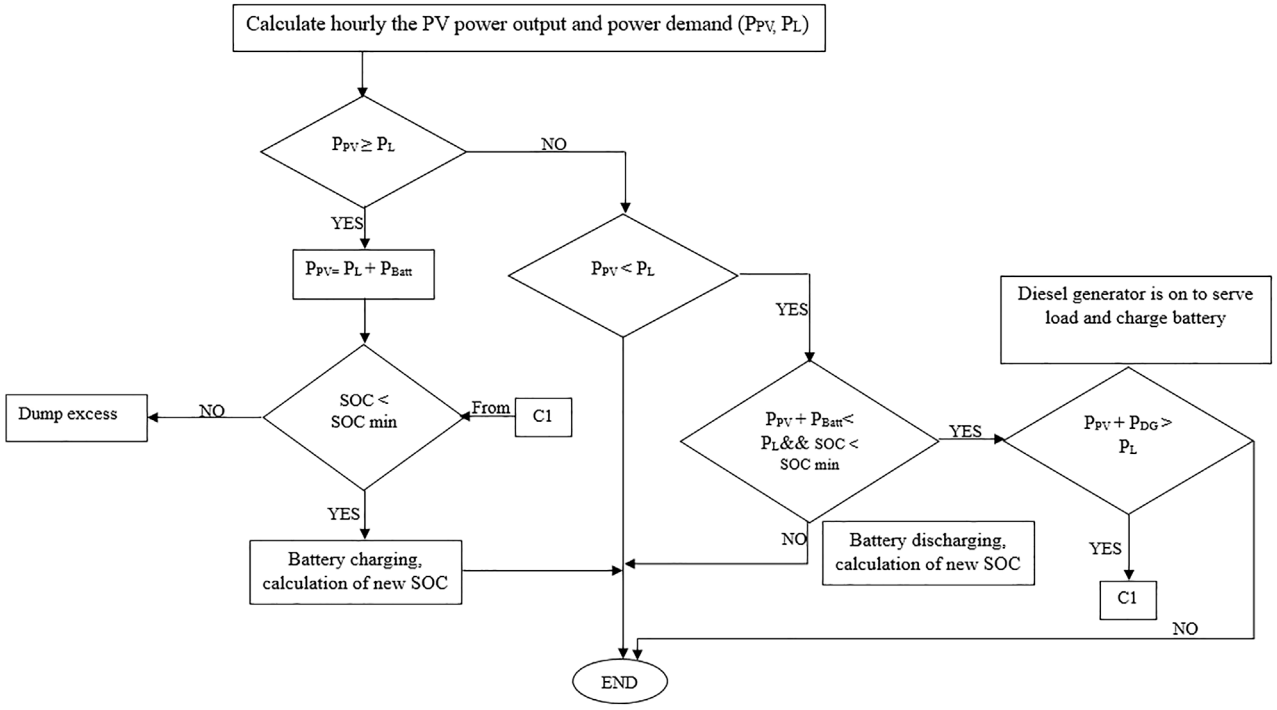

FIGURE 7
Flow chart for CC strategy.

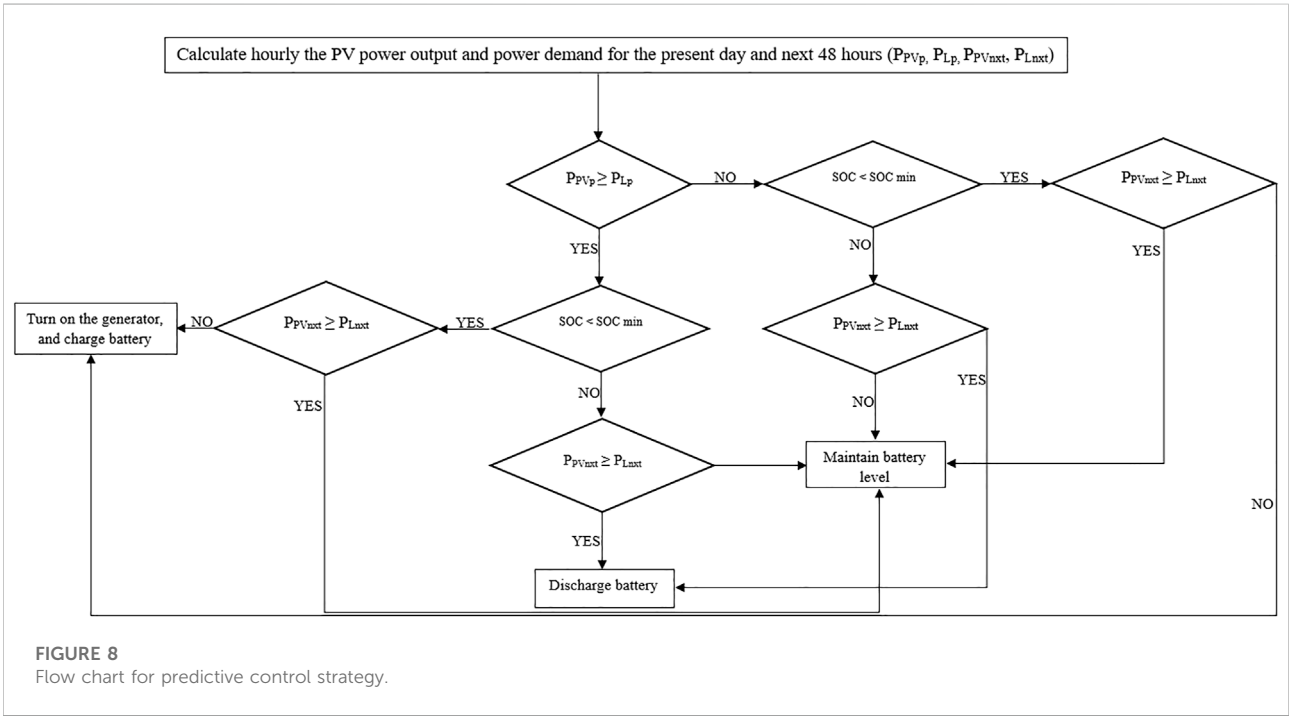

FIGURE 8
Flow chart for predictive control strategy.

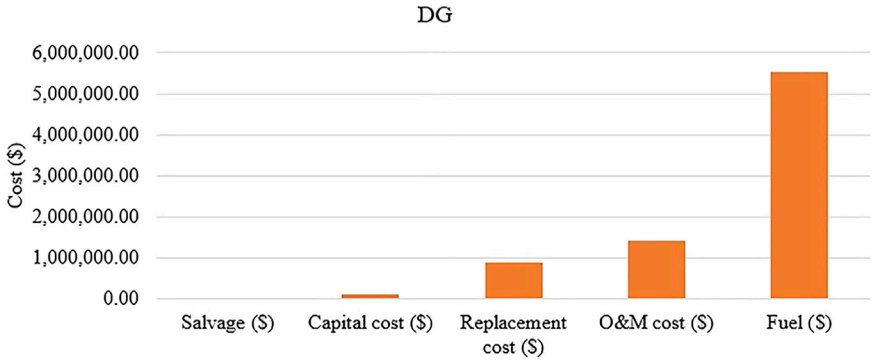

FIGURE 9
Cost summary of the base case.

TABLE 5 Annual GHG emission for the stand-alone diesel system.

Pollutant	Carbon dioxide	Carbon monoxide	Unburned hydrocarbon	Particulate matter	Nitrogen oxide	Sulfur dioxide	Total
Emissions (kg/yr)	1,114,136	7,023	306	42.6	2,728	6,597	1,130,832.6

TABLE 6 Economic performance under different control strategies.

Economic performance	Units	PS strategy	LF dispatch strategy	CC dispatch strategy
NPC	$	3,606,886	3,809,822.54	3,981,010
COE	$/kWh	0.2018	0.2131	0.2234
Operating cost	$	85,294.07	89,251.13	109,107.60
Return on investment	%	18.1	16.6	15.5
Simple payback	Year	4.52	4.83	4.92
Discounted payback	Year	5.42	5.77	5.86

shortage was set to 0%, indicating that all feasible solutions provided by HOMER should be able to meet the demand at all times. Furthermore, the maximum renewable penetration (RP) ranged from 0 to 100%. The day-to-day (5%) and timestep (10%) were considered to compensate for the panel's output due to unpredicted weather changes. The capacity shortage of the system was set to 0. Only systems that can satisfy the load are included in the optimized results. Also, the overall lifetime of the design was set to 25 years.

2.5 Control strategy/energy management

In a hybrid system, a dispatch strategy is employed when renewable resources cannot satisfy the load demand. A dispatch strategy is simply a control algorithm used to switch between the generator and battery bank when the available renewable energy sources cannot satisfy the load demand (Nsafon et al., 2020). By default, HOMER has two control strategies: load following (LF) and cycle charging (CC) (HOMER, 2021). Load following is a strategy in which the generator meets the immediate load demand when other generating sources are insufficient to satisfy the required demand. In this case, charging the battery is the sole responsibility of other generating sources (Nsafon et al., 2020). Renewable energy sources are reserved for lower priority tasks like recharging the storage bank or supplying the deferrable load. The load following strategy uses HOMER to dispatch the system's controllable power sources (generators, grid, and storage bank) to satisfy the operating reserve requirement while providing the primary load and the thermal load at the lowest total cost

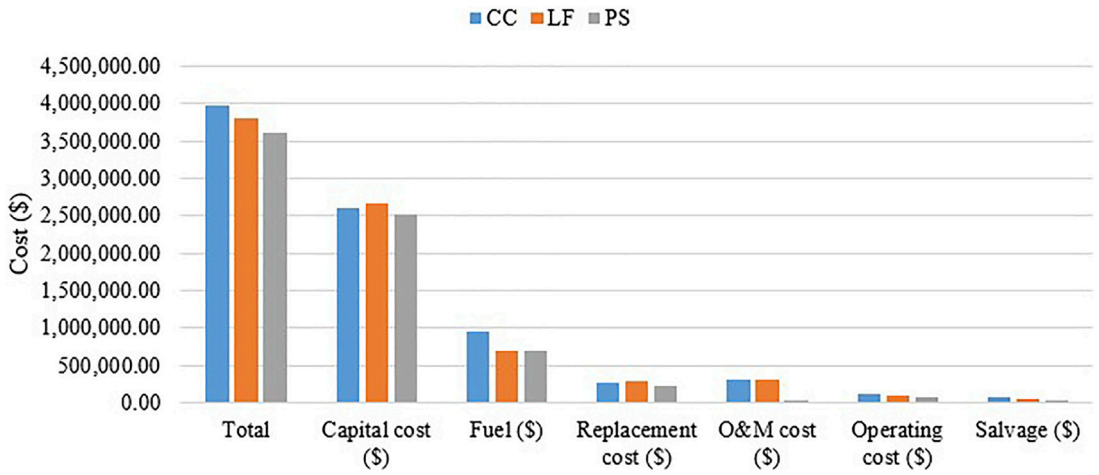

FIGURE 10
Cost summary under the different control strategies.

TABLE 7 Technical performance under different control strategies.

Description	Units	PS strategy	LF dispatch strategy	CC dispatch strategy
System configuration				
Solar PV	kW	972	1,038	1005
Diesel generator	kW	420	420	420
Battery		38	41	39
Converter	kW	400	374	427
Technical performance				
PV electricity production	kWh/year	1,531,510	1,635,623	1,583,331
Diesel generator electricity production	kWh/year	205,438	152,323	284,157
Battery autonomy	hour	19	20.5	31.8
Fuel consumption	L/year	52,839	54,987	72,497
Generator Hours	hours/year	572	705	714
Renewable fraction	%	85.3	89.1	79.7

possible for each time step (HOMER, 2021). Under CC, the generator operates at full power output, providing power to charge the battery and deliver power to the load. With this strategy, a set point of the state of charge can be set for the battery so that the generator continues to charge the battery unless the setpoint is attained before it can be discharged. Excess electricity generation is directed toward lower-priority goals such as, in declining order of priority: feeding the deferred load, charging the storage bank, and serving the electrolyzer. When adopting the cycle charging method, HOMER dispatches the controllable power sources (generators, storage bank, and grid) in a two-step procedure at each simulation time step. HOMER first chooses the best mix of power sources to supply the primary load at the lowest total cost while still meeting the need for operating reserves. Next, the output of each generator in that ideal combination is gradually increased by HOMER until it reaches its rated capacity, or as close to it as feasible without generating too much electricity. The flowchart for FL and CC are presented in Figures 6, 7, respectively.

In this study, a predictive control strategy (PS) was proposed. The upcoming load and availability of resources were predicted from NASA's available solar radiation data for that particular time. In HOMER, this strategy gives a 48 h foresight of the load and available solar resources to harness the excess energy rather than curtail the produced energy (HOMER, 2021). The control algorithm prioritizes discharging the battery rather than turning on the generator in anticipation of harnessing the excess produced by the solar PV. The algorithm for this strategy is

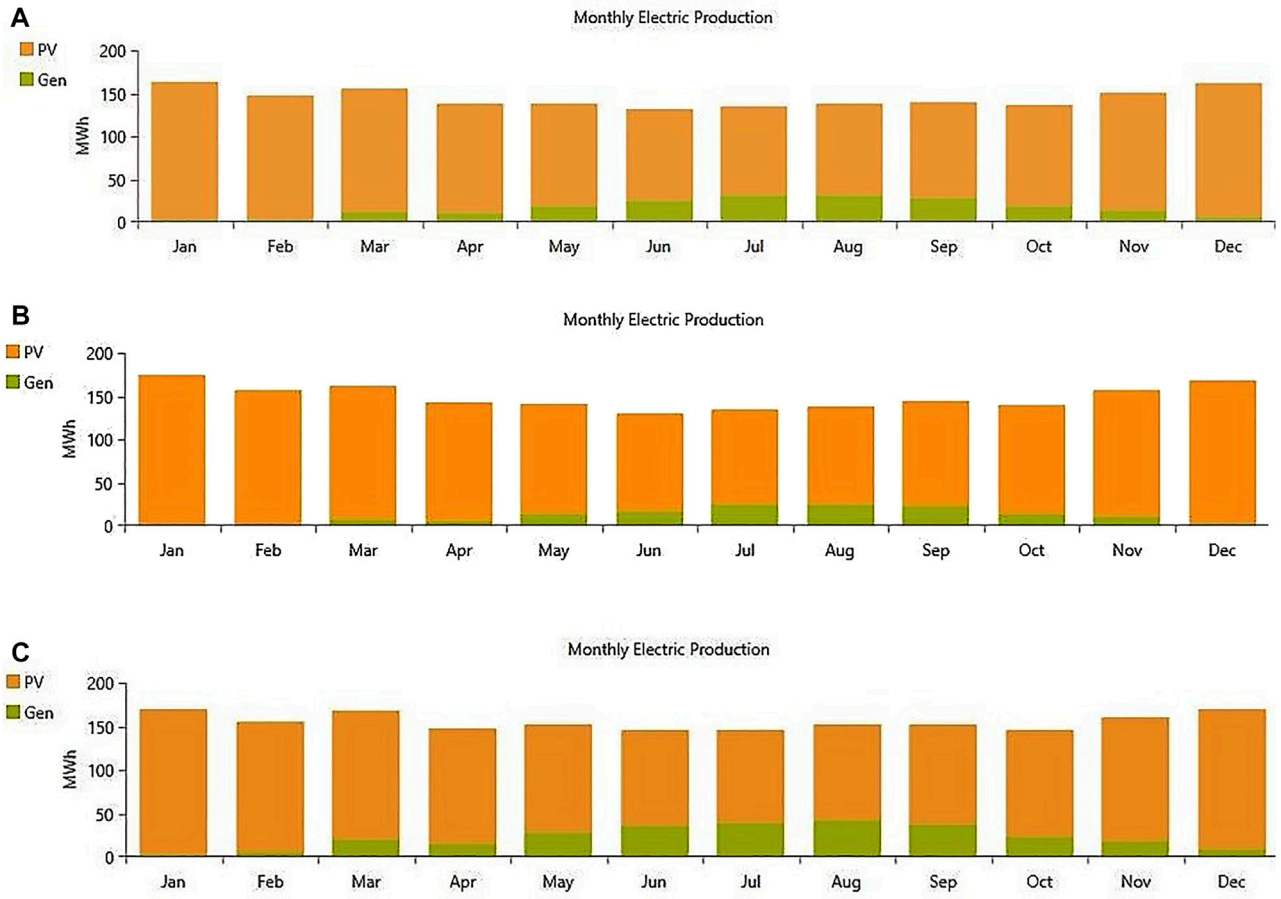

FIGURE 11
Monthly electricity production LF **(A)**, PS **(B)**, CC **(C)**.

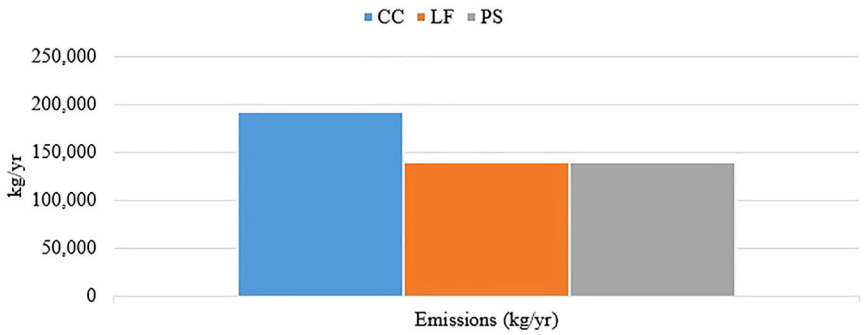

FIGURE 12
Overall emissions of the proposed system under different strategies.

illustrated in Figure 8. This strategy calculates the current load demand and PV power output for the 2 days ahead. Suppose that the resource potential of the next day is greater than the demand of the present day. In this case, the battery is discharged, anticipating the ability to use the excess electricity generated the next day to recharge. However, if the reverse is true, the

TABLE 8 Climate performance under different control strategies.

Climate performance	Units	PS strategy	LF dispatch strategy	CC dispatch strategy
Carbon dioxide	kg/year	137,518	140,357	189,769
Carbon monoxide	kg/year	872	921	1,196
Unburned hydrocarbons	kg/year	38.0	40.2	52.2
Particulate matter	kg/year	5.28	6.45	7.25
Nitrogen oxide	kg/year	339	345	465
Sulfur dioxide	kg/year	819	829	1,124

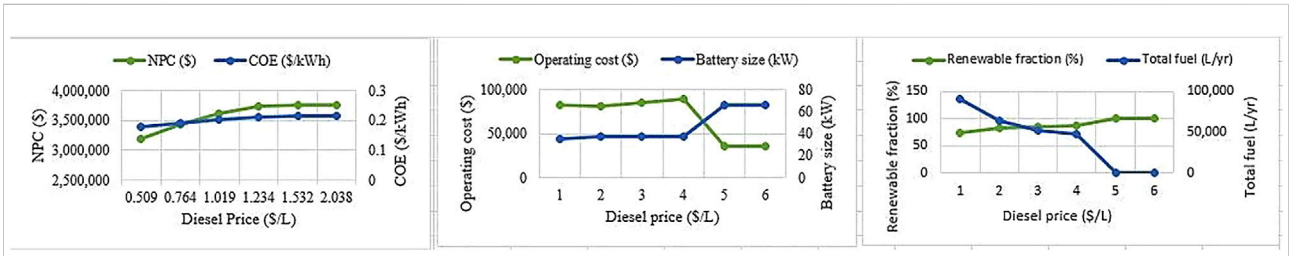

FIGURE 13
Effect of diesel price variation on selected dependent variables.

battery is charged in anticipation of supplying the required load for the following day. This is a control strategy and an energy management strategy, as the excess energy produced by the system is negligible.

3 Results and discussion

In this study, the proposed case under the three strategies was compared to the base case, which comprised only a diesel generator. First, the results of the various systems are presented.

3.1 Base case

The system configuration comprised only a diesel generator with a capacity of 420 kW. The initial investment for the base case was $126,000 because the only component was a 420 kW generator. This system could meet the demands of the refugee camp. The cost summary of this system is presented in Figure 9.

In Cameroon, as of 2020, the price of diesel fuel was 575 FCFA/L ($1.019/L) (Global Petrol Prices, 2021), and as shown in Figure 9 above, the fuel consumption was the highest contributor to the NPC ($7,973,412.00), followed by the O&M cost. The main drawback of this system in financial terms was the cost incurred from the fuel, and the price of fuel fluctuates, implying that the NPC of such a system can increase or decrease. Additionally, because it was a diesel generator, GHG emissions were inevitable in the system. Table 5 lists the various GHGs associated with this system. The total annual GHG emissions were 1,130,832.6 kg/yr.

3.2 Economic dimension

The economic performance of the proposed solar PV/diesel generator/battery system under different control strategies is presented in Table 6, in which essential parameters such as NPC, COE, simple payback, discounted payback, and return on investment (ROI) are highlighted. The NPC of a system is the difference between the present cost incurred from the installation and operation of the various components of the system over their life cycle and the revenues generated during the total life cycle of the project (Ishraque and Ali, 2021). From the analysis, the PS had the lowest NPC and COE, followed by the LF and CC strategies. Figure 10 shows a cost summary of the different designs. Feasibility studies have proven that renewable energy requires high upfront capital. This study is not an exception as one can realise that the initial capital is very high under all the strategies as at least 80% of the total generating capacity is supplied by the solar PV. Also, apart from the initial cost, fuel was the second-highest contributor to the NPC under the CC strategy because it had the highest generator operating hours. Even though the generator's working hours under the CC were only 1.26% higher than those under the LF strategy, their fuel consumption disparity was 24.15%. Under the CC strategy, the generator operated at rated power, whereas under LF, the

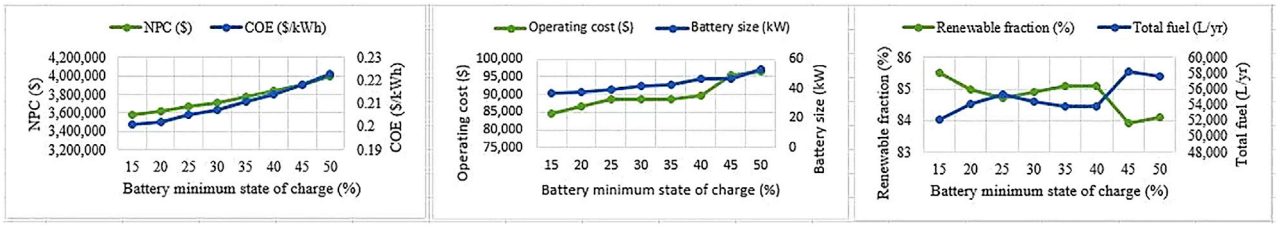

FIGURE 14
Effect of battery minimum state of charge variation on the selected dependent variables.

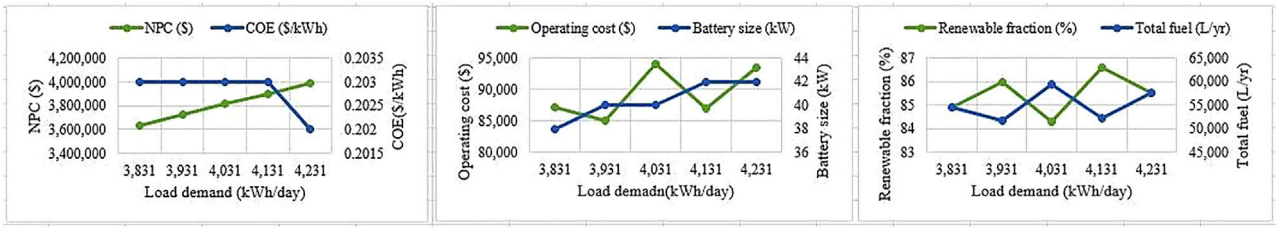

FIGURE 15
Effect of load demand variation of charge on the selected dependent variables.

generator ran to meet the unmet load. In addition, the simple payback period, which is the time for an investor or business to redeem itself on the investments made on a project (Aziz et al., 2021), was the least for the PS (4.52 years) compared to the CC strategy (4.92 4.83 years). Hence, the most viable strategy to implement from an investor's standpoint is the PS.

3.3 Technical dimension

The technical performance was evaluated in this study based on electrical analysis (Table 7; Figure 11). The results show that the three control strategies implemented were able to meet the load demand of the refugee camp. Figures 11A–C present the monthly electric production from various components under the LF, PS, and CC control strategies, respectively. PV/battery catered for the demand from December through February, whereas diesel generators were needed to meet the demand during the other months. The total annual electricity generated by the was 1,736,948 kWh (PS) with 85.3% generated from renewable, 1,787946 kWh (LF) with 89.1% generated by PV alone and finally 1,867,946 kWh (CC) with 79.7% generated by the solar PV respectively. Furthermore, excess electricity was produced during the first 2 months (January and February) and the last month of the year (December) with LF (14.0%), CC (16.8%), and PS (5.7%). The PS had the least excess because this control strategy could predict the solar radiation and load demand; hence, the battery charges and discharges were effectively managed.

3.4 Climate dimensions

In addition, the climate impact of the proposed system under the different strategies was assessed in this study as climate-related issues are now on every development plan in the world, and most seek to take positive actions to combat these issues. Consequently, to develop a reliable and sustainable power system, both techno-economic and climate impacts must be assessed. Generally, the lowest GHG emitter is considered more climate-friendly. The proposed system configuration consists of a diesel generator that uses fuel. Emissions such as carbon dioxide (CO_2), carbon monoxide (CO), nitrogen oxide (NOx), sulfur dioxide (SO_2), unburned hydrocarbons, and particulate matter cannot be avoided but can be controlled (Aziz et al., 2021). The performance evaluation of the effects of the different strategies in terms of their climate impact was investigated, and the results are shown in Figure 12. The total emissions were calculated as 192, 613, 141,357, and 139,592 kg/yr for CC, LF, and PS, respectively. These results confirm that the amount of emission is directly proportional to the quantity of fuel consumed by the generator. The PS had the lowest fuel consumption compared with LF and CC, as indicated in Table 8.

3.5 Sensitivity analysis

Sensitivity performance was carried out to evaluate how the change in different independent variables will affect the proposed

system's dependent variable under the PS strategy because it was the best control strategy financially and environmentally. The independent variables considered in this study were the diesel price, load demand, and battery minimum state of charge (SOC_{min}). In contrast, the dependent variables were the fuel, generator operation, NPC, COE, battery size, and a renewable fraction (Figures 13–15). For the independent parameters, an increase or decrease in the amount was evaluated, except for load demand, which tended to increase due to the rise in the size of the refugee camp. The base case or actual values for diesel price, $SOC_{min,}$ and load demand were \$1.019/L, 20%, and 3830.81 kWh, respectively. Results from the sensitivity analysis show that a rise in diesel price (Figure 13) from \$0.509/L to \$2.02/L had a negligible effect on the generator operation. This strategy prioritized the battery in the configuration as the primary backup supply. At each time, the cost of battery discharge and battery operation were not compared. However, an increase in the diesel price increased the battery size and the expense incurred from fuel purchases. Hence, a 2.518% and 1.3% increase in NPC and COE, respectively, were observed. In addition, the operating cost increased as the diesel price increased and then decreased when the current diesel price was 50% higher than the base price. This is because the system attained a renewable fraction of 100%, which means that solar PV was the sole electricity supplier.

For the SOC_{min} parameter (Figure 14), an increase by a factor of ±5 (from 10 to 50) increased the NPC, COE, operating cost, battery size, and total fuel consumed by approximately 1.287%, 0.275%, 1.746%, 0.16%, and 1.19%, respectively. As the SOC_{min} parameter increased, the reliance of the system on the diesel generator increased. Hence, the renewable fraction was reduced, implying that additional emissions were observed, posing significant climate damage. Looking at the third parameter, which is load demand (Figure 15), increasing the load demand from 3,830.81 to 4,230.81 kWh had the following effects: COE was unaffected, NPC, operating cost, battery size, and total fuel consumed all experienced an increase of 1.793%, 1.483%, 0.008%, and 0.108%, respectively.

4 Conclusion

HRESs have proven to be the most viable and promising solution for meeting the energy demand of the Gado refugee camp, where grid extension is impossible. Furthermore, the hybridization of renewable energy systems promotes energy resilience and sustainability in any country. In this study, an optimal design of a solar PV/diesel generator/battery hybrid system was carried out to provide energy for the Gado refugee camp. Selecting an effective control strategy for a particular design is very important because it affects the performance of various system components. Three different control strategies, LF, CC, and PS, were presented for the solar PV/diesel generator/battery system. A performance comparison was carried out based on the technical, economic, and climate dimensions of the three different control strategies.

The simulation results obtained from the HOMER software indicated that the PS control strategy was best suited for this particular case study. Further performance analysis revealed that the PS strategy was the preferable choice from an investor's point of view because it had the least NPC (\$3,606,886) as compared to the LF control strategy (\$3,809,822.54), CC controlled strategy (\$3,981,010), and the base case (diesel only; \$7,973,412.00). From a technical perspective, all the strategies under study met the demand, with the PS control strategy generating only 5.7% excess electricity compared to the LF (14.0%) and CC (16.8%) control strategies. The stand-alone base case of the diesel generator could meet the demand with no excess generation. From an environmental point of view, the PS strategy was the most climatically friendly as its total emission generation was 139,592.28 kg/yr relative to the 141,357, 192,613 and 1,130,832.6 kg/yr generated by LF, CC, and the base case, respectively. Based on these results, the PS control strategy had the lowest emissions, even though it had a similar climatic impact compared to the LF. It produces less excess energy and has the lowest cost. The optimal design of a hybrid renewable system should be eco-friendly, cost-effective and energy-efficient. With this compromise, the most suitable choice of control strategy for the solar PV/diesel generator/battery hybrid system in this case study is the PS strategy. The proposed approach can considerably increase the energy access and livelihood of similar camps and is an effective energy management technique employed in HRESs.

According to the results of this study, it is vital to develop control strategies that can be applied to the implementation of HRES. Future studies recommend a comparative analysis of the command dispatch and predictive control strategies in combination with other ESS and grid extensions.

Data availability statement

The original contributions presented in the study are included in the article/Supplementary Material, further inquiries can be directed to the corresponding author.

Author contributions

NS: conceptualization, methodology, software, formal analysis, writing–original draft. AY: investigation and data curation. BK: conceptualization, writing—review and editing. AO: writing—review and editing. TM: visualization and revision. DS: software, validation. J-SH: supervision.

Funding

This work was supported by the National Research Foundation of Korea (NRF), a grant funded by the Korean government Ministry of Science and ICT (MSIT) (No. NRF-2021R1A5A8033165); the Korea Institute of Energy Technology Evaluation and Planning

(KETEP) and the Ministry of Trade, Industry & Energy (MOTIE) of the Republic of Korea (No. 20224000000150).

Conflict of interest

The authors declare that the research was conducted in the absence of any commercial or financial relationships that could be construed as a potential conflict of interest.

Publisher's note

All claims expressed in this article are solely those of the authors and do not necessarily represent those of their affiliated organizations, or those of the publisher, the editors and the reviewers. Any product that may be evaluated in this article, or claim that may be made by its manufacturer, is not guaranteed or endorsed by the publisher.

References

Abada, I., Othmani, M., and Tatry, L. (2021). An innovative approach for the optimal sizing of mini-grids in rural areas integrating the demand, the supply, and the grid. *Renew. Sustain. Energy Rev.* 146, 111117. doi:10.1016/j.rser.2021.111117

Aditya, I. A., Aisyah, S., and Simaremare, A. A. (2021). Optimal sizing and sensitivity analysis of hybrid renewable energy systems: A case of ur island in Indonesia. *IOP Conf. Ser. Mat. Sci. Eng.* 1098 (4), 042049. doi:10.1088/1757-899x/1098/4/042049

Ansong, M., Mensah, L. D., and Adaramola, M. S. (2017). Techno-economic analysis of a hybrid system to power a mine in an off-grid area in Ghana. *Sustain. Energy Technol. Assessments* 23, 48–56. doi:10.1016/J.SETA.2017.09.001

Aste, N., Barbieri, J., Berizzi, A., Colombo, E., del Pero, C., Leonforte, F., et al. (2017). Innovative energy solutions for improving food preservation in humanitarian contexts: A case study from informal refugees settlements in Lebanon. *Sustain. Energy Technol. Assessments* 22, 177–187. doi:10.1016/j.seta.2017.02.009

Aziz, A. S., Tajuddin, M. F. N., Adzman, M. R., Ramli, M. A. M., and Mekhilef, S. (2019). Energy management and optimization of a PV/diesel/battery hybrid energy system using a combined dispatch strategy. *Sustain. Switz.* 11, 683–3. doi:10.3390/su11030683

Aziz, A. S., Tajuddin, M. F. N., Hussain, M. K., Adzman, M. R., Ghazali, N. H., Ramli, M. A., et al. (2021). A new optimization strategy for wind/diesel/battery hybrid energy system. *Energy* 239, 122458. doi:10.1016/j.energy.2021.122458

Babaei, R., Ting, D. S.-K., and Carriveau, R. (2022). Feasibility and optimal sizing analysis of stand-alone hybrid energy systems coupled with various battery technologies: A case study of pelee island. *Energy Rep.* 8, 4747–4762. doi:10.1016/j.egyr.2022.03.133

Baranda Alonso, J., Sandwell, P., and Nelson, J. (2021). The potential for solar-diesel hybrid mini-grids in refugee camps: A case study of nyabiheke camp, Rwanda. *Sustain. Energy Technol. Assessments* 44, 101095. doi:10.1016/j.seta.2021.101095

Chand, A. A., Prasad, K. A., Mamun, K. A., Sharma, K. R., and Chand, K. K. (2019). Adoption of grid-tie solar system at residential scale. *Clean. Technol.* 1 (1), 224–231. doi:10.3390/CLEANTECHNOL1010015

Chowdhury, T., Chowdhury, H., Miskat, M. I., Chowdhury, P., Sait, S. M., Thirugnanasambandam, M., et al. (2020). Developing and evaluating a stand-alone hybrid energy system for Rohingya refugee community in Bangladesh. *Energy* 191, 116568. doi:10.1016/j.energy.2019.116568

Das, B. K., and Zaman, F. (2019). Performance analysis of a PV/Diesel hybrid system for a remote area in Bangladesh: Effects of dispatch strategies, batteries, and generator selection. *Energy* 169, 263–276. doi:10.1016/j.energy.2018.12.014

Diesel Generators (2021). Diesel generators | large generators | cat | caterpillar. Available at: https://www.cat.com/en_US/products/new/power-systems/electric-power/diesel-generator-sets.html (Accessed Dec. 23, 2021.

Global Petrol Prices (2021). Cameroon diesel prices, 20-Dec-2021 | GlobalPetrolPrices.com. Available at: https://www.globalpetrolprices.com/Cameroon/diesel_prices/ (Accessed Dec. 24, 2021.

Grafham, O., and Lahn, G. (2018). *The costs of fuelling humanitarian aid*. London: The Royal Institute of International Affairs.

Halabi, L. M., Mekhilef, S., Olatomiwa, L., and Hazelton, J. (2017). Performance analysis of hybrid PV/diesel/battery system using HOMER: A case study sabah, Malaysia. *Energy Convers. Manag.* 144, 322–339. doi:10.1016/J.ENCONMAN.2017.04.070

HOMER (2021). HOMER_Pro_Version_3_7_User_Manual. Available at: www.homerenergy.com (Accessed: Oct. 11, 2021.

IEA (2020). *SDG7: Data and projections*. Paris: IEA. Available at: https://www.iea.org/reports/sdg7-data-and-projections.

I. Renewable Energy Agency (2019). Renewables for refugee settlements: Sustainable energy access in humanitarian situations. Available at: www.irena.org.

Ishraque, M. F., and Ali, M. M. (2021). "Optimized design of a hybrid microgrid using renewable resources considering different dispatch strategies," in 2021 International Conference on Automation, Control and Mechatronics for Industry 4.0 (ACMI), Rajshahi, Bangladesh, 08-09 July 2021. doi:10.1109/ACMI53878.2021.9528096

Jahangiri, M., Souloukngа, M. H., Bardei, F. K., Shamsabadi, A. A., Akinlabi, E. T., Sichilalu, S. M., et al. (2019). Techno-econo-environmental optimal operation of grid-wind-solar electricity generation with hydrogen storage system for domestic scale, case study in Chad. *Int. J. Hydrogen Energy* 44 (54), 28613–28628. doi:10.1016/j.ijhydene.2019.09.130

Jegadeesan, V., Vishnupriyan, J., Raghuraman, R., and Keerthi Vijayadhasan, G. (2020). Techno-economic feasibility investigation on hybrid system using HOMER. *Int. J. Future Generation Commun. Netw.* 13 (1), 1276–1288. Available at: https://www.researchgate.net/publication/346935544.

Karmaker, A. K., Hossain, M. A., Kumar, N. M., Jagadeesan, V., Jayakumar, A., and Ray, B. (2020). Analysis of using biogas resources for electric vehicle charging in Bangladesh: A techno-economic-environmental perspective. *Sustainability* 12 (7), 2579. doi:10.3390/SU12072579

Kehdinga, V. M., and Zacharie, S. (2020). The challenges and measures put in place by some international organizations in charge of the management of refugees in the Eastern Region of Cameroon: Case of Gado Badzere refugee camp in Garoua Boulai. Available at: http://www.ijias.issr-journals.org/.

Kumar, N. M., Ghosh, A., and Chopra, S. S. (2020). Power resilience enhancement of a residential electricity user using photovoltaics and a battery energy storage system under uncertainty conditions. *Energies* 13 (16), 4193. doi:10.3390/EN13164193

Ma, Q., Huang, X., Wang, F., Xu, C., Babaei, R., and Ahmadian, H. (2022). Optimal sizing and feasibility analysis of grid-isolated renewable hybrid microgrids: Effects of energy management controllers. *Energy* 240, 122503. doi:10.1016/j.energy.2021.122503

Mandal, S., Das, B. K., and Hoque, N. (2018). Optimum sizing of a stand-alone hybrid energy system for rural electrification in Bangladesh. *J. Clean. Prod.* 200, 12–27. doi:10.1016/j.jclepro.2018.07.257

Manoj Kumar, N., Chopra, S. S., Chand, A. A., Elavarasan, R. M., and Shafiullah, G. M. (2020). Hybrid renewable energy microgrid for a residential community: A techno-economic and environmental perspective in the context of the SDG7. *Sustainability* 1212 (10), 3944. doi:10.3390/SU12103944

Mubaarak, S., Zhang, D., Liu, J., Chen, Y., Wang, L., Zaki, S. A., et al. (2021). Potential techno-economic feasibility of hybrid energy systems for electrifying various consumers in Yemen. *Sustain. Switz.* 13 (1), 228–324. doi:10.3390/su13010228

Murugaperumal, K., and Ajay D Vimal Raj, P. (2019). Feasibility design and techno-economic analysis of hybrid renewable energy system for rural electrification. *Sol. Energy* 188, 1068–1083. doi:10.1016/J.SOLENER.2019.07.008

Neves, D., Baptista, P., and Pires, J. M. (2021). Sustainable and inclusive energy solutions in refugee camps: Developing a modelling approach for energy demand and alternative renewable power supply. *J. Clean. Prod.* 298, 126745. doi:10.1016/j.jclepro.2021.126745

Nsafon, B. E. K., Owolabi, A. B., Butu, H. M., Roh, J. W., Suh, D., and Huh, J. S. (2020). Optimization and sustainability analysis of PV/wind/diesel hybrid energy system for decentralized energy generation. *Energy Strategy Rev.* 32, 100570. doi:10.1016/j.esr.2020.100570

Olatomiwa, L., Blanchard, R., Mekhilef, S., and Akinyele, D. (2018). Hybrid renewable energy supply for rural healthcare facilities: An approach to quality healthcare delivery. *Sustain. Energy Technol. Assessments* 30, 121–138. doi:10.1016/J.SETA.2018.09.007

Owolabi, A. B., Nsafon, B. E. K., Huh, J. S., and Suh, D. (2019). Validating the techno-economic and environmental sustainability of solar PV technology in Nigeria using RETScreen Experts to assess its viability. *Sustain. Energy Technol. Assessments* 36, 100542. doi:10.1016/j.seta.2019.100542

Pal, P., and Mukherjee, V. (2021). Off-grid solar photovoltaic/hydrogen fuel cell system for renewable energy generation: An investigation based on techno-economic feasibility assessment for the application of end-user load demand in North-East India. *Renew. Sustain. Energy Rev.* 149, 111421. doi:10.1016/j.rser.2021.111421

Rajbongshi, R., Borgohain, D., and Mahapatra, S. (2017). Optimization of PV-biomass-diesel and grid base hybrid energy systems for rural electrification by using HOMER. *Energy* 126, 461–474. doi:10.1016/J.ENERGY.2017.03.056

Ramesh, M., and Prasad Saini, R. (2020). Effect of different batteries and diesel generator on the performance of a stand-alone hybrid renewable energy system. *Energy Sources, Part A Recovery, Util. Environ. Eff.* Available at: https://www.tandfonline.com/loi/ueso20. doi:10.1080/15567036.2020.1763520

Rezaei, M., Dampage, U., Das, B. K., Nasif, O., Borowski, P. F., and Mohamed, M. A. (2021). Investigating the impact of economic uncertainty on optimal sizing of grid-independent hybrid renewable energy systems. *Processes* 9 (8), 1468. doi:10.3390/pr9081468

Richardvigilantebooks (2021). What is the cost of battery storage per kWh? – Richardvigilantebooks.com. Available at: https://richardvigilantebooks.com/what-is-the-cost-of-battery-storage-per-kwh/ (Accessed Dec. 23, 2021.

Seedahmed, M. M. A., Ramli, M. A. M., Bouchekara, H. R. E. H., Shahriar, M. S., Milyani, A. H., and Rawa, M. (2022). A techno-economic analysis of a hybrid energy system for the electrification of a remote cluster in western Saudi Arabia. *Alexandria Eng. J.* 61 (7), 5183–5202. doi:10.1016/j.aej.2021.10.041

Septembre (2014). *CAMEROUN: STATISTIQUES DES PERSONNES RELEVANT DE LA COMPETENCE DU HCR evolution de la population déplacée interne et retournée EVOLUTION DE LA POPULATION (12 DERNIERS MOIS) XXX PDIs XXX Retournes*. UN Refugee Agency (UNHCR). Available at: https://data.unhcr.org/en/country/cmr.

SEPTEMBRE (2021). *INFORMATIONS GENERALES Population totale 28 181 Nombre de secteurs Distance avec la frontière Nombre total d'acteurs Poste de Gendarmerie Coordonnes GPS PERSONNES A BESOINS SPECIFIQUES Hommes Femmes PRINCIPAUX DEFIS 4 102 PBS PROFIL DU SITE DE GADO*. UN Refugee Agency (UNHCR). Available at: https://data.unhcr.org/en/country/cmr.

Sharma, S., Sood, Y. R., Sharma, N. K., Bajaj, M., Zawbaa, H. M., Turky, R. A., et al. (2022). Modeling and sensitivity analysis of grid-connected hybrid green microgrid system. *Ain Shams Eng. J.* 13 (4), 101679. doi:10.1016/j.asej.2021.101679

Shoeb, M. A., and Shafiullah, G. M. (2018). Renewable energy integrated islanded microgrid for sustainable irrigation—a Bangladesh perspective. *Energies* 11 (5), 1283. doi:10.3390/EN11051283

Singh, A., Baredar, P., and Gupta, B. (2017). Techno-economic feasibility analysis of hydrogen fuel cell and solar photovoltaic hybrid renewable energy system for academic research building. *Energy Convers. Manag.* 145, 398–414. doi:10.1016/J.ENCONMAN.2017.05.014

Solar Energy (2022). Solar energy advancements in agriculture and food production systems - google books. Available at: https://books.google.co.kr/books?id=T3dQEAAAQBAJ&pg=PA391&lpg=PA391&dq=-+10.1016/B978-0-323-89866-9.00006&source=bl&ots=UDSrJtePbm&sig=ACfU3U1_KTVmvFGBursS2yYRacP8Jf8V9A&hl=en&sa=X&ved=2ahUKEwj68br61_L4AhVCIIgKHWeEBF4Q6AF6BAgCEAM#v=onepage&q=-%20https%3A%2F%2Fdoi.org%2F10.1016%2FB978-0-323-89866-9.00006&f=false (Accessed Jul. 13, 2022.

Soudan, B., and Masoud Darya, A. (2021). "Modular hybrid energy system for refugee camps," in 2021 6th International Conference on Renewable Energy: Generation and Applications, ICREGA, Al Ain, United Arab Emirates, 02-04 February 2021, 33–38. doi:10.1109/ICREGA50506.2021.9388289

Toopshekan, A., Yousefi, H., and Astaraei, F. R. (2020). Technical, economic, and performance analysis of a hybrid energy system using a novel dispatch strategy. *Energy* 213, 118850. doi:10.1016/j.energy.2020.118850

UNHCR (2021). Document - UNHCR Cameroon - locations of UNHCR persons of concern. Available at: https://data2.unhcr.org/en/documents/details/90018 (Accessed Dec. 30, 2021.

Ur Rashid, M., Ullah, I., Mehran, M., Baharom, M. N. R., and Khan, F. (2022). Techno-economic analysis of grid-connected hybrid renewable energy system for remote areas electrification using homer pro. *J. Electr. Eng. Technol.* 17 (2), 981–997. doi:10.1007/s42835-021-00984-2

van Hove, E., and Johnson, N. G. (2021). Refugee settlements in transition: Energy access and development challenges in Northern Uganda. *Energy Res. Soc. Sci.* 78, 102103. doi:10.1016/j.erss.2021.102103

Zhang, X., Wei, Q. S., and Oh, B. S. (2022). Cost analysis of off-grid renewable hybrid power generation system on Ui Island, South Korea. *Int. J. Hydrogen Energy* 47 (27), 13199–13212. doi:10.1016/j.ijhydene.2022.01.150

Frontiers in Energy Research

Advances and innovation in sustainable, reliable and affordable energy

Explores sustainable and environmental developments in energy. It focuses on technological advances supporting Sustainable Development Goal 7: access to affordable, reliable, sustainable and modern energy for all.

Discover the latest Research Topics

See more →

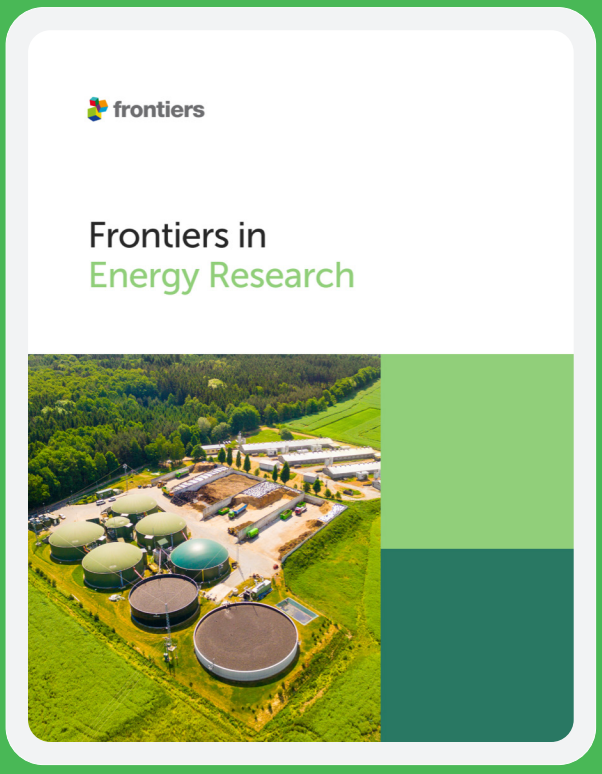

Frontiers

Avenue du Tribunal-Fédéral 34
1005 Lausanne, Switzerland
frontiersin.org

Contact us

+41 (0)21 510 17 00
frontiersin.org/about/contact